STIFFENED PLATING UNDER COMBINED IN-PLANE AND LATERAL LOADING

A thesis submitted for the degree of Doctor of Philosophy in the Faculty of Engineering of the University of London

by

Susan Elizabeth Webb BSc

Imperial College of Science and Technology, London

July 1980

TO MY PARENTS

ABSTRACT

A mathematical formulation is presented for the analysis of eccentrically stiffened plates subjected to the combined or separate actions of lateral and in-plane loading. The formulation allows for both angle and tee section stiffeners as well as rectangular flats, and both material and geometric non-linearities are considered.

To derive the governing equations the stiffeners are replaced by lines of interactive forces which produce the same response in an isotropic plate as the original stiffening members. The equations are then derived by considering the equilibrium and compatibility requirements of a small element of plate under the action of these forces.

Plasticity in the plate is assumed to be governed by a full depth yield criterion whilst in the stiffeners a multilayer approach is adopted. An elastic-perfectly plastic stress-strain curve is used to describe the material behaviour.

The governing equations are solved numerically by the application of Dynamic Relaxation to their finite difference equivalents. The finite difference expressions are generated from a rectangular interlacing network of stress resultants and displacements.

Three stiffened plate models having equal panel slenderness ratios but different stiffener rigidities have been constructed, and one of these has been tested under the combined action of lateral and in-plane loading. A testing rig was designed as part of the work and details of this, together with a description of the models and their instrumentation, is given. Results obtained from the test are discussed and comparisons are made with theoretical predictions. Theoretical results are also given for the two remaining models.

Finally, numerical results are presented for a series of plates stiffened by flats for a wide range of panel slenderness ratios and stiffener rigidities. The effects of initial deformation, combined lateral and in-plane loading and the use of hybrid plates are also investigated.

ACKNOWLEDGEMENTS

This work was carried out in the Department of Civil Engineering at Imperial College under the guidance of Professor P.J. Dowling. The Author is indebted to him for the encouragement and helpful advice she has received throughout the period of research. The Author would also like to express her appreciation to Professor B.G. Neal for providing the opportunity to work in the Department and to the Science Research Council for their financial support.

Special thanks are given to the members of the Structures Laboratory, who,under the direction of Mr J. Neale, enabled the Author to obtain the experimental results. Particular appreciation is expressed to Messrs F. Gould and S. Keir who made numerous contributions towards the design of the testing rig as well as to its construction. The Author would also like to thank Messrs E. Secker and J. Galvin who were jointly involved in the early stages of construction; Mr R. Day who fabricated the pressure bag; the Concrete Department for their assistance in constructing the pressure bag support platform and Mr P.J.D. Guile and the staff of R.M.E. Ltd. who fabricated the models and the testing rig.

The preparation of this thesis would not have been possible without the help of a number of the Author's colleagues and friends. Special thanks are expressed to Miss Judith Barritt who typed the manuscript with great care and patience; Mrs Hazel Guile who skilfully prepared the final drawings; Miss Joyce Gurr and Mr F. Milsom who produced the excellent photographs and Mrs Jean Slatford and the Author's husband Mr K.J. Rutherford for their help in correcting the manuscript. Thanks are also expressed to Mr C.J. Burgoyne with whom the Author had many useful discussions, and to Professor A.K. Basu for his help in deriving the stiffened plate equations.

Finally, the Author wishes to acknowledge the constant help, encouragement and interest shown by her parents.

CONTENTS

CHAPTER 1

INTRODUCTION AND REVIEW OF PREVIOUS WORK

1.1 THE BEHAVIOUR OF PLATED STRUCTURES

Stiffened plate components have been used for a number of years in various forms of engineering construction. They have been employed extensively in the marine and aeronautical fields and more recently as components in box-girder bridges, offshore structures and space structures.

Despite their wide application in practice relatively little is known of their true behaviour and of necessity much design work is based largely on experience. The inadequacy of this is twofold. Firstly, the extrapolation of designs to larger scale structures may be unsafe and secondly, overdesign in existing structures may lead to unnecessarily expensive and heavy components.

To develop reliable design criteria it is necessary to obtain a complete analytical understanding of the problem. It is essential not only to consider such factors as geometric and material properties, imperfections and loading conditions but also the effect of interaction between adjacent elements.

The maximum load which can be carried by a plate, although important for design purposes, cannot be used in isolation to determine safe working conditions. Many structures will become unsatisfactory in use before the ultimate load is reached due to the violation of serviceability requirements, and a complete understanding of the behaviour prior to collapse is therefore essential. Beyond the ultimate load level a stiffened panel may maintain its load carrying capacity or may suffer a violent collapse. In the latter case adjacent panels

are likely to become overloaded with a resulting total failure of the structure, whereas in the former case stability may be maintained. The post-ultimate load behaviour of isolated stiffened panels is therefore also important.

Within an isolated stiffened panel interaction may take place between adjacent plate and stiffener elements. The degree of interaction will depend upon the geometrical properties and instability within one element may precipitate the collapse of another. In Chapter 2, a formulation which allows for the influence of interaction will be presented.

In the following sections the influence of various parameters on the behaviour of plated structures is discussed, currently available methods of analysis are outlined and a review of existing work on the subject is given.

1.1.1 The Effect of Geometrical Properties

Owing to restrictions of weight and economy the panels of stiffened plates are often slender, and if the critical panel buckling stress is less than the yield stress local failure is likely to occur. Although this may violate serviceability requirements, it does not imply immediate collapse since, in many cases, a reserve of strength will exist. This arises from the ability of a section to redistribute sustained loads and the significance of this will depend upon the geometrical properties. If the plate dimensions are such that bifurcation occurs in the elasto-plastic range, the capacity for redistribution will be small and rapid unloading will follow. If the panels are more slender, however, and buckling occurs in the elastic range, stresses will redistribute to stiffer sections of the plate and stability will be maintained. In the latter case the ultimate load will not be reached until either

the rate of unloading exceeds the rate of redistribution, or yielding has occurred in the remaining effective areas of plating.

In the past, the design of stiffened panels has been based on linear buckling theory, with the assumption that the reserve of strength will compensate for loss of capacity due to fabrication tolerances. This approach is particularly unsafe when failure occurs by complex interaction of local panel buckling and yielding, since in this region failure may occur below the critical elastic buckling load.

The development of a local mode does not depend only on the geometry of the panels but also on that of the stiffeners. In slender panels reinforced by flexurally strong and torsionally weak ribs, buckling will occur close to the theoretical critical stress for simply supported plates. With increased torsional stiffness or reduced flexural stiffness, however, the same plate may reach its ultimate stress in the absence of local effects. A high torsional stiffness will provide a partial clamping at the panel edges and thus an increase in the buckling stress, whilst a low flexural stiffness will provide negligible lateral restraint to the panel edges and an overall mode of failure will ensue.

The second type of failure to be discussed is the overall buckling of a stiffened panel between transversals. This can occur in combination with, or in the absence of, a local mode and will involve a flexural or torsional failure of the stiffeners.

For cases in which the stiffeners are flexurally weak and deformation occurs away from the plating, tensile yielding is likely to occur within their extreme fibres. This will lead to a reduction in the flexural capacity and whilst the plating may still be fully elastic, an overall mode of failure will follow.

If buckling occurs towards the plating such that the stiffener outstands are in compression, failure will occur either by yielding of

the stiffeners in the case of stocky sections, or by buckling of the stiffeners[1,2] in more slender sections. The failure of one stiffener within the cross-section will lead to a sudden reduction in overall strength and the remaining stiffeners will be called upon to support a larger proportion of the applied load. Progressive failure across the panel is then likely to follow, and this will lead to the violent collapse often associated with this mode of behaviour.

Lateral buckling of the stiffeners is not only associated with flexural action but may also occur in a compression panel where the stiffeners are torsionally weak. To avoid this situation in practice, the depth to thickness ratio of the stiffeners must be restricted or closed section ribs employed. The latter alternative has been shown[3] to be highly beneficial compared with open section stiffeners of the same cross-sectional area.

The final mode of failure to be noted here applies to compression panels in which both the plating and the stiffeners are stocky. In such cases, the plating will reach full yield in compression and with increased loading will then squash at constant stress. The stiffeners will develop higher tensile stresses to resist additional applied moments and the capacity of the total section will thus decrease.

The modes of failure described above will not usually occur independently and it has been suggested that the optimum design is obtained when the overall mode coincides with the local mode. A recent study[4] indicates, however, that plates within this range are highly imperfection sensitive and since such irregularities cannot be avoided in practice, due consideration must be given to them before a real optimum design can be found. It was further shown[5] that although the highest carrying capacity is often obtained when local buckling occurs in advance of overall buckling, the reverse is true as far as stiffness and therefore serviceability is concerned.

1.1.2 The Effect of Initial Deformation

Initial deformations resulting from fabrication can take a variety of different forms and these will influence both the mode of behaviour and the collapse load. In an eccentrically stiffened welded panel an overall bow will generally be present, and although this will frequently be directed towards the stiffening, the reverse may be true in many cases. The welding of stiffeners to one side of the plate only will often cause a dishing of the panels between the ribs and, in addition, deformations will be present in the stiffeners both locally and in an overall sense along their lengths.

Although the shape of imperfection will not always be sympathetic to the preferred mode of buckling and will therefore not always influence the plate behaviour[6], there are cases where both its magnitude and direction are important. It has been observed[7] that a significant difference in load carrying capacity can exist depending on whether an overall mode of failure occurs towards the plating or towards the stiffeners. The direction of collapse in a compressed panel will depend upon the net eccentricity of the applied load and will therefore be a function of the direction and magnitude of an initial bow.

The significance of any level of initial deformation will depend primarily on the geometrical properties involved. For unstiffened compression panels of low slenderness, where failure occurs in a squash type mode, initial deformation is unlikely to cause a significant reduction in the collapse strength. For very slender panels this is again likely to be the case since large deflections which result under load will mask the presence of initial deformation. For panels of intermediate slenderness, however, where buckling occurs in the elasto-plastic range, much greater imperfection sensitivity is likely to exist.

In stiffened panels, the significance of an overall bow will be influenced by the flexural rigidity of the ribs. In cases where failure is likely to occur by tensile yielding in these members, an overall bow away from the plating will accelerate this process.

To reduce the level of initial deformation and hence its effect on plate behaviour, straightening procedures are often employed. Three methods of straightening have been investigated experimentally by Horne and Narayanan[8,9]. The first method involves localised heating to a sufficient temperature and subsequent cooling to draw the panel back to its required shape. The second method involves the clamping of plate components to predetermined initial curvatures followed by a carefully selected welding sequence, and the third method relies upon mechanical loading. Tests carried out on similar panels straightened by the three different procedures, showed that the method adopted is all important as far as the collapse strength is concerned.

An extensive review of the effect of initial imperfections on the buckling strength of plated structures is given in Reference 10.

1.1.3 The Effect of Residual Stress

Residual stresses resulting from the welding process can have a detrimental effect on the load bearing capacity of plated structures. The area of plating immediately adjacent to a weld is generally stressed to yield in tension, this zone extending some two to four plate thicknesses out from the weld on either side. The remainder of the plate will support a residual compression thereby maintaining overall equilibrium of the system.

As in the case of initial deformations the significance of residual stress will depend upon the geometrical properties. Investigations carried out by Moxham[11] into unstiffened plate behaviour showed that

the effect of residual stress is most severe for panels of intermediate slenderness where interaction between local buckling and yielding occurs. For plate panels of low slenderness, where failure occurs by squashing, residual stresses have negligible effect and the ultimate load capacity will be similar in magnitude to the stress-free case. For panels of high slenderness the presence of residual compression will lower the buckling load,but since the edges are initially stressed to yield in tension a larger post-buckling reserve is likely to exist than in the equivalent stress-free case. It follows therefore that the reduction in ultimate strength is likely to be less than the reduction in buckling strength.

In stiffened panels residual stresses will be present in the ribs as well as in the plating,and investigations by Hasegawa et al[12] show that the smaller the flexural rigidity of the stiffeners, the greater is the drop in strength. Idealised residual stress patterns are shown in Reference 13 where a comparison is made with experimental data.

To reduce the level of residual stress intermittent welding can be used in place of continuous welding. The advantage gained from this however may be insignificant, since the stiffeners will be unsupported between the weld runs and separation may then occur between the members.

1.1.4 The Effect of Loading Type and Boundary Restraint

Stiffened plate components can be subjected to a variety of loading types and boundary constraints in the working state and with different combinations of these parameters, different modes of behaviour are likely to result.

Loading types can be divided into two broad categories, those applied in the plane of the plate and those acting normal to it. In the first group forces may be tensile, compressive or shear and may arise

directly from application, or indirectly from the overall distortion of a structure. Where stresses arise from overall distortion they are likely to vary both along the length and across the width of a member. In the second group, loading will frequently be in the form of a uniformly distributed pressure as in the case of hydrostatic loading on a ship's hull. Often however, concentrated line or point loads will also exist.

In working structures the loading types described will rarely occur in isolation and behaviour under combined loads may be quite different from that under individual loads. The resulting response will depend both on the relative magnitudes of each type of loading and on their order of application. For a plate subjected to both lateral and in-plane loading, where the lateral loading is applied in advance of the compression, in-plane forces are likely to act at a larger mid-span eccentricity than would be the case with compressive loading alone, and this will accelerate the development of an overall mode of failure. The presence of lateral forces may also suppress local buckling within the panels, and if an initial bow opposes the direction of lateral forces the compressive strength of the panel may be enhanced.

The degree of restraint applied to the panel edges both in and out-of-plane, will affect the shape of deformation and hence the response of a structure to a given type of loading. The form of restraint between adjacent members will, in addition, determine the degree of response in one panel from loading applied to another.

In developing analytical techniques it is therefore essential to provide for a variety of combinations of loading types and boundary restraints, if reliable design criteria are to be developed for all possible working conditions.

1.1.5 Material and Geometric Non-Linearities

In any analytical approach a number of simplifying assumptions must be made and in plated structures two of these are related to non-linear behaviour.

In the past, plated structures have been analysed by employing small deflection elastic theory which assumes that deflections remain small in relation to the plate thickness and that the stresses remain in the linear elastic range. In practical structures these assumptions are rarely valid. Under lateral loading, deflections in excess of half the plate thickness are typical and under in-plane loading, for all but the most stocky cross-sections, large deflections are associated with buckling. In reality,therefore, in-plane straining of the middle-plane of the plate will be coupled with flexural action in resisting out-of-plane deformations,and small deflection theory which ignores this coupling effect will predict overconservative results.

The restriction placed on material behaviour is also too stringent for general application, since in all but the most slender cross-sections plasticity will influence the plate strength. This will be particularly significant in the range of panel slenderness where buckling and yielding interact, since here the elastic buckling strength can be reduced by plastic action.

1.2 REVIEW OF EXISTING WORK

In the following sections a review of literature on stiffened plates is given. For the purpose of discussion, the literature is divided into sections according to the analytical approach adopted and an attempt is made to emphasise some of the advantages and disadvantages associated with each. In some cases,however, it should be noted that there may be some degree of overlap owing to the use of two methods in

combination. For example, the finite element method can be used to solve a beam-column or orthotropic plate idealisation as well as a complete structure.

Basic information on the behaviour of plates can be obtained from standard text books[14-16] and attention is drawn to earlier reviews given by Djahani[17] and Mansour[18], the first for stiffened and unstiffened plates and the second for methods of gross panel analysis. Additionally, Smith[19] has investigated some of the methods available with reference to tests on full scale ship grillages.

1.2.1 Orthotropic Plate Theory

In an orthotropic plate analysis a stiffened panel is idealised as a continuum. Stiffeners are smeared across the panel width and orthotropic rigidities are derived for the two orthogonal directions.

The degree of approximation associated with the method depends largely on the panel geometry and the material properties involved. The method provides no facility for the prediction of local panel buckling, and yielding of the orthotropic section will bear little resemblance to that of the real panel. These two limitations restrict the use of the method to plates in which the stiffener spacing is close enough to preclude local panel action and to stresses which remain in the linear elastic range. In addition, the eccentricity of stiffeners can only be included approximately by a modification to the orthotropic rigidities and residual stress distributions cannot be represented accurately. Ultimate load predictions can only be made by employing an approximate collapse criterion and in the real situation behaviour at collapse can take a variety of forms.

The main advantage of the method is its simplicity, and providing it is applied selectively with the above restrictions in mind, a reasonable degree of accuracy will be achieved.

Basic information on orthotropic plate theory can be found in reference 20. The method has been used to study both laterally and uniaxially loaded plates and a number of different boundary conditions have been considered. Early work on the subject has been reviewed in detail by Dowling[21], who employed the method to investigate the behaviour of stiffened plate bridge decks under concentrated wheel loads.

Schade[22] presented small deflection orthotropic solutions for laterally loaded plates orthogonally stiffened by equally spaced ribs, and Falconer and Chapman[23] applied the method to obtain buckling solutions for initially curved compression panels. In these procedures rigidities were determined analytically, whilst in a later analysis presented by Hoppmann[24], rigidities were determined experimentally from bending and twisting tests on steel plates.

Using a series method of solution, Soper[25] applied orthotropic theory to solve the large-deflection problem of laterally loaded orthogonally stiffened plates with both clamped and simply supported edges. Two orthotropic plates were employed, one to deal with out-of-plane effects and the other to deal with membrane effects.

Improving on the above series method of solution, Basu[26] and Basu and Chapman[27] employed a finite difference approach. Modifications were applied to allow for different orthogonal rigidities and a wide range of in-plane and flexural boundary restraints were considered. Aalami[28] and Aalami and Chapman[29] extended the method to study plates under combined lateral and in-plane loading and employed graded meshes to deal more effectively with concentrated loads. Using Aalami's computer program, Williams and Chapman[30] studied the behaviour of double bottom structures with reference to tests on a one-eighth scale steel model loaded both laterally and in-plane. Allowance was made within the theory for reduction in overall flexural stiffness due to local distortions in the plating.

Nishino et al[31] presented an analysis based on the small deflection equilibrium equations for orthotropic plates but allowed for extensibility of the middle-plane in deriving the orthotropic rigidities. Full interaction between the plating and stiffening system was accounted for in deriving the rigidities, and comparisons are given between the torsional term obtained and that used in the less rigorous approach where interaction is ignored.

Although orthotropic theory is essentially limited to the elastic range of stress, some attempt has been made to include the effects of material non-linearity. In an analysis presented by Kagan and Kubo[32] for laterally loaded orthogonally stiffened plates, yielding was considered in the stiffeners but not in the plate. The approach involved the determination of orthotropic plate displacements from which stiffener slopes and hence stiffener bending stresses could be calculated. These stresses were used to check for yielding in the stiffeners and if this had occurred, a reduced area of elastic material was used to calculate rigidities for the next load step.

To study the ultimate load behaviour of box-girder compression flanges, Massonnet and Maquoi[33] adopted orthotropic theory with refined expressions for bending and torsional rigidities. Collapse was assumed to occur when the mean membrane stress along the unloaded edges reached yield, and the ultimate load was obtained by factoring the corresponding mean stress on the loaded edges to allow for local panel buckling.

1.2.2 Beam-Column Theory

In this approach a stiffened panel is idealised as a strut which consists of a single stiffener and an effective width of plating. In general, the analysis involves the determination of moment-thrust-curvature relationships, from which the deflected shape of the plate under any applied loading can be obtained numerically.

This method is satisfactory for the analysis of wide stiffened panels which fail in a single half-wave buckling mode, and allowance can be made for local panel failure by using a reduced effective width of plating or a modified stress-strain curve. For thick plates reinforced by light stiffening or for long narrow plates reinforced by one or two ribs, however, the method is particularly inappropriate since no allowance can be made for biaxial stress conditions.

The main advantage of the approach is the ease with which it can be applied and as a result of this, a number of design proposals have been based on the method.

In an extensive research programme at Lehigh University, beam-column methods of analysis have been developed and results have been compared with experimental data. Ostapenko and Lee[34] presented test results for simply supported panels under combined lateral and in-plane loading, and Kondo and Ostapenko[35] extended the range to include panels with clamped edges. In both cases the unloaded edges were free out-of-plane, and the variables considered were the panel slenderness and the magnitude of applied lateral loading.

To determine the moment-thrust-curvature relationships the stress-strain behaviour of the cross-section must be identified, and assumptions made at this stage in the analysis will determine the range of plates for which the method is applicable. Kondo[36] investigated the buckling of low slenderness panels, assuming a wide column mode and allowing for the non-linear effects of both inelastic action and deformation. An elastic-perfectly plastic stress-strain relationship was assumed and this was modified, where necessary, to take account of residual stress.

Vojta and Ostapenko[37] extended the theory to investigate the

ultimate strength of panels with width to thickness ratios such that panel buckling occurs prior to the ultimate load. For this analysis the stress-strain curve was modified in the following manner. A linear relationship between stress and strain was employed up to the critical panel buckling stress, a non-linear curve according to Koiter was used to describe the elastic post-buckling behaviour, and a horizontal portion was employed to define the maximum stress level based on the mean applied stress when the edges reach yield. Again modifications were applied to take account of residual stress. Using results from this analysis, Vojta and Ostapenko[38] generated design curves from which the dimensions of a panel which will just sustain the simultaneous application of lateral and in-plane loading can be obtained. A further extension to this work was presented by Rutledge and Ostapenko[39] who modified the stress-strain curve to take account of materials which exhibit a non-linear elastic behaviour.

With reference to box-girder bridge construction, Moolani[40] and Moolani and Dowling[41] presented a similar approach for uniaxially loaded compression flanges, taking account of failure both towards the plating and towards the stiffeners. The stress-strain relationships adopted for the plating were obtained from a large-deflection elasto-plastic analysis of individual panels[42], which incorporated a single layer yield criterion and the effect of residual stress. To study the behaviour of multiple bays individual beam-columns were reacted on spring supports.

A simple Ritz solution procedure was adopted by Crisfield[43] to study the beam-column behaviour of plates and, in this approach, the stress-strain characteristics were obtained from a finite element analysis of individual panels. To include the effect of residual stress an approximate method was developed from which the load-shortening

curves obtained for stress free panels, could be modified to generate a family of curves for different levels of residual stress.

Smith[19] adopted a similar approach to compute the collapse loads for two test grillages which failed by flexural buckling of the longitudinal stiffeners. Results are presented for a range of residual stress levels, boundary constraints and initial deformations. Local effects in the plating were again accounted for by employing load-shortening curves derived from the analysis of individual panels, and plasticity in the stiffeners was incorporated by subdividing the cross-section into small elements and limiting the stress at the centroid of each to the yield stress. It was concluded that the collapse loads predicted by this method were reasonably consistent with experimental results.

1.2.3 The Finite Element Method

In the finite element method a stiffened panel is idealised by a series of interconnected elements. These can take the form of orthotropic elements, or bending and stretching plate elements together with beam elements for the stiffeners. The degree of approximation involved will depend primarily on the shape functions selected and on the compatibility conditions applied along the element boundaries.

An adaption of the finite element method is the finite strip approach. Here the structure is idealised by strips which are connected together along two sides whilst the remaining edges form the boundaries of the plate. This reduces the two dimensional problem to one dimension and a considerable saving in computer time results.

Using the finite strip approach, Fukumoto et al[44] have studied the ultimate load behaviour of simply supported compression panels, reinforced by equally spaced ribs of rectangular cross-section. The theory

applies to panels of low width to thickness ratio, where it was assumed that no out-of-flatness exists prior to buckling, and that the ultimate and buckling strengths are identical. Residual stresses were included in both the plate and the stiffeners and their effect on the ultimate load capacity was investigated. Torsional rigidity of the webs was also included and this was shown to enhance the buckling strength. Comparisons were made between theoretical and test results obtained by the authors and in general, satisfactory agreement was achieved. Fukumoto et al[13] subsequently extended this work to obtain solutions for plates stiffened by tee-section ribs. Results showed that compared with a flat type stiffener, the reduction in flexural rigidity due to partial yielding in the stiffeners was much more gradual.

Hasegawa et al[12] also employed the finite strip method to investigate the effect of residual stress on the elasto-plastic buckling strength of multiple stiffened panels. The distribution of residual stress adopted for the plate was similar in form to that employed by Fukumoto et al[13,44]. In the stiffeners, the effect was accounted for by modifying the material stress-strain curve. This consisted of a linear elastic portion reduced to take account of residual stress, a horizontal portion for fully plastic action and a cubic polynomial in between to describe the transition from elastic to plastic behaviour. From this work it was concluded that the drop in buckling strength due to residual stress in the stiffeners is related to the flexural rigidity of these members.

To study the behaviour of laterally loaded plates, Rossow and Ibrahimkhail[45] and Wegmuller[46] adopted the finite element technique. Assuming a linear variation of deformation due to bending Rossow and Ibrahimkhail[45] developed an elastic analysis for stiffened plates with eccentric and concentric stiffeners. Numerical results were obtained

for both types of stiffener and both uniaxial and biaxial ribs were considered. Wegmuller[46] presented a general method capable of predicting the entire load deformation behaviour of stiffened panels under lateral loading. A layered beam-plate model was adopted to describe the process of yielding and the effect of strain hardening was included. Based on the assumption that considerable plastification occurs before deflections become large, a unit load was applied to the structure and the resulting stresses were factored to obtain the load at which first yield occurred. Following this, an incremental technique was employed where stiffnesses were updated at each load stage to allow for the spread of plasticity through the section.

Dowling[47] presented experimental results for a stiffened panel subjected to a central point load. Results obtained show the effect of stiffener yielding on the load-deflection response of the structure.

Tvergaard and Needleman[48] investigated the elasto-plastic buckling and post-buckling behaviour of wide, eccentrically stiffened panels subjected to uniaxial compression. Initial deformations were considered in the shape of a wide column mode and a local mode, and solutions were presented for plates with both simply supported and continuous edge conditions. Plasticity in the plate was assumed to be governed by flow theory with hardening included whilst for the stiffeners, the level of direct stress was employed to predict yielding of the section.

Søreide, Bergan and Moan[49] also adopted flow theory to describe the plastic behaviour of eccentrically stiffened plates, and full details of the formulation are given in reference 50. Using the method, load-deflection curves and deflection profiles were generated and an investigation into the effect of various levels of initial deformation was carried out.

In a non-linear analysis presented by Crisfield[51] the prediction of yield was based on a theory involving stress resultants rather than stresses. The expressions adopted were chosen such that the load at first yield was accurately predicted for full section yielding of the plate and for first fibre yielding of the stiffeners. The formulation was used to analyse eccentrically stiffened wide and narrow panels under the application of in-plane loading.

1.2.4 Discretely Stiffened Plate Theory

In a discretely stiffened plate analysis the plate and stiffeners are treated separately, and by enforcing compatibility and equilibrium along their lines of intersection, the assembly is forced to act in a composite manner. In this way the problem is reduced to the analysis of an unstiffened panel with a line of discontinuity in the loading.

The advantages of this approach are numerous. Both overall buckling of the stiffened section and local buckling of the panels between the ribs can be predicted and interaction between adjacent elements accounted for. Non-linear material effects can be included and allowance can be made for eccentricity of the stiffeners. Further, residual stresses can be incorporated with relative accuracy and different modes of initial deformation can be investigated.

Dean and Omid'varan[52] presented a closed form field approach for the analysis of rectangular plates reinforced by flat section ribs. Small deflection elastic behaviour was assumed throughout and three categories of plate-stiffener interaction were considered. The first approach was a 'composite membrane analysis', in which full composite action was considered in the plane of the plate whilst the flexural capacity of the plating was ignored. The second approach was a 'non-composite flexural analysis', in which in-plane plate deformations and

in-plane continuity were ignored whilst flexural interaction was considered, and the third approach was a 'composite membrane-flexural analysis', in which all interaction components were considered. For each of these categories, the governing equations were solved in closed form to obtain deformations in terms of the applied loading.

An approach similar to the non-composite flexural analysis was adopted by Wah[53] to investigate the effect of torsional stiffness on the buckling strength of compression panels, and the composite membrane-flexural analysis formed the basis of work carried out by Avent and Bounin[54] to investigate the buckling behaviour of ribbed plates.

Hovichitr et al[55] presented a rational small deflection elastic analysis for rectangular plates with eccentric orthogonal stiffening. Governing equations of tenth order were generated and simplified expressions of eighth and fourth order were obtained from them. Using a Fourier series technique, solutions were obtained for a simply supported panel under lateral loading and comparisons were made between the tenth, eighth and fourth order solutions obtained.

Djahani[56] and Basu, Djahani and Dowling[57] investigated the large-deflection elastic behaviour of discretely stiffened plates and developed the governing equations for panels stiffened by rectangular flats in one or both directions. A modified Newton-Raphson technique was used to solve the finite difference forms of these expressions, and solutions were obtained for plates loaded both laterally and in-plane. Djahani[17] later extended this work to include the effects of material non-linearity and residual stress. A full depth yield criterion was adopted for the plate and a multilayer approach was used for the stiffeners. Ignoring transverse bending of the stiffeners and torsional interaction between the plate and stiffeners, Lamas[58] and Lamas and

Dowling[59] used the approach to study the problem of shear lag in wide flanged box-girders. Again a finite difference technique was employed and the equations were solved numerically by the method of Dynamic Relaxation.

1.2.5 Design Methods

Design methods for stiffened plates have been proposed by a number of authors and many of these rely on a beam-column idealisation. Chatterjee and Dowling[60] have reviewed a number of methods recently developed for box-girder compression flanges and have indicated the scope and limitations of each.

Horne and Narayanan[61] proposed a method for axially loaded plates based on a Perry Robertson strut formula. Failure both towards the plating and towards the stiffeners was considered, and allowance was made for reduction in stiffness due to local panel buckling by using a reduced effective width of plate[62]. Residual stresses were included by magnifying the initial deformation level, and the ultimate strength was defined as the load required to cause yield at the middle-plane of the plate or at the extreme fibres of the stiffeners. Comparisons were made between the ultimate loads predicted by this method and test results obtained by the authors.

Murray[63] also proposed a Perry Robertson strut approach and allowed for loss of plate effectiveness when the critical panel buckling stress was less than the Euler stress. The ultimate load was defined as that required to cause yielding at the extreme plate or stiffener fibres, and simple rules were given for panels loaded in bending and in combined bending and axial compression. Test results for nine large scale panels were obtained and these were compared with theoretical predictions.

In a strut approach proposed by Chatterjee and Dowling[64], load-shortening curves were derived from a large-deflection analysis of isolated panels and these were used to allow for loss of plate effectiveness. The peak load position on these curves was used to define a secant stiffness for the plating and from this the effective section was determined. This section was then analysed as a beam-column and yielding at the middle-plane of the plate or extreme fibres of the stiffeners was used to define failure. Chatterjee and Dowling[65] also proposed a method based on orthotropic theory and gave rules for laterally loaded plates, composite steel and concrete compression flanges, and cases in which a variation of axial load exists along the length of a member.

In an approach presented by Dwight[66] and Dwight and Little[67], a fictitious yield approach was adopted to allow for loss of plate effectiveness. Here, the actual yield stress was replaced by a fictitious value which was obtained from plate strength curves for a given panel slenderness. Using this value to define a column curve, the collapse strength was then obtained for the appropriate column slenderness.

Finally, Carlsen[68] discussed two simple strut approaches for stiffened plates. The first of these was an elastic-plastic strut analysis, where collapse was defined as the point of intersection between the elastic and plastic load-deflection curves whilst the second was again a Perry Robertson strut approach.

1.3 SCOPE OF THESIS

From the preceding discussion, it is evident that a greater analytical understanding of stiffened plate behaviour must be acquired before reliable design techniques can be formulated. As a contribution towards this, a theoretical and experimental study on the subject is given in this thesis.

The mathematical formulation developed in Chapter 2, extends the work of Djahani[17] by allowing for tee and angle section stiffeners as well as rectangular flats. Both geometric and material non-linearities are included and interaction between adjacent elements is automatically accounted for. Expressing the governing equations in finite difference form and using the method of Dynamic Relaxation, a computer program has been written and this is discussed in detail in Chapter 3.

To validate a mathematical formulation, comparisons should be made with controlled experimental data and,as part of this work, a series of tests have been designed. A plate testing rig was designed and constructed specifically for the purpose and full details of this, together with a description of the models and their instrumentation,is given in Chapter 4. Of the three models fabricated one only has been tested and the results obtained are compared with theoretical predictions in Chapter 5. In addition, theoretical results are included for the remaining two models.

Finally, a wide range of plate problems have been solved and results are discussed in Chapter 6. The main parameters chosen for investigation were the plate and stiffener slenderness ratios. Smaller scale studies were also undertaken to investigate the effects of initial deformation, combined lateral and in-plane loading and the use of hybrid plates.

CHAPTER 2

MATHEMATICAL FORMULATION

2.1 OUTLINE OF APPROACH AND ASSUMPTIONS

2.1.1 Outline

The equations of equilibrium for discretely stiffened plates are developed by idealising the assembly as an isotropic plate subjected to body forces. This method was first used by Basu, Djahani and Dowling[57] for plates stiffened by flats and here the work is extended to incorporate 'T' and 'L' section ribs.

By considering the equilibrium of a stiffener flange at its intersection with the web and of a stiffener web at its intersection with the plate, and by enforcing displacement continuity between these three elements, expressions are obtained for a set of forces which can be applied to an isotropic plate to simulate the effect of stiffening. The governing equations are then derived by considering the equilibrium of a small element of plate under the action of these forces, and by defining force-displacement relationships for the plate and stiffeners.

To enable an analysis to be carried out in both the elastic and elasto-plastic stress ranges two sets of force-displacement equations are incorporated. For the plate component the Ilyushin[69] yield criterion is used to predict yielding of the cross-section and where this has occurred, total elastic force-displacement relationships are replaced by incremental forms in which the rigidity terms allow for material non-linearity. For the stiffener webs and flanges a simplified form of the Von Mises' yield criterion is used to predict yielding of the cross-section. In the elastic range elastic force-displacement

and moment-curvature relationships are adopted, whilst in the elasto-plastic range a process of numerical integration is used to determine forces and moments.

Finally, for complete definition of the problem a set of boundary conditions is specified.

2.1.2 Assumptions

The formulation presented is based on the following assumptions of thin plate and beam theory:

(a) Direct stresses normal to the middle-plane of the plate and normal to the longitudinal axis of the stiffener are assumed to be negligible.

(b) To comply with the assumption of plane sections remaining plane, transverse shear deformations are ignored both in the plate and in the stiffeners.

(c) Slopes are assumed everywhere to be small by virtue of the fixed co-ordinate system adopted.

It is further assumed that:

(d) The material behaves in an elastic-ideally plastic manner.

(e) The stiffener cross-section does not distort under load.

(f) Shear stresses in the stiffeners are small enough to permit the use of elastic torsional properties throughout the analysis.

2.2 EQUILIBRIUM EQUATIONS IN TERMS OF FORCES

2.2.1 Continuity of Displacements between the Plate and Stiffener

Displacements are defined relative to a fixed system of axes, orientated as shown in Fig. A1, with x and y lying in the middle-plane of the ideally flat plate and z perpendicular to it.

The net components of displacement at the middle-plane of the

plate in the x, y and z directions are defined as u, v and w respectively. A subscript o is used to denote initial deformations and a superscript - to denote total deformations. Stiffener displacements are similarly defined by u, v and w with the addition of subscripts w for web, f for flange, c for centroid and e for the centroid of a small element of the cross-section.

Referring now to Figs A1 and A2 and assuming that the plate is deformed initially only in the z-direction ($u_o = v_o = 0$), the following relationships can be written for stiffener displacements in terms of middle-plane displacements and slopes:

(a) For a point in the web ($y = ehw$; $z = evw$)

$$\left.\begin{aligned}
w_{ew} &= w + ehw.\partial w/\partial y \;;\; w_{oew} = w_o + ehw.\partial w_o/\partial y \\
v_{ew} &= v - evw.\partial w/\partial y \;;\; v_{oew} = -evw.\partial w_o/\partial y \\
u_{ew} &= u - evw.\partial w/\partial x - ehw.\partial v/\partial x \;;\; u_{oew} = -evw.\partial w_o/\partial x \\
\bar{w}_{ew} &= w_{ew} + w_{oew} \;;\; \bar{v}_{ew} = v_{ew} + v_{oew} \;;\; \bar{u}_{ew} = u_{ew} + u_{oew}
\end{aligned}\right\} \quad (1)$$

(b) For a point in the flange ($y = ehf$; $z = evf$)

$$\left.\begin{aligned}
w_{ef} &= w + ehf.\partial w/\partial y \;;\; w_{oef} = w_o + ehf.\partial w_o/\partial y \\
v_{ef} &= v - evf.\partial w/\partial y \;;\; v_{oef} = -evf.\partial w_o/\partial y \\
u_{ef} &= u - evf.\partial w/\partial x - ehf.\partial v/\partial x \;;\; u_{oef} = -evf.\partial w_o/\partial x \\
\bar{w}_{ef} &= w_{ef} + w_{oef} \;;\; \bar{v}_{ef} = v_{ef} + v_{oef} \;;\; \bar{u}_{ef} = u_{ef} + u_{oef}
\end{aligned}\right\} \quad (2)$$

(c) For the web centroid ($y = 0$; $z = cvw$)

$$
\left.
\begin{aligned}
w_{cw} &= w \quad ; \quad w_{ocw} = w_o \\
v_{cw} &= v - cvw.\partial w/\partial y \quad ; \quad v_{ocw} = -cvw.\partial w_o/\partial y \\
u_{cw} &= u - cvw.\partial w/\partial x \quad ; \quad u_{ocw} = -cvw.\partial w_o/\partial x \\
\bar{w}_{cw} &= w_{cw} + w_{ocw} \quad ; \quad \bar{v}_{cw} = v_{cw} + v_{ocw} \quad ; \quad \bar{u}_{cw} = u_{cw} + u_{ocw}
\end{aligned}
\right\} \qquad (3)
$$

(d) For the flange centroid ($y = chf$; $z = cvf$)

$$
\left.
\begin{aligned}
w_{cf} &= w + chf.\partial w/\partial y \quad ; \quad w_{ocf} = w_o + chf.\partial w_o/\partial y \\
v_{cf} &= v - cvf.\partial w/\partial y \quad ; \quad v_{ocf} = -cvf.\partial w_o/\partial y \\
u_{cf} &= u - cvf.\partial w/\partial x - chf.\partial v/\partial x \quad ; \quad u_{ocf} = -cvf.\partial w_o/\partial x \\
\bar{w}_{cf} &= w_{cf} + w_{ocf} \quad ; \quad \bar{v}_{cf} = v_{cf} + v_{ocf} \quad ; \quad \bar{u}_{cf} = u_{cf} + u_{ocf}
\end{aligned}
\right\} \qquad (4)
$$

2.2.2 Interactive Forces and the Equilibrium Equations

The sectional actions associated with a small element of stiffened plate deformed under load are shown in Figs A3 to A5. The web, plate and flange components are detailed separately, interaction between them being preserved by the application of a system of equal and opposite body forces and couples per unit length of the interfaces. These components will be referred to as interactive forces.

The interactive forces at the web-plate interface are defined as FX_w, FY_w, FZ_w and FT_w. The in-plane components, FX_w and FY_w, act within the middle-plane of the deformed plate and the out-of-plane component, FZ_w, acts in the positive z-direction. A directionally similar set of actions, FX_f, FY_f, FZ_f and FT_f are defined at the web-flange interface.

Stiffener internal forces and moments are defined as N and M respectively with the addition of symbols A, H,V and T to denote the axial, horizontal, vertical and torsional components. Again subscripts

w and *f* are employed to distinguish between the web and flange components.

Referring now to Figs A3 to A5, the equations of equilibrium for discretely stiffened plates are developed.

2.2.2.1 *Interactive Forces at the Web-Flange Interface*

Taking moments for the flange about x', y' and z' (a set of axes parallel to x, y and z but with origin at the intersection of the web and flange) and summing flange forces in these directions, a set of expressions is obtained for the interactive forces at the web-flange interface.

Taking moments about x':

$$FT_f = \partial MT_f/\partial x - chf.\partial NV_f/\partial x + \tfrac{1}{2}.t_f.\partial NH_f/\partial x \quad (5)$$

Taking moments about y':

$$NV_f = \partial MV_f/\partial x + \tfrac{1}{2}.t_f.\partial NA_f/\partial x \quad (6)$$

Taking moments about z':

$$NH_f = \partial MH_f/\partial x + chf.\partial NA_f/\partial x \quad (7)$$

Resolving forces in the x' direction:

$$FX_f = \partial NA_f/\partial x \quad (8)$$

Resolving forces in the y' direction:

$$FY_f = \partial NH_f/\partial x + NA_f.\partial^2 \bar{v}_{cf}/\partial x^2 + \partial NA_f/\partial x.\partial \bar{v}_{cf}/\partial x \quad (9)$$

Resolving forces in the z'direction:

$$FZ_f = \partial NV_f/\partial x + NA_f.\partial^2 \bar{w}_{cf}/\partial x^2 + \partial NA_f/\partial x.\partial \bar{w}_{cf}/\partial x - FX_f.\partial \bar{w}/\partial x - FY_f.\partial \bar{w}/\partial y \quad (10)$$

Substituting (6) and (7) into (5):

$$FT_f = \partial MT_f/\partial x - chf.\partial^2 MV_f/\partial x^2 + \tfrac{1}{2}.t_f.\partial^2 MH_f/\partial x^2 \quad (11)$$

Substituting (7) into (9):

$$FY_f = \partial^2 MH_f/\partial x^2 + chf.\partial^2 NA_f/\partial x^2 + NA_f.\partial^2 \bar{v}_{cf}/\partial x^2 + \partial NA_f/\partial x.\partial \bar{v}_{cf}/\partial x \quad (12)$$

Substituting (6) into (10):

$$FZ_f = \partial^2 MV_f/\partial x^2 + \tfrac{1}{2}.t_f.\partial^2 NA_f/\partial x^2 + NA_f.\partial^2 \bar{w}_{cf}/\partial x^2 + \partial NA_f/\partial x.\partial \bar{w}_{cf}/\partial x - FX_f.\partial \bar{w}/\partial x - FY_f.\partial \bar{w}/\partial y \quad (13)$$

Equations (8), (11), (12) and (13) are the required interactive body forces at the web-flange interface.

2.2.2.2 *Interactive Forces at the Web-Plate Interface*

Taking moments for the web about the x, y and z axes and summing forces in these directions, a set of expressions is obtained for the interactive forces at the web-plate interface in terms of stiffener forces and moments:

Taking moments about x:

$$FT_w = FT_f + \partial MT_w/\partial x + FY_f(h_w + \tfrac{1}{2}.t) + cvw.\partial NH_w/\partial x \quad (14)$$

Taking moments about y:

$$NV_w = \partial MV_w/\partial x + cvw.\partial NA_w/\partial x + FX_f(h_w + \tfrac{1}{2}.t) \quad (15)$$

Taking moments about z:

$$NH_w = \partial MH_w/\partial x \quad (16)$$

Resolving forces in the x-direction:

$$FX_w = FX_f + \partial NA_w/\partial x \tag{17}$$

Resolving forces in the y-direction:

$$FY_w = FY_f + \partial NH_w/\partial x + NA_w.\partial^2 \bar{v}_{cw}/\partial x^2 + \partial NA_w/\partial x.\partial \bar{v}_{cw}/\partial x \tag{18}$$

Resolving forces in the z-direction and putting $\bar{w}_{cw} = \bar{w}$:

$$FZ_w = FZ_f + (FX_f - FX_w).\partial \bar{w}/\partial x + (FY_f - FY_w).\partial \bar{w}/\partial y + \partial NV_w/\partial x + NA_w.\partial^2 \bar{w}/\partial x^2 + \partial NA_w/\partial x.\partial \bar{w}/\partial x \tag{19}$$

Substituting (16) into (18):

$$FY_w = FY_f + \partial^2 MH_w/\partial x^2 + NA_w.\partial^2 \bar{v}_{cw}/\partial x^2 + \partial NA_w/\partial x.\partial \bar{v}_{cw}/\partial x \tag{20}$$

Substituting (15) and (17) into (19):

$$FZ_w = FZ_f + (FY_f - FY_w).\partial \bar{w}/\partial y + \partial^2 MV_w/\partial x^2 + cvw.\partial^2 NA_w/\partial x^2 + NA_w.\partial^2 \bar{w}/\partial x^2 + (h_w + \tfrac{1}{2}.t).\partial FX_f/\partial x \tag{21}$$

Substituting (16) into (14):

$$FT_w = FT_f + \partial MT_w/\partial x + FY_f(h_w + \tfrac{1}{2}.t) + cvw.\partial^2 MH_w/\partial x^2 \tag{22}$$

Equations (17), (20), (21) and (22) are the required body forces at the web-plate interface.

2.2.2.3 *Equilibrium Equations for the Stiffened Plate*

The derivation is completed by considering the equilibrium of a small element of plate subjected to load intensities q and $FZ_w/\delta y$ laterally, and $FX_w/\delta y$ and $FY_w/\delta y$ in-plane. The quantity δy defines the width of plating over which the body forces are assumed to be distributed and q represents the intensity of the applied lateral loading.

It is important to note that the line couple, FT_w, cannot be accommodated directly in the formulation and is therefore ignored at this stage in the analysis. It is however included in the numerical procedure and this is explained in Chapter 3, Section 3.1.1.7.

The resulting equations of equilibrium, developed in full by Djahani[56] and quoted below, are found to be identical to those for unstiffened plates subjected to body forces:

In the x-direction:

$$\partial Nx/\partial x + \partial Nxy/\partial y + C1 = 0 \qquad (23)$$

In the y-direction:

$$\partial Ny/\partial y + \partial Nxy/\partial x + C2 = 0 \qquad (24)$$

and in the z-direction:

$$\partial^2 Mx/\partial x^2 + 2.\partial^2 Mxy/\partial x\partial y + \partial^2 My/\partial y^2 + Nx.\partial^2 \bar{w}/\partial x^2 + 2.Nxy.\partial^2 \bar{w}/\partial x\partial y + Ny.\partial^2 \bar{w}/\partial y^2 + q + C3 = 0 \qquad (25)$$

where for stiffened elements:

$$C1 = FX_w/\delta y \; ; \; C2 = FY_w/\delta y \text{ and } C3 = FZ_w/\delta y$$

and for unstiffened elements:

$$C1 = C2 = C3 = 0$$

2.3 FORCE-DISPLACEMENT RELATIONSHIPS

The remaining fourteen equations required for a solution are now obtained by defining force-displacement relationships for the plate and stiffeners. To cover a full range analysis, two sets of expressions are given, the first for application in the elastic range

and the second for application in the elasto-plastic range.

2.3.1 Force-Displacement Relationships for the Plate

Plasticity in the plate is assumed to be governed by the approximate Ilyushin yield criterion given in Appendix A. Known values of the stress resultants are used to evaluate the yield function f (Expression (A3), Appendix A) and from this the state of the material is determined. If at any point within the plate the value of f is equal to unity a condition of yield is assumed to have been reached.

2.3.1.1 *Elastic Force-Displacement Relationships (f < 1)*

In the elastic range, the stress resultants can be expressed in terms of centroidal strains and curvatures, and elastic rigidites as follows:

$$\left.\begin{aligned} Nx &= E1(\varepsilon x + \nu.\varepsilon y) \\ Ny &= E1(\varepsilon y + \nu.\varepsilon x) \\ Mx &= -D(\partial^2 w/\partial x^2 + \nu.\partial^2 w/\partial y^2) \\ My &= -D(\partial^2 w/\partial y^2 + \nu.\partial^2 w/\partial x^2) \\ Nxy &= E1(1-\nu)\varepsilon xy/2 \\ Mxy &= -D(1-\nu).\partial^2 w/\partial x\partial y \end{aligned}\right\} \qquad (26)$$

where:

$$\left.\begin{aligned} \varepsilon x &= \partial u/\partial x + \tfrac{1}{2}(\partial w/\partial x)^2 + \partial w/\partial x.\partial w_o/\partial x \\ \varepsilon y &= \partial v/\partial y + \tfrac{1}{2}(\partial w/\partial y)^2 + \partial w/\partial y.\partial w_o/\partial y \\ \varepsilon xy &= \partial u/\partial y + \partial v/\partial x + \partial w/\partial x.\partial w/\partial y \\ &\quad + \partial w/\partial y.\partial w_o/\partial x + \partial w/\partial x.\partial w_o/\partial y \end{aligned}\right\} \qquad (27)$$

$$E1 = E.t/(1-\nu^2) \quad \text{and} \quad D = E.t^3/12(1-\nu^2) \tag{28}$$

2.3.1.2 *Elasto-Plastic Force-Displacement Relationships (f ≠ 1)*

In the elasto-plastic range the force-displacement and moment-curvature relationships (26) are no longer valid and the non-linear behaviour of the material must be considered. The relationships adopted here were first suggested by Crisfield[70], who, basing his formulation on the 'approximate' Ilyushin yield criterion in conjunction with the 'associated' flow rule, obtained expressions relating incremental stress resultants to incremental strains and curvatures. These expressions, given in full in Appendix B, are as follows:

$$\{\Delta N\} = [C^*]\{\Delta\varepsilon t\} + [cd]\{\Delta\psi t\} \tag{29}$$

$$\{\Delta M\} = [cd]^T\{\Delta\varepsilon t\} + [D^*]\{\Delta\psi t\} \tag{30}$$

where $[C^*]$, $[cd]$ and $[D^*]$ are the elasto-plastic tangential rigidities calculated at current stress levels and:

$$\left.\begin{aligned} \{\Delta\varepsilon t\}^T &= \{\Delta\varepsilon x,\ \Delta\varepsilon y,\ \Delta\varepsilon xy\} \\ \{\Delta\psi t\}^T &= \{\Delta\psi x,\ \Delta\psi y,\ \Delta\psi xy\} \end{aligned}\right\} \tag{31}$$

$$\left.\begin{aligned} \{\Delta N\}^T &= \{\Delta Nx,\ \Delta Ny,\ \Delta Nxy\} \\ \{\Delta M\}^T &= \{\Delta Mx,\ \Delta My,\ \Delta Mxy\} \end{aligned}\right\} \tag{32}$$

These relationships, incorporated in an incremental procedure, can be summed at each load step to obtain values for the total stress resultants. Expressions for the elasto-plastic rigidities and incremental strains and curvatures are given in Appendix B.

2.3.2 Force-Displacement Relationships for the Stiffeners

Yielding of the stiffeners is assumed to be governed by a simplified version of the Von Mises yield criterion. For this it is assumed that all components other than the direct stresses and maximum shear stresses due to bending are negligible, and that the shear stresses do not vary across the thickness or through the depth of the section. Defining the uniaxial yield stresses of the webs and flanges as σo_w and σo_f respectively, the maximum possible strains for elastic behaviour can then be written as follows:

For the webs: $$\varepsilon o_w = (\sqrt{\sigma o_w^2 - 3(NV_w/A_w)^2})/E \quad (33)$$

For the flanges: $$\varepsilon o_f = (\sqrt{\sigma o_f^2 - 3(NH_f/A_f)^2})/E \quad (34)$$

where A_w and A_f are the areas of web and flange respectively and E is Young's modulus.

To determine the state of the material at any point (or small element) within the cross-section, the above two expressions are compared with the following direct strains due to deformation:

For a point in the web:

$$\varepsilon_{ew} = \partial u_{ew}/\partial x + \tfrac{1}{2}(\partial w_{ew}/\partial x)^2 + \partial w_{ew}/\partial x . \partial w_{oew}/\partial x + \tfrac{1}{2}(\partial v_{ew}/\partial x)^2 + \partial v_{ew}/\partial x . \partial v_{oew}/\partial x \quad (35)$$

and for a point in the flange:

$$\varepsilon_{ef} = \partial u_{ef}/\partial x + \tfrac{1}{2}(\partial w_{ef}/\partial x)^2 + \partial w_{ef}/\partial x . \partial w_{oef}/\partial x + \tfrac{1}{2}(\partial v_{ef}/\partial x)^2 + \partial v_{ef}/\partial x . \partial v_{oef}/\partial x \quad (36)$$

where the displacements are given by equations (1) and (2).

2.3.2.1 *Elastic Force-Displacement Relationships*

For any web cross-section where all $|\varepsilon_{ew}| < \varepsilon o_w$ and any flange cross-section where all $|\varepsilon_{ef}| < \varepsilon o_f$, the moments and forces can be obtained from centroidal strains and curvatures, and elastic rigidities as follows:

(a) For the web

$$\left.\begin{aligned} NA_w &= EA_w.\varepsilon_{cw} \\ MV_w &= -EI_{yw}.\partial^2 w_{cw}/\partial x^2 \\ MH_w &= -EI_{zw}.\partial^2 v_{cw}/\partial x^2 \\ MT_w &= -GJ_w.\partial^2 w_{cw}/\partial x\partial y \end{aligned}\right\} \quad (37)$$

where

$$\begin{aligned} \varepsilon_{cw} &= \partial u_{cw}/\partial x + \tfrac{1}{2}(\partial w_{cw}/\partial x)^2 + \partial w_{cw}/\partial x.\partial w_{ocw}/\partial x \\ &\quad + \tfrac{1}{2}(\partial v_{cw}/\partial x)^2 + \partial v_{cw}/\partial x.\partial v_{ocw}/\partial x \end{aligned} \quad (38)$$

$$\left.\begin{aligned} EA_w &= E.h_w.t_w \;; \quad EI_{yw} = E.t_w.h_w^3/12 \\ EI_{zw} &= E.h_w.t_w^3/12 \;; \quad GJ_w = G.\phi.h_w.t_w^3 \end{aligned}\right\} \quad (39)$$

where ϕ is a torsional rigidity factor and the displacements are given by equations (3).

(b) For the flange

$$\left.\begin{aligned} NA_f &= EA_f.\varepsilon_{cf} \\ MV_f &= -EI_{yf}.\partial^2 w_{cf}/\partial x^2 \\ MH_f &= -EI_{zf}.\partial^2 v_{cf}/\partial x^2 \\ MT_f &= -GJ_f.\partial^2 w_{cf}/\partial x\partial y \end{aligned}\right\} \quad (40)$$

where

$$\varepsilon_{cf} = \partial u_{cf}/\partial x + \tfrac{1}{2}(\partial w_{cf}/\partial x)^2 + \partial w_{cf}/\partial x.\partial w_{ocf}/\partial x + \tfrac{1}{2}(\partial v_{cf}/\partial x)^2 + \partial v_{cf}/\partial x.\partial v_{ocf}/\partial x \qquad (41)$$

$$\left.\begin{aligned} EA_f &= E.b_f.t_f \quad ; \quad EI_{yf} = E.b_f.t_f^3/12 \\ EI_{zf} &= E.t_f.b_f^3/12 \quad \text{and} \quad GJ_f = G.\phi.b_f.t_f^3 \end{aligned}\right\} \qquad (42)$$

where ϕ is a torsional rigidity factor and the displacements are given by equations (4).

2.3.2.2 *Elasto-Plastic Force-Displacement Relationships*

For any web cross-section where $|\varepsilon_{ew}| \geq \varepsilon o_w$ and for any flange cross-section where $|\varepsilon_{ef}| \geq \varepsilon o_f$ at one or more points, the direct forces NA and the bending moments MV and MH are obtained by numerical integration. This technique is described in Chapter 3, section 3.1.1.5.

2.4 BOUNDARY CONDITIONS

In addition to satisfying the equations of equilibrium and compatibility, the deflected shape of the plate must also satisfy known boundary conditions at the supported edges.

For unstiffened plates four conditions are required on each side of the plate, two of these being associated with flexural action and two with membrane action. For stiffened plates, however, an additional condition is required at each end of the stiffeners, this being associated with rotation in the horizontal plane (i.e. a plane parallel to the x-y plane).

Assuming now that edges parallel to the ribs are unstiffened, the following boundary conditions can be written for various types of edge support. An edge parallel to the stiffeners is referred to as $y = 0$ and an edge normal to the stiffeners as $x = 0$.

2.4.1 Flexural Boundary Conditions

2.4.1.1 *The Edge y = 0*

Three flexural constraints are considered on this edge, these being simply supported, clamped and free.

(a) Simply Supported Edge:

The edge is restrained laterally but is free to rotate. Thus:

$$w = 0 \quad \text{and} \quad My = 0 \tag{43}$$

(b) Clamped Edge:

The edge of the plate is firmly clamped so that neither rotation nor deflection is possible. Thus:

$$w = 0 \quad \text{and} \quad \partial w/\partial y = 0 \tag{44}$$

(c) Free Edge:

Along the free edge there are no vertical shearing forces and no bending or twisting moments. These three requirements, combined into two by Kirchoff[15] are as follows:

$$My = 0 \quad \text{and} \quad \partial My/\partial y + 2.\partial Mxy/\partial x = 0 \tag{45}$$

2.4.1.2 *The Edge x = 0*

Two flexural constraints only are considered on this edge, these being simply supported and clamped:

(a) Simply Supported Edge:

$$w = 0 \quad \text{and} \quad Mx = 0 \tag{46}$$

(b) Clamped Edge:

$$w = 0 \quad \text{and} \quad \partial w/\partial x = 0 \tag{47}$$

2.4.2 Membrane Boundary Conditions

2.4.2.1 *The Edge y = 0*

On this edge five in-plane constraints are considered, three being related to displacements normal to the edge and two to displacements tangential to the edge. A combination of one normal and one

tangential condition is required for a solution.

(a) Free Displacement Normal to the Edge:

The direct stress resultant normal to the edge must be zero at all points. Thus:

$$Ny = 0 \tag{48}$$

(b) The Constrained Edge:

The edge is constrained to remain straight but is free to translate in-plane. The sum of direct stresses along the edge must therefore be zero. For an edge extending from x = 0 to x = Lx we have

$$\sum_{x=0}^{Lx} Ny.dx = 0 \tag{49}$$

(c) Known Uniform Displacement Normal to the Edge:

At all points along the edge we have:

$$v = \text{constant} \tag{50}$$

(d) Free Displacement Tangential to the Edge:

At all points along the edge the shear force must be zero:

$$Nxy = 0 \tag{51}$$

(e) Full Fixity Tangential to the Edge:

At all points along the edge the displacement must be zero:

$$u = 0 \tag{52}$$

2.4.2.2 *The Edge x = 0*

On this edge three in-plane constraints are considered, two of them related to the normal displacement u and the third to the tangential displacement v. In addition, an edge condition is given to take account of stiffener rotation in the horizontal plane.

(a) Known Uniform Displacement Normal to the Edge:

At all points along the edge we have:

$$u = \text{constant} \tag{53}$$

(b) The Constrained Edge:

As in case 2.4.2.1(b), the resultant normal force on the edge must be zero. Thus for an edge extending from y = 0 to y = Ly we have:

$$\sum_{y=0}^{Ly} Nx.dy + \Sigma NA_w + \Sigma NA_f = 0 \tag{54}$$

(c) Full Fixity Tangential to the Edge:

At all points along the edge the displacement must be zero:

$$v = 0 \tag{55}$$

(d) Rotation of the Stiffener.

The above three constraints are applicable to a plate and stiffener combination which is welded into a rigid end plate, the function of the rigid plate being to prevent shortening tangential to the edge and to constrain the edge to remain straight. This being the case, it can be assumed that for any depth z below the middle-plane of the plate there can be no variation of u_{ew} or u_{ef} with y. Expressions for these displacements, given in section 2.2.1 are:

$$u_{ew} = u - evw.\partial w/\partial x - ehw.\partial v/\partial x$$

and $$u_{ef} = u - evf.\partial w/\partial x - ehf.\partial v/\partial x$$

If u_{ew} and u_{ef} are not to vary with y it follows that they must also be independent of *ehw* and *ehf* and therefore:

$$\partial v/\partial x = 0 \tag{56}$$

This provides the additional condition required at each end of the stiffener.

CHAPTER 3

THE SOLUTION PROCEDURE

3.1 THE METHOD OF SOLUTION

3.1.1 Solution of the Stiffened Plate Equations

The governing equations for discretely stiffened plates are solved numerically by the application of Dynamic Relaxation to their finite difference equivalents. The first order central difference expressions are generated from a rectangular interlacing network of stress resultants and displacements, the arrangement of which is shown in Fig. B1. Background information on the Dynamic Relaxation technique and its application to a number of different structural forms can be found elsewhere[71-84], and discussion here is therefore confined to its application in the solution procedure.

Using this method a computer program has been written, and this is summarised in the form of a flow chart in Appendix C. The main steps involved are as follows:

Step 1: Assume an initial set of plate displacements.

Step 2: Calculate forces and moments in the plate and stiffeners.

Step 3: Calculate the interactive forces and evaluate the equilibrium equations.

Step 4: Apply the Dynamic Relaxation equations to obtain an updated set of plate displacements.

Step 5: Repeat steps (2) to (4) until a convergent solution is obtained.

Step 6: Check for yielding in the plate and stiffeners, determine plate rigidities for the next load increment and repeat the above procedure for a new load level.

With reference to the computer program flow chart, the solution procedure will now be discussed in detail.

3.1.1.1 *Plate Rigidities*

For the initial load increment of the solution procedure elastic rigidities given by expressions (28) are specified for each plate node. For subsequent increments, every node in the plate must be checked for yielding before the appropriate rigidities can be determined.

As outlined in section 2.3.1 the Ilyushin yield criterion (Appendix A) is used to predict yielding in the plate. Current nodal values of the stress resultants are substituted into equation (A3) and numerical values for the yield function f are thus obtained.

At the main nodal positions, stress resultants Nxy and Mxy are required to evaluate (A3) but, owing to the adopted interlacing mesh arrangement, these values are not specified directly. At main internal nodes, therefore, known values at the surrounding interlacing nodes are averaged, whilst along the boundaries the following approximations are employed:

For main nodes on the boundary J = 2 (Fig. B1):

For free tangential displacement,

$$Nxy(I,2)_E = 0 \tag{57}$$

For zero tangential displacement,

$$Nxy(I,2)_E = \tfrac{1}{2}(Nxy(I,2) + Nxy(I-1,2)) \tag{58}$$

For the clamped edge,

$$Mxy(I,2)_E = 0 \tag{59}$$

For the simply supported edge,

$$Mxy(I,2)_E = \tfrac{1}{2}(Mxy(I,2) + Mxy(I-1,2)) \qquad (60)$$

where E denotes boundary mesh points.

Similar expressions are employed along the boundary I = 2.

At interlacing nodes where the quantities Nx,Ny,Mx and My are required, the above averaging process was found to be inaccurate after yielding had occurred at one or more of the surrounding main nodes. Instead therefore, the strains and curvatures were averaged and the additional stress resultants were calculated using expressions (29) and (30).

In general, for nodes at which f is less than unity the elastic rigidities (28) are retained for the next load cycle, whilst for nodes at which f is equal to unity the elasto-plastic rigidities given by expressions (B7) (Appendix B) are employed. In the latter case, however, the finite nature of the loading increment will often result in values of f exceeding unity, and to minimise the error involved the stress resultants are modified before the rigidities are calculated. Comparing the value of the yield function f with the equivalent quantity, fp, obtained at the beginning of the previous load cycle, the required modifications are determined:

(a) For fp < 1 and f > 1

During the previous load increment the material was stressed from a point in the elastic range to a point in the elasto-plastic range. Elastic plate rigidities were employed throughout and the final stress resultants were therefore overestimated. To reduce this error the stress resultants are modified as outlined in reference (70), and these modified values are employed in equations (B7) to obtain the

elasto-plastic rigidities for the next load increment.

(b) For fp = 1 and f > 1

In this case a condition of yield existed both at the beginning and at the end of the previous increment and although elasto-plastic rigidities were employed, their constant nature has resulted in drift from the yield surface. Moving the stress resultants normal to the surface in accordance with the method outlined in Appendix D, the unit yield function is reinstated and the elasto-plastic rigidities can then be obtained as above.

The final possibility to be considered is that of unloading from the yield surface. This condition is investigated by examining the value of the term λ given by equation (B5) (Appendix B), where a negative result indicates that unloading has occurred and that elastic rigidities should be re-introduced for the next load cycle.

3.1.1.2 *Stiffener Rigidities*

To enable analysis in the elasto-plastic range, the stiffener cross-section is divided into a number of small elements having sectional areas δA_w in the webs and δA_f in the flanges (Fig. B2). Each element is checked for yielding, as outlined in Section 2.3.2, at positions along the stiffener corresponding to the main plate nodes. For fully elastic web and flange cross-sections elastic rigidities (39) and (42) are specified for the next load step, whilst for all other cross-sections the need for numerical summation is recorded.

3.1.1.3 *Initial Plate Displacements*

For the first iteration of each load increment a set of plate displacement u, v and w must be specified. For the initial load

increment zero values are assumed for each component, whilst for subsequent increments u, v and w are estimated by linear extrapolation to obtain a starting value closer to the final solution, and hence to speed the convergence process.

3.1.1.4 *Plate Stress Resultants*

The plate rigidities determined in Section 3.1.1.1 are now used in conjunction with the plate displacements to obtain numerical values for the stress resultants. At elastic nodes, equations (26) to (28) are employed, whilst at elasto-plastic nodes these are replaced by the incremental expressions (29) and (30). The unknown strains and curvatures required at main and interlacing nodes to evaluate (29) and (30) are obtained by averaging known surrounding values.

In the elasto-plastic range the plate rigidities [C*], [cd] and [D*] are each functions of the six current stress resultants and should therefore be updated at each infinitesimal load step. As an approximation to this, small finite load steps are employed and the rigidities are maintained at their starting values for the duration of the increment.

3.1.1.5 *Stiffener Internal Forces and Moments*

At all stiffener cross-sections where, in 3.1.1.2, elastic behaviour was indicated, forces and moments are calculated directly using expressions (37) to (42). Elsewhere, however, where one or more elements in the web or flange cross-sections have yielded, the following summation process is adopted:

For the webs:

$$\left.\begin{aligned} NA_w &= \sum_{i=1}^{K_w} E.\varepsilon iw.\delta A_w \\ MV_w &= \sum_{i=1}^{K_w} E.\varepsilon iw.\delta A_w(evw-cvw) \\ MH_w &= \sum_{i=1}^{K_w} E.\varepsilon iw.\delta A_w.ehw \end{aligned}\right\} \quad (61)$$

For the flanges:

$$\left.\begin{aligned} NA_f &= \sum_{i=1}^{K_f} E.\varepsilon if.\delta A_f \\ MV_f &= \sum_{i=1}^{K_f} E.\varepsilon if.\delta A_f(evf-cvf) \\ MH_f &= \sum_{i=1}^{K_f} E.\varepsilon if.\delta A_f(ehf-chf) \end{aligned}\right\} \quad (62)$$

where the strains εiw and εif are obtained from equations (33) to (36) as follows:

$$\left.\begin{aligned} \varepsilon iw &= \varepsilon_{ew} && \text{if} \quad |\varepsilon_{ew}| < \varepsilon o_w \\ \varepsilon iw &= \varepsilon o_w.|\varepsilon_{ew}|/\varepsilon_{ew} && \text{if} \quad |\varepsilon_{ew}| \geq \varepsilon o_w \\ \varepsilon if &= \varepsilon_{ef} && \text{if} \quad |\varepsilon_{ef}| < \varepsilon o_f \\ \varepsilon if &= \varepsilon o_f.|\varepsilon_{ef}|/\varepsilon_{ef} && \text{if} \quad |\varepsilon_{ef}| \geq \varepsilon o_f \end{aligned}\right\} \quad (63)$$

and K_w and K_f represent the number of web and flange elements respectively. The torsional actions MT_w and MT_f are assumed to retain their elastic values throughout.

To calculate stiffener strains and curvatures, in-plane displacement components v are required at main mesh points along the stiffener. These are obtained by averaging the y-direction plate displacements to either side of the stiffener location.

3.1.1.6 *Boundary Conditions Applied as Stresses*

The stiffened plate configurations and loading patterns considered are symmetrical with respect to both x and y. Quarter plate panels are therefore analysed with stress and displacement boundary conditions applied across the centre lines to retain the symmetrical form.

All edge conditions given in Section 2.4, with the exception of (45) and (51), are applied via displacements. Condition (45) was included specifically for the analysis of the models and is discussed in Chapter 5, and condition (51) is given in finite difference form in Appendix F.

3.1.1.7 *Equilibrium Equations and Interactive Forces*

The current stress resultants and deformations are now employed in equations (23) to (25), to obtain the 'out-of-balance' forces at u, v and w nodes respectively. For this purpose, the interactive force component FY_w is assumed to consist of two equal line loads of magnitude $FY_w/2$ acting at both sets of v nodes adjacent to the stiffener. In addition, the line couple FT_w, ignored in the derivation of equations (23) to (25), is included by applying equal and opposite lateral line loads of magnitude $FT_w/2\Delta y$ to the w nodes adjacent to the stiffener.

Replacing the finite distance δy in equations (23) to (25) by the mesh division Δy and incorporating the above changes, the

following modified expressions are obtained for terms C1 to C3, for a plate stiffened along the line y = J (Fig. B1):

$$\left.\begin{array}{lll} C1 = FX_w/\Delta y & \text{for } y = J \\ C1 = 0 & \text{for } y \neq J \end{array}\right\} \quad \text{At u nodes:} \qquad (64)$$

At v nodes:

$$\left.\begin{array}{lll} C2 = FY_w/2\Delta y & \text{for } y = J \text{ and } y = J-1 \\ C2 = 0 & \text{for } J < y < J-1 \end{array}\right\} \qquad (65)$$

At w nodes:

$$\left.\begin{array}{lll} C3 = FT_w/2\Delta y^2 & \text{for } y = J-1 \\ C3 = FZ_w/\Delta y & \text{for } y = J \\ C3 = -FT_w/2\Delta y^2 & \text{for } y = J+1 \\ \text{and} \quad C3 = 0 & \text{for } J+1 < y < J-1 \end{array}\right\} \qquad (66)$$

3.1.1.8 *The Dynamic Relaxation Routine*

The numerical values obtained in 3.1.1.7 provide a set of out-of-balance forces which must reduce to zero for equilibrium. In the Dynamic Relaxation technique these residuals are incorporated as disturbing forces in equations of motion with damping included, and through successive applications of the iterative cycle the ensuing plate oscillations are forced to diminish until a static state is achieved.

Applying the equations of motion in the x,y and z directions and integrating the velocities with respect to time, the following updated displacement components are obtained[76]:

In the x direction:

$$u_{t+\delta t} = u_t + \delta t.\dot{u}_{t+\delta t/2} \qquad (67)$$

where the velocity is given by:

$$\dot{u}_{t+\delta t/2} = \dot{u}_{t-\delta t/2}(1 - \tfrac{1}{2}Kx)/(1 + \tfrac{1}{2}Kx) + \delta t \cdot Px/\rho x(1+\tfrac{1}{2}Kx) \tag{68}$$

Similar expressions are obtained for y and z direction components by interchanging u and x in the above expressions by v and y,and w and z respectively.

Knowing the densities $\rho i = (\rho x, \rho y, \rho z)$, the non-dimensional damping terms $Ki = (Kx, Ky, Kz)$, the residual forces $Pi = (Px, Py, Pz)$ and the time increment δt, displacements can be obtained for the next iteration.

(a) Fictitious Densities and the Time Increment

The fictitious densities ρx, ρy and ρz, evaluated at u, v and w nodes respectively, can be obtained from the following expression[75], with δt set at unity:

$$\rho i = \frac{1}{4} \sum_{j=1}^{n} |Sij| \tag{69}$$

where Sij represents the jth coefficient in a row of the stiffness matrix of nodal displacements; the rows of the matrix being formed from equations (23), (24) and (25) for each u, v and w node respectively. Stiffener interaction terms are included in the rows where applicable, and by considering each row of the matrix in turn fictitious densities are obtained for every node in the plate. Re-calculation of the densities at every tenth iteration was generally found to be adequate for retaining overall numerical stability.

The coefficients Sij, being dependent upon material properties, should be adjusted to take account of material non-linearity. As in

previous work[77], however, this refinement was found to be unnecessary and the elastic relationships were therefore retained throughout.

To illustrate the above procedure, the derivation of ρx for a stiffened node u(I,J) is given in Appendix E.

(b) Damping Factors

In general, for the analysis of unstiffened plates, three damping factors Kx, Ky and Kz are sufficient to depress oscillations in the x, y and z directions respectively. For stiffened plates,however, two additional factors Kx' and Kz' are incorporated. These are applied in place of Kx and Kz at u and w nodes along the stiffeners and have the effect of improving the rate of convergence.

3.1.1.9 *Boundary Conditions Applied as Displacements*

All boundary conditions given in Section 2.4,other than those specified in Section 3.1.1.6,are applied to the plate in the form of displacements. For the cases of lateral and tangential restraint displacements can be applied directly to the edges. For all other conditions the displacements are set on nodes beyond the edges to induce the required edge stresses, average edge displacements, or known curvatures. For completeness, the finite difference expressions adopted are given in Appendix F, where those derived from stress resultants are quoted for the elasto-plastic range.

3.1.1.10 *Convergence*

As a measure of the total kinetic energy of the system the expression $\sum(\dot{u}^2 + \dot{v}^2 + \dot{w}^2)$ is evaluated at each iteration. When this value becomes small,(in the order of 10^{-8}), convergence is assumed to have occurred and the iterative procedure is repeated for a new load level.

If oscillations have not been adequately damped however, further iterations are carried out at the existing load level commencing with the calculation of stress resultants, Section 3.1.1.4.

3.1.2 Initial Distortion and Loading

3.1.2.1 *Initial Deformation and Residual Stresses*

Initial deformations are included in the analysis by specifying a continuous function $w_o(x,y)$ from which each initial nodal displacement can be evaluated. For all examples considered in Chapter 6, the overall sinusoidal form given by the following expression is employed; where wc represents the deformation at the centre of a plate having dimensions Lx and Ly in the x and y directions respectively.

$$w_o(x,y) = wc.\sin(\pi.x/Lx).\sin(\pi.y/Ly) \qquad (70)$$

For the analysis of the stiffened plate models a more complex relationship is adopted, and this will be given in Chapter 5.

The mathematical formulation described in Chapter 2 makes no allowance for the existence of residual stresses and a numerical approach is therefore adopted to include this parameter. Using the distributions of stress and strain[13] shown in Fig. B3.for the plate and stiffeners respectively, numerical values are obtained for Nx at each plate node and for ε_{ew} and ε_{ef} within each stiffener element. These values are then incorporated as data at the beginning of the numerical procedure to define the initial state of stress.

The above distributions are determined such that equilibrium is achieved separately for each initially undeformed plate panel and for each of the webs and flanges, and providing that no initial deformation exists overall equilibrium will be satisfied. In the presence of

initial deformation,however, several cycles of the solution procedure must be carried out under zero applied load to achieve equilibrium for the deformed section. This relaxation procedure will result in a slight modification of the initial deformation levels,and should a specific deformation be required in conjunction with residual stress a process of trial and error must be adopted.

The distribution of strain shown for the flat type stiffener, although in equilibrium for NA_w and MH_w,is not in equilibrium for the moment component MV_w. Since however only first and second differentials of this term appear in the equilibrium equations,and because it is almost constant for the full length of the stiffener, its magnitude does not directly affect the solution.

3.1.2.2 *Applied Loading and the Average Edge Stress*

Uniaxial loads are applied to the plate in terms of displacements rather than stresses. This enables the load-deflection behaviour to be examined beyond the ultimate load position.

The average edge stress σm, resulting from the applied strain εa, is obtained by numerical summation of the stress resultants Nx,and the stiffener forces NA_w and NA_f across the edge,as follows:

$$\sigma m = (\Sigma Nx.\Delta y + \Sigma NA_w + \Sigma NA_f)/(A + \Sigma A_w + \Sigma A_f) \qquad (71)$$

where the summation for Nx is carried out using the Trapesium Rule.

3.2 DISCUSSION OF THE SOLUTION PROCEDURE

3.2.1 The Finite Difference Mesh and Stiffener Elements

3.2.1.1 *The Finite Difference Mesh*

As an alternative to the interlacing mesh arrangement a non-interlacing system could be used, in which all stress resultants and displacements are defined at common mesh points. Although the latter approach is simpler in application it is less accurate, since first differentials must be obtained by taking differences over two mesh divisions whereas in the former approach a single division can often be employed.

The number of mesh divisions required for a given degree of accuracy will depend upon the deformed shape of the plate and will therefore be influenced by the plate and stiffener dimensions. To illustrate this point two plate geometries (Fig. B4) have been analysed, the first being a stocky plate with light stiffening ($b/t = 45$; $Lx/R = 84.3$) and the second a flexible plate with heavy stiffening ($b/t = 75$; $Lx/R = 32.2$). For each of these cases the percentage change in deflection has been plotted against mesh size for two positions on the plate, the (2×2) mesh deflections being chosen as a basis for comparison (Fig. B5).

For the first of these geometries, the plate responds to load by deflecting in an overall sense with negligible deformation of the plating between the stiffeners. Here, a refinement in mesh size from (4×4) to (8×8) leads to a small percentage improvement in both panel and stiffener deflections. In the second case, however, where the plating deforms locally between the ribs, an equivalent mesh refinement leads to a much greater change in panel deflections, and here a finer mesh spacing would be required to reproduce the accuracy achieved above.

Approximation of the interactive couple by two equal and

opposite line loads applied at main nodes adjacent to the stiffener becomes less accurate as the mesh spacing per unit width of panel increases. Ideally, since this is a local effect, the forces should be applied as close to the stiffener as possible. This approximation, together with the division of the interactive force FY_w and the averaging of y-direction displacements at the stiffener location could be represented more accurately by including the facility of graded meshes, although no such refinement has been considered in the present work.

A further point for consideration in assessing the mesh size is the application of residual stresses. The basic stress pattern shown in Fig. B3, cannot be applied directly in the analysis and further idealisation resulting in the form shown in Fig. E4, is necessary. In the latter distribution residual stress levels at the stiffener location are reduced below the specified yield, and this can only be improved upon by refining the mesh spacing.

The degree of mesh refinement provided in any solution must be suitable not only from the point of view of accuracy but also in terms of economy.

Apart from the large number of additional equations which must be solved as a result of mesh refinement, a greater number of cycles of the solution procedure are also necessary to achieve convergence. In Fig. B6 the displacement w at the centre of the plate (b/t = 45; Lx/R = 84.3) is plotted against number of cycles of the solution procedure for three different mesh sizes and with zero applied damping in the z-direction. Similar plots are shown in Fig. B7 for two different geometrical arrangements and for one selected mesh size. It is evident from these curves that although the geometry has little effect on the speed of convergence, the number of mesh divisions is critical and for economy should be kept as low as possible.

All plates analysed by the existing program must be arranged such that the main mesh points coincide with the boundaries, the stiffeners and the centre lines. For a plate stiffened at third points across the width, this dictates an increase from six mesh divisions to nine per quarter plate, with no intermediate refinement being possible. The large amount of additional computer time this generates can be reduced in some cases by retaining a larger mesh division in the direction of the stiffening along which variations in the deflection profiles are often less acute.

3.2.1.2 *Stiffener Elements*

In the elasto-plastic range the stiffener webs and flanges are divided into volume elements by a selected number of horizontal and vertical layers. The number of elements required will depend upon the mode of failure and therefore upon the stiffener dimensions and the loading arrangement.

A stocky plate with flexurally weak stiffening (b/t = 30; Lx/R = 90) has been analysed to compare solutions with two, four, six and eight horizontal layers provided. The stiffeners are of the flat type and failure of the panel is preceded by tensile yielding in their extreme fibres. The applied strain-deflection curves are shown for each case in Fig. B8 where a discrepancy of 25% in the prediction of first yield is observed between the two extreme cases. Between the two yield points the solutions diverge, and although in this case the curves converge again at higher strains it should be noted that, in some cases, delayed prediction of first yield may cause the stresses in the plate to exceed the elastic limit or the critical buckling stress, when in fact this would not occur in practice.

A second study was undertaken to compare the solutions obtained

for different numbers of vertical layers. A similar plate-stiffener arrangement was adopted but with b/t = 80 and Lx/R = 80; a case for which strains were observed to vary across the thickness of the webs. Two, four and six vertical layers were considered, but in all cases discrepancy in the deflections was never greater than 0.2%.

As in the case of the finite difference mesh refinement may be necessary when dealing with residual stresses, the strain distributions shown in Fig. B3 being idealised for application to the element centroids as indicated in Fig. E4. It is clear that the greater the number of horizontal layers provided through the depth of the web, the closer will be the idealisation to the original distribution.

3.2.2 Plate Plasticity and Incremental Loads

The approximate Ilyushin yield criterion has been compared by others with the more rigorous approach of Von Mises[70] in which both surface yielding and the spread of plasticity through the depth of the section are considered. From such comparisons carried out by Frieze[77] in application to unstiffened plates, it was concluded that the maximum discrepancy between the two approaches occurs for plates of slenderness b/t = 55, for which the theoretical elastic buckling stress coincides with the yield stress. In this region the effect of surface yielding is most pronounced and the Ilyushin yield criterion overestimates the collapse load by approximately 3½ percent. Although this inherent inaccuracy should not be ignored in the interpretation of analytical results, the full section yield criterion is beneficial for problems which require a large computer storage capacity, and for this reason it was adopted in the present work.

The elasto-plastic rigidities suggested by Crisfield[70] were developed by applying flow theory and the Ilyushin yield criterion to an elastic-perfectly plastic material. Although the yield criterion

was originally intended for application with deformation theory, it has since been established that its use with flow theory is also permissible.

As discussed in section 3.1.1.1, the averaging of stress resultants to evaluate the yield function at interlacing nodes was not sufficiently accurate and instead equations (29) and (30) were applied. This refinement, although requiring the calculation of additional rigidities, does not significantly affect the solution time or the storage requirements, since each rigidity is calculated once only for every load increment and it is unnecessary to retain the arrays for further use within the iterative cycle.

The stress resultant modifications outlined in Section 3.1.1.1 were generally found to be small in magnitude,and the facility to restore overall equilibrium by the application of further Dynamic Relaxation cycles was therefore not considered. Although this procedure is not strictly correct, the resulting lack of equilibrium will be negligible providing the loading increments are small and the resulting deformation changes are not excessive.

In some cases,however, particularly where a rapid change of mode occurs in the elasto-plastic range, a small increment of applied loading can cause a significant change in the stress levels. Under such circumstances overstressing can occur at plastic nodes through the use of constant rigidities,and this will in turn lead to yield functions far in excess of unity. The modifications given in 3.1.1.1 can then no longer be considered acceptable.

The required sizes of the loading increments were determined in each analysis by a trial solution, from which the applied load at first yield was obtained. Prior to yielding large increments can be used since the solution does not depend upon a variable rigidity. After yielding has occurred,however, the increments must be reduced in

magnitude to prevent the solution deviating too far from the yield surface.

For plates in which stiffener yielding occurs in advance of panel yielding, immediate reduction of the loading increment is not so critical. Once yielding has been established at one or more elements within the cross-section, the spread of plasticity is monitored at each iteration and thus the rigidities are continually updated.

The plastic strain rate multiplier, λ, adopted in the analysis to predict unloading from the yield surface, tended to be inaccurate and led to a situation where some nodes where loading and unloading with successive load increments. This problem was partially overcome by checking for negative λ at two successive increments before re-setting the elastic rigidities.

3.2.3 Iteractive Forces and Equilibrium Equations

The equilibrium and interactive force equations expressed in terms of stress resultants rather than displacements, are applicable in both the elastic and elasto-plastic ranges. This is of considerable advantage in programming, since to extend the analysis into the elasto-plastic range, it is simply a matter of re-defining stress resultants and in some cases modifying the boundary conditions. The separated forms of the equilibrium and force-displacement equations also enables boundary conditions to be applied, with relative ease, either in the form of stresses or as displacements.

3.2.4 Damping Factors, Iterations and Convergence

As outlined in section 3.1.1.8(b), a total of five damping factors are required to depress oscillations in the x, y and z directions, three of these being associated with plate nodes and two with

stiffener nodes. Direct calculation of these coefficients is not possible and the interdependence of one with another prevents a systematic study of their variation with structural properties and mesh size. As a result, the procedure adopted is based largely on conjecture.

For each analysis undertaken a trial solution involving one load increment was carried out,with zero damping factor Kz' applied along the stiffeners and estimated values applied elsewhere. Plotting the out-of-plane stiffener deformations at mid-span against the number of iterations, a first estimate of Kz' was obtained[72]. Additional trial solutions were then undertaken to improve upon this estimate and to modify, where necessary, the remaining four coefficients.

The initial guessing of four interrelated values is less burdensome than might at first be envisaged. Oscillations at the stiffener nodes have a much longer wavelength than those elsewhere in the plate,and for successful damping of the entire system it is this wavelength which dictates the required number of iterations. It follows therefore, that at most nodes within the structure, the number of iterations provided is far greater than would be required for critical damping and in consequence,a fairly wide band of damping coefficients exist from which a successful solution would be obtained.

In general, the number of iterations required for convergence can be reduced considerably by the estimation of plate displacements as outlined in Section 3.1.1.3. For increments within which a mode change occurs,however, no benefit can be obtained from this facility, and the possibility of increasing the number of cycles over part of the analysis was therefore considered essential.

CHAPTER 4

THE EXPERIMENTAL PROGRAMME

4.1 DESCRIPTION OF MODELS AND INSTRUMENTATION

4.1.1 Geometry and Construction Sequence

To enable comparisons between the theoretical and experimental results three stiffened plate models have been designed. Details of these are shown in Figs C1 and C2, where the dimensions quoted are as specified to the frabricators.

All models have a panel slenderness b/t = 60 and the stiffener slenderness, Lx/R, was varied for the study. The three values considered were Lx/R = 49, 65 and 77 and these were varied by changing the stiffener dimension only. The plating was nominally 5 mm thick and for uniformity was drawn from the same batch of steel. Tee-section stiffeners were adopted throughout and these were fabricated from 5 mm and 8 mm steel plates, cut to size and joined together by a continuous fillet weld. Thick steel sections were welded across the ends of each model to provide a stiff medium for load transfer.

Each of the models was fabricated in the following sequence. Stiffener webs and flanges were cut to size, clamped flat and welded together. Large imperfections resulting from the welding process were then removed by the application of heat spots to selected points along their lengths. With the plate and stiffeners clamped flat the stiffeners were welded into position on the plate, starting with those at the centre and finishing with those at the edges. The ends of the stiffeners were then trimmed and the end plates were welded into position. Finally, deformations in excess of the specified ±2 mm were removed by a further application of heat spots.

4.1.2 Material Properties

Steel plating having a yield stress within the range 300-400 N/mm² was specified for each model. Tensile tests carried out on the steel obtained, however, showed this value to be in excess of 500 N/mm², and to ensure failure within the rig capacity the strength was lowered by a process of heat treatment. From preliminary tests on samples of the steel, the following process was found to reduce the yield stress of the material close to the nominal value specified in BS4360 (355 N/mm² for grade 50B plate up to 16 mm thick).

Normalise at 900°C for 15 minutes.

Air cool and stress relieve at 650°C for 1 hour.

4.1.3 Residual Strain Measurement

Weld induced residual strains were measured in the standard way by taking extensometer readings between fixed locations in the plate. These positions are shown in Figs C3 and C4, for the plate panels and stiffeners respectively.

For the stiffener components, extensometer readings were recorded both before and after fabrication of the tee-sections and again after welding to the plate, and these results are tabulated in Figs C11 and C12. For models SP1 and SP2, strain readings on the webs could not be obtained since the clearance between stiffener flanges and the plating was inadequate for the measuring equipment.

Transverse and longitudinal residual strains were recorded on both sides of the plating and results are tabulated in Figs C5 to C10. The final differences shown have been adjusted to compensate for temperature variations and readings which are suspect have been indicated.

4.1.4 Initial Deformation Measurement

Initial deformations were measured on the unstiffened side of each model relative to the four selected datum points shown in Fig C14. Four steel blocks were located adjacent to these points and were used to support two rectangular bars which were positioned along the lines B1 and B9. A third flat bar was then clamped over the two end bars and, using a depth micrometer, relative deformations of the model surface were measured along the section A1. The bar was then positioned over each of the remaining sections (A2 to A21) in turn and relative deformations were thus obtained for every point shown on the grid. The readings were subsequently reduced to give values close to zero at the datum points and these are plotted for each of the three models in Figs C15 to C23.

4.1.5 The Strain Gauge Arrangement

Electrical resistance strain gauges having a 5 mm length were located on each of the models at the positions shown in Figs C24 to C26. These are liberally positioned over one-quarter of the plate surface and check gauges are provided elsewhere to investigate the symmetry of the system. The linear gauges at the model ends enable the difference in stress between the loading and reaction edges to be investigated, and thus the accuracy of analysing one-quarter of the stiffened panel to be determined.

For a panel of aspect ratio 5:1 and slenderness ratio b/t = 60, buckling is likely to occur in a five half-wave mode form. With this in mind, the gauge arrangement was based on a 300 mm grid, the theoretical length of one half-wave. Panel gauges adjacent to the stiffeners were positioned a distance of 20 mm from the web centre lines. This was specified in order to avoid the most heavily weld affected zone close to the ribs.

After the gauges were bonded to the models each was coated with a layer of wax to protect them from dampness. This precaution is advisable in the present tests where lateral pressure is applied by a water filled bag and dampness can arise either from leakage or from condensation.

4.1.6 Deflection Measurement

Out-of-plane deformations were measured throughout by a series of 35 transducers mounted over the model at the positions shown in Fig C27. Additionally, a dial gauge was located at the centre of the plate to enable the rate of deformation under load to be rapidly assessed.

The transducers were mounted on an independent frame which was fabricated from rolled hollow section and supported directly on the model end plates. At the reaction end of the model the frame was supported on two fixed point landings whilst at the loading end a single roller bearing was used. This mode of support ensures that the readings are unaffected by lateral movements elsewhere in the rig, and that the model can shorten in-plane without load being transmitted into the frame.

In-plane shortening of the model ends was measured by the four dial gauges D1, D2, D5 and D6 shown in Fig C27. These were clamped to the pressure bag support platform and were reacted against the model end plates.

Finally, two dial gauges, D3 and D4, were mounted against the model end plates to enable transverse movements to be detected and thus eliminated.

4.2 DESCRIPTION OF THE PLATE TESTING RIG

Constructional details and photographs of the plate testing rig are shown in Figs C28 to C50. The structure consists of two independent loading arrangements, the first for the application of lateral pressure and the second for the application of uniaxial compression.

To apply the lateral loading component a water pressure system was adopted. This was selected on the basis of its low compressibility, the air alternative being considered unsuitable owing to its highly elastic nature. With a water pressure arrangement it is necessary to load the model in the horizontal plane to ensure a constant pressure over its surface, and this dictates that the uniaxial loading is also applied in the horizontal plane. High in-plane forces must therefore be reacted either by shear restraints in the strong floor or through a self contained reaction arrangement, and in the present work the latter alternative was adopted.

A full account of the two loading arrangements is now given commencing with that for lateral pressure.

4.2.1 The Lateral Loading System

Lateral loading is applied to the unstiffened side of the model via a pressurised rubber bag which is contained between the model and a stiff supporting platform. The bag is pressurised by water from a variable head tank, and lateral constraint to the model edges is provided through a series of vertically placed load cells and a stiff overhead frame.

4.2.1.1 *The Overhead Reaction Frame and Vertical Load Cells*

The overhead reaction frame and vertical load cells are shown in Figs C30 and C39 respectively. The structure consists of a stiff square frame which is fabricated from rolled hollow section and carried on two cross-beams by four hangers. The beams are in turn supported on four short columns which are stressed down to the floor, each to a load of 50 tons. The stressing down procedure ensures full clamping action at floor level and at the beam-column intersections and thus minimises the amount of deformation due to rotation at these points. The interfaces between the square frame and the cross-beams are coated with a layer of epoxy resin filler. This compensates for irregularities in the two surfaces and provides a full contact area for load transfer.

To transfer thrust to the overhead frame, a set of spherical ended mild steel compression cells are positioned vertically between the perimeter of the model and the ring beam. The spherical ends ensure freedom of rotation and unrestrained in-plane movement of the model edges, whilst the 260 mm length allows end shortening to take place without excessive loss of lateral restraint. The cells can be adjusted vertically via the threaded spherical seatings shown in Fig C39 and these are tightened prior to testing to give uniform strain readings throughout.

4.2.1.2 *The Pressure Bag Support Platform*

The pressure bag support platform shown in Figs C36 and C37 is of composite steel and concrete construction. The permanent steel formwork is fabricated from a built up channel section which is welded to a 6 mm thick steel plate. Shear studs are located at 100 mm centres across the plate and a nominal mesh is provided in the compression zone.

The eight jacking points provided around the perimeter of the platform enable the pressure bag to be lowered away from the face of the model after a period of testing. This facility prevents an accumulation of condensation on the underside of the models and thus prevents the gauges from being damaged.

The water inlet is formed of a steel tube cast into the concrete and is positioned off centre towards the stationary end of the model. At this position the relative movement between the model and the platform is small, and by locating the inlet at this position the probability of damaging the bag is reduced.

The bag is constrained around its edges by steel angle sections which are bolted to the platform at 75 mm intervals. Allowance was made in the spacing of the angles for 15 mm of model end shortening to take place. The concrete is covered by a layer of varnished ply-wood to provide a smooth supporting surface for the bag, and a rubber angle section placed inside the steel angles gives added protection to the bag edges.

To prevent the strain gauge wiring from becoming trapped between the angle constraints and the model, and to reduce gaps between these two surfaces, a rubber strip is glued around the model perimeter. This separates the angle sections from the plating and is cut back, where necessary, to accommodate the wiring.

4.2.1.3 *The Pressure Bag and Water Pressure System*

Details of the pressure bag are shown in Fig. C37. The bag is fabricated from 1 mm thick latex rubber sheets, which are joined together along the edges and at the corners by rubber strips. The sealing strips are folded so as to minimise the number of rubber thicknesses in direct contact with the model, and the area of bag adjacent to the water inlet is reinforced by hessian and rubber solution. A rubber bleed tube attached to an inside edge of the bag and extending through the water pressure system to the exhaust, provides a means through which trapped air can be expelled from the system.

The water pressure system is shown schematically in Fig. C38. The variable head tank is fed by water from the mains and a ball valve ensures immediate flow into the tank to compensate for head loss due to model deformation. Prior to testing, the bag is filled with water at low pressure to expel air from the system. A transparent pipe provided between the air bleed and the exhaust enables the operator to observe when this has been achieved. Bag pressure is adjusted by raising and lowering the tank on an arrangement of pulleys, and pressure levels are monitored by a dial gauge at the level of the bag and by a pressure transducer incorporated in the system.

4.2.2 The Axial Loading System

A plan view of the axial loading system is shown in Fig. C28. The loading is applied by nineteen 20 tonf capacity hydraulic jacks which are situated between beam A and the loading beam.. The jack forces cause translation of the loading beam and this in turn applies a uniform displacement to the models.

To eliminate the problem of resisting horizontal shear forces on the laboratory strong floor a self contained reaction system was

adopted. This consists of the two beams A and B (Figs C33 and C34) and two pairs of tie plates (Fig C35). The beams react against stiff bearing plates which are welded to the ties, and in this way applied horizontal forces are transmitted into the tie plates. The resulting tensile forces balance the applied in-plane loading and overall equilibrium is thus achieved in the absence of constraint from the floor. A layer of epoxy resin filler was poured between the bearing plates and the beam flanges to develop a full contact area for load transfer, and each of the beams was propped along its longitudinal axis to prevent transverse movement due to misalignment of the jacks.

At the loading end of the rig the model is subjected to uniform applied displacement, and deflections which occur across beam A are counteracted by travel of the jacks. At the reaction end of the rig, however, there is no such compensating facility, and if the model were to be reacted directly against beam B differential deflections across its span would destroy the symmetry of end loading. To minimise this effect the model is reacted against the deflection beam, which is supported at points 0.233× beam length from its ends. This is the required position for minimum deflection and hence the most favourable position for symmetry of loading.

The loading beam and parallel arm mechanism which were modified for the purpose of these tests, were originally designed for the testing of stiffened steel grillages[85]. For this reason some of the dimensions quoted in the figures are in imperial units.

The loading beam is designed to move freely in the direction of the applied load on the system of rollers shown in Figs C31 and C32. To prevent rotation about the longitudinal axis the beam is held down by two solid rectangular sections on rollers. These react against thick plates which are bolted loosely to the strong floor as

shown in Fig. C31. Sideways movement is prevented by a nib at the centre of the beam which passes through an adjustable slot in the web and is attached to a plate on the strong floor. Smooth guide rails were later added at each end of the beam to provide additional control. The final degree of freedom to be eliminated is that of twisting in the horizontal plane and this is achieved through the parallel arm mechanism shown in Fig C32. Should one side of the model sustain a greater load than the other, the resulting inbalance on the loading beam will be reacted by forces in the arms and connecting tie bars. The arms will retain their parallel configuration and the loading beam will be forced to remain horizontal.

Applied loads are transferred from the loading beam to the model through twenty-one spherical ended aluminium load cells (Fig C39). Threaded sockets at the loading beam end provide the horizontal adjustment facility, and bearing pads with elongated slots on the model end plates provide the vertical adjustment facility. An identical arrangement of cells is also provided at the reaction end of the model.

To provide restraint in the transverse direction, the model end plates are propped by four short pins (Fig C34). These are reacted at one end by the deflection beam and at the other end by the loading beam. By using the loading beam as one of the supports the pins are forced to remain parallel to the end plates, since model end-shortening which results under load will be followed by an equivalent movement of the beam.

To elevate the beams and to provide clearance between the floor and the tie plates, the rig is supported on the arrangement of base plates shown in Fig C29. Full details of these members are given in Fig C35.

Finally, to provide overall stability to the system each of the beams is held loosely to the floor. This is achieved by locating floor bolts through the webs of the beams at the positions shown in Figs C33 and C34.

4.2.3 Construction Sequence

The testing rig was assembled in the following sequence:

(a) The base plates were located on the strong floor as shown in Fig C29 and were packed on the underside, where necessary, to correct for warping. Base plates BP4, BP5 and BP6 were then stressed down.

(b) The tie plates were located in position and reaction beams A and B were slotted through.

(c) The loading beam was lowered over the central restraining nib and was rotated into position between the tie plates. The parallel arm mechanism was fitted and the turnbuckles on the connecting ties were adjusted until the parallel configuration was achieved. The hydraulic jacks were then positioned.

(d) The deflection beam was lowered into position, and the bearings between this and beam B were formed.

(e) The pressure bag support platform was located mid-way between the loading beam and the deflection beam and the pressure bag was positioned on the smooth supporting surface. The connection between the bag and the water pressure system was then made.

(f) The model was placed in position over the pressure bag and the transducer frame was located above. The horizontal load cells were then inserted at each end of the model.

(g) The overhead frame was assembled by lowering the cross-beams and ring beam, in a single unit, over the supporting columns. The vertical load cells were located and each of the columns was stressed to the floor.

(h) Finally, epoxy resin filler was poured between the ring beam and cross-beams, and between the end reaction beams and the tie plate connectors.

4.2.4 Levelling and Performance Testing

To ensure overall stability of the in-plane loading system, the beam centre lines should coincide with the plane of load application. Optical levelling equipment was used to investigate the discrepancy involved and,on the basis of this, the necessary adjustments were made. Beams A and B, and the deflection beam were elevated as required on packing pieces between the base plates and beam flanges, and the loading beam was adjusted by lengthening or shortening the roller bearing arms..

The hydraulic jacks and the horizontal load cells were aligned in the horizontal plane by using electronic levelling equipment. The cells were then set parallel to each other by slightly adjusting the bearing pads on the model end plates.

With these adjustments made, the system was load tested to 350 tonf axial compression against concrete blocks. At each load stage measurements were taken at selected points along the beams in both the lateral and transverse directions. From the lateral measurements final adjustments were made to the beam levels,whilst from the transverse measurements additional constraints were found to be necessary. These were provided in the form of heavily greased guide rails which were positioned at each end of all beams in the system.

The pressure bag was sandwiched between the support platform and a stiff board and was pressurised by water from the overhead tank. The response to a sudden loss of head was investigated and pressures were found to return rapidly to normal.

4.2.5 The Setting Up Procedure

Prior to testing, the following setting up procedure was adopted:

The model was hung in position on the four corner ties and the pressure bag support platform was raised to the required level by means of the eight jacking points around its perimeter. A small gap was left between the model and the support platform to minimise the drop in stress due to frictional resistance between the two ends, and care was taken to ensure that the bag could not become trapped within the space allowed.

With the model in this position, the vertical load cells were adjusted by hand until each was just in contact with the model. A small head of water was then applied to the model and the strains resulting in each load cell were recorded. Adjustments were made to each of the cells until an approximately symmetrical distribution of strain was obtained and their positions were then fixed by tightening the lock nuts.

Adjustment of the horizontal load cells was carried out in a similar manner. A small pressure was applied by the jacks and the cells were adjusted under this load until a symmetrical pattern of strains was achieved both across the width of the model and between its two ends. The lock nuts were then tightened to fix their positions.

4.3 INITIAL MEASUREMENTS

4.3.1 Tensile Tests

Tensile tests were conducted in accordance with BS.18:Pt 2, 1971. Specimens of the plating were cut from material remaining after fabrication and additional coupons were cut from the model after testing. Typical stress-strain curves and material properties are shown in Fig C52.

As observed from these curves, the yield stress of the material has been lowered by the heat treatment process to a value within the range specified to the fabricators. The process does not appear to have adversely affected the stress-strain response and all material appears to have been equally treated.

4.3.2 Residual Strains

Residual stresses arise from the heating and subsequent cooling of material in the vicinity of a weld run. The area of material immediately adjacent to the weld sustains a tensile stress of magnitude close to the yield stress, whilst for equilibrium remaining areas are forced into a state of residual compression.

The distribution of residual stress is difficult to assess in theoretical terms since it is dependent upon a number of factors. The degree of constraint applied during welding will alter the amount of differential movement which can take place between the separate components, and will therefore affect the distributions of stress and the degree of bending present in the completed structure. Stops and starts in the welding process will lead to irregularities in the stress distributions, since cooling in the vicinity of a part weld run will induce stresses and distortions elsewhere in the structure.

In an eccentrically stiffened steel panel a weld run is

applied to one side of the plating only, and this leads to distortion of the panels between the ribs and an overall bending along the ribs. The distribution of stress obtained will therefore contain a bending component and this will be dependent upon the initial shape of the members.

A stiffening member constructed from welded steel plate will be in a state of residual stress before it is welded to the plating. On fabrication of the complete structure this existing state of stress will be altered.

In typical structures, initial deformations and distortions due to welding are often in excess of specified tolerances. Straightening procedures are then employed and further changes to the stress patterns result.

For each of the three models fabricated, residual strains were measured in both the transverse and longitudinal directions, as outlined in Section (4.1.3). Results are tabulated in Figs C5 to C12 and longitudinal strains across the centre lines are plotted in Fig C13.

(a) *Longitudinal Residual Strains*

Longitudinal residual strains are plotted for each of the three models in Fig C13, where the values shown are the average of those measured to the north and south of the centre lines. For model SP1, each panel sustains a similar distribution of compression strain, where the magnitude of strain at the centre of each is generally less than in the vicinity of the stiffeners. For models SP2 and SP3, the distributions are less regular and the strain sustained is generally lower than that observed for model SP1.

In general, the longitudinal residual strains measured on the unstiffened face of each model are tensile whereas those measured

on the stiffened side are compressive. This reflects a net curvature away from the stiffeners due to welding and this will be discussed in section (4.3.3).

(b) *Transverse Residual Strains*

Transverse residual strain readings are tabulated in Figs C8 to C10. These values are generally small in magnitude although at some locations they are comparable in size with the longitudinal measurements. The most random distribution of strain occurs for model SP3: this was the only model which required straightening after fabrication and this could have influenced the results obtained.

In general, the strains recorded on the stiffened sides of the plates are tensile whereas those on the unstiffened sides are compressive. This indicates a bending of the individual panels towards the stiffeners, and this mode of deformation will be discussed in section (4.3.3).

(c) *Stiffener Residual Strains*

During fabrication stiffener residual strains were recorded at two stages, firstly after the webs were welded to the flanges and secondly after the stiffeners were welded to the plate. Both sets of readings are tabulated in Figs C11 and C12.

In all cases a compressive residual strain was recorded at the edges of the stiffener flange plates and this is in agreement with the theoretical distribution given in reference 13 . The magnitudes of these strains are however quite random, and there appears to be no correlation between the stiffener dimensions and the resulting strain pattern.

Comparing the readings taken before the stiffeners were welded to the plate with those taken afterwards, significant changes in

strain are observed to have occurred at some locations. In most cases the compressive strain present in the flanges was reduced and this could imply a net deflection of the stiffeners away from the plating during the second welding process. Additionally, in some cases a greater reduction in compressive strain occurred on one side of the stiffener than on the other. This could result from the bending of a stiffener in the horizontal plane due to welding along one side of a web before the other.

4.3.3 Initial Deformations

Distortions in steel plating arise from the initial rolling process and from welding during fabrication. These are likely to influence both the mode of collapse and the ultimate strength, and to enable comparisons with the theory extensive measurements have therefore been taken. These are shown graphically in Figs C15 to C23, where the shapes adopted in the numerical analyses are also indicated.

In this section, the distortions expected to occur during the welding process will be discussed and comparisons will then be made with measurements taken on each of the models.

4.3.3.1 *Distortions due to Welding*

(a) The Stiffeners

The tee-section stiffeners were fabricated in the following sequence:

(i) The web and flange plates were cut to size and clamped in position.

(ii) The two plates were tack welded together.

(iii) A continuous fillet weld was passed along both sides of the webs.

(iv) After cooling, the clamps were removed.

Immediately adjacent to the weld run, the material will expand during welding. Since the ends are clamped compression will result, and eventually yielding and then squashing will occur. On cooling, contraction will take place and a stress equal to yield in tension will be set up along the web-flange junction. The resulting forces are reacted by the end clamps, but when these are removed the force eccentricity in the tee-section stiffener will result in a bending of the member away from the flange plate.

(b) The Stiffened Plate

If a perfectly straight stiffening member is welded to a plate, a net deformation towards the stiffener would be expected to occur after welding. If however a stiffener is initially deformed as described above, a clamping moment must be provided at its ends before the weld run can be applied. The direction of this moment will oppose that set up by the tensile forces due to welding, and if it predominates, a net curvature away from the stiffeners will result when the clamps are removed.

Tensile forces will also be present in the plating in the transverse direction and again, owing to load eccentricity, bending will result towards the stiffeners. A sagging of the plate panels will then be superimposed on an overall positive or negative deformation at the stiffener locations.

4.3.3.2 *Measured Distortions*

The initial deformations measured on model SP1 are given in Figs C15 to C17, and the relevant cross-sections are shown in Fig C14. As observed, all stiffeners are bowed in the negative direction (i.e. towards the plate) and this is in agreement with the expected mode of

distortion discussed in 4.3.3.1(a). Referring back to the residual strain table, Fig C11, the compressive strains resulting from stiffener fabrication were generally seen to reduce after welding to the plate. This would occur under the action of the combined moments discussed in section 4.3.3.1(b).

From cross-sections B1 to B9, the sagging of the plate panels between the ribs can be observed. These distortions are fairly regular at the centre of the plate but are less regular at the two ends where the profiles have been subsequently distorted by the end plate welds.

Deformation profiles for model SP2 are shown in Figs C18 to C20. Again the stiffeners are observed to bow in the negative direction although from sections B1 to B9, an overall bow towards the stiffeners is observed in the transverse direction. This curvature is thought to have been imposed during the welding of the end plates to the model, since these members are also bowed in the positive direction.

Figures C21 to C23 show the deformation profiles for model SP3. These are similar in nature to those discussed above for model SP1 although the distortions along the stiffeners are greater in magnitude.

The deflection profiles shown in these figures for use in the numerical analyses will be discussed in Chapter 5, where details of the test results are given and comparisons are made between the experimental data and the theoretical results.

CHAPTER 5

TEST RESULTS AND ANALYSIS OF MODELS

5.1 PARAMETERS USED IN MODEL ANALYSES

5.1.1 The Finite Difference Idealisation

To analyse the models, the finite difference mesh arrangement shown in Fig. D1 was adopted. The mesh covers one-quarter of the stiffened panel and provides four equal spacings between the stiffeners in the y-direction and eight over the half-span in the x-direction.

To accommodate this mesh arrangement the overall width of the panel was increased from 1600 mm to 1650 mm. This was necessary in order to locate a line of main mesh points along the plate boundary, J = 2. As an alternative, the mesh spacing Δy could have been reduced from 75 mm to 50 mm; this would have eliminated the small error in geometry but would have increased the required computer time.

The span of the models was assumed to equal the distance centre to centre of the two end plates. These plates were included in the analyses as members which exert a torsional constraint to the panel edges (Section 5.1.2).

The number of stiffener elements provided within each cross-section is shown in Fig. D1. The webs are divided vertically into four layers and horizontally into five, whilst the flanges are divided vertically into five layers and horizontally into four.

5.1.2 Boundary Conditions

5.1.2.1 *Boundary Conditions on I = 2*

(a) Flexural Conditions

Although the models were constrained laterally on the two end

plates by load cells which allowed free rotation, it is not generally realistic to assume that the moment Mx is equal to zero at all points along the edge. At the intersection of the two lines of lateral constraint (I = 2 and J = 3) rotation cannot occur and the two end plates are thus effectively clamped in position. As the model is loaded, torsional moments are transmitted to the end plates and the resulting rotations vary from zero at the clamped ends to a maximum at the centre. The flexibility of the end plates determines the degree of rotation and hence the flexural constraint imposed along the model edges. For low stiffness end plates the condition Mx = 0 is likely to yield reliable results whereas for high stiffness end plates a fully clamped condition would be more realistic.

Referring now to the diagram shown below, an expression is obtained from which the fictitious displacements w(1,J) can be calculated. The force and moment components in the loaded end plate are defined as N_s, M_s and T_s, and the distance from the centroid of the end plate to the position of the applied moment M is defined as e_s.

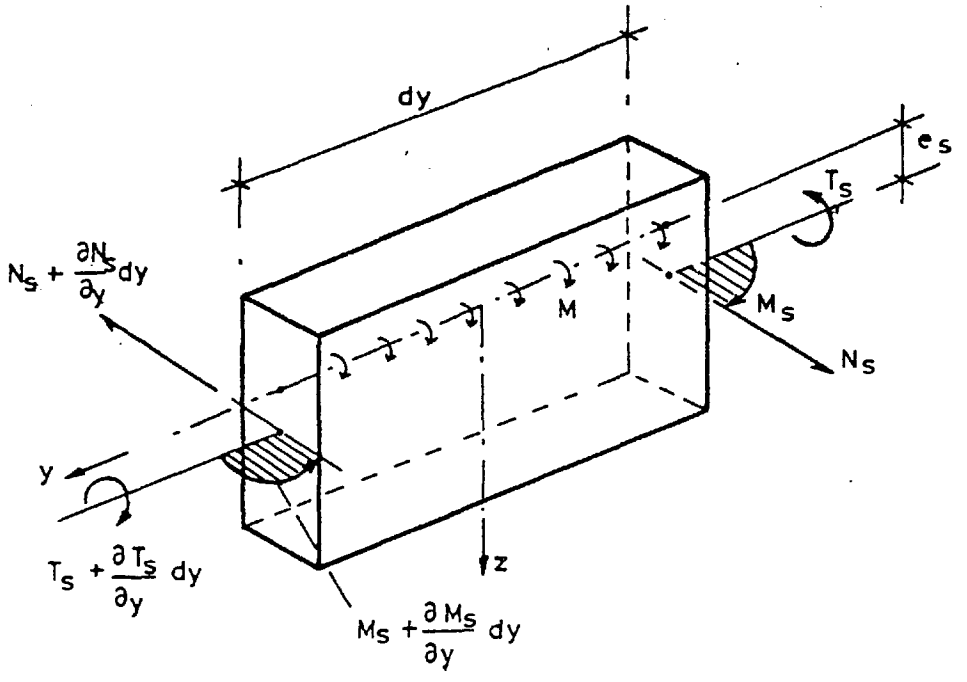

Taking moments about axis y:

$$\partial T_s/\partial y + e_s.\partial N_s/\partial y + M = 0 \qquad (72)$$

Taking moments about axis z:

$$N_s = \partial M_s/\partial y \qquad (73)$$

Combining (72) and (73):

$$\partial T_s/\partial y + e_s.\partial^2 M_s/\partial y^2 + M = 0 \qquad (74)$$

Elastic moment-curvature relationships for the section give:

$$T_s = -GJ_s.\partial^2 w/\partial x\partial y \qquad (75)$$

$$M_s = -EI_s(\partial^2 u/\partial y^2 - e_p.\partial^3 w/\partial x\partial y^2). \qquad (76)$$

where GJ_s and EI_s represent the torsional and flexural rigidities of the end plate, and e_p represents the distance from the centroid of the end plate to the middle-plane of the plate.

Combining (74), (75) and (76) and noting that $\partial^2 u/\partial y^2 = 0$:

$$-GJ_s.\ \partial^3 w/\partial x\partial y^2 + EI_s.e_s.e_p.\partial^5 w/\partial x\partial y^4 + M = 0 \qquad (77)$$

Expression (77) (with moment M expressed in terms of displacements) can be written in finite difference form and re-arranged to give a relationship between the nodal displacements w(1,J), known displacements and elastic rigidites.

(i) *The Applied Moment M at Unstiffened Nodes:*

At unstiffened nodes the applied moment M is assumed to equal the plate moment Mx, and the distance e_s is assumed to equal the separation between the centroid of the end plate and the middle-plane of the plate. Thus, assuming elastic behaviour is retained throughout, expression (77) can be re-written as follows:

$$-GJ_s.\partial^3w/\partial x\partial y^2 + EI_s.e_s.e_p.\partial^5w/\partial x\partial y^4 - D.\partial^2w/\partial x^2 = 0 \quad (78)$$

(ii) *The Applied Moment M at Stiffened Nodes:*

At stiffened nodes the applied moment M is assumed to act at the centroid of a section consisting of a stiffener and a mesh width of plating. The rigidity D' for this section is calculated about the assumed position of moment application. Thus:

$$-GJ_s.\partial^3w/\partial x\partial y^2 + EI_s.e_s.e_p.\partial^5w/\partial x\partial y^4 - D'.\partial^2w/\partial x^2 = 0 \quad (79)$$

In this analysis, it is assumed that the forces NA_w, NA_f and Nx do not contribute to the value of the applied moment, and these forces were also ignored in defining the simply supported edge condition given in Chapter 2. Although this is incorrect, no satisfactory method of incorporating the effect has been established and further work is therefore required to simulate the edge condition more accurately.

(b) In-plane Conditions

The model end plates were assumed to be sufficiently rigid to prevent shortening of the model in the y-direction. Further it was assumed that bending of the plating in the x-y plane was negligible. On the basis of these assumptions, the edge conditions given by expressions (53) to (55) in Chapter 2 were employed. Expression (54) was applied during the relaxation of residual stresses and for lateral load application, and expression (53) was used to apply the uniaxial compression.

5.1.2.2 *Boundary Conditions on J = 2 and J = 3*

(a) Flexural Conditions

In the testing programme lateral movements along the edge

stiffeners were prevented by a series of vertically placed load cells. Thus on the mesh line J = 3:

$$w(I,3) = 0 \qquad (80)$$

To obtain displacements w along the mesh line J = 2, the free edge conditions given by equations (45) in Chapter 2 were employed as follows:

(i) Fictitious displacements w(I,1) were obtained from:

$$My(I,2) = 0 \qquad \text{(Eqn. 45, Ch. 2)}$$

(ii) Moments My(I,1) were obtained from:

$$(\partial My/\partial y + 2.\ \partial Mxy/\partial x)(I,2) = 0 \qquad \text{(Eqn. 45, Ch. 2)}$$

(iii) Knowing these terms, the following equilibrium equation was then employed to obtain the required displacements w(I,2):

$$\{\partial^2 Mx/\partial x^2 + 2.\partial^2 Mxy/\partial x\partial y + \partial^2 My/\partial y^2 + Nx.\partial^2\bar{w}/\partial x^2 + FT_w/2\Delta y^2\}(I,2) = 0 \qquad (81)$$

In expression (81) the lateral load term q was omitted since the pressure bag did not extend beyond the edge stiffeners.

(b) In-plane Conditions

The edges of the plate were unrestrained in both the tangential and normal directions. Expressions (48) and (51) given in Chapter 2, were therefore employed along the mesh line J = 2.

5.1.3 Initial Deformations and Residual Stress

5.1.3.1 *Initial Deformations*

Initial deformations can be specified at each node point by reading the measured values directly, or by defining a relationship from which the nodal displacements can be calculated. In the present work

the latter approach was employed.

The shape of deformation adopted is a combination of an overall sine wave and a local sine wave. This can be represented in the following form:

$$w_o(I,J) = wc.\sin\alpha.\sin\beta + wpan.\sin\alpha.|\sin\gamma| \qquad (82)$$

where

wc is the amplitude of the overall sine wave

wpan is the amplitude of the local sine wave

$$\left.\begin{aligned} \alpha &= \pi.\Delta x(I-2)/Lx \\ \beta &= \pi.\Delta y\ (J-3)/(Ly - 2\Delta y) \\ \text{and}\quad \gamma &= \pi.\Delta y\ (J-3)/b \end{aligned}\right\} \qquad (83)$$

For each of the models the curves were fitted such that good agreement was achieved between the theoretical and experimental values at the centre of the plate. The amplitudes wc and wpan are tabulated in Fig D3, and the theoretical deformation profiles are plotted in Figs C15 to C23. In all three cases the out-of-plane deformations along the panel edges were ignored since no allowance was made for them in the formulation.

In general, the theoretical profiles agree well with measured values although for model SP2 the correlation is less satisfactory. The anticlastic curvature present in this model cannot be represented theoretically unless an initial deformation is included along the panel edges.

5.1.3.2 *Residual Stresses*

The residual stress patterns incorporated in each analysis are shown in Fig D2. All panels of each model were assumed to carry an identical compressive stress and these were calculated from the longitudinal strain levels indicated in Fig C13. At the stiffener

locations a stress of magnitude equal to yield in tension was assumed.

The basic stress patterns were then idealised for application to the finite difference mesh and the forms shown in Fig D2 were obtained. Across the panels the stress levels remained unaltered whilst at the stiffener locations significant reductions followed. This problem can only be eliminated by refining the mesh spacing and this was not considered viable in terms of computation time.

In the stiffener webs and flanges measured strains were irregular, and insufficient readings were available to enable the correct distributions to be used in the theoretical studies. For each case, therefore, the stiffeners were assumed to be residual stress free.

5.1.4 Geometry and Material Properties

Before testing, measurements were taken on each model to compare the actual dimensions with those specified for fabrication. Correlation between the two sets of dimensions was good and specified values (Fig D3) were therefore used in the analyses.

The material properties quoted in Fig D3 were obtained by averaging the tensile test results discussed in Chapter 4. In all cases Poisson's Ratio was assumed to equal 0.3.

5.2 TEST RESULTS

5.2.1 The Loading Sequence

Model SP3 was positioned in the rig as outlined in Chapter 4 and was subjected to an initial in-plane compression of 190 kN. This load was applied in order to maintain contact between the model and the horizontal load cells during lateral load application.

Lateral loading was then applied to the model in increments

of approximately 15 kN/m², with a maximum of 133.7 kN/m². Checks were then made to ensure that the bow under lateral pressure was sufficient to promote a failure towards the stiffeners.

The model was then subjected to in-plane loading in increments of 190 kN, this value being reduced to 38 kN close to failure. A maximum load of 3344 kN was sustained by the model.

5.2.2 Logging of Results

At each load stage, transducer and strain gauge results were recorded and dial gauge readings were taken. The latter readings were not however monitored beyond 3268 kN for reasons of safety, and in future tests it would therefore be advantageous to replace the dial gauges by transducers.

Between each load increment adequate time was allowed for the model to settle down at the new stress level before scanning took place. This was not completely satisfactory close to failure where straining of the model occurred at constant stress.

Selected areas of the model were monitored throughout the test by plotting deflections and strains against applied load. In addition, a Southwell plot was used to predict collapse. This is shown in Fig D23 where the slope of the curve gives the collapse load prediction. The change in slope which is observed near failure probably results from plasticity developing in the model.

5.2.3 Experimental Behaviour of Model SP3

5.2.3.1 *Strains in the Plating*

Strains recorded on both sides of the plating are shown in Figs D5 to D13, where the relevant sections are indicated in Fig D4. The uniaxial yield strain of the material is approximately 1900 $\mu\varepsilon$.

(a) Longitudinal Strains across Section 1-1

Longitudinal strains recorded across section 1-1 are shown in Fig D5 where,under lateral pressure, tension develops on the unstiffened face of the model whilst compression develops on the stiffened face. This distribution of strain reflects the clamping action which is induced along the model edge by the end plate.

Under in-plane loading the strains initially increase in a uniform manner, with higher compressive components being carried on the stiffened side of the plating than on the unstiffened side. This is again evidence of torsional constraint along the edge.

Towards failure the distribution becomes less regular and redistribution starts to occur. In panels P1, P3 and P5 a greater increase in compression occurs on the unstiffened side than on the stiffened side, whilst in panels P2 and P4 the reverse occurs. This change in form indicates a buckling of panels P1, P3 and P5 towards the stiffeners and a sympathetic buckling of panels P2 and P4 towards the plating.

This mode change was probably promoted by surface yielding in the model. The uniaxial yield strain of 1900 $\mu\varepsilon$ has been exceeded at a number of locations,and plasticity will generally occur at a strain less than that for uniaxial yield.

(b) Longitudinal Strains across Section 2-2

Figure D6 shows the distribution of longitudinal strain at mid-span on both the stiffened and unstiffened sides of the model.

Under lateral pressure compressive straining occurs on both faces, the magnitude of this being greatest on the unstiffened side since bending takes place towards the stiffeners. Bending action also results in higher values of compression across the centre of the plate

than around its edges.

Under in-plane loading the strains increase uniformly until approximately 80% of the maximum load is carried at which stage redistribution starts to take place. In panels P1, P3 and P5 increased compression is carried on the unstiffened side whilst a reduction occurs on the stiffened side. Conversely, in panels P2 and P4 unloading occurs on the unstiffened side whilst additional compression is carried on the stiffened side. This reflects a sympathetic buckling of panels P1, P3 and P5 towards the stiffeners and P2 and P4 towards the plating.

Compressive yielding has occurred in the plating over the two central stiffeners and has probably penetrated the full depth. This effect would have created a hinge at each side of panel P3 and would thus have reduced its buckling strength.

(c) Transverse Strains across Section 2-2

Figure D7 shows the distribution of transverse strain across the plating at mid-span. On the stiffened side of the model high tensile strains occur in the panels whilst over the stiffeners compressive strains result. Conversely, on the unstiffened side tensile strains result over the stiffeners whilst compressive straining occurs in the panels. This distribution of strain reflects the sagging of the panels between the stiffeners and the hogging of the panels over the stiffeners.

The tensile strains which occur on the stiffened side of the model are greater in magnitude than the compressive components on the unstiffened side. This indicates the existence of membrane forces which develop as deflections become large in a constrained panel.

(d) Longitudinal and Transverse Strains across Section 3-3

Longitudinal strains across section 3-3 are shown in Fig D8. Behaviour here is similar to that described above for section 2-2, although at failure there is negligible change in the distribution of strain.

The transverse strains for this section are shown in Fig D9. Again behaviour is similar to that at mid-span and further discussion is therefore omitted.

(e) Longitudinal Strains across Section 4-4

Figure D10 shows the distribution of strain across a section 600 mm to the south of the model centre line. This section is fairly close to the model ends where the resulting distribution of strain is quite different from that at mid-span. At the stiffener positions the level of strain is virtually constant throughout the depth of the plating; this indicates an absence of bending and is probably close to the point of contraflexure. In the panels, however, significant bending occurs towards the stiffeners, and this can be seen by comparing the strains on the stiffened side with those on the unstiffened side.

At the maximum load, unloading starts to occur on the stiffened side of the model in panel P4. This is the reverse of behaviour noted for sections 2-2 and 3-3, and indicates a deformation of panel P4 towards the stiffeners.

(f) Transverse Strains across Section 4-4

Transverse strains across section 4-4 are shown in Fig D11. The form of these curves is similar to those shown in Figs D7 and D9, although less difference exists between the tensile and compressive

strains across the plate thickness. This indicates a smaller tensile membrane action which would be expected close to the model ends where deflections are restrained.

(g) Longitudinal Strains across Section 5-5

Figure D12 shows the distribution of longitudinal strain at the reaction end of the model. Between sections 4-4 and 5-5 a considerable increase in compression has occurred on the stiffened side of the model whilst a reduction has occurred on the unstiffened side. This is again indicative of clamping action which is induced along the model edge by the end plates. Comparing these curves with those shown in Fig D5 for the loading end of the model, a similar behaviour is observed. Similarity is greater under lateral pressure than under in-plane loading, however, where it appears that a greater clamping action exists at the reaction end. This could result from a slight difference in positioning of the horizontal load cells or from differences in the shape of the initial deformation.

(h) Longitudinal Strains along Section 6-6

Figure D13 shows the distribution of longitudinal strain along the centre line of panel P3. The clamping action at the model ends can be seen clearly and strains are initially quite symmetrical about the centre line. The loss of symmetry which occurs at failure is probably a function of the difference in end constraints noted above.

5.2.3.2 *Strains in the Stiffeners*

(a) Longitudinal Strains along the Flange Centre Lines

Figure D14 shows the variation in longitudinal strain which occurs along the stiffening members S4 and S5. The gauges are located

on the stiffener flange plates and are positioned along their centre lines.

Under lateral pressure stiffener S4 sustains a tensile strain at its extreme fibres, this reducing with bending action towards the edges of the plate. With the addition of in-plane loading tensile strains at mid-span reduce until, at failure, the bending component predominates and additional tensile straining results. At the end plate position where the bending component is negligible, the flanges support high compressive strains throughout.

The behaviour of stiffener S5 is similar to that of S4, although under lateral pressure there is greater evidence of clamping at the model ends and lower tensile strains are induced at mid-span. Also, under in-plane loading higher compressive strains result at the end plate positions owing to the greater fixing moment.

(b) Longitudinal Strains across the Stiffener Flange Plates

Figure D15 shows the variation in longitudinal strain which occurs across the stiffener flange plates at mid-span.

The strains shown for stiffeners S2 and S5 vary almost linearly and the distributions are quite symmetrical across the centre line. Tensile strains are greatest on edges adjacent to the model boundaries since rotations occur in this direction.

For stiffener S4, less variation of strain occurs across the width of the flange and this implies a smaller horizontal bending component. This would be expected close to the centre of a plate where the slope of an overall deformation is small. The degree of variation remains almost constant until the ultimate load is reached at which point a greater twisting component develops. This probably occurs as the two adjacent panels buckle in sympathy.

Longitudinal strains across the edge stiffener S6 are predominantly compressive owing to lateral constraint provided at these locations. Here, there is also greater evidence of bending than in the cases discussed previously, since the maximum plate rotations occur at the edges. Most of the rotation occurs under lateral pressure as indicated by the parallel nature of the in-plane loading curves.

5.2.3.3 *Deformation under Load*

Figure D16 shows the load-deflection response along a section 400 mm to the north of the model centre line. Under lateral pressure a linear response is observed and the degree of symmetry achieved is good. With the addition of in-plane forces, however, there is some loss of symmetry and a less linear behaviour develops.

Loss of symmetry under in-plane load can be attributed to three possible causes. Firstly, the initial deformations shown in Figs C21 to C23 are not symmetrical and the eccentricity of applied load will therefore vary across the section. Secondly, the loading beam was moving at a slight angle to the model edge and was therefore applying a higher load on one side of the plate than on the other and thirdly, the positioning of the horizontal load cells may have been in error.

Corresponding deflections to the south of the centre line are shown in Fig D18. Under lateral pressure deflections are almost identical to those shown in Fig D16 although there is some lack of symmetry prior to the addition of in-plane forces. This is thought to result from irregularities in the model geometry and, in particular, from the spacing of the stiffeners. Again, under in-plane loading the response is similar to that observed in Fig D16 although the magnitude of deflection at the centre of panel P3 is much reduced. This is

thought to result from the differences in initial deformation which can be seen from sections B3 and B7 in Fig C21. Also, deformation of the plating away from the stiffeners which occurred in panels P2 and P4 in Fig D16 did not occur at this end of the model. There was however some evidence of stiffening at these locations prior to collapse.

The load-deflection behaviour at mid-span is shown in Fig D17. Deflections are greater in magnitude than those observed above although the general response to load is similar. At failure panels P2 and P4 stiffened and snapped through, whilst in adjacent panels greater positive out-of-plane deflections resulted.

Figures D19 to D22 show the deflected shape of the plate at a number of cross-sections. Insufficient data is however available to detect local buckling in panels P1, P2, P4 and P5,and in future tests it would therefore be advisable to modify the present arrangement of transducers. The local mode of deformation for panel P3 can however be seen in Figs D19 and D21.

5.2.3.4 *Behaviour at Collapse*

Just prior to collapse deflections started to increase rapidly and significant straining occurred at constant stress. The mode of deformation observed at failure is indicated in Fig D24 where five half-waves developed across the width. The number of half-waves within the span appears also to be five in number although this cannot be stated with certainty owing to the lack of relevant data. The maximum load sustained by the model was 3344 kN.

As buckling occurred and deflections became large,the horizontal load cells tilted upwards and applied a downward force to the loading beam. Damage resulted in the roller bearing connections and with this the beam dropped in level. This in turn resulted in a shear force being

applied to the bearing pads on the model end plates and movement of the pads followed. A large eccentric load was thus applied to the model ends and the developing buckling mode was destroyed.

For future tests,therefore, some modifications must be carried out,and proposals for this are given in Chapter 7.

5.2.4 Horizontal and Vertical Load Cells

5.2.4.1 *Horizontal Load Cells*

Forces in the horizontal load cells are shown graphically in Fig D25. Similar distributions are seen across the two ends and the loss of load due to frictional resistance is small (5%).

Summation of forces to the left and right of the longitudinal centre line gives a 6% difference in load between the two sides; this results from a slight misalignment of the parallel arm mechanism which forced the beam to move at a small angle to the model edge.

In both sets of load cells higher forces are observed in the vicinity of the stiffeners than across the panels,and the applied edge displacement was therefore not uniform as originally assumed. This results from deformation of the model end plates under the applied load, and can only be reduced by adopting a much stiffer section.

5,2.4.2 *Vertical Load Cells*

Forces resulting in the vertical load cells under lateral pressure are shown in Fig D26. The degree of symmetry achieved is good, where the discrepancies are only 4.5% between the north and south sides and 3.9% between the east and west sides.

Along the east and west sides the reactions are approximately equal to the loading supported by one-half panel whilst along the north and south sides they are considerably greater. Most of the applied

load is transmitted via the panels to the stiffeners and is thus carried to the north and south end plates.

At the corners of a panel there is a tendency for uplift to occur under lateral pressure. This effect can be seen in Fig D26 where tensile reactions occur at these locations.

5.3 ANALYTICAL SOLUTIONS AND COMPARISONS

The three stiffened plate models were analysed using the parameters discussed in Section 5.1. For each case two initial states of stress were considered, these being zero residual stress and applied residual stress.

The level of lateral load applied to model SP3 was identical to that used in the test, whilst for models SP1 and SP2 the loading was determined such that deflections of magnitude similar to those of SP3 were induced. The behaviour of model SP1 will now be discussed in detail and the major differences between this and the remaining models will then be noted. Comparisons will also be made between the theoretical and test results obtained for model SP3.

5.3.1 Analysis of Model SP1

5.3.1.1 *Load-Shortening Curves and Ultimate Strength*

Load-shortening curves are shown for both initial states of stress in Fig D27. The two solutions are identical up to $\sigma m/\sigma o = 0.510$ when yielding occurs in the plating and the two solutions begin to diverge. In both cases the load-shortening response is quite linear and unloading occurs suddenly.

In the absence of residual stress yield zones develop as shown in Fig D28. First yield occurs at the stress level $\sigma m/\sigma o = 0.437$ where, owing to lateral constraint and bending in the x-y plane, plasti-

city results in the edge stiffener flanges. Plate yielding occurs at the stress level $\sigma m/\sigma o = 0.613$ over the stiffening member S3; it then develops over stiffening member S2 and finally spreads into the panels. The ultimate load is then reached as buckling occurs in the elasto-plastic range where there is negligible capacity for stress redistribution.

Under the application of residual stress the process of yielding is quite different. The flanges of the edge stiffeners again yield at $\sigma m/\sigma o = 0.437$, but this is followed by yielding of the plating along the free edges as shown in Fig D29. This commences at $\sigma m/\sigma o = 0.510$ where the two solutions were observed to diverge. With a further addition of in-plane loading yield occurs in panels P1, P2 and P3 where compressive residual stresses are present. Overall unloading then follows whilst the plating over the stiffeners is still elastic, capacity being lost in the panels more rapidly than redistribution can take place.

The unloading curve shown in Fig D27 for the case of applied residual stress is not entirely accurate, since the yield function vastly exceeded unity at some locations. This portion of the curve has however been included to indicate the sudden loss in carrying capacity associated with this type of failure. For the case of zero residual stress divergence occurred at the peak load and no post-ultimate response is therefore shown.

5.3.1.2 *Load-Deflection Behaviour*

The load-deflection response of model SP1 is shown graphically in Figs D30 and D31. The first of these figures relates to zero residual stress and the second to applied residual stress. In addition, selected deflection profiles are shown in Fig D32.

Referring to Fig D30 a linear load-deflection response is seen under lateral pressure, the maximum deflection on stiffener S3 being 1.25 times plate thickness and that on panel P3 being 1.45 times plate thickness.

Under in-plane loading, the observed response is much less linear. The out-of-plane deflections, and hence the eccentricity of load at mid-span, increase with each successive load increment and the non-linear relationship between applied load and deformation is thus produced.

As yielding occurs at the stiffener locations deflections at mid-span become suddenly large, and the seven half-wave buckling mode indicated in Fig D30 develops along the span. Each of the panels deflects in the same mode and no sympathetic rotation occurs across the stiffeners.

Referring now to Fig D31 the load-deflection behaviour is seen for the case of applied residual stress. Initially the response is identical to that described above, but at the ultimate load, snap through occurs in all panels at mid-span and a series of nine alternating buckles appear along the length.

The number of half-waves which develop along the span will depend upon the aspect ratio of the panels and the degree of clamping afforded by the stiffeners. In the absence of residual stress plasticity developed over the stiffeners and hinges were formed along the panels. The clamping action was thus reduced and this probably gave rise to the different mode forms obtained in the two analyses.

5.3.1.3 *Stresses in the Plating and Stiffeners*

(a) Stresses in the Plating

Direct stresses at selected sections in the plating are shown

in Figs D33 and D34, sections 2-2, 3-3 and 4-4 showing distributions across the width and section 6-6 the distribution on the longitudinal centre line.

At sections 2-2 and 3-3 similar distributions of stress are observed, concentration being slightly greater in the vicinity of the stiffeners than across the panels where local bending occurs.

At section 4-4 which is close to the model boundary a different distribution of stress is observed. Local depressions in the stress curves are less pronounced owing to the smaller panel deflections, whilst an overall depression results across the plate width. This form of distribution is typical close to the edge of a plate which is forced to remain straight.

The distribution of stress along the centre of panel P3 shows an increase in compression towards the centre of the plate where maximum bending occurs. In addition, the tensile stresses which develop at the supports due to partial clamping action can be observed under lateral pressure.

(b) Stresses in the Stiffeners

Extreme fibre stresses are shown for stiffeners S4 and S5 in Fig D35.

Under lateral pressure bending action causes tensile straining at mid-span. The magnitude of this is greater for stiffener S4 than for S5 since higher rotations can occur at the edges. The effect of rotational restraint at the boundary can be seen clearly for stiffener S5, where increased compression is observed to occur with an addition of applied pressure.

Under in-plane loading the stiffener flanges initially carry a proportion of the applied compression at mid-span. As

deflections increase, however, and the bending action starts to predominate, further tensile straining results.

Figure D36 shows the variation in direct stress which occurs across the stiffener flange plates at mid-span.

Under lateral pressure negligible variation of stress occurs across stiffener S4 and only slight changes of slope are observed during in-plane load application. Variation of stress results from the rotation of a stiffener due to an overall deformation of the plate, and from horizontal bending of a stiffener in the x-y plane. This stiffener is located close to the centre of the plate where the slope of an overall deformation is small, and hence where negligible rotation occurs.

A greater variation in stress is observed across the flange of stiffener S5, where tension increases towards the model edge. This reflects the twisting of the stiffener which occurs as the model deforms out-of-plane.

The edge stiffener S6, unlike members S4 and S5, supports compressive loading along its full length owing to the application of lateral restraint. The stresses do however vary in a manner similar to those of S5, although the slopes are greater owing to the higher degree of rotational freedom.

5.3.2 Analysis of Model SP2

5.3.2.1 *Load-Shortening Curves and Ultimate Strength*

Load-shortening curves are shown for model SP2 in Fig D37. The two solutions are almost linear and are identical until close to collapse when, in both cases, sudden unloading occurs.

Unlike model SP1 where the application of residual stress was seen to reduce the ultimate strength a slight

increase in capacity is achieved. This result can be explained by observing the yield diagrams in Figs D38 and D39.

For the case of zero residual stress, plasticity occurs first in the edge stiffener flanges at the stress level $\sigma m/\sigma o = 0.178$. This stress is far below that for first yield in model SP1 owing to the lower strength of the stiffener material. Plasticity in the plating occurs at $\sigma m/\sigma o = 0.557$ and, as for model SP1, this develops over the stiffening member S3. Yielding then develops over stiffener S2 and finally the ultimate load is reached as yielding spreads into the panels. The behaviour observed for this case is therefore similar in nature to that described for model SP1.

For the case of applied residual stress yielding starts at the free edge of the plating at the stress level $\sigma m/\sigma o = 0.572$. This spreads along the length of the edge until, at $\sigma m/\sigma o = 0.616$, yielding suddenly occurs across the full width of the plate and collapse follows.

For model SP2, the residual stress is lower than that applied to model SP1 and compressive yielding in the panels therefore occurs at a higher stress level. This increase in strength combined with delayed yielding at the stiffener locations due to tensile residual stress, creates a situation in which plasticity occurs simultaneously over the stiffeners and in the panels. Higher stresses are therefore sustained than in the residual stress free case where failure occurred by partial yielding of the section.

5.3.2.2 *Load-Deflection Behaviour*

Load-deflection curves and deflection profiles are shown for model SP2 in Figs D40 to D42. Deflections under lateral load are again linear with a maximum value of 1.34 times plate thickness on stiffener S3 and 1.6 times plate thickness at the centre of panel P3. Comparing

these curves with those shown for model SP1, a similar response is observed. Deflections are however smaller in magnitude owing to the higher flexural stiffness involved. The buckling modes are also similar in form and again no sympathetic rotation occurs across the stiffeners.

5.3.2.3 *Stresses in the Plating and Stiffeners*

In general, the stress distributions for both the plating and the stiffeners are similar to those described in Section 5.3.1.3 for model SP1. Discussion is therefore omitted here although the distributions have been included for future comparison with test results (Figs D43 to D46).

5.3.3 Analysis of Model SP3 and Comparisons with Experimental Results

5.3.3.1 *Load-Shortening Curves and Ultimate Strength*

Theoretical and experimental load-shortening curves for model SP3 are shown in Fig D47. A description of the theoretical results will be given first and comparisons will then be made with the experimental data.

(i) Theoretical Results

The load-shortening characteristics of model SP3 are similar in form to those described for model SP2. Here,however, the response is slightly stiffer owing to the greater rigidity involved.

For zero residual stress plasticity develops as described for model SP2 in section 5.3.2, first yield occurring over stiffening member S3 at the stress level $\sigma m/\sigma o = 0.501$. This process is shown in Fig D48 where at failure plasticity has spread into the upper fibres of stiffeners S2 and S3.

For the case of applied residual stress, first yield occurs at the centre of the plate at the stress level $\sigma m/\sigma o = 0.563$. As shown in Fig D49, this is followed almost immediately by collapse, as extensive yielding occurs across the full width of plating. Again an increase in ultimate strength was achieved over the residual stress free case, as the full capacity of the section was utilised at failure.

(ii) Test Results

The load-shortening curve obtained experimentally is shown in Fig D47 where, as in the theoretical work, a fairly linear behaviour is seen. Here, however, the response is stiffer and this could result from both inaccuracies in the test set up and in the analytical approach.

In carrying out the test it was necessary to locate the horizontal load cells at the centroid of the model cross-section. Since however the model ends had been deformed during the welding process, this position was almost impossible to determine. The initial deformation diagrams shown in Figs C21 and C22 indicate a distortion at the two ends towards the plating, and the application of a load to the theoretical centroid would therefore probably result in a fixing moment at the model ends. With this, an overestimation of the model stiffness would result.

As noted in Section 5.1.2.1, forces NA_w and NA_f were ignored in defining the moment constraint. These components would however contribute to the bending action and this may have led to an underestimation of the stress-strain capabilities.

The maximum stress sustained in the test was 0.590 of the yield stress and the equivalent theoretical values were 0.573 and 0.559 of yield, for the cases of applied residual stress and zero residual stress respectively. Good agreement was therefore achieved in the

collapse strengths, although further experimental verification is essential.

The experimental load-shortening curve could not be monitored in the final stages of the test owing to reasons of safety. In future tests, therefore, it would be sensible to replace the existing dial gauges by transducers through which remote control is possible.

5.3.3.2 *Load-Deflection Behaviour*

(i) Theoretical Results

Load-deflection curves for model SP3 are shown in Figs D50 to D53 where, for clarity, deflections at the stiffener locations are shown separately from those in the panels. Load-deflection profiles are also shown for two cross-sections in Fig D54.

Under lateral pressure a linear load-deflection response is observed, the maximum deflection on stiffener S3 being 1.32 times plate thickness and that at the centre of panel P3 being 1.71 times plate thickness. The deflections are smaller in magnitude that those seen for models SP1 and SP2, but in general the response is similar. Close to the ultimate load local buckling occurs and the wave forms shown in Figs D51 and D53 develop. These are identical to the modes of deformation obtained for models SP1 and SP2.

(ii) Experimental Results

Deflections obtained experimentally are shown in Figs D50 to D54 where comparisons are made with the theoretical results.

Under lateral pressure a linear load-deflection response is seen both experimentally and theoretically. The experimental values are however smaller in magnitude, the maximum value on stiffener S3 being 1.2 times plate thickness and that in panel P3 being 1.38 times

plate thickness. This gives an error of 10% in the calculation of stiffener deflections and 24% in the calculation of panel deflections.

The magnitude of the overall bow will be influenced significantly by the flexural constraint imposed along the model edge. In Fig D59 results are shown for three different edge conditions, these being clamped, simply supported and partially constrained by an edge member. Between the two extreme cases a ratio of 5:1 is seen in the deflections.

At the simply supported end of the range a panel is particularly sensitive to a small rotational constraint, and small changes in torsional stiffness can therefore lead to large changes in deflection. In the analysis of model SP3, torsional stiffness was assumed to be a function of the edge beam alone whereas, in reality, part of the plate would act compositely with the beam. By including this component in the analysis, lower deflections would undoubtedly result.

In the derivation of expressions (78) and (79), the influence of forces NA_w and NA_f was ignored. To investigate the error introduced here the panel was re-analysed as a beam consisting of a single stiffener with a width of plating based on Faulkner's effective breadth formula . The deflection obtained is shown in Fig D59 where the result is seen to agree closely with the simply supported plate analysis. Assuming that the effective breadth is sufficiently accurate, this indicates that the effect of forces NA_w and NA_f is quite small.

Panel deflections relative to the stiffeners are overestimated in the analysis, being in the order of twice those measured in the test. This discrepancy is thought to arise from two main sources, the first being the finite difference mesh and the second being the panel slenderness ratio.

The first of these was investigated by analysing a single

panel with clamped edges under lateral loading, for three different mesh sizes. The results are shown in Fig D59, where a deflection of 1.314 mm is obtained for the 5 × 11 mesh used in the model analysis and a deflection of 0.928 mm is obtained with the refined 9 × 11 mesh. If a similar improvement was obtained in a total panel analysis, the calculated deflection would reduce from 1.49 mm to 1.05 mm

Despite the above improvement, the calculated deflection is still larger than the measured value of 0.72 mm. In the analysis the deflecting width of the panel is assumed to equal the distance centre to centre of the stiffening members. In reality, however, the width of plating over a web and the welded zone around it cannot deflect relative to the stiffener. This reduces the deflecting width from 300 mm to 286 mm, from which an estimated 17% reduction in deflection would follow.

Under in-plane loading a stiffer load-deflection response is observed in the test than in the analysis, this resulting from the problems discussed in Section 5.3.3.1. The vertical portion shown at the beginning of each of the in-plane loading curves results from the initial application of compressive forces.

At failure the model started to buckle into the alternating wave form shown in Fig D24. This form was not predicted in either of the analyses although in both cases a change of mode did occur. It was however shown in the numerical work that the addition of a small residual stress can give rise to a different buckling mode. Thus, if the residual stress input was modified and the analysis repeated, it is possible that the experimental mode of failure would be predicted.

5.3.3.3 *Stresses in the Plating and Stiffeners*

In general, the observations made in Section 5.3.1.3 for model SP1 apply equally to model SP3. Detailed discussion is

therefore omitted although comparisons are given between the test results and the theoretical solutions.

(a) Stresses in the Plating

Stresses obtained in the plating both experimentally and theoretically are shown in Figs D55 and D56. In general the agreement achieved is good, particularly over the central region where the effect of boundary constraints is small.

During the application of lateral load, the measured stresses are slightly in excess of the calculated values; this results from the initial application of an in-plane load equivalent to an average stress of 13 N/mm^2.

(b) Stresses in the Stiffeners

Stresses in the stiffener flange plates, obtained both theoretically and experimentally are shown in Figs D57 and D58.

Referring first to Fig D57 the variation in stress along stiffeners S4 and S5 can be seen. Under lateral pressure, higher tensile stresses are predicted in the analysis than observed in the test, and under in-plane loading less applied compression is supported by the stiffeners at mid-span. This arises from the overestimation of deflections which produces higher bending stresses under lateral load and a greater eccentricity of in-plane load.

Figure D58 shows the variation in direct stress across the stiffener flange plates at mid-span. In general, the predicted behaviour is similar to that observed in the test although again, owing to the overestimation of deflections, stresses do not agree well in magnitude.

CHAPTER 6

NUMERICAL SOLUTIONS

6.1 SCOPE OF NUMERICAL SOLUTIONS

The governing equations for discretely stiffened plates have been used to solve a wide range of plate problems. The results obtained will be presented in this chapter.

The main study undertaken investigates the influence of geometrical properties on the serviceability and collapse behaviour of stiffened plating. An identical geometrical configuration was adopted for each of the panels, and the plate and stiffener slenderness ratios were varied for the study by altering the plate thickness and web dimensions only.

Several smaller scale investigations were also carried out on plate geometries selected from the main study. The first of these considers the effect of initial deformation on plates of slenderness $b/t = 30$. In all cases an overall sinusoidal deformation profile was selected and the magnitude of the bow was varied for the study.

A second study investigates the concept of hybrid plates for which the yield stress of the stiffener material is different from that of the plate. Panels of $b/t = 60$ were selected, and the stiffener slenderness ratios were varied between the limits $Lx/R = 30$ and $Lx/R = 90$.

In all the cases analysed above loading was applied to the plate as a uniaxial in-plane displacement in the direction of the stiffening. To examine the effect of combined loading one plate was selected from the group ($b/t = 60$; $Lx/R = 30$) and was subjected to an initial level of lateral load followed by in-plane load to failure. Three different levels of lateral load were applied, these ranging from 0 to 105 kN/m^2 (0 to 15 psi).

In Chapter 5 the theory was compared with test results and here comparisons are made with existing analytical solutions. Few solutions are however available for comparison, and those quoted here are taken exclusively from a similar but less general formulation presented by Djahani[17].

6.2 COMPARISONS WITH EXISTING WORK

6.2.1 A Plate with an Eccentrically Placed Central Stiffener

The first of the comparisons undertaken is for a simply supported plate divided into two panels of aspect ratio 2:1 by a central rectangular stiffener. The loading is applied in the plane of the plate as a uniform edge displacement in the direction of the stiffening. The initial deformation is sinusoidal in shape and has an amplitude of 10 mm in the positive z-direction. All dimensions, material properties and boundary conditions used, are quoted in Fig E1.

Both the elastic and the elasto-plastic behaviour have been investigated and the load-shortening relationships obtained are shown in Fig E2. Good agreement is achieved for the elastic analysis and the ultimate loads obtained are almost identical. In the post-ultimate range, however, agreement is less satisfactory, and this is thought to result from either different degrees of convergence or from the size of the loading increments. If loading increments are too large the stiffness of the section will be overestimated and this could account for the discrepancy involved.

6.2.2 A Stiffened Plate with Residual Stresses

The second analytical solution available for comparison was taken from a series of tests conducted by Fukomoto et al[44]. The model selected for analysis is shown in Fig E3 together with a listing of the material properties and boundary conditions used. The plating is

divided into four panels by three equally spaced rectangular stiffeners which are welded eccentrically to the plate. Loading is applied as a controlled edge displacement and the initial deformation is sinusoidal in shape.

The model has been analysed for two separate conditions. The first of these assumes a zero residual stress level in both the plate and stiffeners whilst the second allows for a residual compressive stress in both components of 0.4 times yield stress. The assumed residual stress blocks are shown in Fig E4 together with the idealised distributions used in the numerical procedure.

The load-shortening curves obtained are given in Fig E5, where the equivalent curves obtained by Djahani and the test result obtained by Fukomoto et al. are also shown. A discrepancy of approximately five per cent exists between the two analytical failure loads, and this is thought to arise from the boundary restraint applied along the loaded edges. In the present work this edge was assumed to be fully fixed tangentially ($v = 0$), whilst in the Djahani solution a shear free edge was adopted.

To investigate this problem further, an unstiffened plate was analysed for which the alternative boundary condition could be easily applied. The example chosen for analysis was first solved by Moxham[11] and the relevant data is shown in Fig E6. Four solutions have been obtained, two of these for a residual stress level of 0.1225 times yield and the second pair for a zero residual stress level. The first in each pair was analysed with a shear free edge whilst the second was analysed with a fixed edge. As observed from Fig E7, the two cases for $Nxy = 0$, agree well with the results presented by Djahani, whereas the two cases with $v = 0$ show a reduction in capacity similar in magnitude to that observed in Fig E5.

For both analytical solutions the ultimate load obtained is

greater than that observed in the test. It was however noted by Fukomoto et al[44] that in some cases the test results fell below their predictions, and this they attributed partly to a difference between the actual and assumed residual stress levels.

6.3 PARAMETRIC STUDIES

The remainder of this chapter is devoted to the presentation and discussion of a series of new solutions. In most cases the analyses have been extended into the post-ultimate range, although for some geometries this was not possible owing to the effects of numerical instability. Since all plates could not be analysed beyond the peak stress the decision was made to curtail all solutions close to the ultimate load, thereby economising on computer time and enabling a greater range of plate types to be considered.

The number of mesh divisions required for a given degree of accuracy will depend upon the deformed shape of the plate and hence upon the plate and stiffener dimensions. In the following studies, therefore, where for economy a constant mesh spacing is used throughout, a lesser degree of accuracy is assigned to cases which fail in a panel buckling mode than to cases which fail in an overall mode.

6.3.1 A Study of Various Failure Modes

The basic plate geometry selected for the study is shown in Fig E8. The plate is subdivided into three panels of aspect ratio 3:1 by two longitudinal webs which have a fixed depth to thickness ratio of ten. Simply supported, non-deflecting edges are assumed and in all cases the unloaded boundaries are free to move in the x and y directions. On the loaded edges a uniform in-plane displacement is applied whilst in the tangential direction full restraint is assumed. The selected initial deformation profile is sinusoidal in shape and has an amplitude of 5 mm

in the positive z-direction. All material properties for the plate apply equally to the stiffeners, and the lateral load and residual stress levels are set at zero. Six mesh divisions are adopted in each direction for the quarter plate analysed, and the stiffeners are divided horizontally into five layers and vertically into four.

The plate and stiffener slenderness ratios b/t and Lx/R are varied for the study by altering the plate thickness and web dimensions only. The range of ratios considered, together with the relevant plate and stiffener dimensions, are tabulated in Fig E9.

Results from the study are shown graphically in Figs E10 to E51. The first group of curves, E10 to E15, show the load-shortening relationships for the total cross-section and the load-shortening relationships at mid-span for the webs alone. Where poor convergence was observed or where the yield function exceeded reliable proportions these curves are shown as discontinuous. In Fig E16 the peak loads are summarised graphically and three approximate zones of plate behaviour have been identified. A discontinuous curve is again adopted where sharp changes in curvature occur and no results have been obtained to identify the relationships accurately.

Figures E17 to E26 show the distributions of direct stress in the plating at mid-span for a range of applied strain and for each combination of b/t and Lx/R considered. Figures E27 to E46 show a selected number of load-deflection curves and deflection profiles. Within the latter group, Fig E 42 shows the effect of web torsional stiffness, and Fig E45 the effect of shear restraint along the loaded edge, on the plate behaviour. Discontinuous curves are used in these figures only for reasons of clarity. The final group of figures, E47 to E51, describe the areas of stiffened plate which have reached yield by the ultimate load.

The zones of plate behaviour shown in Fig E16 indicate the predominant mode of failure which was observed in each case. These can be summarised as follows:

In Zone I: Failure occurs by squashing of the cross-section before extensive buckling occurs.

In Zone II: Failure occurs in an overall mode following flexural failure of the stiffeners.

In Zone III: Failure is preceded by panel buckling in three half-wave mode form.

In addition, Zone III is divided into three subzones A, B and C, where different arrangements of the three half-wave mode buckles were observed.

With reference to this diagram the results will now be discussed, commencing with plates in Zone I.

6.3.1.1 *Plates in Zone I*

The following discussion is presented in two sections, the first for plates of slenderness b/t = 30 and the second for plates of slenderness b/t = 50. In each section the behaviour is described in detail for Lx/R = 30, and differences between these and the more slender cross-sections are indicated.

(a) b/t = 30; Lx/R = 30

Referring to the load-shortening curve(Fig E10) a linear stress-strain relationship is seen. The peak load is reached soon after first yield in the plate and subsequent unloading occurs gradually. Over the range of strain considered the direct stress at mid-span (Fig E17) remains fairly uniform across the width, and at the peak load almost full yield in compression is sustained. The corresponding area of yield is shown in Fig E47, where the webs are seen to yield in compression.

Although the plating alone can carry almost full squash loading,

the total cross-section fails at 95% of this value. This reduction results from bending action which accelerates with increasing deformation. Beyond the peak load additional applied strain will lead to squashing of the plate at constant stress, and deflections will increase owing to the load eccentricity. To balance the resulting additional applied moment a greater tensile component is required from the stiffeners and this, combined with constant stress in the plate, will lead to overall unloading. This can be observed visually in Fig E10, where the compressive stress in the stiffeners is seen to reach a maximum value of approximately 62% of yield, after which gradual unloading occurs as the increase in tension outweighs that in compression.

Load-deflection curves and deflection profiles are shown in Fig E27 for the locations indicated in Fig E8. As expected for panels of these dimensions negligible deformation occurs in the plating between the stiffeners, and overall the deflections remain small by virtue of the stiff webs employed.

Extending the discussion to Lx/R = 50 and Lx/R = 60 we refer to the load-shortening relationships Figs E11 and E12, and the direct stress curves Fig E17. In each case the direct stress at mid-span is similar to that for Lx/R = 30 although for both cases lower ultimate load levels are reached. The lower peak loads observed again result from loss of stiffener in-plane capacity due to flexural action, the maximum web stresses seen from Figs E11 and E12 to be only 19% of yield for Lx/R = 50, and just 6% of yield for Lx/R = 60.

The loss of effectiveness with reducing stiffness can also be observed from the yield diagrams (Fig E47). For Lx/R = 30 and Lx/R = 50 the deflections remain small and the webs yield in compression. For Lx/R = 60, however, where greater deformations occur, the webs yield in tension. Although the ultimate strength is not significantly affected by this since the majority of the web depth is still fully

effective, its influence becomes more pronounced in the post-peak range where a faster rate of unloading is observed.

(b) b/t = 50; Lx/R = 30

The load-shortening relationship for this case is shown in Fig E10. Comparing this with the curve for b/t = 30; Lx/R = 30, a lower ultimate load level is reached and a sharper rate of unloading is seen in the post-peak range. These differences in behaviour can be explained by observing the direct stress curves and deflection curves in Figs E19 and E30 respectively. For an applied strain ratio less than unity both the overall and local panel deformations are small and the stress distribution is fairly uniform across the plate. Beyond this ratio, however, the panel deformations become suddenly large with a resulting loss of in-plane capacity. This effect can be seen clearly in Fig E19 for the strain ratio $\varepsilon a/\varepsilon o = 1.11$. Beyond the ultimate load, yielding across the plate width prevents stress redistribution and the rapid unloading observed in Fig E10 follows.

At the strain ratio $\varepsilon a/\varepsilon o = 1.01$, small depressions are observed in the stress curves in the vicinity of the webs (Fig E19). These are thought to result from high transverse moments which develop as the plate panels buckle, the required moment capacity being provided at the expense of in-plane capacity to maintain unit yield function at these nodes.

It is of further interest to note that the stress supported by the stiffeners (Fig E10) is almost identical to that for b/t = 30; Lx/R = 30. This indicates that the total reduction in compressive capacity can be attributed to panel buckling and, further, that the behaviour of the stiffeners is virtually unaffected by this change in plate behaviour.

The lower ultimate capacities obtained for Lx/R = 50 and

Lx/R = 60 can again be accounted for by flexural action as discussed in section 6.3.1.1(a). Detailed discussion is therefore omitted although load-shortening curves E11 and E12, direct stress curves E19 and yield diagrams E48 have been included for completeness, together with the deflection curves E31, for Lx/R = 60.

6.3.1.2 *Plates in Zone II*

As seen from Fig E16, all plates within this zone are stiffened by webs of low flexural rigidity. The smaller the web rigidity in relation to the plate stiffness, the less is the interaction between the plate and webs, and the closer the behaviour becomes to that of an unstiffened section of three times the basic panel slenderness. This change from three panel to single panel behaviour occurs gradually with increasing Lx/R, and plates close to the boundary of Zones I and II possess behavioural characteristics of both the stiffest and weakest sections. In order therefore to avoid unnecessary repetition, attention will be focussed on the highest Lx/R ratio considered, and points of significance will be noted for the remaining plates. Load-shortening curves, direct stress curves and yield diagrams have, however, been included for all cases to enable the reader to trace this change in behaviour visually. Deflection curves are also included for a selected number of cases.

(a) b/t = 30; Lx/R = 90

Referring to the load-shortening relationship (Fig E15) and comparing this with the relationship for b/t = 30; Lx/R = 30 (Fig E10), a less linear load path is observed and a much lower ultimate stress is sustained. The less linear load path results from the lower flexural stiffness involved, applied strain being absorbed more readily through out-of-plane deformation than through in-plane shortening.

The direct stress curves (Fig E18) indicate a fairly uniform distribution of stress across the plate for low applied strains. As the strain level increases, however, and deflections become more pronounced, effectiveness is lost at the centre of the plate and additional loading is then carried only by the stiffer edge sections. Edge strip loading continues whilst losses are incurred at the centre of the plate until the edges reach yield. At this stage there is no further capacity for stress redistribution and overall unloading follows.

The load-deflection curves shown in Fig E29 are again less linear than those given for b/t = 30; Lx/R = 30 (Fig E27), and the deflection profiles show little evidence of interaction between the plate and stiffeners. The deflections are observed to increase more rapidly following tensile yielding in the webs, and this is reflected in the load-shortening relationship where an obvious change of curvature is apparent. At the ultimate load level the mid-span sections of the webs have reached almost full yield in tension (Fig E47) and their effectiveness as load carrying members is therefore terminated.

For b/t = 30 and Lx/R = 70 and 80 behaviour is similar, although with the stiffer sections involved buckling occurs at a higher stress level. The load-shortening relationships for these plates are given in Figs E13 and E14, and the direct stress curves in Fig E18. Additionally, deflection curves are shown for the case Lx/R = 70 in Fig E28, and yield diagrams are shown in Fig E47.

(b) b/t = 50; Lx/R = 90

As discussed in section 6.3.1.2(a), a low stiffener rigidity gave rise to an overall mode of failure and the deflection curves (Fig E33) again show this to be the case. For this plate, however, the stress distribution is also influenced by local panel deformations, and this effect can be seen by comparing the direct stress curves for

Lx/R = 90 in Figs E18 and E20. In the latter case small depressions arising from local panel deformations are superimposed on the larger depression due to overall bending.

Referring to the load-shortening curve (Fig E15) and comparing this relationship with that described in 6.3.1.2(a) for b/t = 30; Lx/R = 90, an initially flatter unloading curve is observed. It was found here that the plating was fully elastic at the peak load (Fig E48), and continued to accept additional loading beyond the ultimate strain by redistributing stresses to stiffer sections of the plate. This, however, combined with an increased tension in the webs due to bending, led to a slight overall reduction in capacity, the two effects, one positive and one negative, combining to give the flat appearance at the peak load.

The remaining plates of slenderness b/t = 50 are not considered in detail here since their behaviour is covered by combinations of the local elasto-plastic response discussed in section 6.3.1.1(b) for Lx/R = 30, and the predominently overall mode of behaviour discussed above for Lx/R = 90. Load-shortening curves E13 and E14, direct stress curves E20, deflection curves E32 and yield diagrams E48, have however been included for completeness.

(c) Plates of slenderness b/t = 60 and b/t = 70

The remaining plates within this zone behave in a similar manner to that described in section 6.3.1.2(b) for b/t = 50, and no further discussion is therefore considered necessary. Reference is made however to the load-shortening curves E14 and E15, the direct stress curves E22 and E24, the deflection curves E36 and E40 and the yield diagrams E49 and E50.

6.3.1.3 *Plates in Zone III*

For all geometries within this zone, the theoretical critical panel buckling stress is less than the yield stress and deflections along the stiffeners are relatively small. The response to load is therefore similar to that obtained for three individual panels of aspect ratio 3:1, laterally restrained along their edges.

(a) SUBZONE A

The general mode of behaviour for plates in subzone A is described in detail for the case b/t = 80; Lx/R = 80, for which the load-deflection curves and deflection profiles are shown in Fig E46. As seen from these curves a change of mode occurs at the stress level $\sigma m/\sigma o = 0.44$, which is almost identical to the theoretical critical stress for simply supported panels ($\sigma m/\sigma o = 0.46$). The outer panels, being simply supported along one side and partially clamped at the stiffener, have a lower critical stress than the middle panel which is partially clamped along both sides. The outer panels thus control the mode of deformation and the central panel deflects in sympathy with them. The standard three half-wave form can be seen in section 3-3 and the sympathetic wave form in section 4-4, of Fig E46.

Beyond the buckling strain the stress distribution at mid-span becomes less uniform (Fig E26), and with this an obvious change of slope results in the load-shortening curve (Fig E14). Additional applied loading is then supported by the plating at the edges and in the vicinity of the webs until, at the stress ratio $\sigma m/\sigma o = 0.546$, loss of capacity in the panels overrides the gains at these locations. Overall unloading then commences whilst the plating is still predominantly elastic (Fig E51).

The effect of the mode change is also felt by the stiffeners and this can be seen from Fig E14 where, at the buckling stress, a

reduction in the resultant tensile force is observed. As the panels buckle the out-of-plane deformations on the stiffeners at mid-span are retarded, and their capacity for resisting direct stress is thus enhanced.

The remaining plates within subzone A behave in a similar manner, although with decreasing b/t the mode change occurs at a higher average stress level. The least slender of these cases (b/t = 60; Lx/R = 70) starts to buckle at the peak load. This would be expected since the ultimate load occurs close to the boundary of zones II and III, the dividing line between an overall mode of failure and a panel mode of failure. Load-shortening curves E13 to E15, direct stress curves E22, E24 and E26, and yield diagrams E49 to E51 are included for each of these three cases, and deflection curves E35 and E39 are shown for b/t = 60 and b/t = 70.

The final point of interest to be noted for subzone A is the apparent small increase in ultimate strength which occurs across the boundary of zones II and III in Fig E16, on the curves for Lx/R = 80 and Lx/R = 90. To the left of the boundary the webs yield in tension and an overall mode of failure results, whereas to the right of the boundary higher panel slendernesses are involved and local panel buckling occurs in advance of yielding. With this change in mode form the stiffener deformations are retarded, and the resulting delay in tensile yielding gives rise to the observed increase in ultimate strength.

(b) SUBZONE B

The behaviour of plates in subzone B is described in detail for the case b/t = 80; Lx/R = 60, for which the load-deflection curves are shown in Fig E44. At the stress level $\sigma m/\sigma o = 0.43$ a stiffening effect was observed at the plate corners, and at $\sigma m/\sigma o = 0.47$ snap-through occurred at these locations. In response, a sympathetic stiffening was

observed at the centre of the plate (curve C) whilst in the outer panels at mid-span and in the central panel close to the loaded ends, deflections grew more rapidly in the positive z-direction.

This mode of deformation is the reverse of that seen in subzone A and this has been shown to result from the destabilising effect of shear forces along the loaded edges. To prove this point the same plate was re-analysed with the shear stress component, Nxy, set at zero on the first line of nodes inside the boundary. The resulting out-of-plane deformations are compared with those from the original analysis in Fig E45, where it is observed that the mode reverts to the standard form discussed in section 6.3.1.3(a) when shear restraint is ignored.

The load-shortening curves are shown in Fig E12 and the direct stress at mid-span in Fig E25. The latter curves show the drop in strength which occurs with local panel buckling and this is reflected in the load-shortening curve where, at the buckling stress, a change of slope is observed. The effect of the mode change on the stiffeners is also evident from Fig E12, where the compressive stress in the webs is seen to increase after buckling occurs in the plate.

For b/t = 80 and Lx/R = 50 and 70, behaviour is similar to that described above and discussion here is therefore omitted. Reference can be made however to the load-shortening curves E11 and E13, the direct stress curves E25 and E26, the deflection curves E43 for Lx/R = 50 and the yield diagrams E51.

Load-shortening curves for plates of slenderness b/t = 60 are shown in Figs E10 to E12 and the direct stress curves are shown in Fig E21. In these cases buckling occurs close to the peak load, and as seen from Fig E21 rapid unloading then follows. The distributions of direct stress plotted for strains beyond the ultimate are likely to be inaccurate owing to poor convergence and overstressing at some plastic

nodes. They have however been included to explain the sudden drop in capacity which occurs in the load-shortening curves beyond the peak stress. Deflection curves are shown for Lx/R = 50 in Fig E34,where the sympathetic stiffening which occurs at mid-span as the corners snap through can be seen in curve C. In this case, however, the mode described previously is not fully developed at the ultimate stress owing to the lower panel slendernesses involved.

For plates of slenderness b/t = 70, the relevent load-shortening curves can be found in Figs E11 to E13 and the direct stress curves in E23 and E24. Deflection curves (Fig E38) are again plotted for the case Lx/R = 50,where behaviour is seen to be similar to the case b/t = 60; Lx/R = 50 considered above. The chief difference in these curves is the magnitude of deformations, buckling occurring at a lower average stress level for b/t = 70 than for b/t = 60.

For all plate panels within subzone B, the analyses were terminated soon after the peak load owing to poor convergence and drift from the yield surface. The former problem is thought to be associated with the superimposition of two mode forms. If snap-through occurs in subzone A form in the presence of an existing shear mode buckle, a complex wave pattern will result and a much finer mesh spacing will be required.

(c) SUBZONE C

The final mode of deformation to be encountered applies to plate geometries in subzone C, for which the load-shortening curves are shown in Fig E10. The behaviour will be discussed in detail for b/t = 80; Lx/R = 30 and,for completeness, direct stress curves, deflection curves and yield diagrams are shown for b/t = 70; Lx/R = 30 in Figs E23, E37 and E50 respectively.

As observed from Fig E41, the behaviour of this plate is initially similar to that described previously for geometries in subzone B. As the shear mode develops, however, the sympathetic buckle seen previously at the centre of the plate does not follow and instead an additional upward buckle forms in the central panel close to the loaded ends. In response, all three panels at mid-span suffer greater positive out-of-plane deformations, and this can be seen from the load-deflection curves A and C in Fig E41. To identify the reason for a mode change between subzones B and C, the same plate was re-analysed with the interactive couple FT_w set at zero for the full length of the stiffener. In the absence of torsional restraint the deformations take the form shown in Fig E42, and this will be recognized as the mode form obtained for plates in subzone B. The effect of the torsional restraint is to prevent sympathetic rotations across the webs and this leads to the change of mode observed.

The load-shortening curve (Fig E10) and the direct stress curves (Fig E25) indicate a fairly linear stress-strain response prior to buckling. As the mode form changes, however, and the plate panels lose strength a less linear response is observed, and the ultimate load is reached as yielding of the plate occurs in the vicinity of the stiffeners and along the boundaries (Fig E51).

Finally, it is of interest to note the parallel nature of curves within zone III (Fig E16), this suggesting that the disposition of the buckles has a negligible influence on the ultimate load achieved.

6.3.2 A Study of the Effect of Initial Deformation

As a small contribution towards the understanding of the effect of initial deformation on plate behaviour, panels of slenderness $b/t = 30$ and $Lx/R = 30$ to 80 have been re-analysed for two additional imperfection levels. The overall sinusoidal bow used in the main study is retained and, apart

from the magnitude of this parameter, all other variables remain unaltered.

In a realistic structure, dishing of the panels between the ribs may be present, and although this type of deformation has not been considered, it is thought that its presence would not significantly affect the ultimate strength. From the main study it was found that panels of these dimensions failed by squashing or by buckling in an overall sense, and these modes of failure would not be sympathetic to a local mode of deformation.

The peak loads obtained for each level of imperfection considered are summarised graphically in Fig E52. It is apparent from these curves that sensitivity to imperfections increases with Lx/R; a 4 mm increase in the initial bow giving rise to a 5% reduction in capacity for Lx/R = 30 and a 25% reduction for Lx/R = 80. The behaviour of these plates will now be discussed for the two extreme cases.

(a) b/t = 30; Lx/R = 30

Load-shortening curves for the stiffeners and for the total cross-section are shown in Fig E53, and the distributions of direct stress across the plate are shown in Fig E55. Over the range of deformation considered the load sustained by the plating remains virtually constant, and at the peak load almost full squash conditions are achieved (Fig E55). The overall ultimate strength is however influenced by the initial bow and, as observed from Fig E53, this results from a difference in compressive strengths afforded by the stiffeners. In an eccentrically loaded compression panel out-of-plane deformations will result from bending action, and the larger the eccentricity of applied load the greater will be this component. For wc = 5 mm, therefore, a greater moment of resistance must be provided at mid-span to balance the applied moment than for wc = 1 mm. This dictates an increased tensile component in the stiffeners

and hence a reduction in compressive capacity.

(b) b/t = 30; Lx/R = 80

Load-shortening curves for these plates are shown in Fig E54 and the distributions of direct stress at mid-span in Fig E56.

For the lowest level of deformation (wc = 1 mm) the plating is seen to yield in advance of the stiffeners, and at the peak load it sustains a stress level comparable with that for b/t = 30; Lx/R = 30. In contrast, for the higher levels of deformation, yielding occurs first in the stiffeners owing to the higher tensile stresses which develop under the greater bending action (Fig E54). For wc = 3 mm, the plating is still able to develop almost full yield capacity since the stiffeners do not yield until close to the peak load. Beyond this stress, however, unloading proceeds rapidly as deflections grow large in the elasto-plastic range. For wc = 5 mm, tensile yielding in the webs occurs far in advance of plate yielding and deflections grow large prior to the peak load. The plating is then used to provide some of the flexural resistance required and the loss of in-plane capacity seen in Fig E56 follows.

The summary of peak stresses given in Fig E52 shows a fairly linear reduction in capacity with Lx/R for wc = 1 mm, and the three curves remain quite parallel between Lx/R = 30 and Lx/R = 60. None of these plates were influenced by tensile yielding in the stiffeners, and providing this effect can be eliminated, a less severe reduction in capacity will result than seen currently for Lx/R = 80 on the curves wc = 3 mm and wc = 5 mm. This can be realised in practice by adopting a material of higher yield stress for the webs than for the plate, and this is investigated in the following section.

6.3.3 A Study on the Use of Hybrid Plates

The advantage to be gained from the use of hybrid plates was investigated for geometries b/t = 60 and Lx/R = 30 to 90. All parameters adopted for these plates in the main study were retained with the exception of the stiffener yield stress, which was set at 1000 N/mm² to ensure elastic action throughout.

The peak loads obtained are summarised graphically in Fig E57 and the load-shortening curves are shown in Fig E58 where, in both cases, the solutions are compared with those obtained in the main study.

For Lx/R = 30 compressive yielding in the webs was suppressed and a slight increase in the ultimate strength was thus achieved. This gave rise to a more linear relationship between the ultimate strength and the stiffener slenderness, as seen from Fig E57.

Between Lx/R = 40 and Lx/R = 60 yielding of the stiffeners did not occur in the main study, and the two sets of solutions are therefore identical.

For Lx/R = 70 to Lx/R = 90 tensile yielding in the stiffeners was suppressed and higher ultimate capacities were therefore reached. The summary of peak stresses for hybrid plates is almost linear, and from this it can be concluded that in the absence of web yielding zone II shown in Fig E16 would not exist. For Lx/R = 70 tensile yielding occurred close to the ultimate load and the increase in strength achieved by using the hybrid plate was therefore quite small. For Lx/R = 80 and Lx/R = 90, however, much greater increases in capacity were achieved.

Load-deflection curves and distributions of direct stress at mid-span are shown for Lx/R = 90 in Fig E59, where comparisons are made with the results obtained in the main study. From the latter curves it is evident that in the absence of tensile yielding the plating can sustain a higher compressive stress for a given applied strain, and in the post-peak range the rate of unloading is much more gradual (Fig E58).

Finally, the load-deflection curves for the hybrid plate indicate a change in the direction of deformation at point A close to the peak load. This is further evidence of the elimination of zone II, this mode of deformation being characteristic of plates within zone III, subzone A.

6.3.4 A Plate Under Combined In-Plane and Lateral Loading

The final study investigates the behaviour of plated structures under the combined action of lateral and in-plane loading. The geometrical properties selected are as given in the main study for $b/t = 60$; $Lx/R = 30$, and a central deformation of 1 mm was adopted.

The behaviour of this plate was first investigated under the action of in-plane load alone, and the load-shortening curves and load-deflection curves obtained are shown in Figs E60 and E61 respectively. Under this type of loading the plate was found to buckle in the mode form associated with plates in subzone C, and yielding occurred at the centre and at the corners of the plate (Fig E60).

The same plate was then subjected to three different levels of lateral load followed by in-plane loading to failure, and again the relevant load-shortening and load-deflection curves are shown in Figs E60 and E61. In each case the deflections are seen to increase linearly under lateral load, and under in-plane load each plate deflects at approximately the same rate. The mode of deformation is however different from that observed for $q = 0$. Referring to Fig E61, the panel deflections at mid-span are seen to increase at a reducing rate with successive load increments and close to the peak load the deflections start to reduce. This mode form is the reverse of that observed above for the case of zero lateral load and is thought to result as the shear mode buckle is suppressed by the lateral pressure.

For the pressure level q = 105 KN/m² yielding has occurred in the plating along the majority of the stiffener length. This reduces the clamping action provided by the stiffeners, and results in the sudden small increase in deformation seen in Fig E61 at the stress level $\sigma m/\sigma o = 0.6$

CHAPTER 7

CONCLUSIONS AND FUTURE WORK

7.1 CONCLUSIONS

7.1.1 The Mathematical Formulation and Solution Procedure

A formulation has been presented for the analysis of plates reinforced in one direction by stiffeners of tee, angle or rectangular cross-section. Both material and geometric non-linearities were considered and account was taken of residual stress and initial deformation.

The equations generated are identical to those for isotropic plates subjected at the stiffener locations to a set of body forces. Interaction between adjacent elements is automatically accounted for and local buckling of the plate panels can be predicted. In this respect the formulation surpasses the alternative beam-column and orthotropic approaches, where interaction is ignored and local effects can only be treated approximately.

The governing equations were expressed in finite difference form and were solved numerically by the Dynamic Relaxation procedure. An interlacing mesh system was adopted to obtain maximum accuracy for a given mesh spacing.

In the solution procedure the equilibrium equations were expressed in terms of stress resultants rather than displacements. This approach is ideally suited to both the elastic and elasto-plastic stress ranges, since to extend the analysis into the non-linear range simply requires a re-definition of the stress resultant expressions.

The stiffening members can be located along any main mesh line in the system with the exception of those at the plate edges. If local effects are to be detected, however, at least four spacings should

be provided between adjacent stiffeners.

In general the degree of convergence achieved was satisfactory and it was possible to establish both the ultimate load level and the post-ultimate load behaviour. Convergence problems did arise however for plates of intermediate slenderness where local buckling action interacted with yielding.

Prior to the application of each load increment current stress resultants were modified to correct for drift from the yield surface. No additional relaxation cycles were carried out after modification since the resulting lack of equilibrium was generally small. In cases where buckling occurred in the non-linear material range, however, the magnitude of the yield function could not be controlled and the analyses were therefore terminated close to the ultimate load.

Each plastic node was checked before the application of a new load increment to determine whether unloading from the yield surface had occurred. The method adopted was not totally successful and further investigations are therefore considered necessary.

Suitable damping factors were established for each of the analyses by trial and error. Their magnitudes were found to be influenced significantly by the mesh spacing but only slightly by changes in geometry.

7.1.2 Test Results and Theoretical Predictions

7.1.2.1 *Theoretical Predictions*

The three stiffened plate models have each been analysed for two conditions these being residual stress free and a level of stress approximating to the measured values. In both cases a zero stress was assumed in the stiffener webs and flanges.

The adopted initial deformation profiles were similar in form

to the measured values but were calculated from the combination of two sine wave relationships. The maximum discrepancy between measured and calculated values occurred close to the model edges.

In developing boundary conditions for the analysis, an attempt was made to mirror the real behaviour. These conditions were not however totally satisfactory and further work is therefore considered necessary.

For model SP1 the addition of residual stress was found to lower the ultimate strength. This resulted as premature yielding occurred in the panels under the higher compressive stress.

In contrast, for models SP2 and SP3 an increased ultimate strength was achieved. In these cases compressive yielding in the panels coincided with yielding along the stiffeners, and close to optimum efficiency was therefore achieved.

In all three cases the addition of residual stress was found to change the collapse mode from seven alternating half-waves along the span to nine. This is thought to result from delayed yielding at the stiffener positions owing to the presence of tensile residual stress.

Under lateral loading a linear load-deflection response was observed for all models, the deflections being greatest for model SP1 owing to the lighter stiffening involved.

For all three models a rapid rate of unloading was observed at the ultimate load as yielding interacted with buckling. It was therefore not possible to predict the unloading characteristics of these plates with accuracy.

7.1.2.2 *Test Results and Comparisons with Theory*

The testing programme was in general very successful and until the model started to fail, the rig responded according to plan. Some

damage did however occur at failure and before models SP1 and SP2 can be tested, some minor modifications are necessary. Proposals for this are given in Section 7.2.

Strains recorded in the horizontal and vertical load cells were almost symmetrical and loss of load through frictional resistance was small. There was however a slight variation of strain across the model ends owing to a misalignment of the parallel arm mechanism. During in-plane loading the vertical load cells were observed to slant as model shortening and stretching of the rig took place. There was however no significant loss of lateral restraint.

The primary cause for concern in the test was the positioning of the horizontal load cells,where a slight eccentricity of load relative to the centroid would result in a bending moment being applied to the model ends. This position is almost impossible to determine in a section which is initially deformed,and errors introduced here have probably affected the correlation between theoretical and experimental results.

Test results obtained for model SP3 have been compared with theoretical predictions and in general the degree of correlation is good. The collapse loads agree to within 6% for the case of zero residual stress and 3% for the case of applied residual stress,and the load-shortening curves are in both cases fairly linear.

Although the load-deflection response obtained theoretically is of a similar form to that seen in the test, the magnitude of deformation is overestimated. This is thought to arise chiefly from inaccuracies in the flexural boundary constraint at the loaded end and from the coarsness of the finite difference mesh. The geometry and positioning of the horizontal load cells may also have affected the result.

At failure the test model had yielded at a number of locations and a five half-wave buckling mode appeared to develop along the length with sympathetic rotations occurring across the stiffeners. This wave form was not observed theoretically although local panel buckling did occur.

With the exception of areas close to the plate boundaries, good agreement was achieved between the theoretical and experimental stress levels in the plating. For the stiffeners,however, correlation was less satisfactory owing to the overestimation of out-of-plane deformations.

7.1.3 Numerical Studies

Results from the computer program have been compared with two existing analytical solutions. These were obtained from a similar formulation and,in general, satisfactory correlation was achieved. The application of a tangential restraint along the loaded edge of a panel was found to reduce its collapse strength.

The main parametric study undertaken investigated the influence of geometrical properties on the serviceability and collapse behaviour of stiffened plating. A wide range of slenderness ratios were considered and loading was applied in the plane of the plate. Stiffeners of rectangular cross-section were employed throughout.

From the study three basic forms of collapse behaviour were identified. In zone I failure occurred by squashing of the cross-section before extensive buckling occurred. In zone II an overall mode of failure was initiated by tensile yielding in the stiffeners, and in zone III failure was triggered by local buckling of the plate panels. The arrangement of the local buckles was found to be influenced by the torsional stiffness of the ribs and by the shear

restraint applied along the loaded edges. The collapse strength did not however appear to be influenced by this change in arrangement.

To investigate the effect of initial deformation, a small number of plates from the main study were re-analysed for two additional imperfection levels. Imperfection sensitivity was found to be most significant for plates with light stiffening where failure was initiated by tensile yielding. In such cases the use of hybrid plates was shown to be beneficial.

Finally, one plate from the main study was re-analysed under the combined action of lateral and in-plane loading. Three different levels of lateral load were applied followed by the application of in-plane load to failure. It was established that an initial application of lateral load can lead to a significant reduction in compressive capacity, and that the mode of deformation resulting from compressive forces alone can be altered by the addition of lateral pressure.

7.2 FUTURE WORK

1. The formulation should be extended to include biaxial stiffening. This would enable the degree of interaction between two or more adjacent uniaxially stiffened panels to be evaluated.

2. Edge stiffening should be included at the plate boundaries to enable a more exact analysis of the stiffened plate models.

3. Initial distortion of the stiffener webs and flanges could be included by re-defining expressions (1) to (4) in Chapter 2. Both a local mode of deformation and an overall bow should be incorporated.

4. The present formulation takes no account of failure caused by tripping of the stiffeners. Flexural failures towards the plating can

only therefore be predicted with accuracy when stocky stiffeners are involved,and in compression panels stiffener dimensions must be limited to prevent this form of instability. Detailed work is therefore required to investigate this form of collapse mode.

5. It would be beneficial to re-write the computer program in terms of graded meshes. This would enable local effects in the vicinity of the stiffeners to be determined with greater accuracy. Further, it would provide the facility to locate a stiffener at any position across the plate width.

6. Detailed work is required to investigate the problem of numerical instability which was encountered in a number of the analyses. Elimination of this problem would enable more solutions to be extended into the post-ultimate range where a knowledge of the carrying capacity is important when considering the collapse behaviour of a total structure.

7. The existing computer program should be used to investigate a wider range of plate parameters. Consideration should be given to loading types, boundary constraints, aspects ratio, residual stress, initial deformation, material properties and stiffener type. In particular, more emphasis should be placed on the analysis of plates reinforced by tee and angle section stiffeners.

8. It would be interesting to compare solutions obtained from the present formulation with alternative calculations based on beam-column theory and orthotropic theory. This study would indicate the range of plate parameters for which the alternative,less time consuming methods,could be employed with confidence.

9. For a wide panel where large numbers of stiffeners are involved, a full plate analysis would be expensive since a large number of mesh divisions are required. It would therefore be interesting to investigate the minimum number of stiffeners and associated panel widths which would accurately predict the wide panel result.

10. More experimental work is required to validate the theoretical predictions. Greater emphasis should be placed on creating physical boundary conditions which can be mirrored exactly in the analysis,and the problem associated with the location of horizontal load cells should be investigated more fully.

11. For future use of the testing rig the following modifications should be carried out:

(i) The rollers on the underside of the loading beam should be replaced by members of a higher load-bearing capacity. Solid steel cylinders located between the beam and the base plates would fulfil this requirement.

(ii) The bearing pads on the model end plates should be fixed more permanently into position to prevent the sliding action which occurred as model SP3 reached failure.

12. Finally, theoretical results should be compared with currently available design recommendations and new criteria established where necessary.

REFERENCES

1. FOK, W.C., RHODES, J., WALKER, A.C. "Local buckling of outstands in stiffened plates". Aeronautical Quarterly, Vol. 27, Pt. 4, Nov. 1976, pp.277-291.
2. FOK, W.C., WALKER, A.C., RHODES, J. "Buckling of locally imperfect stiffeners in plates". Journal of Eng. Mech. Div., Proc. ASCE, Vol. 103, No. EM5, Oct. 1977, pp. 895-911.
3. DUBAS, P. "Plated structures with closed-section stiffeners". Steel plated structures; an international symposium. Crosby Lockwood Staples, London, 1977.
4. TVERGAARD, V. "Imperfection sensitivity of a wide integrally stiffened panel under compression". Int. J. Solids Structures, Vol. 9, 1973, pp. 177-192.
5. TVERGAARD, V. "Influence of post-buckling behaviour on optimum design of stiffened panels". Int. J. Solids Structures, Vol. 9, 1973, pp. 1519-1533.
6. DOWLING, P.J. "Strength of steel box-girder bridges". Journal of Struct. Div., Proc. ASCE, Vol. 101, No. ST9, Sept. 1975, pp. 1929-1946.
7. MURRAY, N.W. "Buckling of stiffened panels loaded axially and in bending". The Structural Engineer, Vol. 51, No. 8, Aug. 1973, pp. 285-301.
8. HORNE, M.R., NARAYANAN, R. "The strength of straightened welded steel stiffened plates". The Structural Engineer, Vol. 54, No. 11, Nov. 1976, pp. 437-443.
9. HORNE, M.R., NARAYANAN, R. "Ultimate strength of stiffened panels under uniaxial compression". Steel plated structures; an international symposium. Crosby Lockwood Staples, London, 1977.
10. EGGWERTZ, S. "Effect of initial imperfections on the buckling strength of plate structures". SSF project 5619, The Swedish Ship Research Foundation, 1977.

11. MOXHAM, K.E. "Theoretical prediction of the strength of welded steel plates in compression". University of Cambridge, Report No. CUED/C-Struct./TR2, 1971.

12. HASEGAWA, A., OTA, K., NISHINO, F. "Buckling strength of multiple stiffened plates". Procs. National Struct. Eng. Conf., ASCE Struct. Div. Special Conf. on Methods of Structural Analysis, Vol. 2, 1976, pp. 937-956.

13. FUKUMOTO, Y., USAMI, T., YAMAGUCHI, K. "Inelastic buckling strength of stiffened plates in compression". IABSE Periodica, 3/1977, August 1977.

14. BLEICH, F. "Buckling strength of metal structures". McGraw-Hill Book Co., New York, 1952.

15. TIMOSHENKO, S., WAINOWSKY-KRIEGER, S. "Theory of plates and shells". McGraw-Hill Book Co., New York, 1959.

16. TIMOSHENKO, S., GERE, J. "Theory of elastic stability". McGraw-Hill Book Co., New York, 1961.

17. DJAHANI, P. "Large-deflection elasto-plastic analysis of discretely stiffened plates". PhD Thesis, University of London (Imperial College), 1977.

18. MANSOUR, A.E. "Gross panel strength under combined loading". Mansour Engineering Inc., Berkeley, California, Project SR-225, Final Report.

19. SMITH, C.S. "Compressive strength of welded ship grillages". Trans. RINA, Vol. 117 (Spring Meeting), 1975.

20. BARES, R., MASSONNET, C. "Analysis of beam grids and orthotropic plates". Crosby Lockwood and Sons Ltd., London, 1968.

21. DOWLING, P.J. "The behaviour of stiffened plate bridge decks under wheel loading". PhD Thesis, University of London (Imperial College), 1968.

22. SCHADE, H.A. "The orthogonally stiffened plate under uniform lateral load". ASME Transactions, Vol. 62, Dec. 1940, pp. A143-A146.

23. FALCONER, B.H., CHAPMAN, J.C. "Compressive buckling of stiffened plates". The Engineer, Vol. 195, Nos 5080 and 5081, June 1953, pp 789-791 and 822-825.

24. HOPPMANN, W.H. "Bending of orthogonally stiffened plates". Journal of Applied Mechanics, Vol. 22, June 1955, pp. 267-271.

25. SOPER, W.G. "Large-deflection of stiffened plates". Journal of Applied Mechanics, Vol. 25, Dec. 1958, pp. 444-448.

26. BASU, A.K. "The theory of orthotropic plates under lateral pressure and its application to corrugated plates". PhD Thesis, University of London (Imperial College), 1964.

27. BASU, A.K., CHAPMAN, J.C. "Large-deflection behaviour of transversely loaded rectangular orthotropic plates". Proc. Instn. Civ. Engrs., Vol. 35, Pt. 2, Sept. 1966, pp. 79-110.

28. AALAMI, B. "Non-linear behaviour of rectangular orthotropic plates under transverse and in-plane loads". PhD Thesis, University of London (Imperial College), 1967.

29. AALAMI, B., CHAPMAN, J.C. "Large-deflection behaviour of ship plate panels under normal pressure and in-plane loading". Trans. RINA, Vol. 114, March 1972, pp. 155-181.

30. WILLIAMS, D.G., CHAPMAN, J.C. "Tests on a one-eighth scale model of the double bottom structure". Trans. RINA, Vol. 116, No. 4, Nov. 1974, pp 329-345.

31. NISHINO, F., PAMA, R.P., LEE, S. "Orthotropic plates with eccentric stiffeners". IABSE Periodica, Vol. 34, No. II, 1974, pp 117-129.

32. KAGAN, H.A., KUBO, G.G. "Elasto-plastic analysis of reinforced plates". Journal of Struct. Div., Proc. ASCE, Vol. 94, No. ST4, April 1968, pp. 943-958.

33. MASSONNET, C., MAQUOI, R. "New theory and tests on the ultimate strength of stiffened box girders". Steel Box-Grider Bridges. Proceedings of the International Conference. Instn. Civ. Engrs., 13-14 Feb. 1973, pp 131-143.

34. OSTAPENKO, A., LEE, T. "Tests on longitudinally stiffened plate panels subjected to lateral and axial loading". Lehigh University Pennsylvania, Fritz Eng. Lab. Report, No. 248.4, Aug. 1960.

35. KONDO, J., OSTAPENKO, A. "Tests on longitudinally stiffened plate panels with fixed ends". Lehigh University Pennsylvania, Fritz Eng. Lab. Report, No. 248.12, July 1964.

36. KONDO, J. "Ultimate strength of longitudinally stiffened plate panels subjected to combined axial and lateral loading". Lehigh University Pennsylvania, Fritz Eng. Lab. Report, No. 248.13, Aug. 1965.

37. VOJTA, J.F., OSTAPENKO, A. "Ultimate strength design of longitudinally stiffened plate panels with large b/t". Lehigh University Pennsylvania, Fritz Eng. Lab. Report, No. 248.18, Aug. 1967.

38. VOJTA, J.F., OSTAPENKO, A. "Ultimate strength design curves for longitudinally stiffened plate panels with large b/t". Lehigh University Pennsylvania, Fritz Eng. Lab. Report, No. 248.19, Aug. 1967.

39. RUTLEDGE, D.R., OSTAPENKO, A. "Ultimate strength of longitudinally stiffened plate panels (large and small b/t, general material properties)". Lehigh University Pennsylvania, Fritz Eng. Lab. Report, No. 248.24, Sept. 1968.

40. MOOLANI, F.M. "Ultimate load behaviour of steel box-girder stiffened compression flanges". PhD Thesis, University of London (Imperial College), 1976.

41. MOOLANI, F.M., DOWLING, P.J. "Ultimate load behaviour of stiffened plates in compression". Steel plated structures; an international symposium. Crosby Lockwood Staples, London, 1977.

42. FRIEZE, P.A., DOWLING, P.J., HOBBS, R.E. "Parametric study on plates in compression". Engineering Structures Laboratories, Civ. Eng. Dept., Imperial College, London. CESLIC Report BG39, Jan. 1975.

43. CRISFIELD, M.A. "Full-range analysis of steel plates and stiffened plating under uniaxial compression". Proc. Instn. Civ. Engrs., Vol. 59, Pt. 2, Dec. 1975, pp 595-624.

44. FUKUMOTO, Y., USAMI, T., OKAMOTO, Y. "Ultimate compressive strength of stiffened plates". ASCE Speciality Conference on Metal Bridges, St. Louis, Nov. 12-13, 1974, pp. 201-230.

45. ROSSOW, M.P., IBRAHIMKHAIL, A.K. "Constraint method analysis of stiffened plates". Comput. Struct., Vol. 8, No.1, Feb. 1978, pp. 51-60.

46. WEGMULLER, A.W. "Full range analysis of eccentrically stiffened plates". Journal of Struct. Div., Proc. ASCE, Vol. 100, No. ST1, Jan. 1974, pp. 143-159.

47. DOWLING, P.J. "The behaviour of orthotropic steel deck bridges". Developments in bridge design and construction. Proceedings of the International Conference at University College Cardiff, 1971. Crosby Lockwood, London, 1972.

48. TVERGAARD,V., NEEDLEMAN, A. "Buckling of eccentrically stiffened elastic-plastic panels on two simple supports or multiply supported". Int. J. Solids Structures, Vol. 11, 1975, pp. 647-663.

49. SØREIDE, T.H., BERGAN, P.G., MOAN, T. "Ultimate collapse behaviour of stiffened plates using alternative finite element formulations". Steel plated structures; an international symposium. Crosby Lockwood Staples, London, 1977.

50. SØREIDE, T.H., MOAN, T. "Non-linear material and geometric behaviour of stiffened plates". The Norwegian Institute of Technology, The University of Trondheim, Report No SK/M31, Division of Ship Structures, April 1975.

51. CRISFIELD, M.A. "Large-deflection elasto-plastic buckling analysis of eccentrically stiffened plates using finite elements". Department of the Environment, TRRL Report No. 725, Crowthorne, Berkshire, 1976.

52. DEAN, D.L., OMID'VARAN, C. "Analysis of ribbed plates". Journal of Struct. Div., Proc. ASCE, Vol. 95, No. ST3, March 1969, pp. 411-440.

53. WAH, T. "Buckling of longitudinally stiffened plates". Aeronautical Quarterly, Vol. 18, Feb. 1967, pp. 85-99.

54. AVENT, R., BOUNIN, D. "Discrete field stability analysis of ribbed plates". Journal of Struct. Div., Proc. ASCE, Vol. 102, No. ST9, Sept. 1976, pp. 1917-1938.

55. HOVICHITR, I., KARASUDHI, P., NISHINO, F., LEE, S. "A rational analysis of plates with eccentric stiffeners". IABSE Periodica, 4/1977, Nov. 1977.

56. DJAHANI, P. "Large deflection elastic analysis of discretely stiffened plates subject to transverse and/or in-plane loading". MSc Thesis, University of London (Imperial College), 1974.

57. BASU, A.K., DJAHANI, P., DOWLING, P.J. "Elastic post-buckling behaviour of discretely stiffened plates". International Colloquium on Stability of Steel Structures, Leige, 13-15 April 1977.

58. LAMAS, A.R.G. "Influence of shear lag on the collapse of wide-flange girders". PhD Thesis, University of London (Imperial College), 1979.

59. LAMAS, A.R.G., DOWLING, P.J. "Effect of shear lag on the inelastic buckling behaviour of thin-walled structures". Proceedings of the International Conference on Thin-Walled Structures, University of Strathclyde, Glasgow, April 1979.

60. CHATTERJEE, S., DOWLING, P.J. "Design of stiffened compression flanges in steel box girders". ECCS Task Group 8/3: Plate Buckling, Imperial College, London, Oct. 1975.

61. HORNE, M.R., NARAYANAN, R. "An approximate method for the design of stiffened steel compression panels". Proc. Instn. Civ. Engrs., Vol.59, Pt. 2, Sept. 1975, pp. 501-514.

62. HORNE, M.R., NARAYANAN, R. "Strength of axially loaded stiffened panels". Simon Engineering Laboratories, University of Manchester, August 1974.

63. MURRAY, N.W. "Analysis and design of stiffened plates for collapse load". The Structural Engineer, Vol. 53, No. 3, March 1975, pp. 153-158.

64. CHATTERJEE, S., DOWLING, P.J. "The design of box girder compression flanges". Steel plated structures; an international symposium. Crosby Lockwood Staples, London, 1977.

65. CHATTERJEE, S., DOWLING, P.J. "Proposed design rules for longitudinal stiffeners in compression flanges of box girders". Engineering Structures Laboratories, Civ. Eng. Dept., Imperial College, London, CESLIC Report BG40, May 1975.

66. DWIGHT, J.B. "Stiffened compression panels". Journal of Australian Inst. of Steel Construction, Vol. 9, No. 3, 1975.

67. DWIGHT, J.B., LITTLE, G.H. "Stiffened steel compression flanges - a simpler approach". The Structural Engineer, Vol. 54, No. 12, Dec. 1976, pp. 501-509.

68. CARLSEN, C.A. "Simplified collapse analysis of stiffened plates". Norwegian Maritime Research, Vol. 5, No. 4, 1977, pp. 20-36.

69. CRISFIELD, M.A. "Some approximations in the non-linear analysis of rectangular plates using finite elements". Department of the Envrionment, TRRL Supplementary Report 51UC, Crowthorne, Berkshire, 1974.

70. CRISFIELD, M.A. "Large-deflection elasto-plastic buckling analysis of plates using finite elements". Department of the Environment, TRRL Report LR593, Crowthorne, Berkshire, 1973.

71. OTTER, J.R.H., CASSELL, A.C., HOBBS, R.E. "Dynamic Relaxation". Proc. Instn. Civ. Engrs., Vol. 35, 1966, pp. 633-656.

72. RUSHTON, K.R. "Dynamic-relaxation solutions of elastic plate problems". Journal of Strain Analysis, Vol. 3, No. 1, 1968, pp. 23-32.

73. CASSELL, A.C., KINSEY, P.J., SEFTON, D.J. "Cylindrical shell analysis by dynamic relaxation". Proc. Instn. Civ. Engrs., Vol. 39, Jan. 1968, pp. 75-84.

74. RUSHTON, K.R. "Dynamic-relaxation solution for the large deflection of plates with specified boundary stresses". Journal of Strain Analysis, Vol. 4, No. 2, 1969, pp. 75-80.

75. CASSELL, A.C. "Shells of revolution under arbitrary loading and the use of fictitious densities in dynamic relaxation". Proc. Instn. Civ. Engrs., Vol. 45, Jan.1970, pp 65-78.

76. CASSELL, A.C., HOBBS, R.E. "Dynamic relaxation". High Speed Computing of Elastic Structures, Proceedings of the Symposium of International Union of Theoretical and Applied Mechanics, Leige, August 23-28, 1970.

77. FRIEZE, P.A. "Ultimate load behaviour of steel box girders and their components". PhD Thesis, University of London (Imperial College), 1975.

78. HARDING, J.E. "Bolted spliced panels and stress redistribution in box girder components up to collapse". PhD Thesis, University of London (Imperial College), 1975.

79. HARDING, J.E., HOBBS, R.E., NEAL, B.G. "The elasto-plastic analysis of imperfect square plates under in-plane loading". Proc. Instn. Civ. Engrs., Vol. 63, Pt. 2, March 1977, pp. 137-158.

80. FRIEZE, P.A., DOWLING, P.J. "Interactive buckling analysis of box sections using dynamic relaxation". Computers and Structures, Vol. 9, 1978, pp. 431-439.

81. FRIEZE, P.A., HOBBS, R.E., DOWLING, P.J. "Application of dynamic relaxation to the large deflection elasto-plastic analysis of plates". Computers and Structures, Vol. 8, April 1978, pp. 301-310.

82. TURVEY, G.J. "Large deflection of tapered annular plates by dynamic relaxation". Journal of Eng. Mech. Div., ASCE, Vol. 104, No. EM2, April 1978, pp. 351-366.

83. FRIEZE, P.A. "Elasto-plastic buckling in short thin-walled beams and columns". Proc. Instn. Civ. Engrs., Vol. 65, Pt. 2, Dec. 1978, pp. 857-874.

84. HARDING, J.E. "The elasto-plastic analysis of imperfect cylinders". Proc. Instn. Civ. Engrs., Vol. 65, Pt. 2, Dec. 1978, pp. 875-892.

85. DEAN, J.A. "The collapse behaviour of steel plating subject to complex loading". PhD Thesis, University of London (Imperial College), 1975.

NOTATION

(a) Notation Subscripted by *w* and *f*

The following terms appear in the text, subscripted by *w* or *f*. Subscript *w* indicates the web and subscript *f* the flange.

A	cross-sectional area
b	breadth of section
EA	extensional rigidity
EI_y	flexural rigidity of the web/flange about a y-direction axis through its own centroid
EI_z	flexural rigidity of the web/flange about a z-direction axis through its own centroid
FT	interactive couple per unit length of stiffener
FX; FY; FZ	interactive forces per unit length of stiffener in the x, y and z directions
GJ	torsional rigidity
h	height of section
K	number of elements in the web/flange
MH; MV; MT	bending and twisting moments in the stiffener
NA; NH; NV	axial and shear forces in the stiffener
t	thickness of section
u_c; v_c; w_c	net centroidal displacements of the web/flange
u_e; v_e; w_e	net displacements of an element of web/flange
u_{oc}; v_{oc}; w_{oc}	initial centroidal displacements of a web/flange
u_{oe}; v_{oe}; w_{oe}	initial displacements of an element of web/flange
$\bar{u}_c$; $\bar{v}_c$; $\bar{w}_c$	total centroidal displacements of a web/flange
$\bar{u}_e$; $\bar{v}_e$; $\bar{w}_e$	total displacements of an element of web/flange
δA	cross-sectional area of an element of web/flange

ε_c	direct strain at the centroid of the web/flange
ε_e	direct strain at the centroid of an element of web/flange
εo	modified yield strain
σo	stiffener yield stress
σ_R	stiffener residual stress

(b) Non-Subscripted Notation

A	cross-sectional area of the plating
b	breadth of plating between stiffeners
chf	horizontal separation between the web and flange centroids
cvf; cvw	distance from the flange and web centroids to the middle-plane of the plate
D	flexural rigidity of the plate
dx; dy	dimensions of a small element of plate in the x-y plane
E	Young's modulus
E1	extensional rigidity of the plate
ehf; ehw	horizontal separation between the web centroid and small elements in the flange and web
evf; evw	vertical distances from the middle-plane of the plate to small elements in the flange and web
f; fp	current and previous values of the yield function
G	shear modulus
I, J	finite difference mesh lines
Kx; Ky; Kz	plate damping factors at u, v and w nodes respectively
Kx'; Kz'	damping factors at u and w nodes along the stiffeners

Lx; Ly	plate dimensions in the x and y directions
Mx; My	bending moments per unit length of plate about the y and x axes
Mxy; Myx	twisting moments per unit length of plate about the x and y axes
$\bar{N}$; $\overline{MN}$; $\bar{M}$	quadratic stress intensities
Nx; Ny	axial forces per unit length of plate in the x and y directions
Nxy; Nyx	shear forces per unit length of plate in the y and x directions
Px; Py; Pz	numerical values of the x, y and z direction equilibrium equations
q	applied lateral load per unit area
Qx; Qy	normal shear forces per unit length of plate
R	radius of gyration
t	plate thickness
u; v; w	net middle-plane displacements in the x, y and z directions
u_o; v_o; w_o	initial middle-plane displacements in the x, y and z directions
$\bar{w}$	total middle-plane displacement in the z-direction
$\dot{u}$; $\dot{v}$; $\dot{w}$	middle-plane velocities in the x, y and z directions
wc	initial deformation at the centre of the plate
x; y; z	co-ordinate axes
δy	finite width of plate adjoining stiffener
δt	time increment
Δx; Δy	finite difference mesh divisions in the x and y directions
εa	applied edge strain

$\varepsilon x;\ \varepsilon y;\ \varepsilon xy$	plate direct and shear strains (equivalent incremental values are prefixed by Δ)
εo	plate yield strain
λ	plastic strain rate multiplier
ν	Poisson's ratio
$\rho x;\ \rho y;\ \rho z$	fictitious densities at u, v and w nodes respectively
σm	average edge stress
σo	plate yield stress
σR	plate residual stress
ϕ	torsional rigidity factor
$\psi x;\ \psi y;\ \psi xy$	plate curvatures (equivalent incremental values are prefixed by Δ)

Matrices

$[C^*];[cd];[D^*]$	elasto-plastic tangential rigidities
$[E]$	$\frac{E}{(1-\nu^2)}\begin{bmatrix} 1 & \nu & 0 \\ \nu & 1 & 0 \\ 0 & 0 & (1-\nu)/2 \end{bmatrix}$
$[I]$	3×3 unit matrix

Vectors

$\{\Delta M\};\ \{\Delta N\}$	incremental stress resultants per unit length of plate: $\{\Delta M\}^T = \{\Delta Mx,\ \Delta My,\ \Delta Mxy\}$ $\{\Delta N\}^T = \{\Delta Nx,\ \Delta Ny,\ \Delta Nxy\}$
$\{\Delta \varepsilon t\};\ \{\Delta \psi t\}$	incremental plate strains and curvatures: $\{\Delta \varepsilon t\}^T = \{\Delta \varepsilon x,\ \Delta \varepsilon y,\ \Delta \varepsilon xy\}$ $\{\Delta \psi t\}^T = \{\Delta \psi x,\ \Delta \psi y,\ \Delta \psi xy\}$

APPENDIX A

The Ilyushin Yield Criterion

The exact Ilyushin yield criterion was developed for the analysis of thin shells by employing the Von Mises yield criterion in conjunction with the 'associated' flow rule. A summarised translation of this work has been presented by Crisfield[69] and the resulting yield surface has been generated in full by Frieze[77].

From the exact yield criterion, Ilyushin proposed a simpler approximate surface which compares exactly for the conditions of 'in-plane' only and 'bending' only. This surface is given by:

$$f = (\bar{N}/t^2 + 4.\overline{MN}/\sqrt{3}.t^3 + 16\bar{M}/t^4)/\sigma o^2 \leqslant 1 \qquad (A1)$$

where:

$$\left.\begin{aligned} \bar{N} &= Nx^2 + Ny^2 - Nx.Ny + 3Nxy^2 \\ \overline{MN} &= Mx.Nx + My.Ny - \tfrac{1}{2}\,Mx.Ny - \tfrac{1}{2}My.Nx + 3\,Mxy.Nxy \\ \text{and} \quad \bar{M} &= Mx^2 + My^2 - Mx.My + 3Mxy^2 \end{aligned}\right\} \qquad (A2)$$

Following this work, Crisfield[69] compared the two criteria for the condition of uniaxial stress, and found that closer overall agreement could be obtained by applying the following modified form of equation (A1):

$$f = (\bar{N}/t^2 + 4.S.\overline{MN}/\sqrt{3}.t^3 + 16\bar{M}/t^4)/\sigma o^2 \leqslant 1 \qquad (A3)$$

where $S = \overline{MN}/|\overline{MN}|$ unless $\overline{MN}$ is small in which case S is set equal to zero.

Small $\overline{MN}$ is defined by the relationship:

$$|4\overline{MN}/\sqrt{3}.t^3.\sigma o^2| < 10^{-4} \qquad (A4)$$

APPENDIX B

Incremental Force-Displacement Relationships

An elastic-perfectly plastic body, in a state of stress defined by a point on the yield surface, will respond to load in a manner which is partially elastic and partially plastic.

The elastic strain component will lead to a redistribution of the stress resultants in such a way that there is no variation in the value of the yield function f (i.e. $\delta f = 0$).

On the basis of this and with the yield function f and the quadratic stress intensities as defined in Appendix A we have:

$$\delta f = \{fn\}^T\{\Delta N\} + \{fm\}^T\{\Delta M\} = 0 \tag{B1}$$

where

$$\left.\begin{aligned} \{fn\} &= \{\partial\bar{N}/\partial N\}/t^2 + 2.S\{\partial\bar{M}/\partial M\}/\sqrt{3}.t^3 \\ \text{and} \\ \{fm\} &= 2.S\{\partial\bar{N}/\partial N\}/\sqrt{3}.t^3 + 16\{\partial\bar{M}/\partial M\}/t^4 \end{aligned}\right\} \tag{B2}$$

Assuming that the flow rule and the normality condition can be applied in stress resultant space, expressions can be written for increments of plastic strain and curvature as follows:

$$\left.\begin{aligned} \{\Delta\varepsilon p\} &= \lambda\{fn\} \\ \{\Delta\psi p\} &= \lambda\{fm\} \end{aligned}\right\} \tag{B3}$$

where λ is a positive scalar quantity.

Assuming also that a proportional relationship exists between elastic strain increments and stress resultant increments, we obtain:

$$\left.\begin{aligned} \{\Delta N\} &= t\,[E]\{\{\Delta\varepsilon t\} - \{\Delta\varepsilon p\}\} \\ \text{and} \\ \{\Delta M\} &= t^3\,[E]\{\{\Delta\psi t\} - \{\Delta\psi p\}\}/12 \end{aligned}\right\} \qquad \text{(B4)}$$

where $\{\Delta\varepsilon t\}$ and $\{\Delta\psi t\}$ are the sum of elastic and plastic components.

Substituting (B3) into (B4) and using equation (B1) an expression is obtained for the scalar quantity λ:

$$\left.\begin{aligned} \lambda &= \left[t\{fn\}^T[E]\{\Delta\varepsilon t\} + t^3\{fm\}^T[E]\{\Delta\psi t\}/12\right]/(m+n) \\ \text{where} \quad n &= t\{fn\}^T[E]\{fn\} \quad \text{and} \quad m = t^3\{fm\}^T[E]\{fm\}/12 \end{aligned}\right\} \qquad \text{(B5)}$$

Substituting (B5) into (B3) and using these results in (B4), the following expressions are obtained for the stress resultant increments in terms of incremental strains and curvatures and elasto-plastic tangential rigidities $[C^*]$, $[cd]$ and $[D^*]$:

$$\left.\begin{aligned} \{\Delta N\} &= [C^*]\{\Delta\varepsilon t\} + [cd]\{\Delta\psi t\} \\ \text{and} \\ \{\Delta M\} &= [cd]^T\{\Delta\varepsilon t\} + [D^*]\{\Delta\psi t\} \end{aligned}\right\} \qquad \text{(B6)}$$

$$\left.\begin{aligned} [C^*] &= t[E]\left[[I] - [N][E]t/(m+n)\right] \\ [cd] &= -t^4[E][NM][E]/12(m+n) \\ [D^*] &= t^3[E]\left[[I] - [M][E]t^3/12(m+n)\right]/12 \end{aligned}\right\} \qquad \text{(B7)}$$

$$\left.\begin{aligned} [N] &= \{fn\}\{fn\}^T \\ [NM] &= \{fn\}\{fm\}^T \\ [M] &= \{fm\}\{fm\}^T \end{aligned}\right\} \qquad \text{(B8)}$$

The incremental strains and curvatures $\{\Delta\varepsilon t\}$ and $\{\Delta\psi t\}$, resulting from a small change of displacement from (up,vp,wp) to

(up+Δu,vp+Δv,wp+Δw) are given by the following expressions:

$$\{\Delta\varepsilon t\}^T = \{\Delta\varepsilon x,\ \Delta\varepsilon y,\ \Delta\varepsilon xy\} \tag{B9}$$

where

$$\Delta\varepsilon x = \partial\Delta u/\partial x + \partial wp/\partial x.\partial\Delta w/\partial x + \tfrac{1}{2}(\partial\Delta w/\partial x)^2 + \partial\Delta w/\partial x.\partial w_o/\partial x \tag{B10}$$

$$\Delta\varepsilon y = \partial\Delta v/\partial y + \partial wp/\partial y.\partial\Delta w/\partial y + \tfrac{1}{2}(\partial\Delta w/\partial y)^2 + \partial\Delta w/\partial y.\partial w_o/\partial y \tag{B11}$$

$$\Delta\varepsilon xy = \partial\Delta u/\partial y + \partial\Delta v/\partial x + \partial\Delta w/\partial x.\partial\overline{wp}/\partial y + \partial\Delta w/\partial y.\partial\overline{wp}/\partial x \tag{B12}$$

and

$$\{\Delta\psi t\}^T = \{\Delta\psi x,\ \Delta\psi y,\ \Delta\psi xy\} \tag{B13}$$

where

$$\Delta\psi x = -\partial^2\Delta w/\partial x^2 \tag{B14}$$

$$\Delta\psi y = -\partial^2\Delta w/\partial y^2 \tag{B15}$$

$$\Delta\psi xy = -2.\partial^2\Delta w/\partial x\partial y \tag{B16}$$

APPENDIX C

The Computer Program Flow Chart

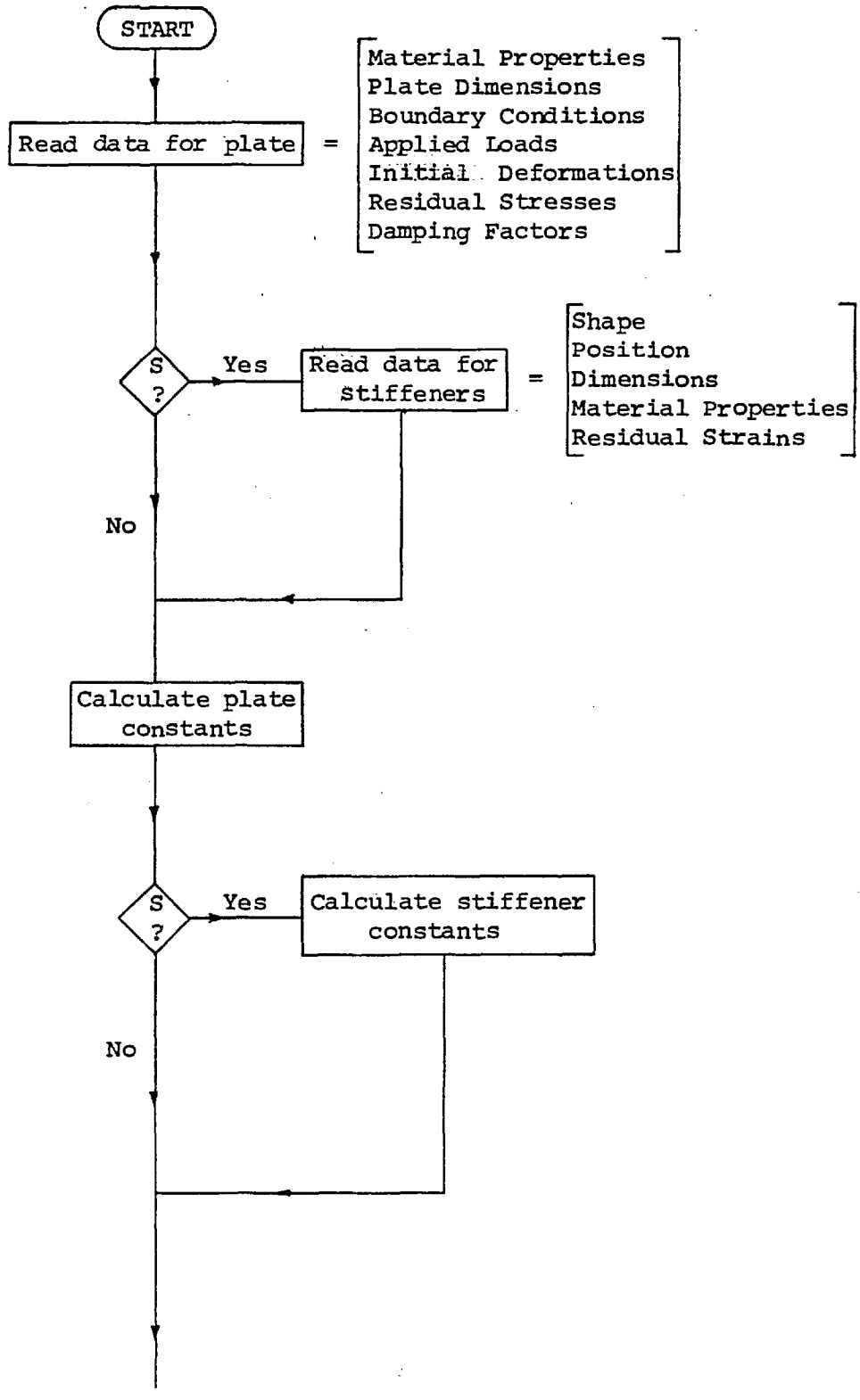

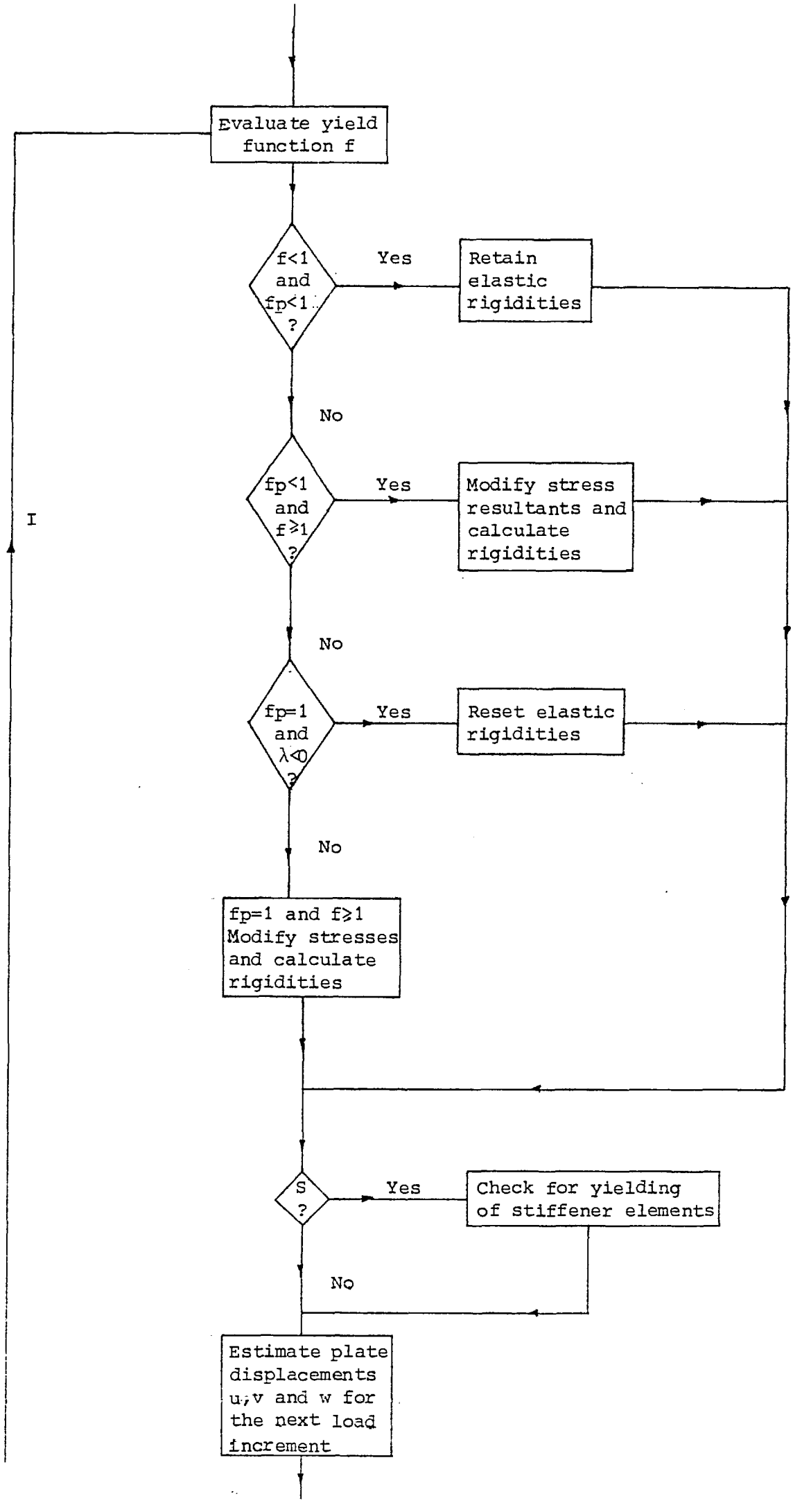
Evaluate yield function f
f<1 and fp<1 ?
Yes
Retain elastic rigidities
No
fp<1 and f≥1 ?
Yes
Modify stress resultants and calculate rigidities
No
fp=1 and λ<0 ?
Yes
Reset elastic rigidities
No
fp=1 and f≥1 Modify stresses and calculate rigidities
S ?
Yes
Check for yielding of stiffener elements
No
Estimate plate displacements u, v and w for the next load increment
I

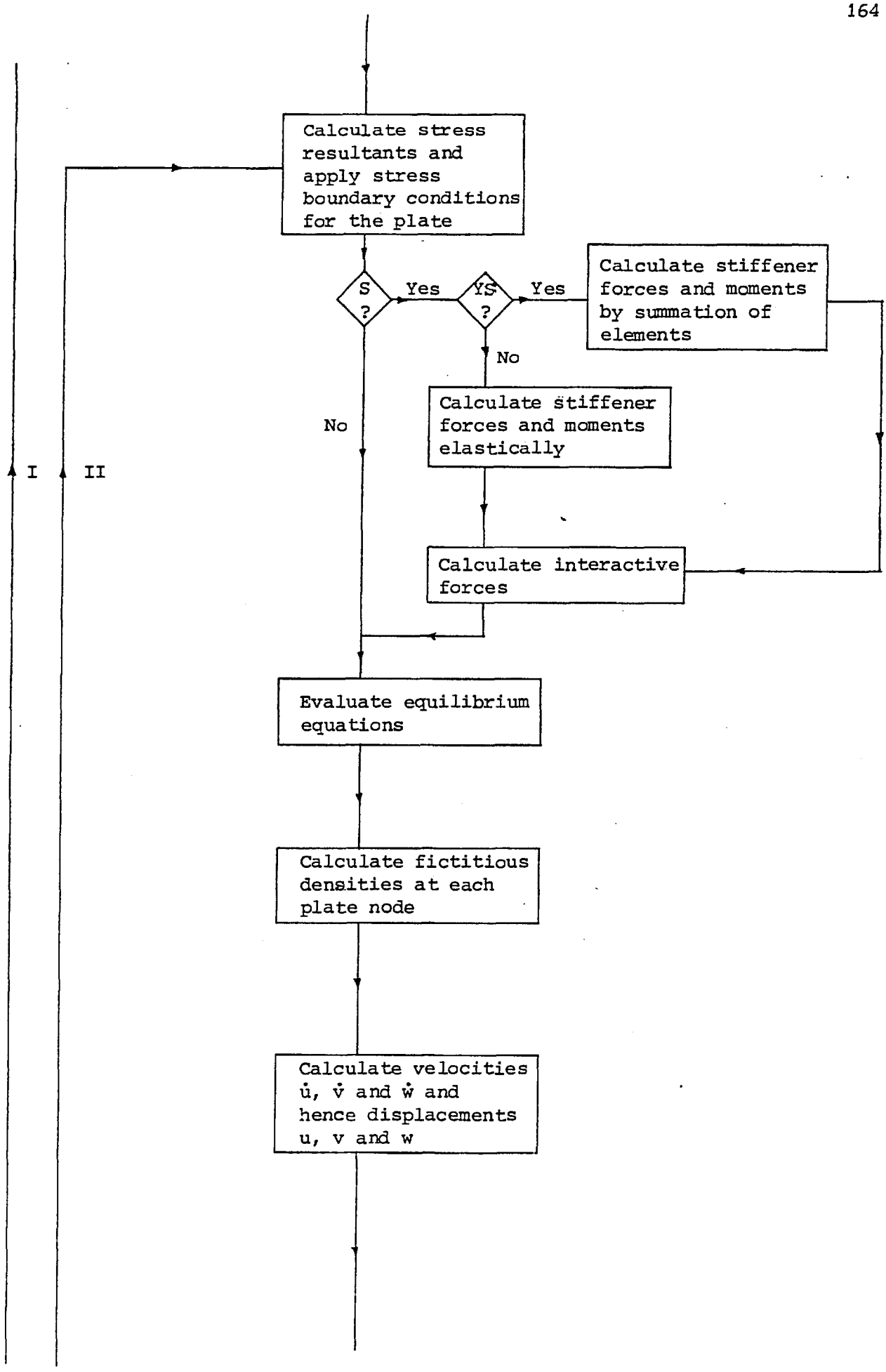
Calculate stress resultants and apply stress boundary conditions for the plate
S ?
Yes
YS ?
Yes
Calculate stiffener forces and moments by summation of elements
No
No
Calculate stiffener forces and moments elastically
Calculate interactive forces
Evaluate equilibrium equations
Calculate fictitious densities at each plate node
Calculate velocities u̇, v̇ and ẇ and hence displacements u, v and w
I
II

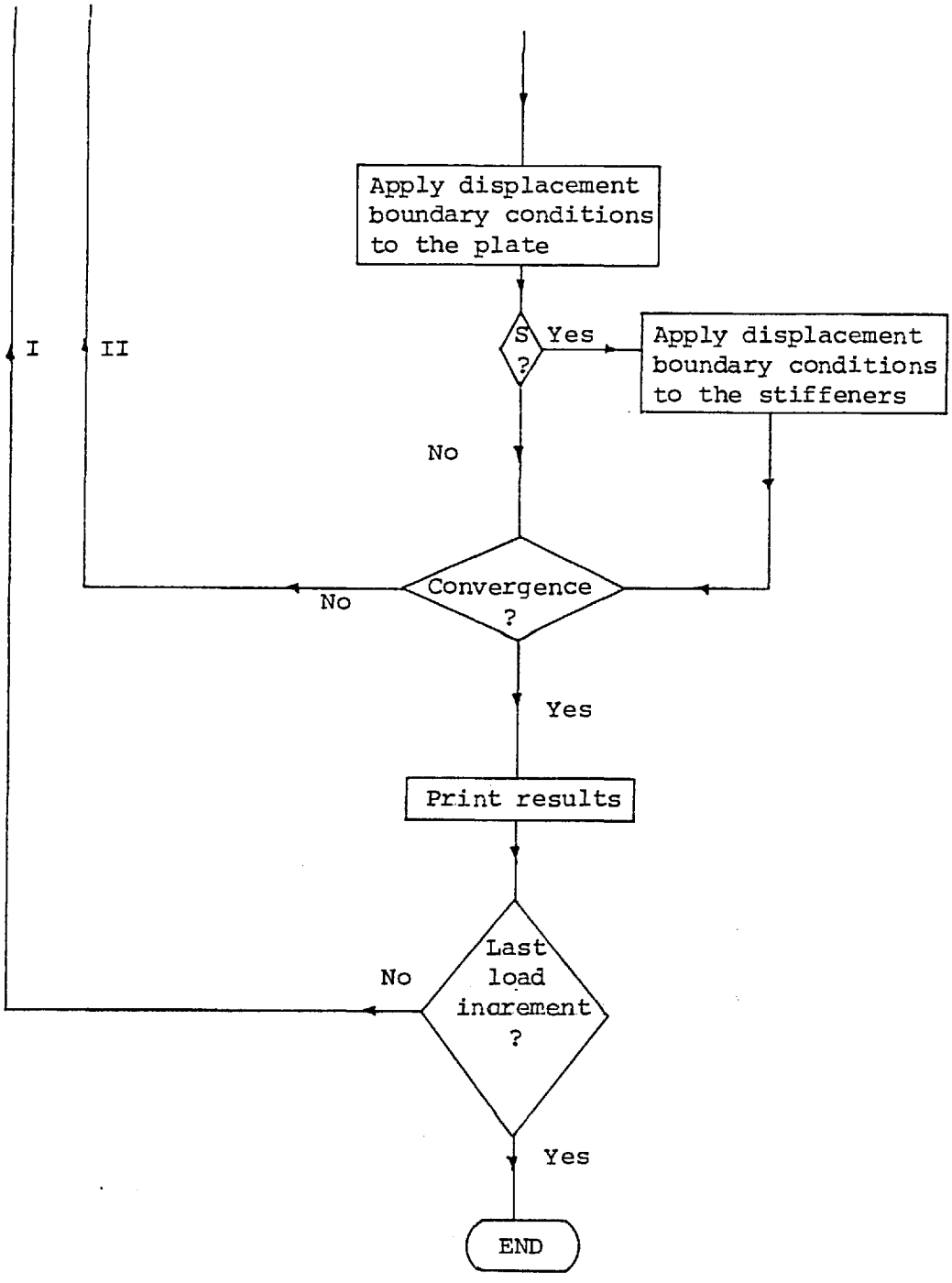

Notation

S denotes stiffeners

f denotes current value of the yield function

fp denotes previous value of the yield function

λ denotes unloading parameter (Appendix B)

YS denotes stiffener yield

APPENDIX D

Adjustment of Stresses Normal to the Yield Surface

Let $\{\delta n\}$ and $\{\delta m\}$ be components of the non-dimensional stress resultants which act normal to the yield surface and let the deviation from the yield surface due to these components be δf. Then for small changes:

$$\delta f = (\partial f/\partial nx)\delta nx + (\partial f/\partial ny)\delta ny + (\partial f/\partial nxy)\delta nxy + (\partial f/\partial mx)\delta mx + (\partial f/\partial my)\delta my + (\partial f/\partial mxy)\delta mxy$$

or in scalar product notation:

$$\delta f = \underset{\sim}{r}.\delta\underset{\sim}{s} \tag{D1}$$

where

$$\underset{\sim}{r} = (\partial f/\partial nx)i_1 + (\partial f/\partial ny)i_2 + (\partial f/\partial nxy)i_3 + (\partial f/\partial mx)i_4 + (\partial f/\partial my)i_5 + (\partial f/\partial mxy)i_6 \tag{D2}$$

and

$$\delta\underset{\sim}{s} = (\delta nx)i_1 + (\delta ny)i_2 + (\delta nxy)i_3 + (\delta mx)i_4 + (\delta my)i_5 + (\delta mxy)i_6 \tag{D3}$$

Observing that both $\underset{\sim}{r}$ and $\delta\underset{\sim}{s}$ are normal to the yield surface expression (D1) can be re-written as follows:

$$\delta f = r\delta s \quad \text{or} \quad \delta s = \frac{\delta f}{r} \tag{D4}$$

Also, since $\delta\underset{\sim}{s}$ and $\underset{\sim}{r}$ act in the same direction, $\delta\underset{\sim}{s}$ can be expressed in terms of the unit vector $\hat{\underset{\sim}{r}}$:

$$\delta\underset{\sim}{s} = \delta s\,\hat{\underset{\sim}{r}} = \delta s\,\underset{\sim}{r}/r \tag{D5}$$

Combining (D4) and (D5) the following expression is obtained:

$$\delta \underset{\sim}{s} = \underset{\sim}{r}\, \delta f / r^2 \qquad \text{(D6)}$$

where
$$r^2 = (\partial f/\partial nx)^2 + (\partial f/\partial ny)^2 + (\partial f/\partial nxy)^2 + (\partial f/\partial mx)^2 + (\partial f/\partial my)^2 + (\partial f/\partial mxy)^2 \qquad \text{(D7)}$$

Then from expressions (D2), (D3) and (D6):

$$\begin{Bmatrix} \delta nx \\ \delta ny \\ \delta nxy \\ \delta mx \\ \delta my \\ \delta mxy \end{Bmatrix} = \frac{\delta f}{r^2} \begin{Bmatrix} \partial f/\partial nx \\ \partial f/\partial ny \\ \partial f/\partial nxy \\ \partial f/\partial mx \\ \partial f/\partial my \\ \partial f/\partial mxy \end{Bmatrix} \qquad \text{(D8)}$$

Equations (D8) are employed in Section 3.1.1.1(b), to adjust the stress resultants back to the yield surface after drift has occurred. The necessary procedure is given here for the stress resultant Nx:

1. Differentiate the yield function and substitute known quantities to obtain numerical values for the vector {r} and the term r^2.
2. Subtract unity from the current value of the yield function to determine the amount of drift, δf.
3. Calculate and apply the following adjustment to Nx.

   $\delta nx = (\partial f/\partial nx)\, \delta f/r^2$

   Nx modified = Nx - $\delta nx.\sigma o.t$

APPENDIX E

Fictitious Density ρx for a Stiffener Node u(I,J)

To obtain ρx for a stiffener node u(I,J) we consider the coefficients of displacement contained in the expression:

$$(\partial Nx/\partial x)_{(I,J)} + (\partial Nxy/\partial y)_{(I,J)} + (FX_w/\Delta y)_{(I,J)} = 0 \qquad (E1)$$

The summation can be carried out most simply by first obtaining the sums of coefficients in Nx, Nxy, NA_w and NA_f separately and then combining them according to the above expression.

(a) *Sum of Coefficients of Nx at Main Node (I,J)*

Defining the sum of coefficients as CNx(I,J) and referring to equations (26) and (27) we obtain:

$$CNx(I,J) = E1(2+\alpha_1)/\Delta x + \nu.E1(2+\alpha_2)/\Delta y \qquad (E2)$$

where α_1 and α_2, given by the following expressions, are evaluated at the main node (I,J).

$$\alpha_1 = |\partial w/\partial x| + |\partial w_o/\partial x| \; ; \; \alpha_2 = |\partial w/\partial y| + |\partial w_o/\partial y|$$

(b) *Sum of Coefficients of Nxy at Interlacing Node (I,J)*

Defining the sum of coefficients as CNxy(I,J) and referring to equations (26) and (27) we obtain

$$CNxy(I,J) = E1(1-\nu)((1+\alpha_3)/\Delta y + (1+\alpha_4)/\Delta x) \qquad (E3)$$

where α_3 and α_4, given by the following expressions, are evaluated at the interlacing node (I,J).

$$\alpha_3 = |\partial w/\partial x| + |\partial w_o/\partial x| \quad \text{and} \quad \alpha_4 = |\partial w/\partial y| + |\partial w_o/\partial y|$$

(c) *Sum of Coefficients of NA_f at Main Node (I,J)*

Defining the sum of coefficents as $CNA_f(I,J)$ and referring to equations (40) and (41) we obtain

$$CNA_f(I,J) = EA_f(2+4.cvf/\Delta x + \beta_1.\alpha_5 + \beta_2(\alpha_6 + 4.chf/\Delta x))/\Delta x \qquad (E4)$$

where α_5 and α_6, given by the following expressions, are evaluated at the main node (I,J):

$$\alpha_5 = |\partial w_{cf}/\partial x| + |\partial w_{ocf}/\partial x|$$

$$\alpha_6 = |\partial v_{cf}/\partial x| + |\partial v_{ocf}/\partial x|$$

and $\beta_1 = (1 + chf/\Delta y)$ and $\beta_2 = (1 + cvf/\Delta y)$

(d) *Sum of Coefficients of NA_w at Main Node (I,J)*

The sum of coefficients, $CNA_w(I,J)$, is obtained from expression (E4) by replacing all flange components by equivalent terms for the web.

The Resulting Density Expression

The coefficients obtained above are now used in equation (E1) to obtain the value of $\sum_{j=1}^{n} |Sxj|$ for the row of the matrix corresponding to node u(I,J), and hence the density expression (E5) is obtained from equation (69):

$$\rho x(I,J) = (CNx/\Delta x + CNxy/\Delta y + CNA_w/\Delta x.\Delta y + CNA_f/\Delta x.\Delta y)/2 \qquad (E5)$$

where $CNx = \frac{1}{2}(CNx(I,J) + CNx(I+1,J))$

$CNxy = \frac{1}{2}(CNxy(I,J-1) + CNxy(I,J))$

$CNA_w = \frac{1}{2}(CNA_w(I,J) + CNA_w(I+1,J))$

$CNA_f = \frac{1}{2}(CNA_f(I,J) + CNA_f(I+1,J))$

APPENDIX F

Boundary Conditions Applied to the Finite Difference Mesh

1. Boundary Conditions Applied as Stresses

Free tangential displacement on J = 2

$$Nxy(I,1) = -Nxy(I,2) \tag{F1}$$

2. Boundary Conditions Applied as Displacements

(a) *Lateral Restraint*

(i) on J = 2 $\quad w(I,2) = 0$ (F2)

(ii) on I = 2 $\quad w(2,J) = 0$ (F3)

(b) *Clamped Edges*

(i) on J = 2 $\quad \partial w/\partial y = 0 \; ; \quad w(I,1) = w(I,3)$ (F4)

(ii) on I = 2 $\quad \partial w/\partial x = 0 \; ; \quad w(1,J) = w(3,J)$ (F5)

(c) *Simply Supported Edges*

(i) on J = 2, My = 0:

Using equations (30) with rigidities expressed as:

$$[cd] = \begin{bmatrix} cd_{11} & cd_{12} & cd_{13} \\ cd_{21} & cd_{22} & cd_{23} \\ cd_{31} & cd_{32} & cd_{33} \end{bmatrix} \quad \text{and} \quad [D^*] = \begin{bmatrix} D_{11} & D_{12} & D_{13} \\ D_{21} & D_{22} & D_{23} \\ D_{31} & D_{32} & D_{33} \end{bmatrix} \tag{F6}$$

and $R1 = cd_{12}.\Delta\varepsilon x + cd_{22}.\Delta\varepsilon y + cd_{32}.\Delta\varepsilon xy + D_{21}.\Delta\psi x + D_{23}.\Delta\psi xy$

we obtain

$$w(I,1) = -w(I,3) + R1.\Delta y^2/D_{22} + wp(I,3) + wp(I,1) \tag{F7}$$

where R1 and D_{22} are evaluated at main nodes (I,2) and wp is defined

in Appendix B.

(ii) On I = 2, Mx = 0

Using equations (30) with rigidities expressed by (F6) and

$R2 = cd_{11}.\Delta\varepsilon x + cd_{21}.\Delta\varepsilon y + cd_{31}.\Delta\varepsilon xy + D_{12}\Delta\psi y + D_{13}\Delta\psi xy$

we obtain:

$$w(1,J) = -w(3,J) + R2.\Delta x^2/D_{11} + wp(3,J) + wp(1,J) \qquad (F8)$$

where R2 and D_{11} are evaluated at main nodes (2,J)

(d) *Free Displacement Normal to the Edge J = 2*

On J = 2, Ny = 0

Using equations (29) with [cd] defined by (F6) and

$$[C^*] = \begin{bmatrix} C_{11} & C_{12} & C_{13} \\ C_{21} & C_{22} & C_{23} \\ C_{31} & C_{32} & C_{33} \end{bmatrix} \qquad (F9)$$

and $R3 = C_{21}.\Delta\varepsilon x + C_{23}.\Delta\varepsilon xy + cd_{21}.\Delta\psi x + cd_{22}.\Delta\psi y + cd_{23}.\Delta\psi xy$

we obtain:

$$v(I,1) = v(I,2) + \Delta y(R3/C_{22} + \tfrac{1}{2}.w_y^2 + w_y.\, w_{oy} - \tfrac{1}{2}.wp_y^2 - wp_y.w_{oy} - vp_y) \qquad (F10)$$

where R3 and C_{22} are evaluated at main edge nodes (I,2) and

$$\left.\begin{aligned} w_y &= (w(I,3) - w(I,1))/2\Delta y \\ w_{oy} &= (w_o(I,3) - w_o(I,1))/2\Delta y \\ wp_y &= (wp(I,3) - wp(I,1))/2\Delta y \\ vp_y &= (vp(I,2) - vp(I,1))/\Delta y \end{aligned}\right\} \qquad (F11)$$

where vp and wp are defined in Appendix B.

(e)*Constrained Edge Conditions*

(i) On $J = 2$, $\sum_{I=2}^{IK-1} Ny = 0$

Defining the uniform edge displacement as $\frac{1}{2}(v(I,2) + v(I,1))$ and using equations (29) we obtain:

$$v(I,1) = -v(I,2) + \Delta y \sum_{I=2}^{IK-1} (R3 + R4) / \sum_{I=2}^{IK-1} C_{22} \qquad \text{(F12)}$$

where:

$$R4 = C_{22}(2\, v(I,2)/\Delta y + \tfrac{1}{2}w_y^{\,2} + w_y.w_{oy} - \tfrac{1}{2}wp_y^2 - wp_y.w_{oy} - vp_y)$$

and C_{22}, R3 and terms in R4 are defined in Section (d).

(ii) On $I = 2$, $\sum_{J=2}^{JK-1} Nx + \sum_{JS=1}^{n/2} (NA_w + NA_f)/\Delta y = 0$

where JS = 1, n represents the number of stiffeners across the plate width. Defining the uniform edge displacement as $\frac{1}{2}(u(1,J) + u(2,J))$ and using equations (29) with:

$$R5 = C_{12}.\Delta\varepsilon y + C_{13}.\Delta\varepsilon xy + cd_{11}.\Delta\psi x + cd_{12}.\Delta\psi y + cd_{13}.\Delta\psi xy$$

we obtain:

$$u(1,J) = -u(2,J) + \Delta x\Big\{ \sum_{J=2}^{JK-1} (Nxp + R5 + R6) + \sum_{JS=1}^{n/2} (NA_w + NA_f)/\Delta y \Big\} / \sum_{J=2}^{JK-1} C_{11} \qquad \text{(F13)}$$

where Nxp are the values of Nx for the previous load increment and

$$R6 = C_{11}(2u(2,J)/\Delta x + \tfrac{1}{2}w_x^{\,2} + w_x.w_{ox} - \tfrac{1}{2}wp_x^2 - wp_x.w_{ox} - up_x)$$

$$\left.\begin{aligned} w_x &= (w(3,J) - w(1,J))/2\Delta x \\ w_{ox} &= (w_o(3,J) - w_o(1,J))/2\Delta x \\ wp_x &= (wp(3,J) - wp(1,J))/2\Delta x \\ up_x &= (up(2,J) - up(1,J))/\Delta x \end{aligned}\right\} \qquad \text{(F14)}$$

where wp and up are the previous increment values given in Appendix B.

(f) *Applied Displacement Normal to the Edges*

(i) On J = 2 for uniform applied displacement VE:

$$v(I,1) = 2VE - v(I,2) \qquad \text{(F15)}$$

(ii) On I = 2 for uniform applied displacement UE:

$$u(1,J) = 2UE - u(2,J) \qquad \text{(F16)}$$

(g) *Full Fixity Tangential to the Edge*

(i) On J = 2 $\quad u(I,2) = 0$ (F17)

(ii) On I = 2 $\quad v(2,J) = 0$ (F18)

(h) *Flexural Edge Condition for the Stiffener*

On stiffener edge nodes $\partial v/\partial x = 0$

$$v(1,J) = v(3,J) \qquad \text{(F19)}$$

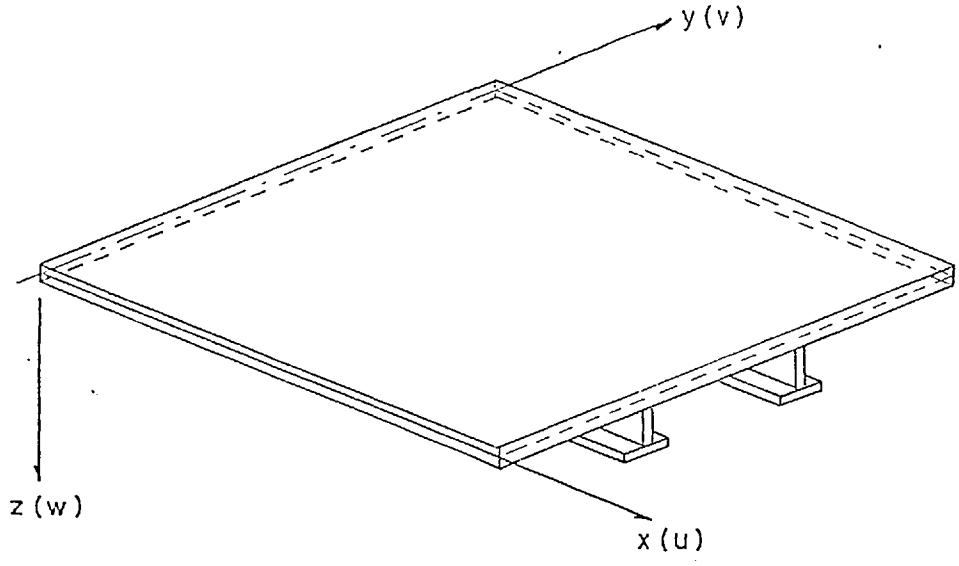

ORIENTATION OF AXES

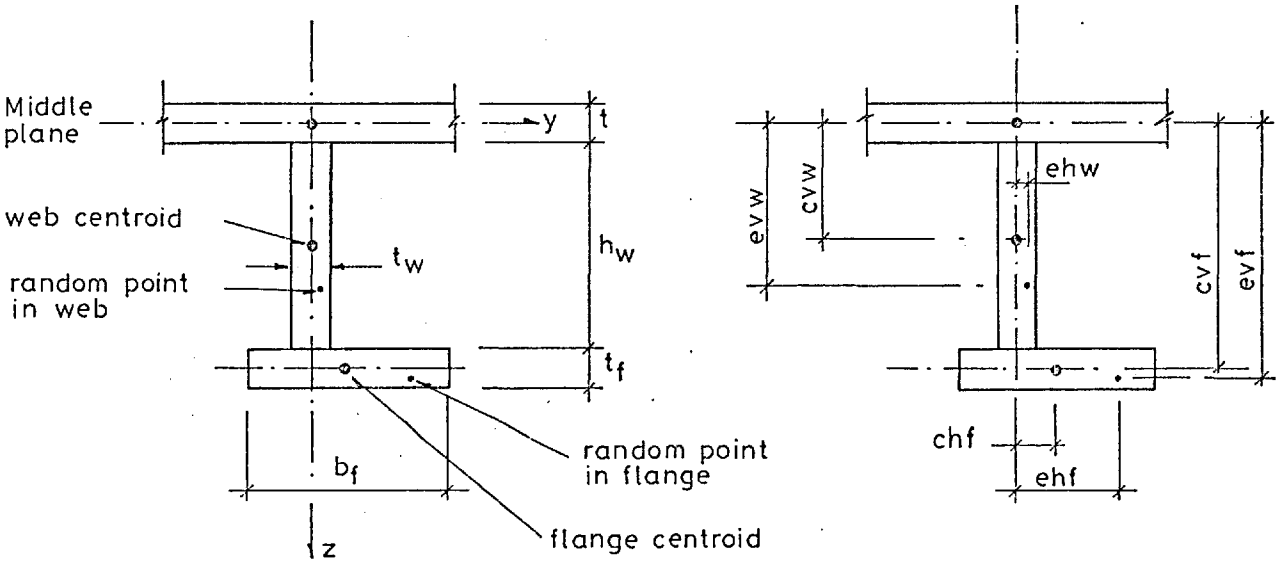

CROSS-SECTIONAL DIMENSIONS

Fig A1

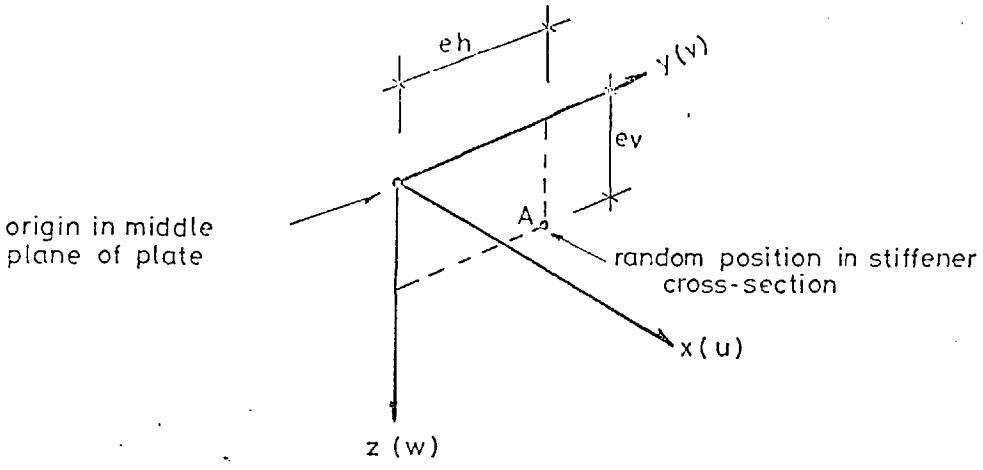

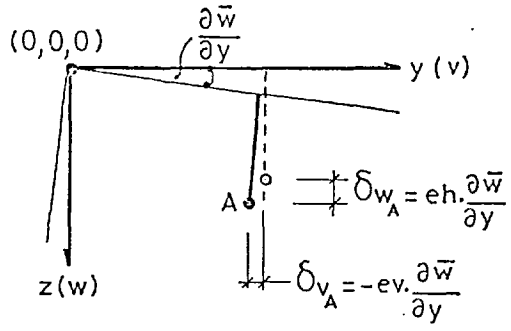

ROTATION ABOUT X-AXIS

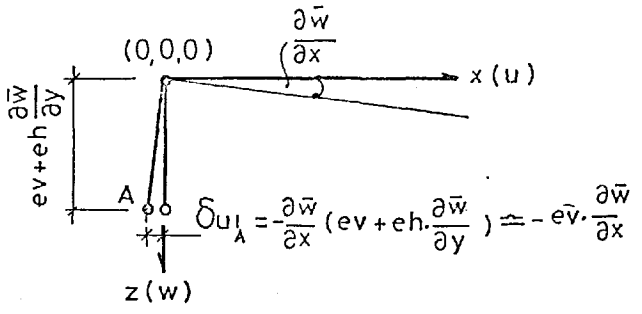

ROTATION ABOUT Y-AXIS

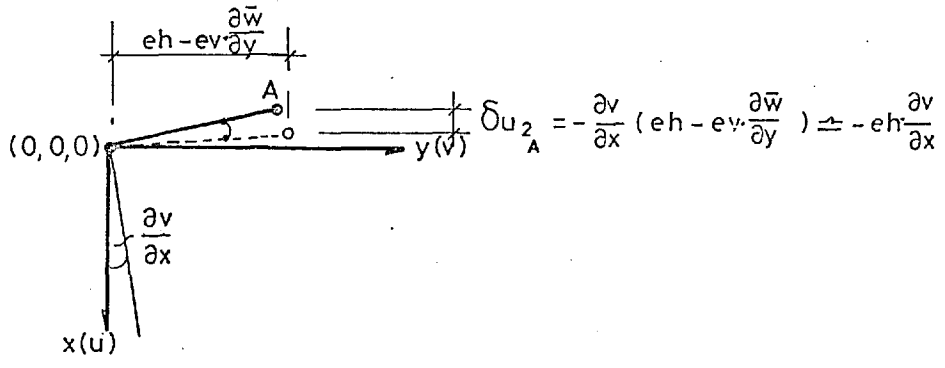

ROTATION ABOUT Z-AXIS

$$\left\{\begin{array}{lll} \delta_{u_A} = & -ev\cdot\partial\bar{w}/\partial x & -\ eh\cdot\partial v/\partial x \\ \delta_{v_A} = & -ev\cdot\partial\bar{w}/\partial y & \\ \delta_{w_A} = & +eh\cdot\partial\bar{w}/\partial y & \end{array}\right\}$$

Fig A2 Displacements of a point in the stiffener due to rotation of the middle-plane of the plate

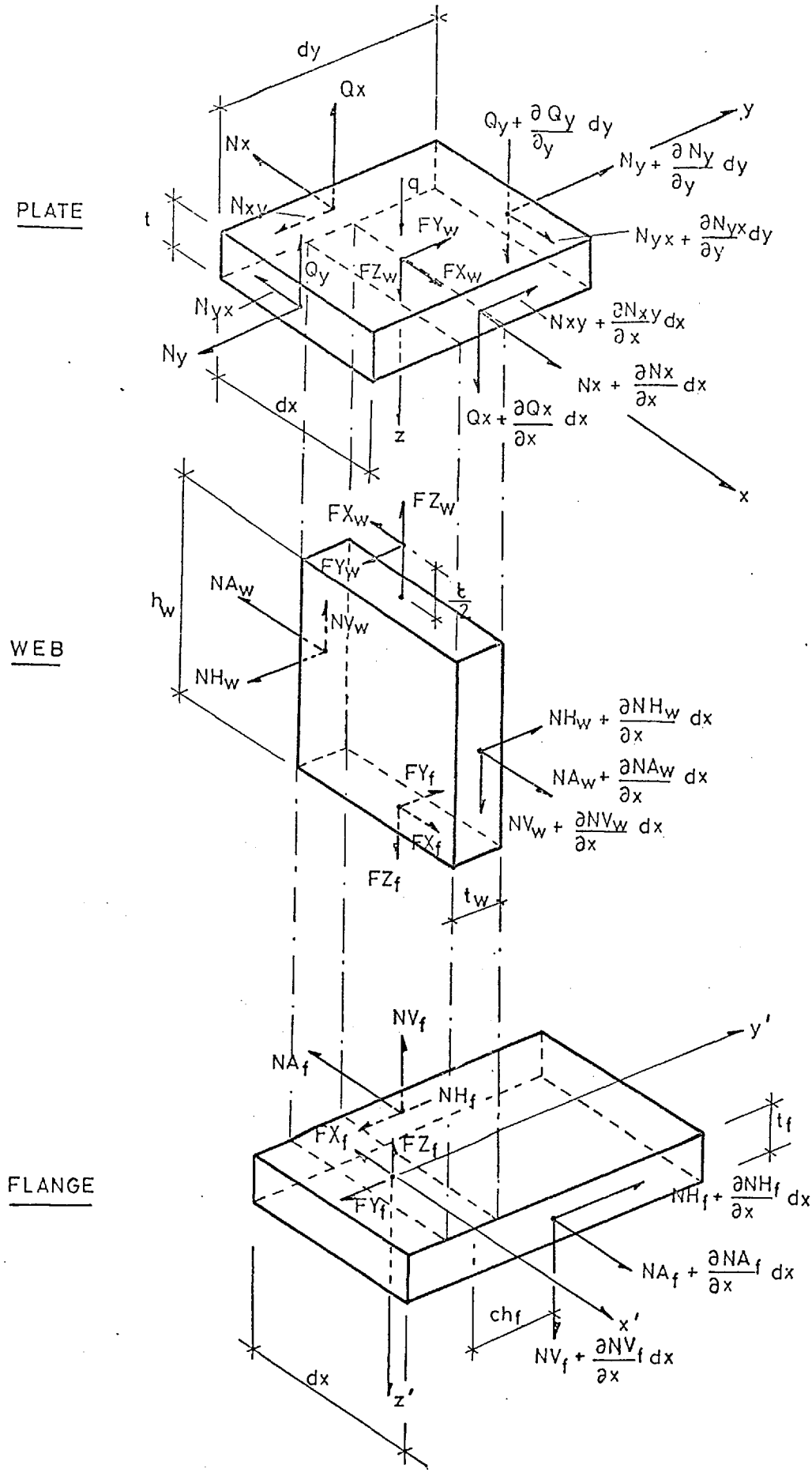

Fig A3 Forces in a deformed element of stiffened plate

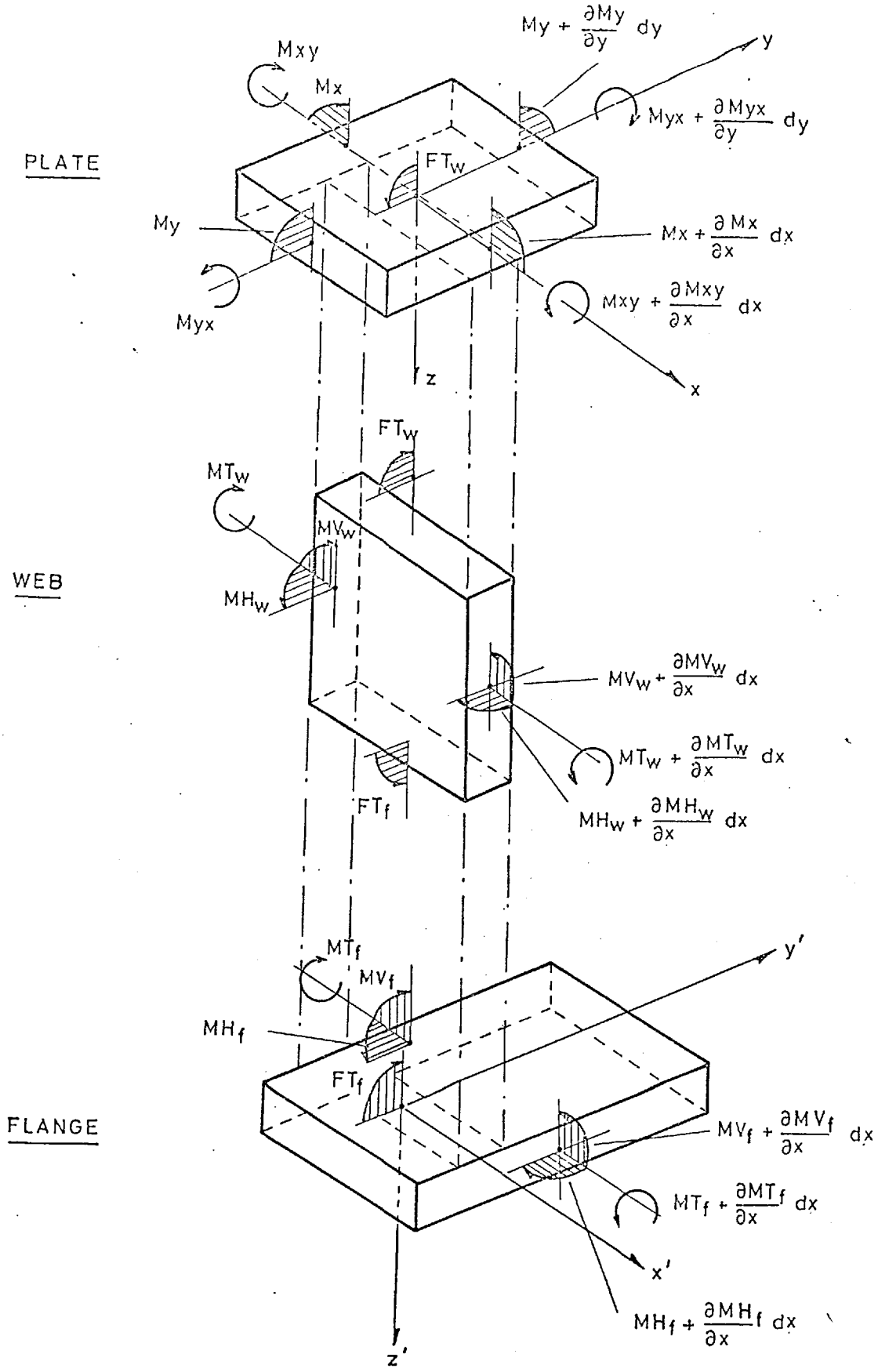

Fig A4 Moments in a deformed element of stiffened plate

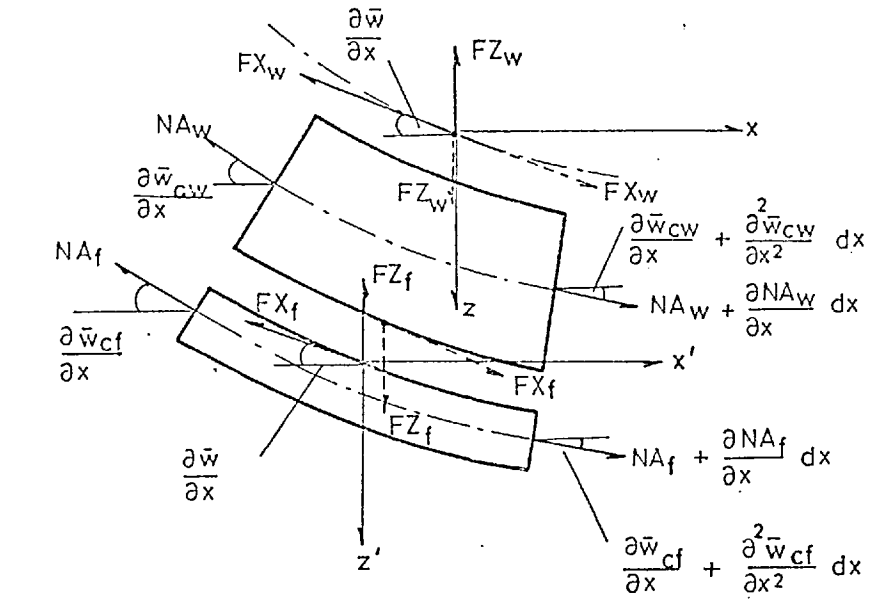

PLANE - XZ AND X'Z'

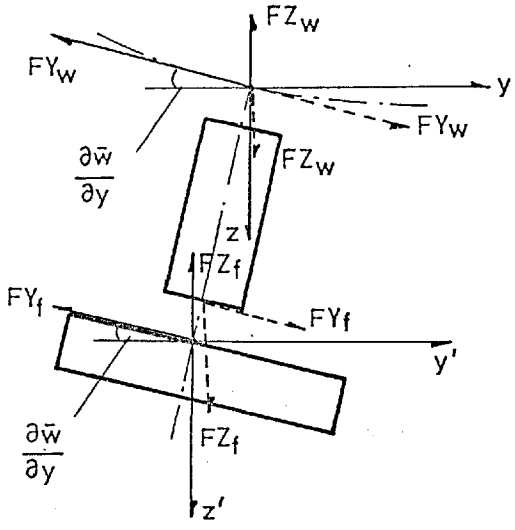

PLANE - YZ AND Y'Z'

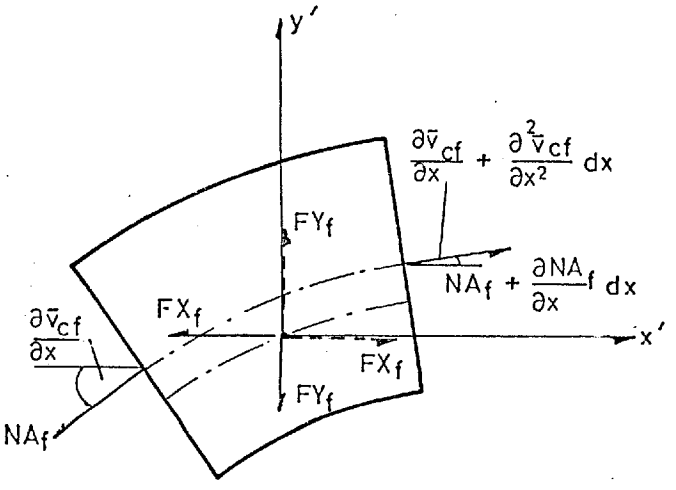

PLANE - X'Y'

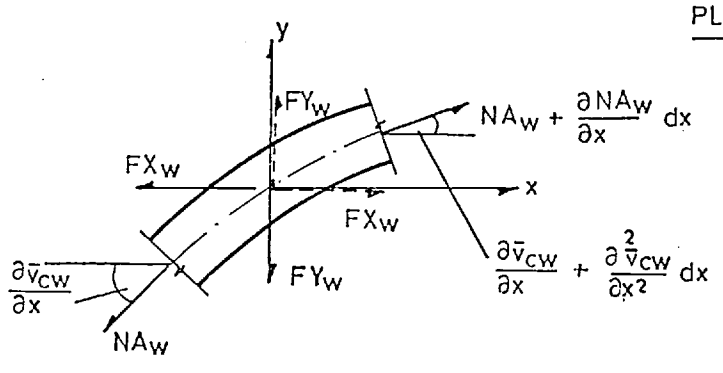

PLANE - XY

Fig A5 Stiffener axial and interactive forces shown relative to the fixed co-ordinate system

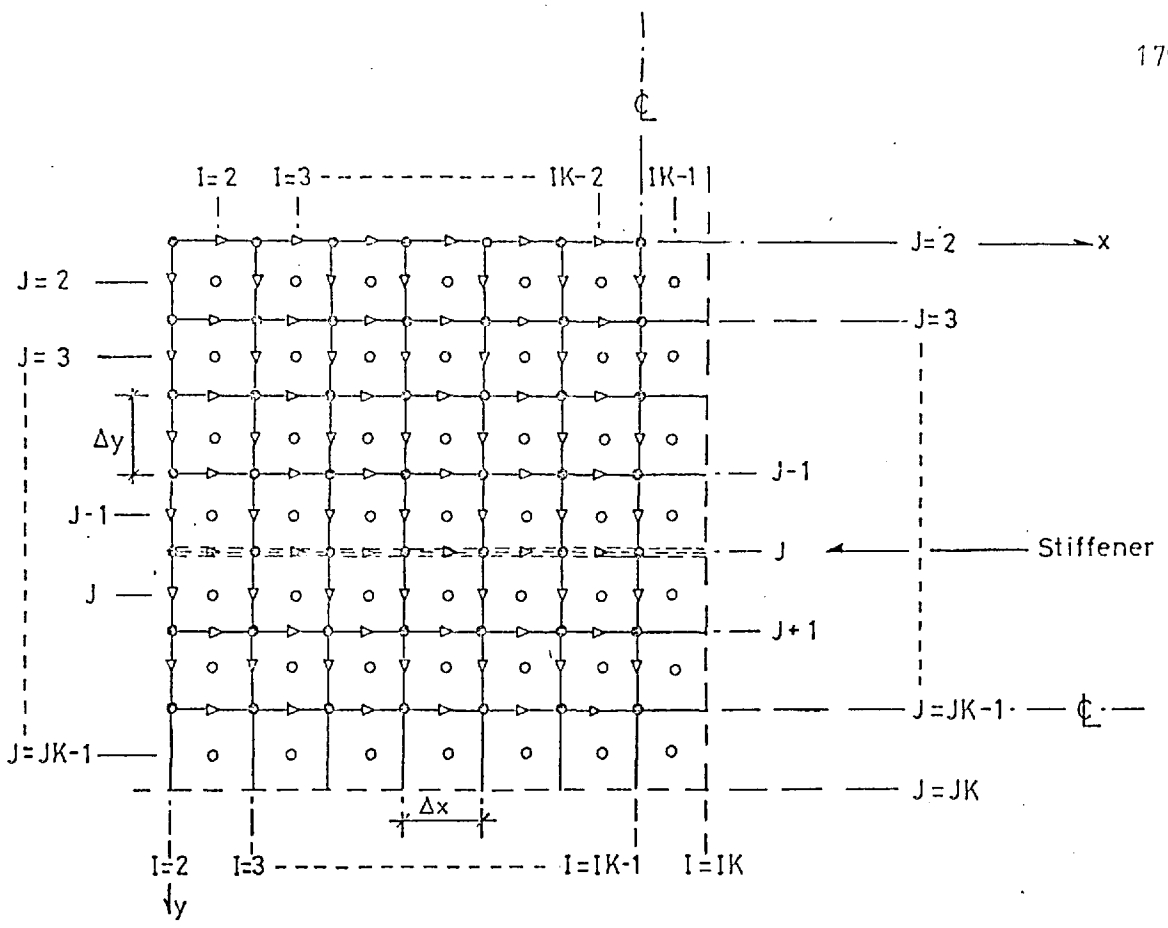

NODE TYPE	SYMBOL	DISPLACEMENTS	FORCES
MAIN	•	W	Nx, Ny, Mx, My FY_w, FZ_w, FT_w
INTER-LACING	○		Nxy Mxy
U NODES	→	U	FX_w
V NODES	↓	V	

THE INTERLACING MESH SYSTEM

Fig B1

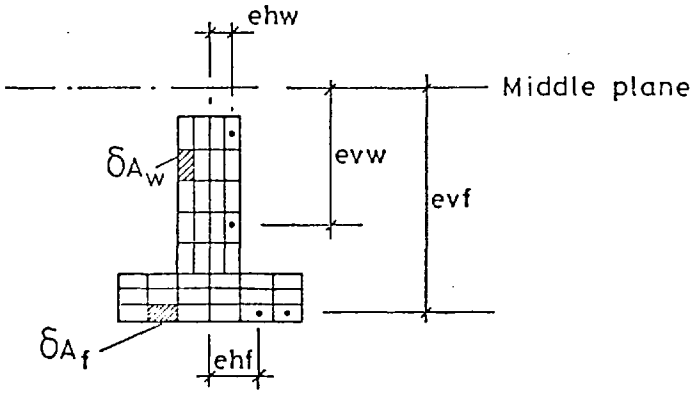

STIFFENER DIVIDED INTO ELEMENTS FOR ELASTO-PLASTIC ANALYSIS

Fig B2

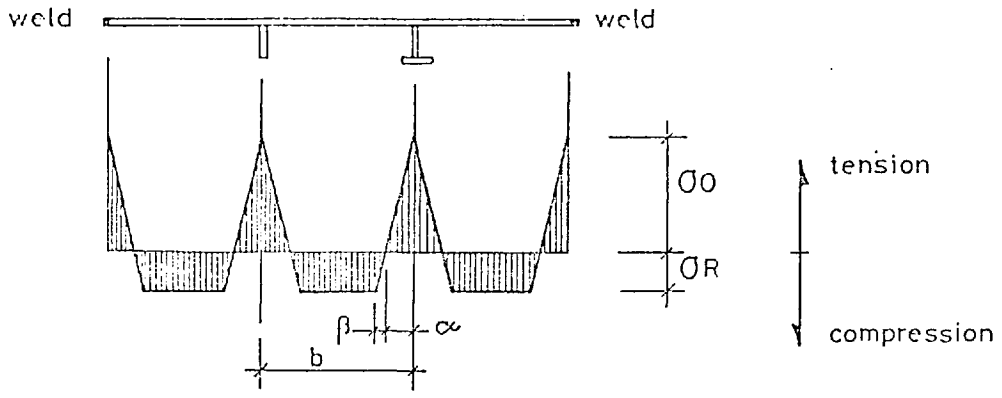

$$\beta = (b \cdot \sigma R^2) / (\sigma 0 + \sigma R)^2 \; ; \quad \alpha = (\beta \cdot \sigma 0) / (\sigma R)$$

PLATE RESIDUAL STRESSES

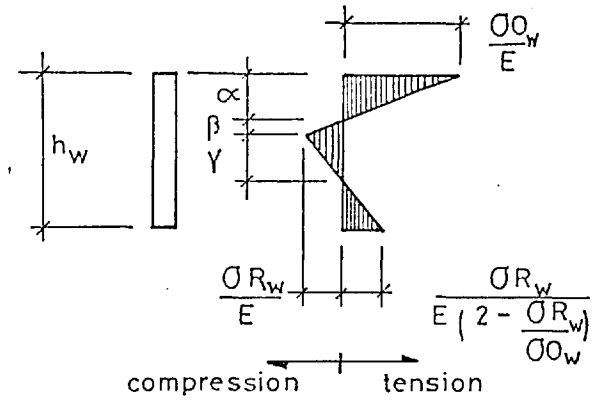

$$\alpha = \frac{h_w \, \sigma R_w}{2 (\sigma 0_w + \sigma R_w)}$$

$$\beta = \frac{h_w \, \sigma R_w^2}{2 \, \sigma 0_w (\sigma 0_w + \sigma R_w)}$$

$$\gamma = \frac{h_w (2\sigma 0_w - \sigma R_w)^2}{2 \, \sigma 0_w (3 \sigma 0_w - \sigma R_w)}$$

RESIDUAL STRAINS FOR FLAT

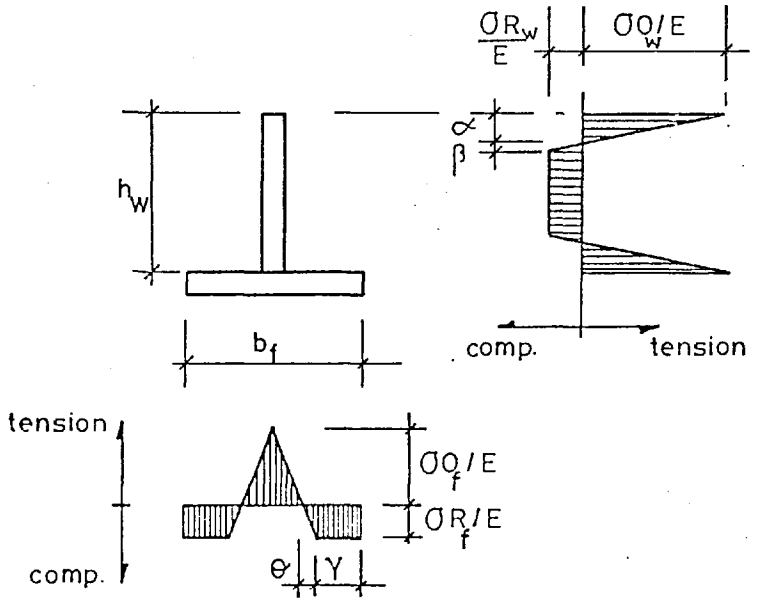

$$\beta = \frac{h_w \, \sigma R_w^2}{(\sigma 0_w + \sigma R_w)^2}$$

$$\alpha = \frac{\beta \, \sigma 0_w}{\sigma R_w}$$

$$\gamma = \frac{b_f (\sigma 0_f - \sigma R_f)}{2 (\sigma R_f + \sigma 0_f)}$$

$$\theta = \frac{b_f \, \sigma R_f^2}{(\sigma R_f + \sigma 0_f)^2}$$

RESIDUAL STRAINS FOR 'T' SECTION

Fig B3 Residual stress patterns (ref. 13)

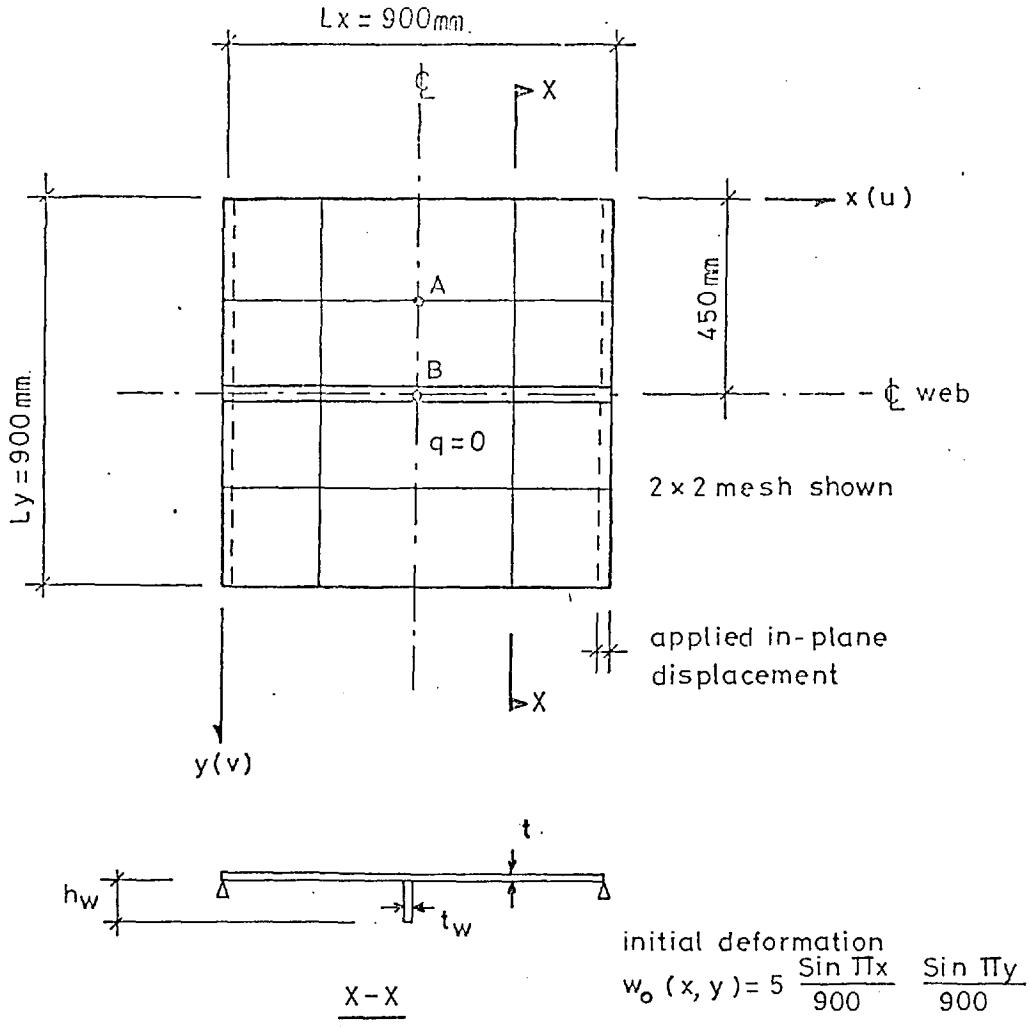

GEOMETRY (mm)							
b/t = 45 Lx/R = 84·3				b/t = 75 Lx/R = 32·2			
b	t	h_w	t_w	b	t	h_w	t_w
450	10	60	6	450	6	100	10

Material properties	
σ_0	250 N/mm^2
σ_{0_w}	250 N/mm^2
E	205000N/mm^2
ν	·3

Boundary conditions	
y = 0	w = My = 0 Ny = Nxy = 0
x = 0	w = Mx = V = 0 u = applied

Fig B4 Stiffened plate arrangement for Figs B5, B6 and B7

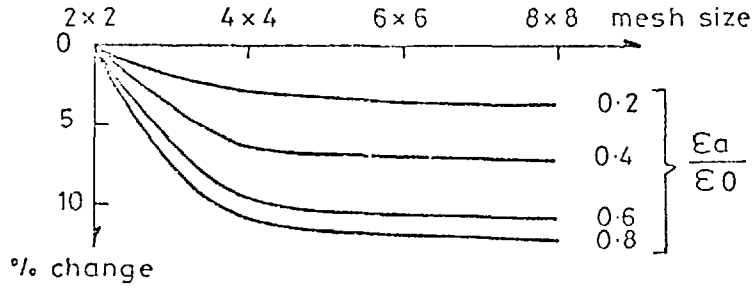

b/t	45·0
Lx/R	84·3

PANEL DEFLECTION AT 'A'

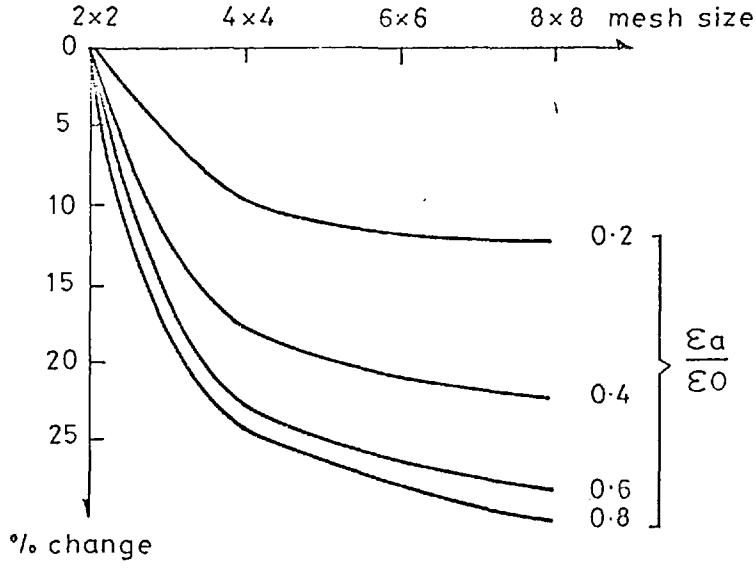

b/t	75·0
Lx/R	32·2

PANEL DEFLECTION AT 'A'

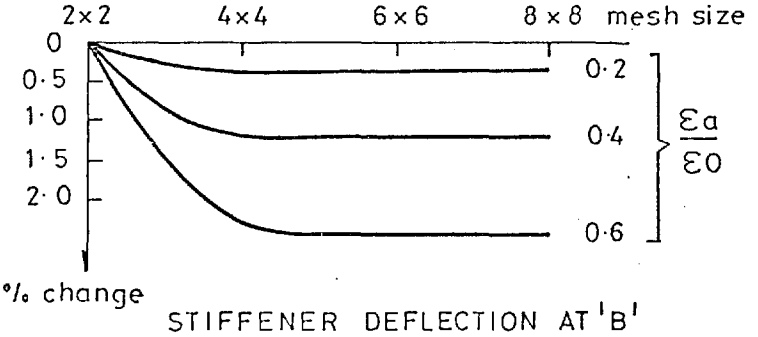

b/t	45·0
Lx/R	84·3

STIFFENER DEFLECTION AT 'B'

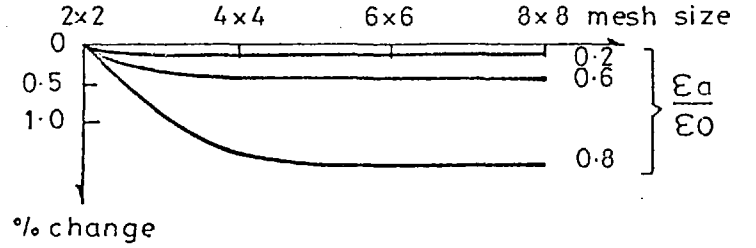

b/t	75·0
Lx/R	32·2

STIFFENER DEFLECTION AT 'B'

Fig B5 Percentage change in deflection resulting from a refinement of the basic 2 × 2 mesh

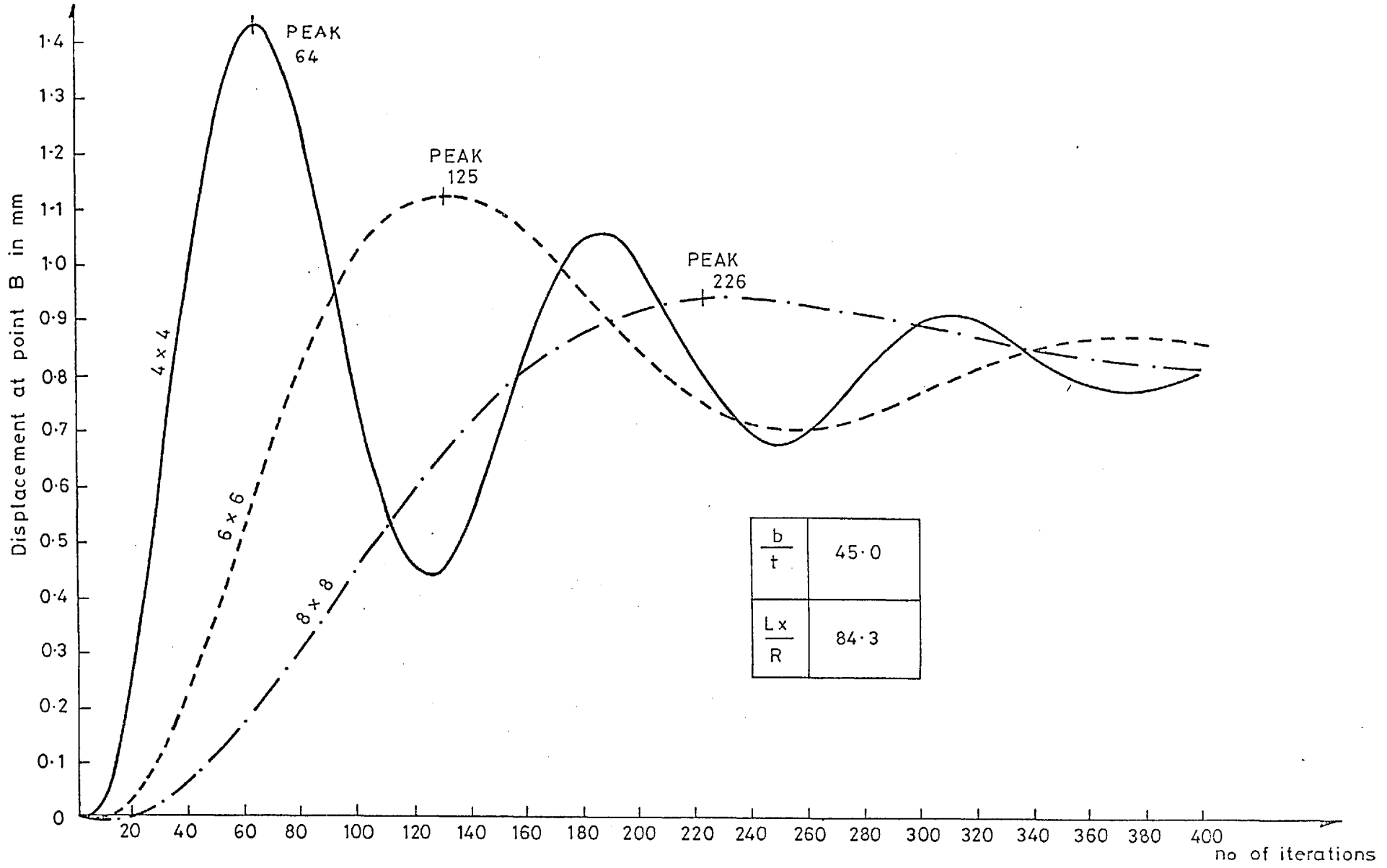

Fig B6 · Undamped oscillations at the stiffener location 'B' for three different mesh sizes

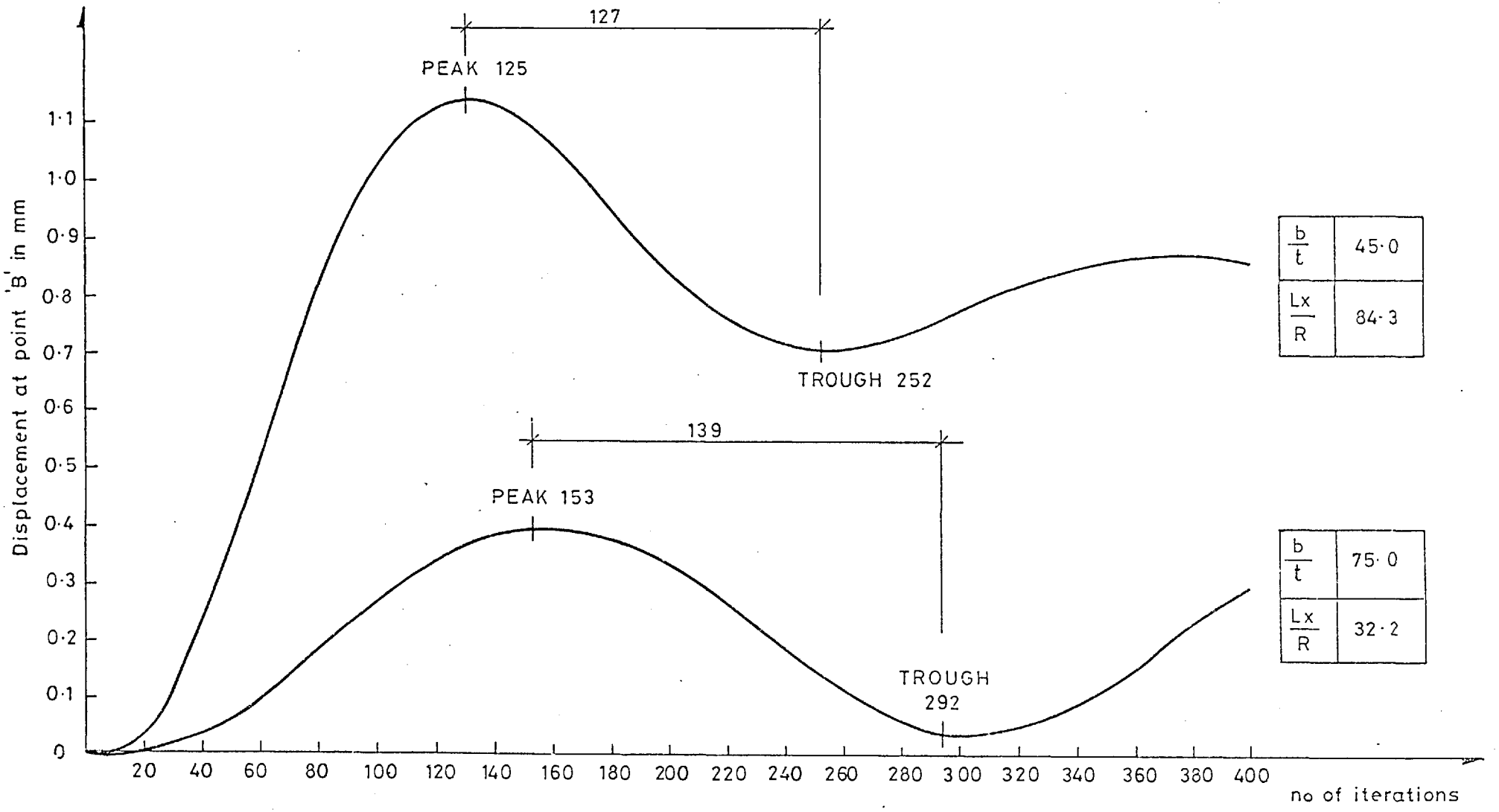

Fig B7 Undamped oscillations at the stiffener location 'B' for two different geometrical arrangements

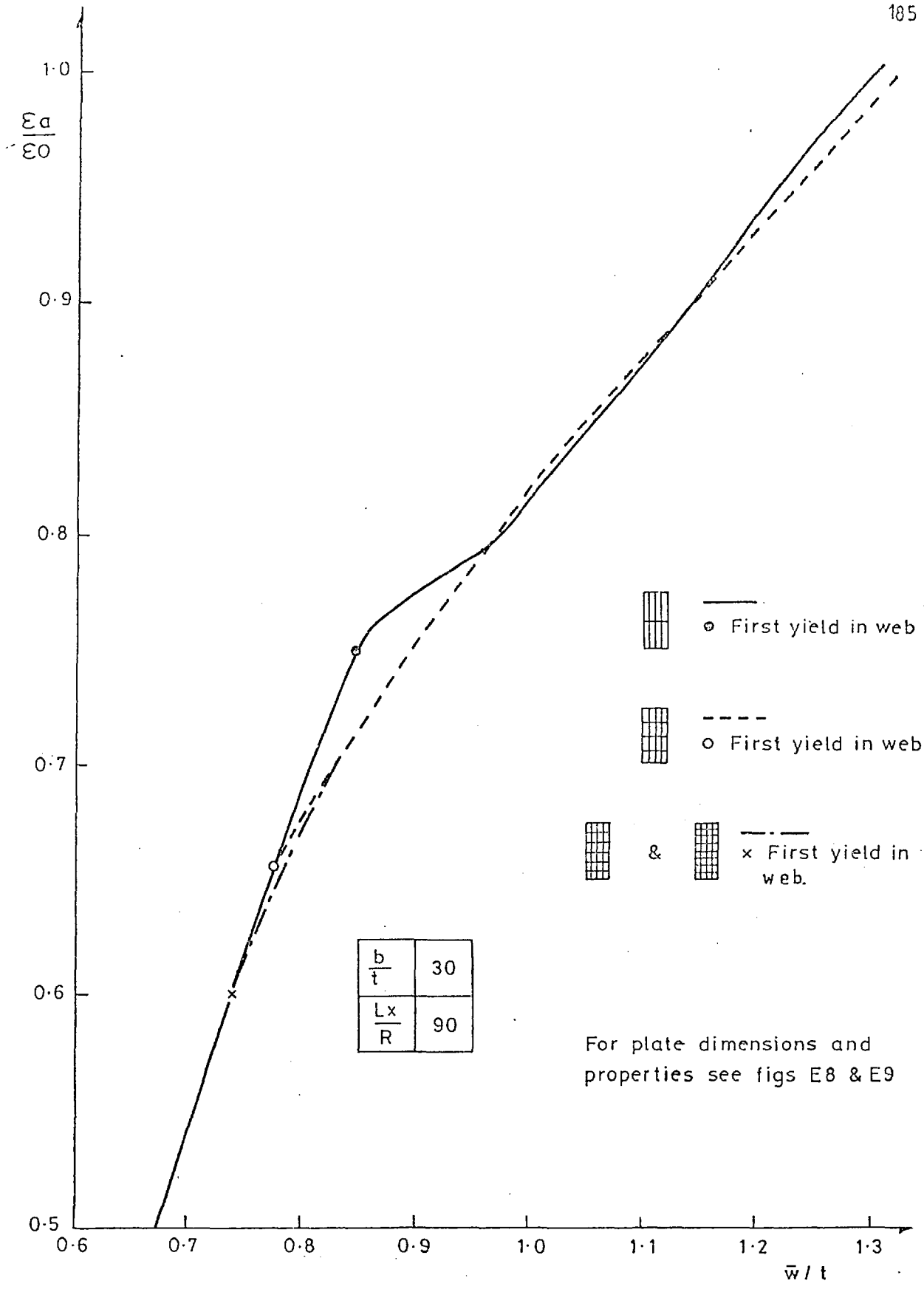

Fig B8 Variation of the load-deflection path with an increase in the number of web elements

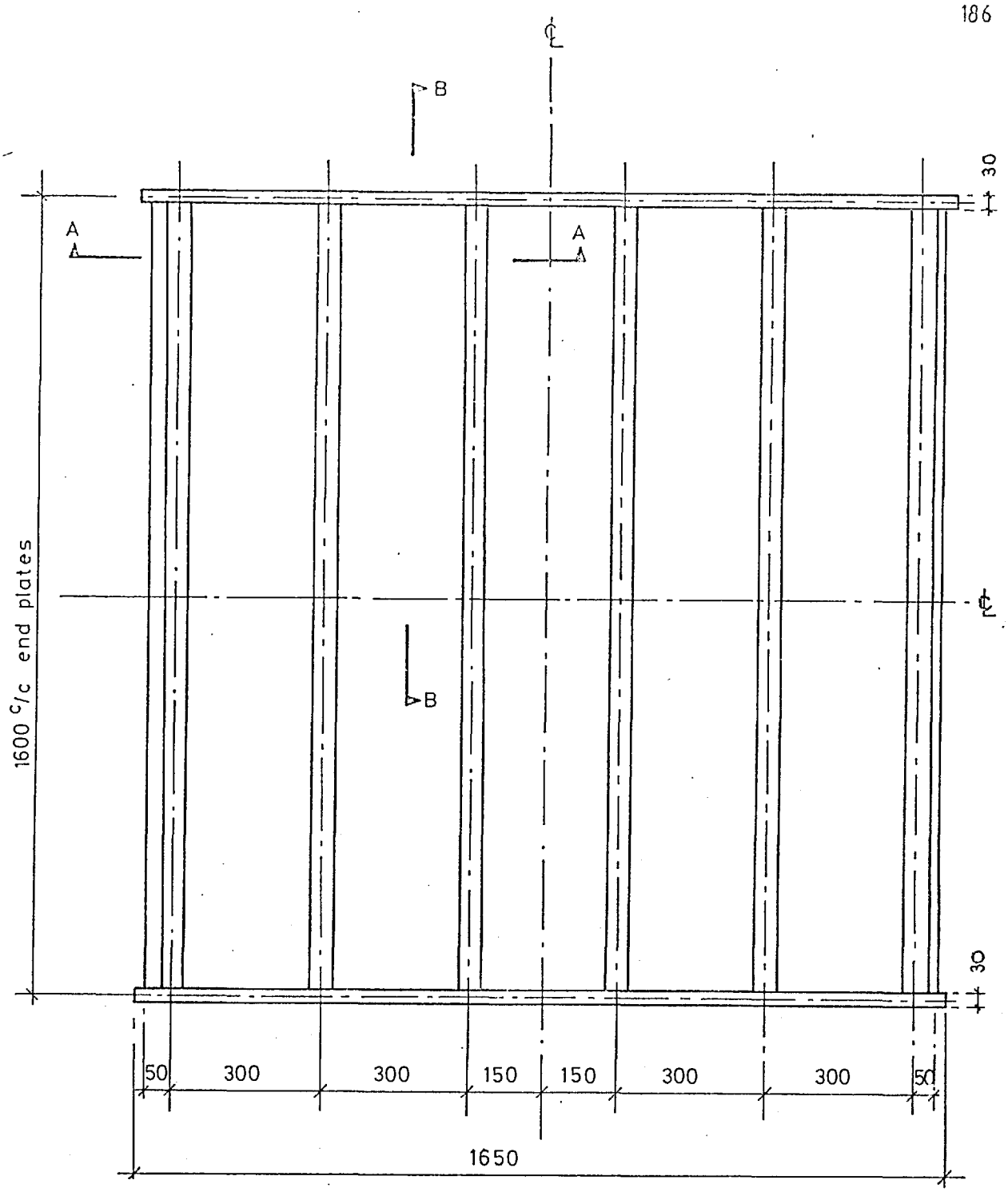

see fig. C2 for cross sections

Fig. C1 Plan of stiffened plate models SP1, SP2 & SP3

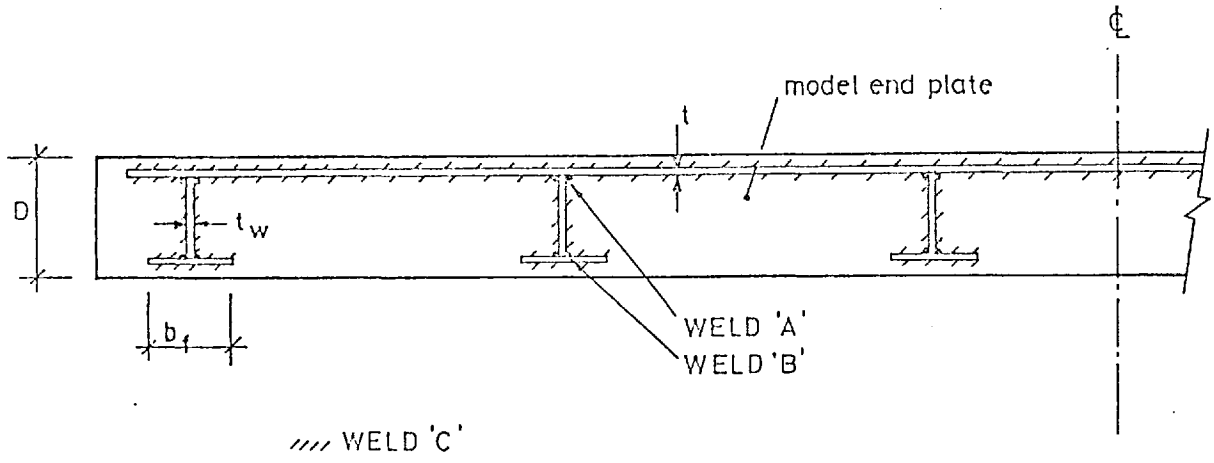

SECTION A-A

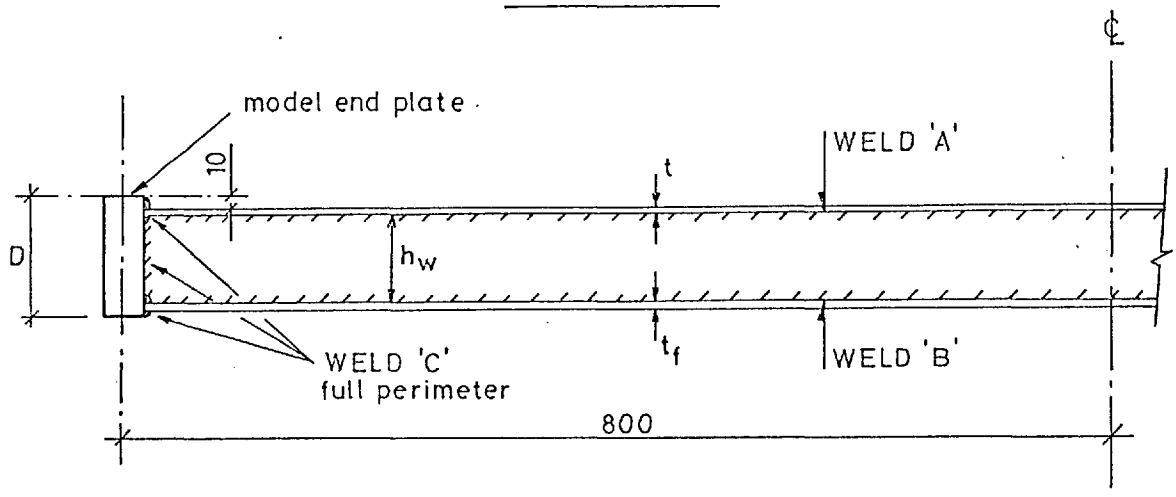

SECTION B-B

MODEL No.	t mm	h_w mm	t_w mm	b_f mm	t_f mm	DEPTH D mm	WELD A mm	WELD B mm	WELD C mm
SP 1	5·0	50·0	5·0	60·0	5·0	80·0	3·0	3·0	8·0
SP 2	5·0	55·0	8·0	50·0	8·0	90·0	3·0	5·0	8·0
SP 3	5·0	70·0	8·0	70·0	8·0	100·0	3·0	5·0	8·0

Fig C2. Stiffened plate models

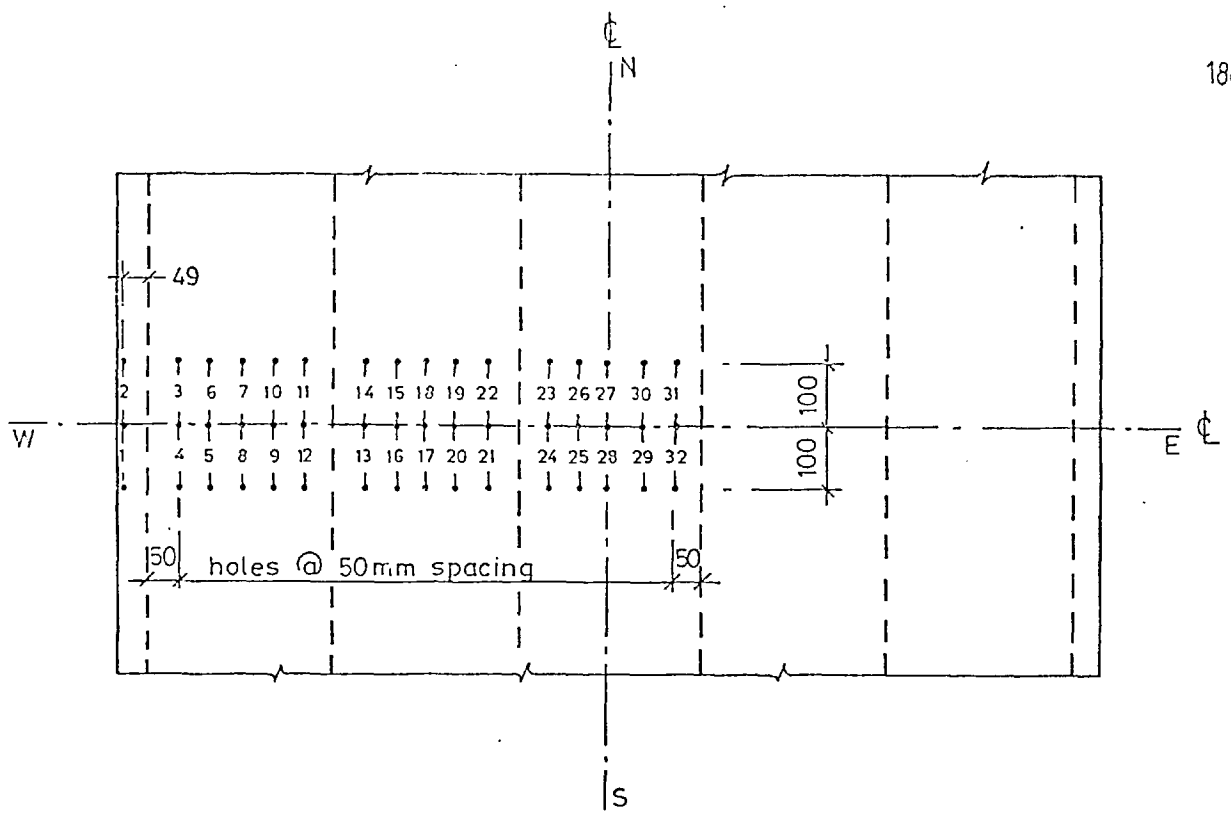

LONGITUDINAL RESIDUAL STRAIN MEASUREMENT POSITIONS
(Unstiffened side shown)

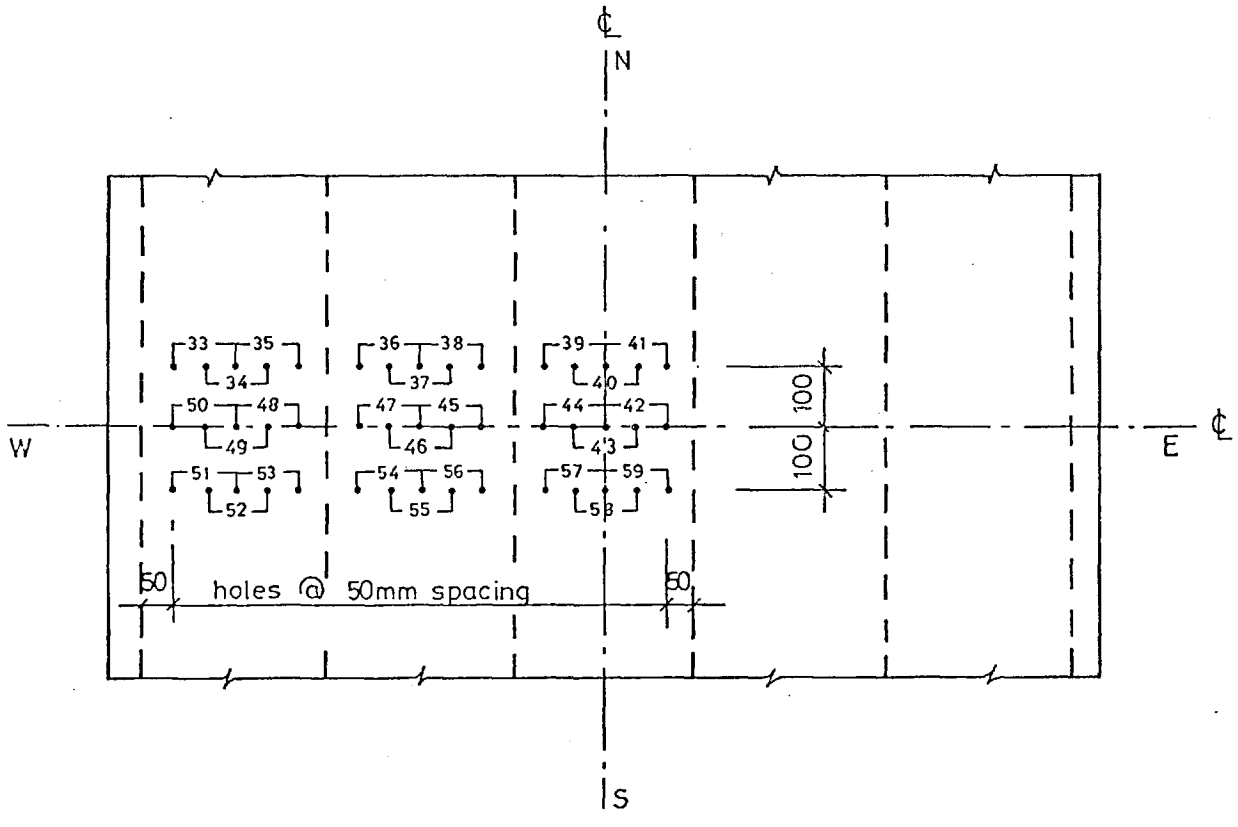

TRANSVERSE RESIDUAL STRAIN MEASUREMENT POSITIONS
(Unstiffened side shown)

Fig C3.

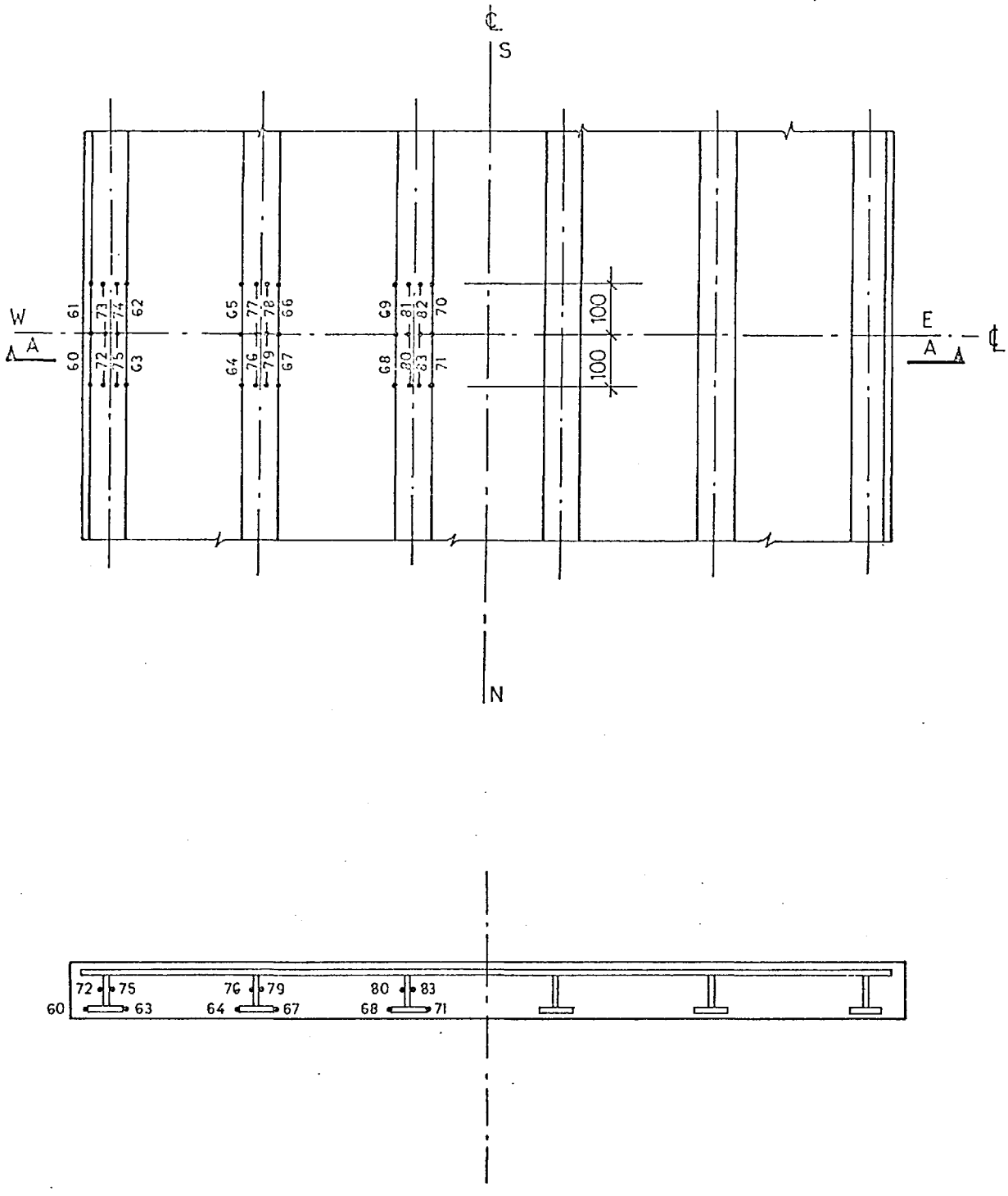

SECTION A-A

Fig C4. Stiffener residual strain measurement positions

Ref No.	Stiffened Side			Unstiffened Side			Mean Diff.	Corrected Mean Diff.	Centre Line Average Diff.
	Before Weld.	Diff.	After Weld.	Before Weld.	Diff.	After Weld.			
D	1451	+1	1452	1452	0	1452	+1	Mean Diff. -2	
TC1	0815	0	0815	0815	0	0815	0		
TC2	0864	+1	0865	0863	+2	0865	+2		
TC3	0938	+1	0939	0939	+2	0941	+2		
TC4	0721	-1	0720	0720	+7	0727	+3		
* 1	0759	-40	0719	0808	+17	0825	-12	-14	-14
* 2	0594	-24	0570	0917	+3	0920	-11	-13	
* 3	0956	-32	0924	0791	+12	0803	-10	-12	-10
* 4	0798	-26	0772	0917	+17	0934	-5	-7	
5	1010	-26	0984	0836	+14	0850	-6	-8	-8
6	0715	-24	0691	0800	+12	0812	-6	-8	
7	0877	-21	0856	0743	+10	0753	-6	-8	-7
8	0932	-23	0909	0794	+17	0811	-3	-5	
9	1096	-23	1073	0791	+10	0801	-7	-9	-10
10	0566	-26	0540	0815	+10	0825	-8	-10	
*11	0742	-27	0715	0740	+13	0753	-7	-9	-10
*12	1029	-26	1003	0869	+10	0879	-8	-10	
*13	1281	-19	1262	0860	+7	0867	-6	-8	-8
*14	0367	-20	0347	0799	+10	0809	-5	-7	
15	0550	-25	0525	0889	+10	0899	-8	-10	-12
16	1086	-21	1065	0828	0	0828	-11	-13	
17	0901	-17	0884	0861	+5	0866	-6	-8	-10
18	0563	-21	0542	0960	+4	0964	-9	-11	
19	0709	-19	0690	0888	+3	0891	-8	-10	-10
20	0829	-16	0813	0903	+2	0905	-7	-9	
*21	1200	-19	1181	0869	+4	0873	-8	-10	-12
*22	0674	-18	0656	0954	-6	0948	-12	-14	
*23	1017	-26	0991	1186	-2	1184	-14	-16	-13
*24	1056	-14	1042	0739	-1	0738	-8	-10	
25	1092	-17	1075	0759	+1	0760	-8	-10	-11
26	0815	-16	0799	1152	-3	1149	-10	-12	
27	-	-	-	-	-	-	-	-	-
28	-	-	-	-	-	-	-	-	
29	0823	-17	0806	0839	-3	0836	-10	-12	-12
30	0802	-14	0788	0920	-5	0915	-10	-12	
*31	1005	-22	0983	0937	-4	0933	-13	-15	-11
*32	0680	-6	0674	0892	-3	0889	-5	-7	

* Suspect readings close to stiffeners

TC = Temperature compensation

D = Dummy

True strain = Diff. × 2.02 × 10^{-5}

Fig. C5

Model SP1 Longitudinal residual strains

Ref No.	Stiffened Side			Unstiffened Side			Mean Diff.	Corrected Mean Diff.	Centre Line Average Diff.
	Before Weld.	Diff.	After Weld.	Before Weld.	Diff.	After Weld.			
D	1452	0	1452	1453	-1	1452	-1	Mean Diff. +3	
TC1	0816	-1	0815	0817	-2	0815	-2		
TC2	0866	-3	0863	0867	-4	0863	-4		
TC3	0939	0	0939	0941	-2	0939	-1		
TC4	0716	-1	0715	0721	-6	0715	-4		
* 1	0891	-37	0854	1077	+11	1088	-13	-10	-10
* 2	0821	-29	0792	0410	+4	0414	-13	-10	
* 3	0898	-22	0876	0678	+5	0683	-9	-6	-6
* 4	0753	-34	0719	0918	+19	0937	-8	-5	
5	0760	-26	0734	0973	+16	0989	-5	-2	-2
6	0876	-18	0858	0657	+9	0666	-5	-2	
7	0948	-22	0926	0669	+5	0674	-9	-6	-5
8	0679	-27	0652	0975	+15	0990	-6	-3	
9	0776	-29	0747	0967	+16	0983	-7	-4	-4
10	0802	-19	0783	0743	+8	0751	-6	-3	
*11	0949	-18	0931	0680	+5	0685	-7	-4	-4
*12	0743	-31	0712	0926	+17	0943	-7	-4	
*13	0722	-29	0693	0824	+11	0835	-9	-6	-5
*14	0837	-20	0817	0777	+7	0784	-7	-4	
15	0843	-23	0820	0944	+5	0949	-9	-6	-5
16	0779	-22	0757	0725	+9	0734	-7	-4	
17	0576	-25	0551	0964	+7	0971	-9	-6	-5
18	1074	-19	1055	0964	+6	0700	-7	-4	
19	0988	-50	0938	0624	0	0624	-25	-22	-14
20	0689	-19	0670	0972	+4	0976	-8	-5	
*21	0695	-21	0674	0763	+1	0764	-10	-7	-8
*22	0949	-24	0925	0855	+2	0857	-11	-8	
*23	1120	-19	1101	0969	+4	0973	-8	-5	-5
*24	0665	-12	0653	0713	-2	0711	-7	-4	
25	0535	-15	0520	0723	-1	0722	-8	-5	-5
26	1000	-15	0985	0877	+1	0878	-7	-4	
27	-	-	-	-	-	-	-	-	-
28	-	-	-	-	-	-	-	-	
29	0393	-71	0322	0853	-5	0848	-38	-35	-19
30	1220	-11	1209	0812	-1	0811	-6	-3	
*31	1119	-16	1103	0461	0	0461	-8	-5	-7
*32	0482	-13	0469	1206	-8	1198	-11	-8	

* Suspect readings close to stiffeners

TC = Temperature compensation

D = Dummy

True strain = Diff. × 2.02 × 10^{-5}

Fig. C6

Model SP2 Longitudinal residual strains

Ref No.	Stiffened Side			Unstiffened Side			Mean Diff.	Corrected Mean Diff.	Centre Line Average Diff.
	Before Weld.	Diff.	After Weld.	Before Weld.	Diff.	After Weld.			
D	1454	-1	1453	1452	+1	1453	0	Zero Correction	
TC1	0818	-1	0817	0816	+1	0817	0		
TC2	0869	-4	0865	0867	+1	0868	-2		
TC3	0941	+1	0942	0939	+1	0940	+1		
TC4	0720	+1	0721	0719	+2	0721	+2		
* 1	0698	-40	0658	0865	+2	0867	-19		-17
* 2	1111	-20	1091	0819	-7	0812	-14		
* 3	0891	-16	0875	0873	+8	0881	-4		-5
* 4	0960	-24	0936	0949	+15	0964	-5		
5	0896	-25	0871	0746	+14	0760	-6		-2
6	0949	+1	0950	0910	+2	0912	+2		
7	1023	-21	1002	0943	+11	0954	-5		-4
8	0837	-24	0813	0856	+18	0874	-3		
9	0935	-88	0847	0803	+17	0820	-35		-23
10	0864	-12	0852	0909	-7	0902	-10		
*11	0898	-14	0884	0948	+5	0953	-5		-5
*12	0875	-30	0845	0764	+21	0785	-5		
*13	0826	-26	0800	0772	+16	0788	-5		-5
*14	0910	-10	0900	1112	+2	1114	-4		
15	0900	-8	0892	0931	+4	0935	-2		-3
16	0875	-22	0853	0814	+15	0829	-4		
17	0749	-20	0729	0835	+28	0863	+4		-12
18	1105	-55	1050	0671	+1	0672	-27		
19	0949	+122	1071	0819	+8	0827	+65		+17
20	0804	-81	0723	0789	+20	0809	-31		
*21	0767	-29	0738	0762	+16	0778	-7		-4
*22	0953	-7	0946	0855	+5	0860	-1		
*23	1207	-12	1195	0821	0	0821	-6		-4
*24	0736	-17	0719	0657	+13	0670	-2		
25	0749	-11	0738	0784	+11	0795	0		0
26	0946	-6	0940	0853	+6	0859	0		
27	-	-	-	-	-	-	-		-
28	-	-	-	-	-	-	-		
29	0945	-17	0928	0861	+1	0862	-8		-6
30	0745	-6	0739	0757	-1	0756	-4		
*31	0688	-5	0683	0637	-2	0635	-4		-10
*32	0978	-31	0947	1033	-1	1032	-16		

* Suspect readings close to stiffeners

TC = Temperature compensation

D = Dummy

True strain = Diff. × 2.02 × 10^{-5}

Fig. C7

Model SP3 Longitudinal residual strains

Ref No.	Stiffened Side			Unstiffened Side			Mean Diff.	Corrected Mean Diff.
	Before Weld.	Diff.	After Weld.	Before Weld.	Diff.	After Weld.		
D	1451	+1	1452	1452	0	1452	+1	Mean Diff. -2
TC1	0815	0	0815	0815	0	0815	0	
TC2	0864	+1	0865	0863	+2	0867	+2	
TC3	0938	+1	0939	0939	+2	0941	+2	
TC4	0721	-1	0720	0729	+7	0727	+3	
33	1035	+10	1045	1006	+1	1007	+6	+4
34	0511	+11	0522	0819	-1	0818	+5	+3
35	0697	+20	0717	0808	-5	0803	+8	+6
36	0631	+20	0651	0841	-13	0828	+4	+2
37	0982	+20	1002	0248	-15	0233	+3	+1
38	0917	+24	0941	0825	-15	0810	+5	+3
39	0400	+19	0419	0544	-5	0539	+7	+5
40	0350	+18	0368	0355	-6	0349	+6	+4
41	0802	+26	0828	0930	-15	0915	+6	+4
42	-	-	-	-	-	-	-	-
43	0355	+18	0373	0524	-15	0509	+2	0
44	-	-	-	-	-	-	-	-
45	1140	+19	1159	0965	-17	0948	+1	-1
46	0983	+23	1006	0180	-15	0165	+4	+2
47	0520	+21	0541	0369	-16	0353	+3	+1
48	0816	+16	0832	0835	-10	0825	+3	+1
49	0572	+13	0585	0840	-10	0830	+2	0
50	0763	+10	0773	1005	-4	1001	+3	+1
51	0841	+3	0844	0999	+1	1000	+2	0
52	0575	+14	0589	0823	-8	0815	+3	+1
53	0784	+13	0797	0749	-9	0740	+2	0
54	0592	+20	0612	0366	-13	0353	+4	+2
55	0954	+19	0973	0247	-17	0230	+1	-1
56	1191	+22	1213	0901	-15	0886	+4	+2
57	0198	+17	0215	0716	-17	0699	0	-2
58	0429	+19	0448	0443	-13	0430	+3	+1
59	1126	+19	1145	1145	-16	1031	+2	0

TC = Temperature compensation

D = Dummy

True strain = Diff. × 2.02×10^{-5}

Fig. C8

Model SP1 Transverse residual strains

Ref No.	Stiffened Side			Unstiffened Side			Mean Diff.	Corrected Mean Diff.
	Before Weld.	Diff.	After Weld.	Before Weld.	Diff.	After Weld.		
D	1452	0	1452	1453	-1	1452	-1	Mean Diff. +3
TC1	0816	-1	0815	0817	-2	0815	-2	
TC2	0866	0	0866	0867	-4	0863	-2	
TC3	0939	+1	0940	0941	-2	0939	-1	
TC4	0716	-1	0715	0721	-6	0715	-4	
33	0818	+6	0824	0680	+1	0681	+4	+7
34	0824	+9	0833	0918	-4	0914	+3	+6
35	0860	+12	0872	0864	-13	0851	-1	+2
36	0958	+21	0979	0710	-13	0697	+4	+7
37	0577	+15	0592	0641	-19	0622	-2	+1
38	0828	+13	0841	0658	-14	0644	-1	+2
39	1023	+21	1044	0897	-18	0879	+2	+5
40	0930	+23	0953	0906	-19	0887	+2	+5
41	0862	+17	0879	0786	-21	0765	-2	+1
42	-	-	-	-	-	-	-	-
43	1019	+22	1041	1120	-24	1096	-1	+2
44	-	-	-	-	-	-	-	-
45	0500	+16	0516	0768	-16	0752	0	+3
46	0660	+19	0679	0786	-21	0765	-1	+2
47	0928	+16	0944	0576	-19	0557	-2	+1
48	0900	+25	0925	1132	-17	1115	+4	+7
49	0731	+12	0743	0885	-15	0870	-2	+1
50	0715	+10	0725	0433	-8	0425	+1	+4
51	0878	+14	0892	0603	-9	0594	+3	+6
52	0691	+19	0710	0807	-17	0790	+1	+4
53	0594	+23	0617	0945	-21	0924	+1	+4
54	0712	+20	0732	0596	-52	0544	-16	-13
55	0549	+21	0570	0832	-17	0815	+2	+5
56	0496	+19	0515	0763	-20	0743	-1	+2
57	0886	+28	0914	0916	-19	0897	+5	+8
58	0969	+27	0996	0886	-18	0868	+5	+8
59	1110	+23	1133	0610	-22	0588	+1	+4

TC = Temperature compensation

D = Dummy

True strain = Diff. $\times$ 2.02 $\times$ 10^{-5}

Fig. C9

Model SP2 Transverse residual strains

Ref No.	Stiffened Side			Unstiffened Side			Mean Diff.	Corrected Mean Diff.
	Before Weld.	Diff.	After Weld.	Before Weld.	Diff.	After Weld.		
D	1454	-1	1453	1452	+1	1453	0	Zero Correction
TC1	0818	-1	0817	0816	+1	0817	0	
TC2	0869	-4	0865	0867	+1	0868	-2	
TC3	0941	+1	0942	0939	+1	0940	+1	
TC4	0720	+1	0721	0719	+3	0721	+2	
33	0831	0	0831	0141	+14	0155	+7	
34	0814	-3	0811	0532	+11	0543	+4	
35	0919	+6	0925	0960	+1	0961	+4	
36	0766	-27	0739	0698	+3	0701	-12	
37	0797	0	0797	0566	0	0566	0	
38	0962	-3	0959	0598	+5	0603	+1	
40	0694	+12	0706	0759	-6	0753	+3	
41	0734	+11	0745	0876	-96	0780	-43	
42	-	-	-	-	-	-	-	
43	0764	+5	0769	0760	-15	0745	-5	
44	-	-	-	-	-	-	-	
45	1108	+3	1111	0576	+10	0586	+7	
46	0859	-15	0844	0704	-5	0699	-10	
47	0588	+12	0600	0809	0	0809	+6	
48	0934	+10	0944	1090	+4	1094	+7	
49	0916	-60	0856	0543	-1	0542	-31	
50	0721	+6	0727	0137	+7	0144	+7	
51	0858	+13	0871	0394	+12	0406	+13	
52	0775	+16	0791	0682	-1	0681	+8	
53	0909	+12	0921	0959	-6	0953	+3	
54	0947	+9	0956	0607	+5	0612	+7	
55	0984	+6	0990	0810	+4	0814	+5	
56	0695	+2	0697	0822	-7	0815	-3	
57	0576	+23	0599	0893	-13	0880	+5	
58	0630	+20	0650	0553	-10	0543	+5	
59	0866	-14	0852	0503	+5	0508	-5	
39	0722	+9	0731	0774	-3	0771	+3	

TC = Temperature compensation

D = Dummy

True strain = Diff. × 2.02 × 10^{-5}

Fig. C10

Model SP3 Transverse residual strains

Ref No.	Before Weld. (A)	After Web/Flg. Weld & Straight (B)	After Weld to Plate (C)	Diff. (B)-(A)	Diff. (C)-(B)	Diff. (C)-(A)	Corrected Diff. (C)-(A)	Centre Line Average Diff.
D	1453	1451	1454	-2	+3	+1	Diff. -2	
TC1	0816	0814	0817	-2	+3	+1		
TC2	0866	0865	0867	-1	+2	+1		
TC3	0940	0938	0942	-2	+4	+2		
TC4	0717	0716	0719	-1	+3	+2		
60	0888	0856	0875	-32	+19	-13	-15	-13
61	0847	0817	0838	-30	+21	-9	-11	
62	0857	0824	0829	-33	+5	-28	-30	-28
63	0786	0755	0762	-31	+7	-24	-26	
64	0787	0758	0761	-29	+3	-26	-28	-38
65	0921	0885	0875	-36	-10	-46	-48	
66	0821	0790	0790	-31	0	-31	-33	-40
67	0891	0862	0847	-29	-15	-44	-46	
68	0840	0809	0820	-31	+11	-20	-22	-26
69	0820	0781	0792	-39	+11	-28	-30	
70	0841	0811	0803	-30	-8	-38	-40	-25
71	0931	0937	0923	+6	-14	-8	-10	

TC = Temperature compensation; D = Dummy; True strain = $2.02 \times \text{Diff.} \times 10^{-5}$

Model SP1 Stiffener residual strains

Ref No.	Before Weld. (A)	After Web/Flg. Weld & Straight (B)	After Weld to Plate (C)	Diff. (B)-(A)	Diff. (C)-(B)	Diff. (C)-(A)	Corrected Diff. (C)-(A)	Centre Line Average Diff.
D	1456	1453	1453	-3	0	-3	Diff. +2	
TC1	0821	0817	0819	-4	+2	-2		
TC2	0871	0873	0870	+2	-3	-1		
TC3	0945	0942	0944	-3	+2	-1		
TC4	0724	0719	0721	-5	+2	-3		
60	0939	0866	0869	-73	+3	-70	-68	-63
61	0722	0657	0663	-65	+6	-59	-57	
62	0795	0749	0751	-46	+2	-44	-42	-41
63	0874	0834	0832	-40	-2	-42	-40	
64	1015	0919	0908	-96	-11	-107	-105	-101
65	0814	0713	0715	-101	+2	-99	-97	
66	0836	0781	0779	-55	-2	-57	-55	-50
67	0875	0835	0829	-40	-6	-46	-44	
68	0918	0830	0830	-88	0	-88	-86	-66
69	0743	0696	0695	-47	-1	-48	-46	
70	0825	0791	0791	-34	0	-34	-32	-37
71	0850	0806	0807	-44	+1	-43	-41	

TC = Temperature compensation; D = Dummy; True strain = $2.02 \times \text{Diff.} \times 10^{-5}$

Model SP2 Stiffener residual strains

Fig. C11

Ref No.	Before Weld. (A)	After Web/Flg. Weld & Straight (B)	After Weld to Plate (C)	Diff. (B)-(A)	Diff. (C)-(B)	Diff. (C)-(A)	Corrected Diff. (C)-(A)	Centre Line Average Diff.	
D	1456	1453	1454	-3	+1	-2	Diff. +2		
TC1	0820	0817	0818	-3	+1	-2			
TC2	0871	0870	0868	-1	-2	-3			
TC3	0943	0942	0942	-1	0	-1			
TC4	0721	0720	0719	-1	-1	-2			
60	0816	0780	0811	-36	+31	-5	-3	-10	Flange
61	0871	0833	0853	-38	+20	-18	-16		
62	0824	0795	0818	-29	+23	-6	-4	-27	
63	0889	0815	0838	-74	+23	-51	-49		
64	0913	0862	0895	-51	+33	-18	-16	-194	
65	1249	0849	0875	-400	+26	-374	-372		
66	0923	0871	0892	-52	+21	-31	-29	-30	
67	0820	0759	0787	-61	+28	-33	-31		
68	0812	0754	0785	-58	+31	-27	-25	-24	
69	0834	0788	0810	-46	+22	-24	-22		
70	0860	0790	0820	-70	+30	-40	-38	-39	
71	0905	0824	0864	-81	+40	-41	-39		
72	0854	0825	0876	-29	+51	+22	+24	-1	Web
73	0957	0900	0915	-57	+15	-42	-40		
74	0885	0851	0902	-34	+51	+17	+19		
75	0880	0866	0871	-14	+5	-9	-7		
76	1014	1008	1027	-6	+19	+13	+15	+27	
77	0793	0772	0892	-21	+120	+99	+101		
78	0855	0831	0852	-24	+21	-3	-1		
79	0986	0948	0977	-38	+29	-9	-7		
80	1001	0988	1006	-13	+18	+5	+7		
81	0773	0753	0762	-20	+9	-11	-9	-7	
82	0841	0813	0829	-28	+16	-12	-10		
83	0881	0845	0865	-36	+20	-16	-14		

TC = Temperature compensation

D = Dummy

True strain = Diff. × 2.02×10^{-5}

Fig. C12

Model SP3 Stiffener residual strains

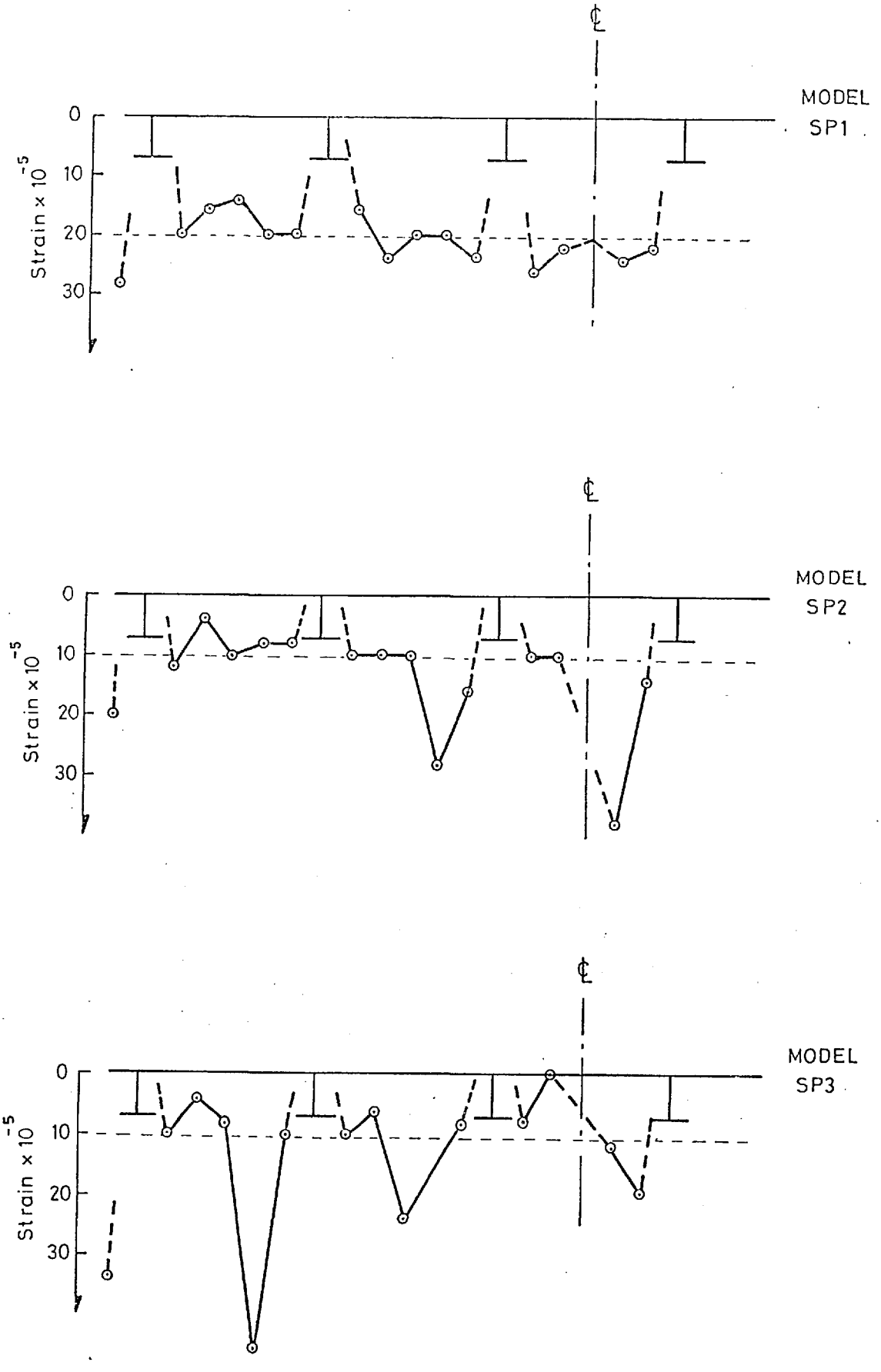

Fig C13 Longitudinal residual strains plotted across centre lines

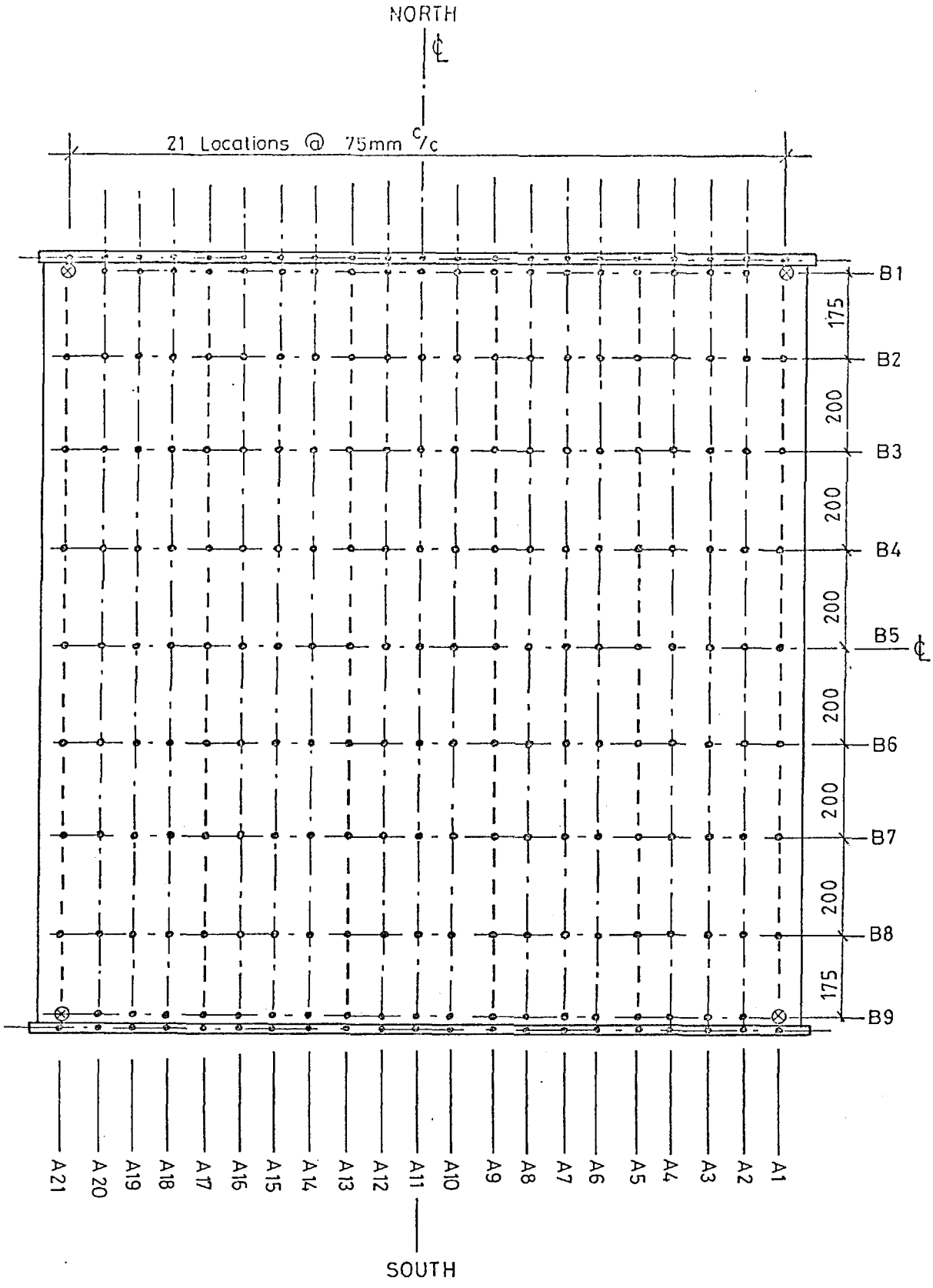

Fig C14 Initial deformation measurement positions
(measured on unstiffened side of panel)

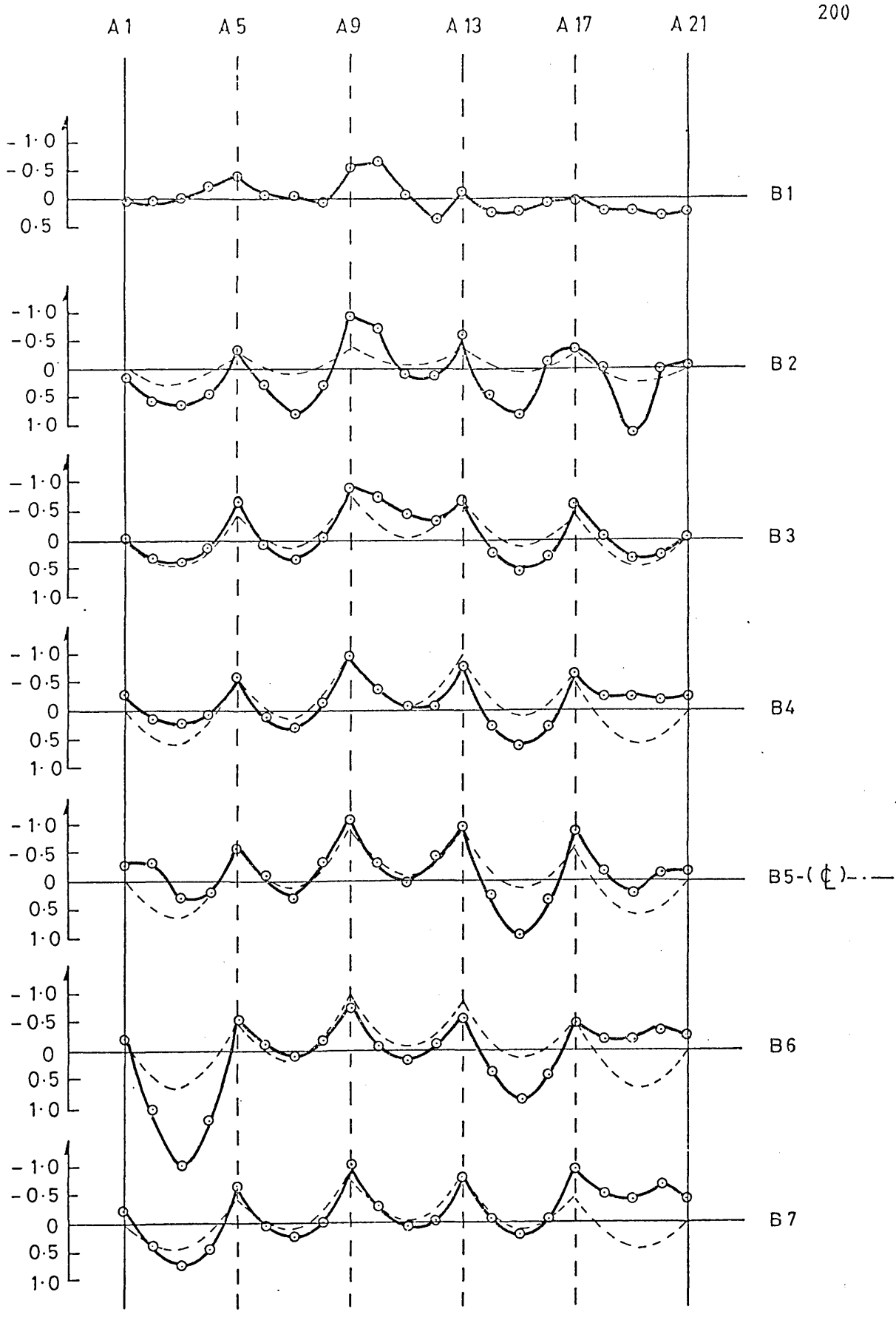

Scale in mm

---- Distribution used in theoretical study
negative deflections are towards plate

Fig C15 Model SP1 initial deformations

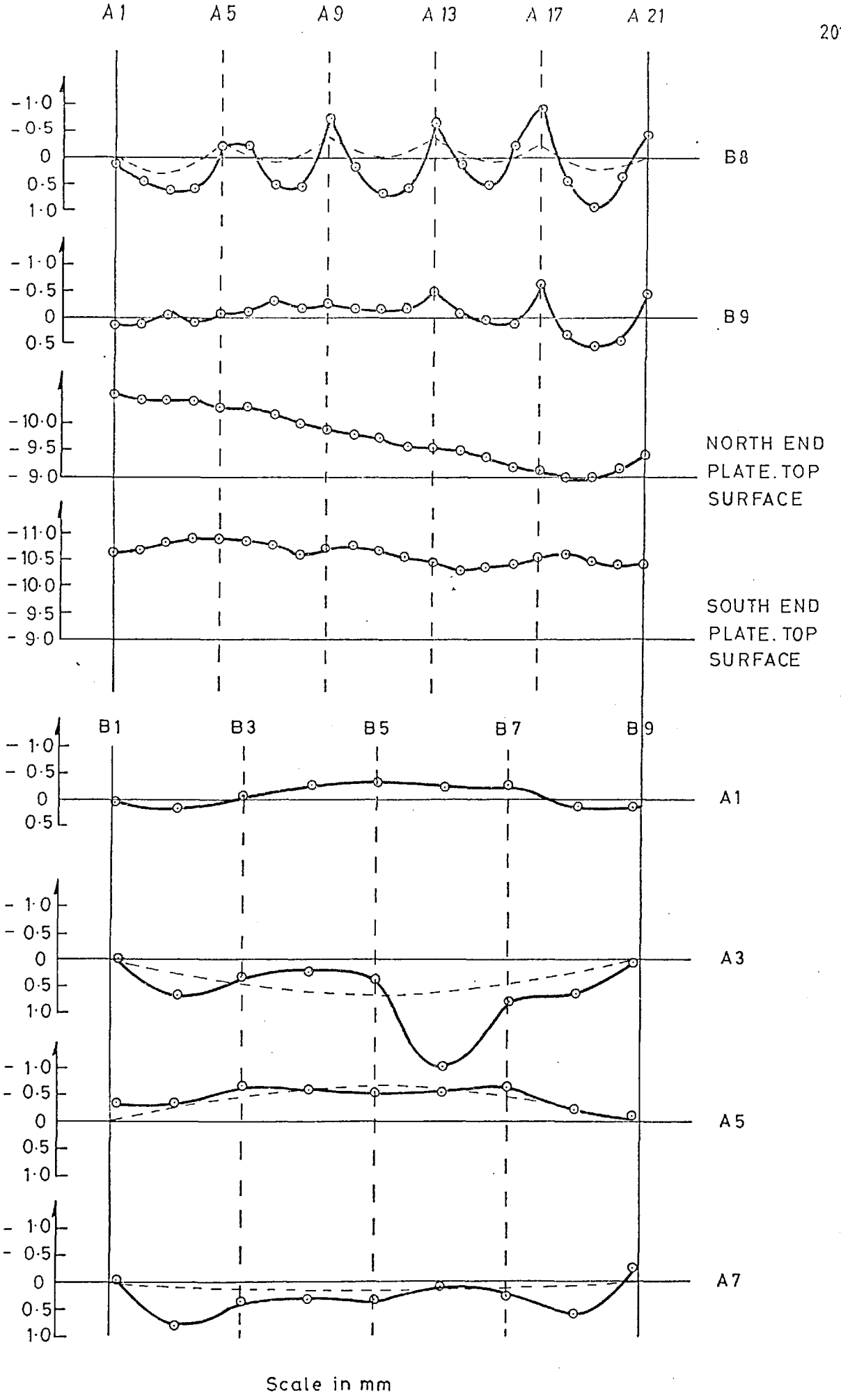

Fig C16 Model SP1 initial deformations continued

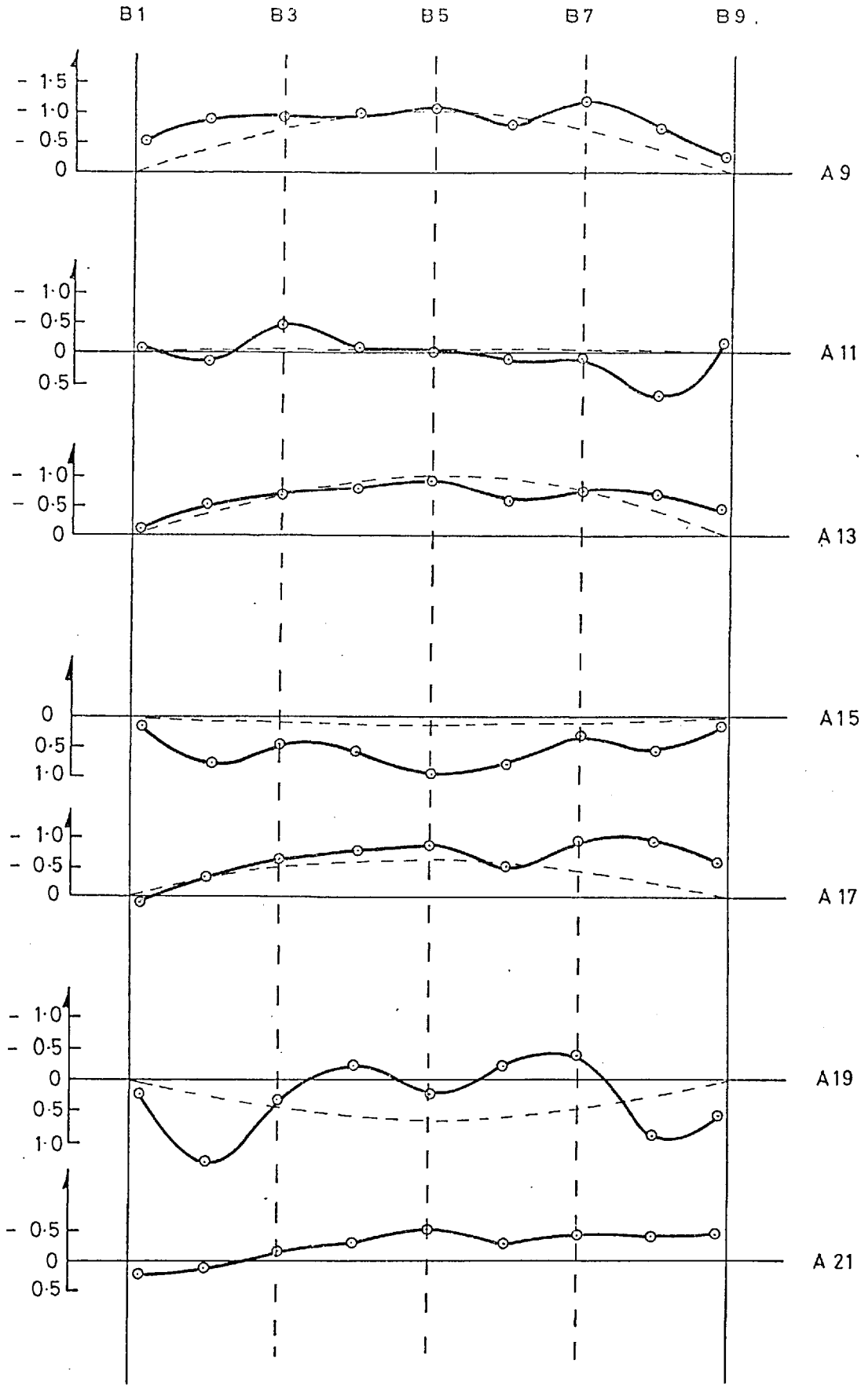

Fig C17 Model SP1 initial deformations continued

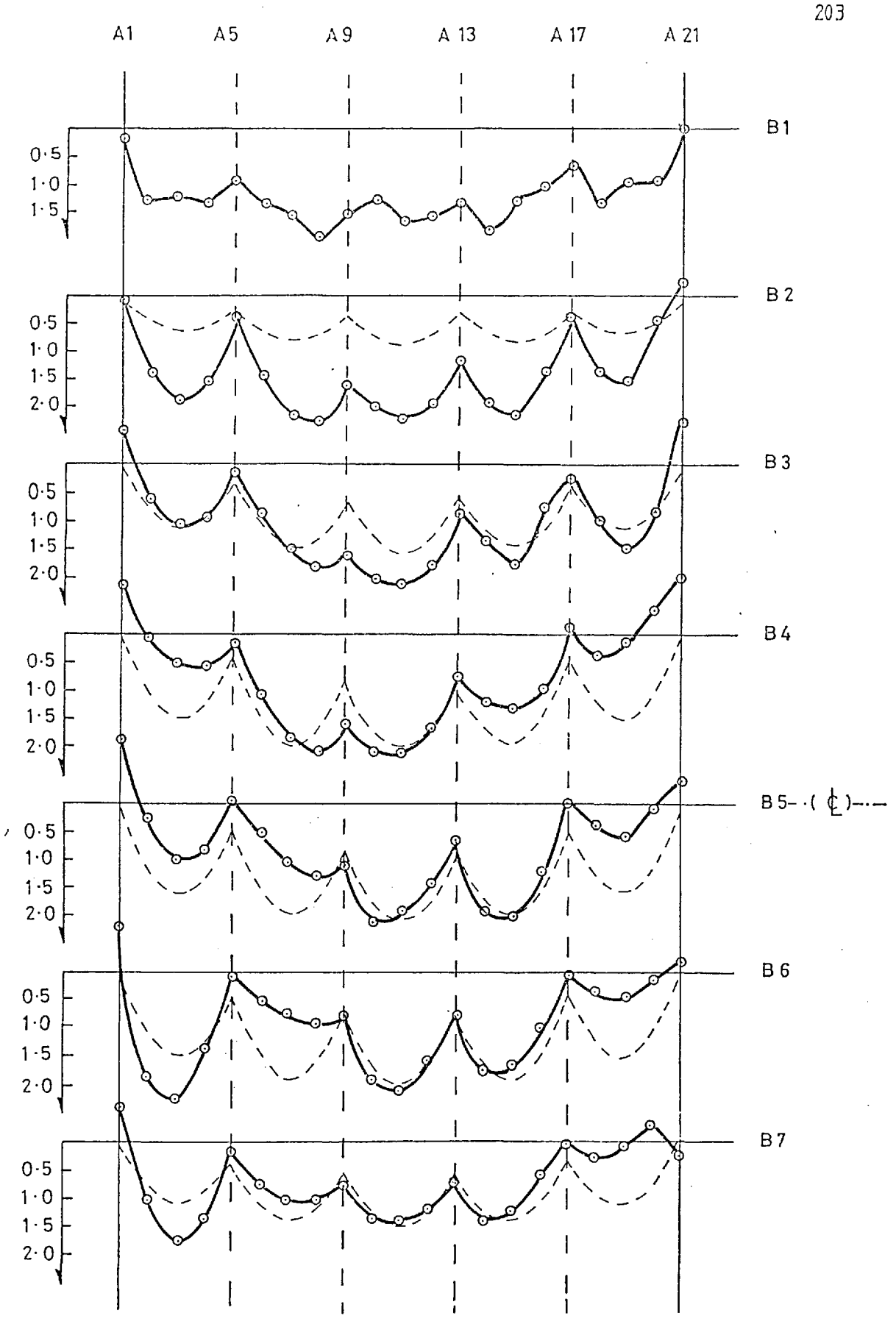

Fig C18 Model SP2 initial deformations

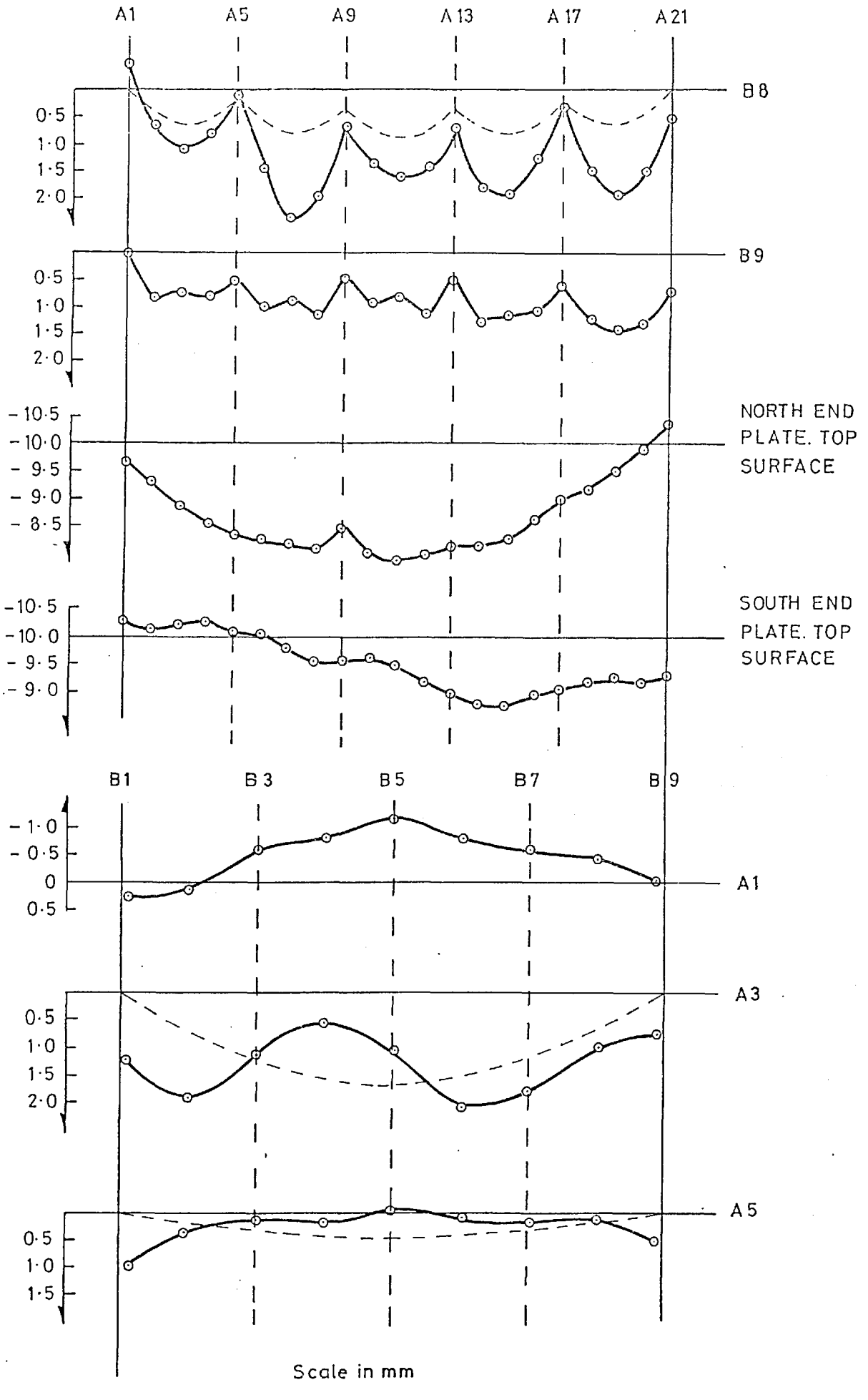

Fig C19 Model SP2 initial deformations continued

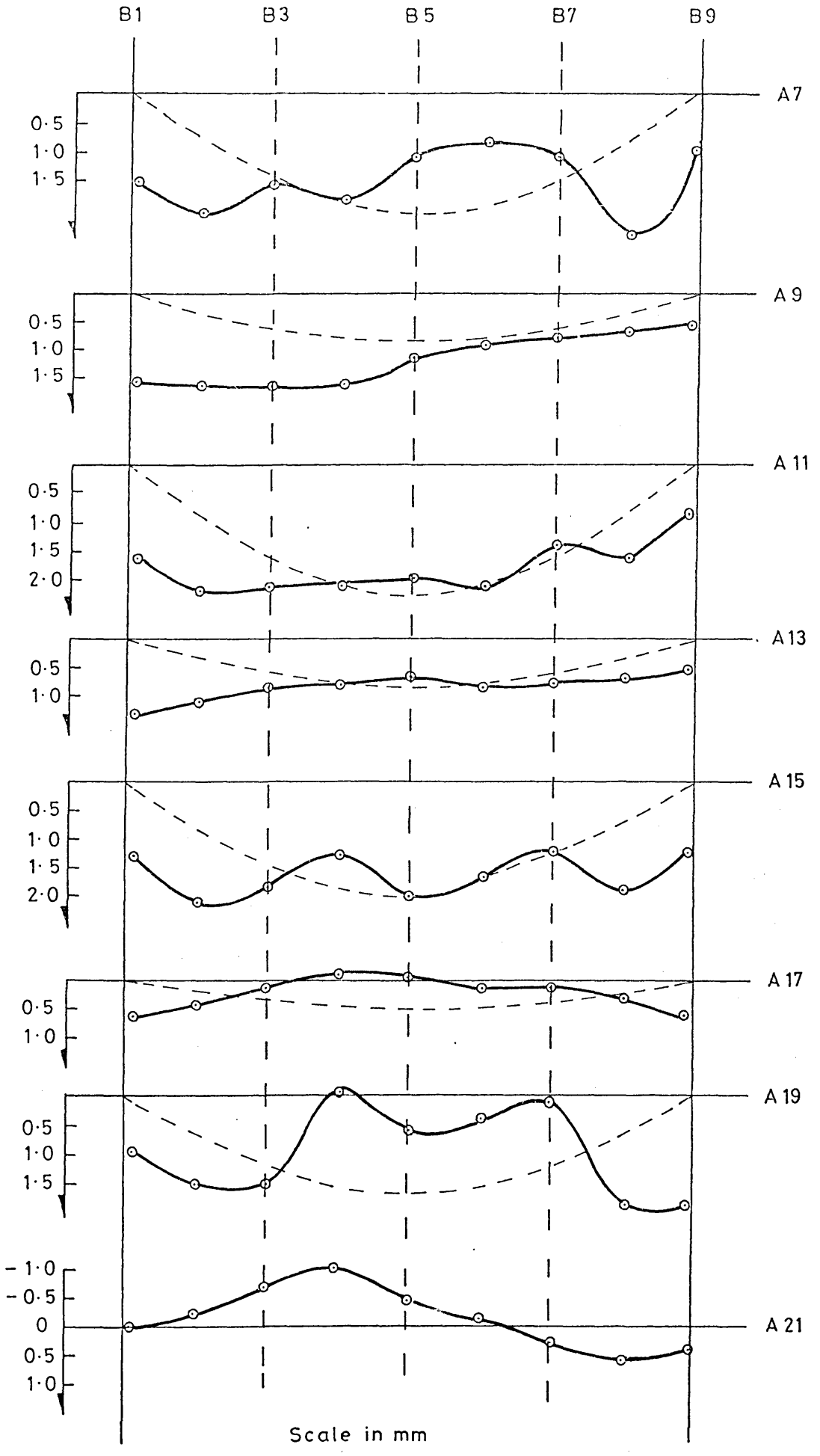

Fig C20 Model SP2 initial deformations continued

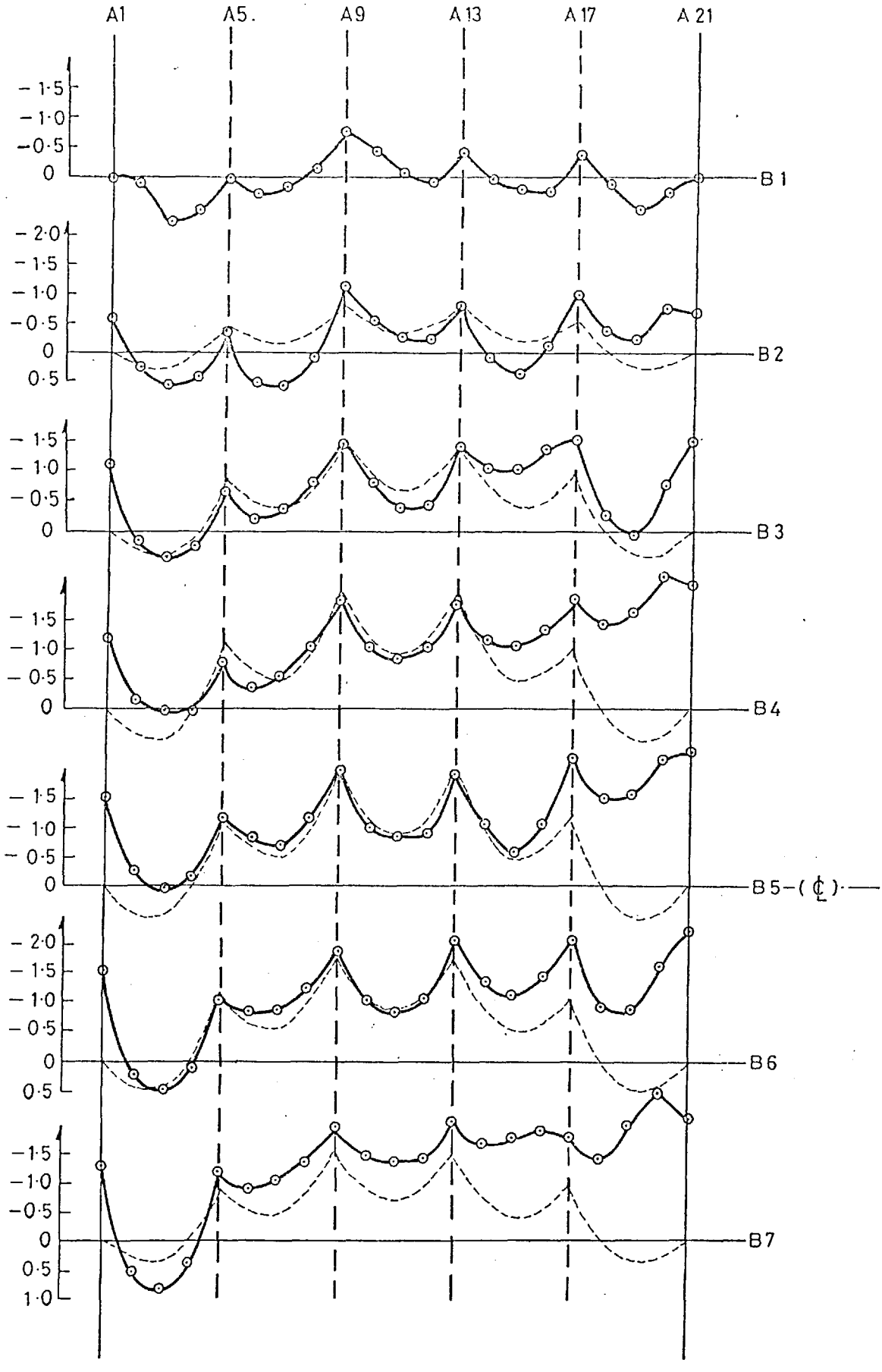

Fig C21 Model SP3 initial deformations

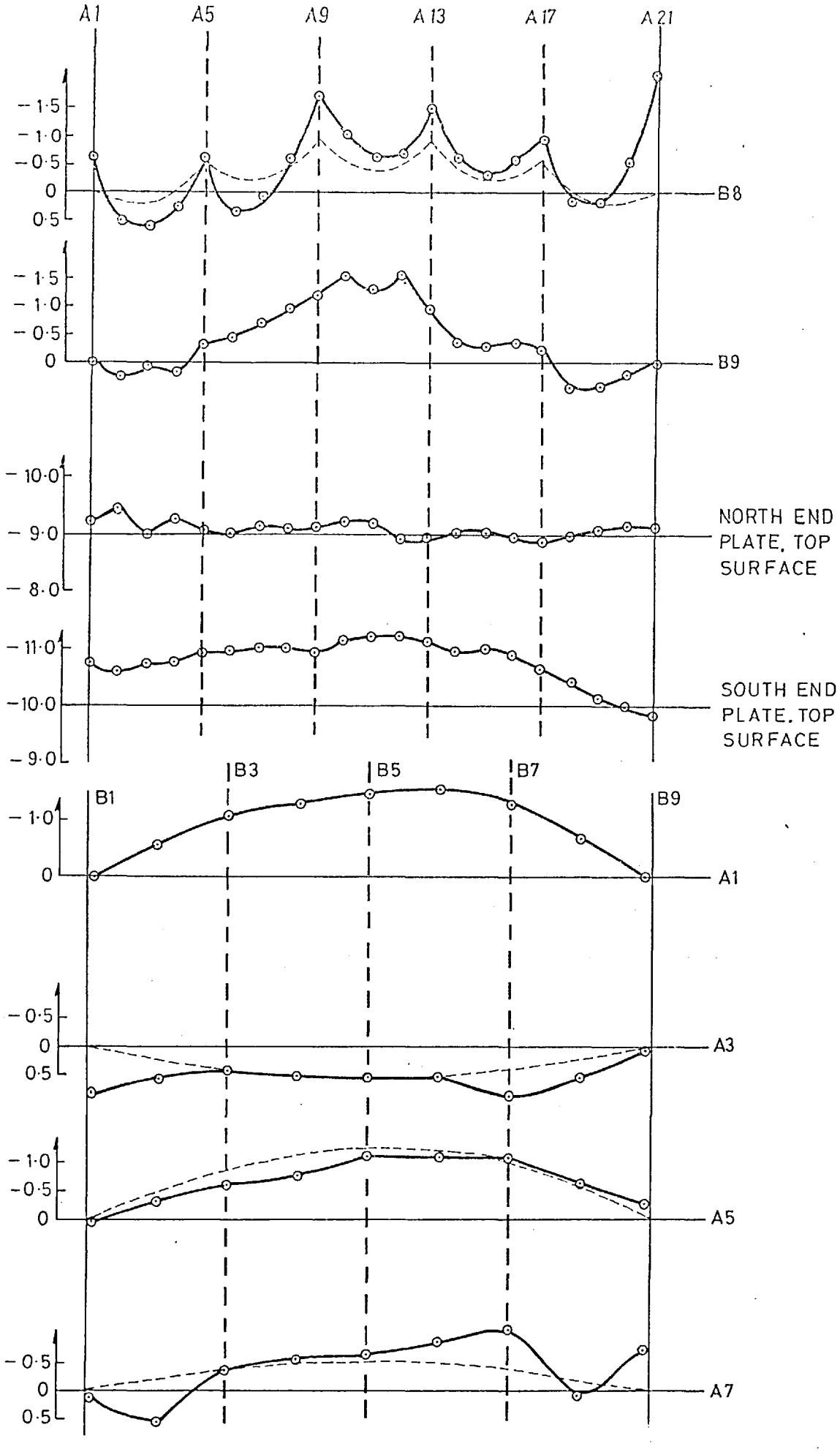

Scale mm

Fig C22 Model SP3 initial deformations continued

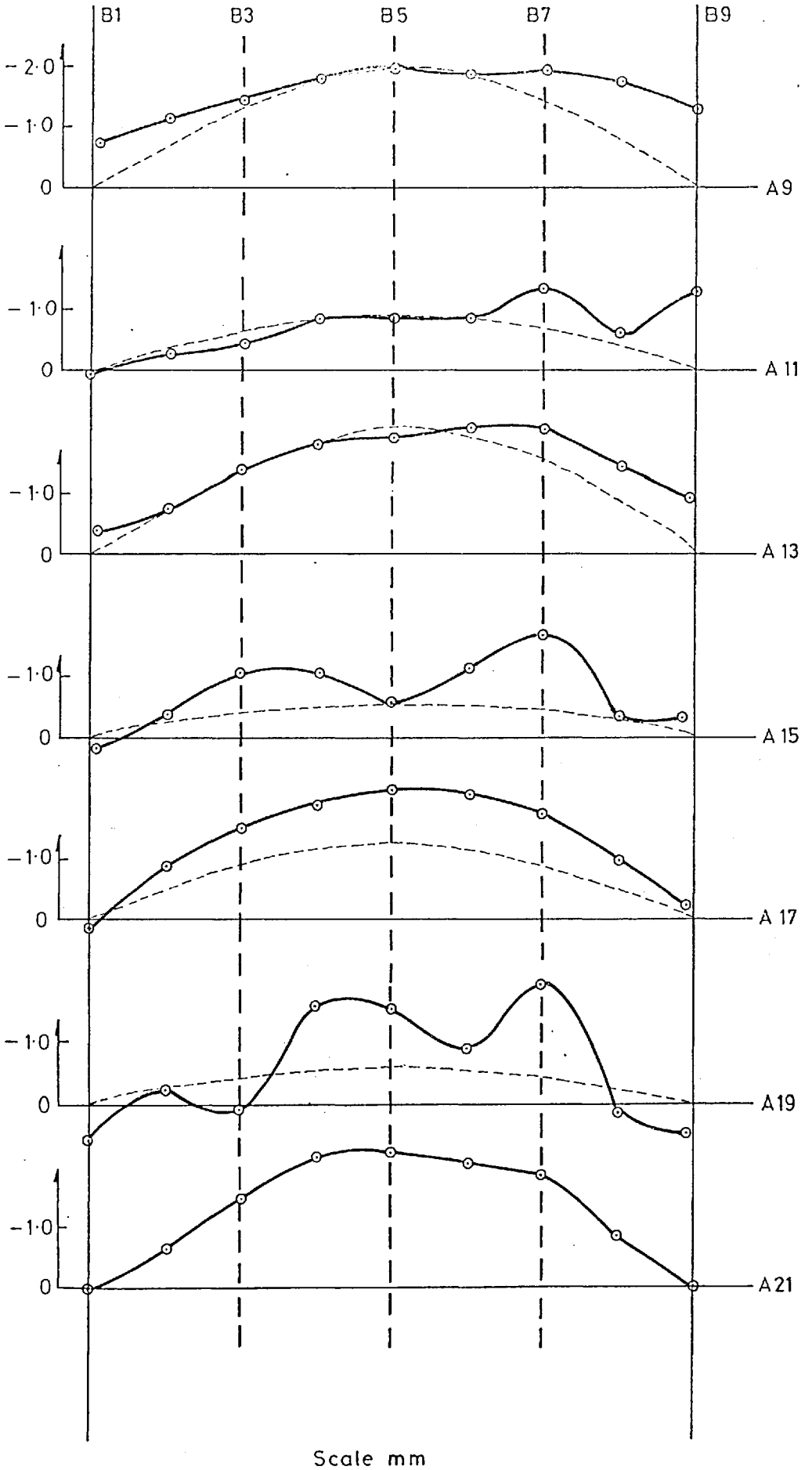

Fig C23 Model SP3 initial deformations continued

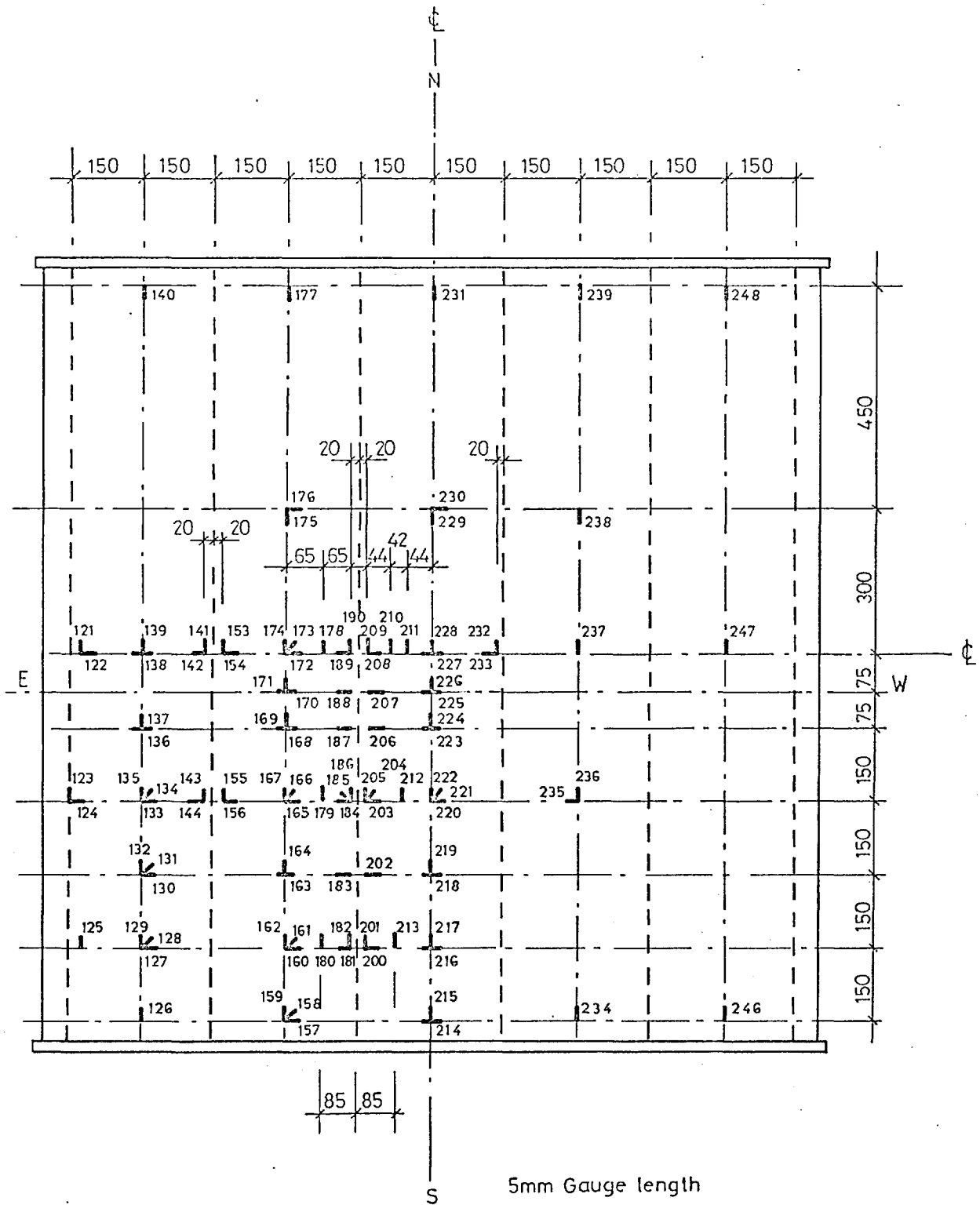

STIFFENED FACE

Fig C 24 Strain gauge positions and numbering

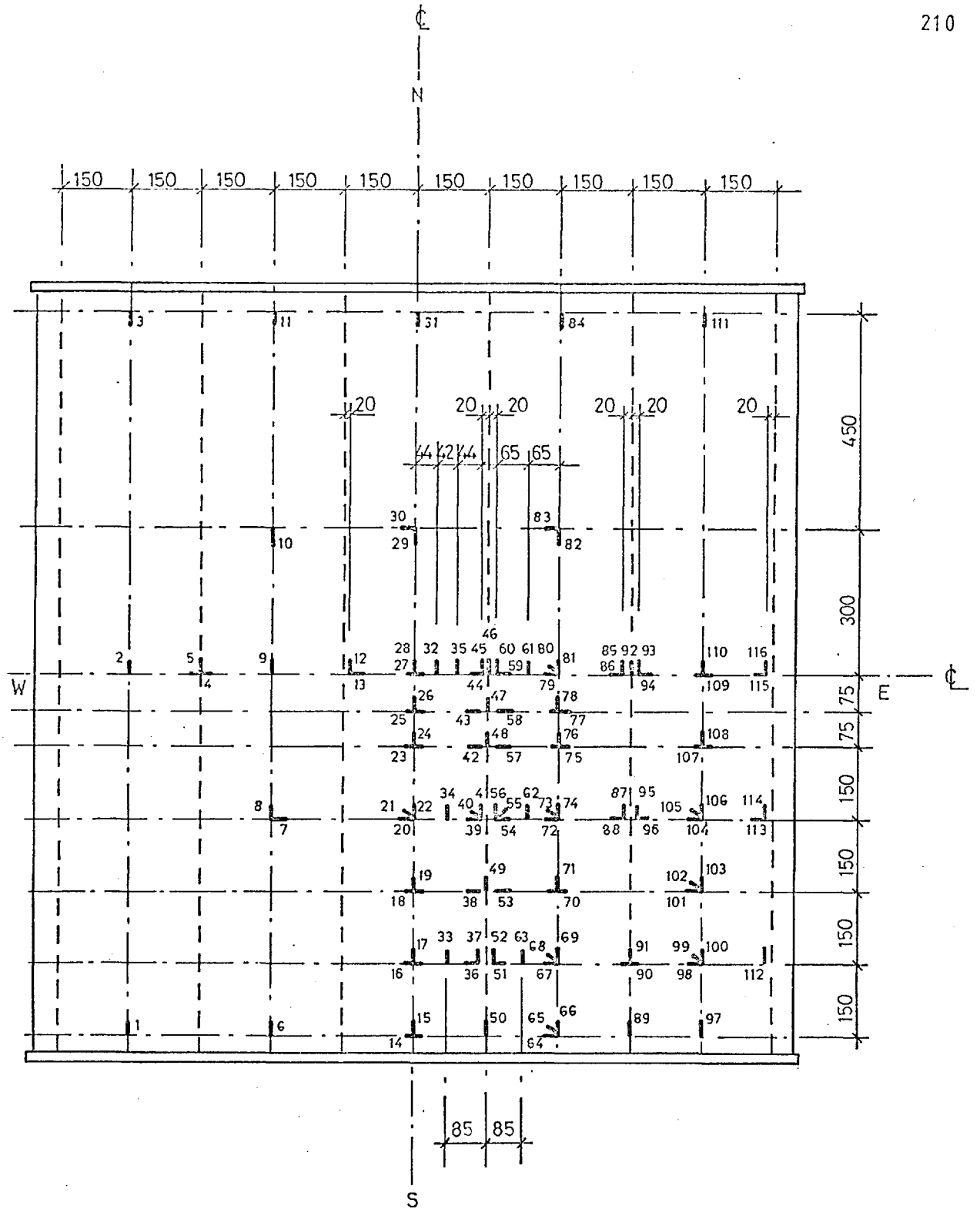

UNSTIFFENED FACE

Fig C25 Strain gauge positions and numbering

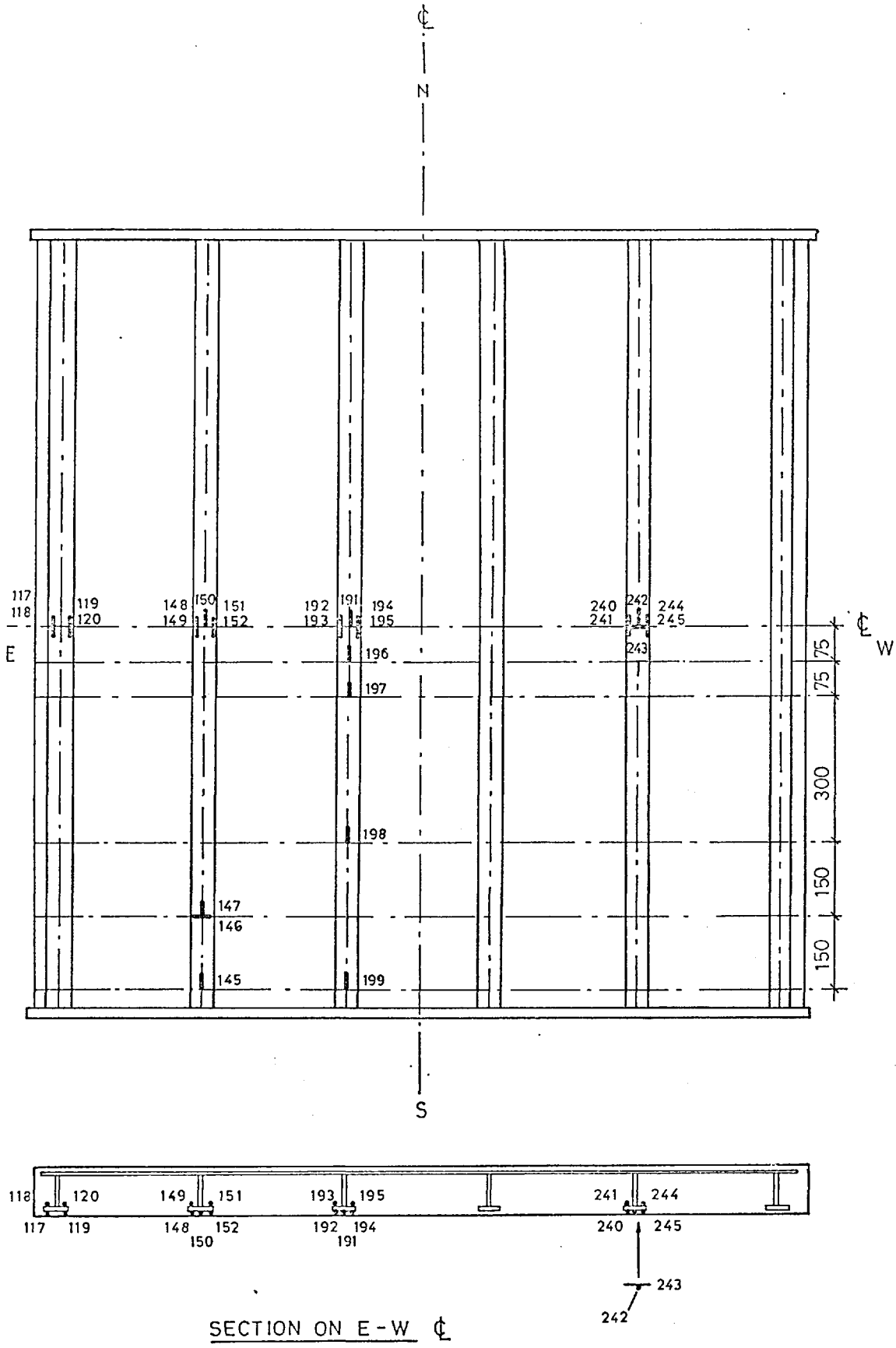

5mm Gauge length

Fig C26 Strain gauge positions and numbering for stiffeners

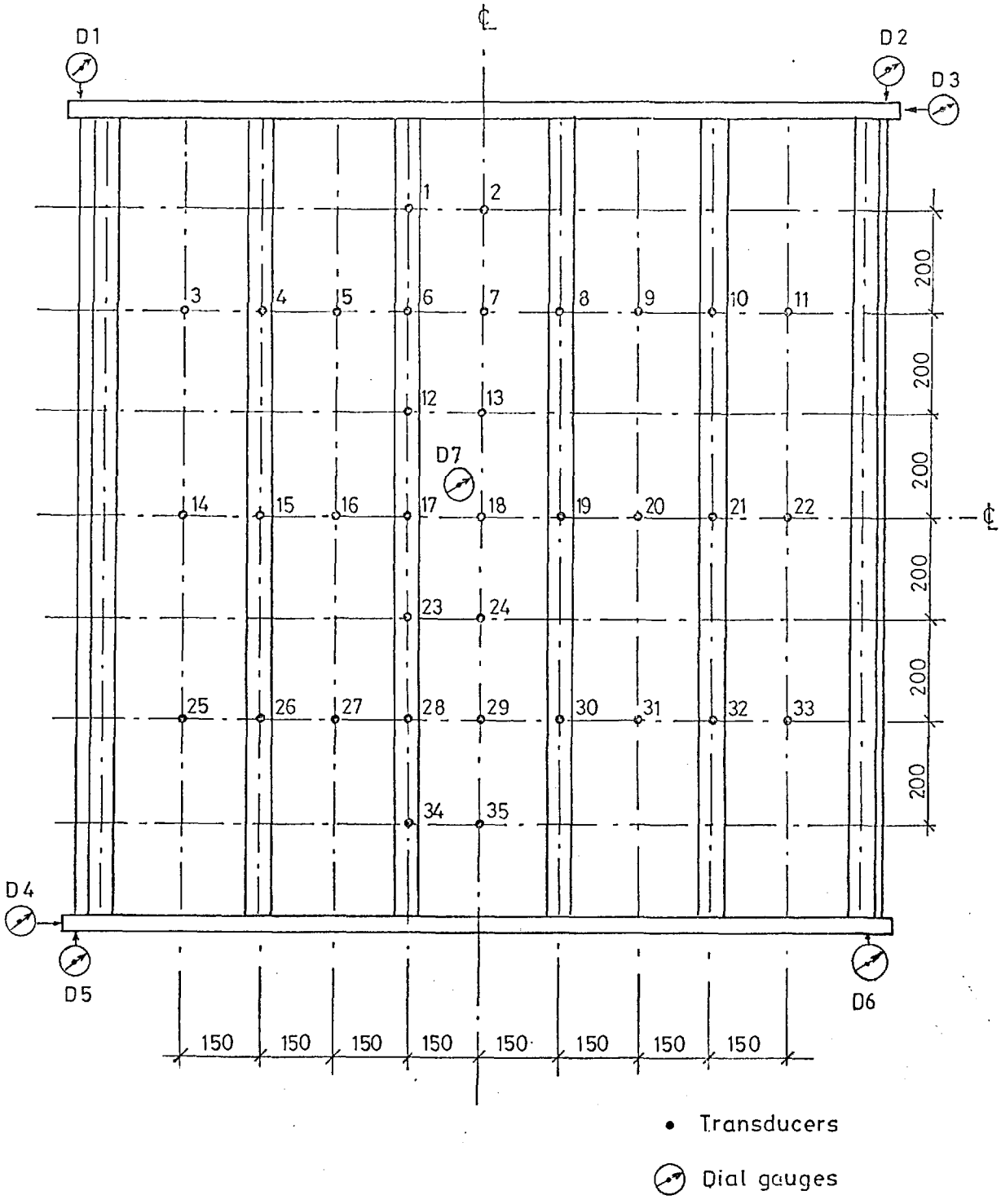

DEFLECTION MEASUREMENT

Fig C27 Transducer and dial gauge positions

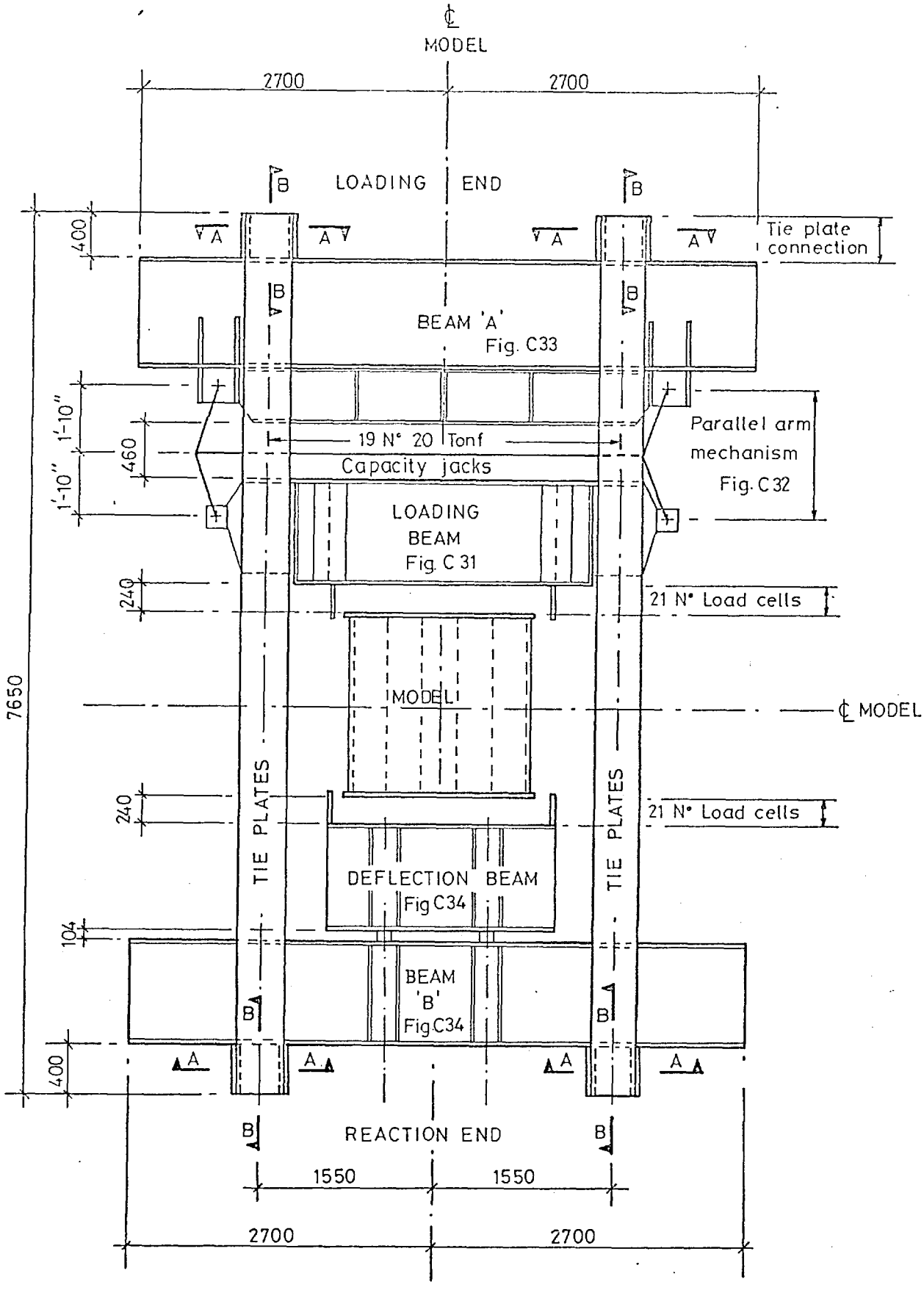

note : 1) see fig C35 for sections A-A and B-B

Fig C28 In-plane loading frame

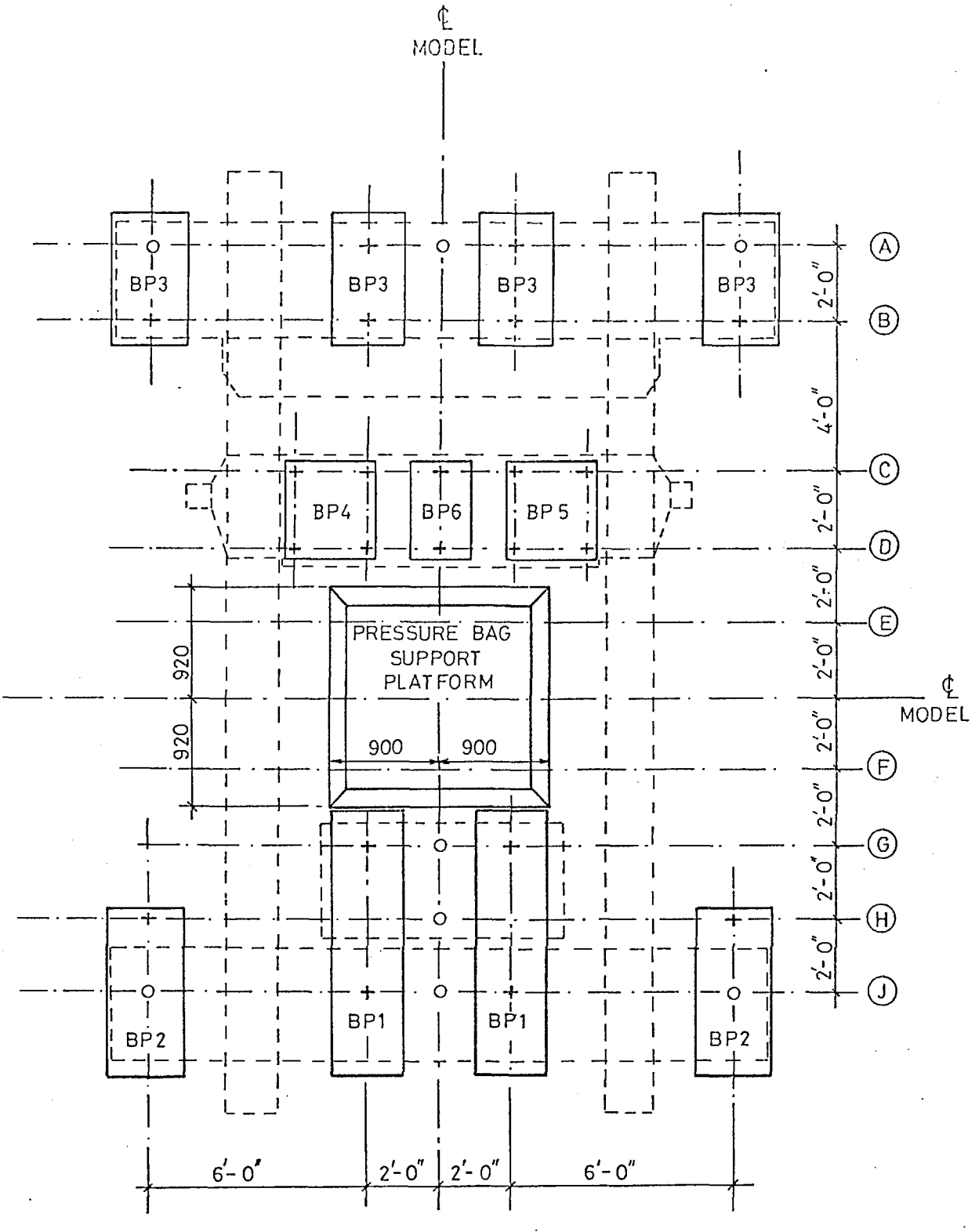

note : 1) see figC35 for base plate details
2) see figC36 for platform details

o Beam holding down bolts
\+ Base plates bolted to floor

Fig C 29 Location of base plates and pressure bag support platform

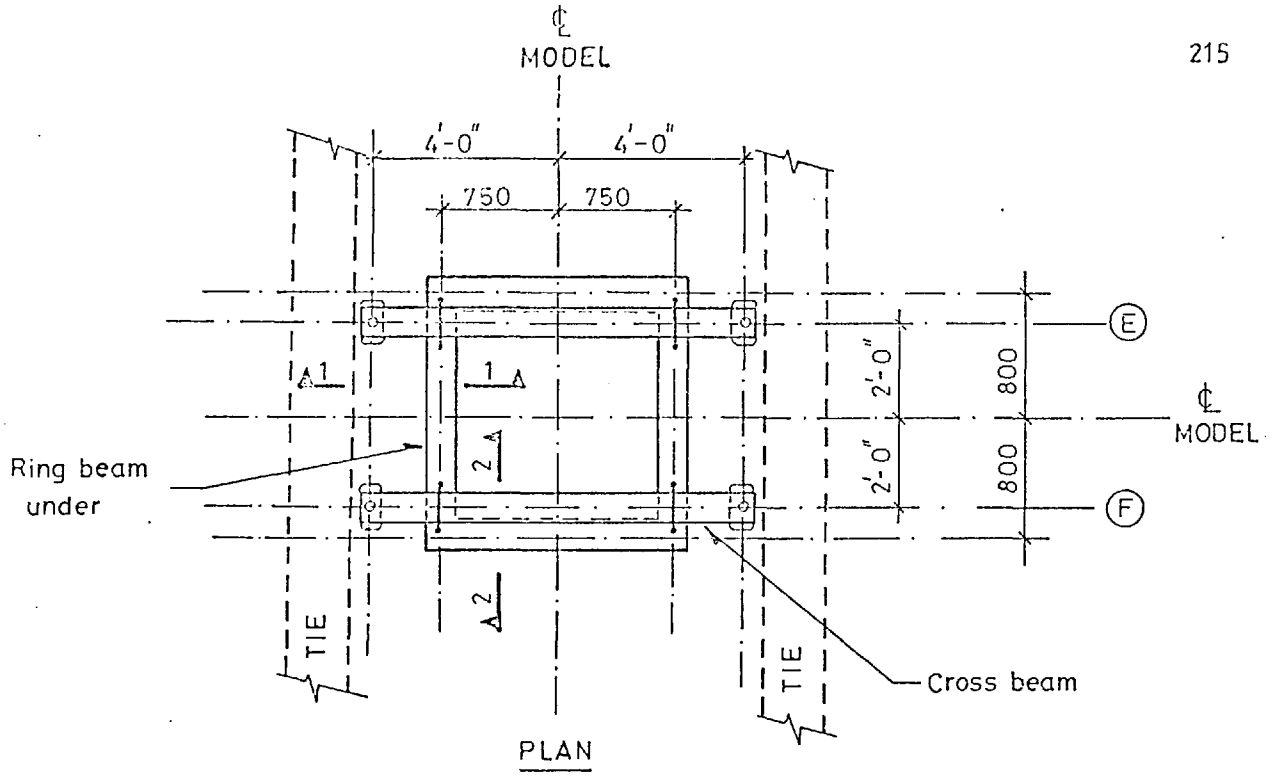

PLAN

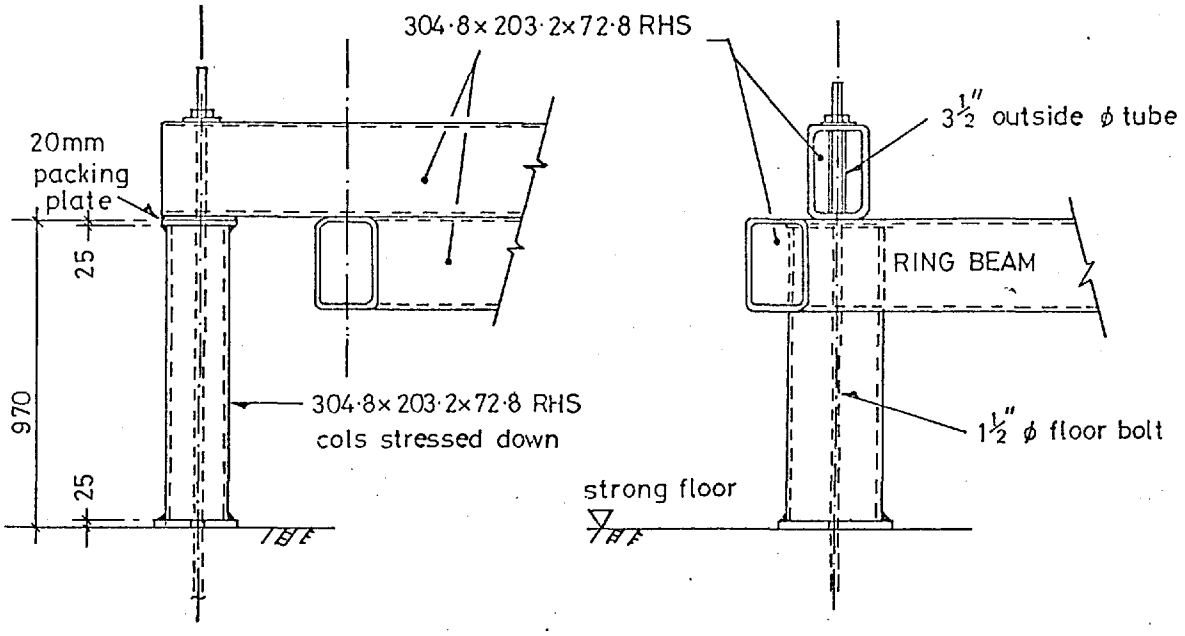

SECTION 1-1

SECTION 2-2

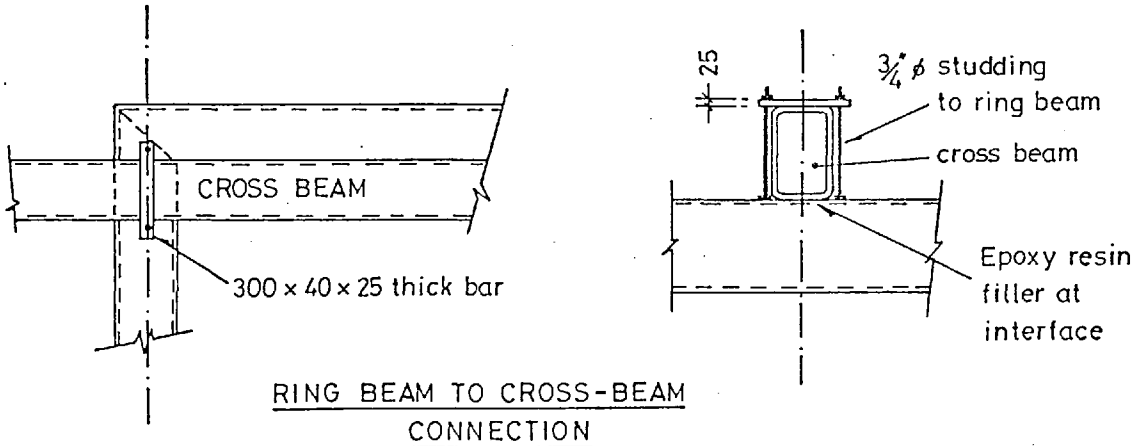

RING BEAM TO CROSS-BEAM
CONNECTION

Fig C30 Lateral load reaction frame

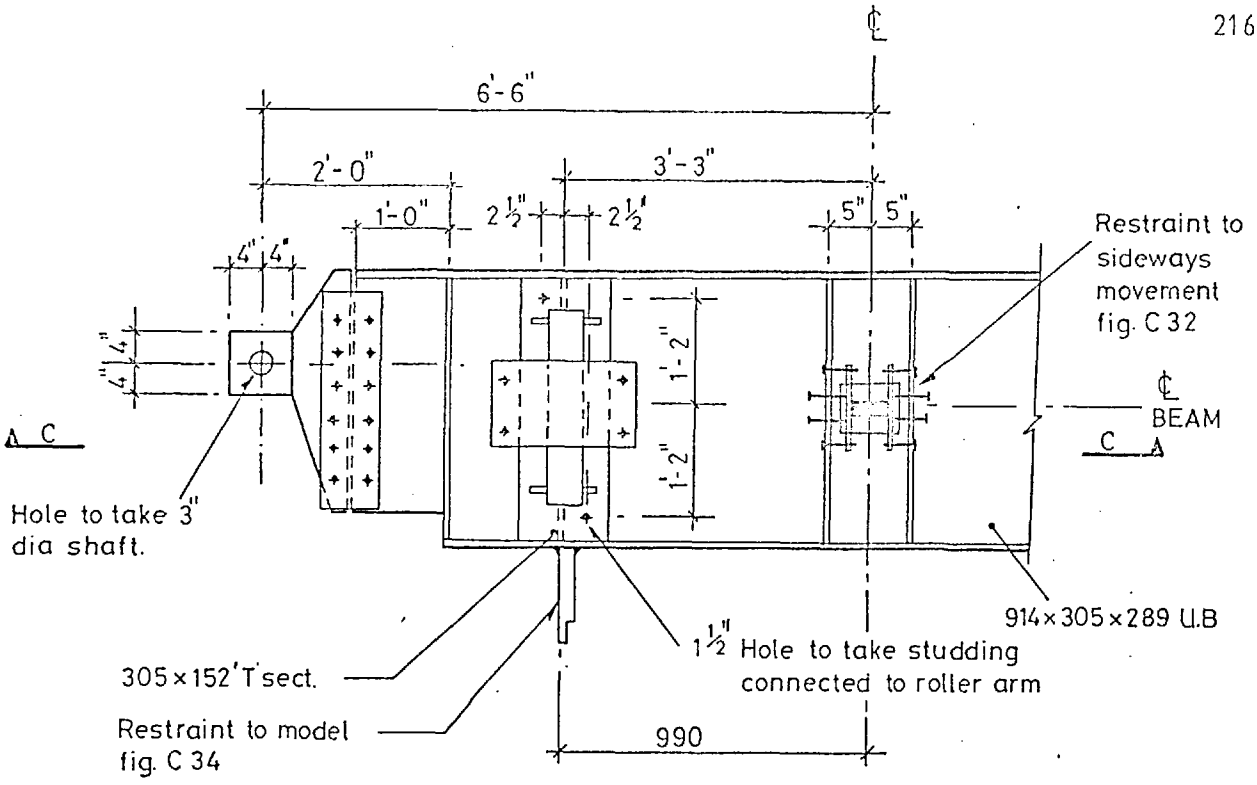

LOADING BEAM - SECTION A-A

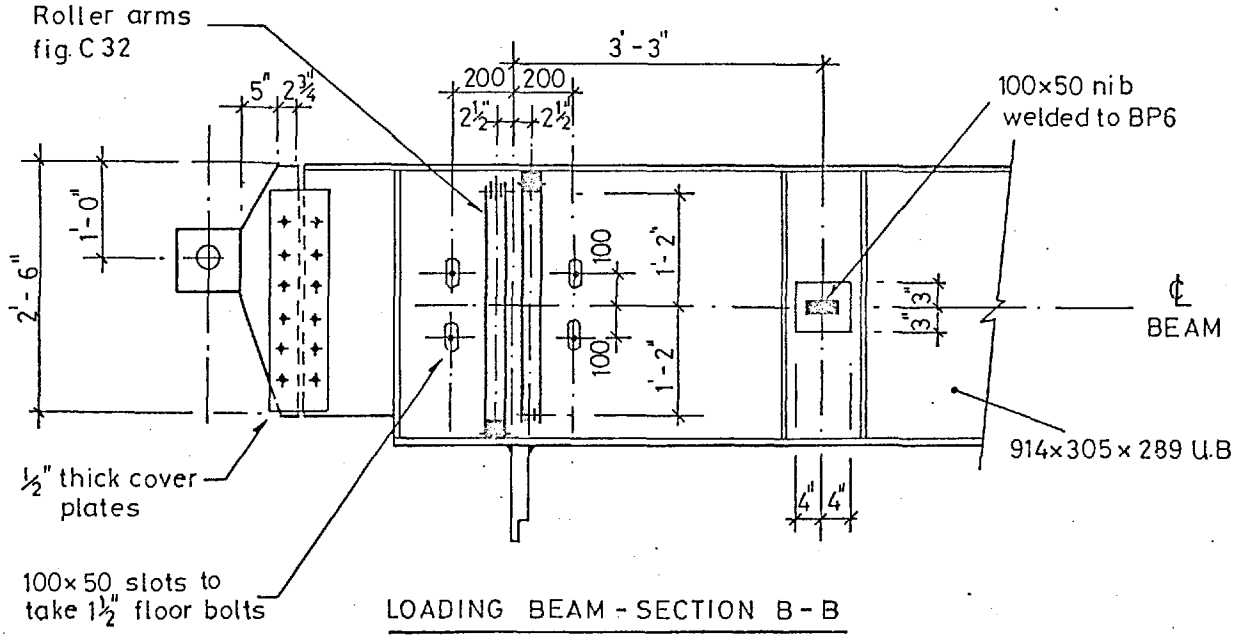

LOADING BEAM - SECTION B-B

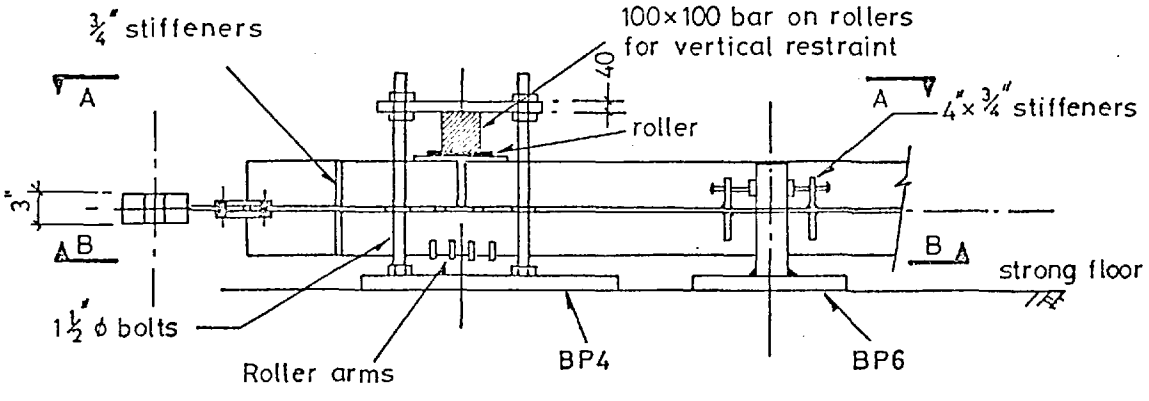

LOADING BEAM - SECTION C-C

Fig C 31 Loading beam details

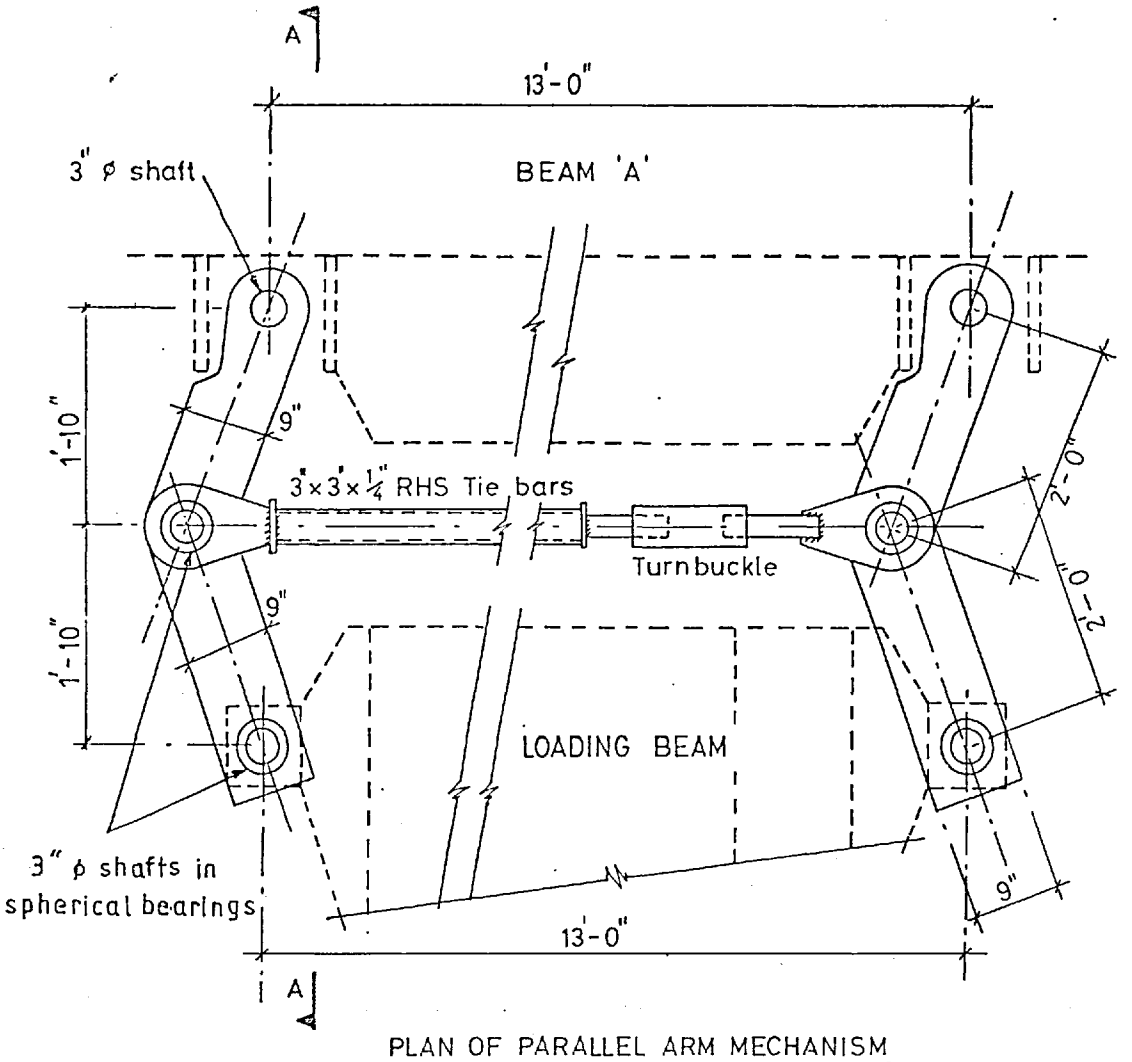

PLAN OF PARALLEL ARM MECHANISM

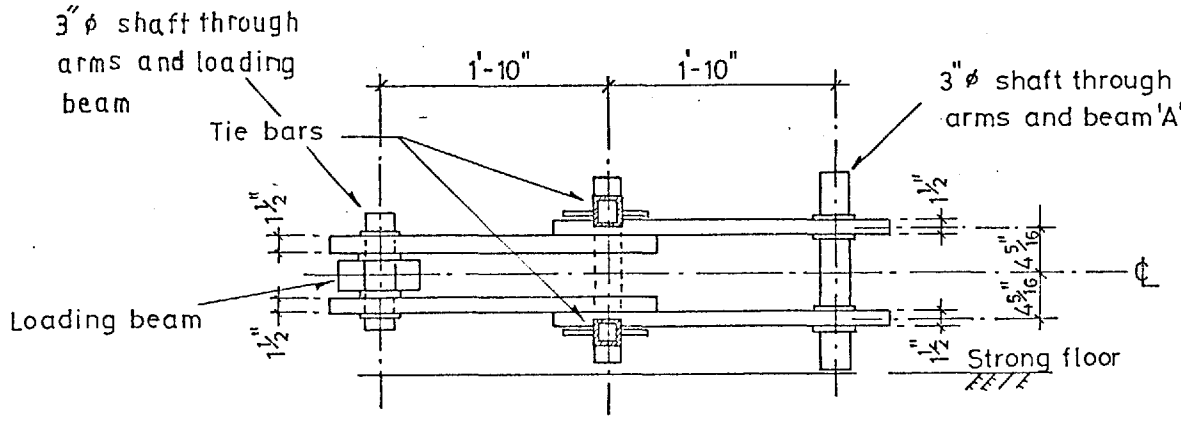

SECTION A-A

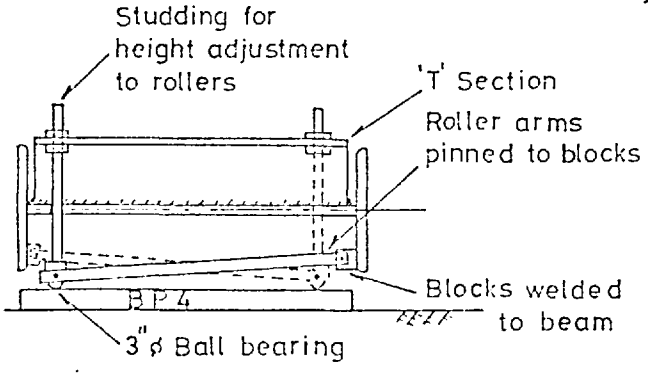

LOADING BEAM ROLLERS

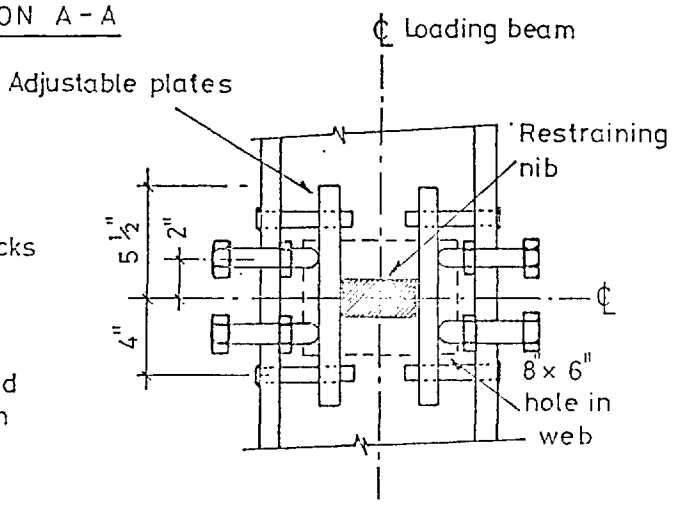

SIDEWAYS RESTRAINT TO LOADING BEAM

Fig C32

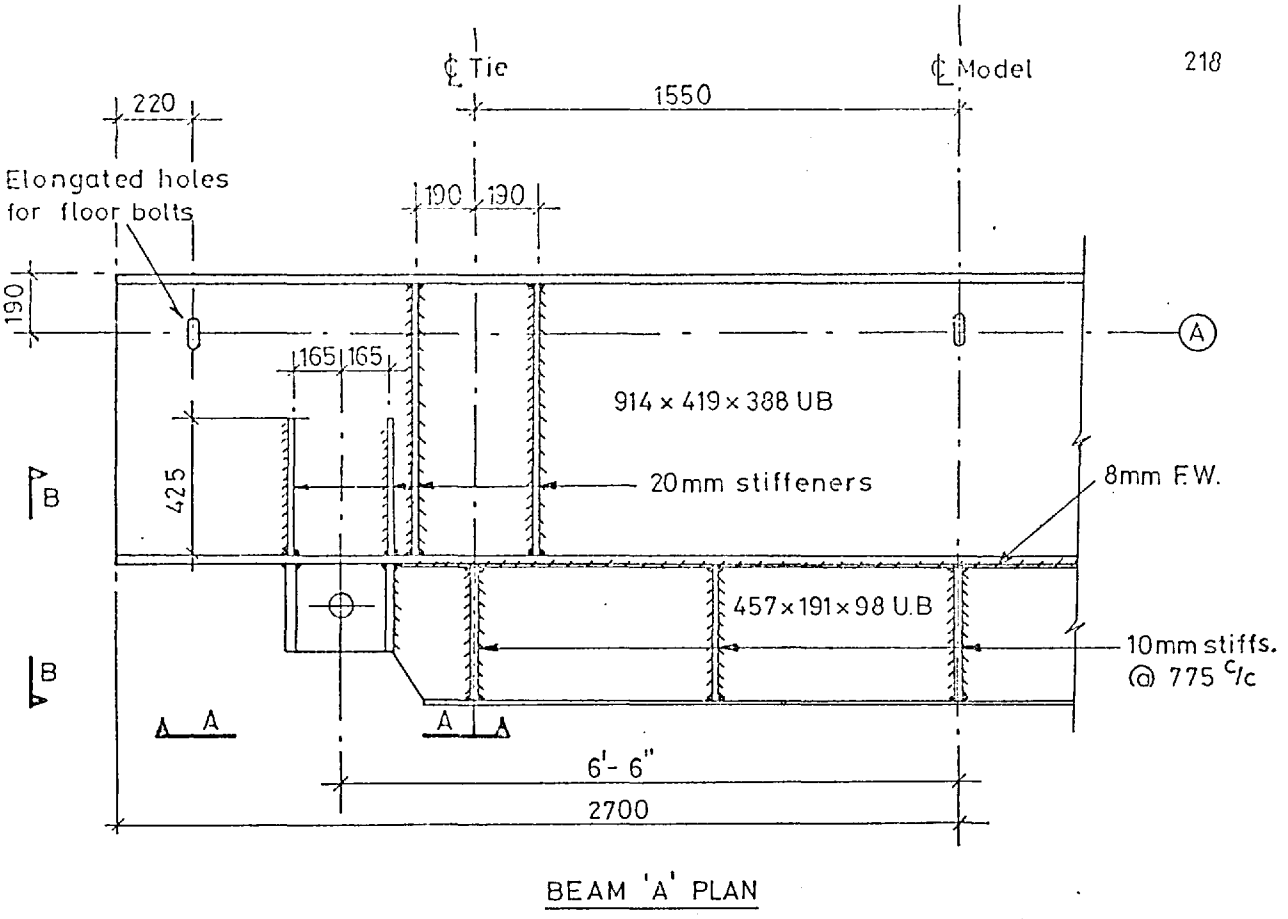

BEAM 'A' PLAN

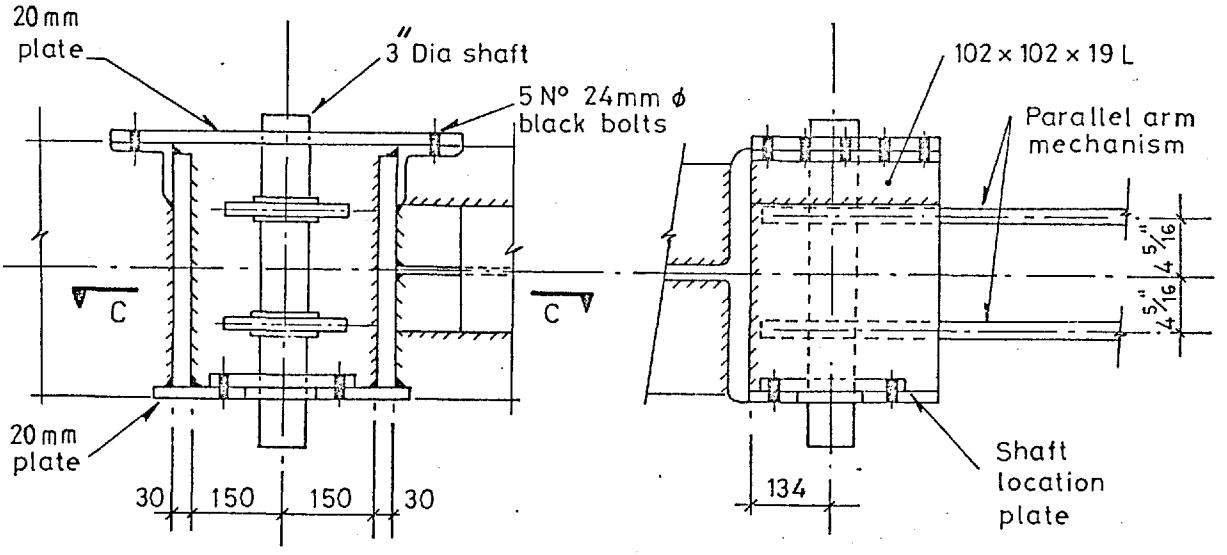

ELEVATION A – A

ELEVATION B-B

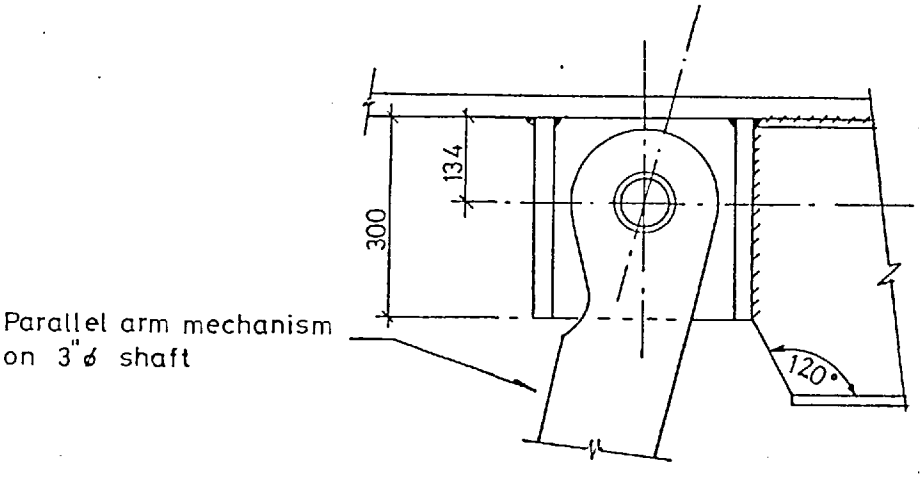

SECTION C-C

Note:
All welds are 6mm continuous, unless shown otherwise

Fig C33 Beam 'A' details

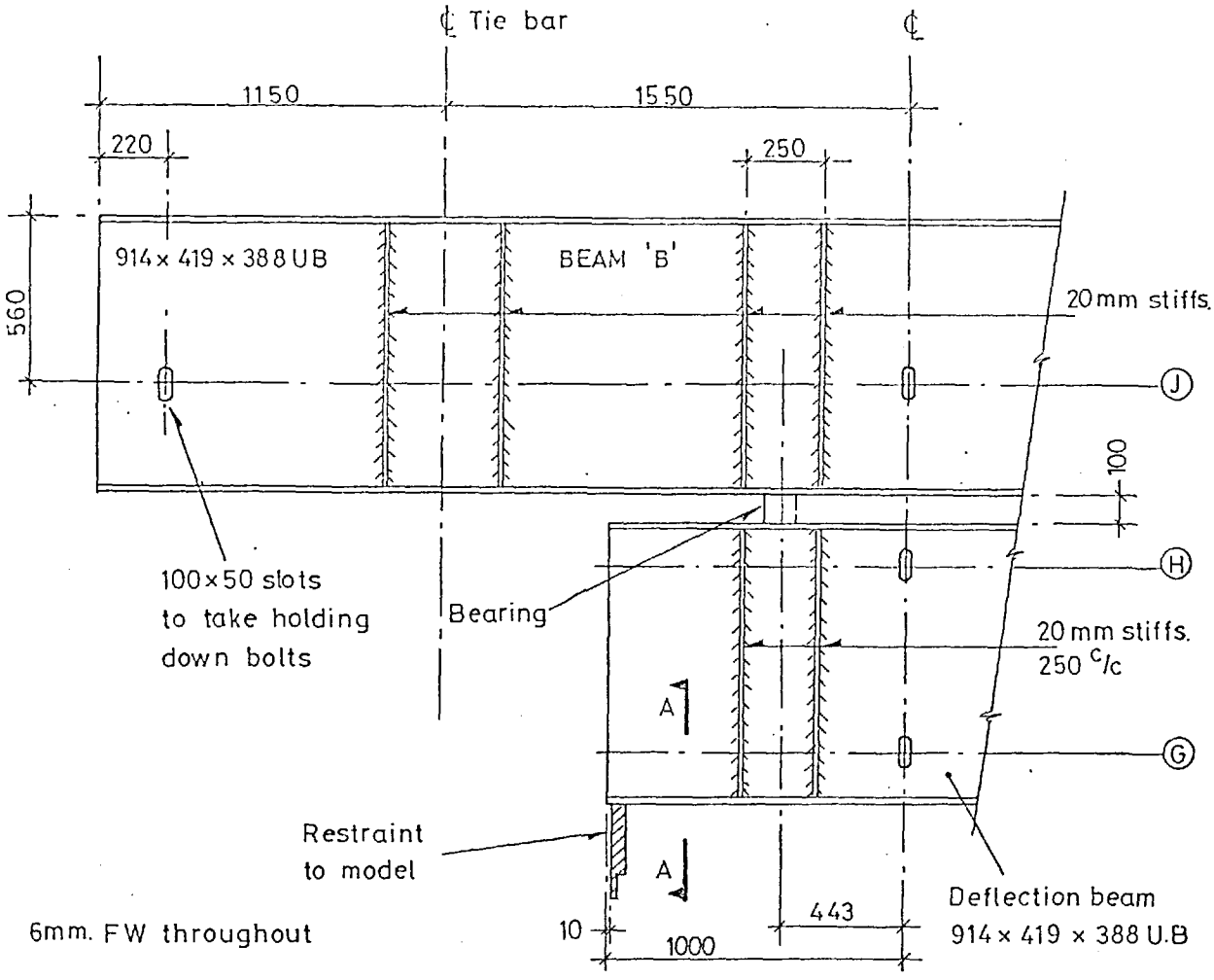

BEAM 'B' AND DEFLECTION BEAM

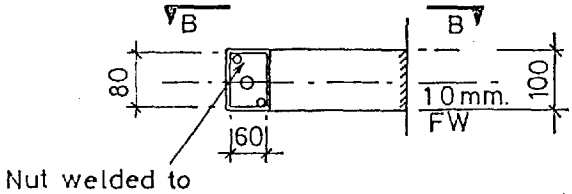

A - A

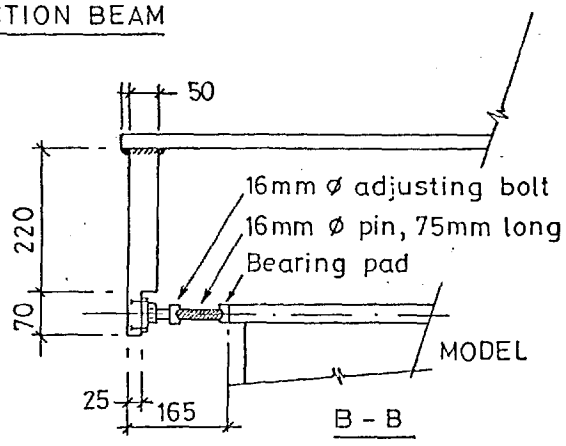

B - B

HORIZONTAL RESTRAINT TO MODEL

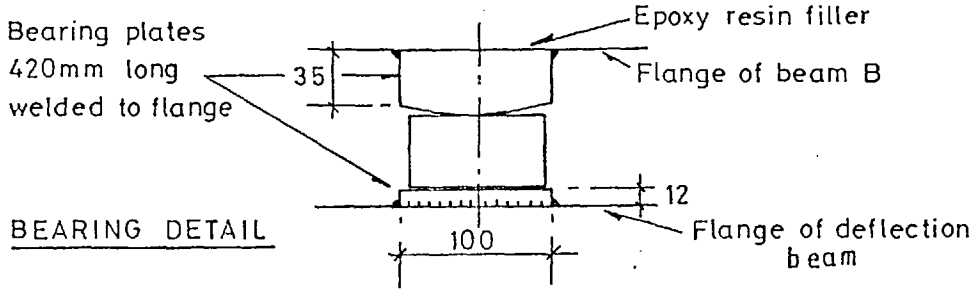

BEARING DETAIL

Fig C34

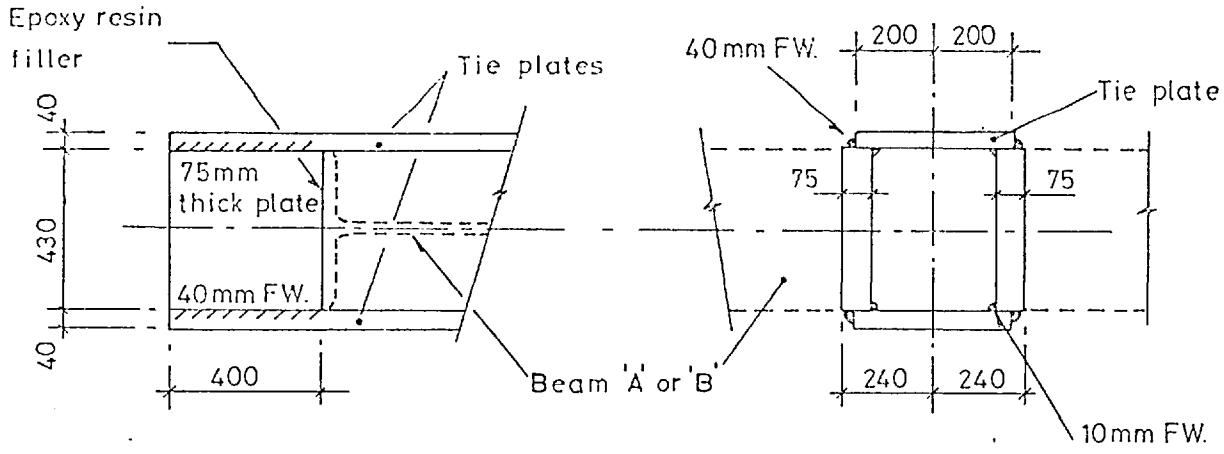

SECTION B-B
(see figC28)

SECTION A-A
(see figC28)

TIE PLATE CONNECTION DETAILS

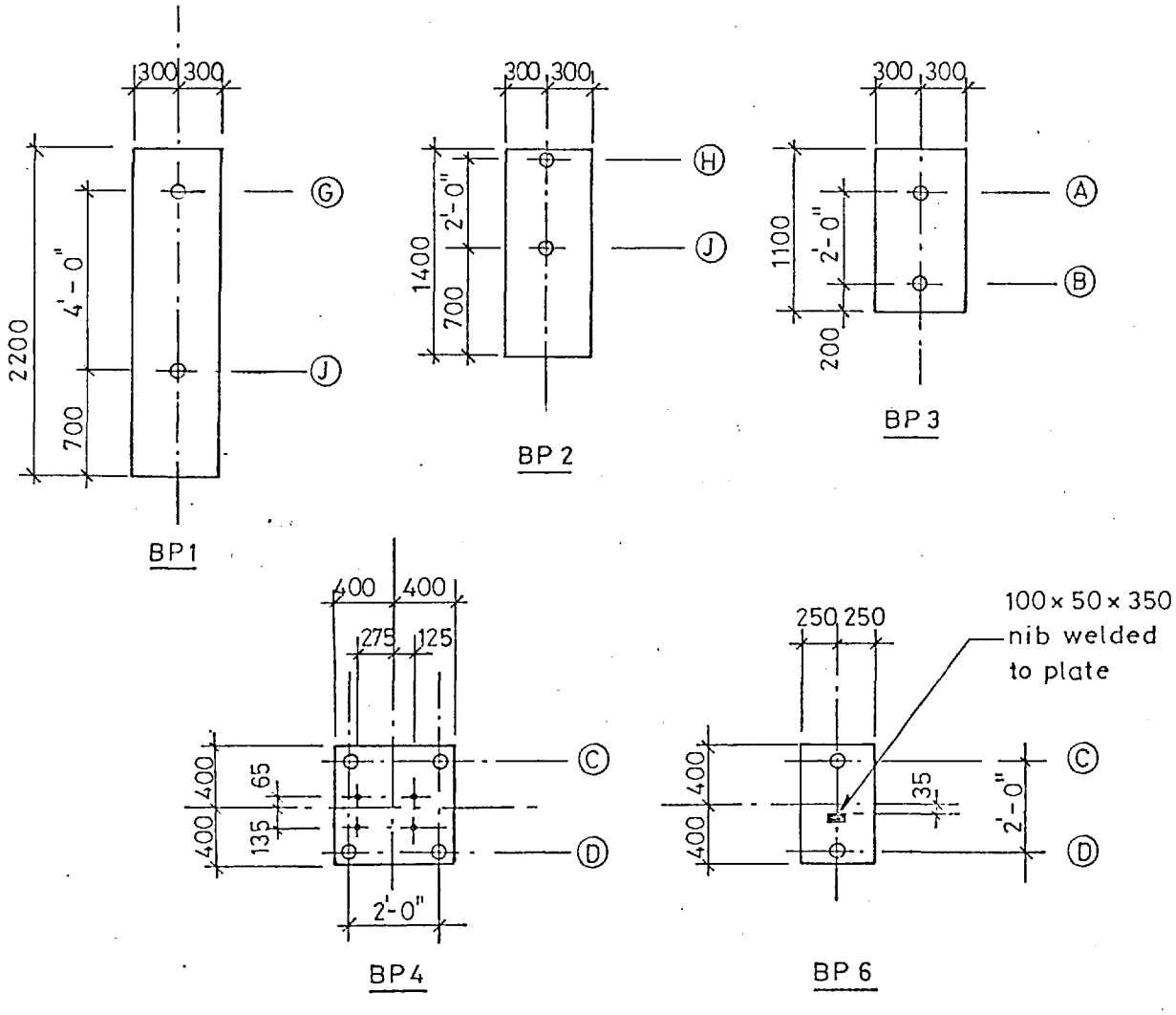

(BP5 similar but handed)

Note

1. All plates 50mm thick
2. ⊕ Holes to take 1½" ø floor bolts
3. + 1½" ø nuts welded to plates BP4 & BP5

BASE PLATE DETAILS

Fig C35

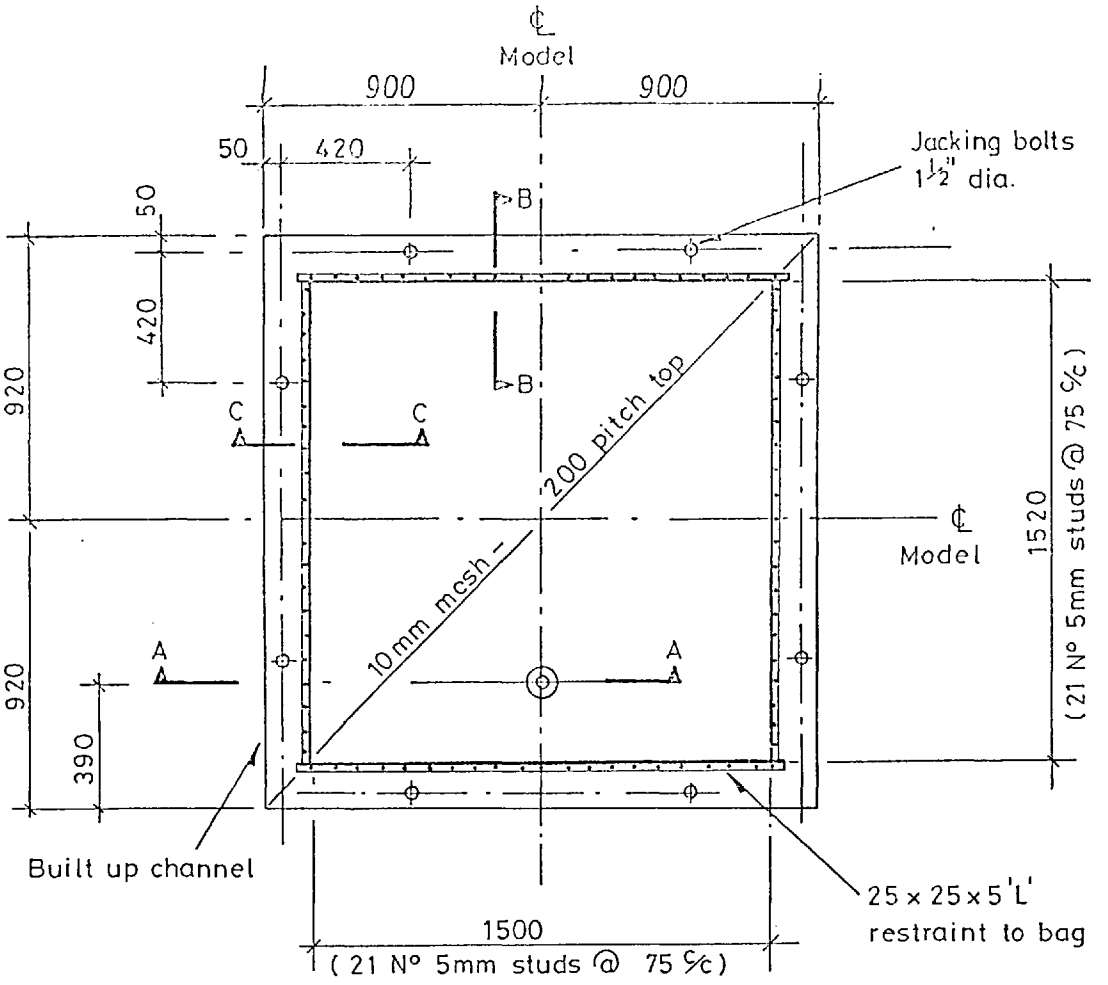

PLAN

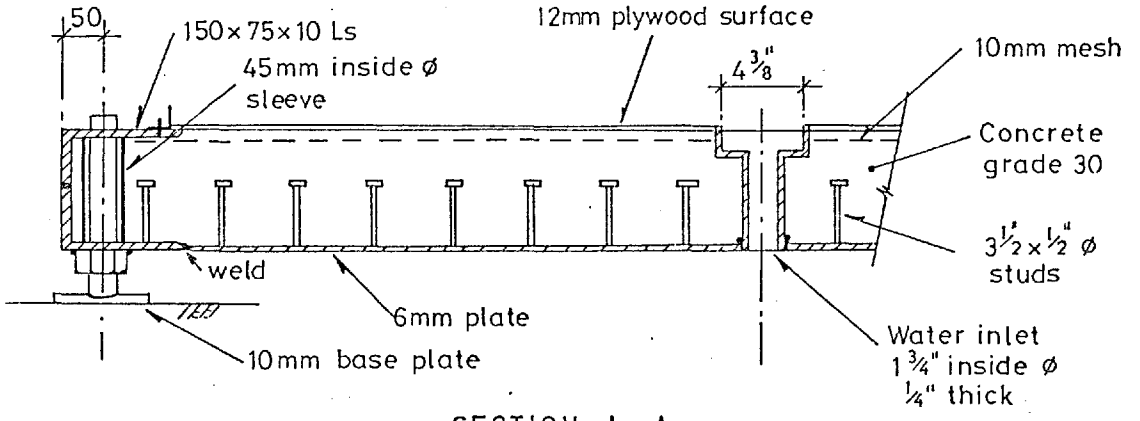

SECTION A-A

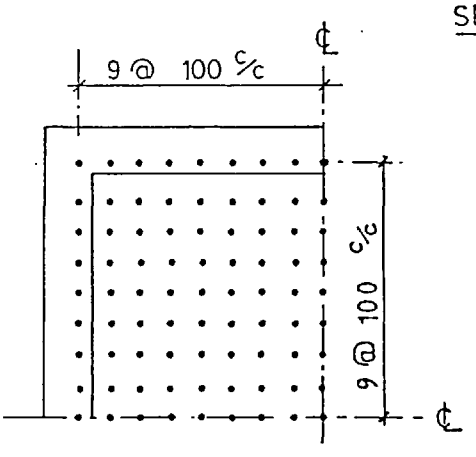

STUD POSITIONS

Note

For sections B-B & C-C
see fig C 37

PRESSURE BAG SUPPORT PLATFORM

Fig. C36

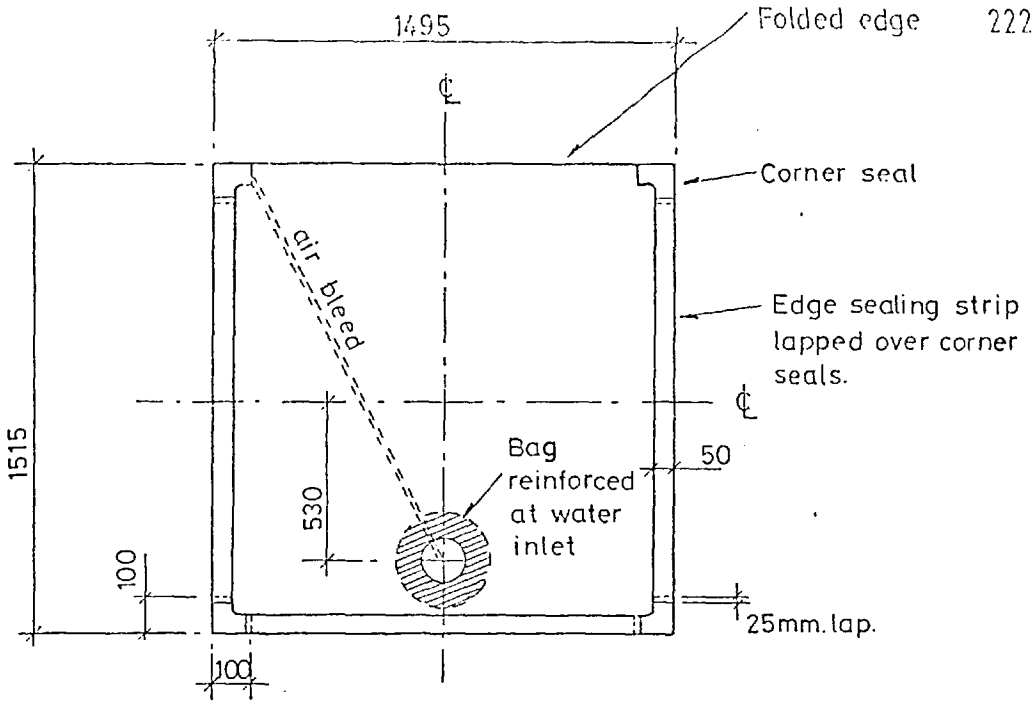

UNDER SIDE OF PRESSURE BAG

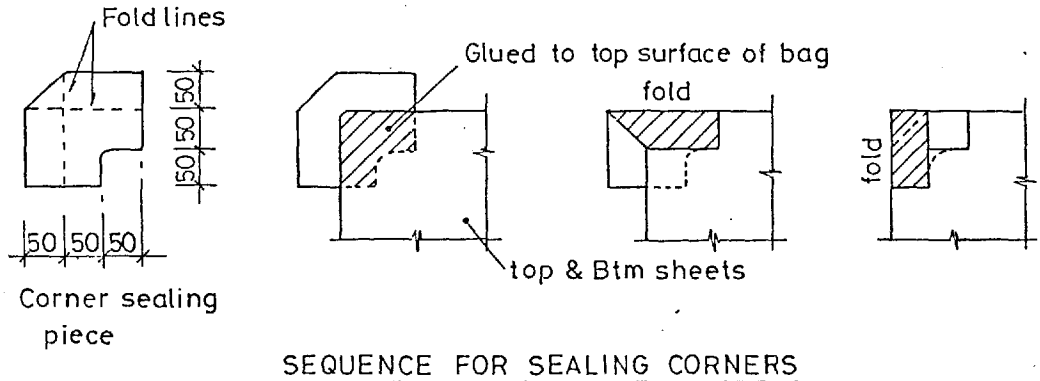

SEQUENCE FOR SEALING CORNERS

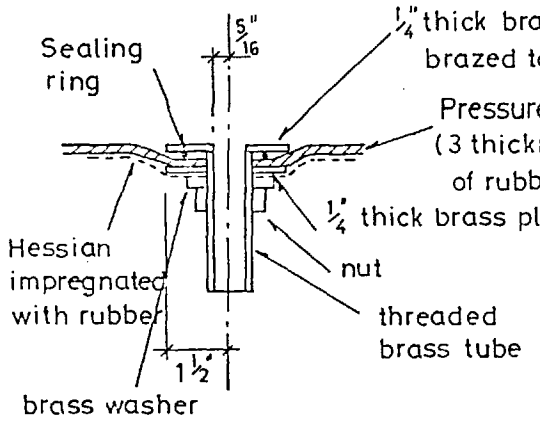

SECTION THROUGH WATER INLET

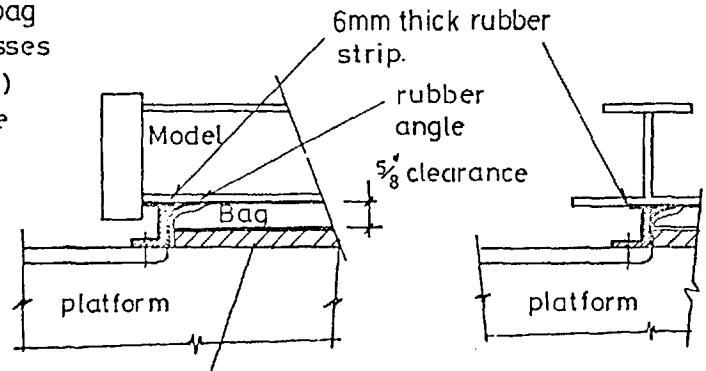

1/2" thick varnished ply-wood

SECTION B-B
(see fig C36)

SECTION C-C
(see fig C36)

Fig C37

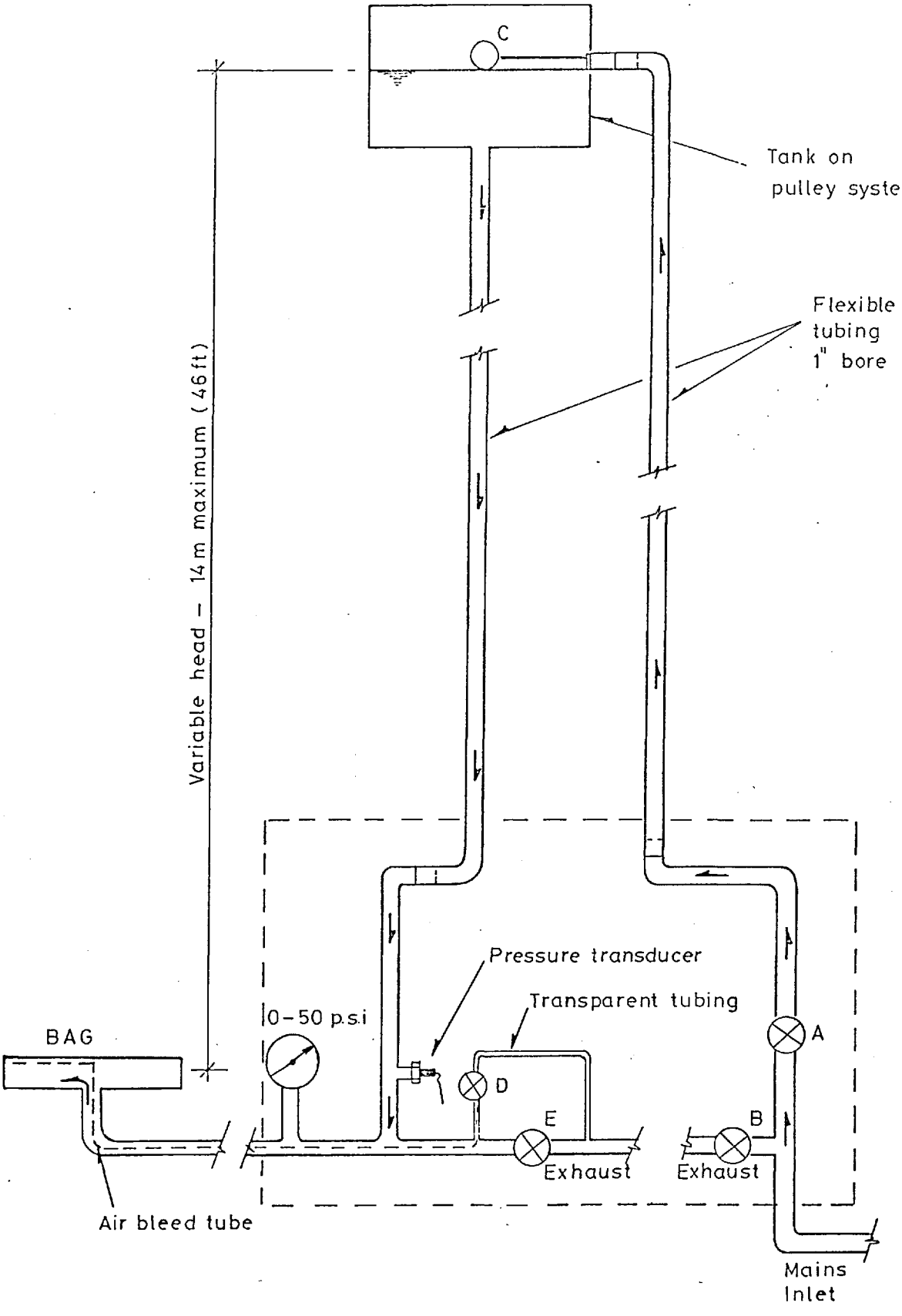

Fig C 38 Water pressure system

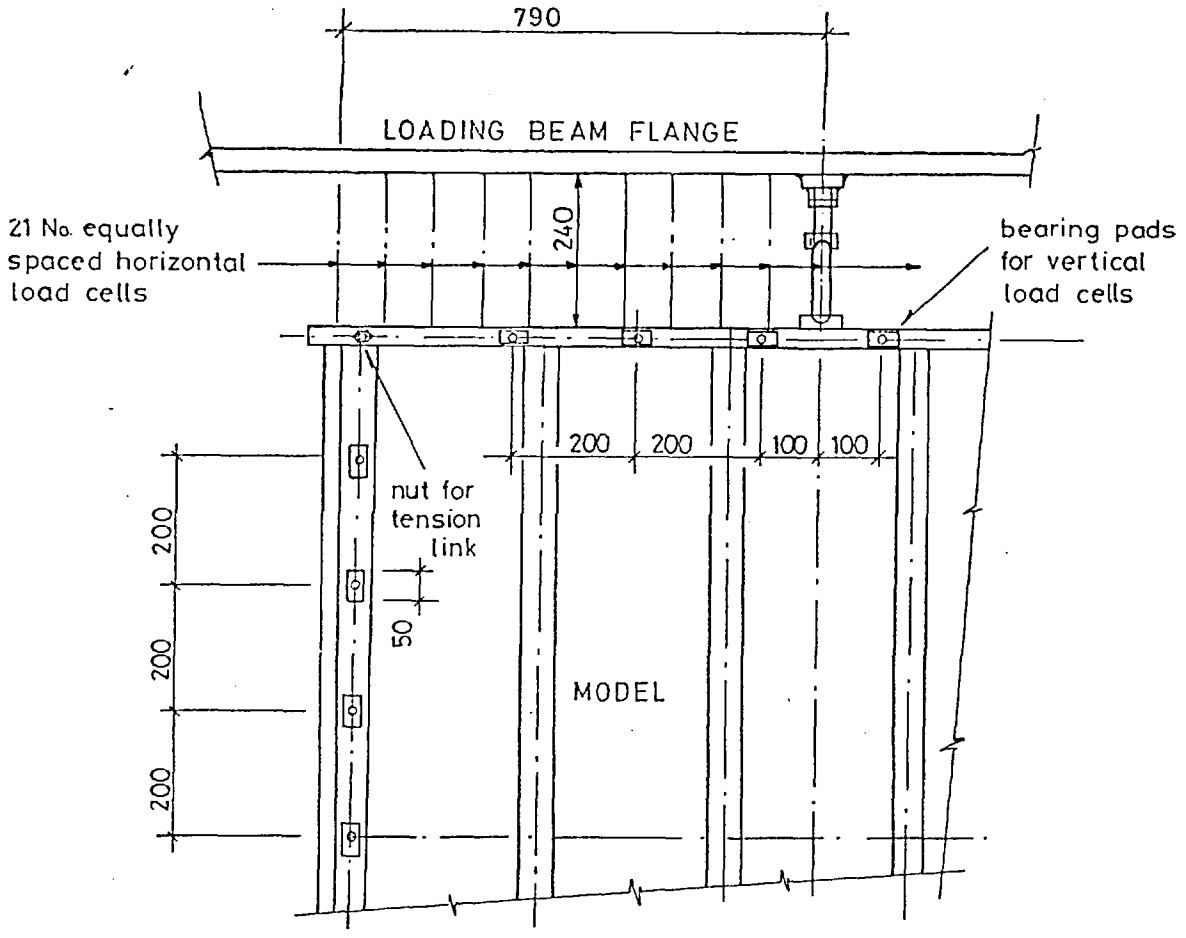

LOAD CELL POSITIONS

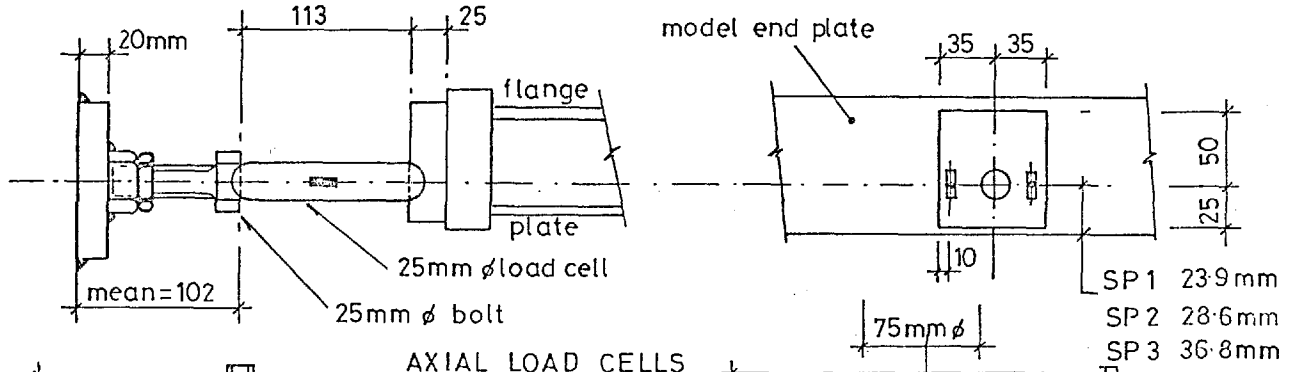

AXIAL LOAD CELLS

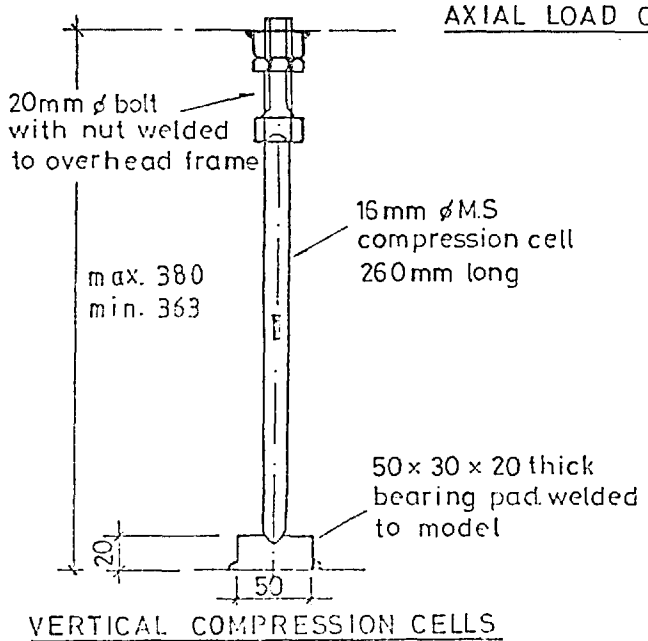

VERTICAL COMPRESSION CELLS

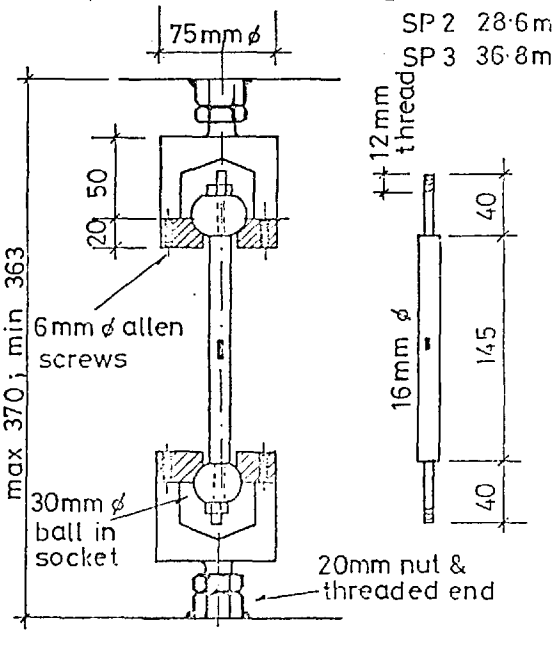

CORNER TIES

Fig C39

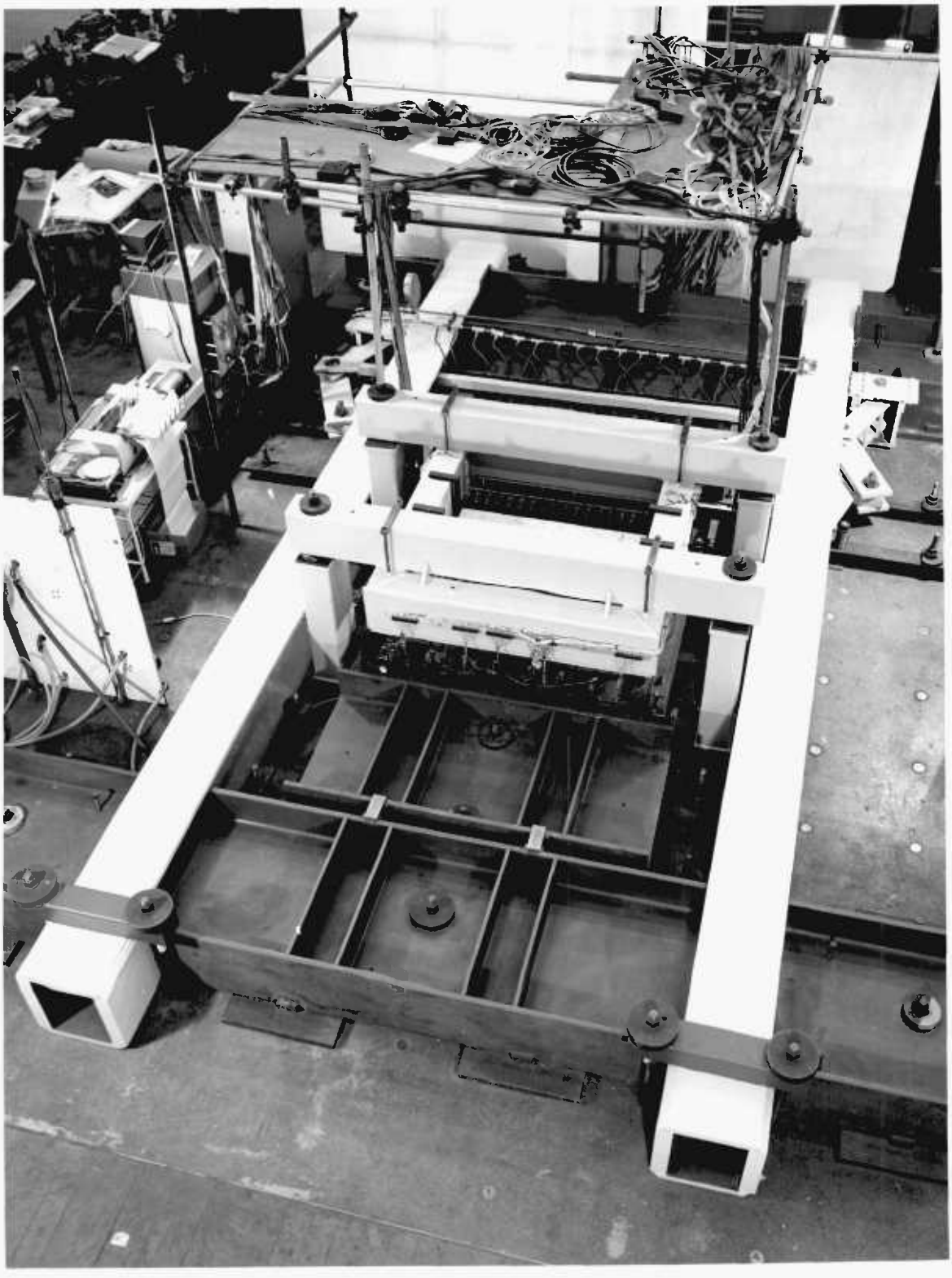

Fig C40 Testing rig viewed from the stationary end

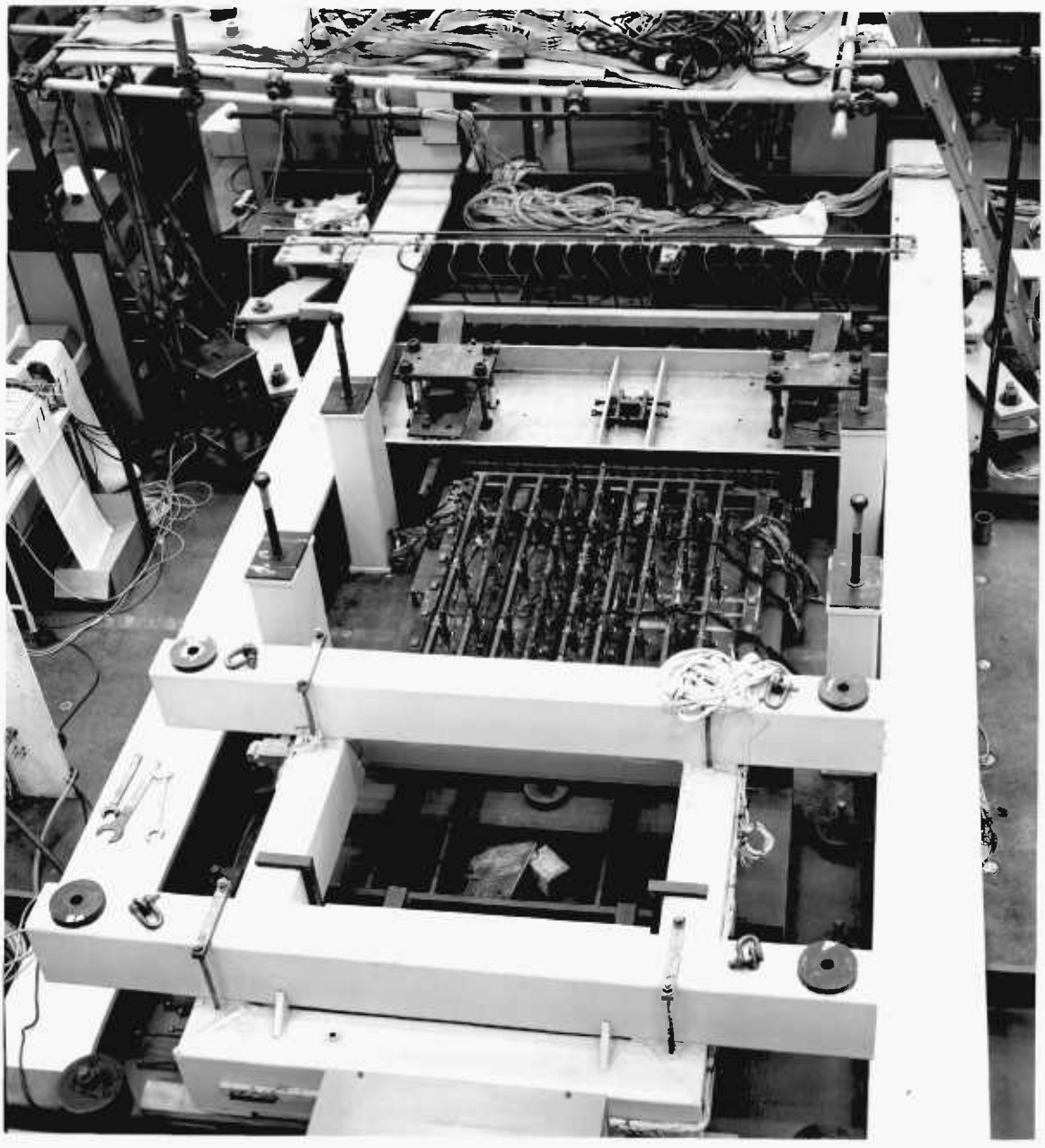

Fig C41 Testing rig with overhead reaction frame removed

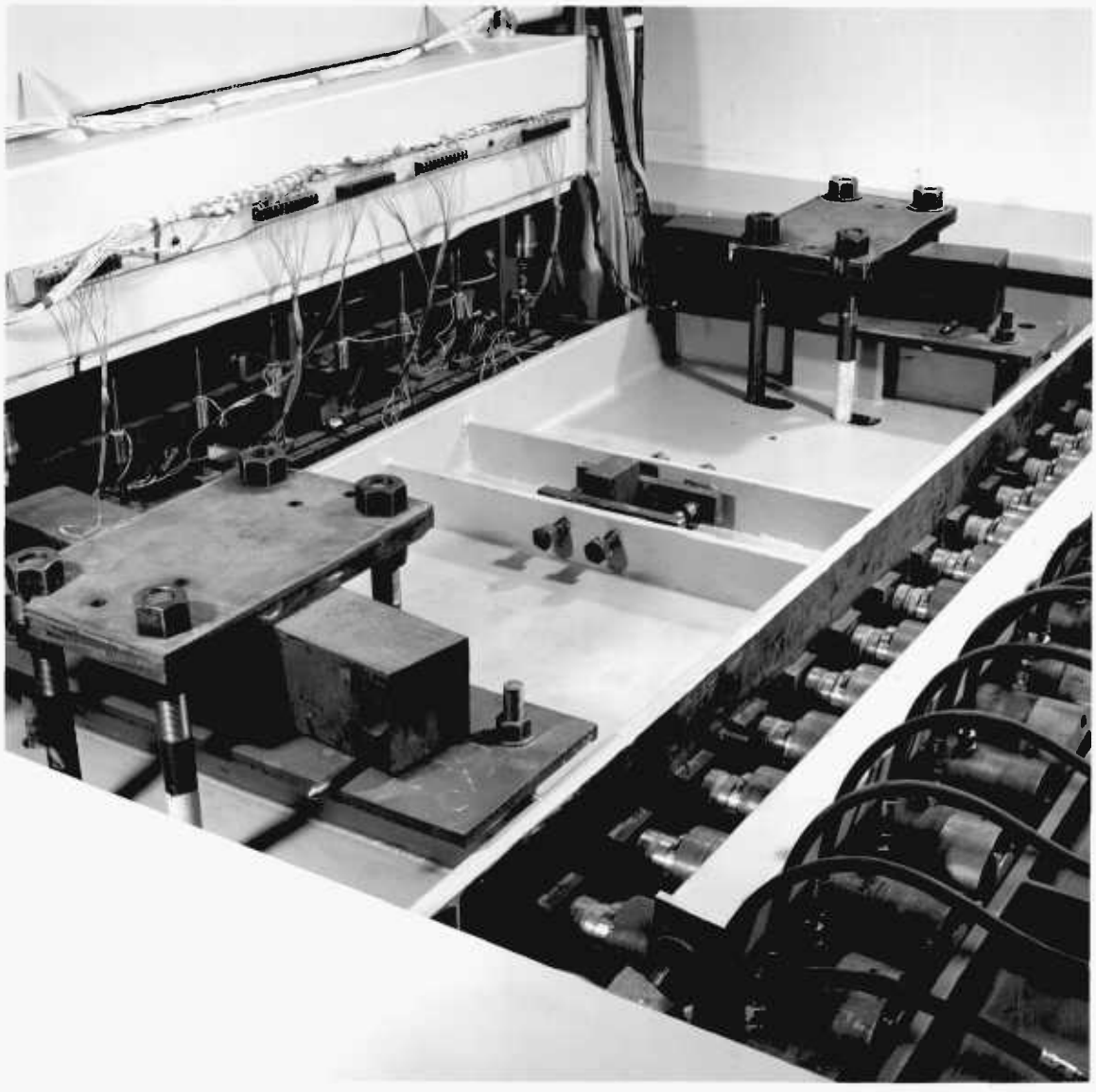

Fig C42 Loading beam showing the central nib constraint and the holding down arrangement

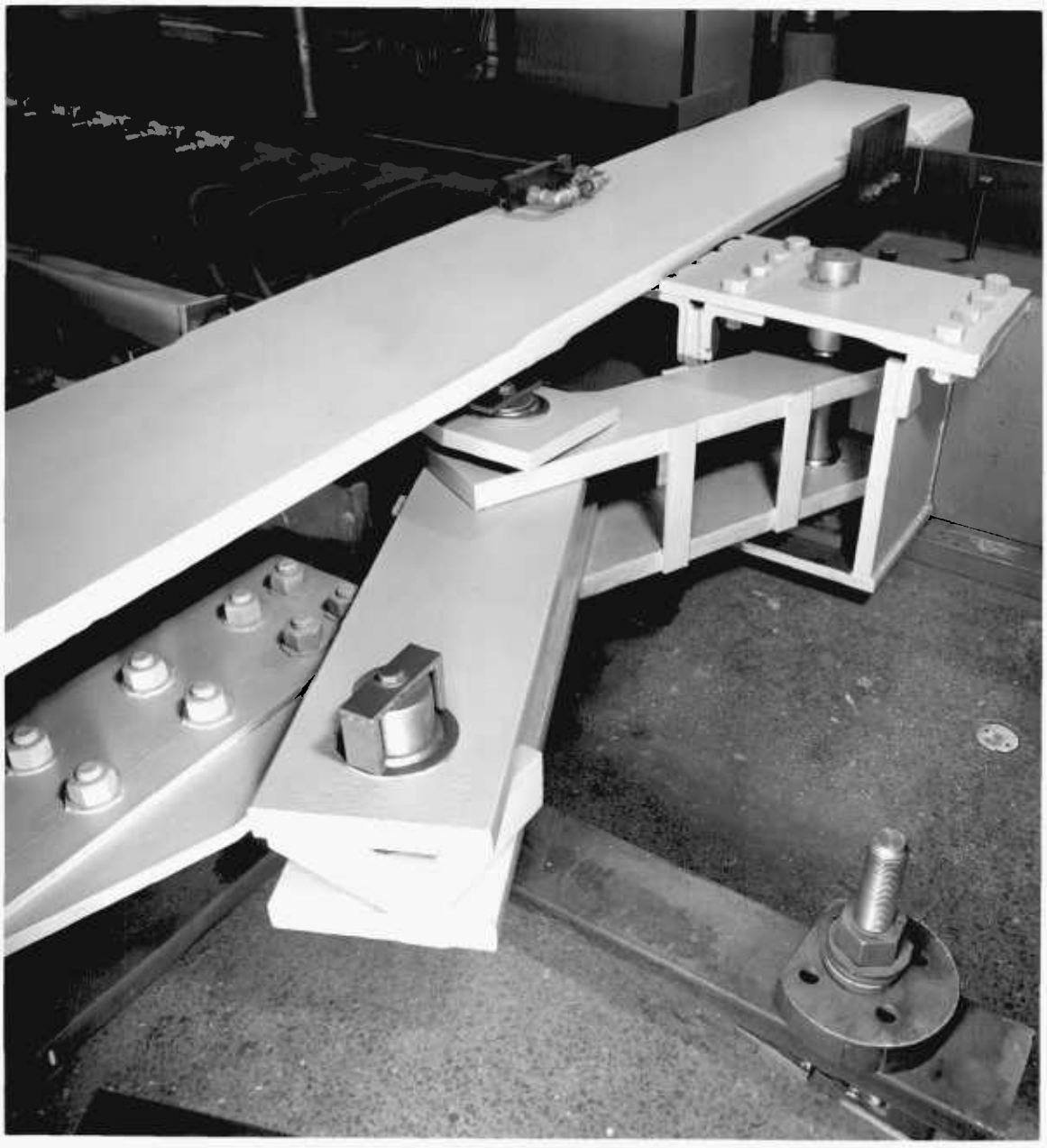

Fig C43 Parallel arm mechanism showing connections to beam A and the loading beam

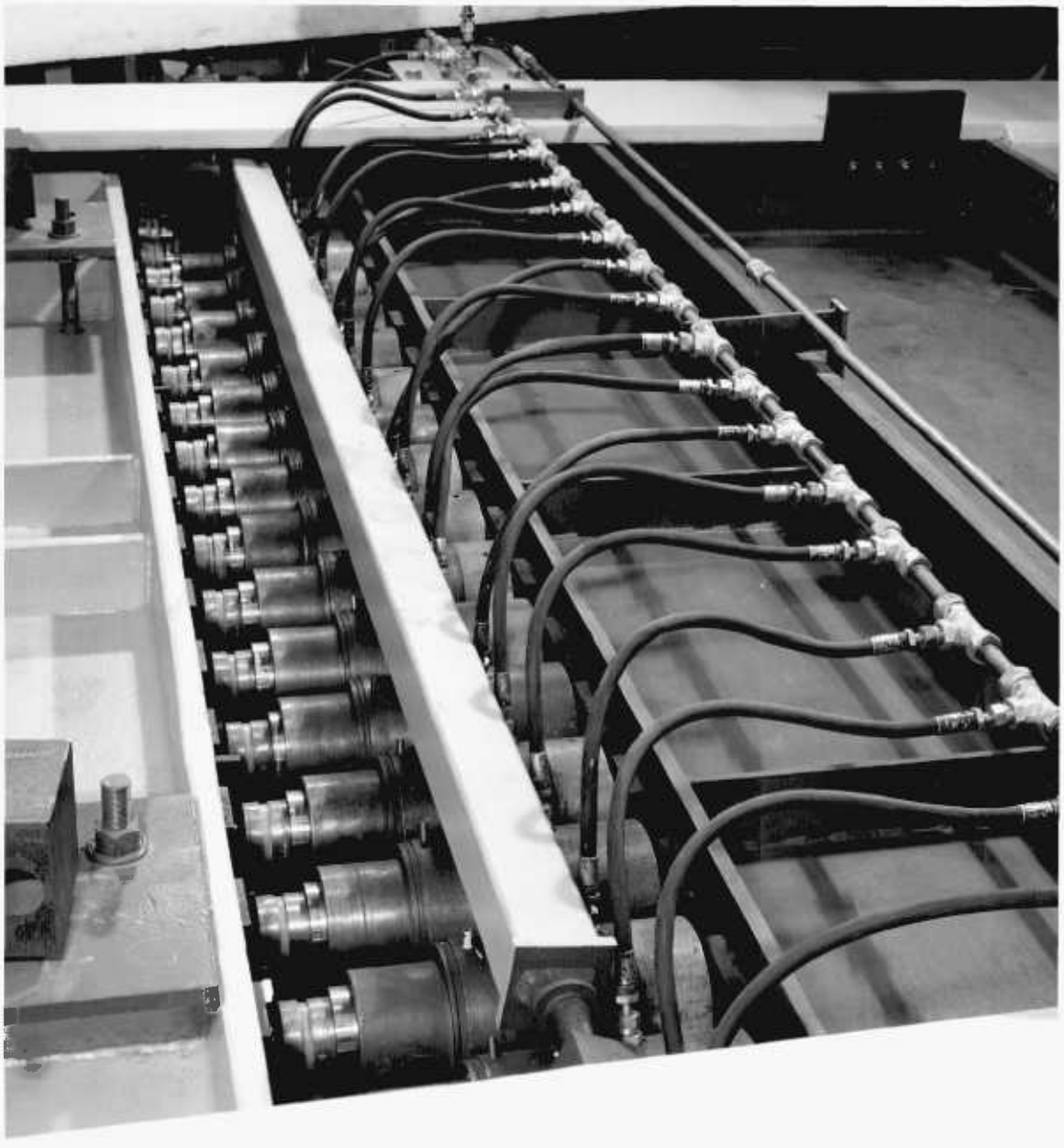

Fig C44 Arrangement of jacks between beam A and the loading beam

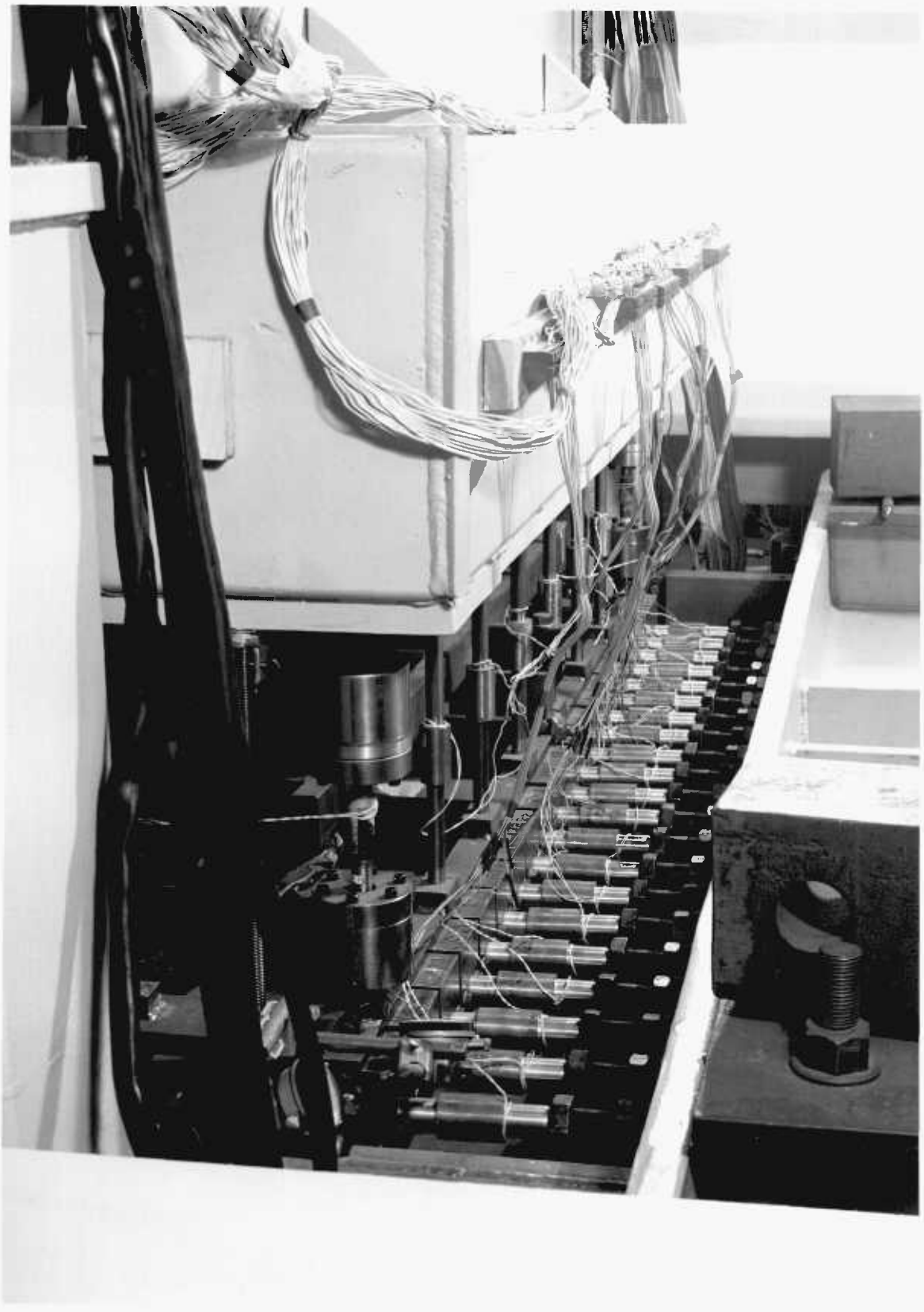

Fig C45 The arrangement of horizontal and vertical load cells

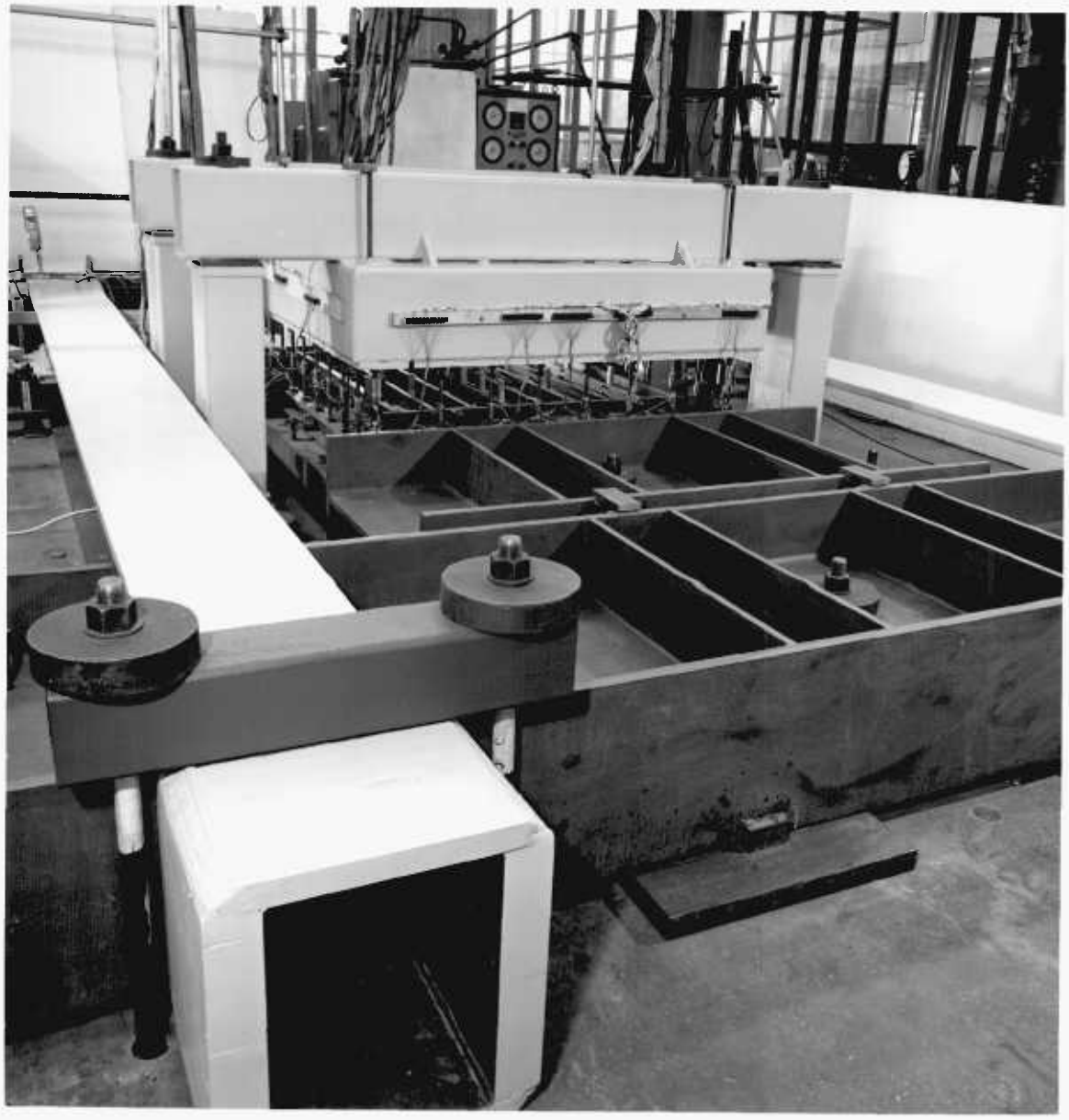

Fig C46 Tie plate connection detail at beam B

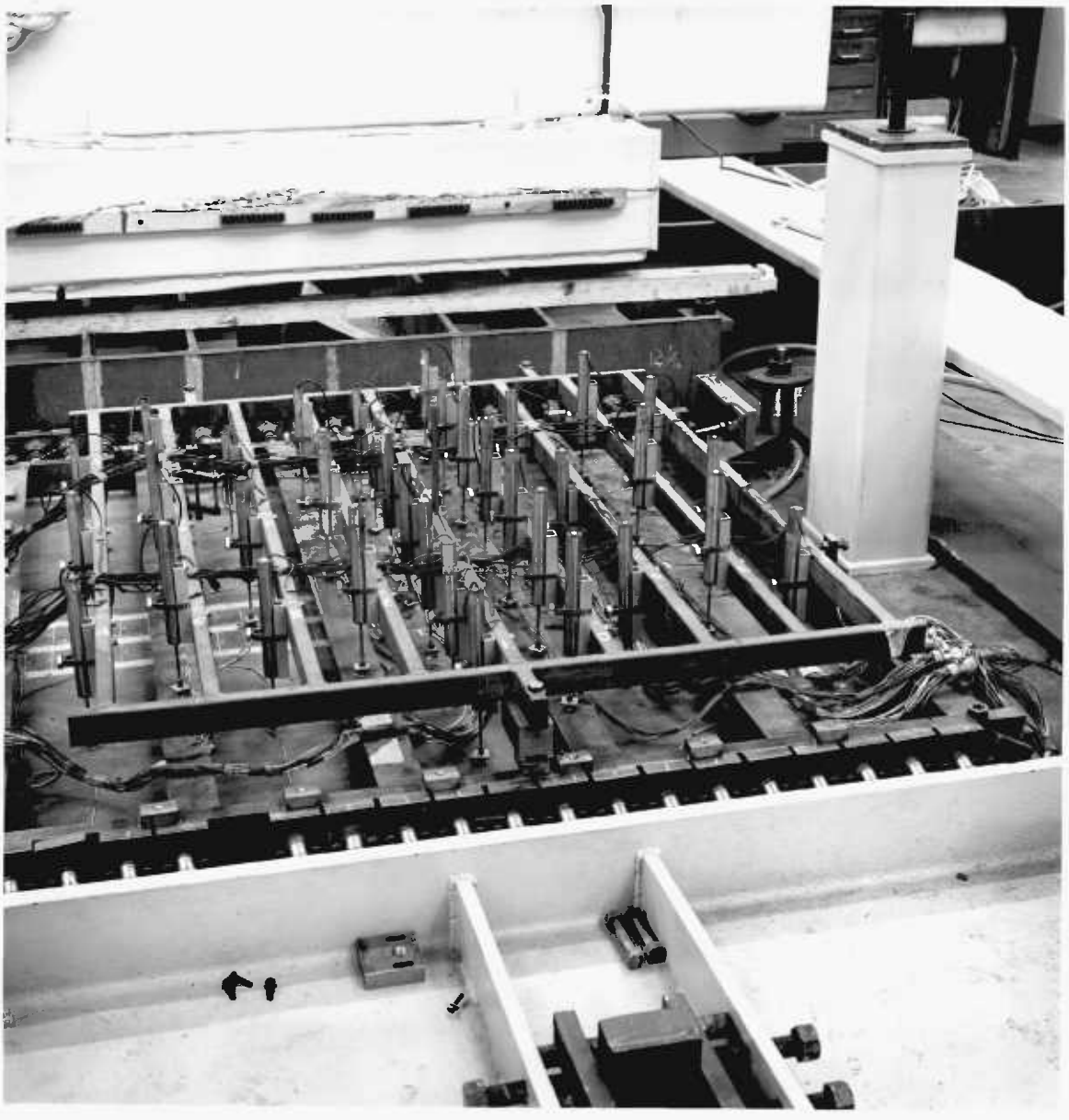

Fig C47 Model in rig with transducer frame over
(overhead frame and vertical load cells removed)

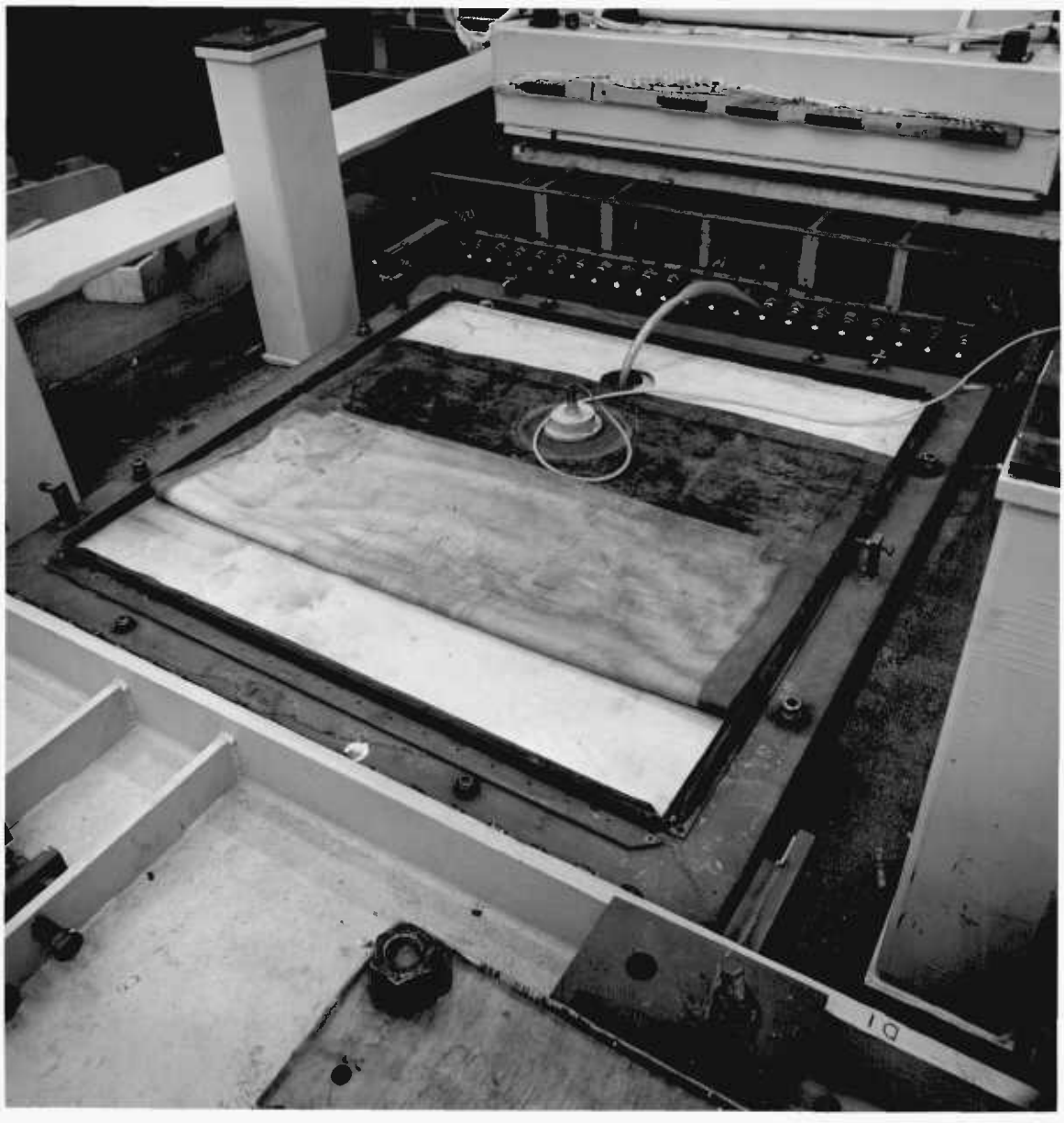

Fig C48 Pressure bag shown folded back on the support platform

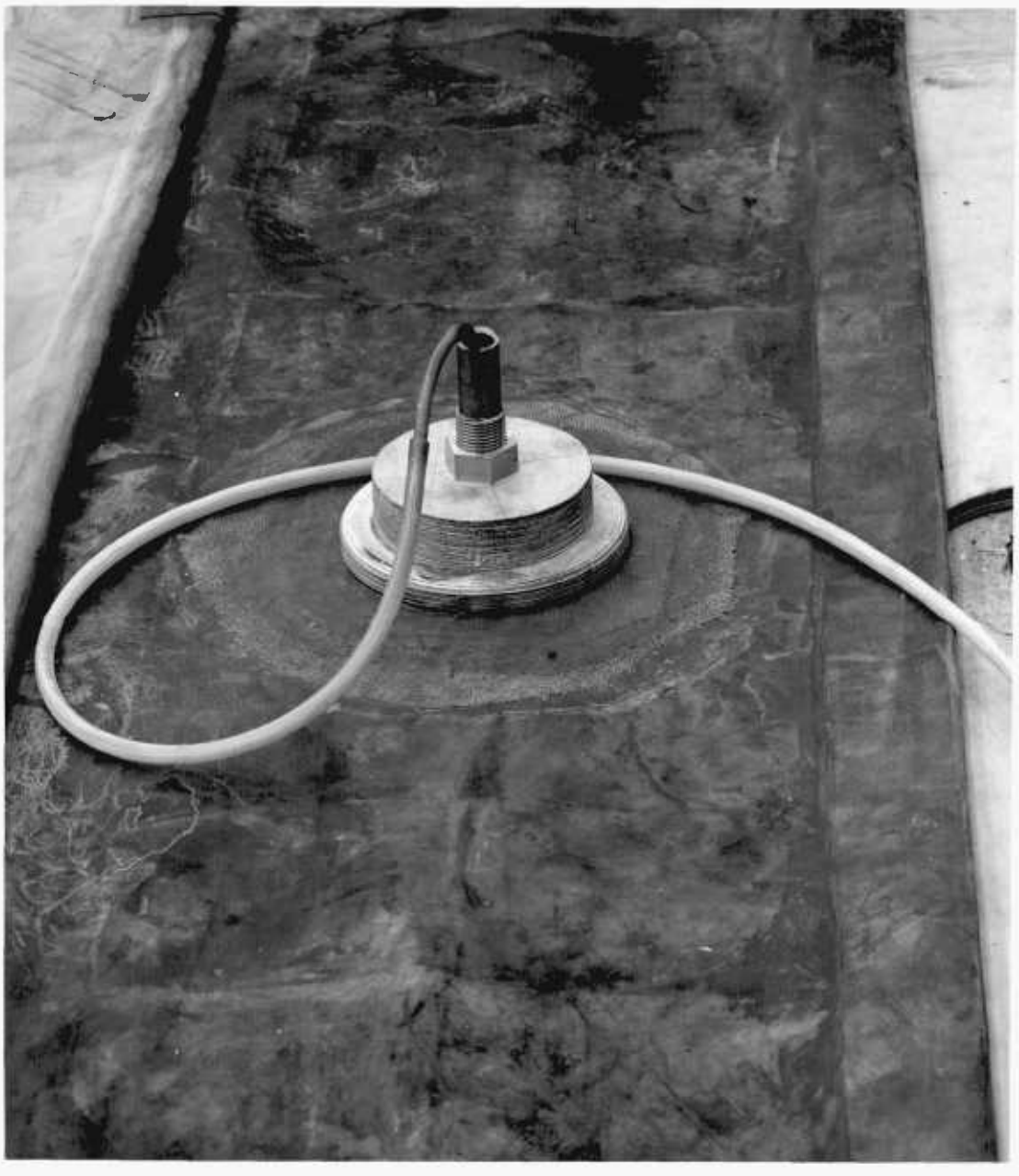

Fig C49 Detail of inlet to pressure bag

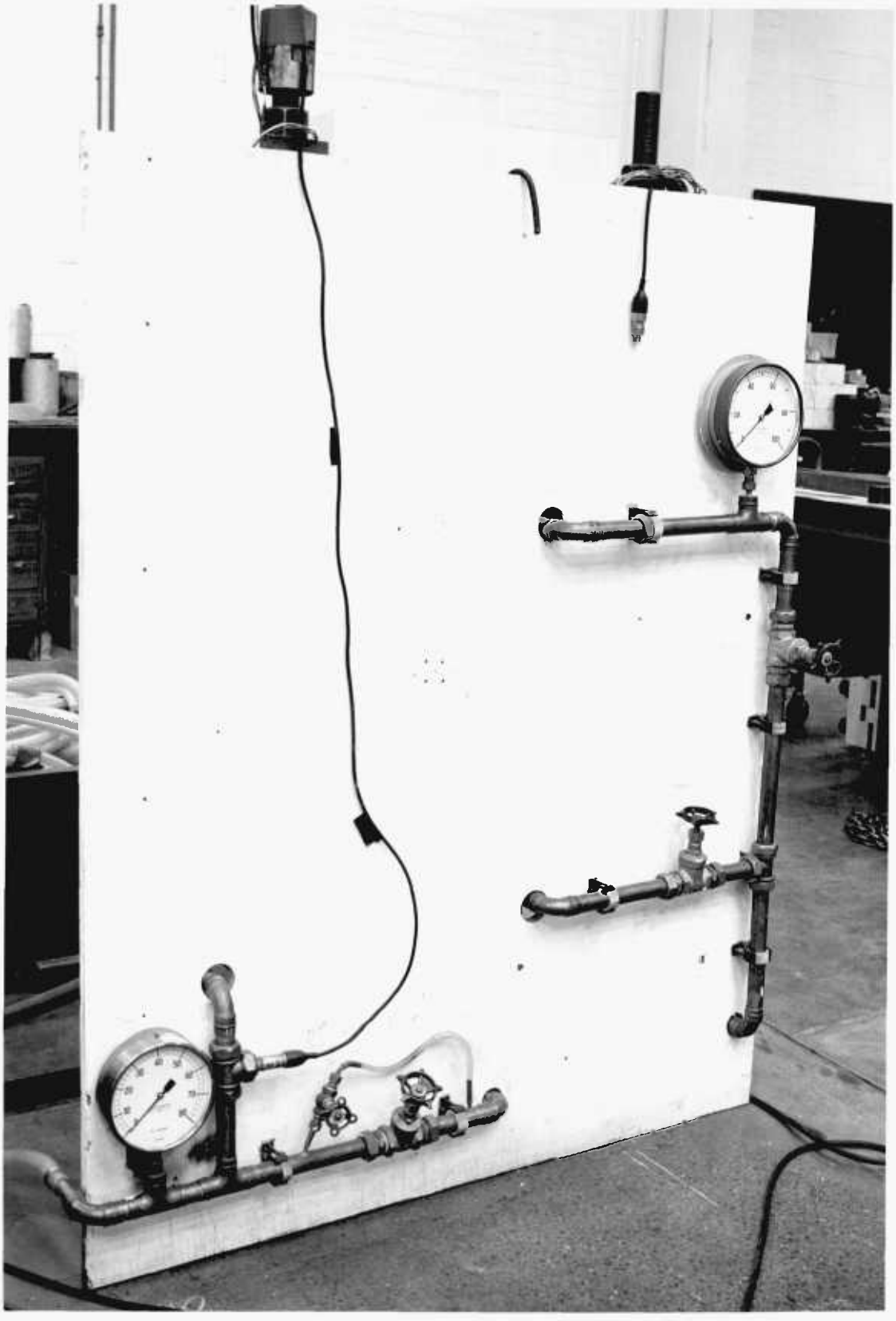

Fig C50 The water pressure control panel

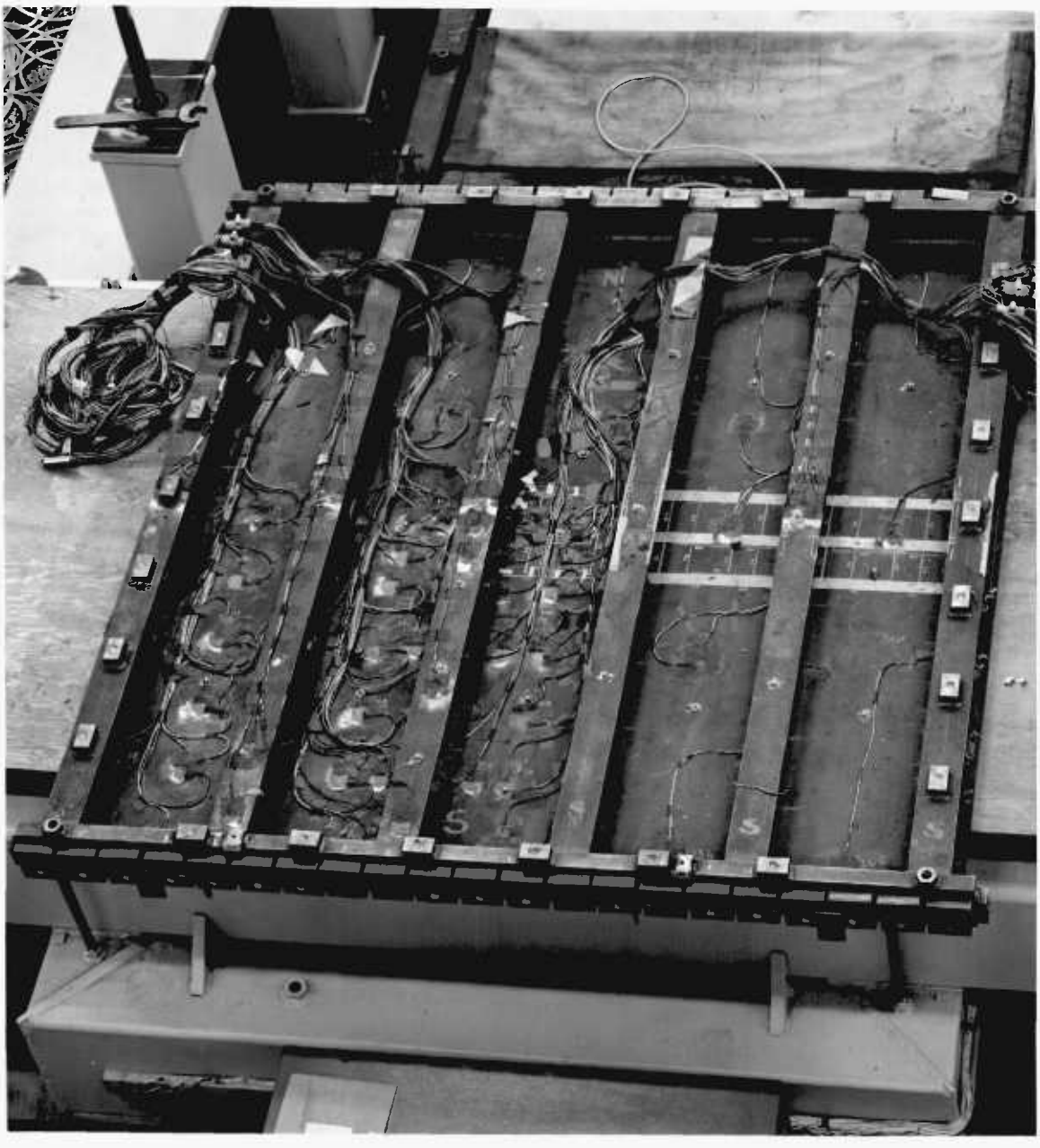

Fig C51 Stiffened plate model SP3

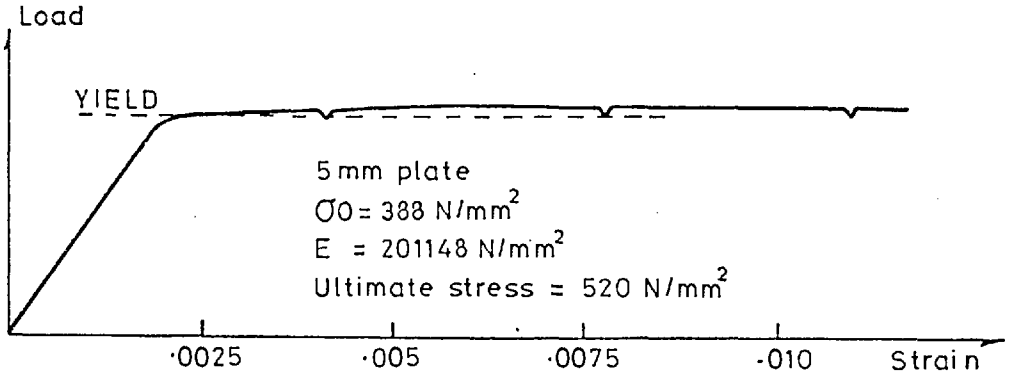

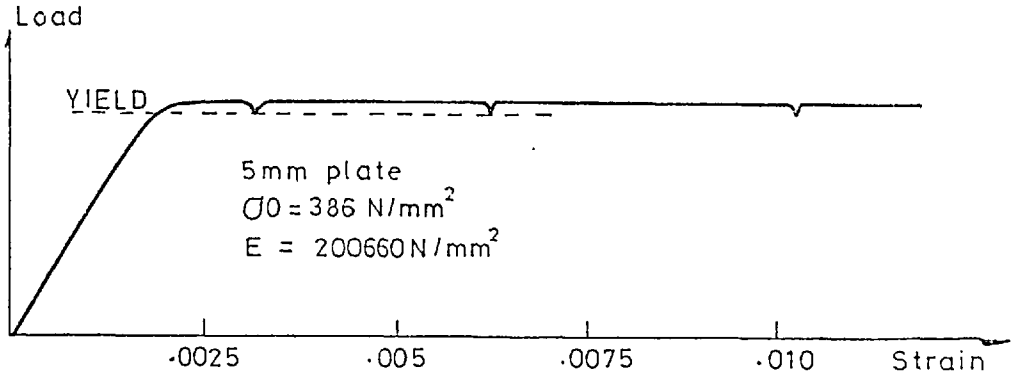

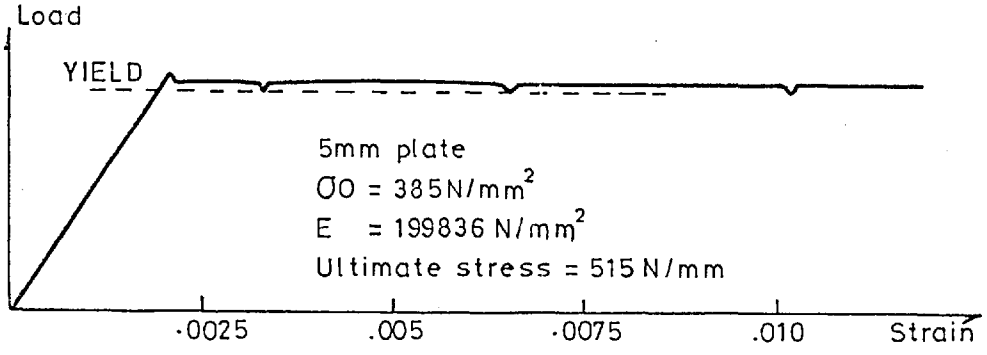

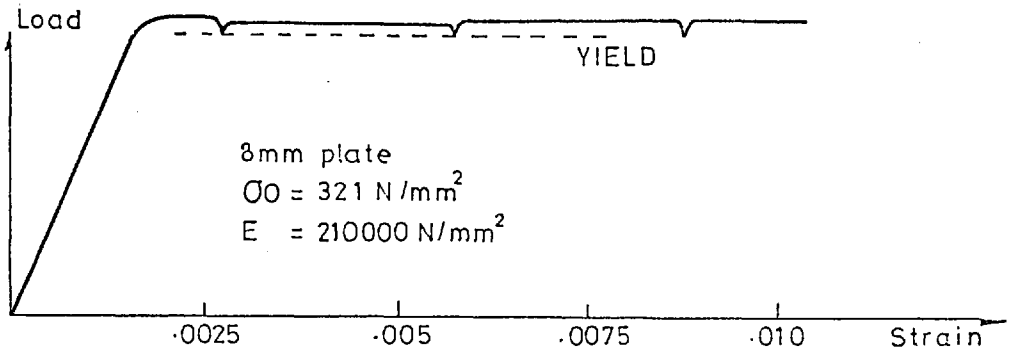

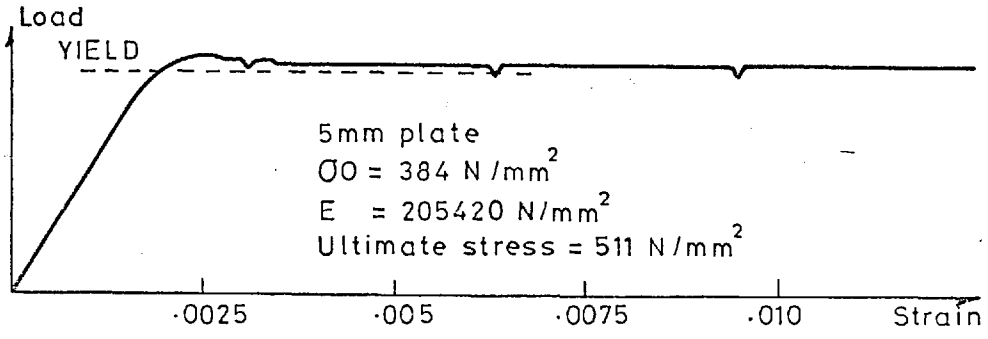

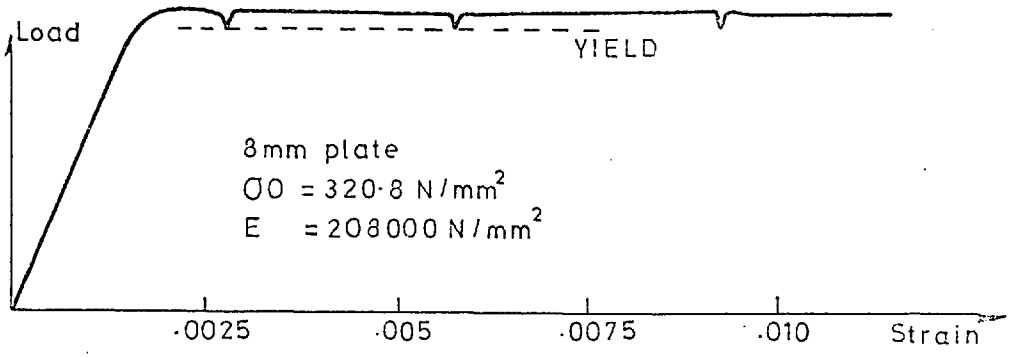

Fig.C.52 Tensile test results for 5mm and 8mm thick plating

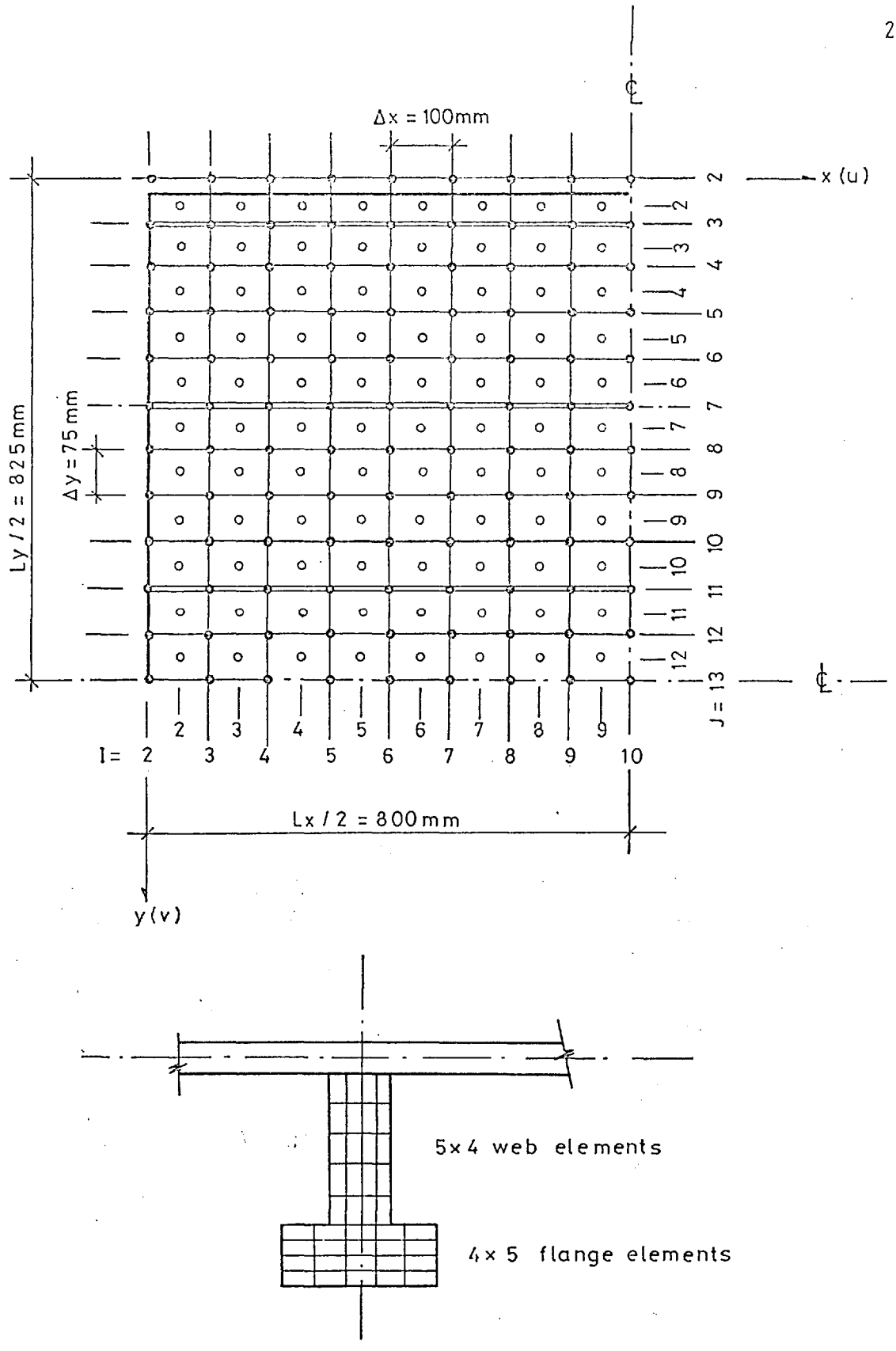

Fig D1 Finite difference mesh and stiffener elements assumed for analysis of models

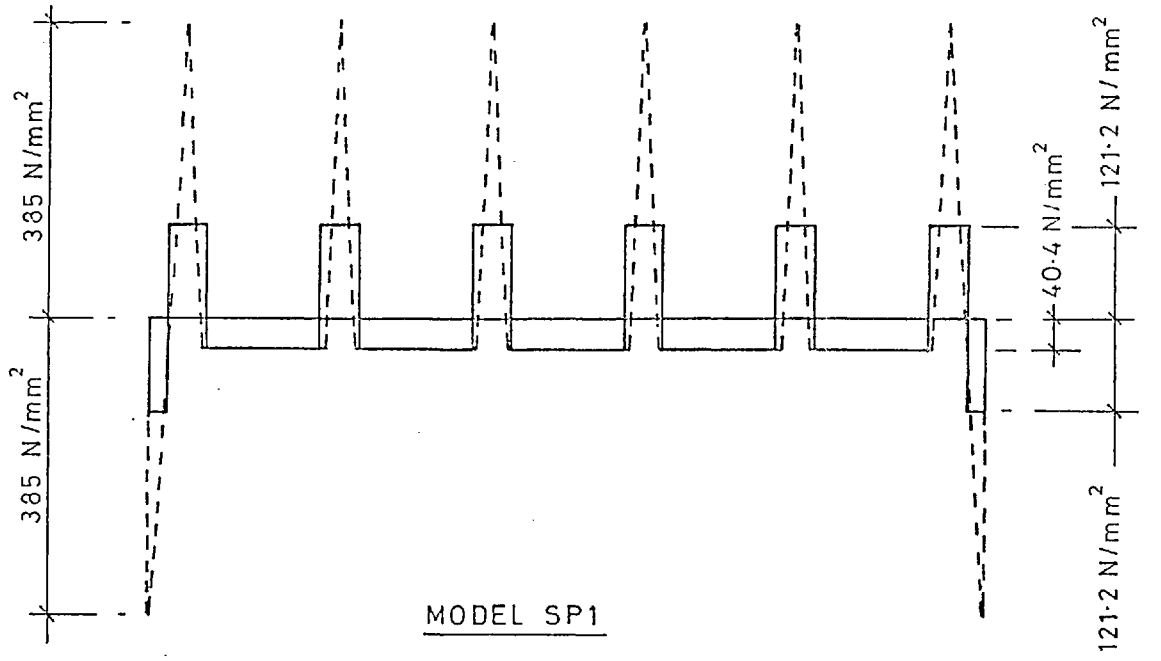

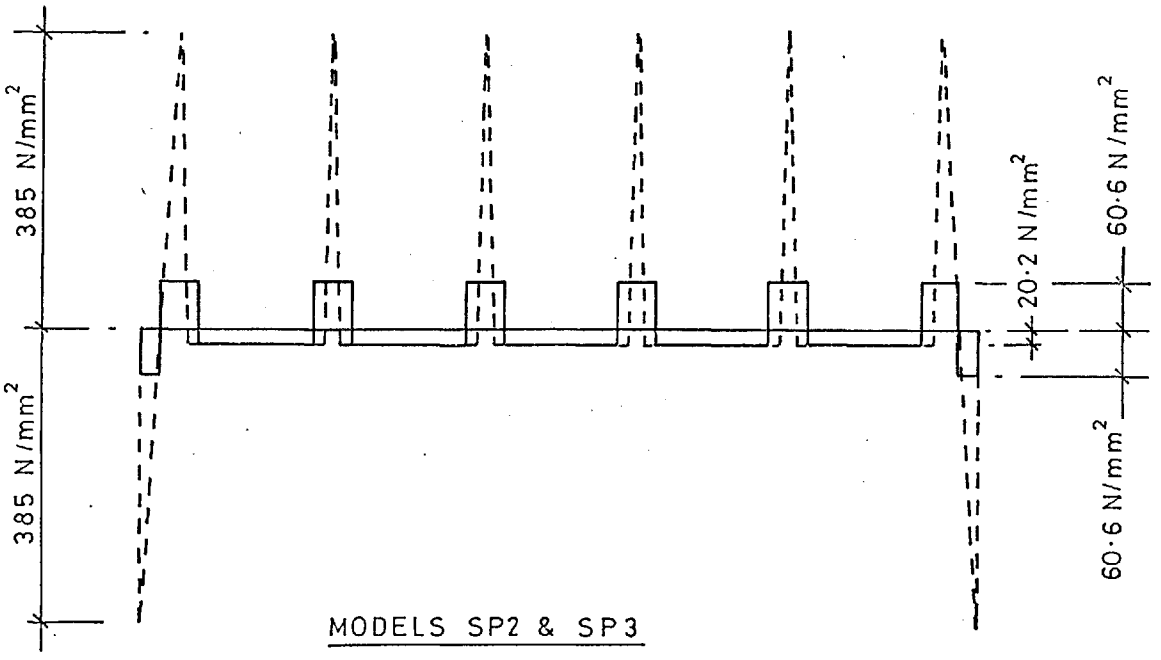

------ assumed stress pattern

——— idealised stress pattern

Fig. D 2 Assumed and idealised residual stress blocks used in analysis of stiffened plate models

MODEL	Lx mm	Ly mm	b mm	t mm	h_w mm	t_w mm	b_f mm	t_f mm	b / t	Lx / R
SP1	1600·0	1650·0	300·0	5·0	50·0	5·0	60·0	5·0	60·0	76·9
SP2	1600·0	1650·0	300·0	5·0	55·0	8·0	50·0	8·0	60·0	65·1
SP3	1600·0	1650·0	300·0	5·0	70·0	8·0	70·0	8·0	60·0	48·9

MODEL	$\sigma 0$ N/mm^2	$\sigma 0_w$ N/mm^2	$\sigma 0_f$ N/mm^2	E N/mm^2	V	σR N/mm^2	wc mm	wpan mm	q KN/m^2
SP1	385·0	385·0	385·0	202000·0	0·3	40·4	−1·05	+1·0	50·0
SP2	385·0	321·0	321·0	202000·0	0·3	20·2	+0·85	+1·4	80·0
SP3	385·0	321·0	321·0	202000·0	0·3	20·2	−2·1	+1·2	133·7

Fig.D3 Dimensions and properties used for analysis of models

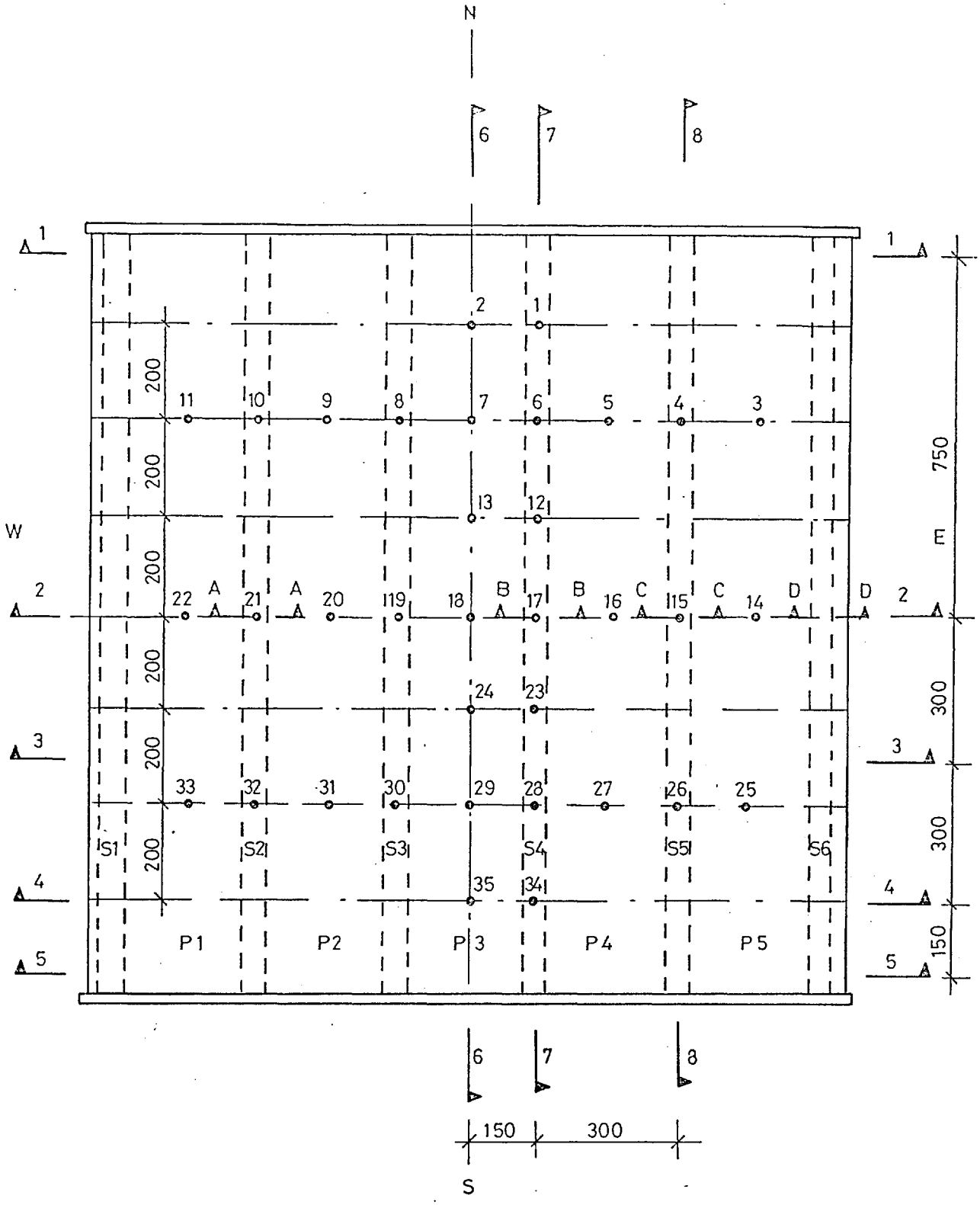

Fig D4. Cross-sections and plate locations shown in Figs. D5 to D22

(Viewed from unstiffened side)

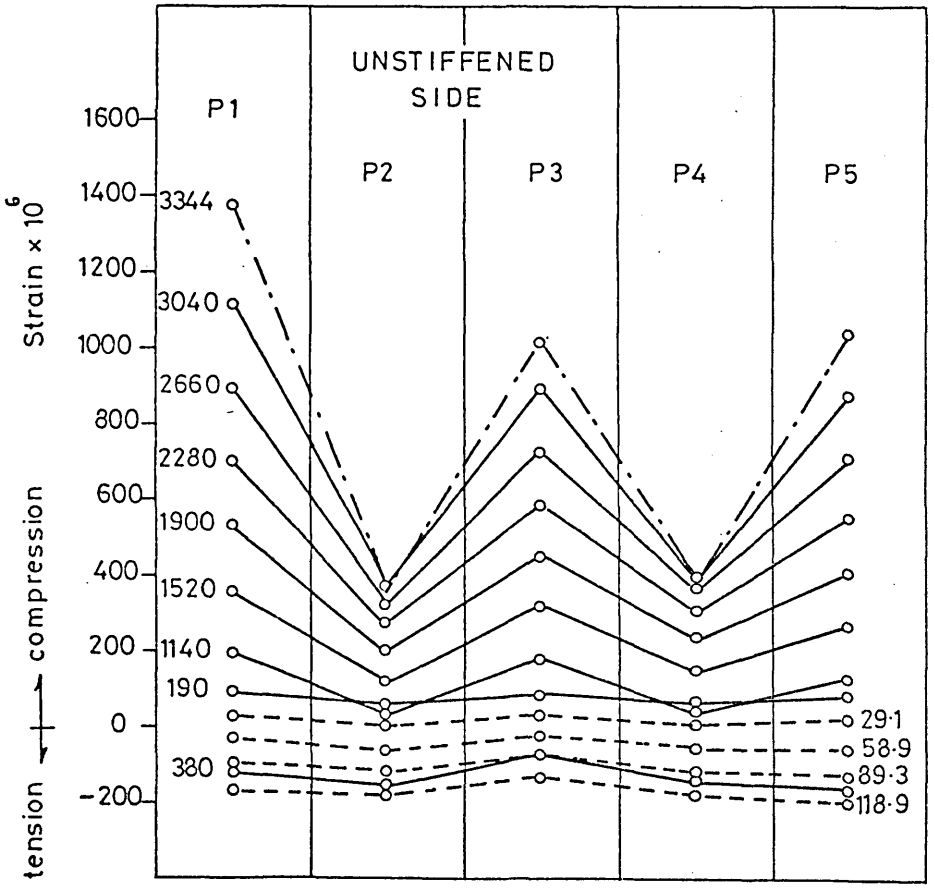

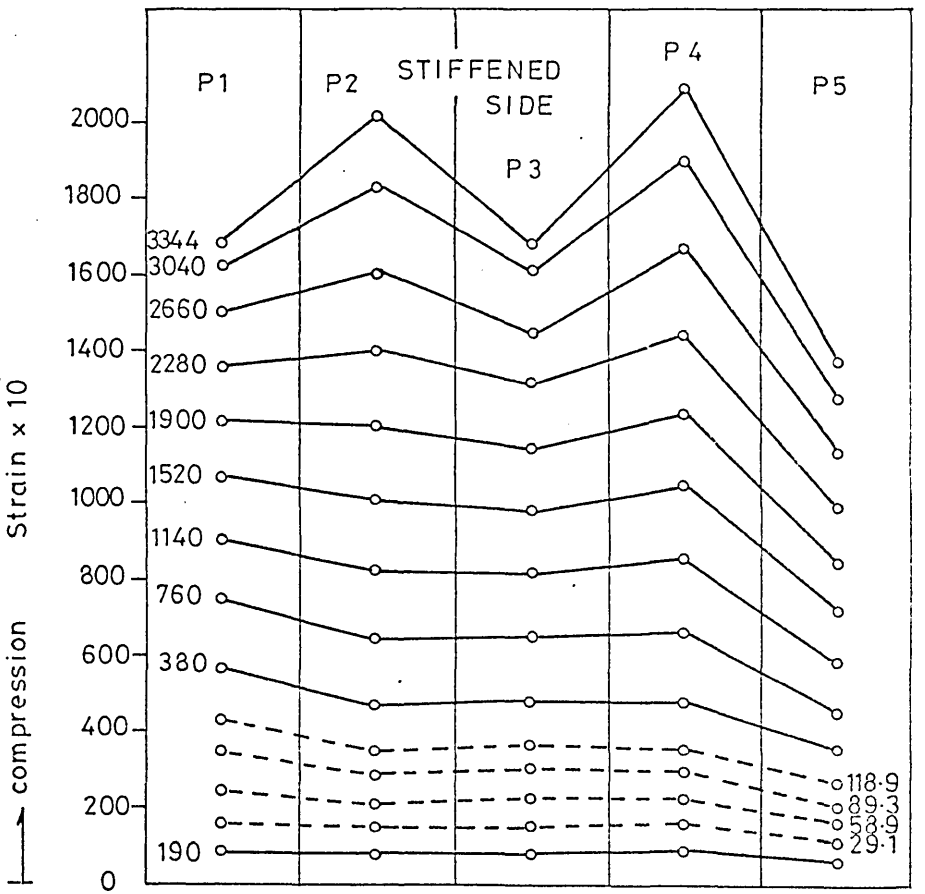

Fig D5. Model SP3. Measured longitudinal strains at section 1-1 (see fig D4)

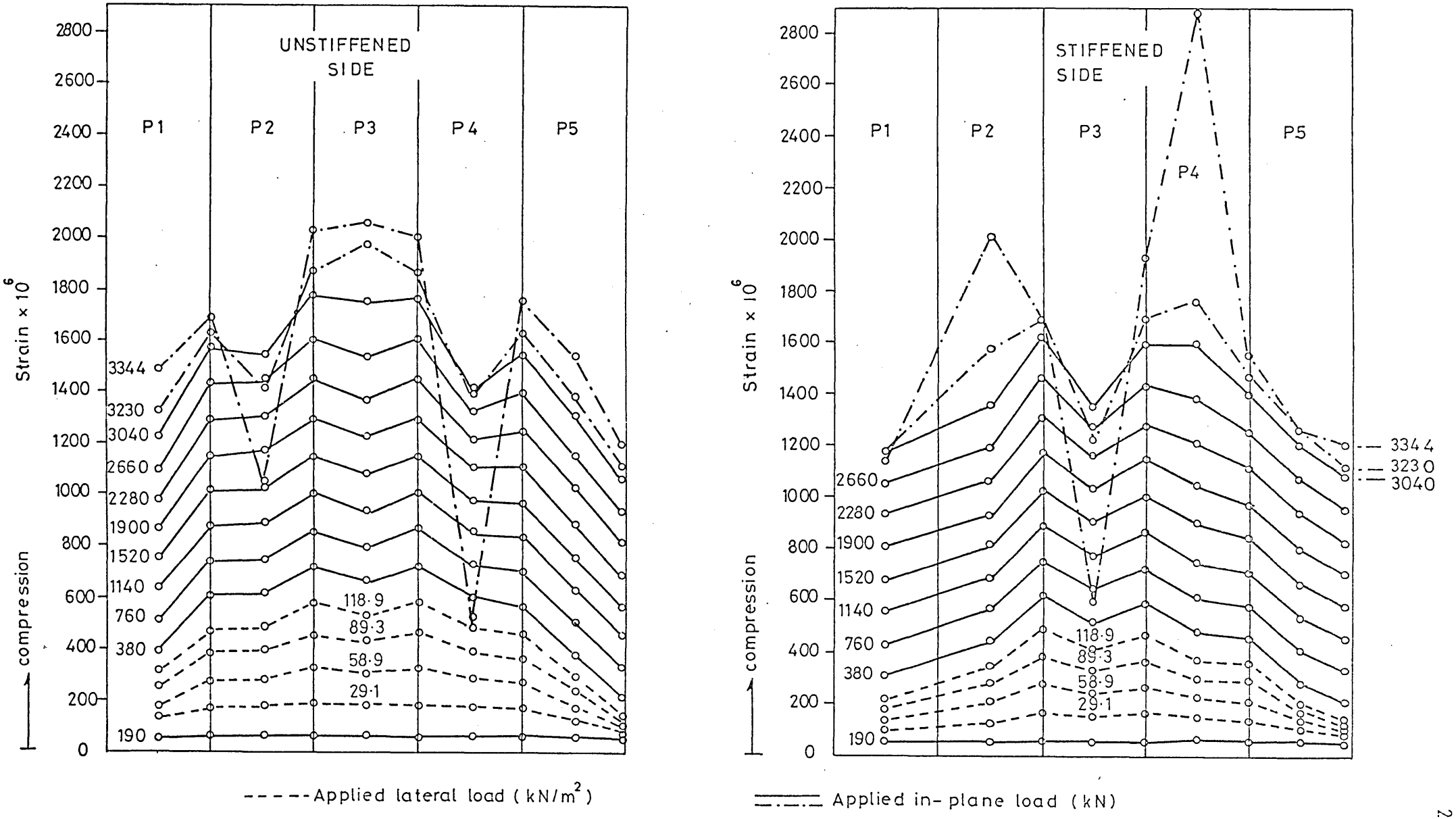

Fig D6 Model SP3. Measured longitudinal strains at section 2-2 (see fig D4)

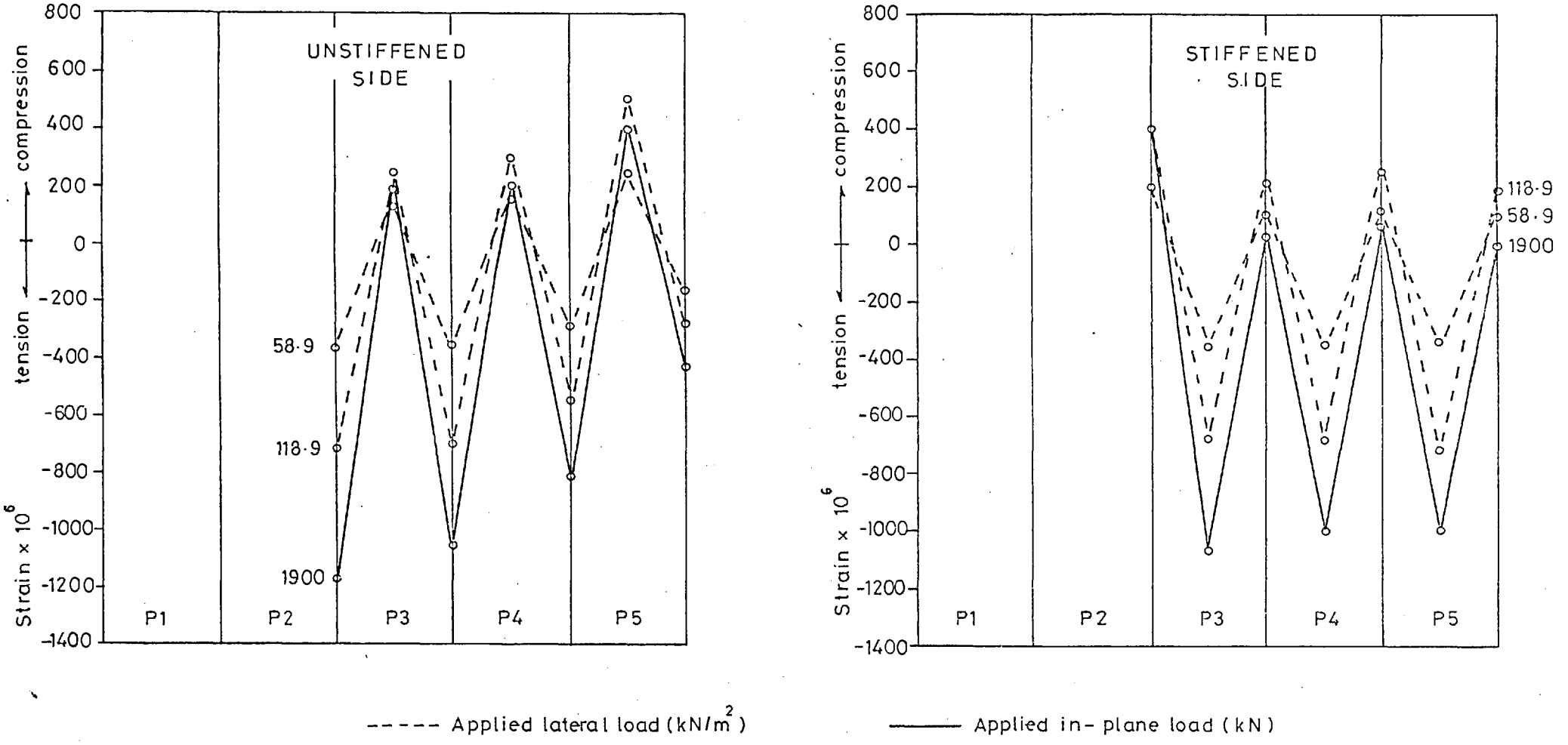

Fig D7 Model SP3. Measured transverse strains at section 2-2 (see fig D4)

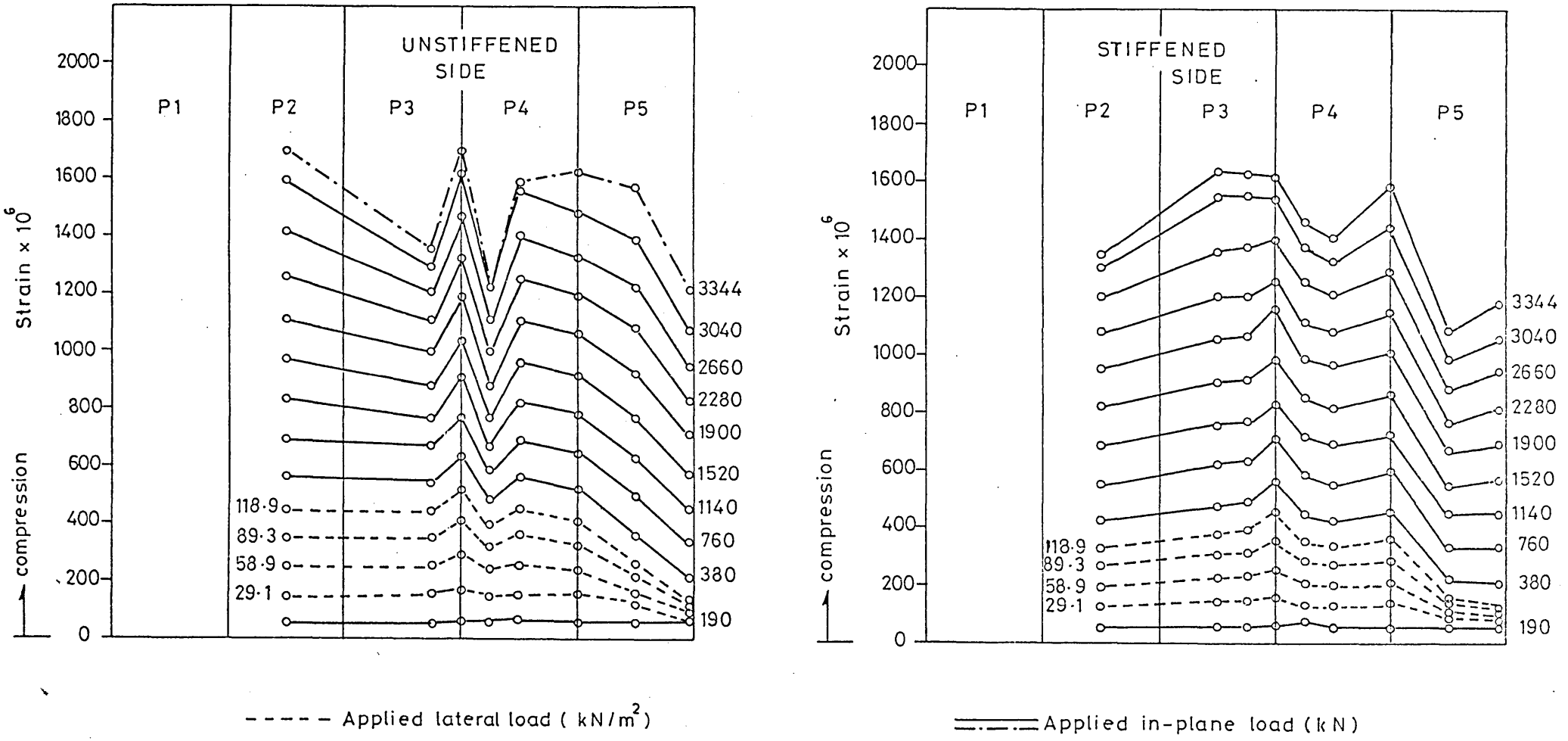

Fig D8. Model SP3. Measured longitudinal strains at section 3-3 (see fig D4)

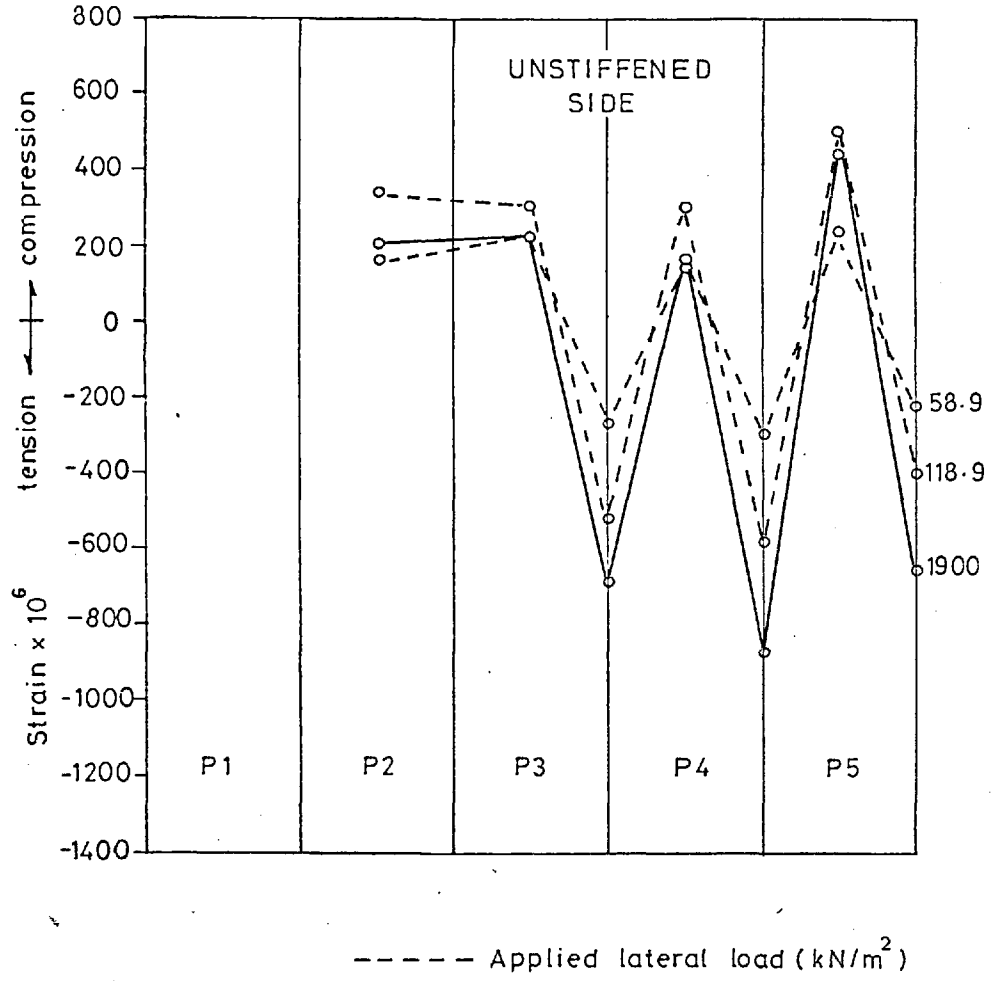

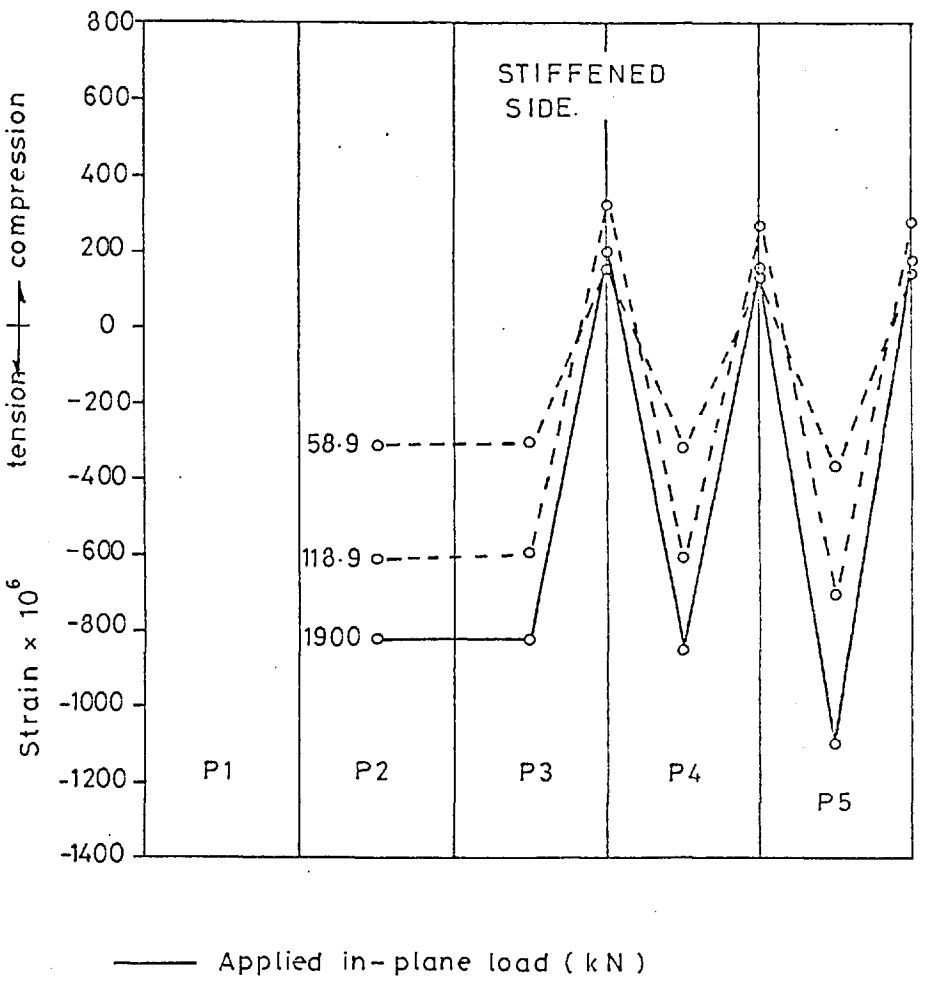

Fig D9. Model SP3. Measured transverse strains at section 3-3 (see fig D4)

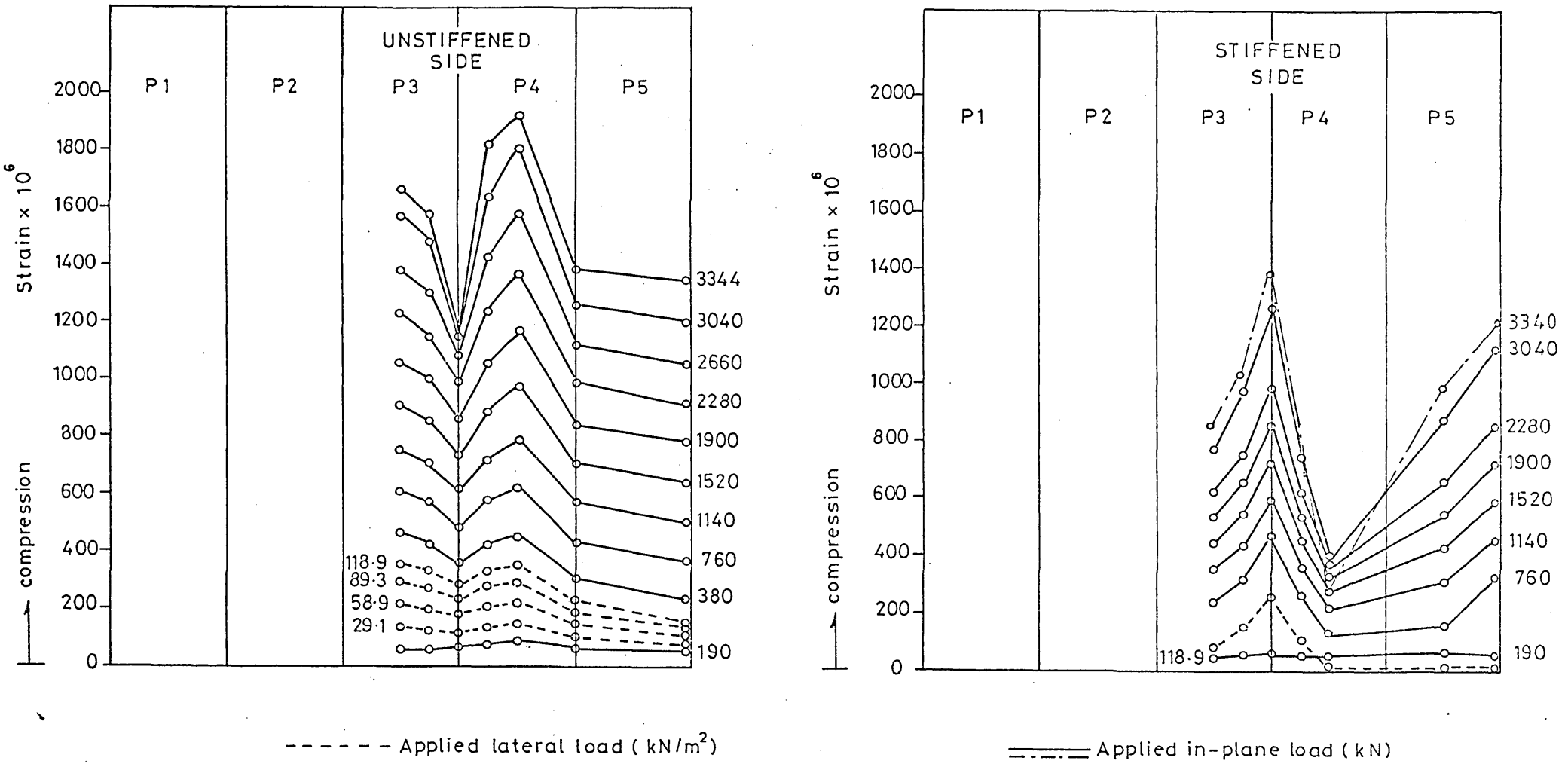

Fig D10 Model SP3. Measured longitudinal strains at section 4-4 (see fig D4)

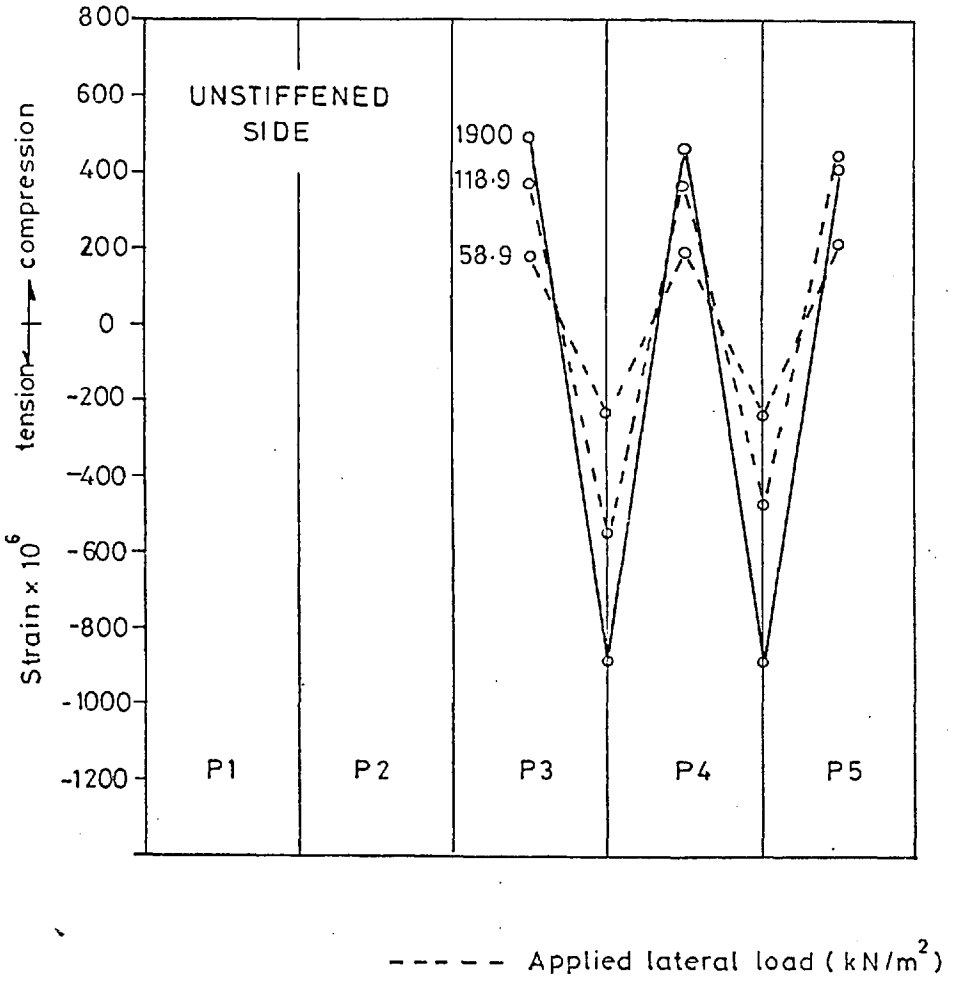

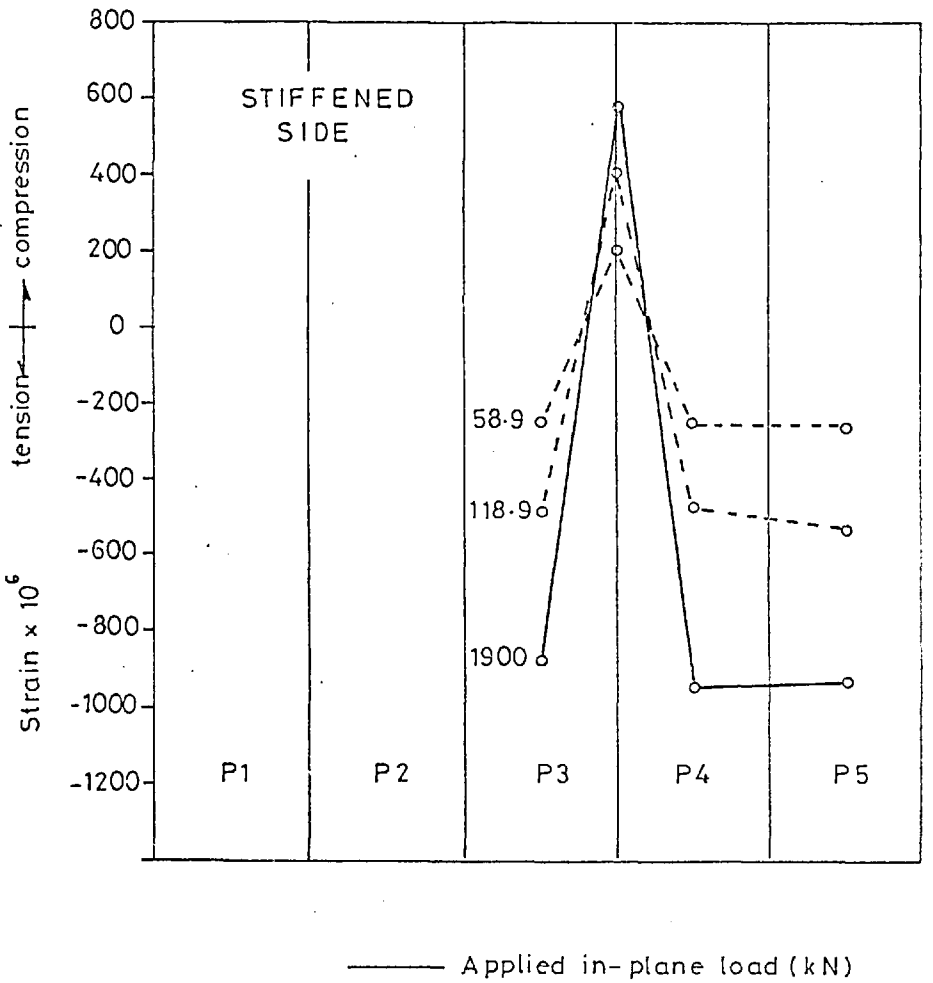

Fig D11. Model SP3. Measured transverse strains at section 4-4 (see fig D4)

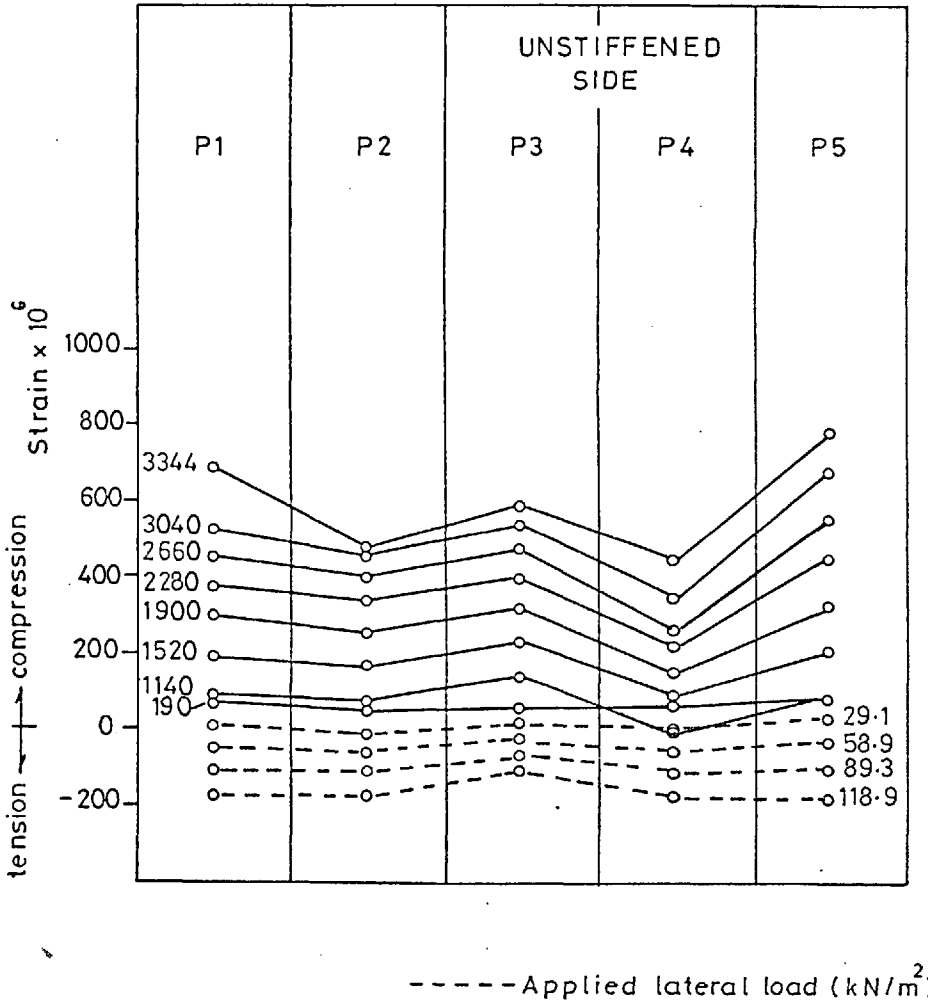

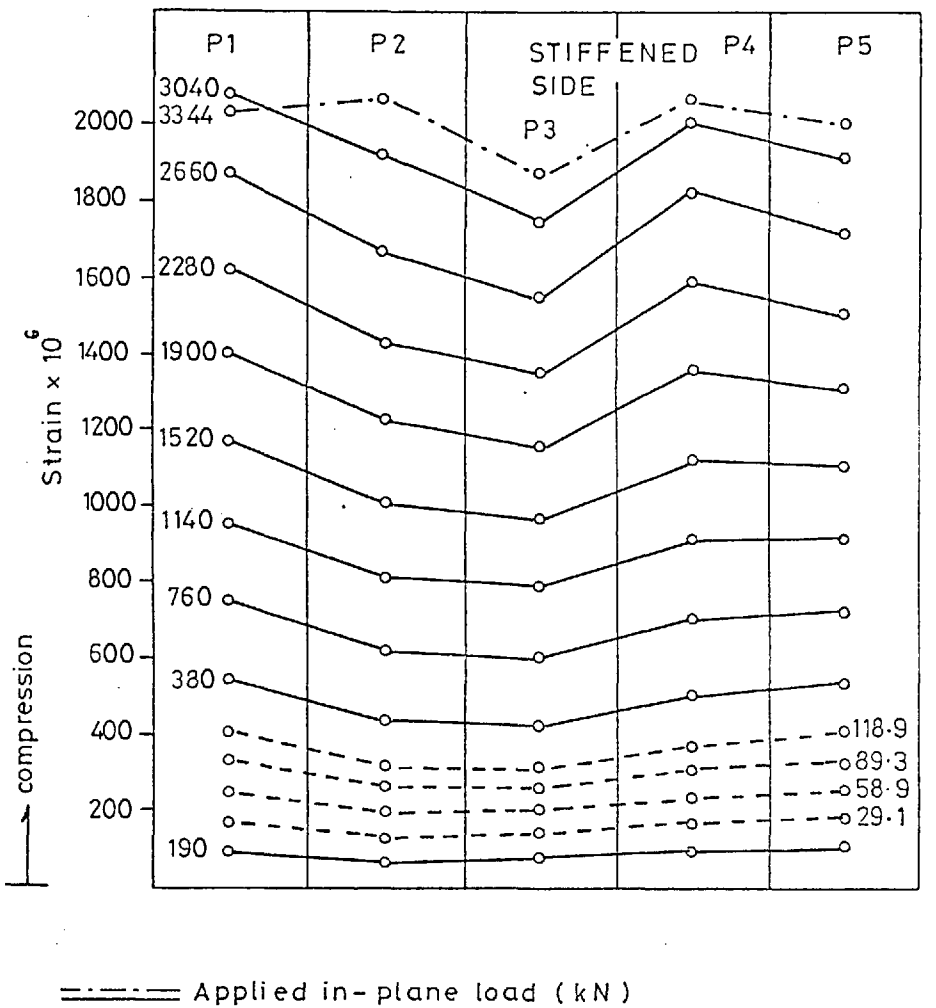

Fig D12 Model SP3. Measured longitudinal strains at section 5-5 (see fig D4)

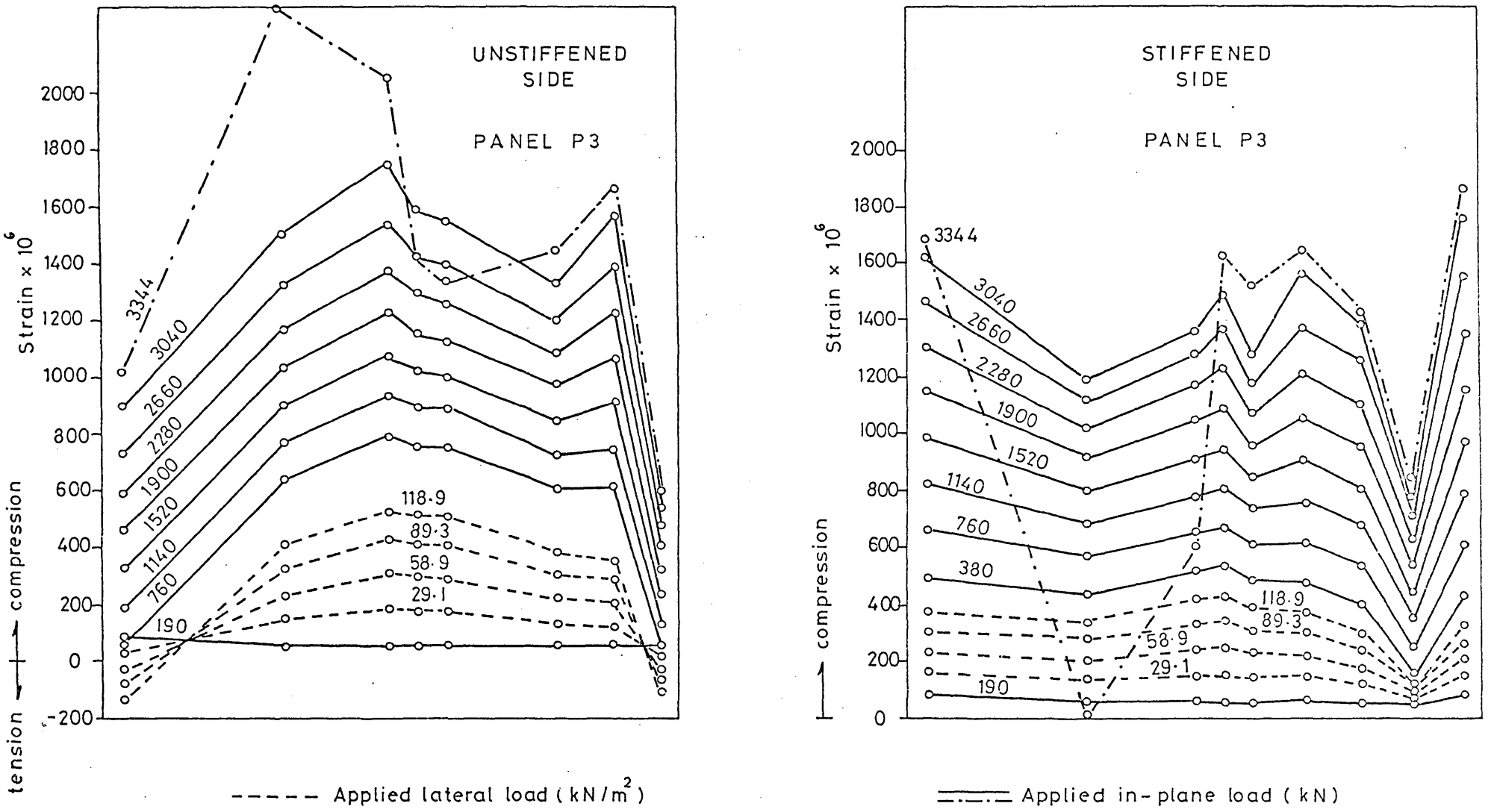

Fig D13 Model SP3. Measured longitudinal strains at section 6-6 (see fig D4)

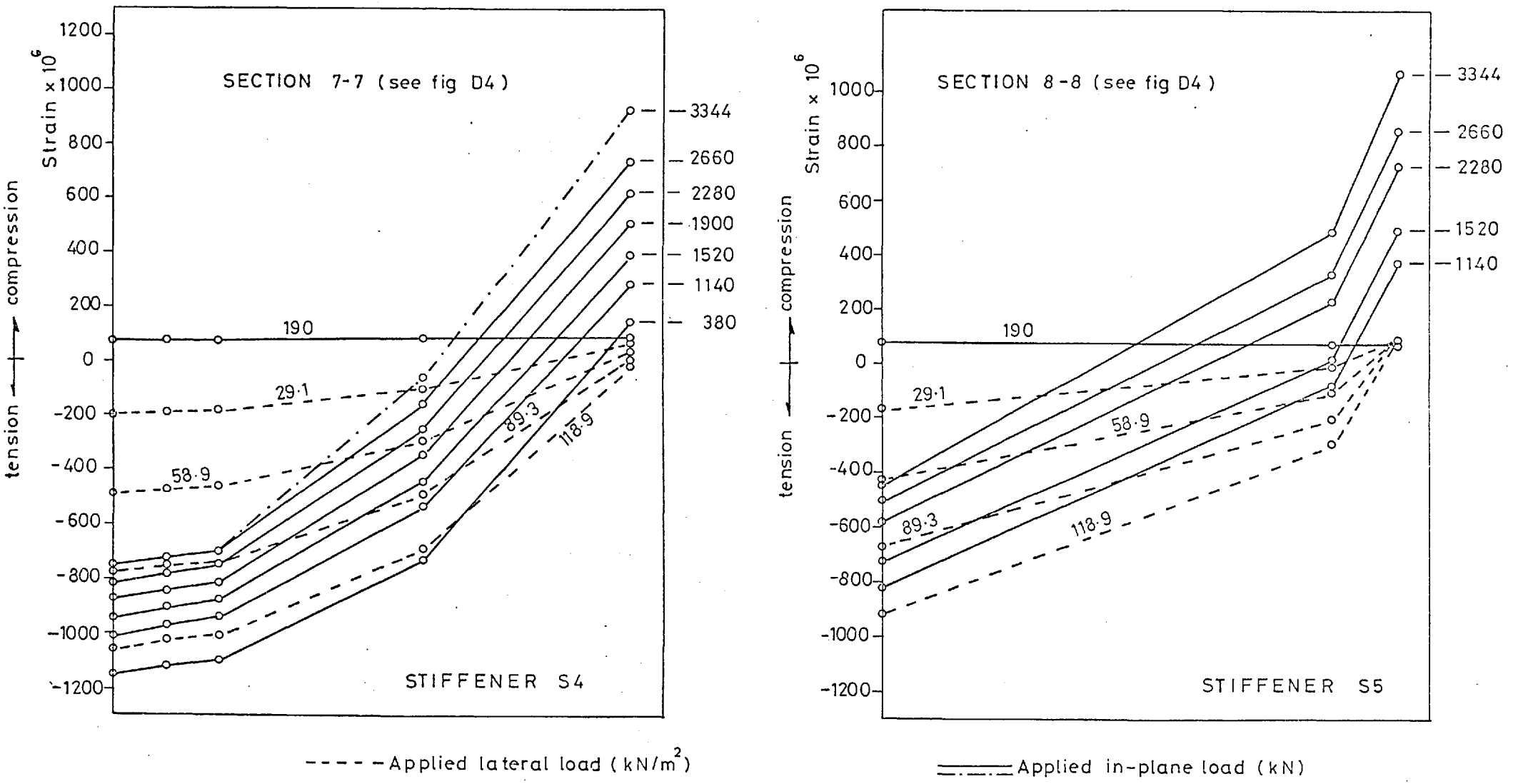

Fig D14 Model SP3. Longitudinal strains measured on stiffener flange plates

(Drawn as viewed from unstiffened side)

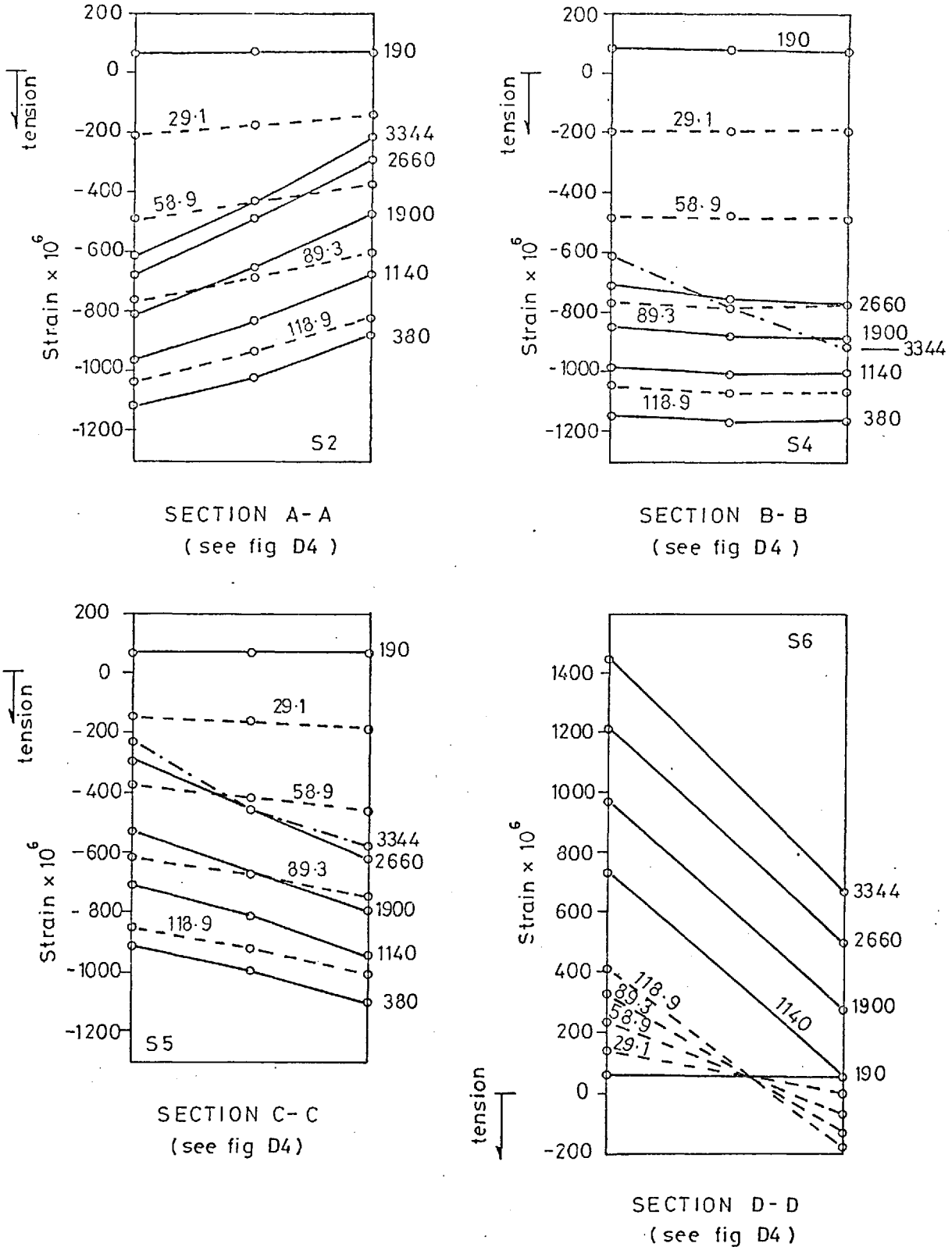

Fig D15 Model SP3. Variation of longitudinal strain across stiffener flange plates

(Drawn as viewed from unstiffened side)

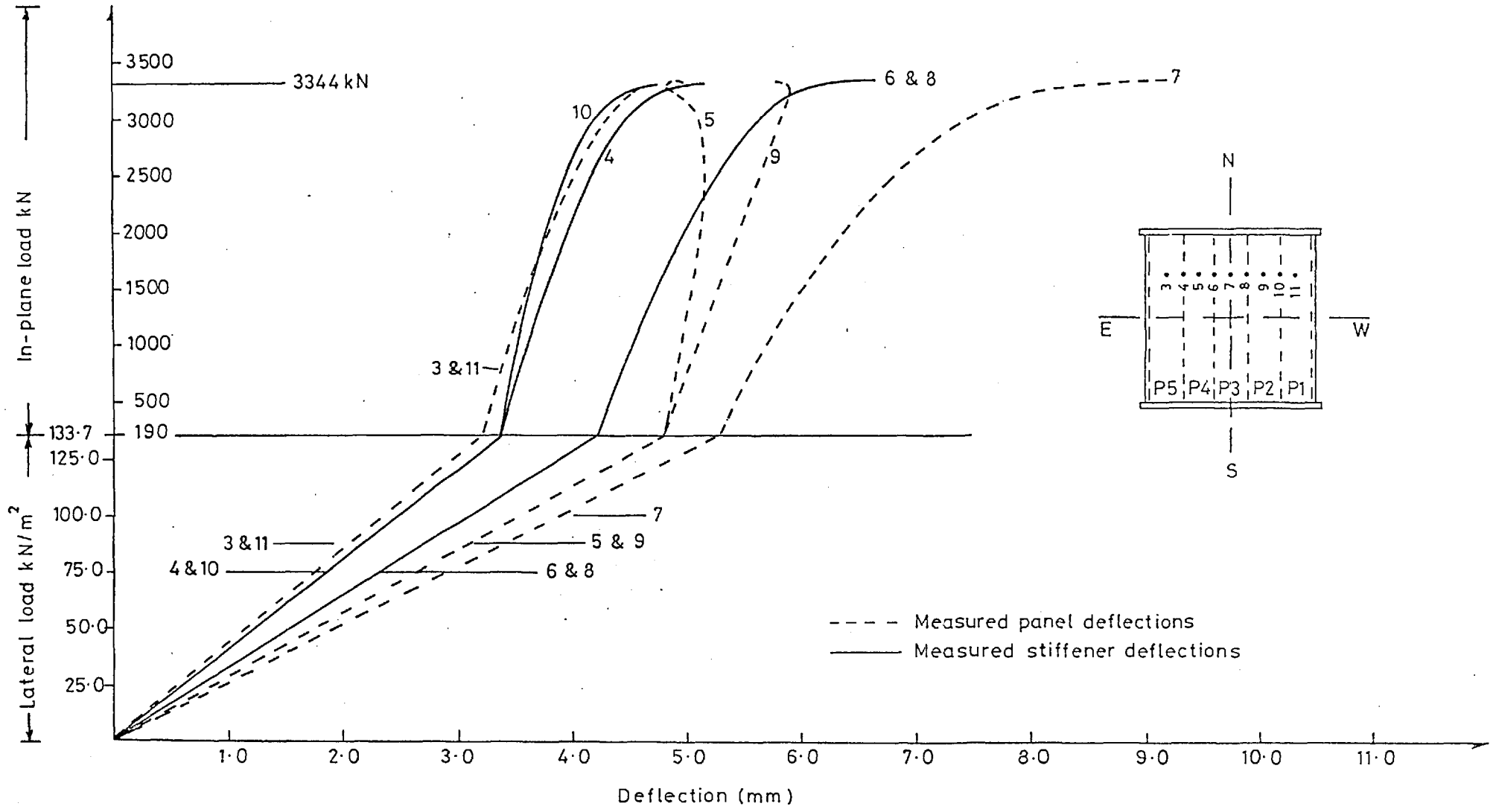

Fig D16 Load-deflection curves for model SP3.

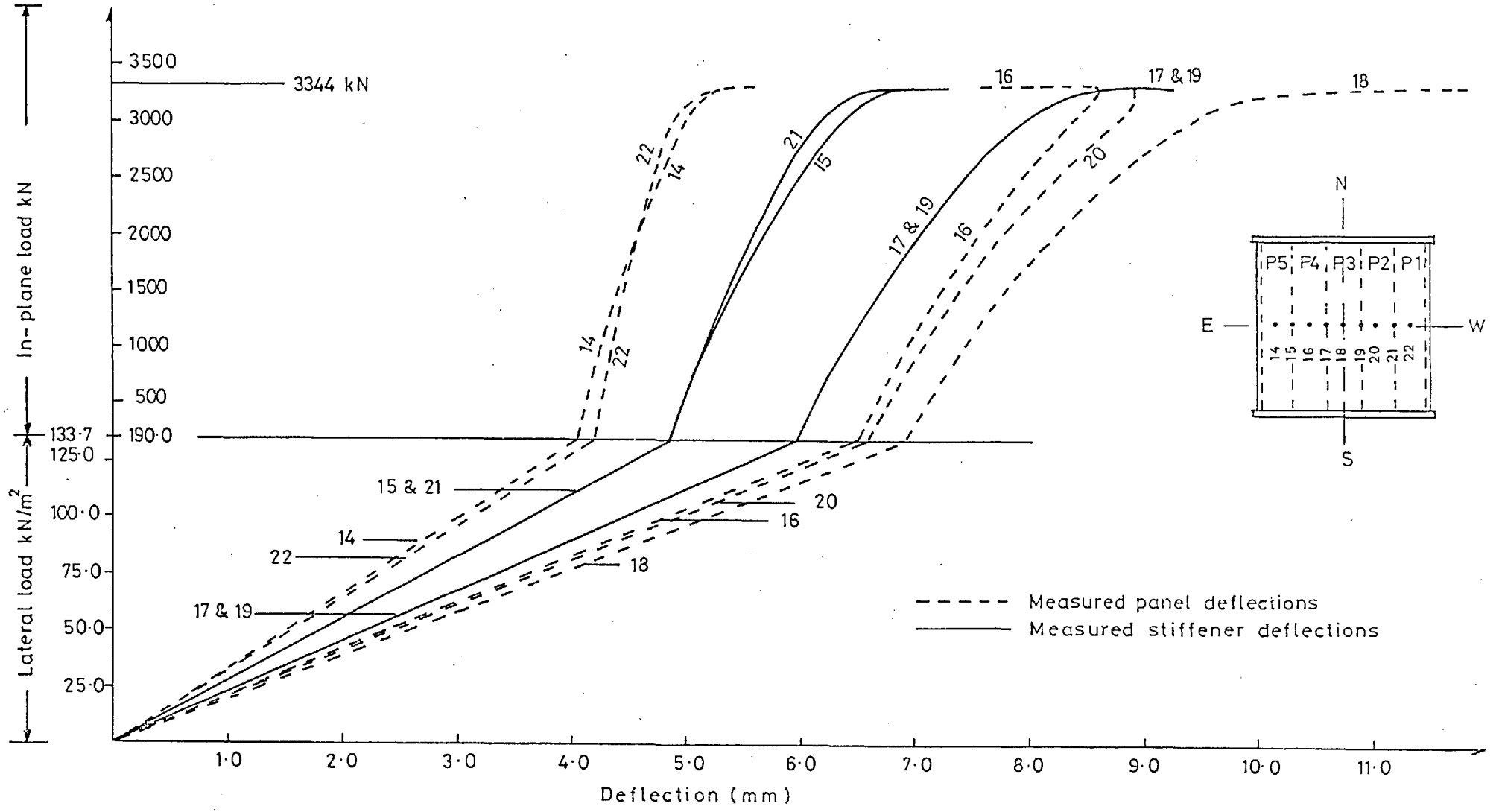

Fig D17 Load-deflection curves for model SP 3

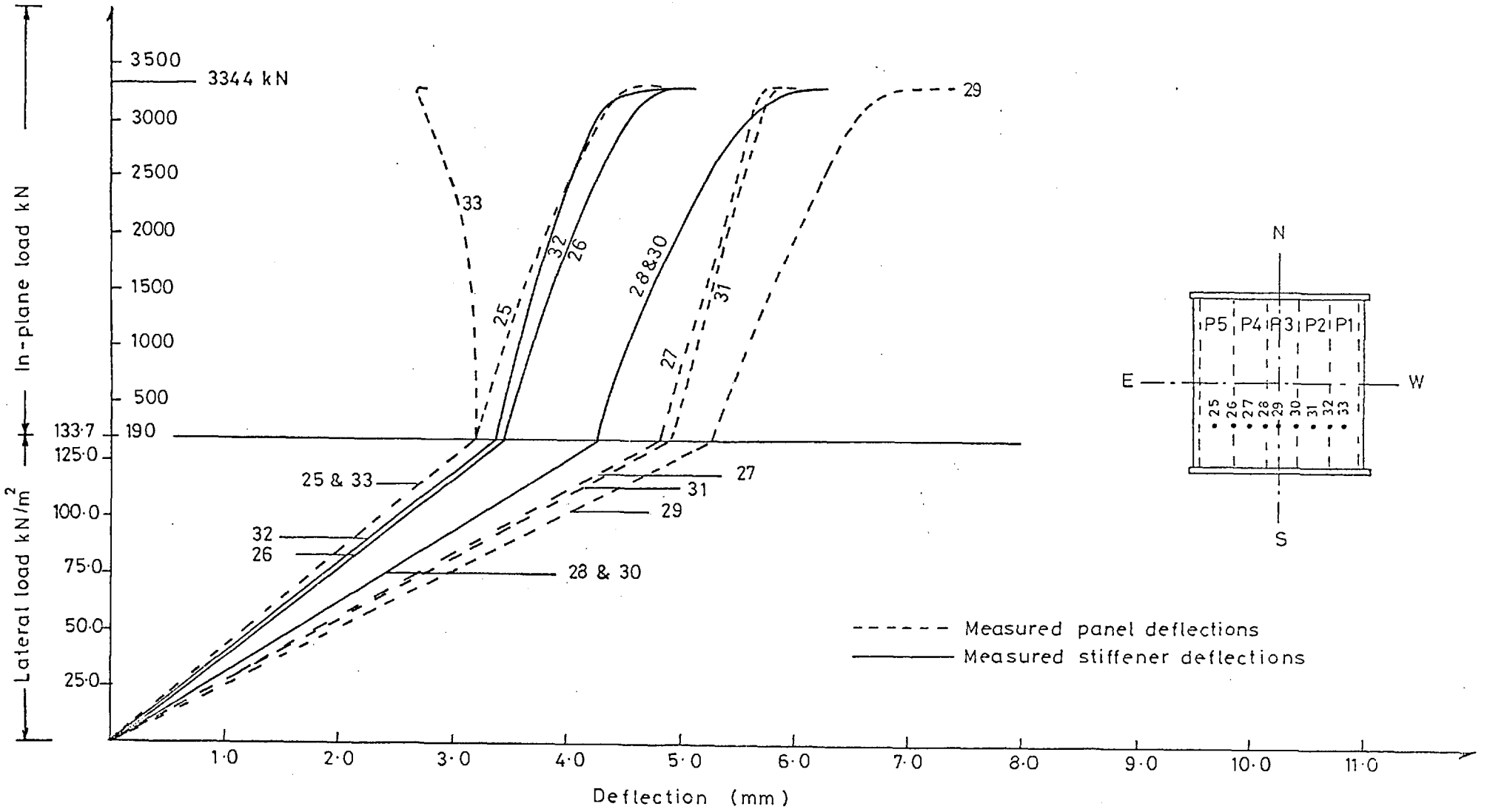

Fig D 18 Load-deflection curves for model SP3

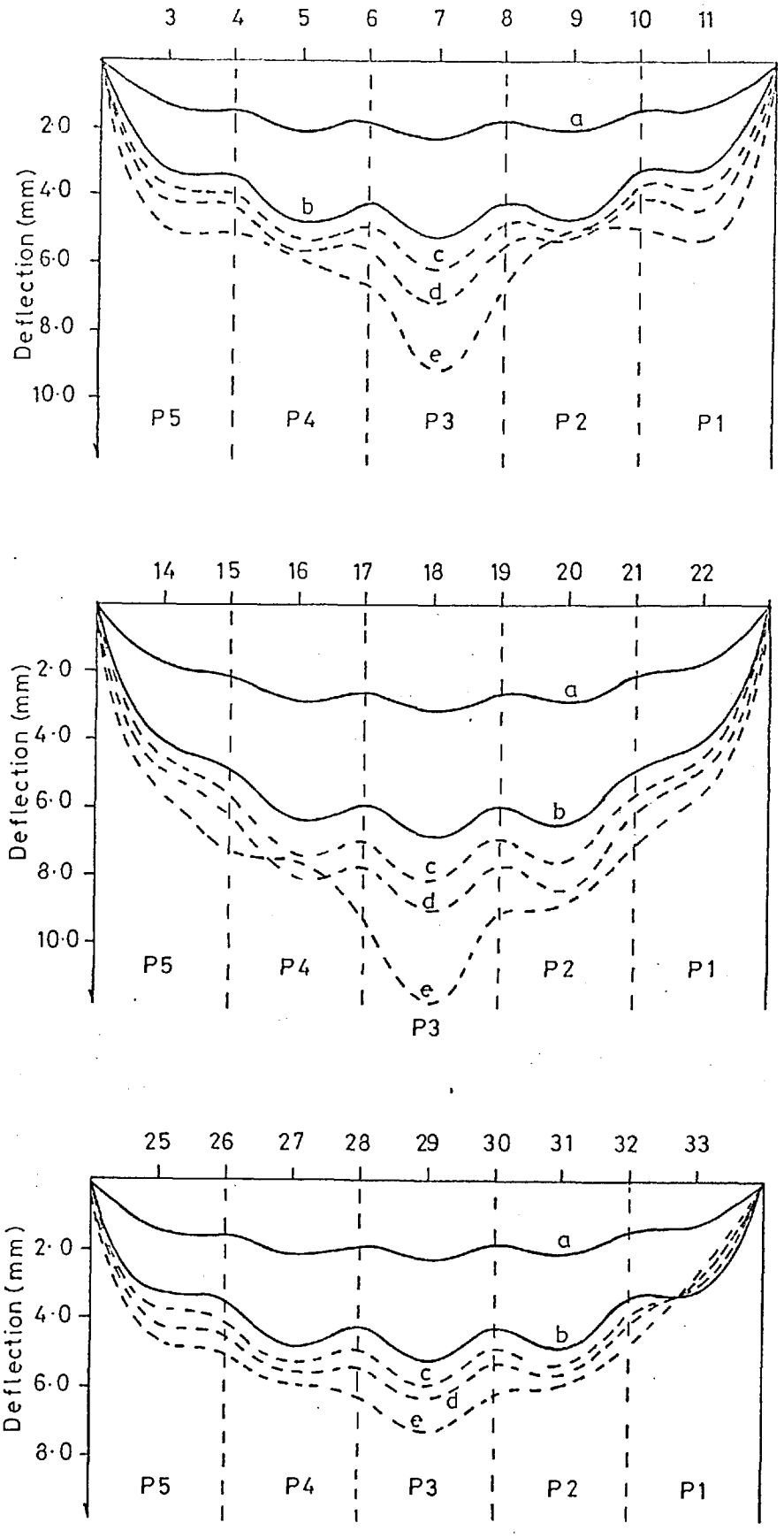

——— Applied lateral load

- - - - - Applied in-plane load

Locations shown in fig D4

Applied load	
a	58·9 kN/m^2
b	133·7 kN/m^2
c	1900 kN
d	2850 kN
e	3344 kN

Fig D 19 Model SP3. Measured deflections

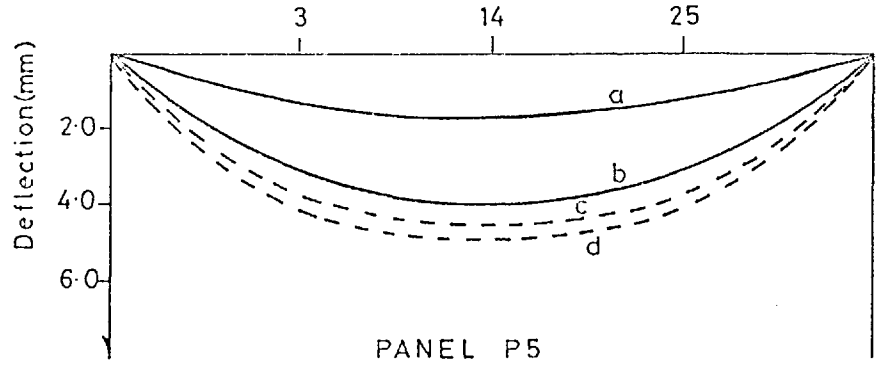

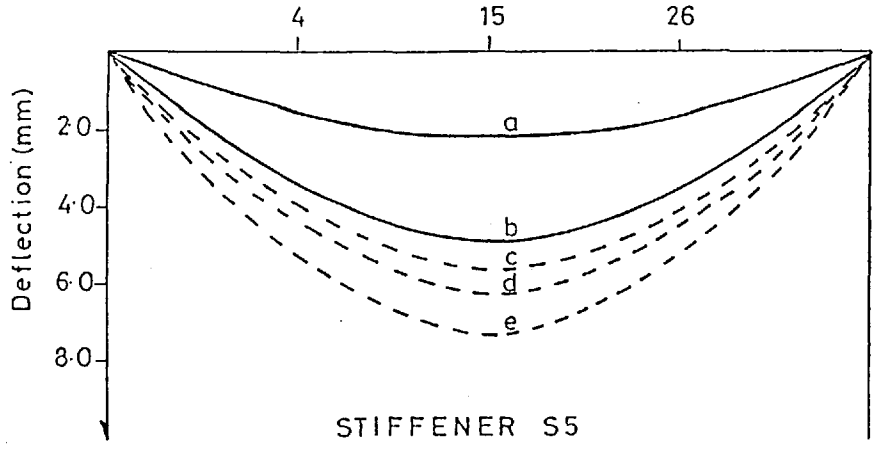

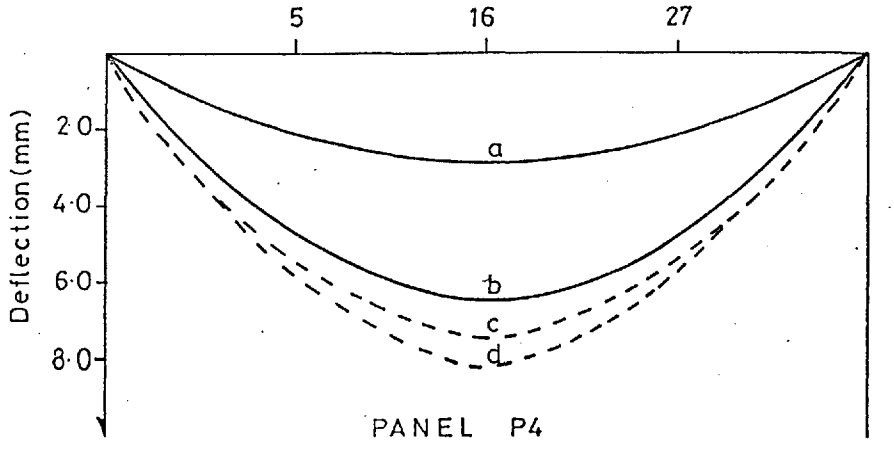

——— Applied lateral load
- - - - Applied in-plane load

Locations shown in fig D4

Applied load	
a	58·9 kN/m^2
b	133·7 kN/m^2
c	1900 kN
d	2850 kN
e	3344 kN

Fig D20 Model SP3 Measured deflections

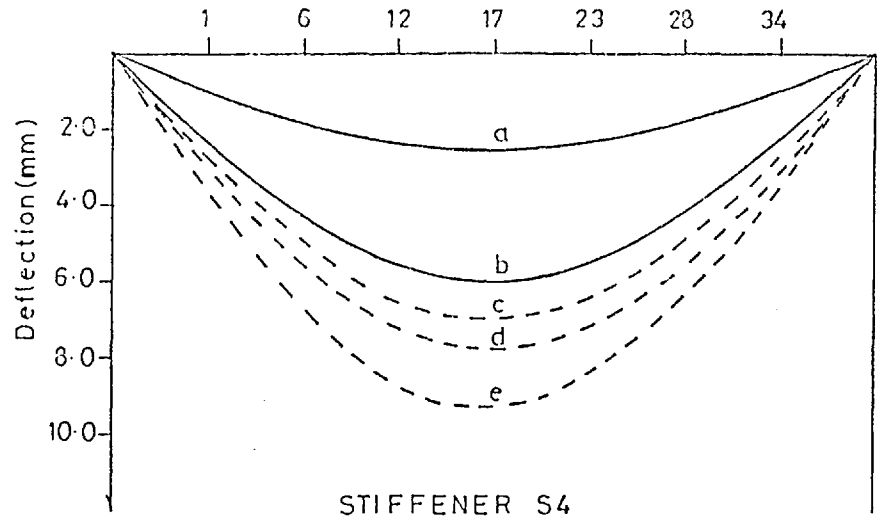

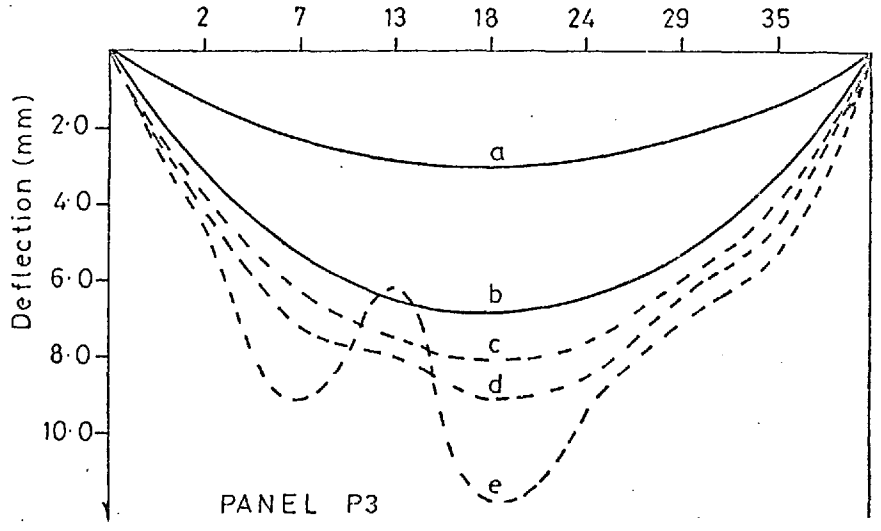

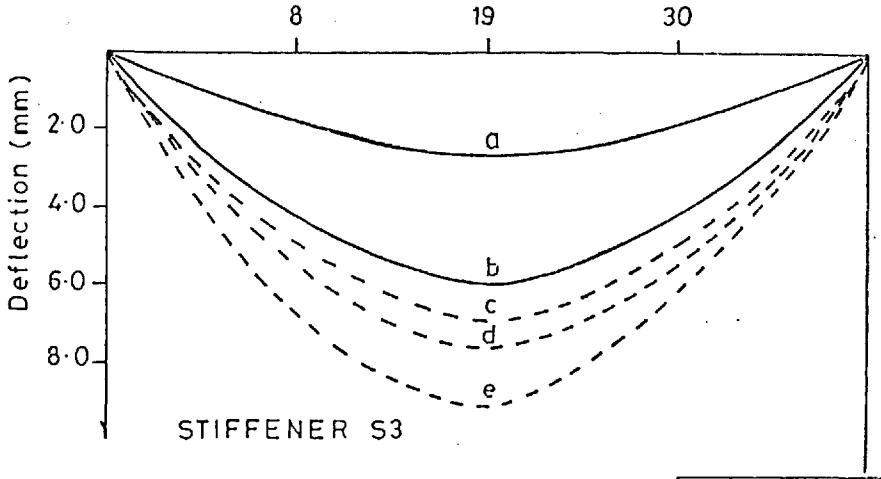

——— Applied lateral load
- - - - - Applied in-plane load
Locations shown in fig D4

Applied load	
a	58·9 kN/m^2
b	133·7 kN/m^2
c	1900 kN
d	2850 kN
e	3344 kN

Fig D21 Model SP3. Measured deflections

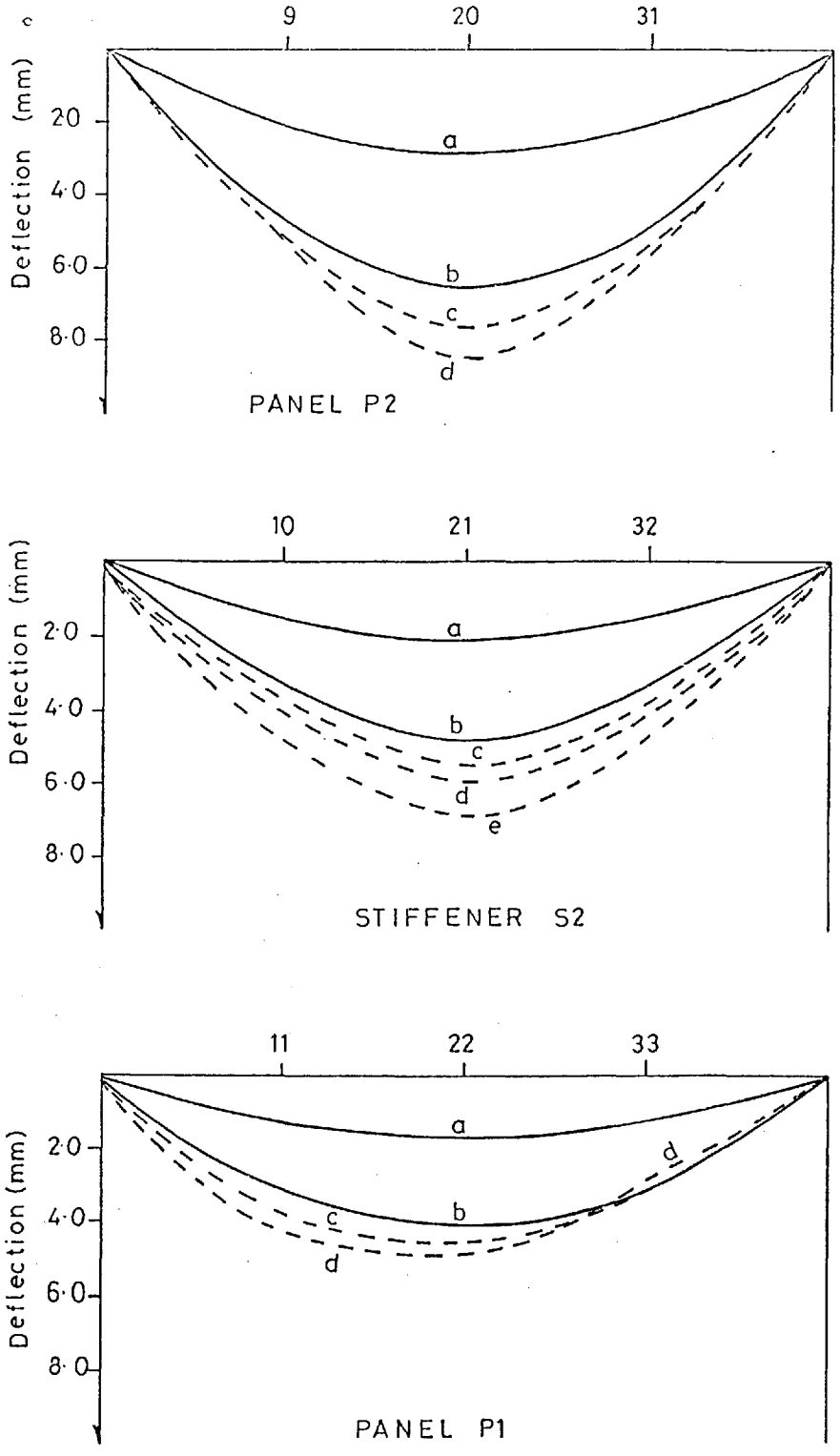

——— Applied lateral load

- - - - Applied in-plane load

Locations shown in fig D4

Applied load	
a	58·9 kN/m²
b	133·7 kN/m²
c	1900 kN
d	2850 kN
e	3344 kN

Fig D22 Model SP3. Measured deflections

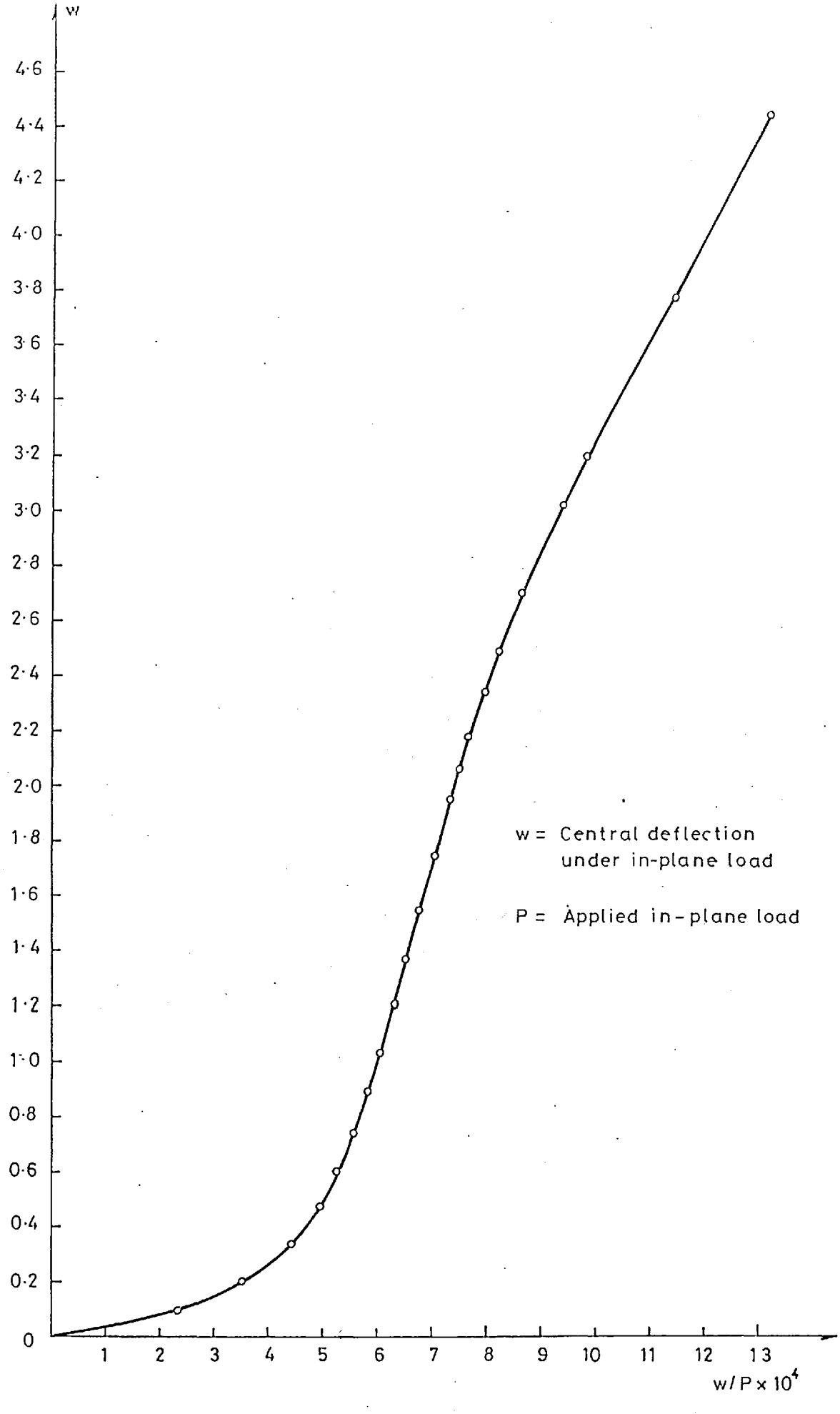

Fig D 23 Southwell plot based on central deflection

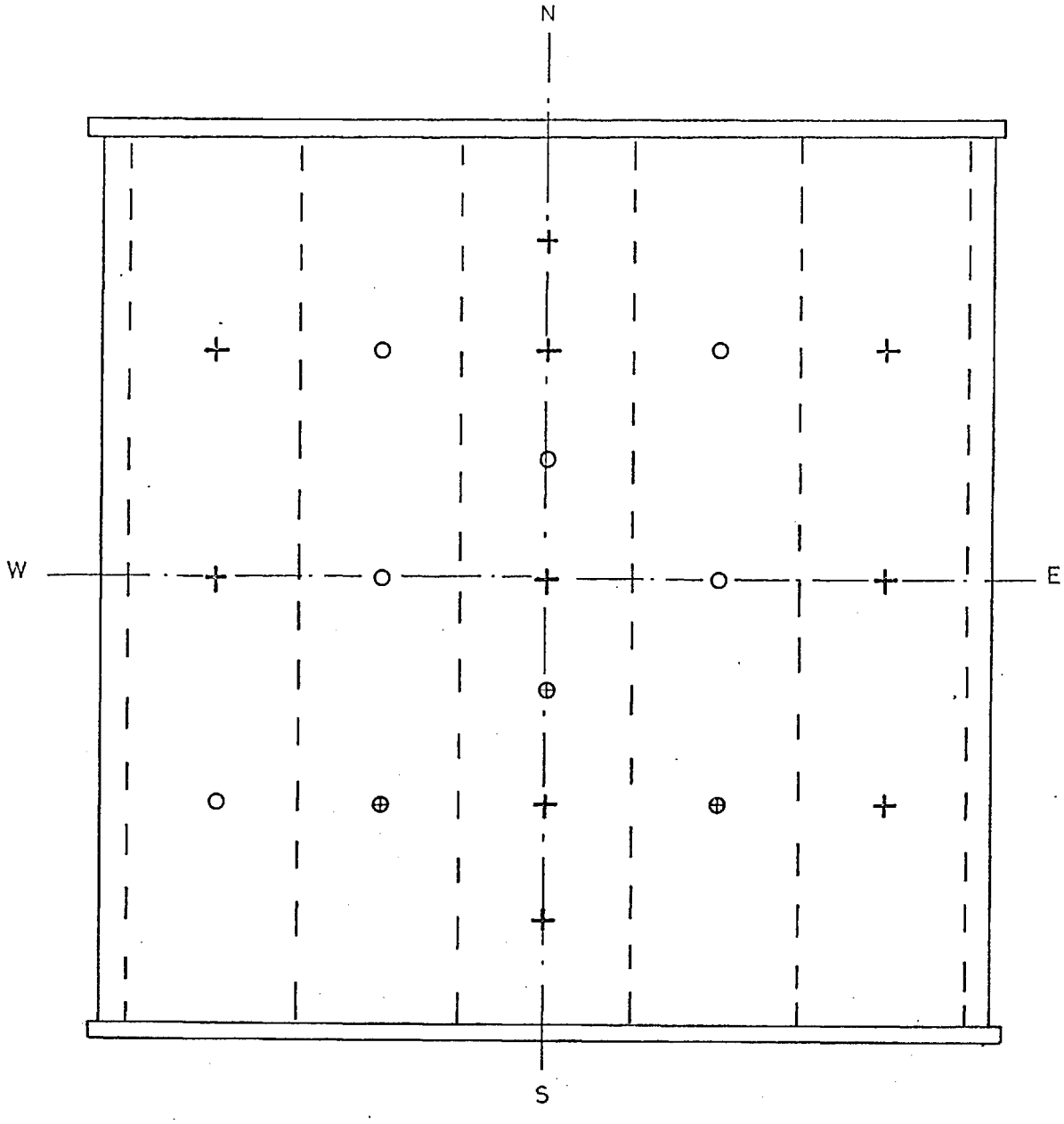

Fig D24 Measured failure mode of model SP3

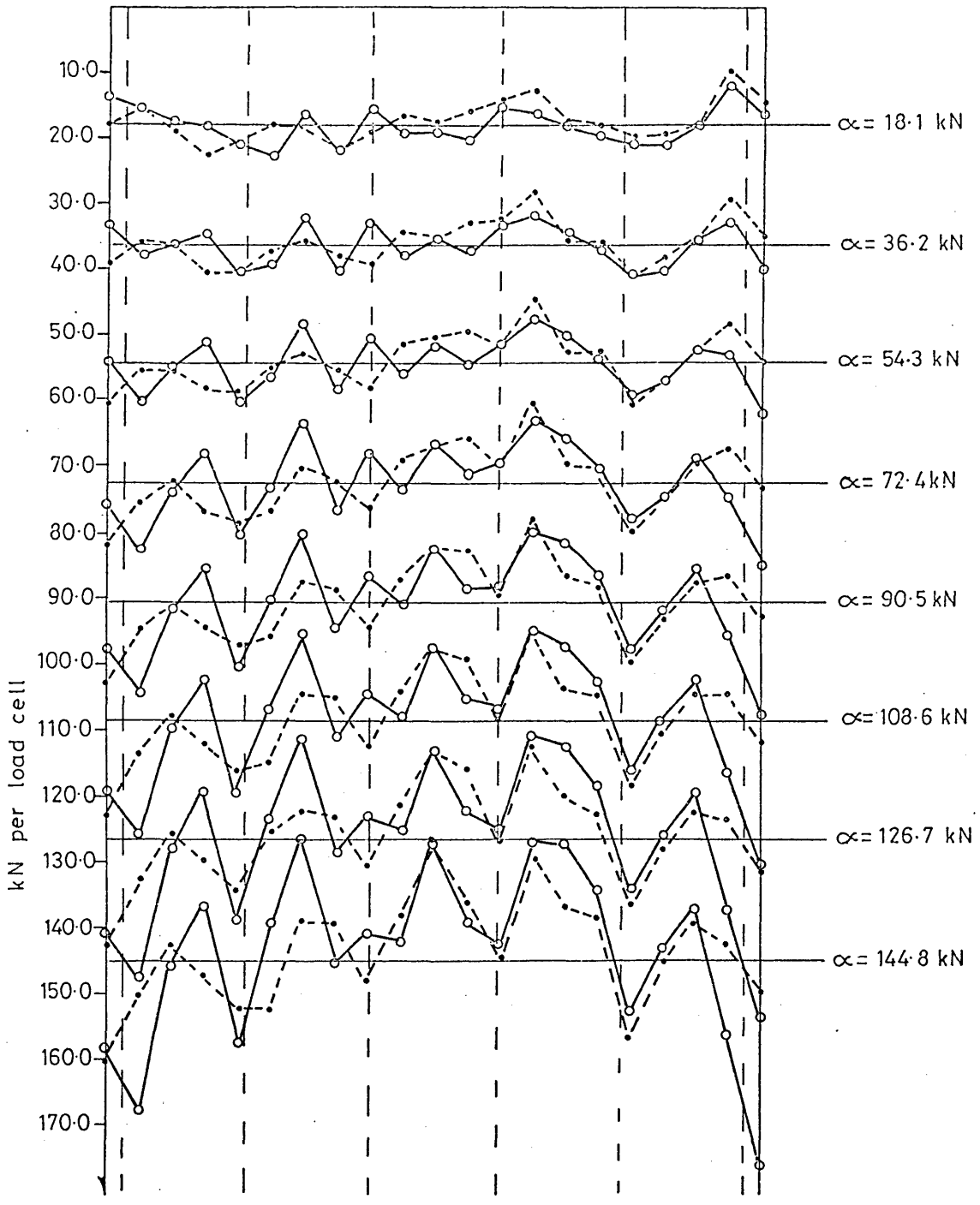

Fig D25 Distribution of force in horizontal load cells at loading and reaction ends of model

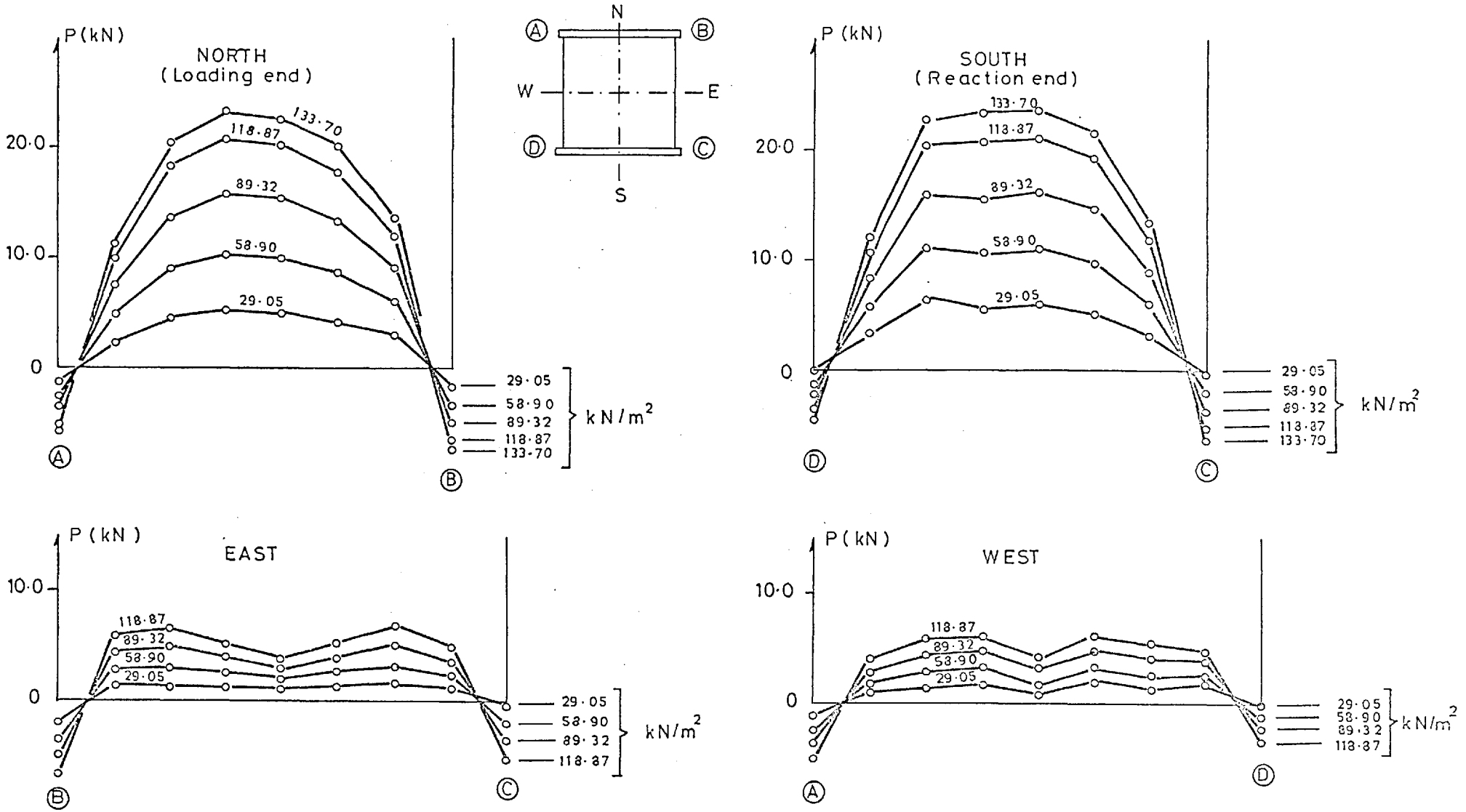

Fig D26 Forces in vertical load cells resulting from lateral pressure

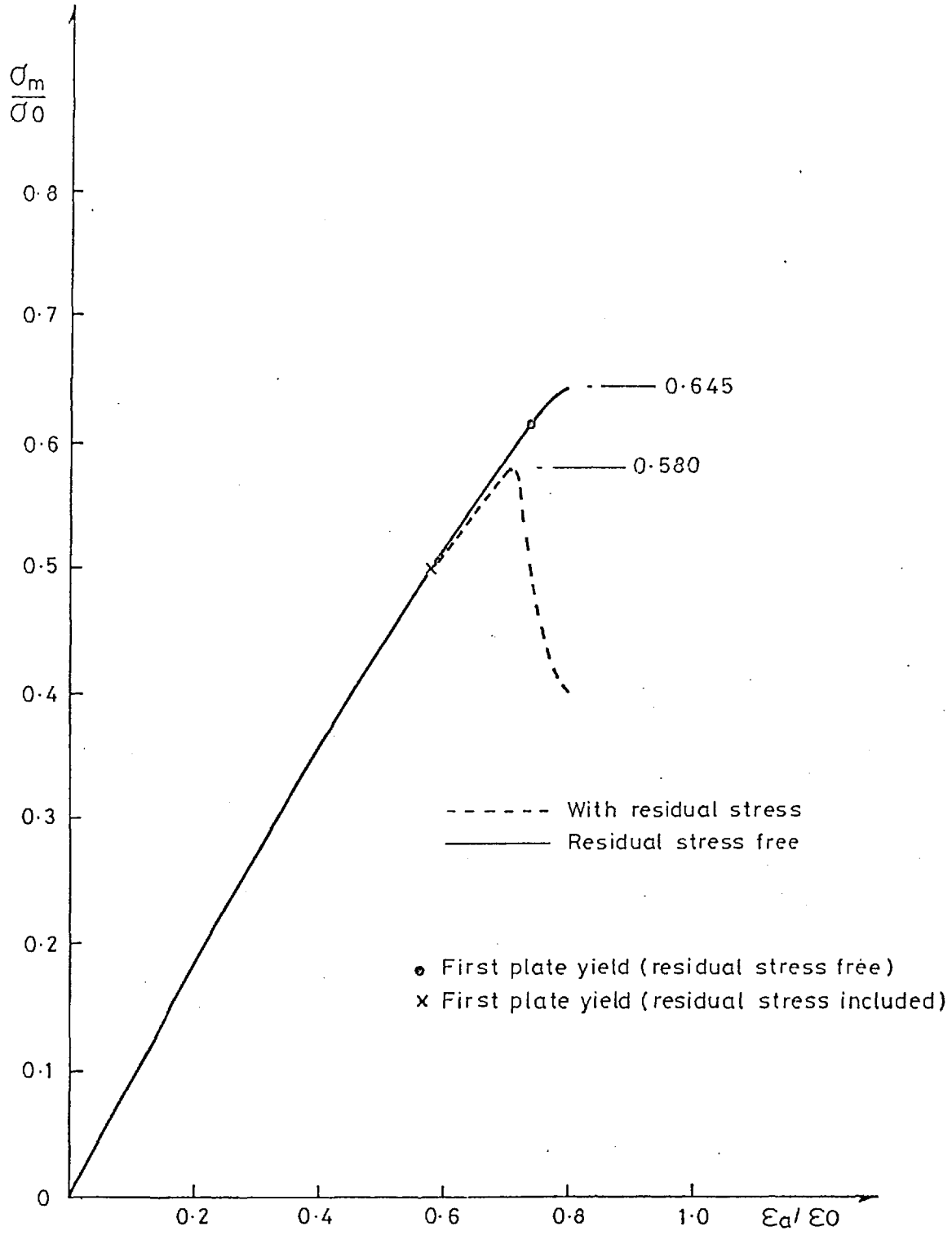

Fig D27 Model SP1 Load-shortening curves

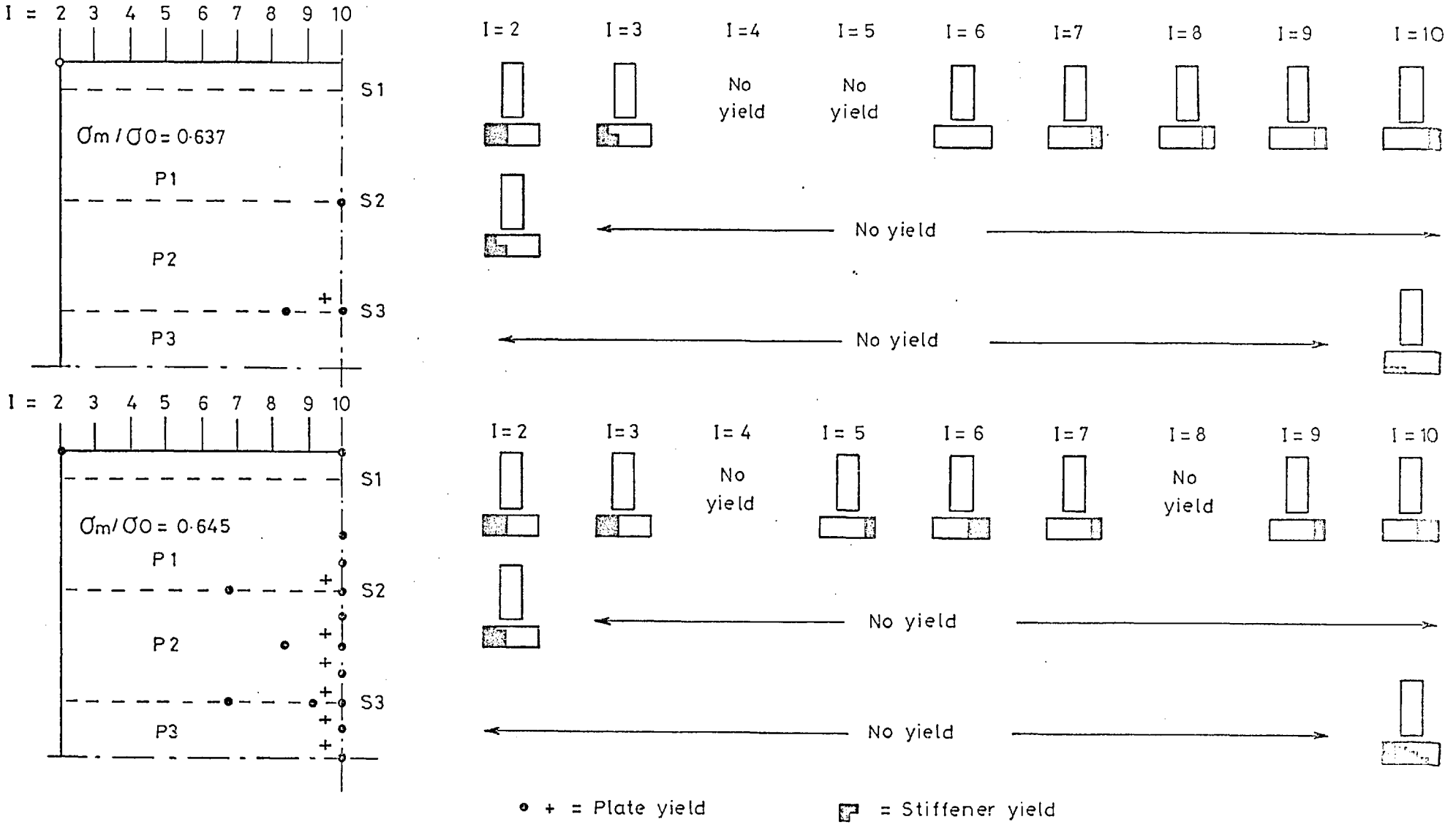

Fig D28 Model SP1. Zero residual stress. Predicted yield zones

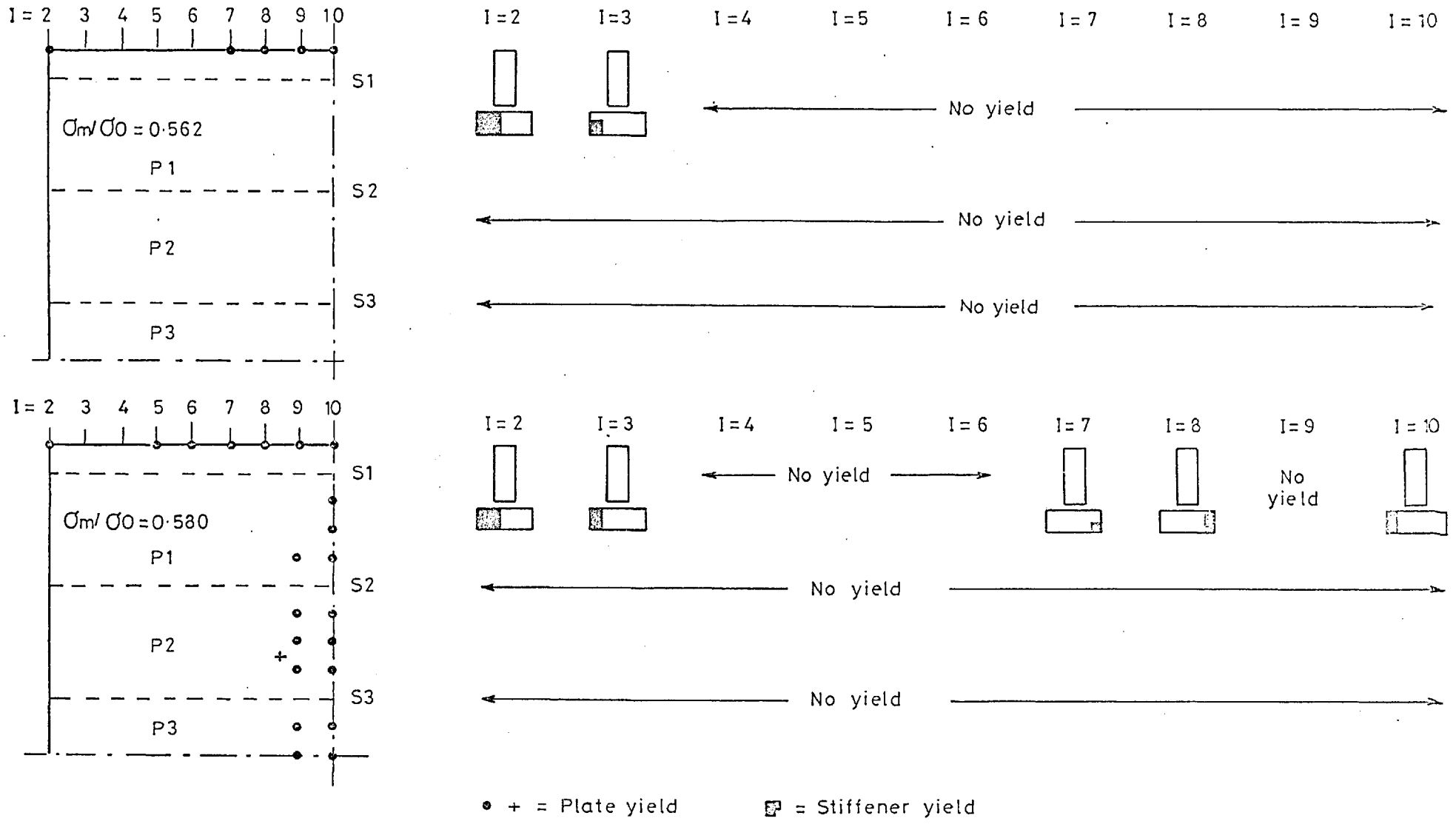

Fig D29 Model SP1. Residual stress applied. Predicted yield zones

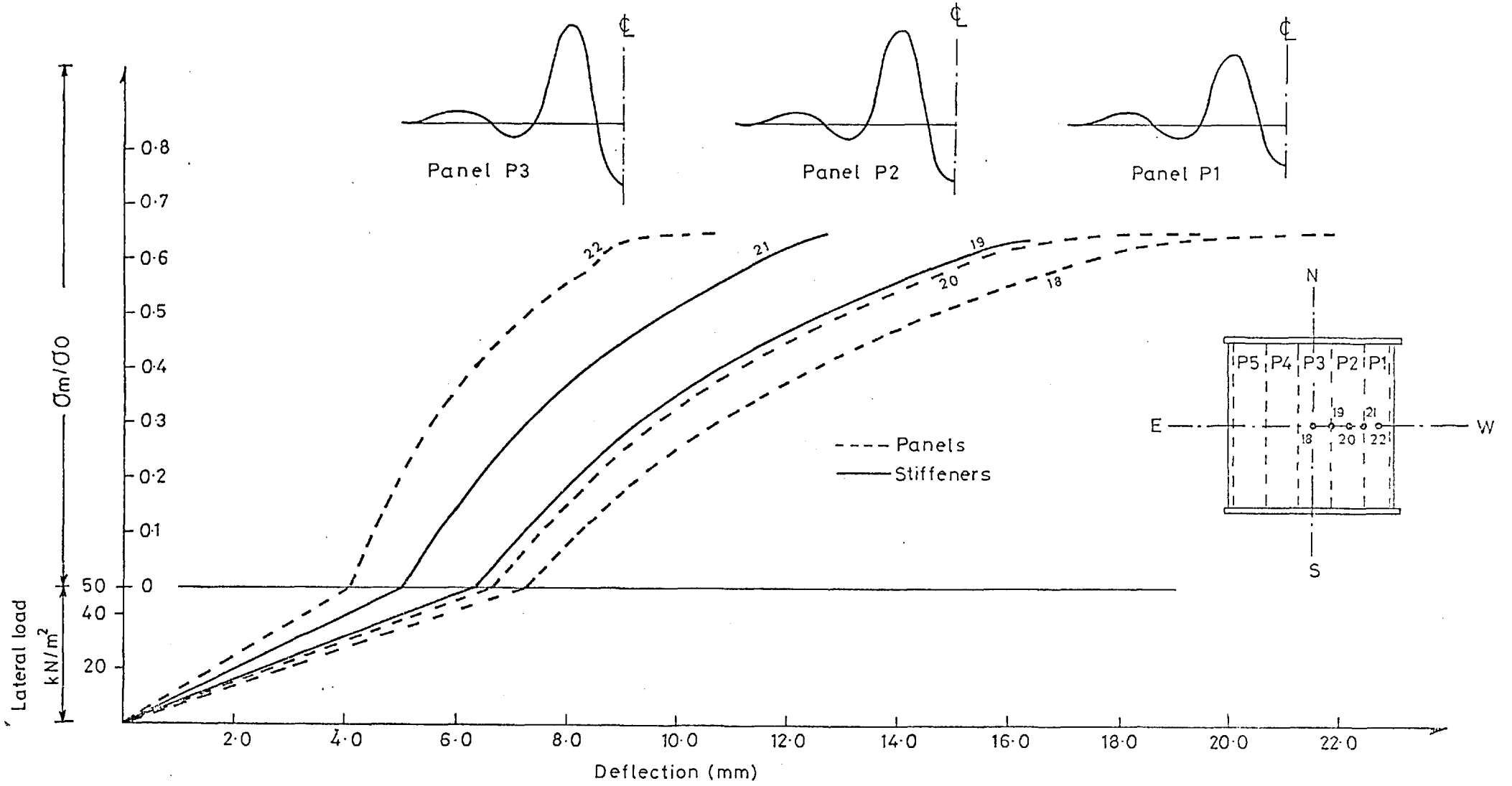

Fig D30 Model SP1. Load - deflection curves (zero residual stress)

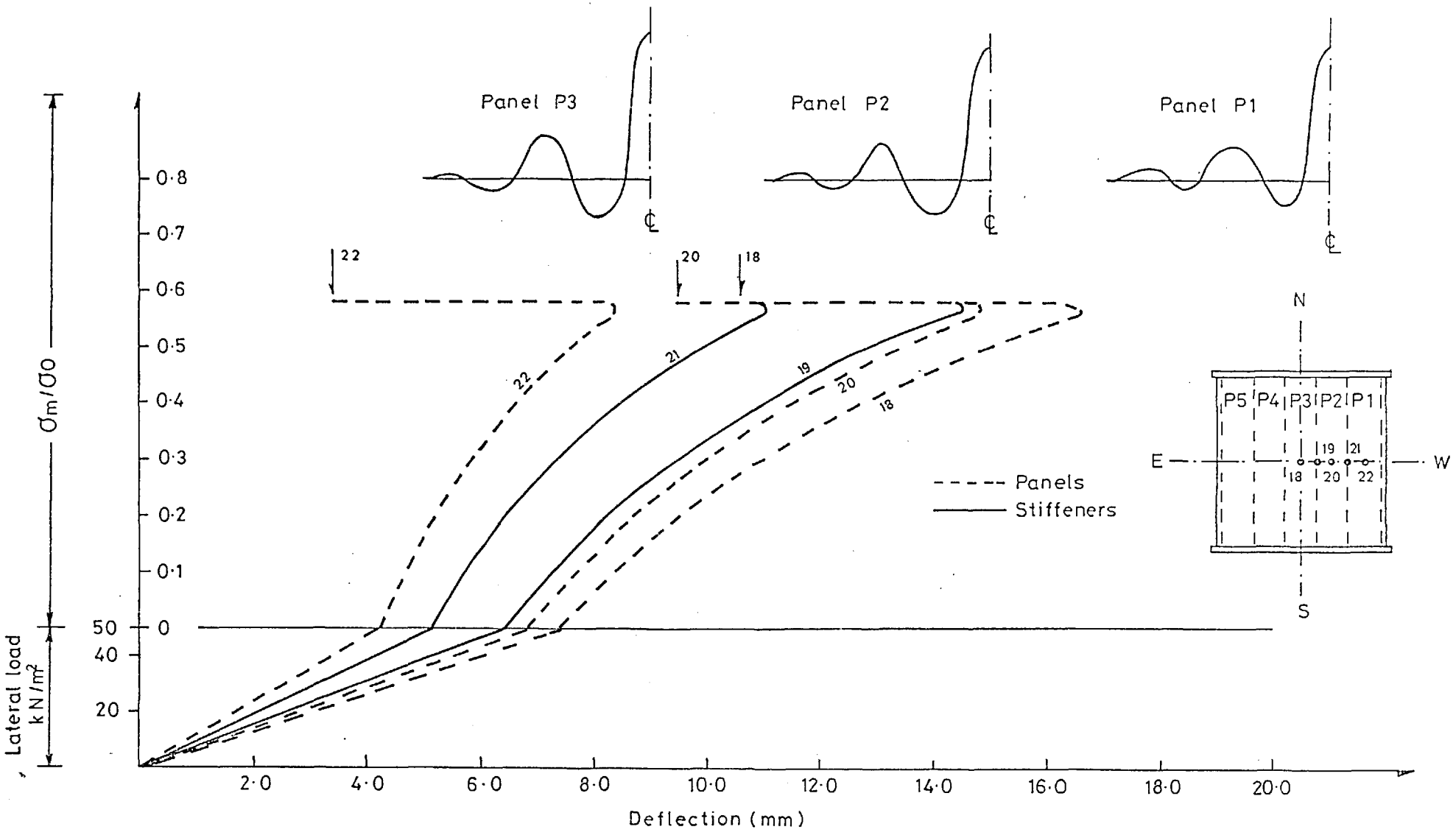

Fig D31 Model S P1. Load-deflection curves (residual stress as shown in fig D2)

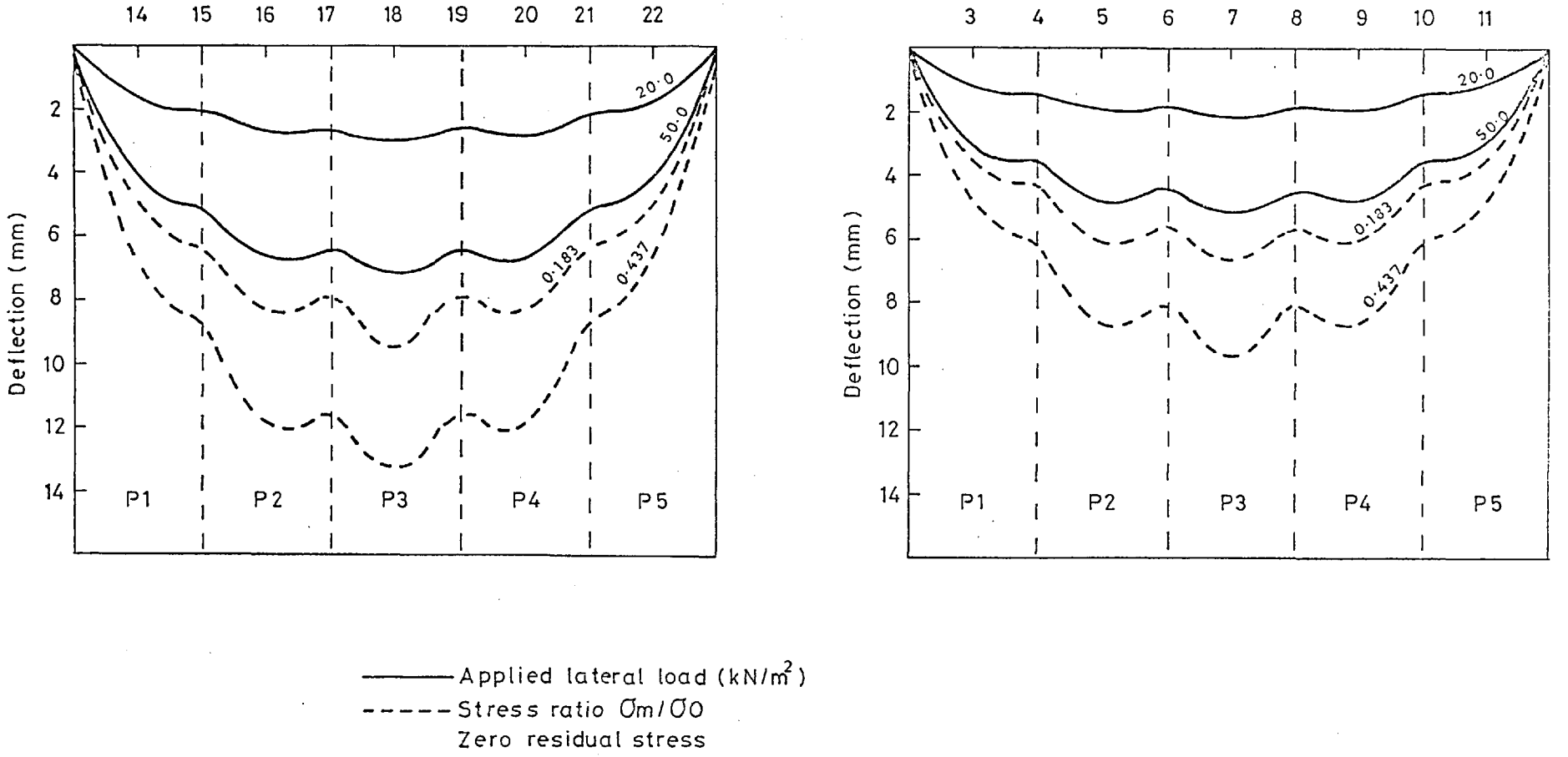

Fig D32 Model SP1. Deflection profiles (locations shown in fig D4)

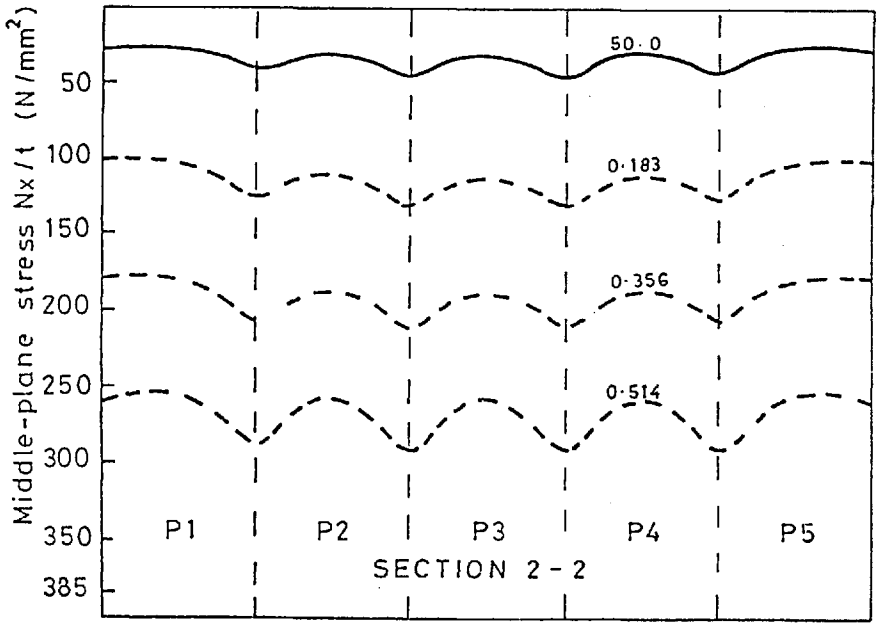

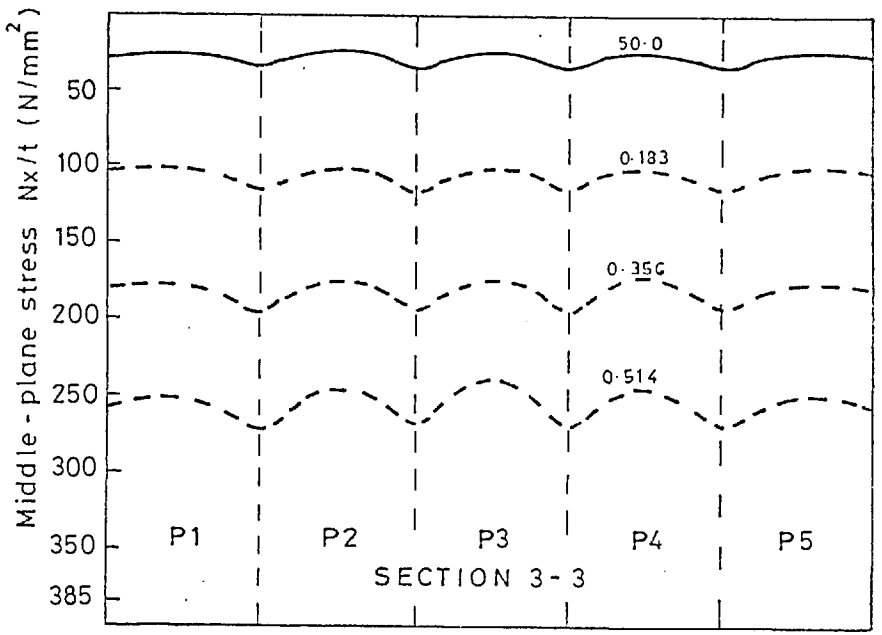

——— Applied lateral load (kN/m²)

------ Stress ratio σm/σ0

Zero residual stress

Fig D33 Model SP1. Distributions of direct stress across plate (sections shown in fig D4)

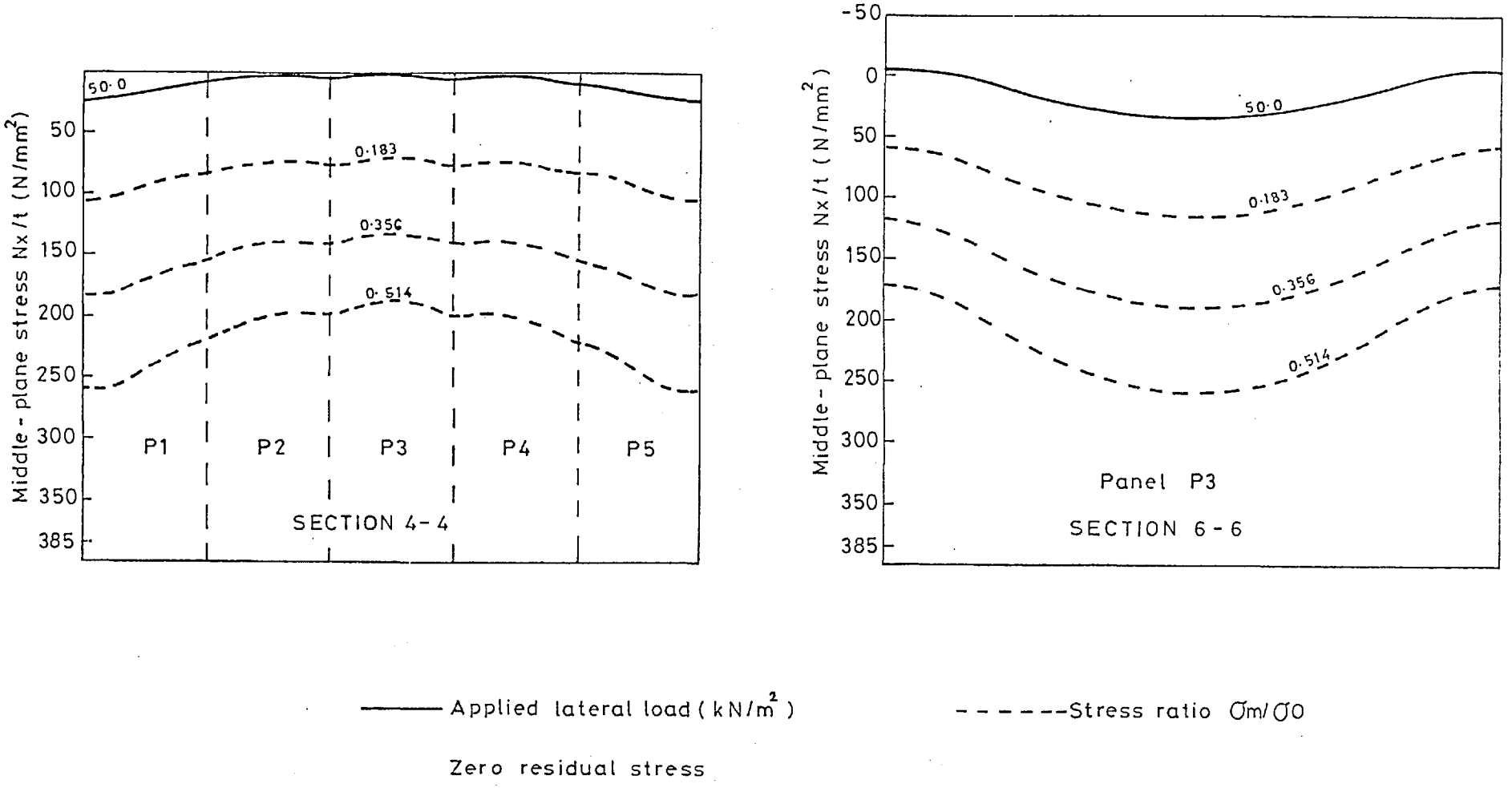

Fig D34 Model SP1. Distributions of direct stress across plate (sections shown in fig D4)

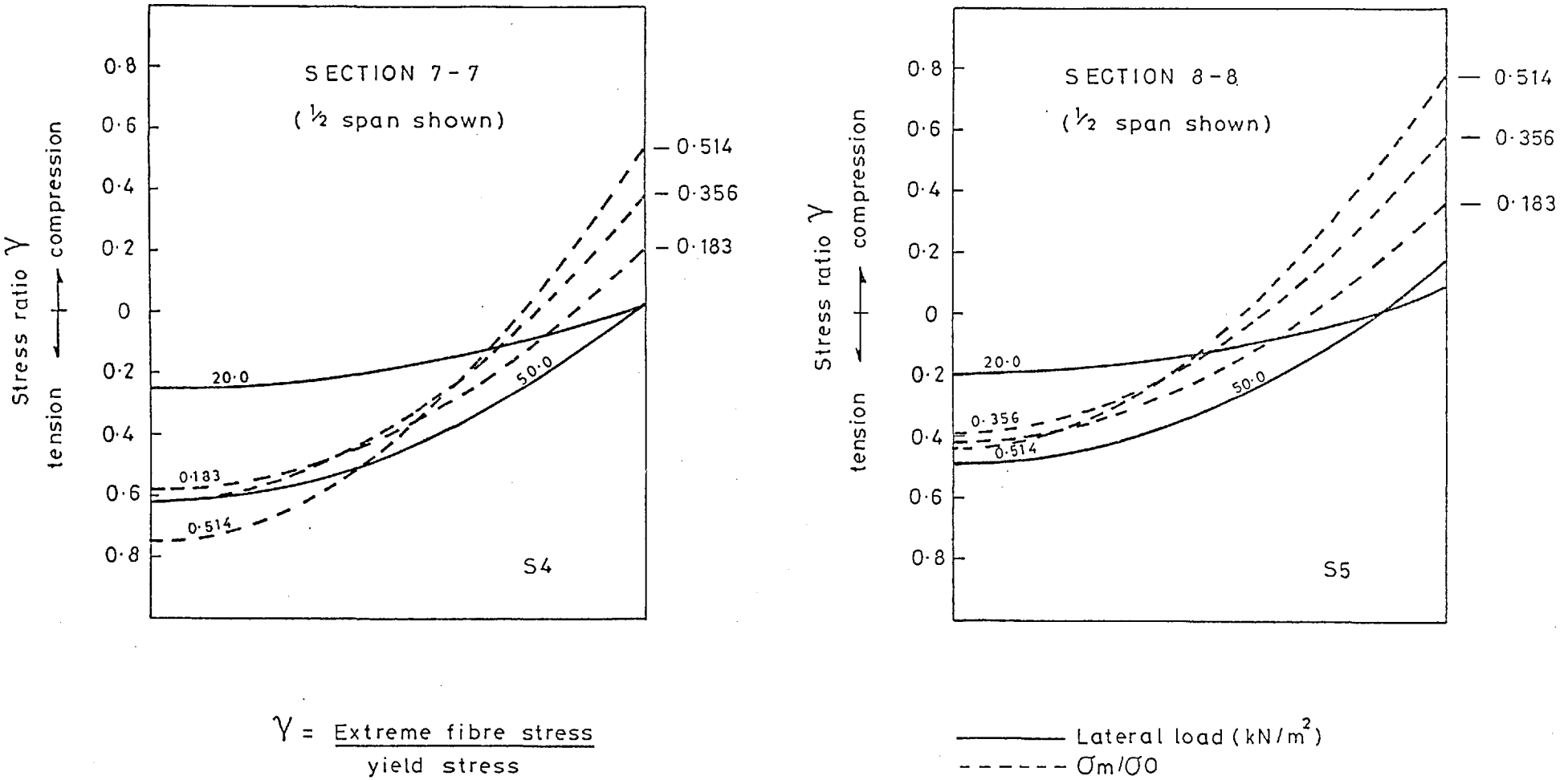

Fig D 35 Model SP1. Extreme fibre stresses in the stiffener flanges (sections shown in fig D4)

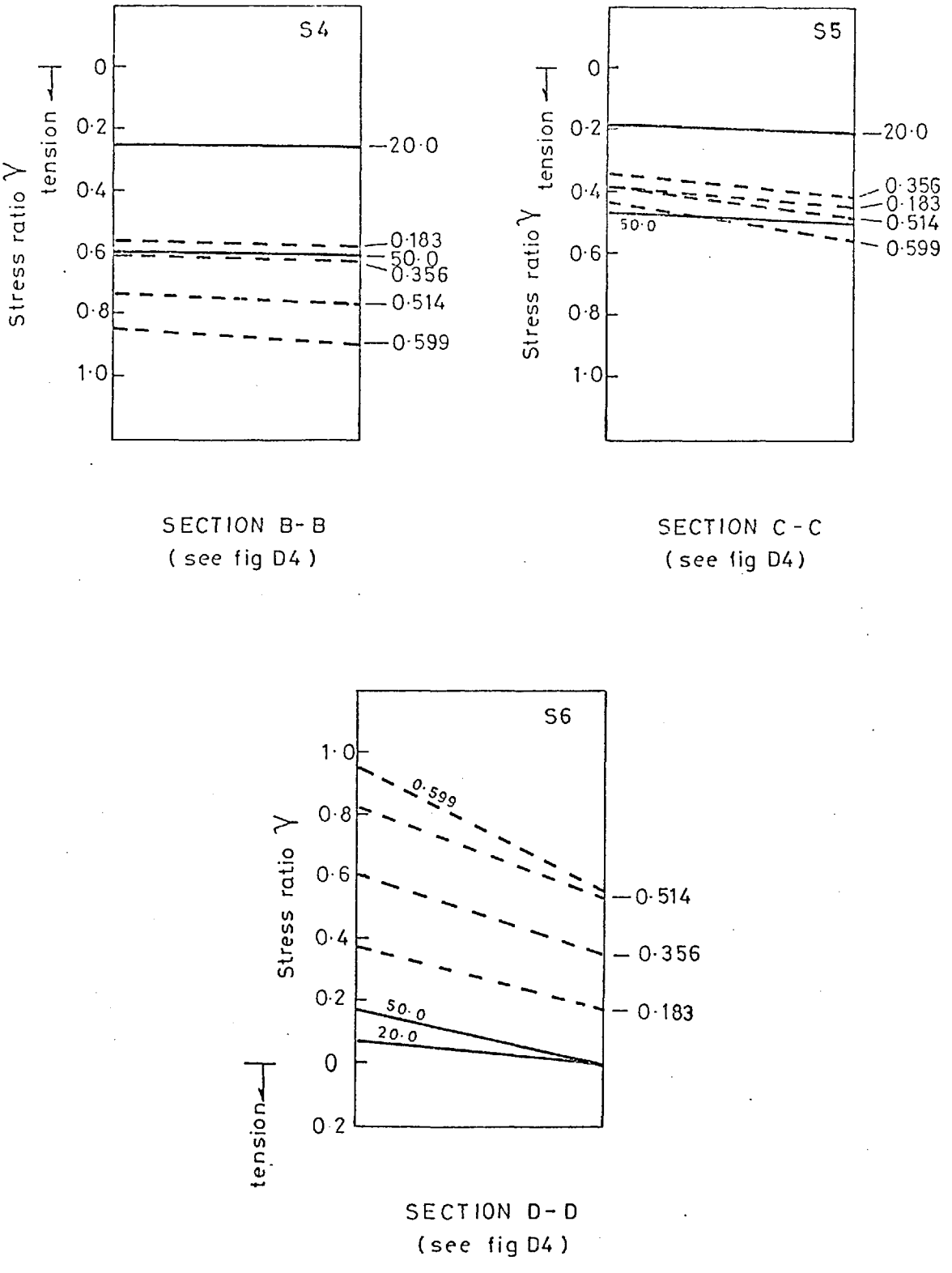

Fig D36 Model SP1. Variation of longitudinal stress across stiffener flange plates

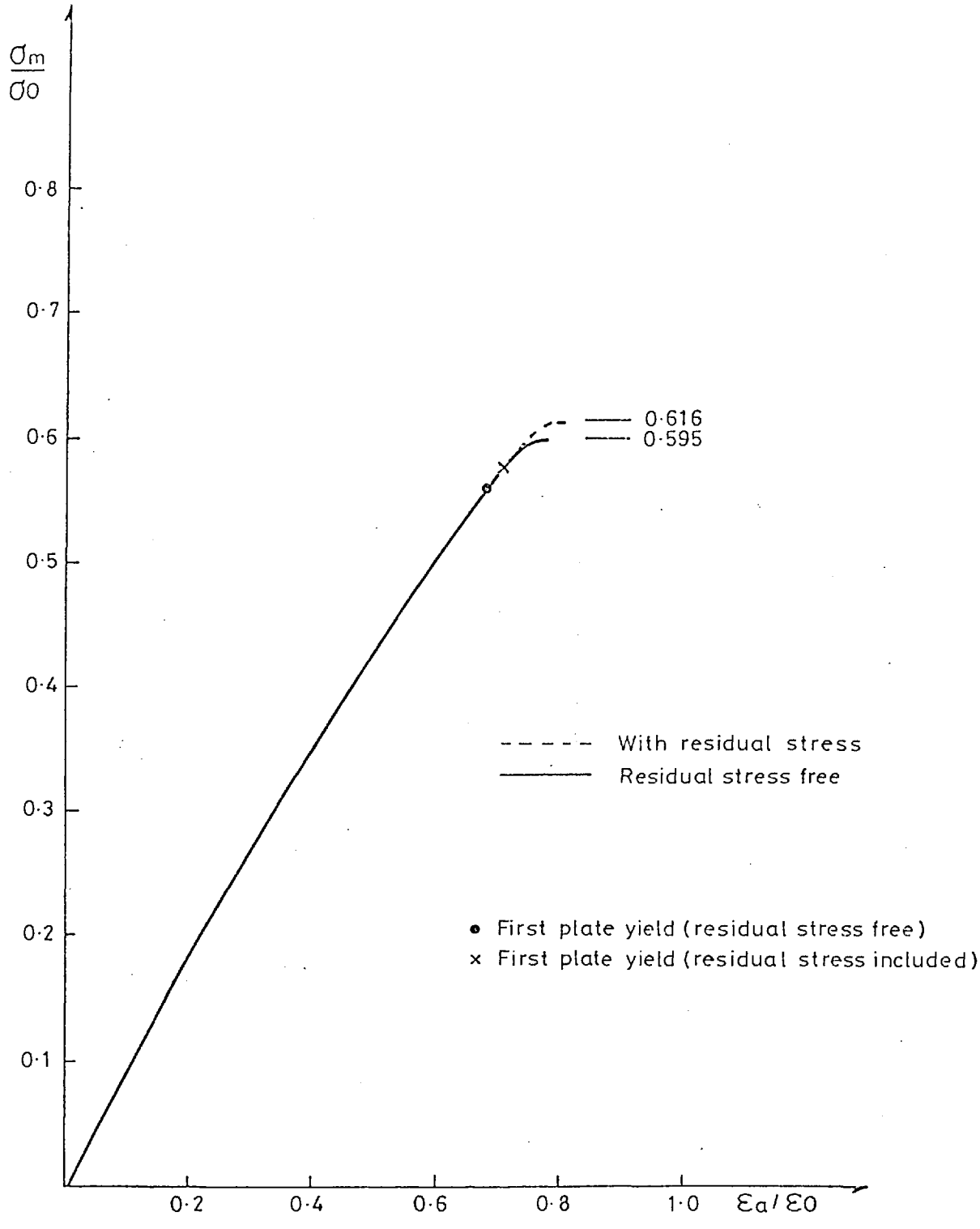

Fig D37 Model SP2. Load-shortening curves

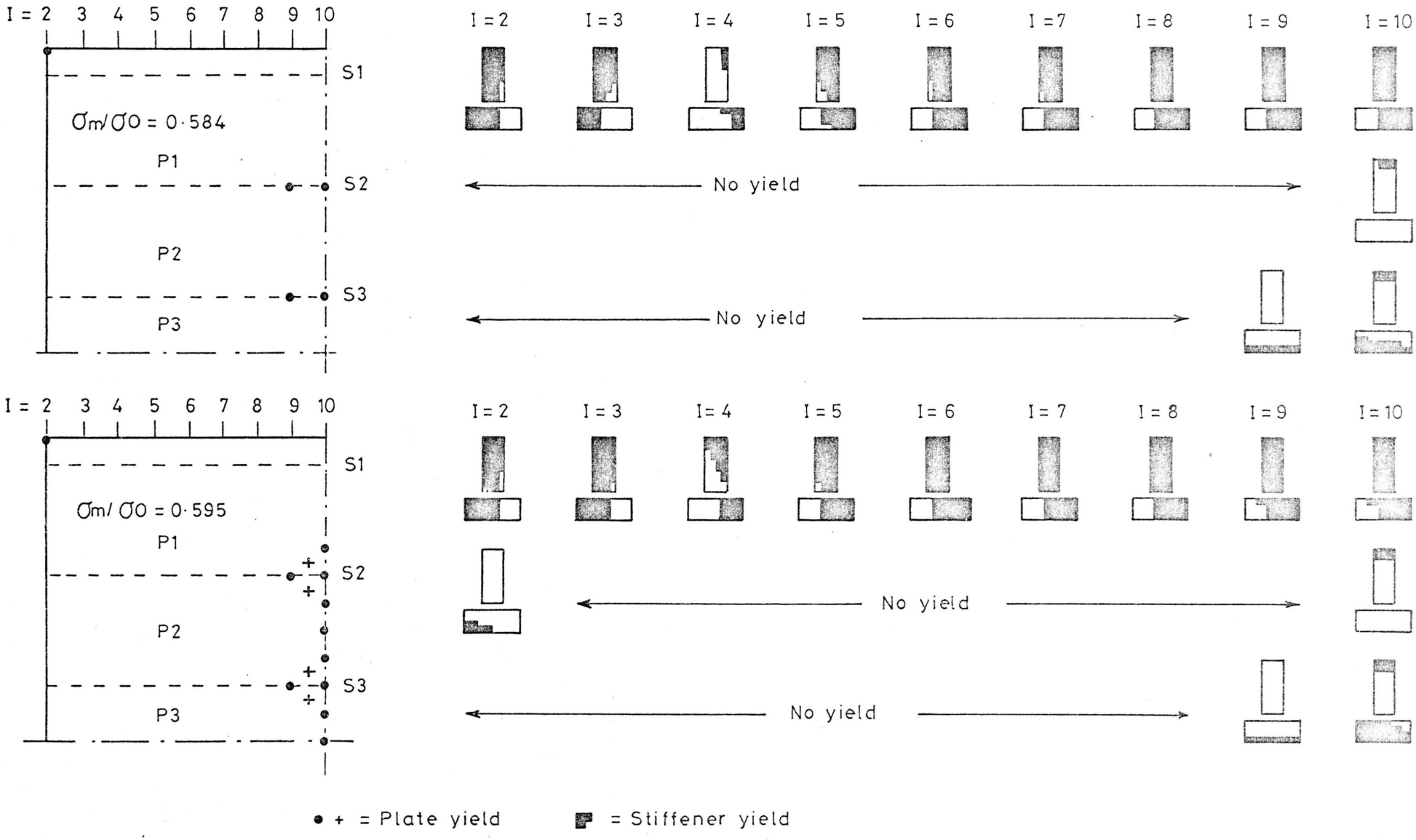

Fig D38 Model SP2. Zero residual stress. Predicted yield zones

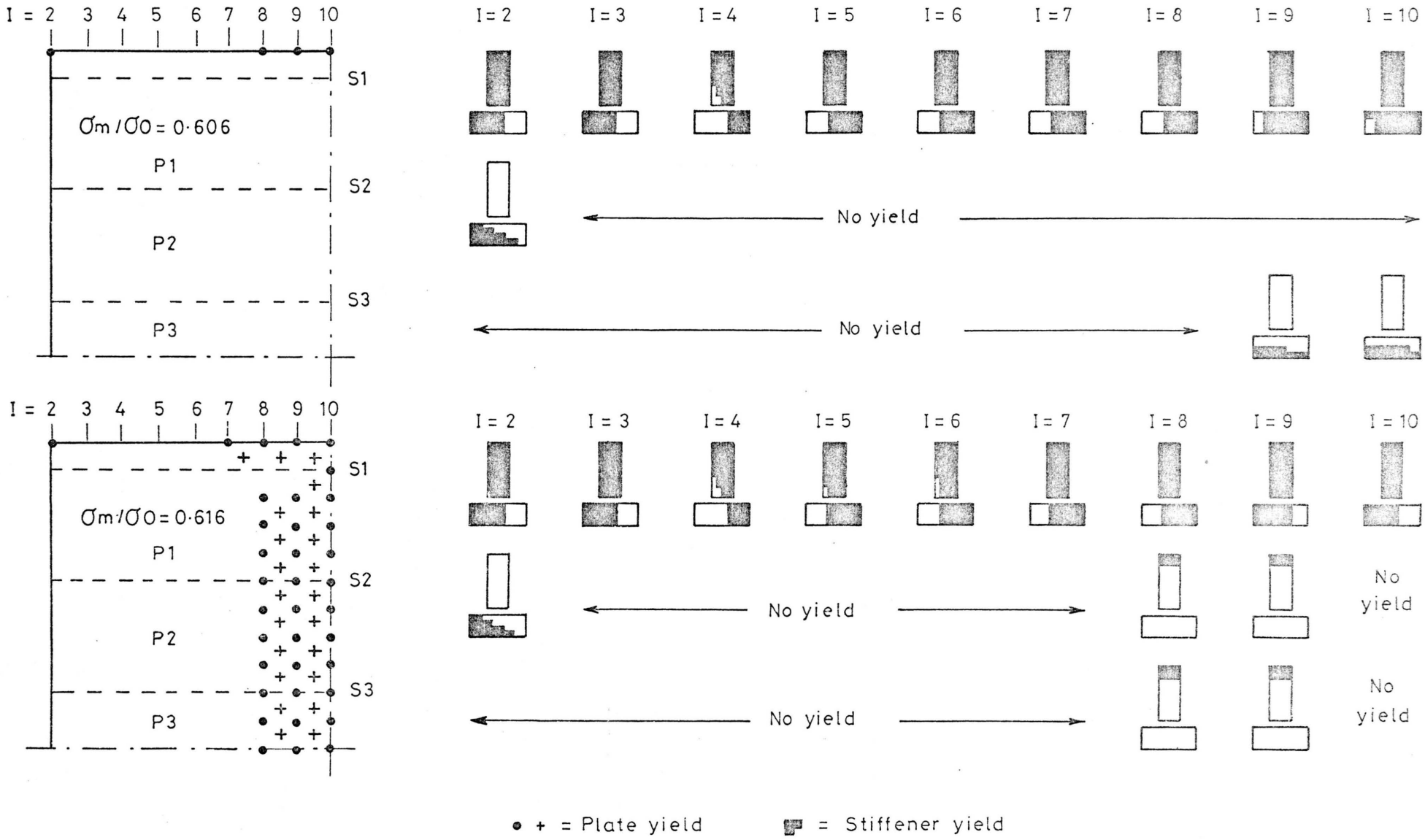

Fig D39 Model SP2. Residual stress applied. Predicted yield zones

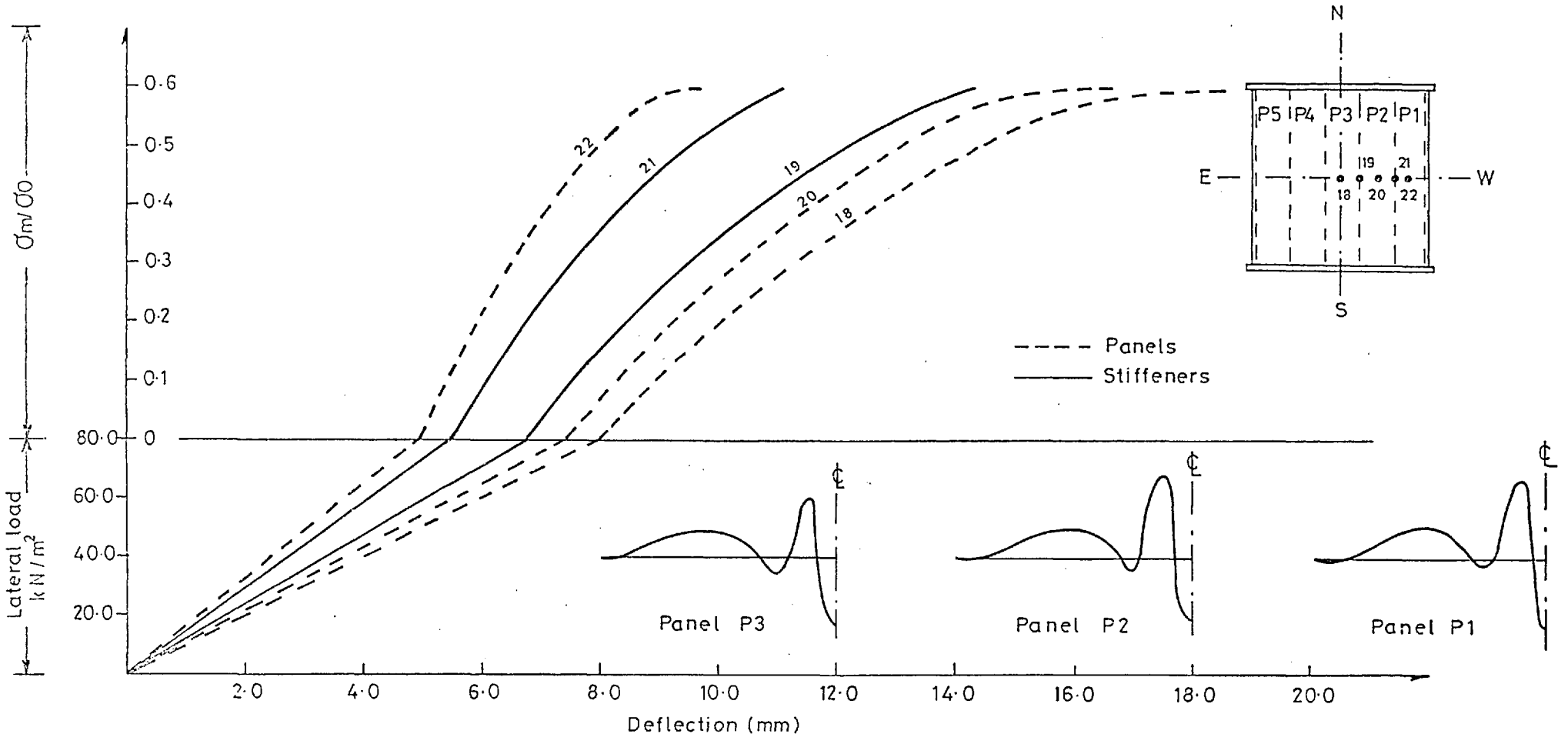

Fig D40 Model SP2 Load-deflection curves (zero residual stress)

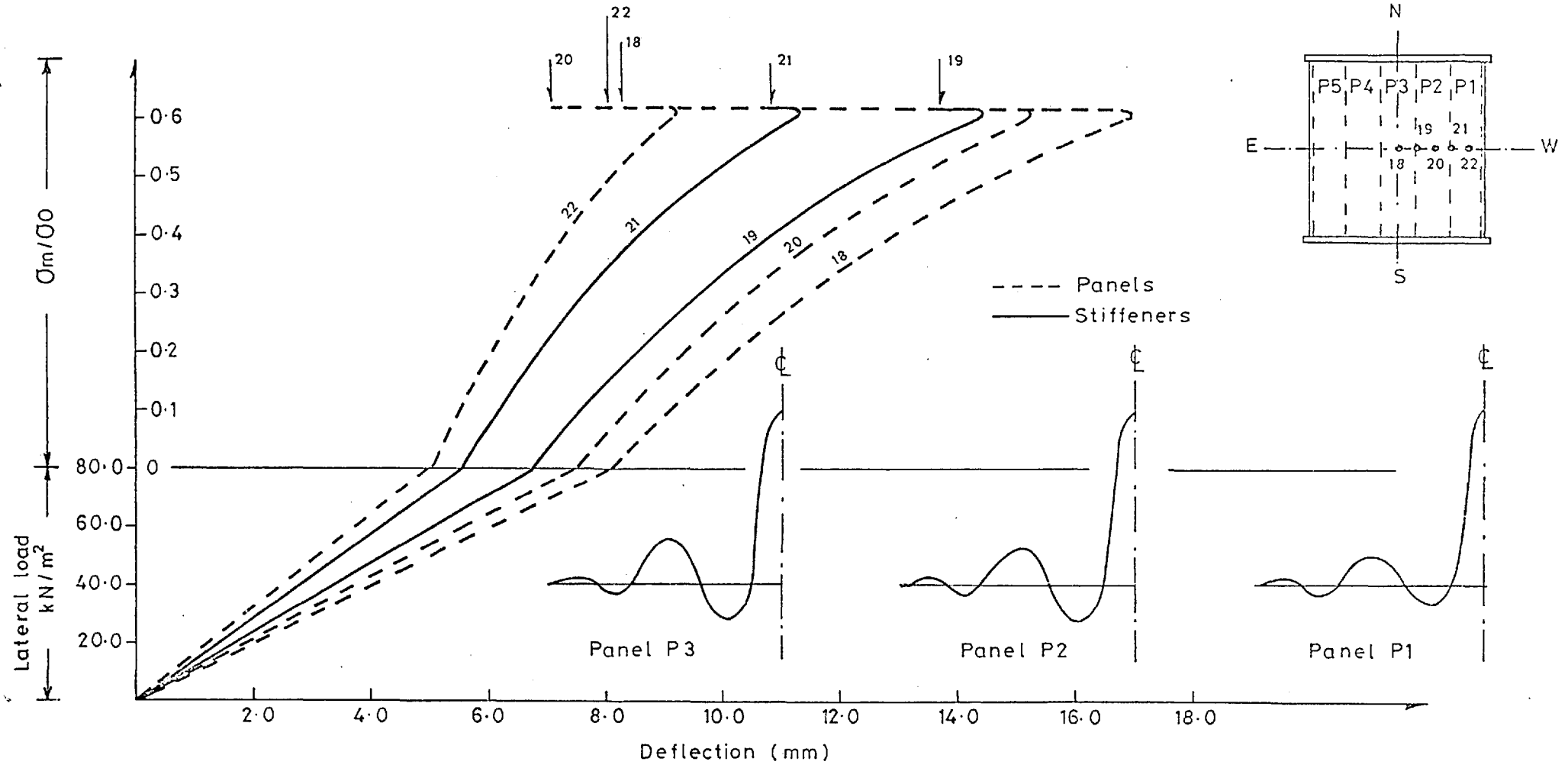

Fig D 41 Model SP2 Load-deflection curves (residual stress as shown in fig D2)

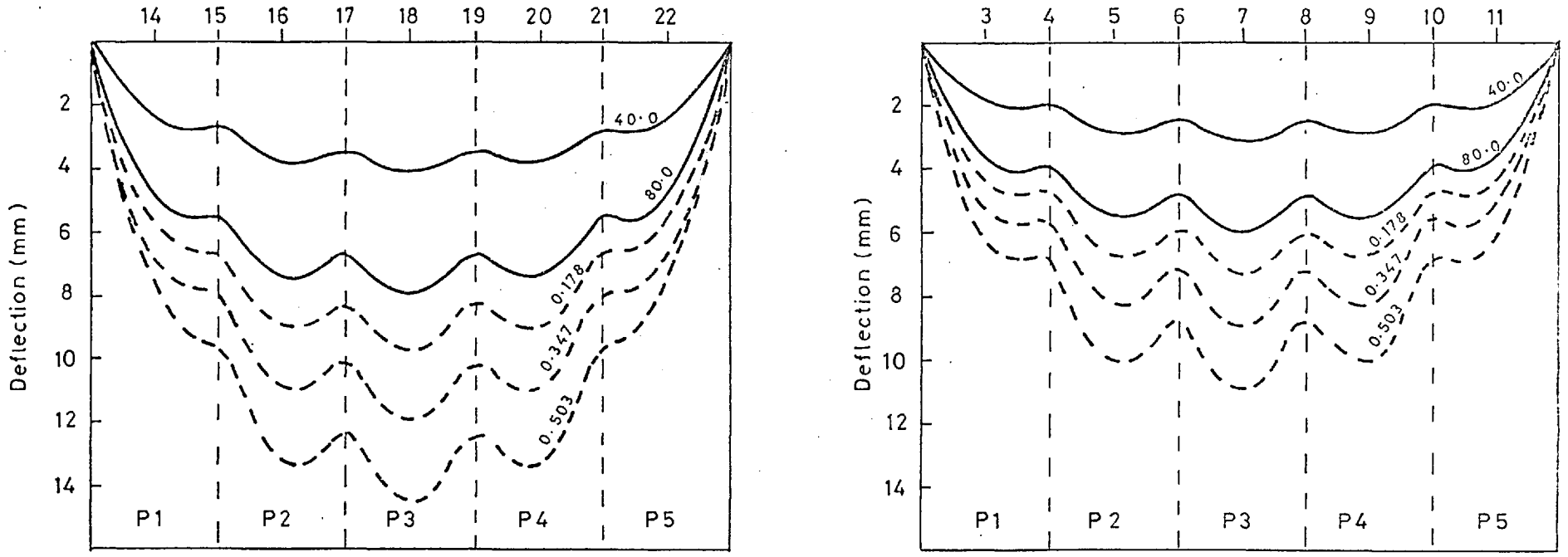

Applied lateral load (kN/m^2)

Stress ratio σ_m/σ_0

Zero residual stress

Fig D42 Model SP2. Deflection profiles (locations shown in fig D4)

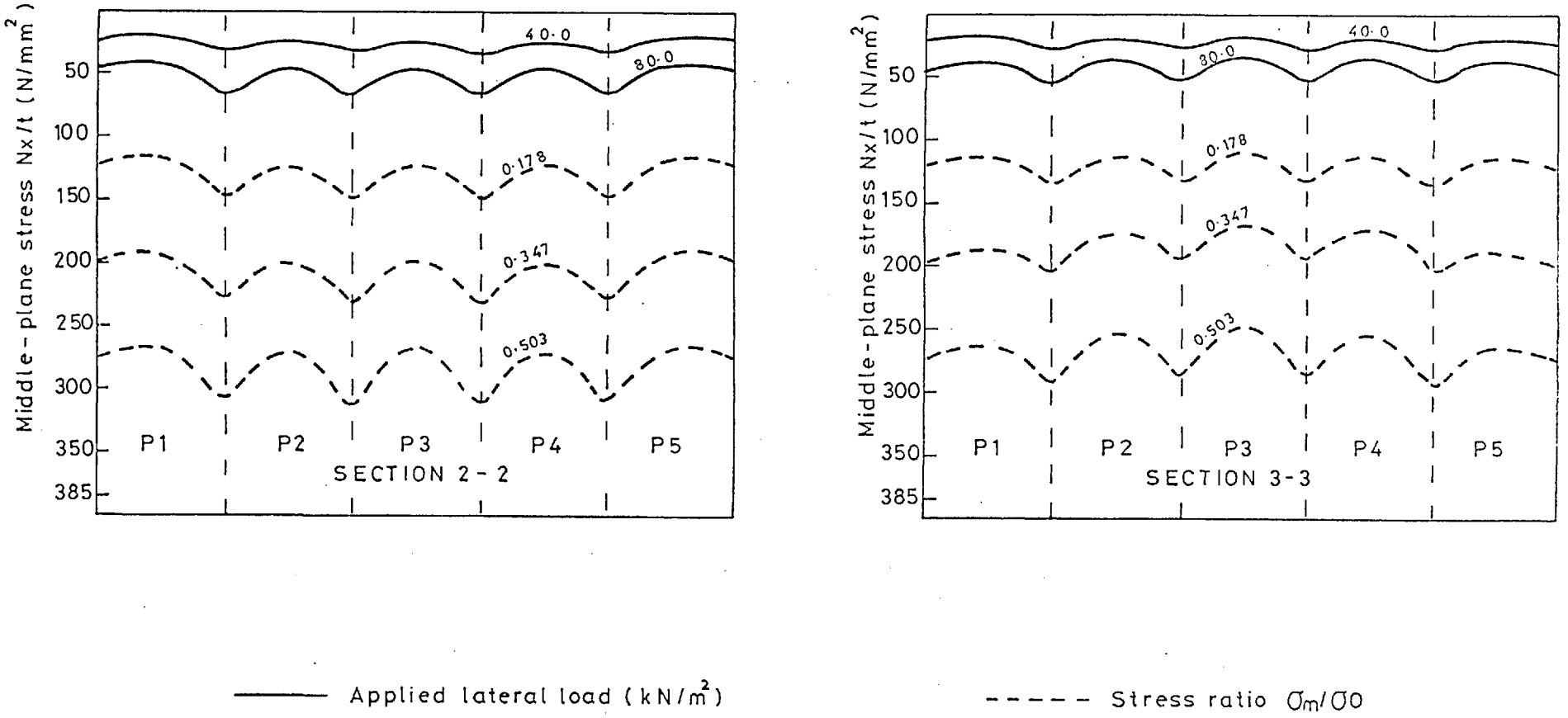

Fig D43 Model SP2 Distributions of direct stress across plate (sections shown in fig D4)

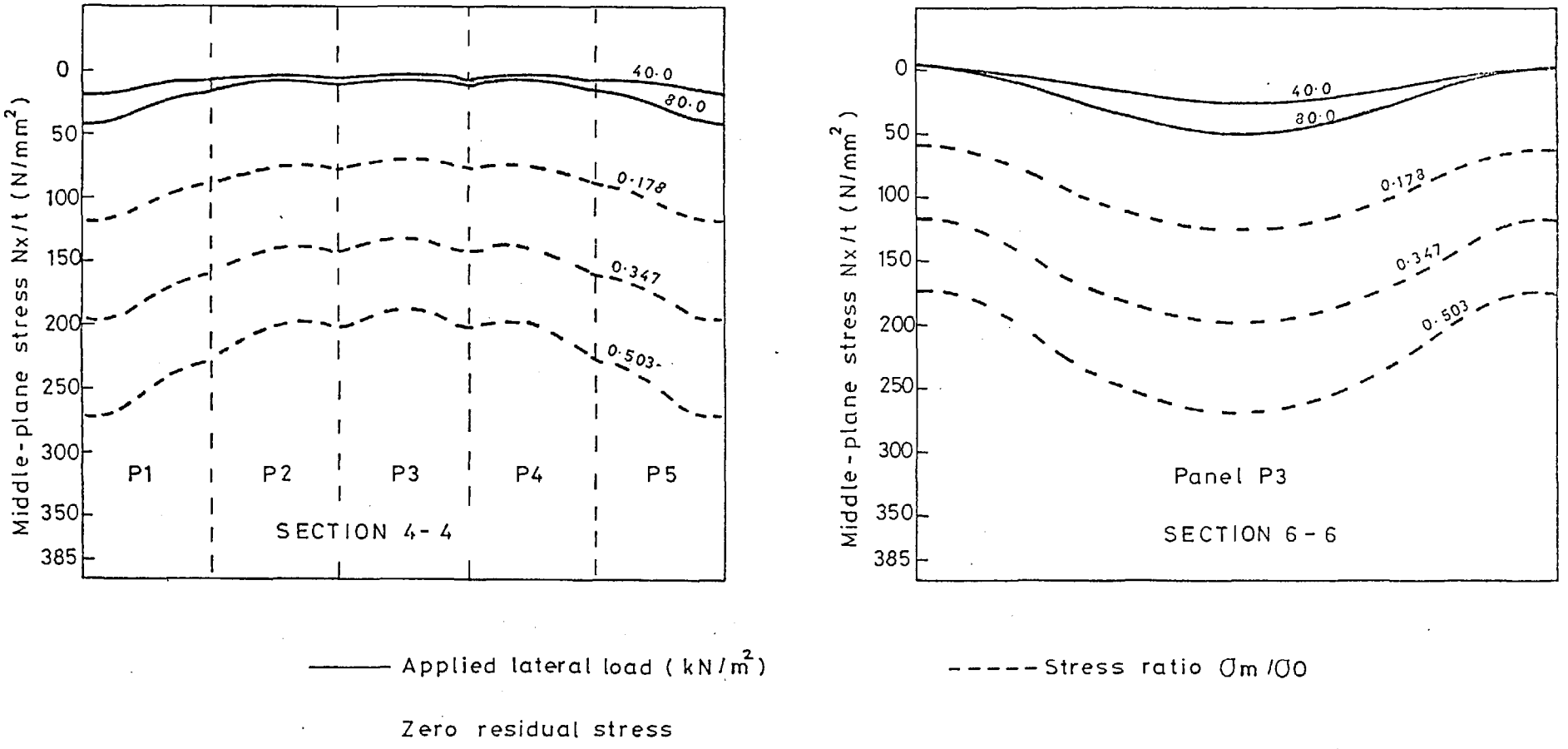

Fig D44 Model SP2 Distributions of direct stress across plate (sections shown in fig D4)

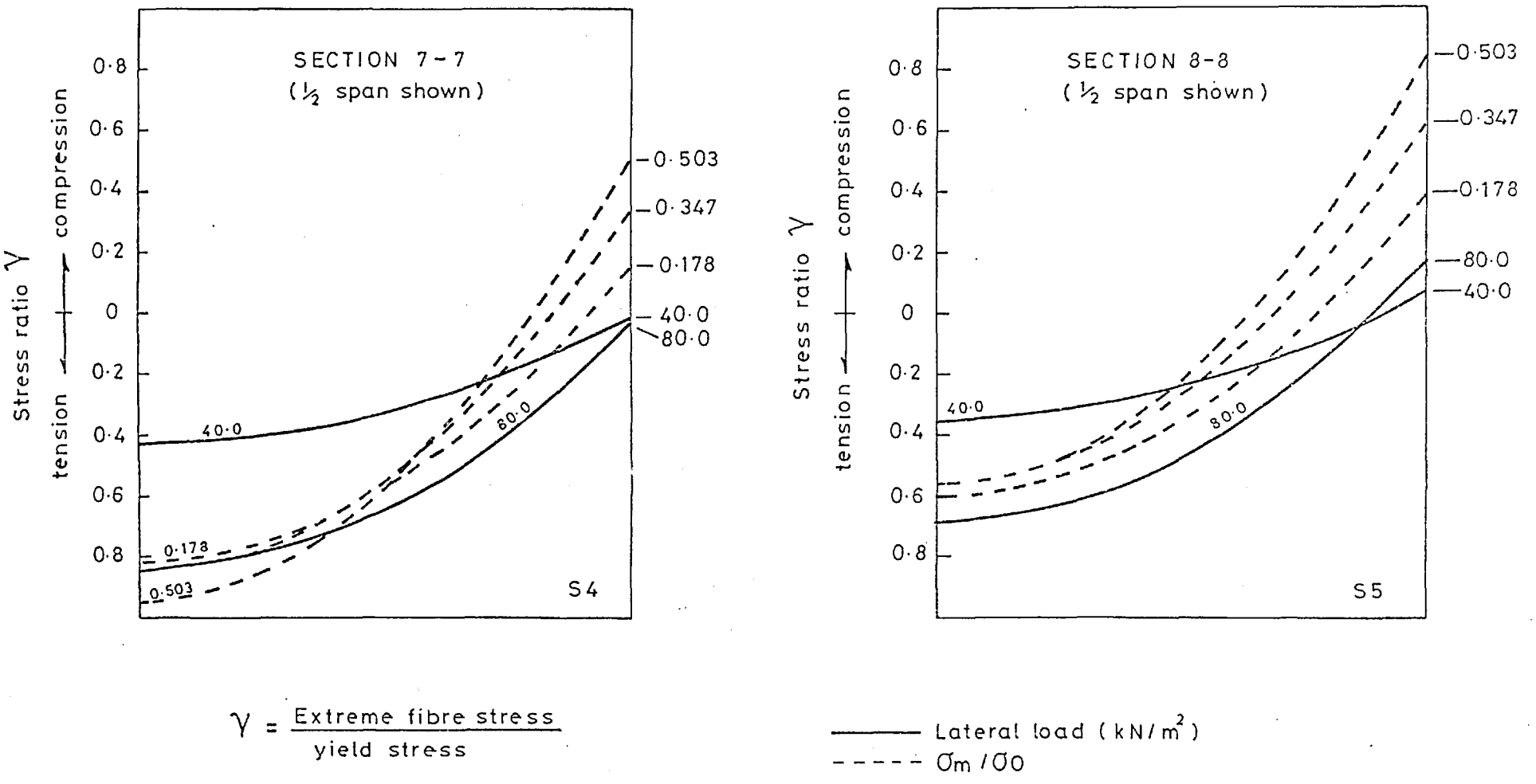

Fig D45 Model SP2. Extreme fibre stresses in the stiffener flanges
(sections shown in fig D4)

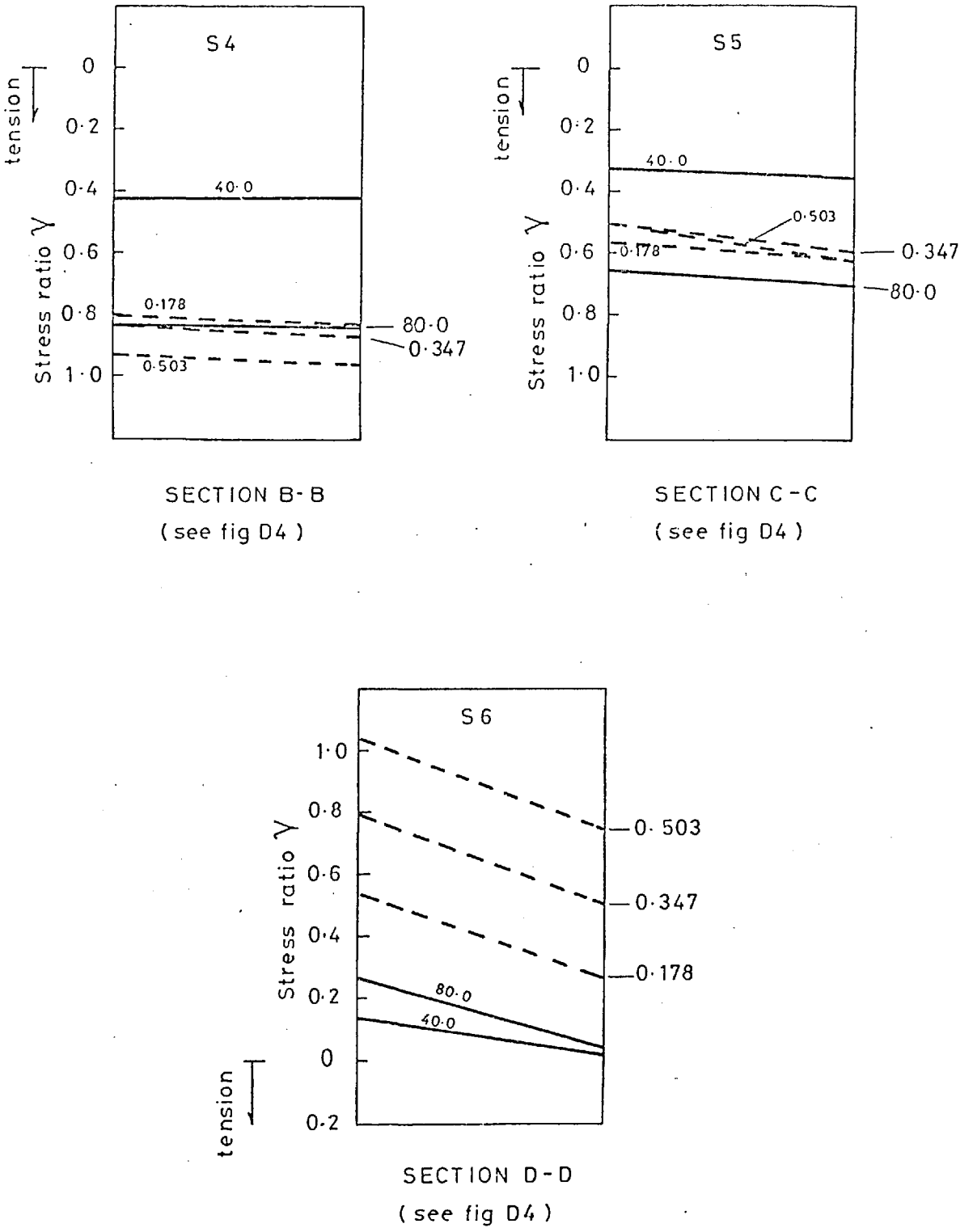

Fig D46 Model SP2 Variation of longitudinal stress across stiffener flange plates

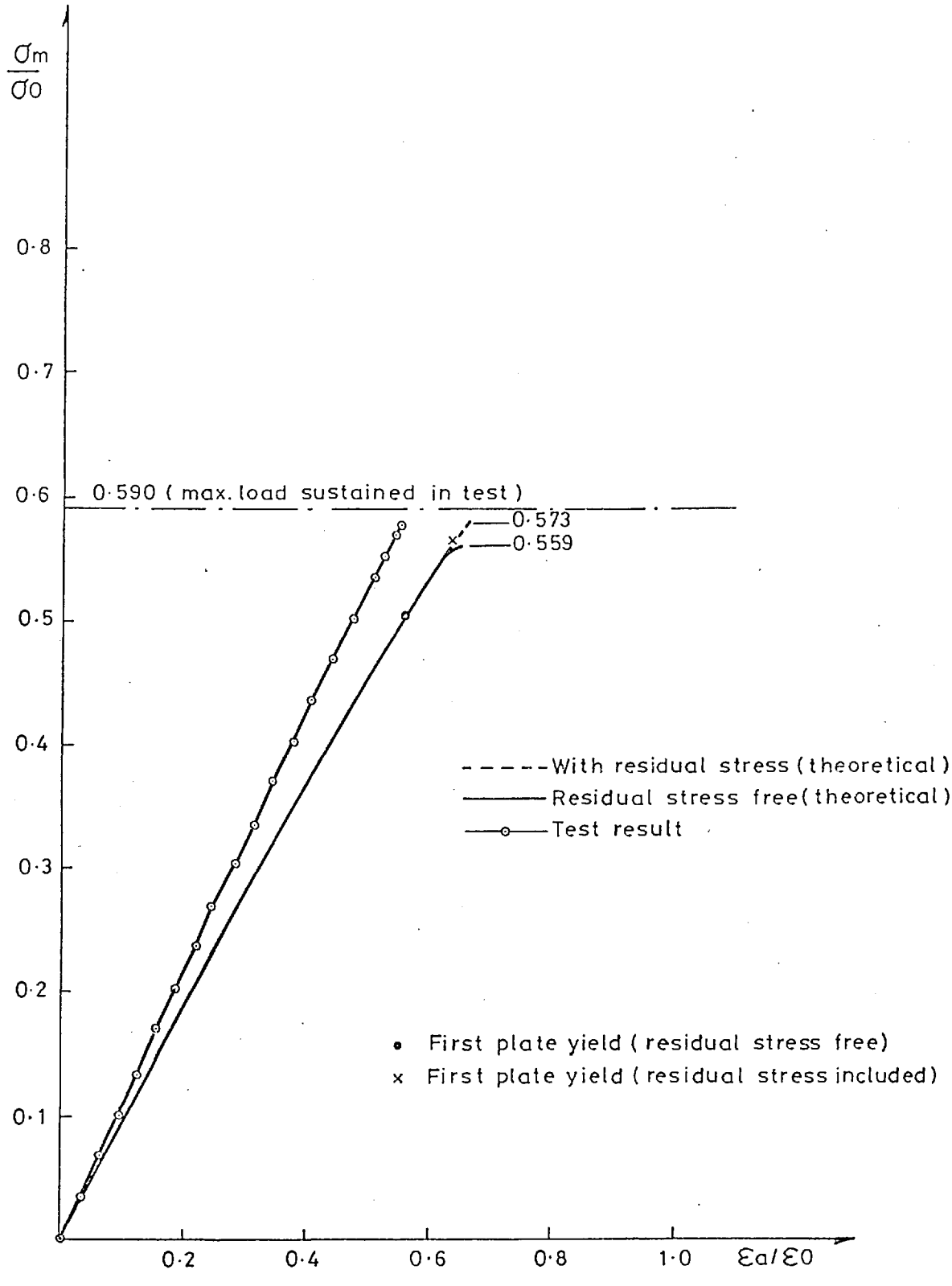

Fig D47 Model SP3 Load- shortening curves

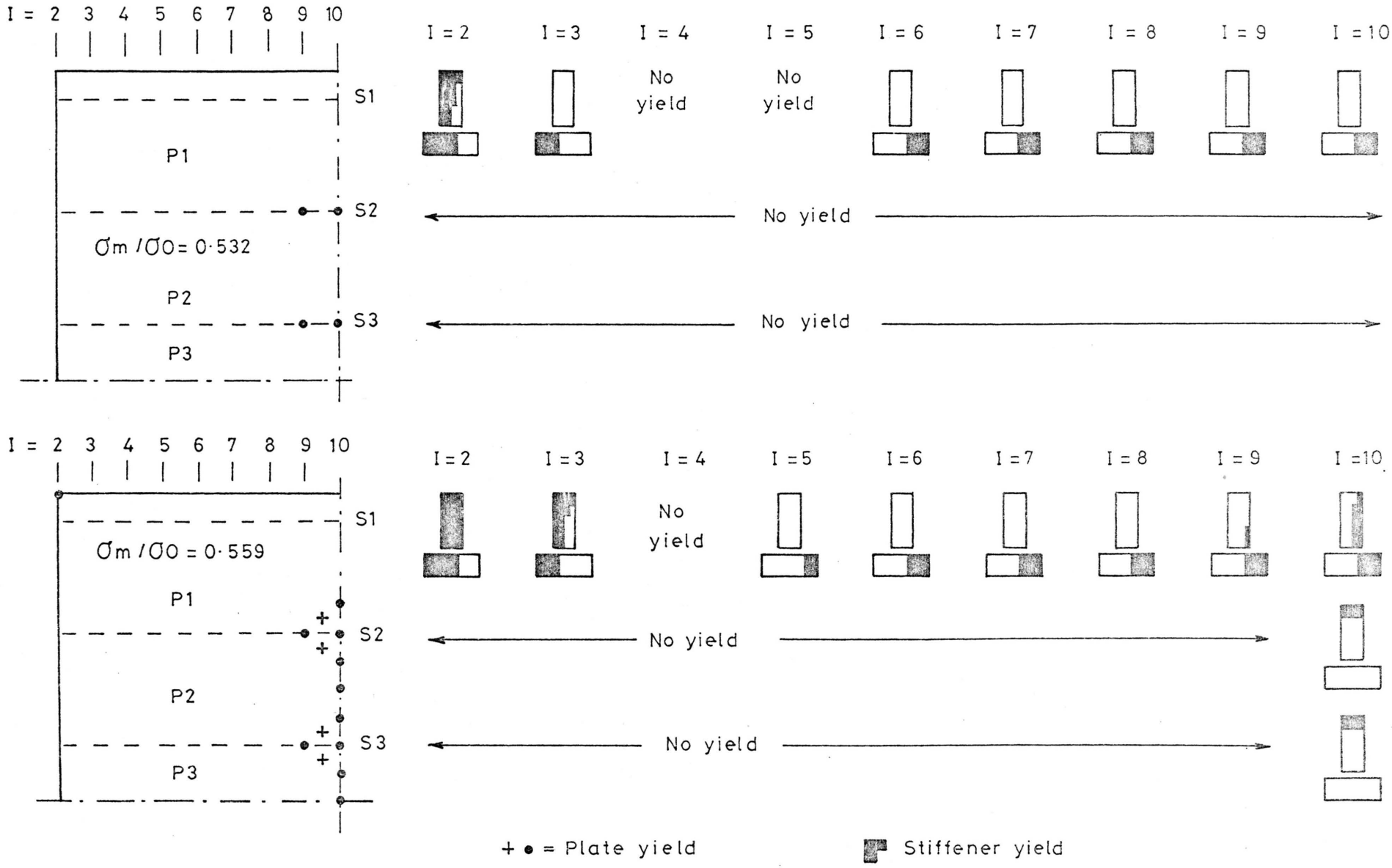

Fig D48 Model SP3. Zero residual stress. Predicted yield zones

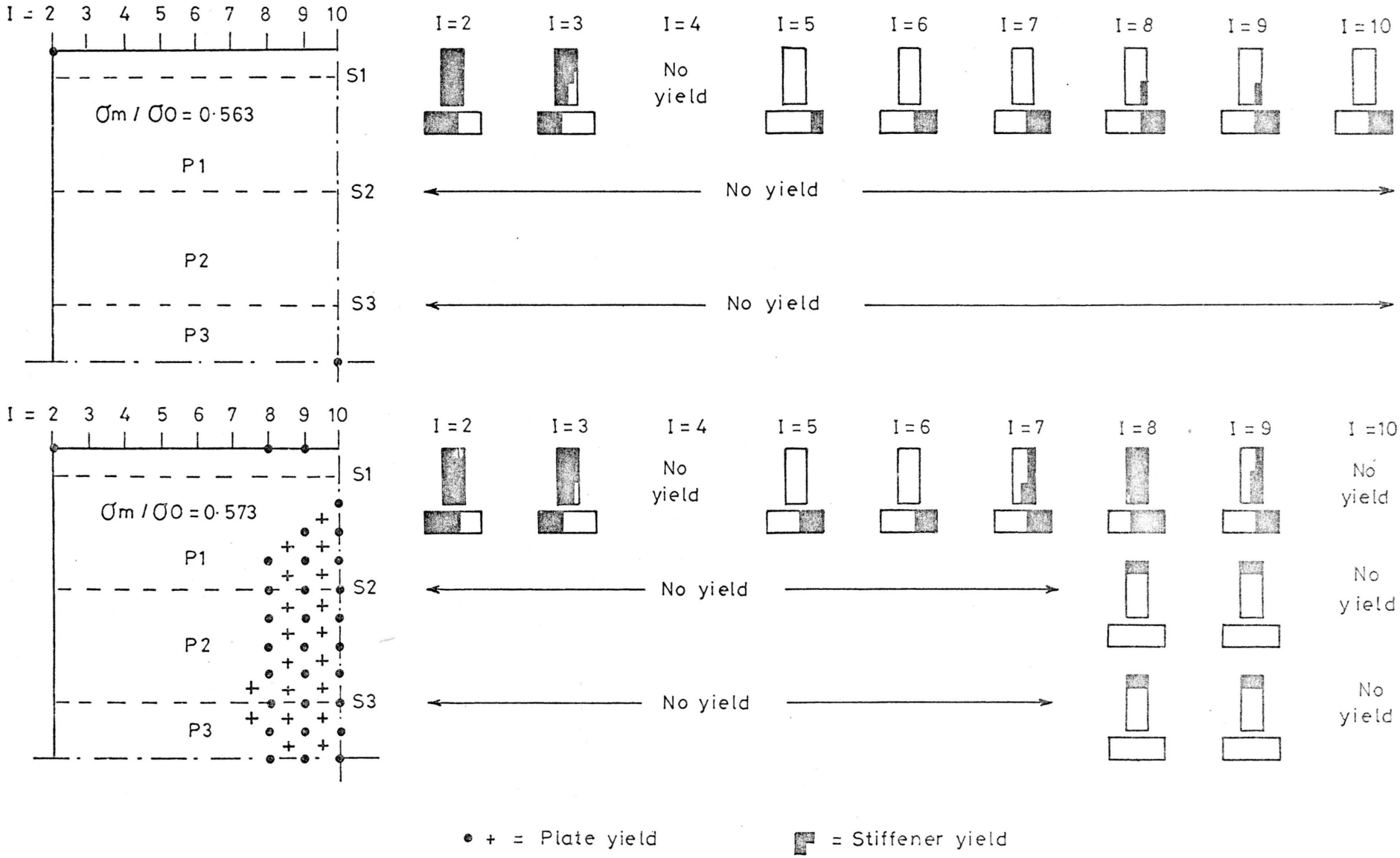

Fig D49 Model SP3 Residual stress applied. Predicted yield zones

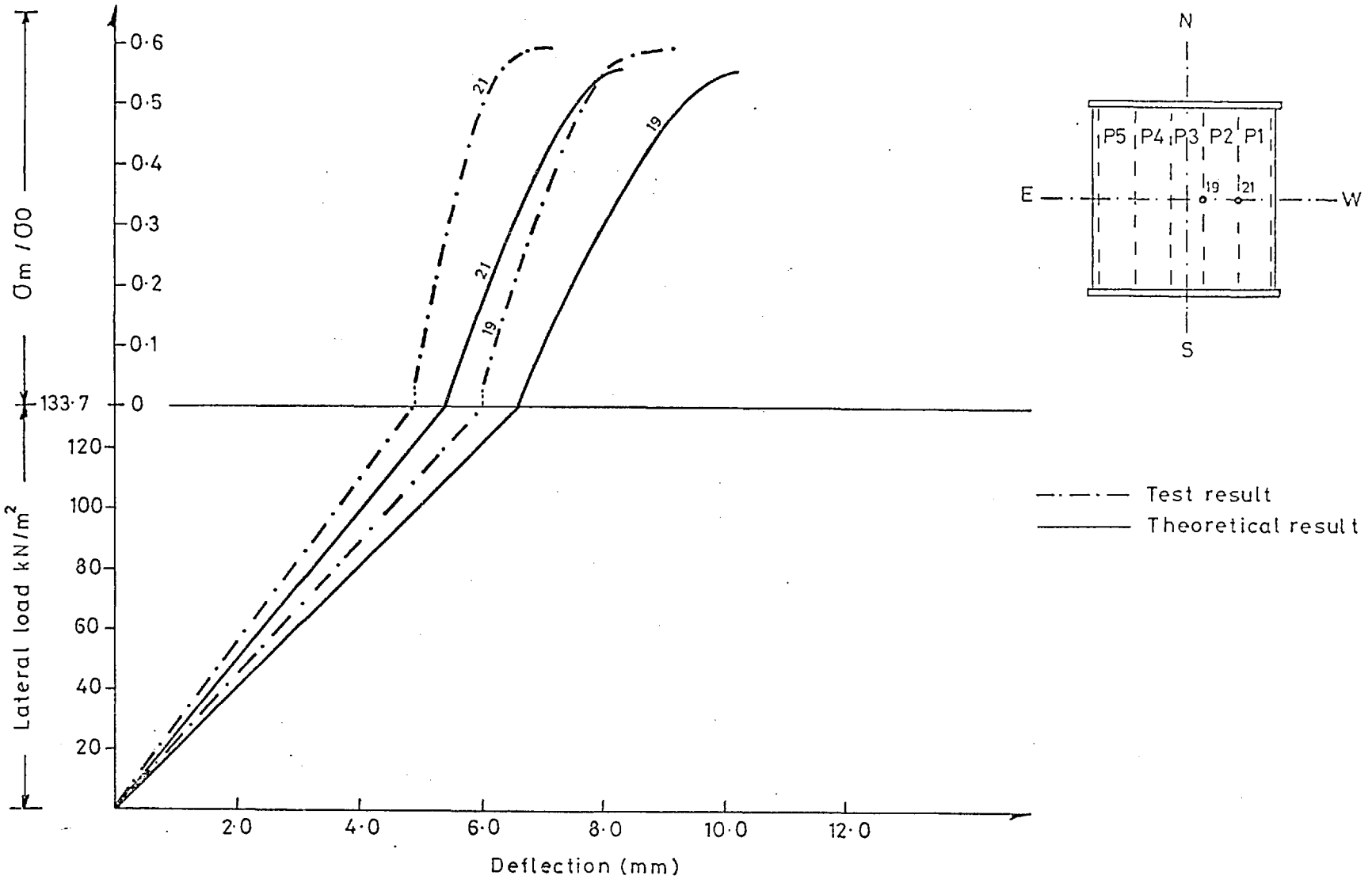

Fig D50 Model SP3 Load-deflection curves (zero residual stress)

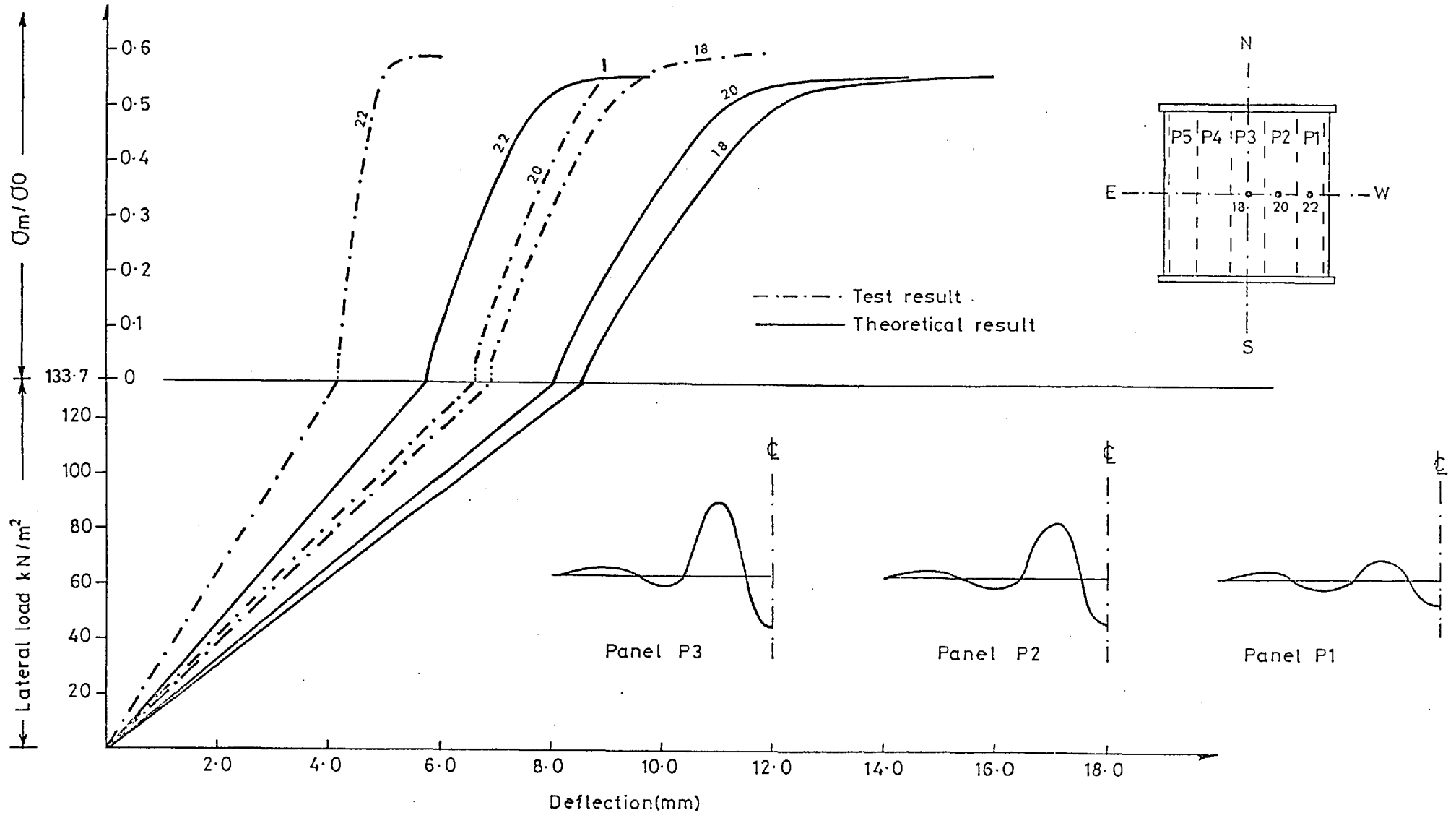

Fig D51 Model SP3 Load-deflection curves (zero residual stress)

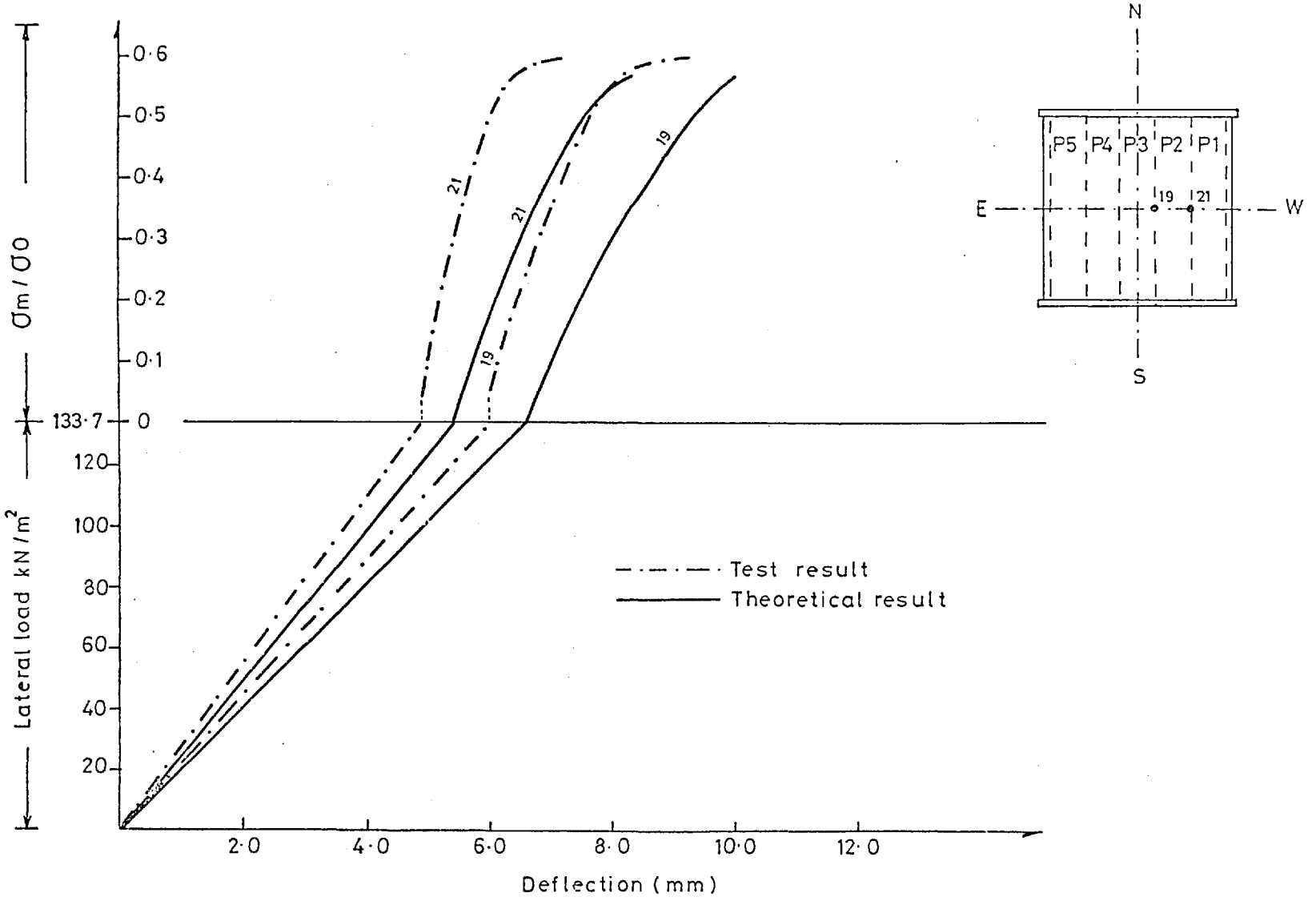

Fig D52 Model SP3 Load-deflection curves (residual stress as shown in fig D2)

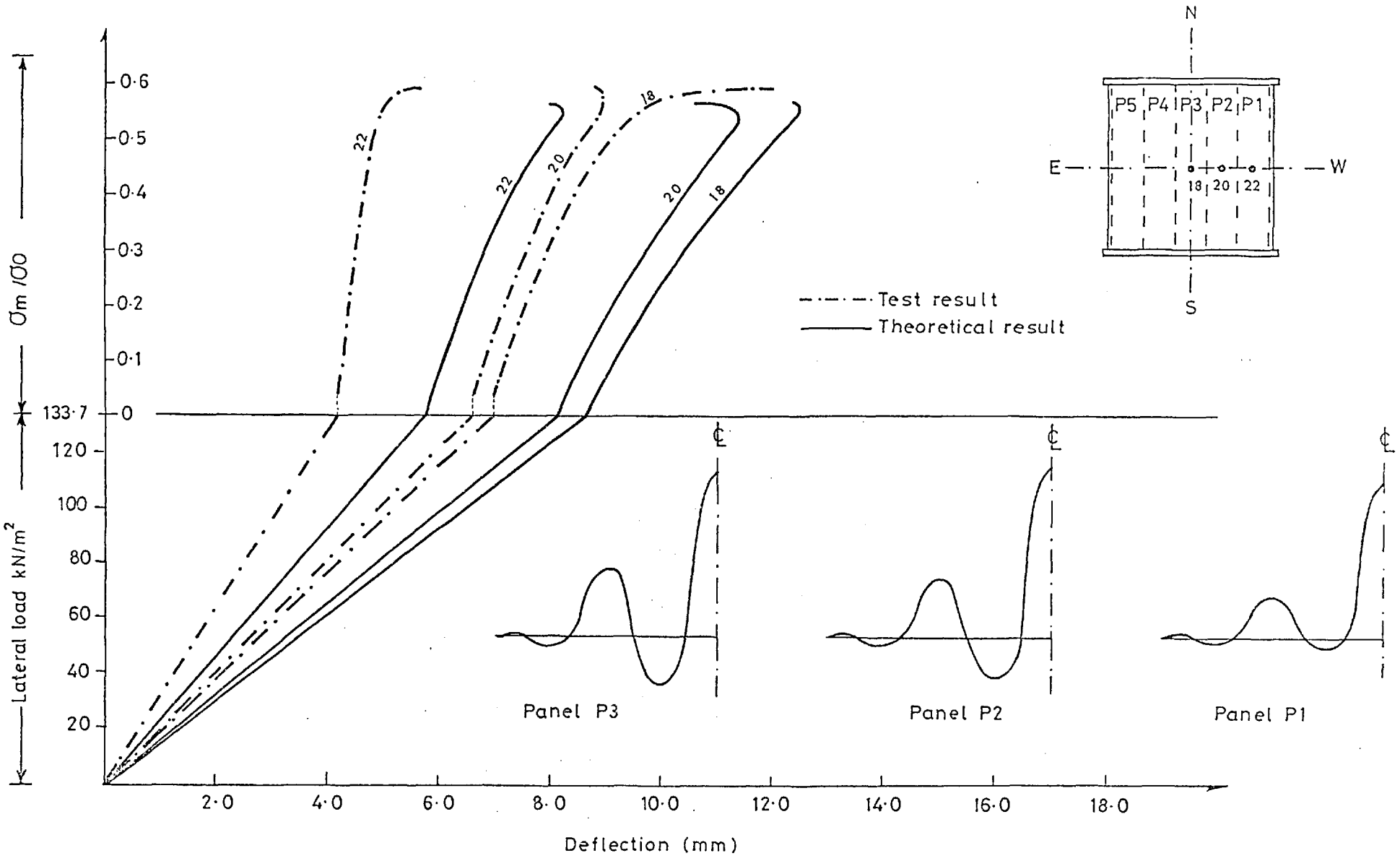

Fig D 53 Model SP3 Load-deflection curves (residual stress as shown in fig D2)

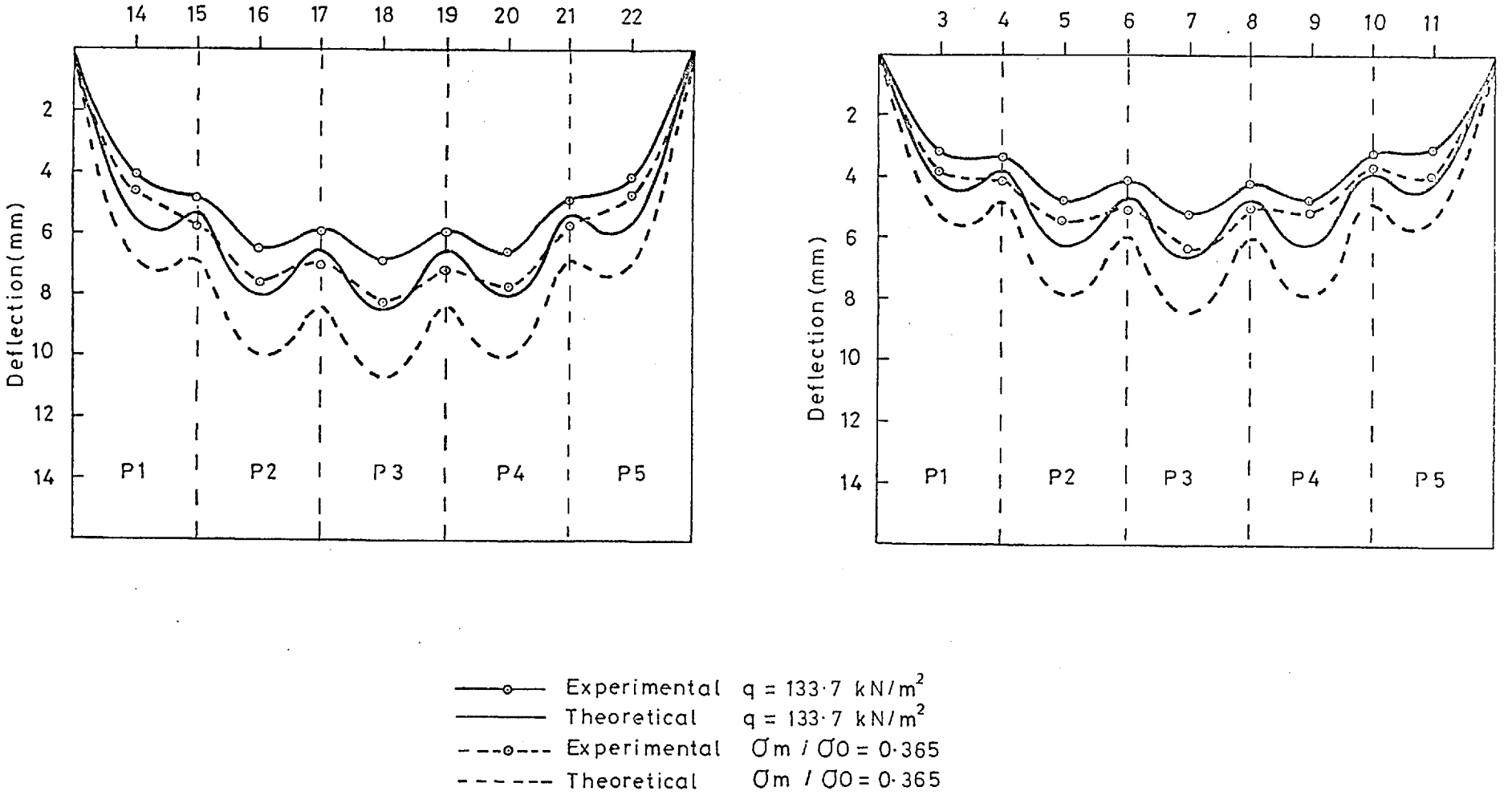

Fig D54 Model SP3 Deflection profiles (locations shown in fig D4)

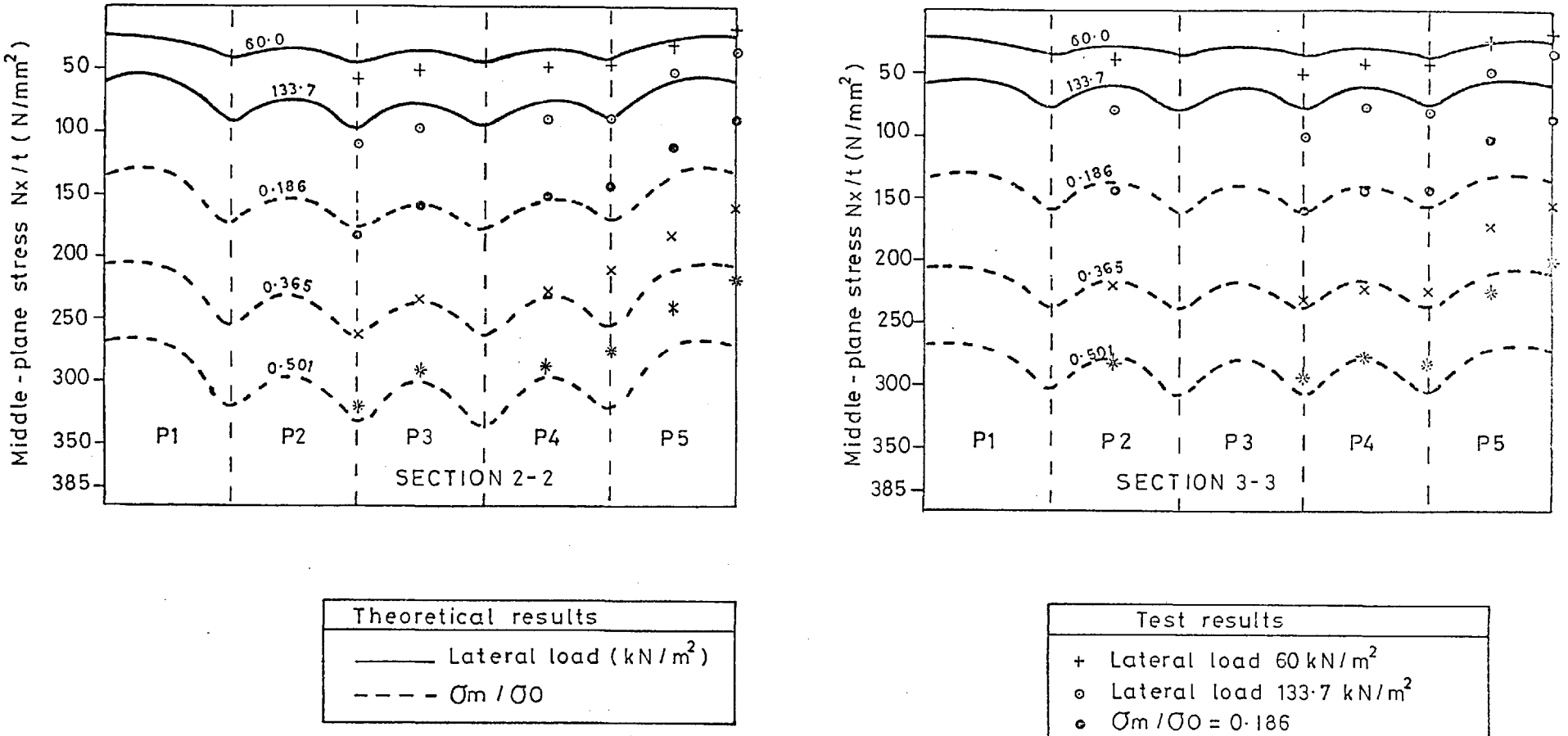

Fig D55 Model SP3 Distributions of direct stress across plate (sections shown in fig D4)

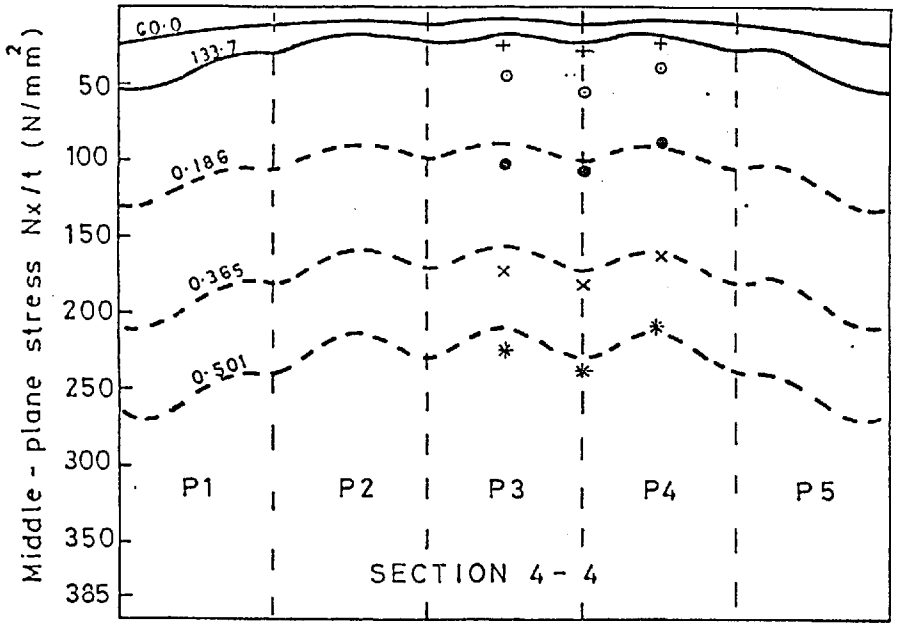

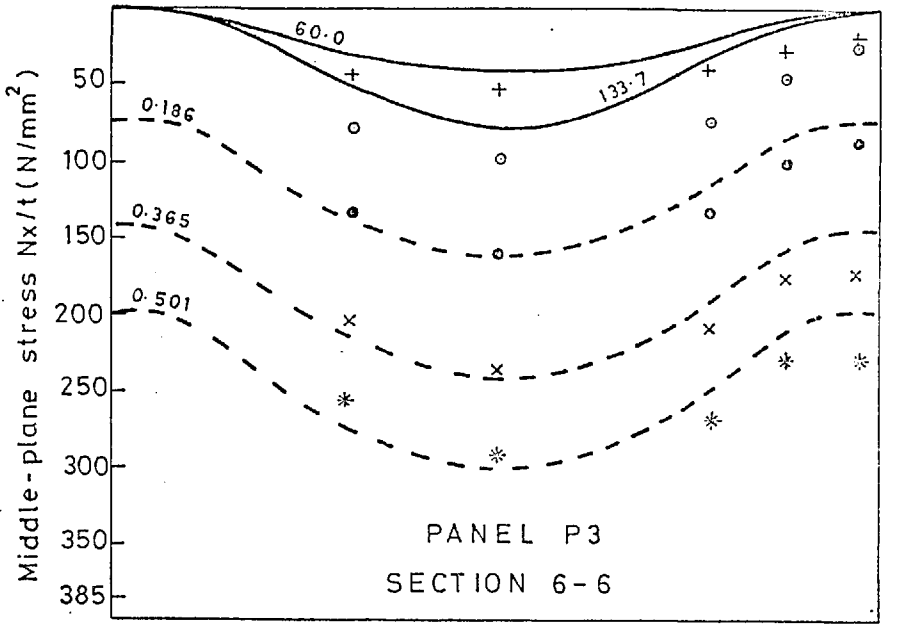

Theoretical results
——— Lateral load kN/m²
- - - - - σm / σ0

Test results
+ Lateral load 60 kN/m²
⊙ Lateral load 133·7 kN/m²
o σm / σ0 = 0·186
× σm / σ0 = 0·365
✳ σm / σ0 = 0·501

Fig D56 Model SP3. Distributions of direct stress across plate (sections shown in fig D4)

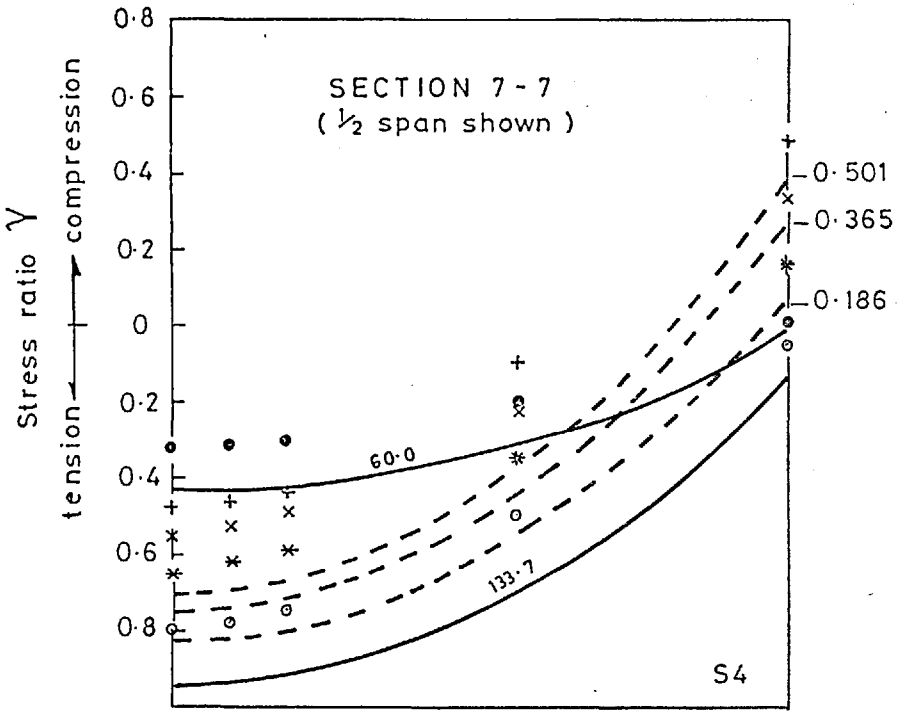

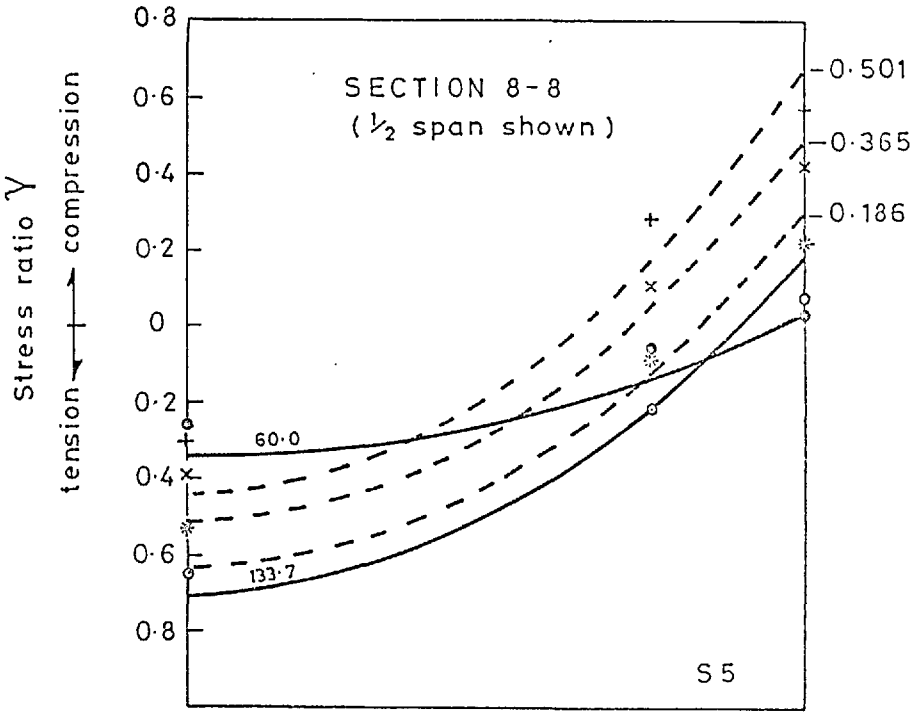

$$\gamma = \frac{\text{Extreme fibre stress}}{\text{yield stress}}$$

Theoretical results
—— Lateral load kN/m²
– – – σm /σ0

Test results
○ Lateral load 60 kN/m²
⊙ Lateral load 133·7 kN/m²
✳ σm / σ0 = 0·186
× σm / σ0 = 0·365
+ σm / σ0 = 0·501

Fig D57 Model SP3. Extreme fibre stresses in the stiffener flanges (sections shown in fig D4)

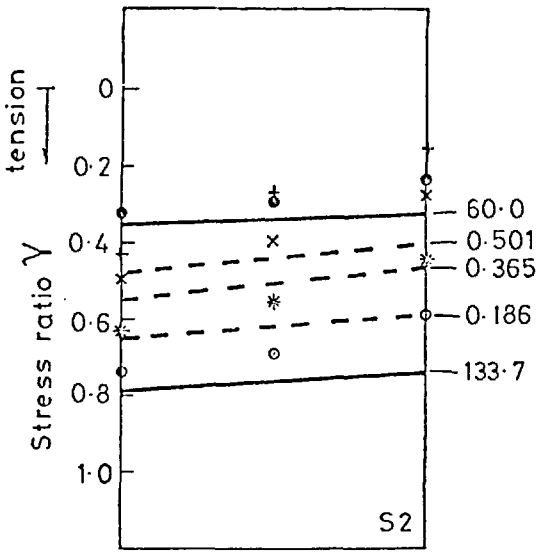

SECTION A-A
(see fig D4)

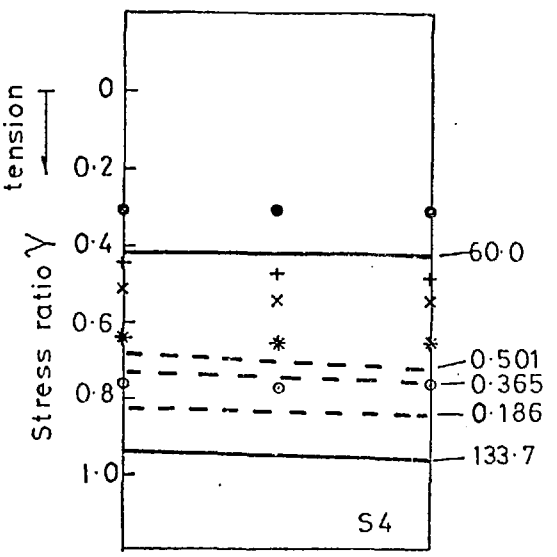

SECTION B-B
(see fig D4)

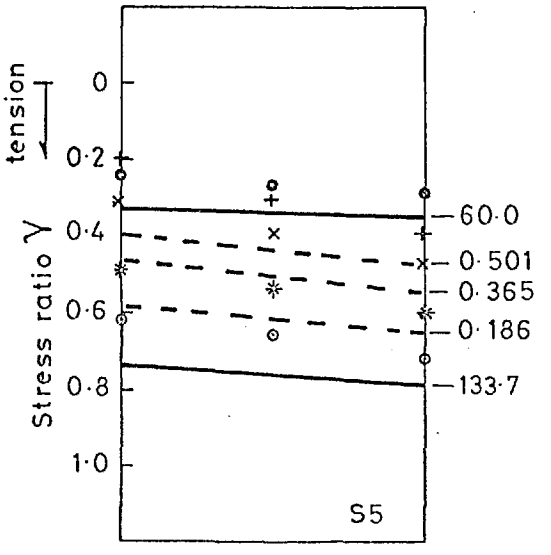

SECTION C-C
(see fig D4)

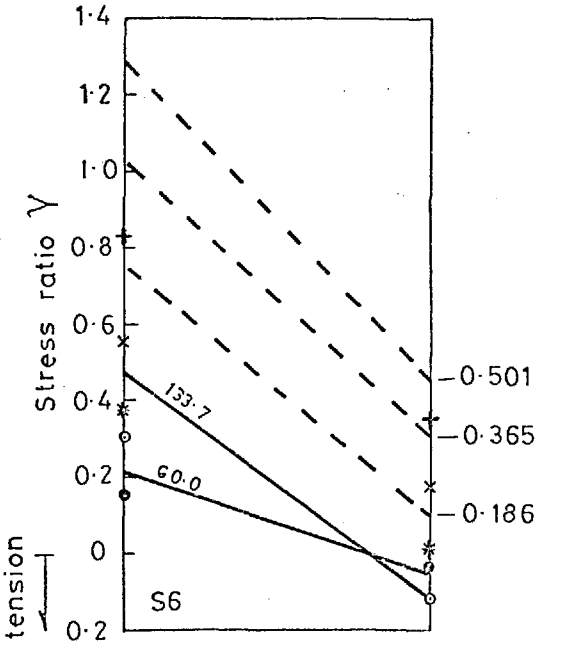

SECTION D-D
(see fig D4)

γ = Extreme fibre stress / yield stress

Theoretical results
—— Lateral load kN/m²
---- $\sigma m / \sigma 0$

Test results
∘ Lateral load 60 kN/m²
⊙ Lateral load 133·7 kN/m²
✳ $\sigma m / \sigma 0$ = 0·186
× $\sigma m / \sigma 0$ = 0·365
+ $\sigma m / \sigma 0$ = 0·501

Fig D 58 Model SP3. Variation of longitudinal stress across stiffener flange plates

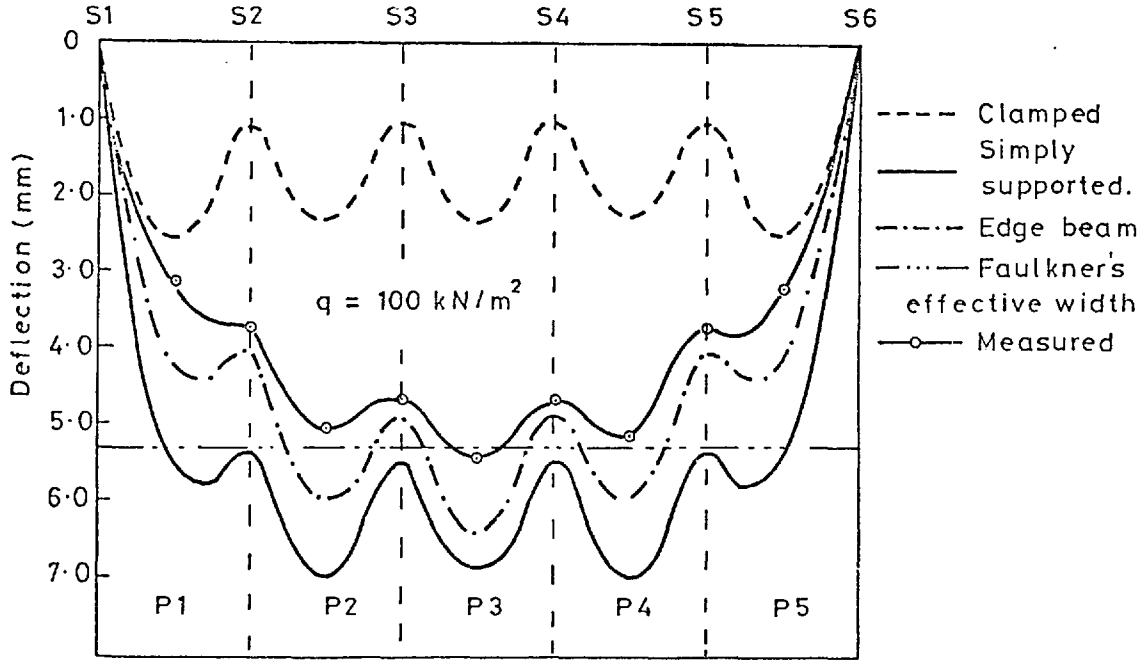

COMPARISON OF CENTRE LINE DEFLECTIONS FOR DIFFERENT FLEXURAL CONSTRAINTS ON BOUNDARY I = 2

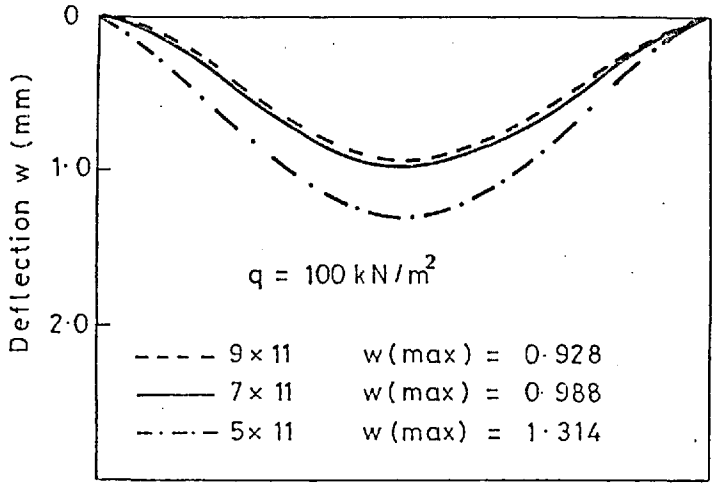

DEFLECTIONS OF A SINGLE PANEL FOR DIFFERENT MESH SIZES

Fig D 59

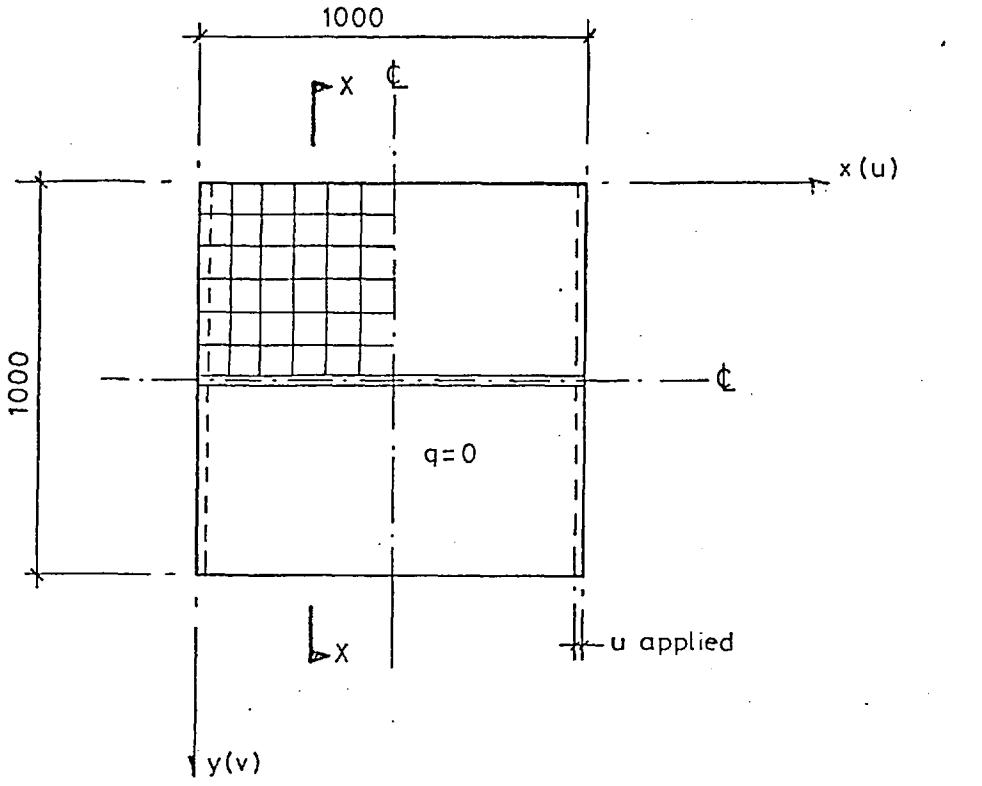

X – X

Material properties	
$\sigma 0$	250 N/mm^2
$\sigma 0_w$	250 N/mm^2
E	205000N/mm^2
V	·3

Boundary conditions	
y = 0	w = My = 0 Ny = Nxy = 0
x = 0	w = Mx = 0 Nxy = 0 u applied

Dimensions shown are in mm

Fig E1 Stiffened plate arrangement and properties for fig E2

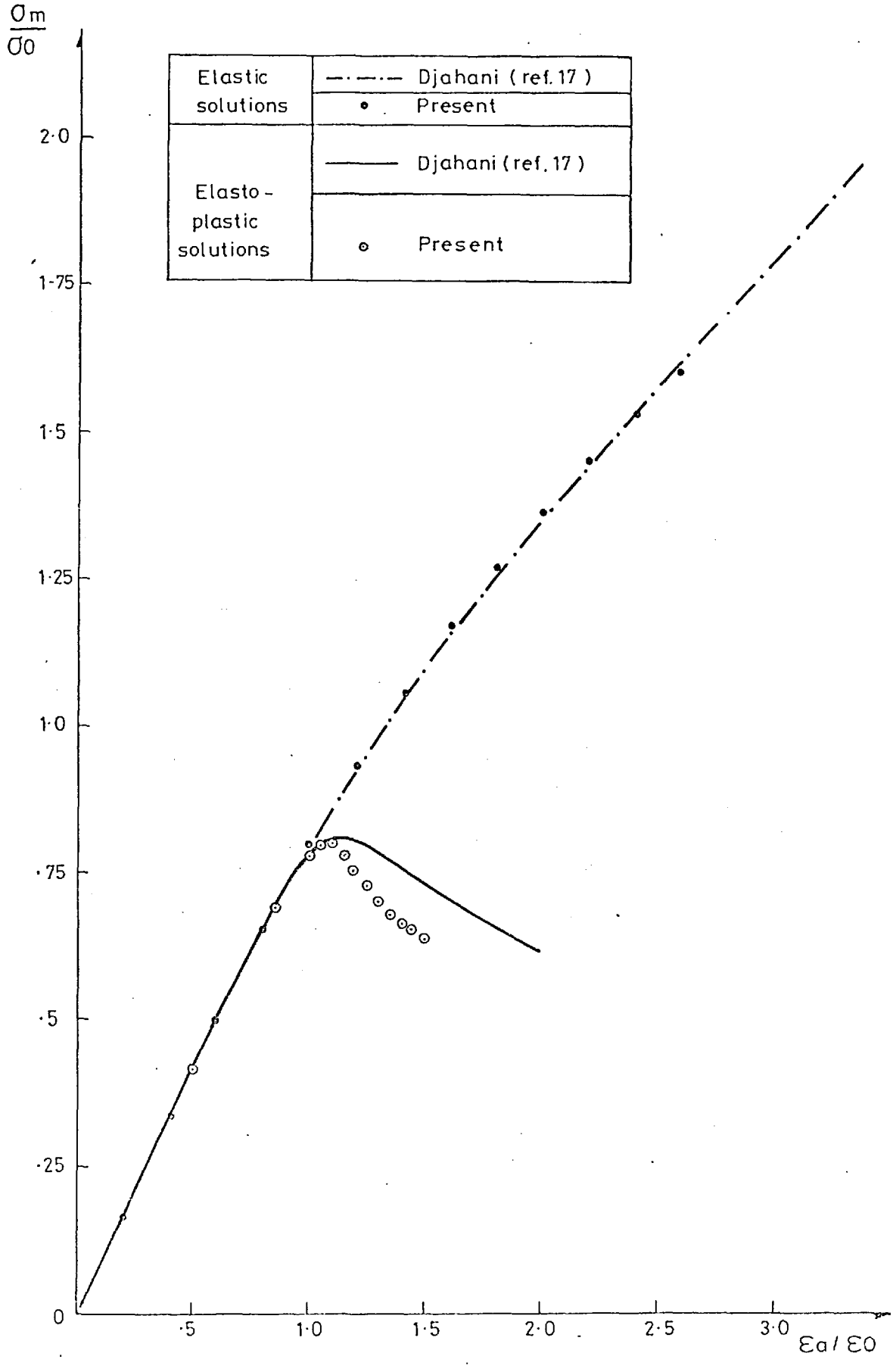

Fig E2 Relationship between mean edge stress and applied strain

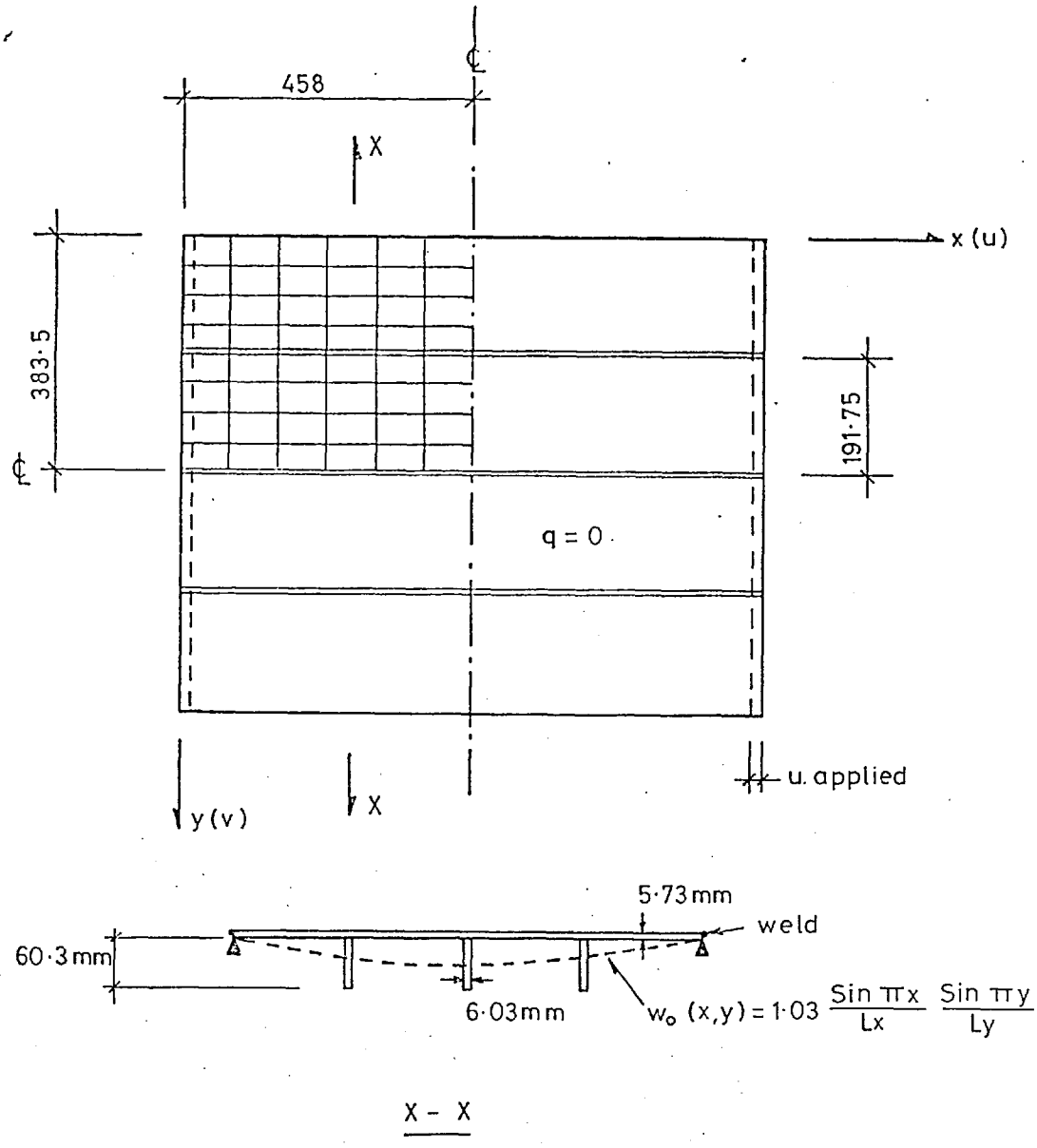

X - X

Material properties	
σ_0	348 N/mm^2
σ_{0_w}	348 N/mm^2
E	210000 N/mm^2
V	·3
σ_R	·4 σ_0
σ_{R_w}	·4 σ_{0_w}

Boundary conditions	
y=0	w = My = 0 Ny = Nxy = 0
x=0	w = Mx = 0 v = 0 u applied

Fig E3 Stiffened plate arrangement and properties for figs. E4 & E5

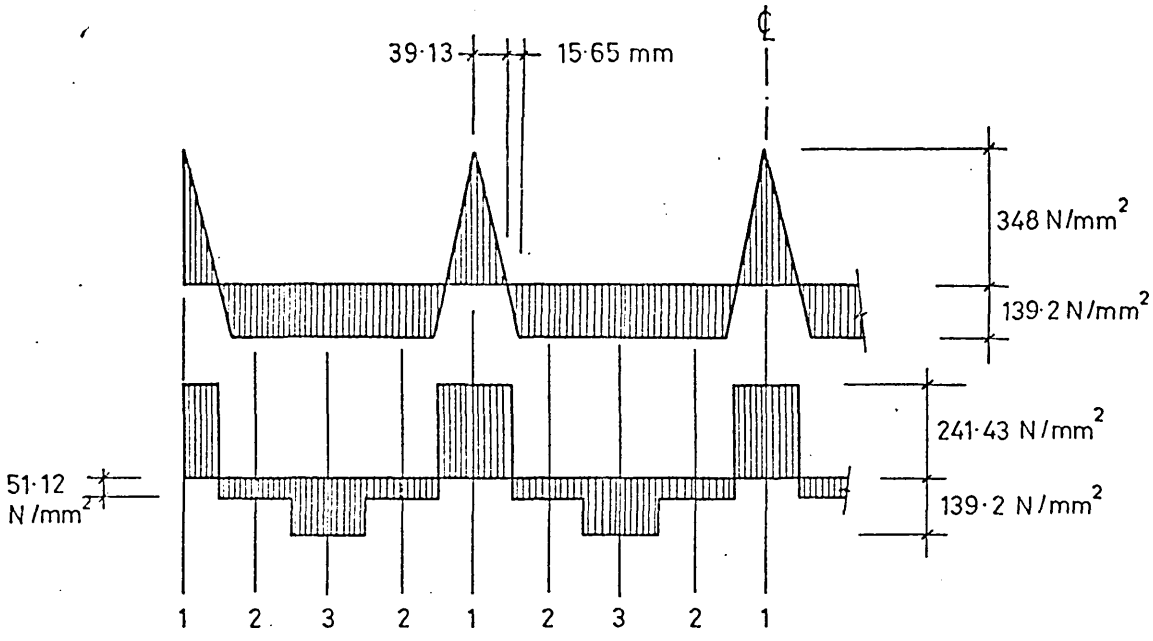

$N_x(1) = +1383{\cdot}4$ N/mm ; $N_x(2) = -292{\cdot}92$ N/mm ; $N_x(3) = -797{\cdot}62$ N/mm

INITIAL AND IDEALISED RESIDUAL
STRESS DISTRIBUTIONS IN THE PLATE

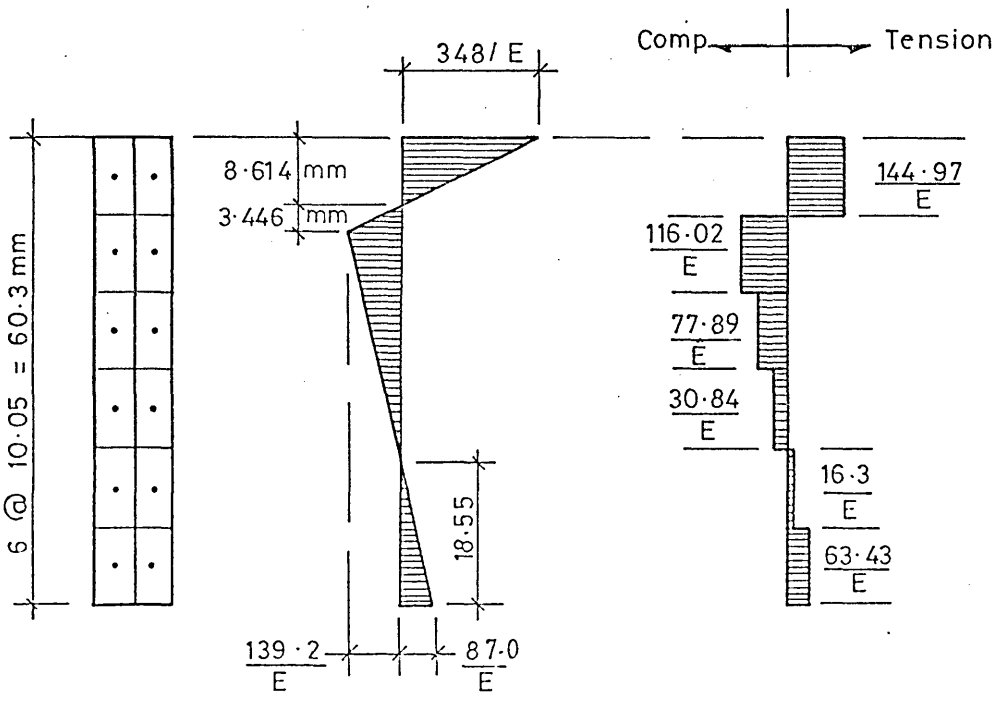

INITIAL AND IDEALISED RESIDUAL
STRAIN DISTRIBUTIONS IN THE WEBS

Fig E4 Weld induced residual stresses

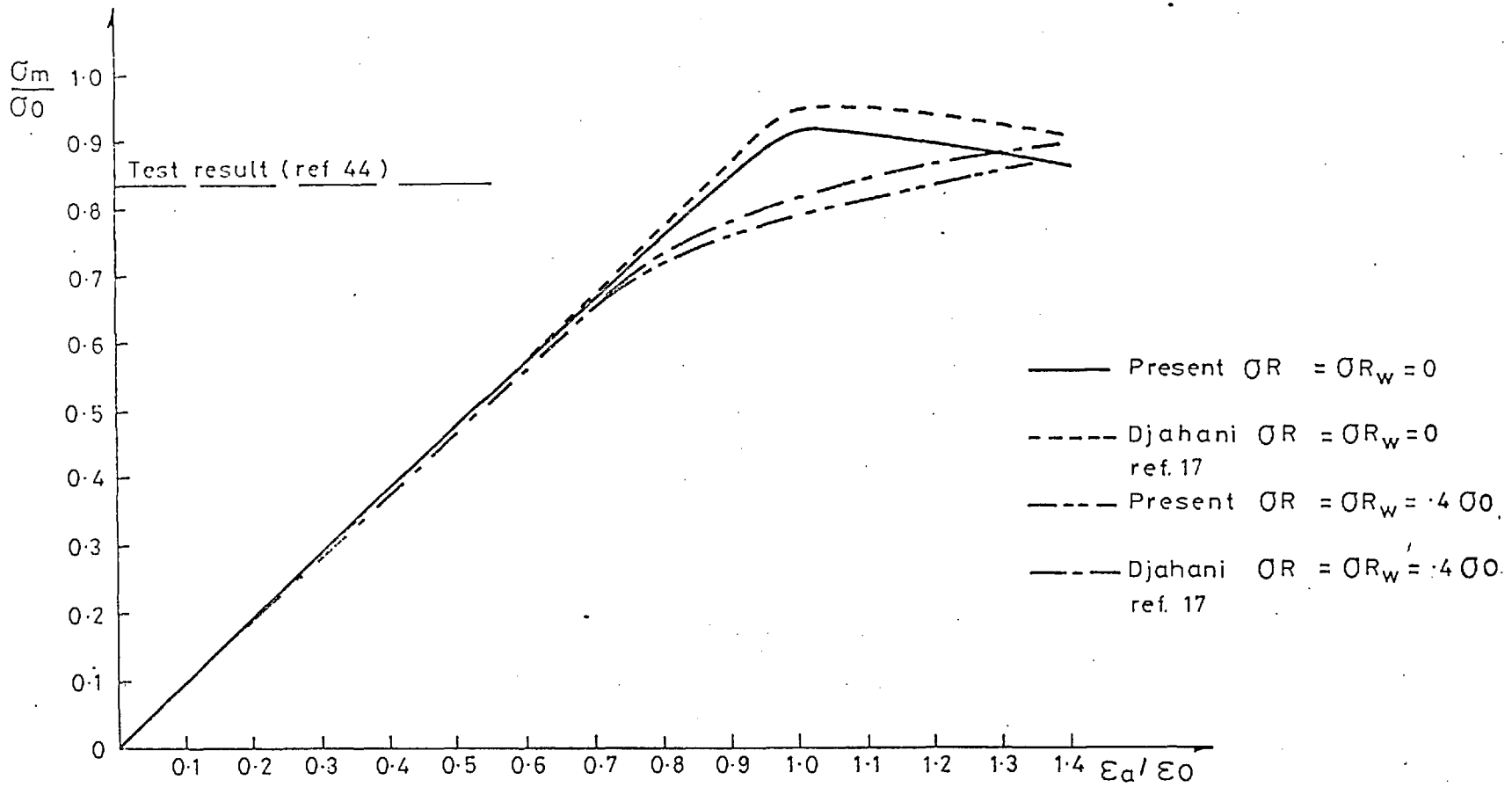

Fig E5 Relationship between mean edge stress and applied strain

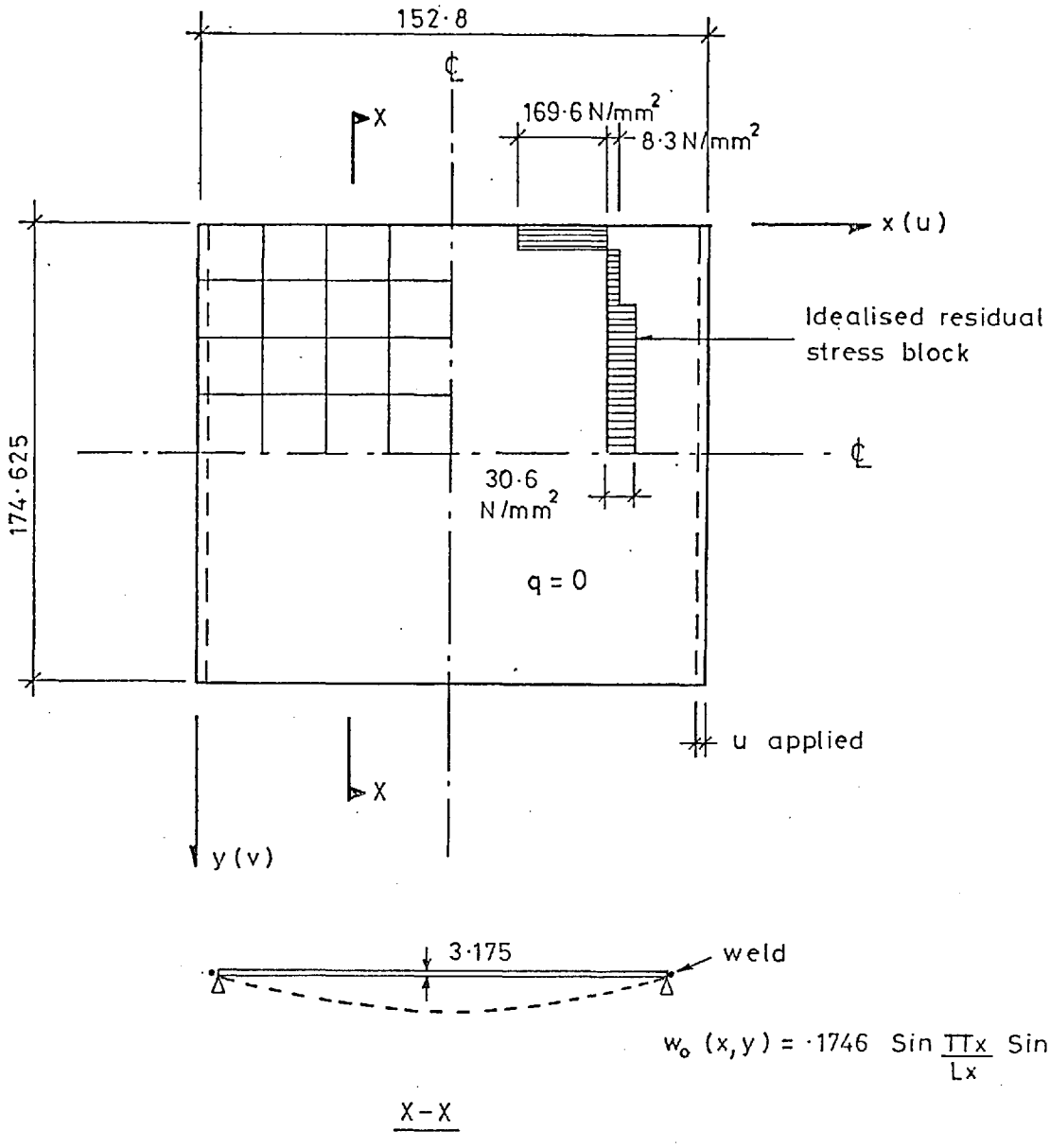

$$w_o(x,y) = \cdot 1746 \ \text{Sin}\frac{\pi x}{Lx} \ \text{Sin}\frac{\pi y}{Ly}$$

Material properties	
σ_0	250 N/mm
σ_R	0·1225 σ_0
E	206200 N/mm²
V	·3

Boundary conditions	
y=0	w = My = 0 Ny = Nxy = 0
x=0 Case I	w=Mx=0 Nxy = 0 u applied
x=0 Case II	w=Mx=0 v = 0 u applied

Fig E6 Plate arrangement and properies for Fig E7

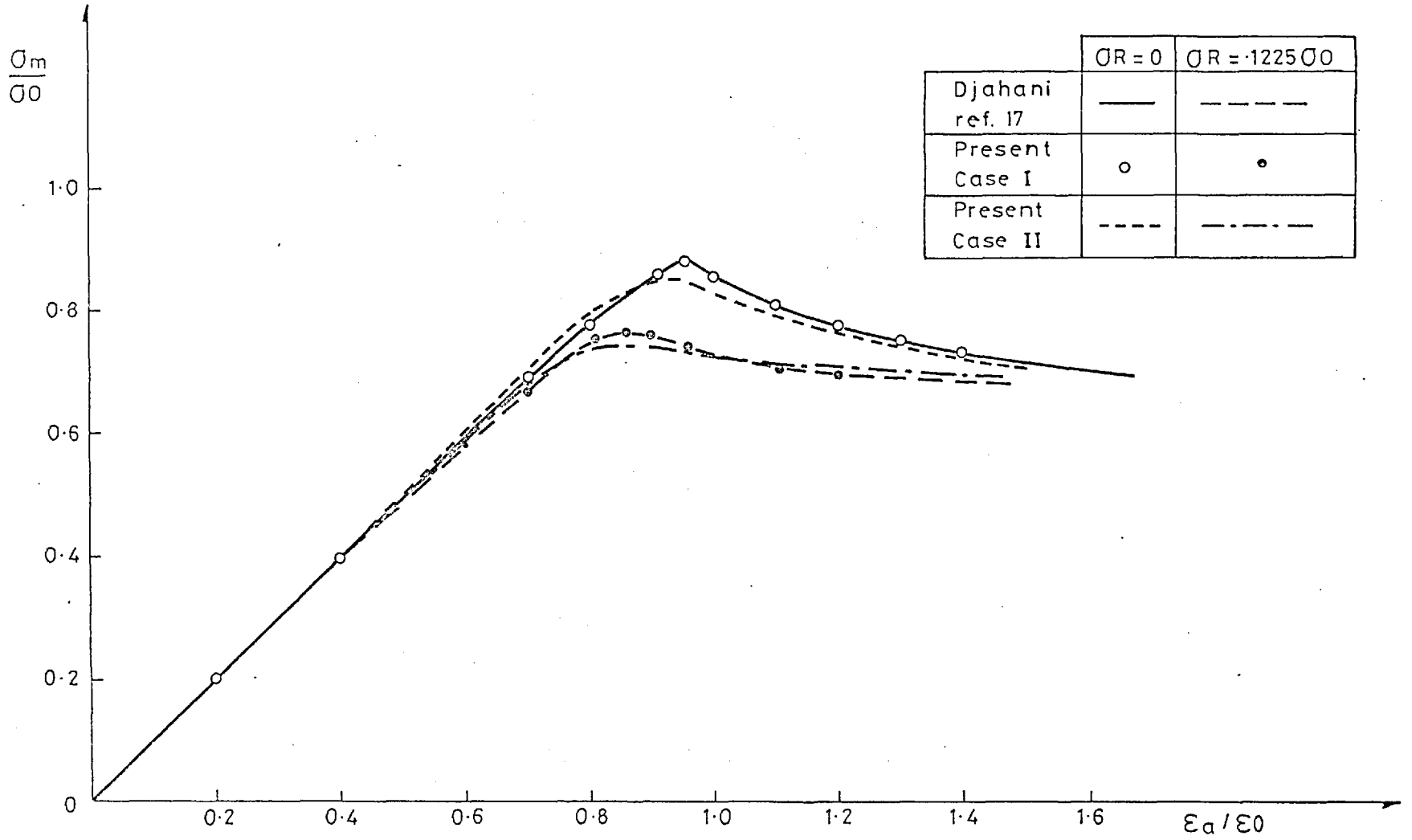

Fig E7 Relationship between mean edge stress and applied strain

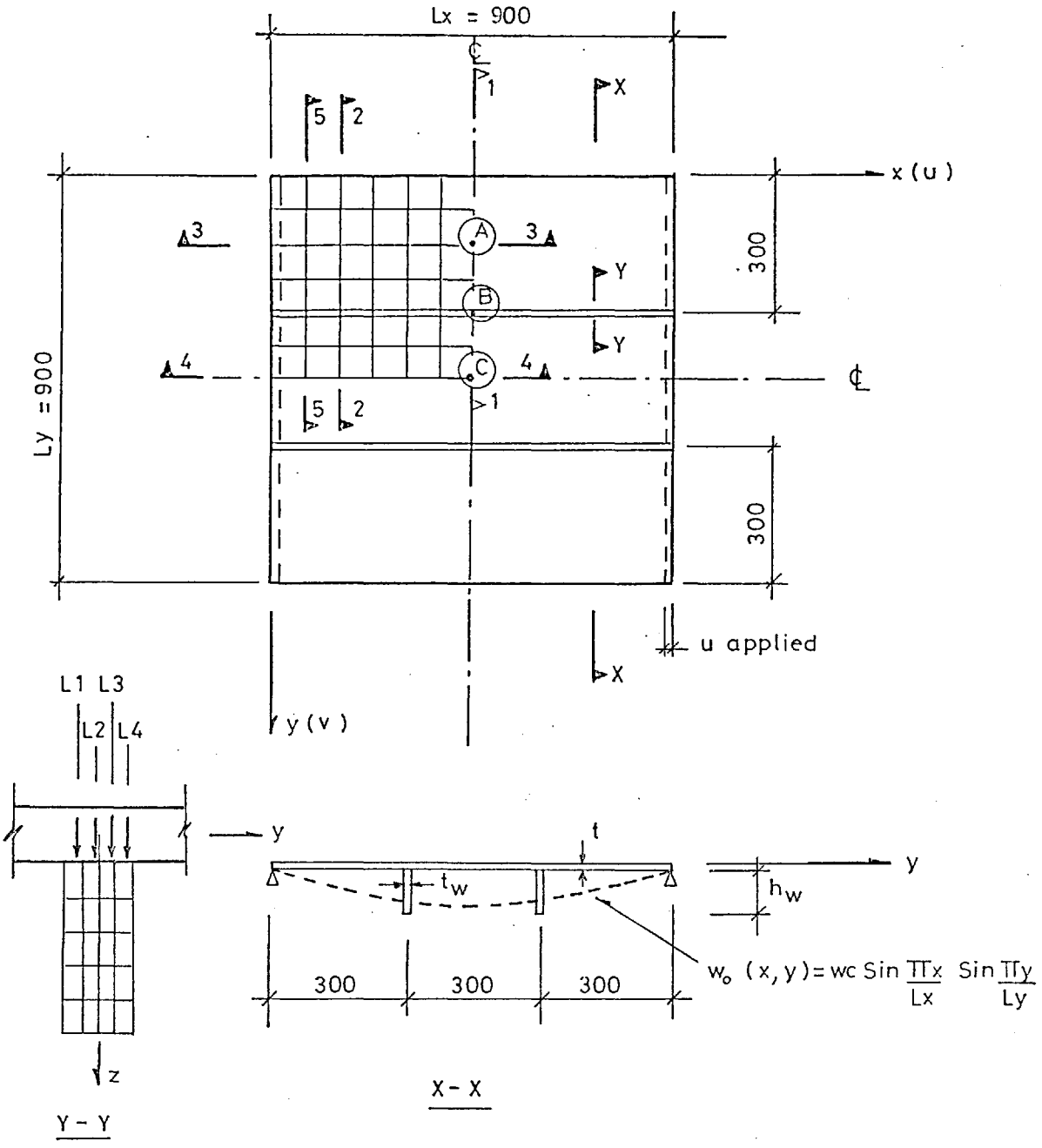

Material properies applicable to all cases	
σ_0	250 N/mm^2
E	205000 N/mm^2
V	·3

Boundary conditions	
y = 0	w = My = 0 Ny = Nxy = 0
x = 0	w = Mx = 0 v = 0 u applied

Fig E8 General plate arrangement and properties used in parametric studies

b/t	Lx/R	b mm	t mm	h_w mm	t_w mm
30	30	300.0	10.0	104.9	10.49
	50			75.2	7.52
	60			67.1	6.71
	70			61.0	6.10
	80			56.1	5.61
	90			52.2	5.22
50	30	300.0	6.0	98.3	9.83
	50			69.4	6.94
	60			61.9	6.19
	70			56.3	5.63
	80			51.9	5.19
	90			48.4	4.84
60	30	300.0	5.0	96.2	9.62
	50			67.4	6.74
	60			60.0	6.00
	70			54.6	5.46
	80			50.3	5.03
	90			46.9	4.69
70	30	300.0	4.2857	94.7	9.47
	50			65.8	6.58
	60			58.5	5.85
	70			53.1	5.31
	80			48.9	4.89
	90			45.6	4.56
80	30	300.0	3.75	93.5	9.35
	50			64.5	6.45
	60			57.2	5.72
	70			51.9	5.19
	80			47.2	4.72
	90			44.5	4.45

Fig. E9

Plate and stiffener dimensions for the range of parameters, b/t and Lx/R

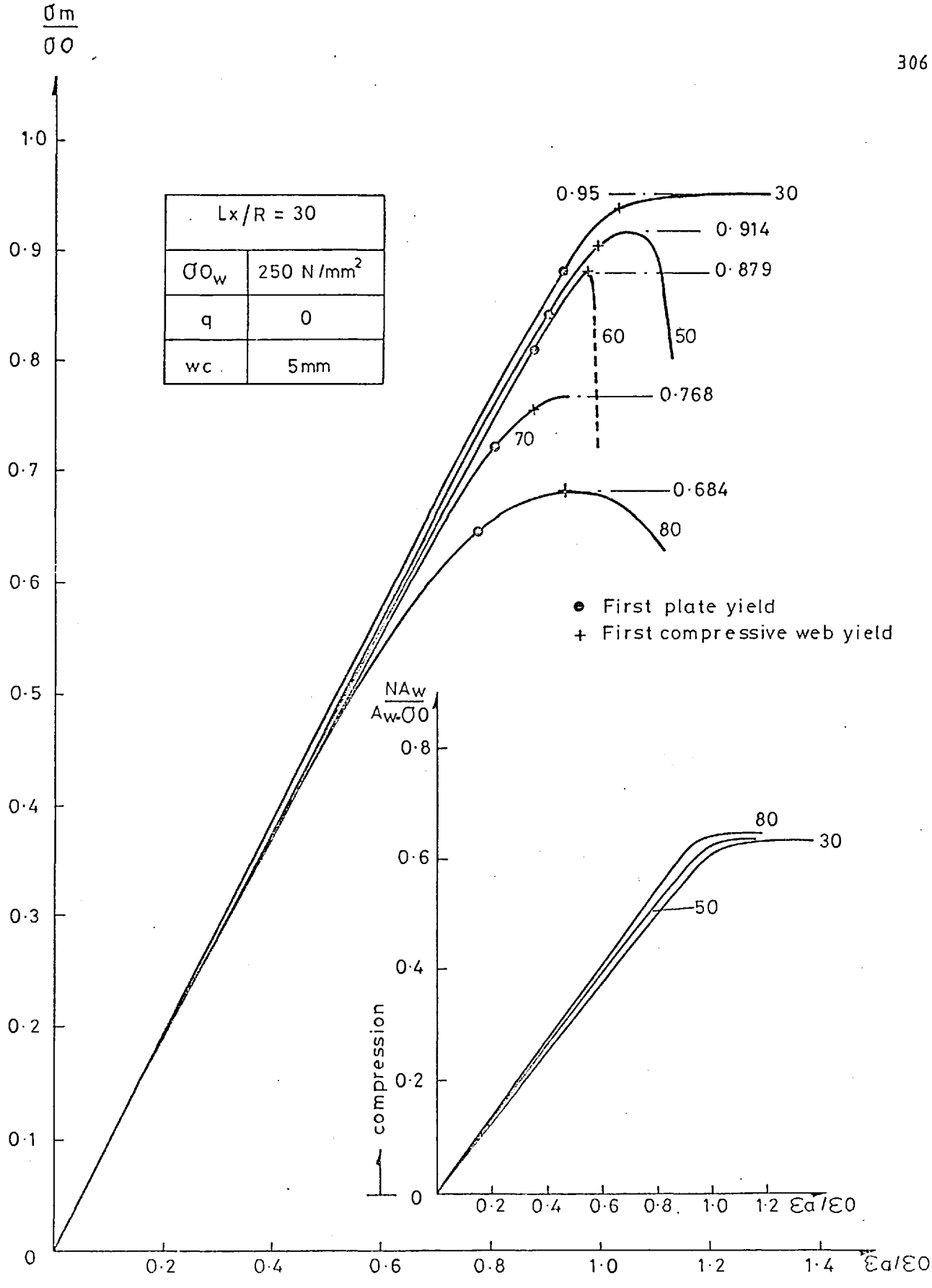

Fig E10 Mid-span stress in the webs and mean edge stress in the gross section versus applied strain, for plates of b/t = 30 to 80 and Lx/R = 30

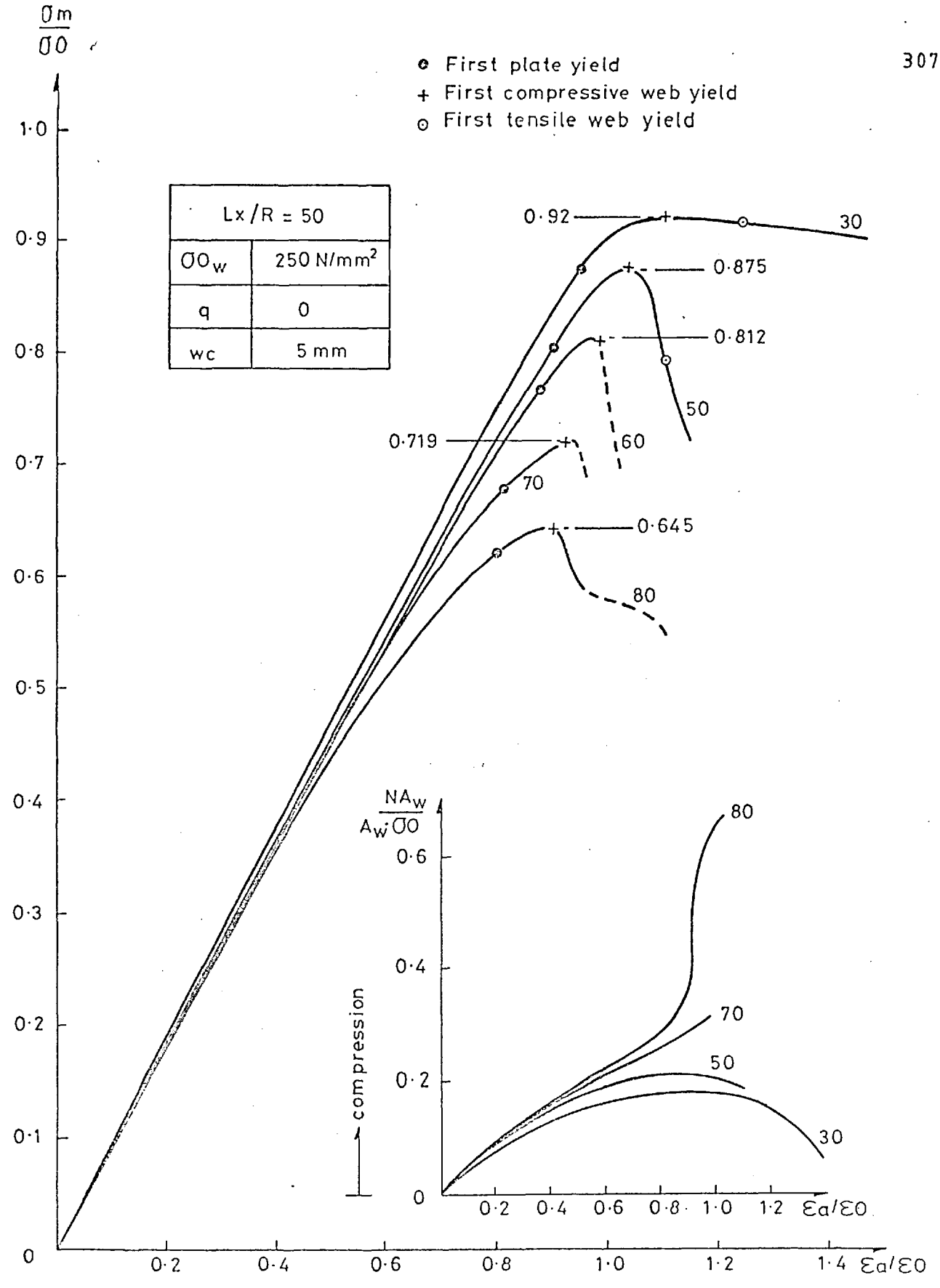

Fig E11 Mid-span stress in the webs and mean edge stress in the gross section versus applied strain, for plates of b/t = 30 to 80 and Lx/R = 50

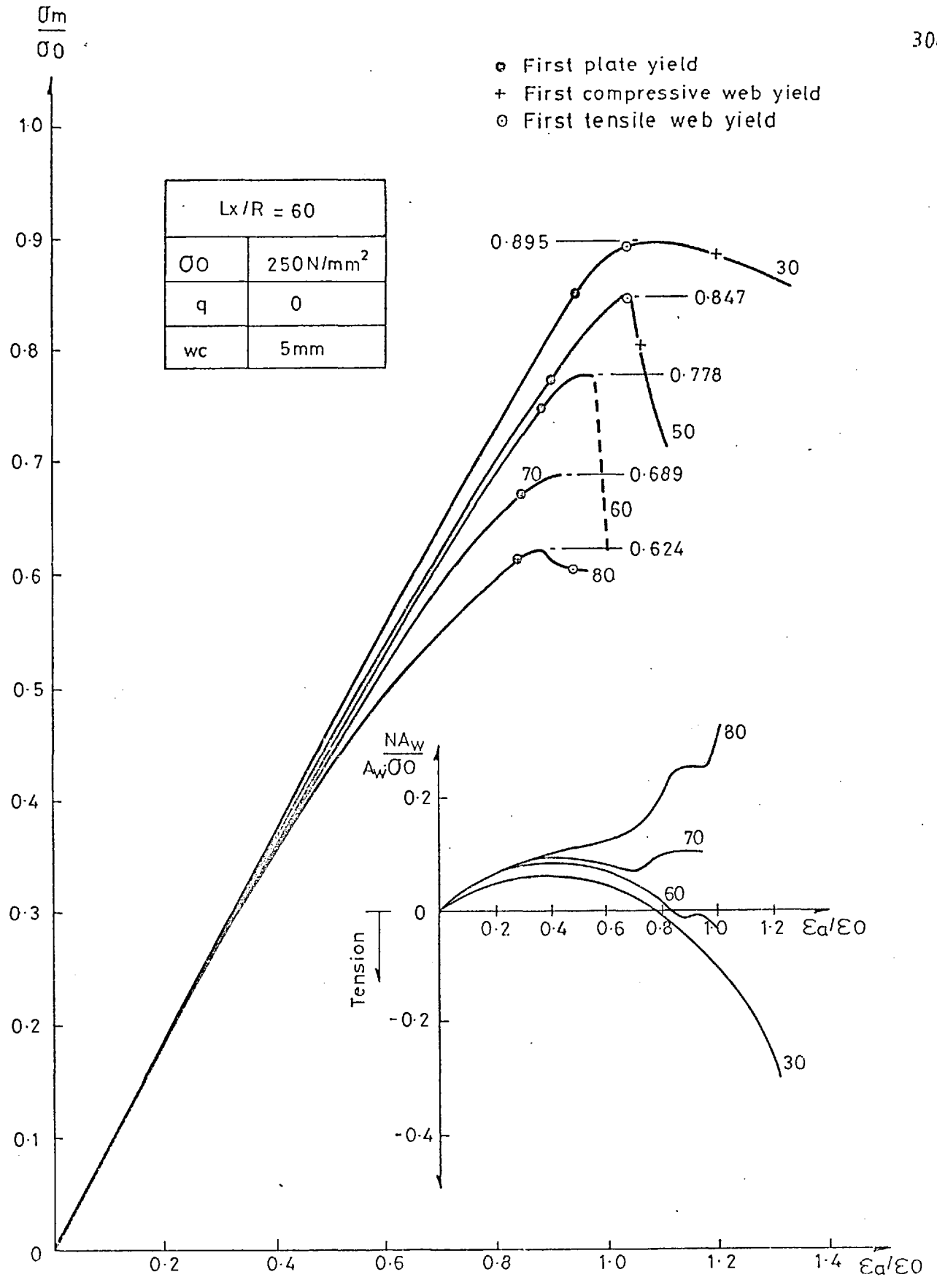

Fig E12 Mid-span stress in the webs and mean edge stress in the gross section versus applied strain, for plates of b/t = 30 to 80 and Lx/R = 60

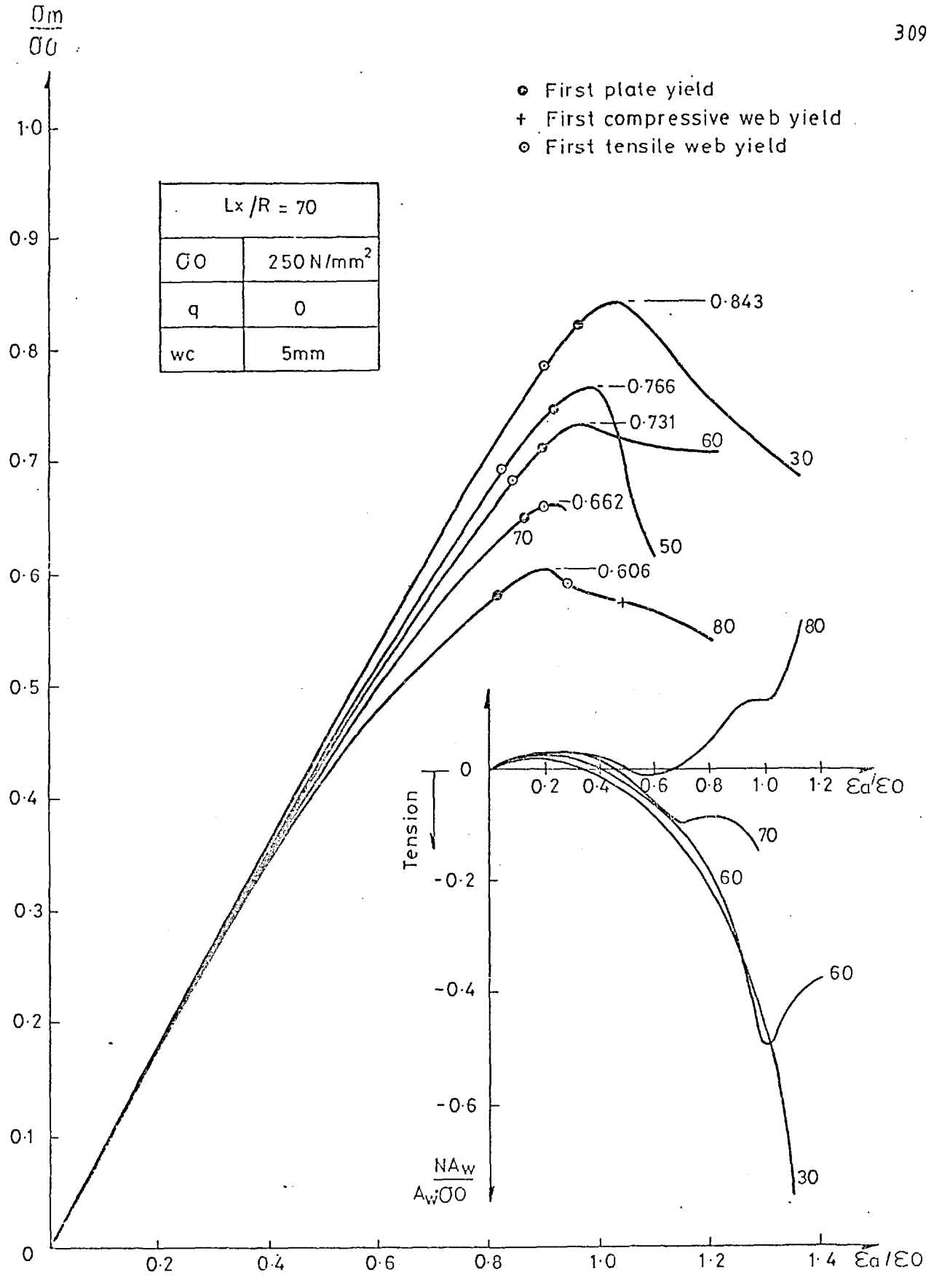

Fig E 13 Mid-span stress in the webs and mean edge stress in the gross section versus applied strain, for plates of b/t = 30 to 80 and Lx/R = 70

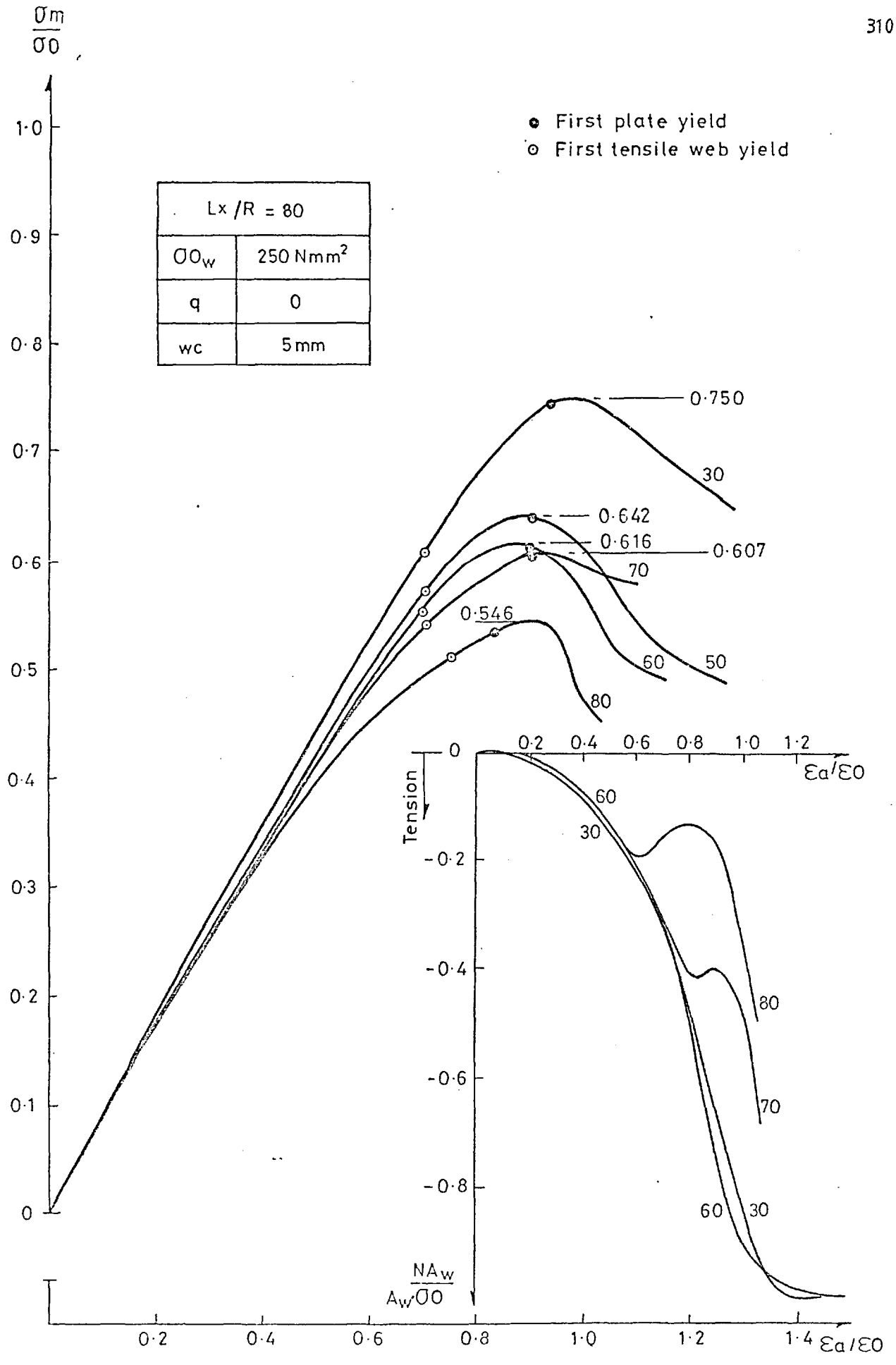

Fig E14 Mid-span stress in the webs and mean edge stress in the gross section versus applied strain, for plates of b/t = 30 to 80 and Lx/R = 80

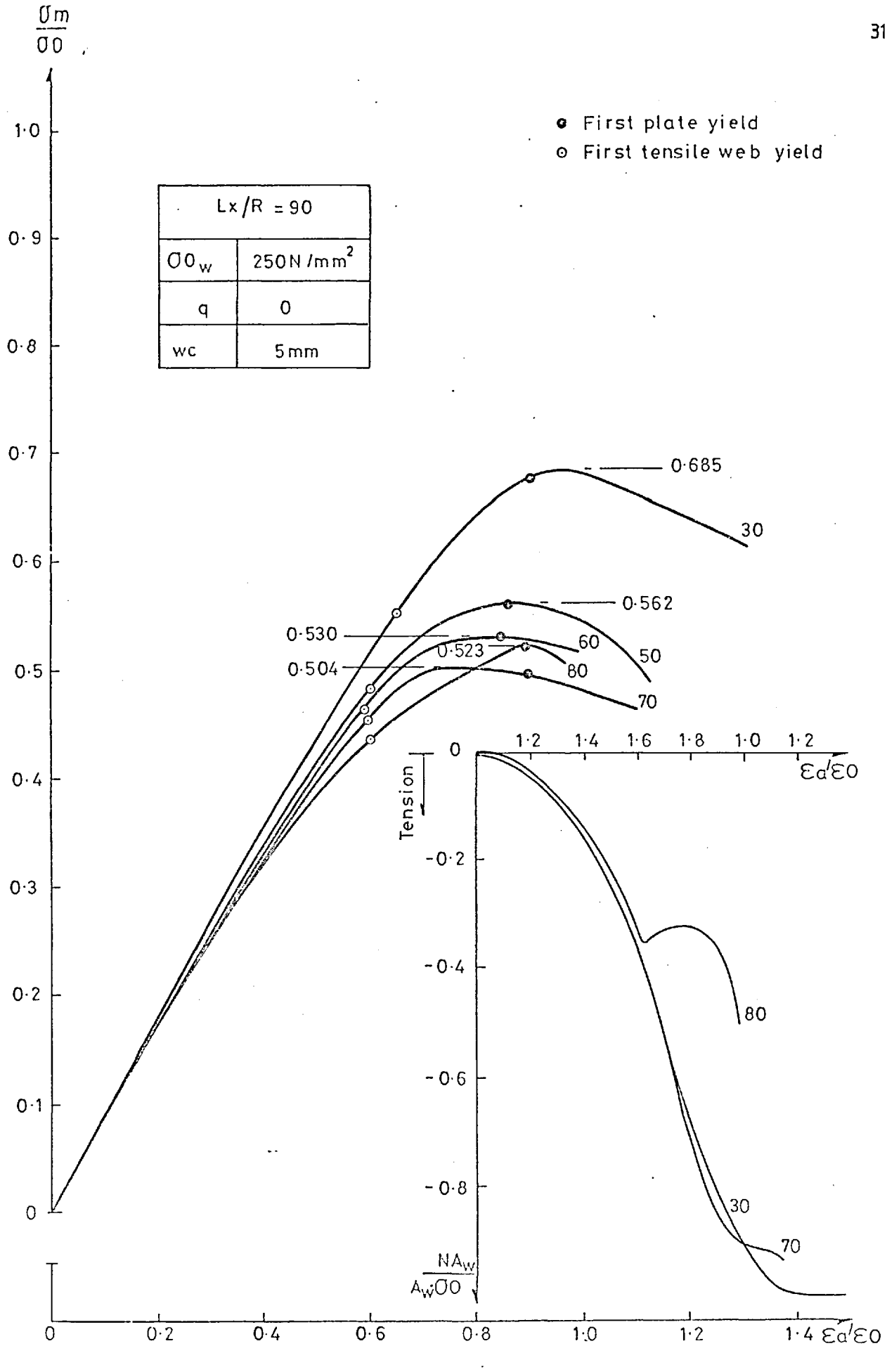

Fig E15 Mid-span stress in the webs and mean edge stress in the gross section versus applied strain, for plates of b/t = 30 to 80 and Lx/R = 90

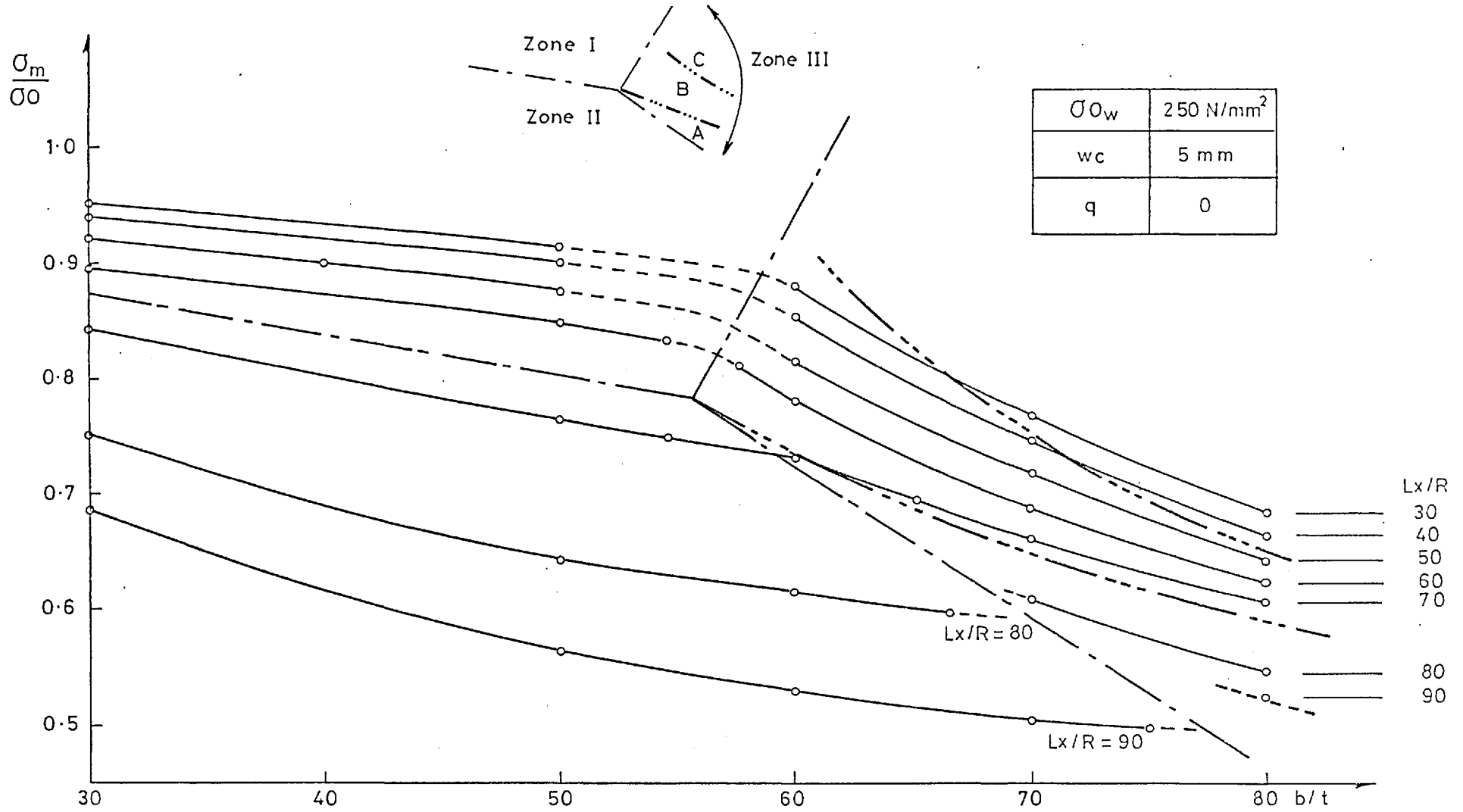

Fig E16 Summary of peak loads for plates of b/t = 30 to 80 and Lx/R = 30 to 90

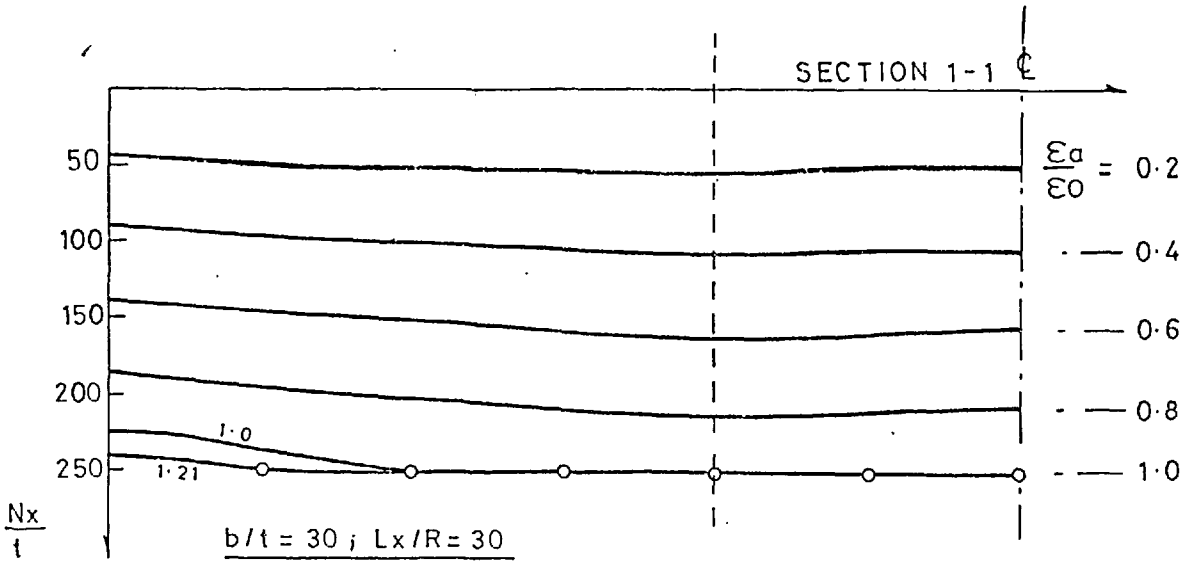

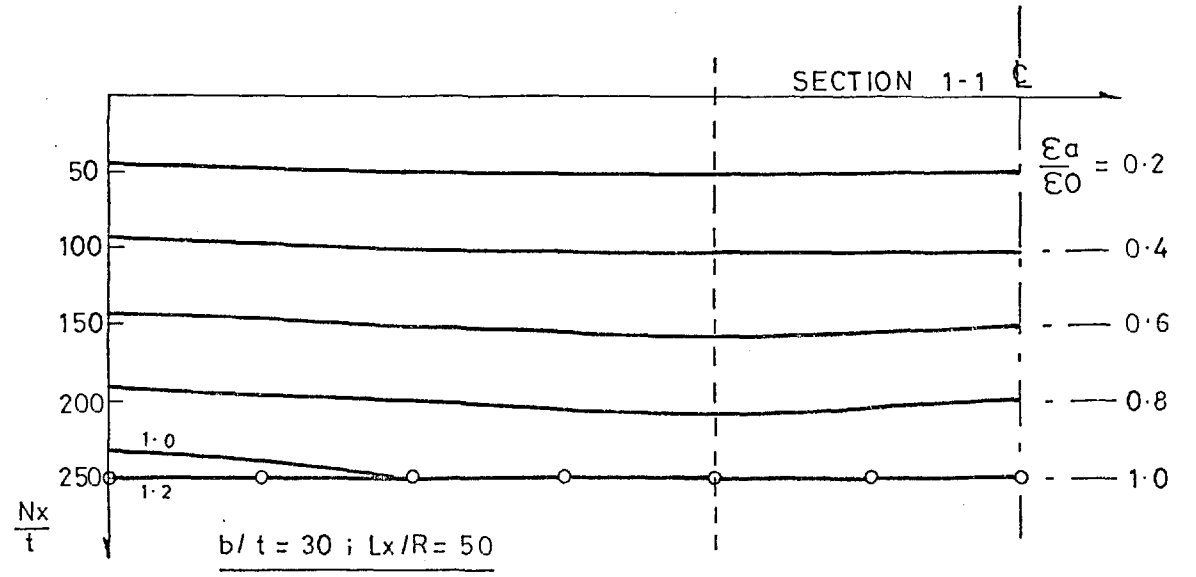

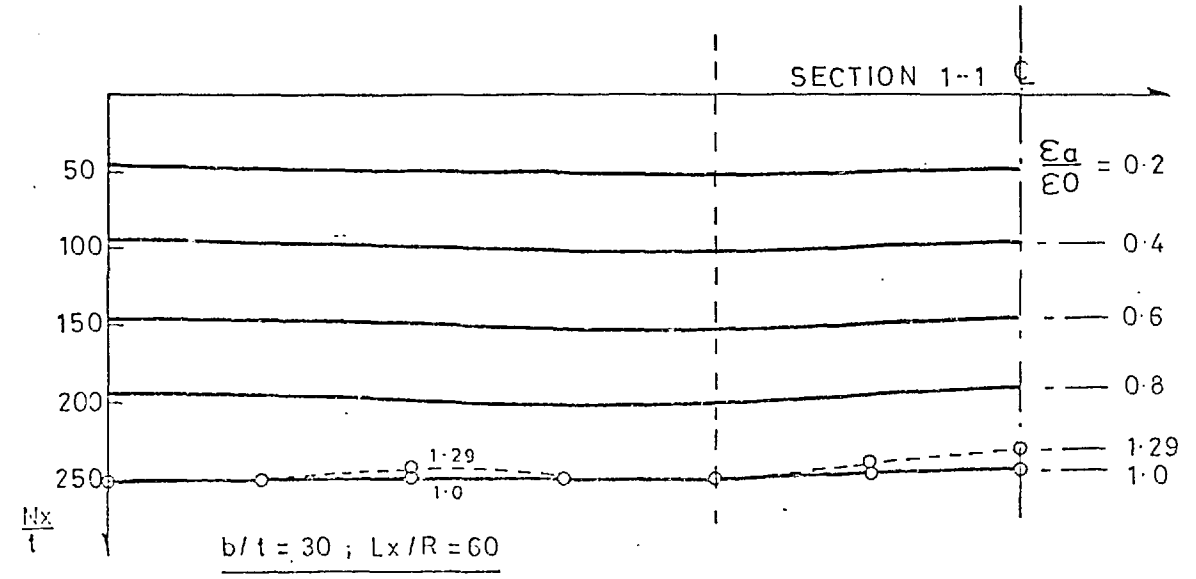

o Plastic nodes

Fig E17 Direct stresses at mid-span for increments of applied strain

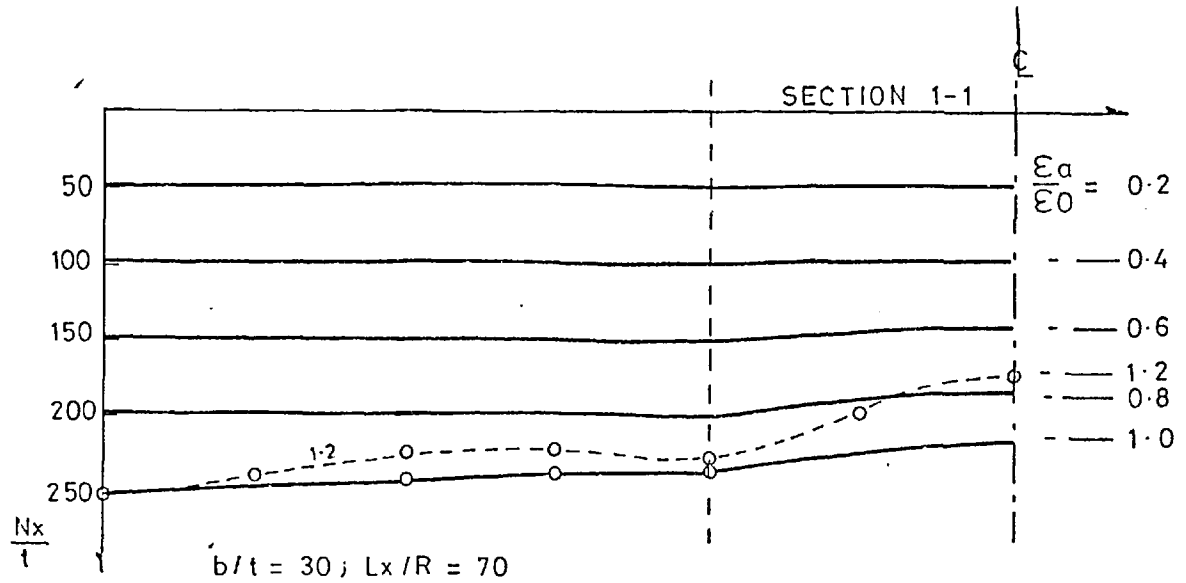

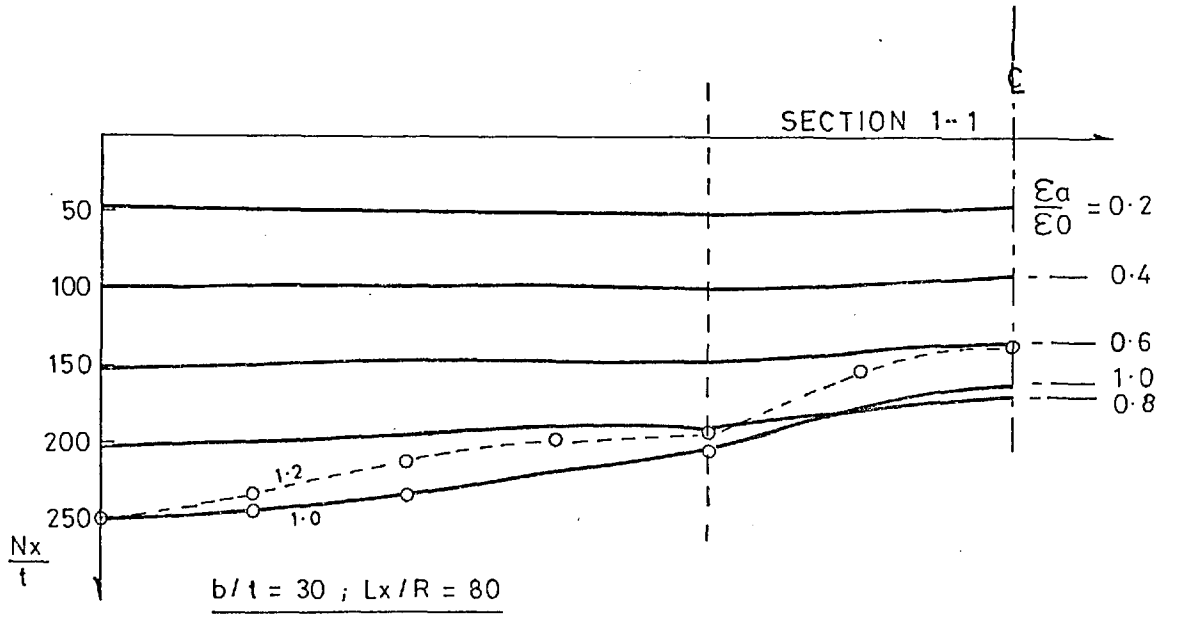

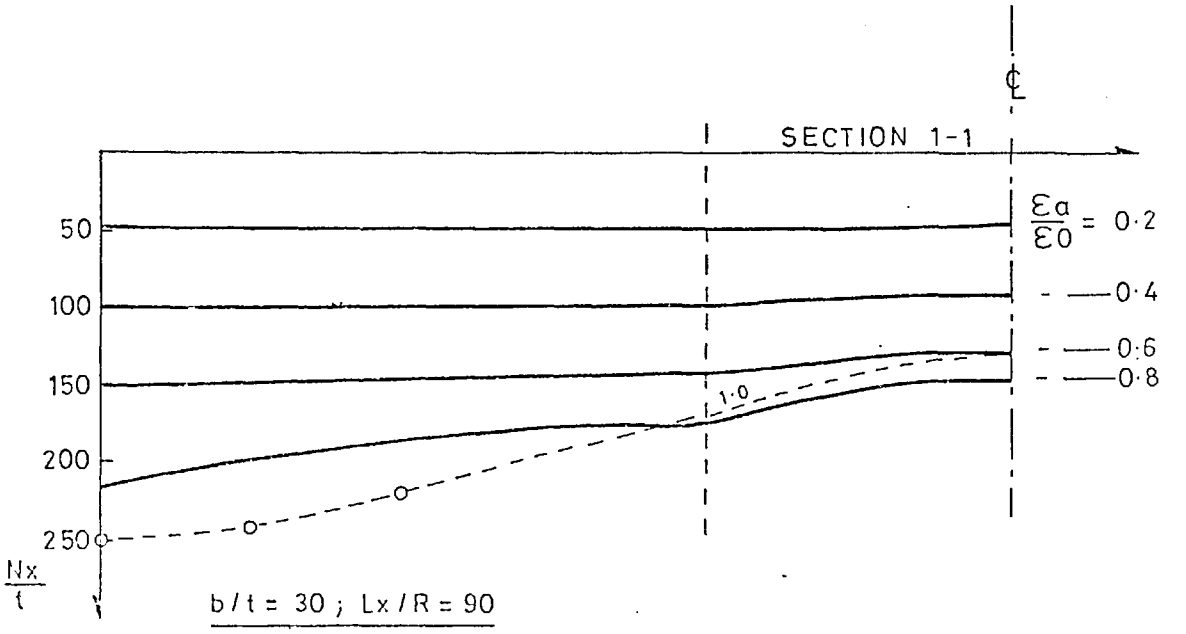

o Plastic nodes

Fig E18 Direct stresses at mid-span for increments of applied strain

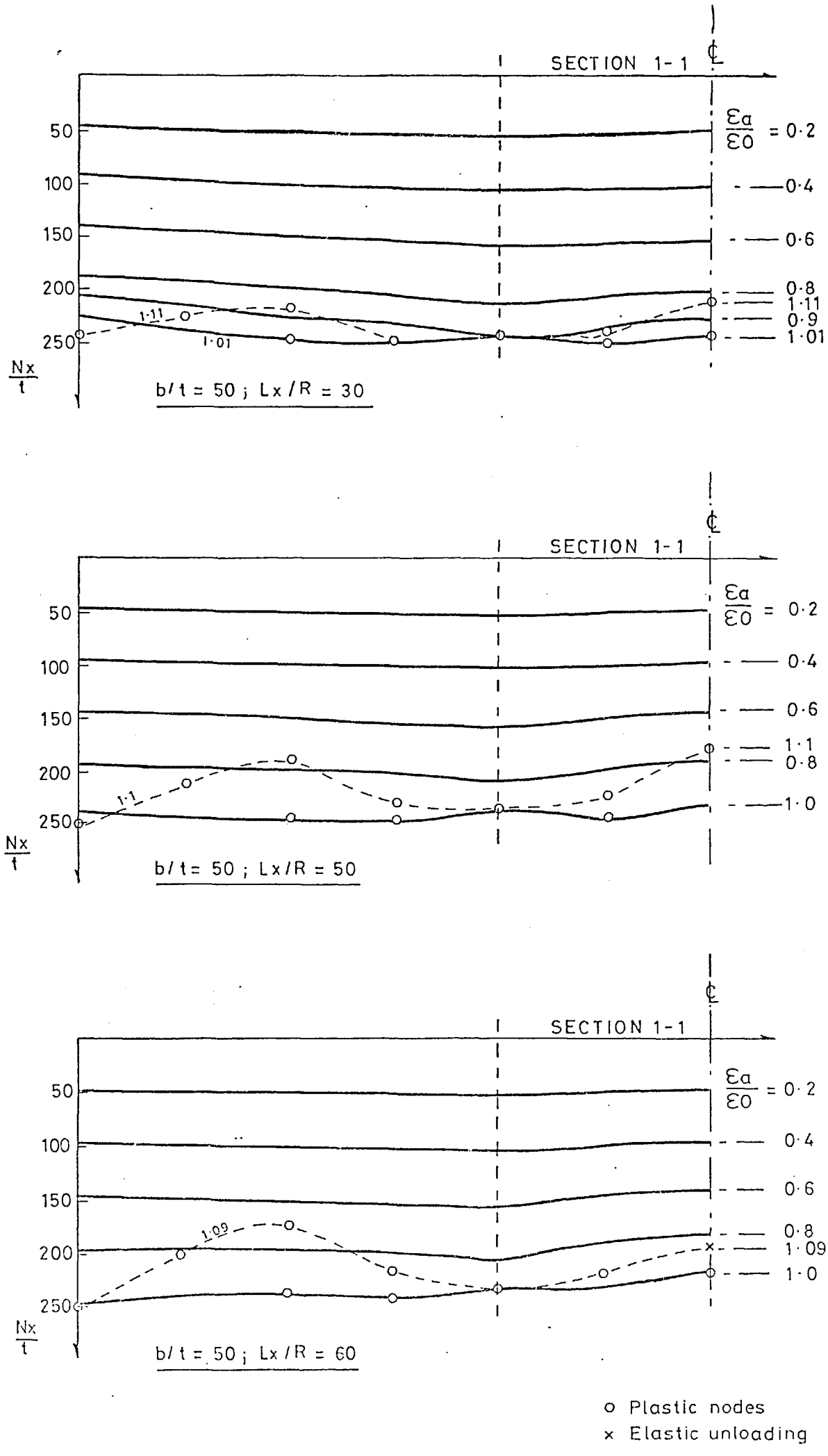

Fig E19 Direct stresses at mid-span for increments of applied strain

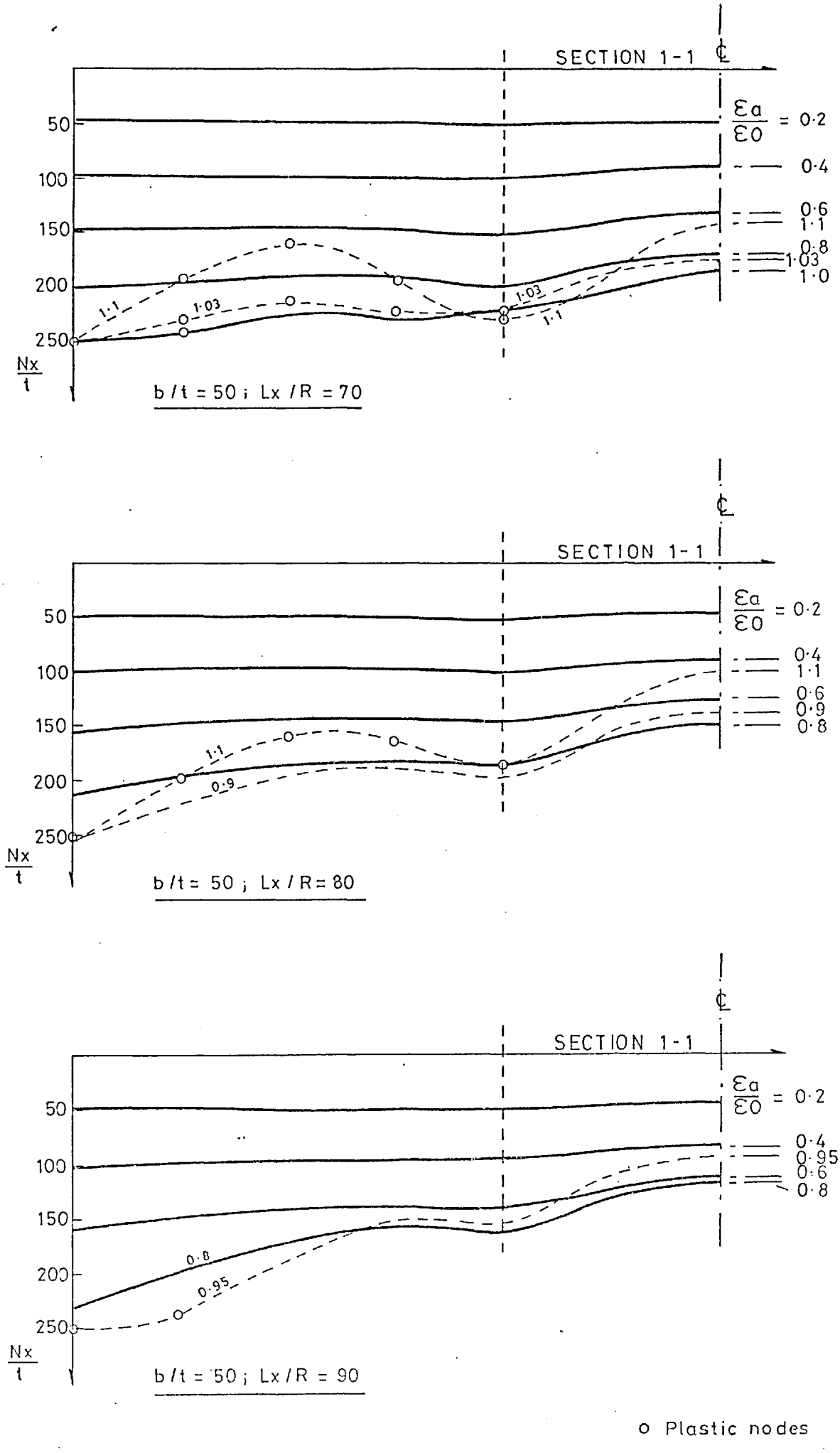

Fig E20 Direct stresses at mid-span for increments of applied strain

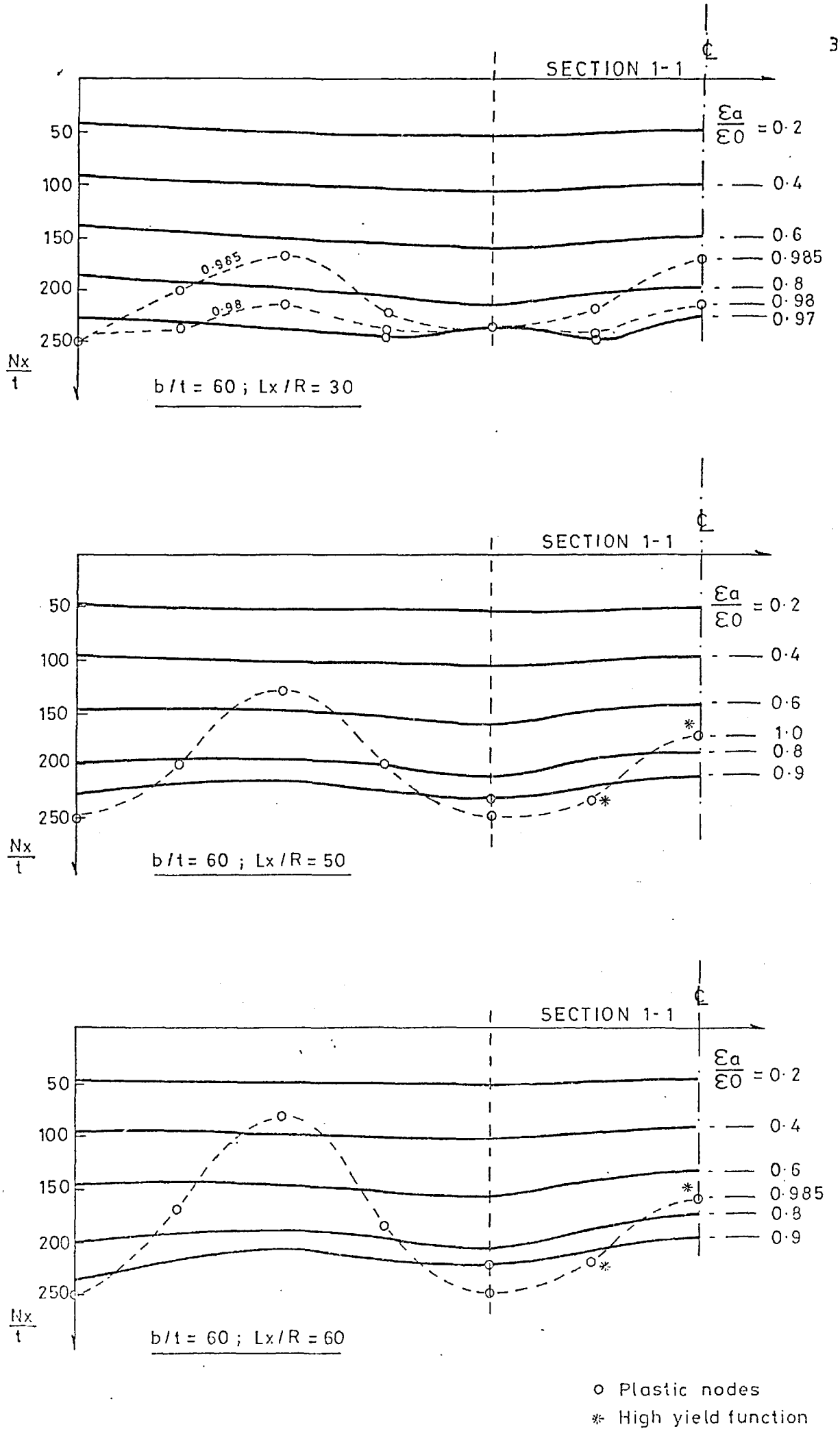

Fig E21 Direct stresses at mid-span for increments of applied strain

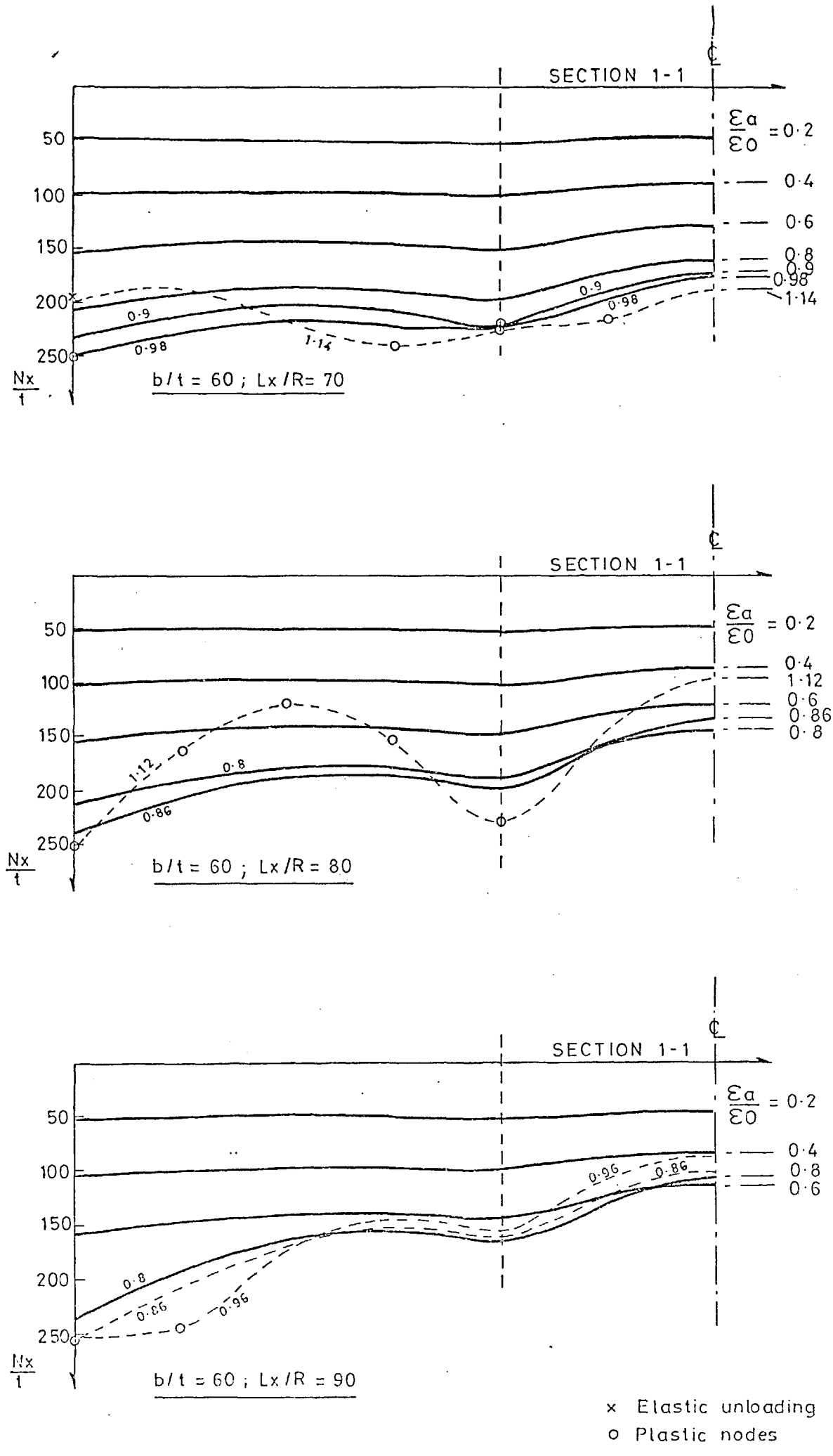

Fig E22 Direct stresses at mid-span for increments of applied strain

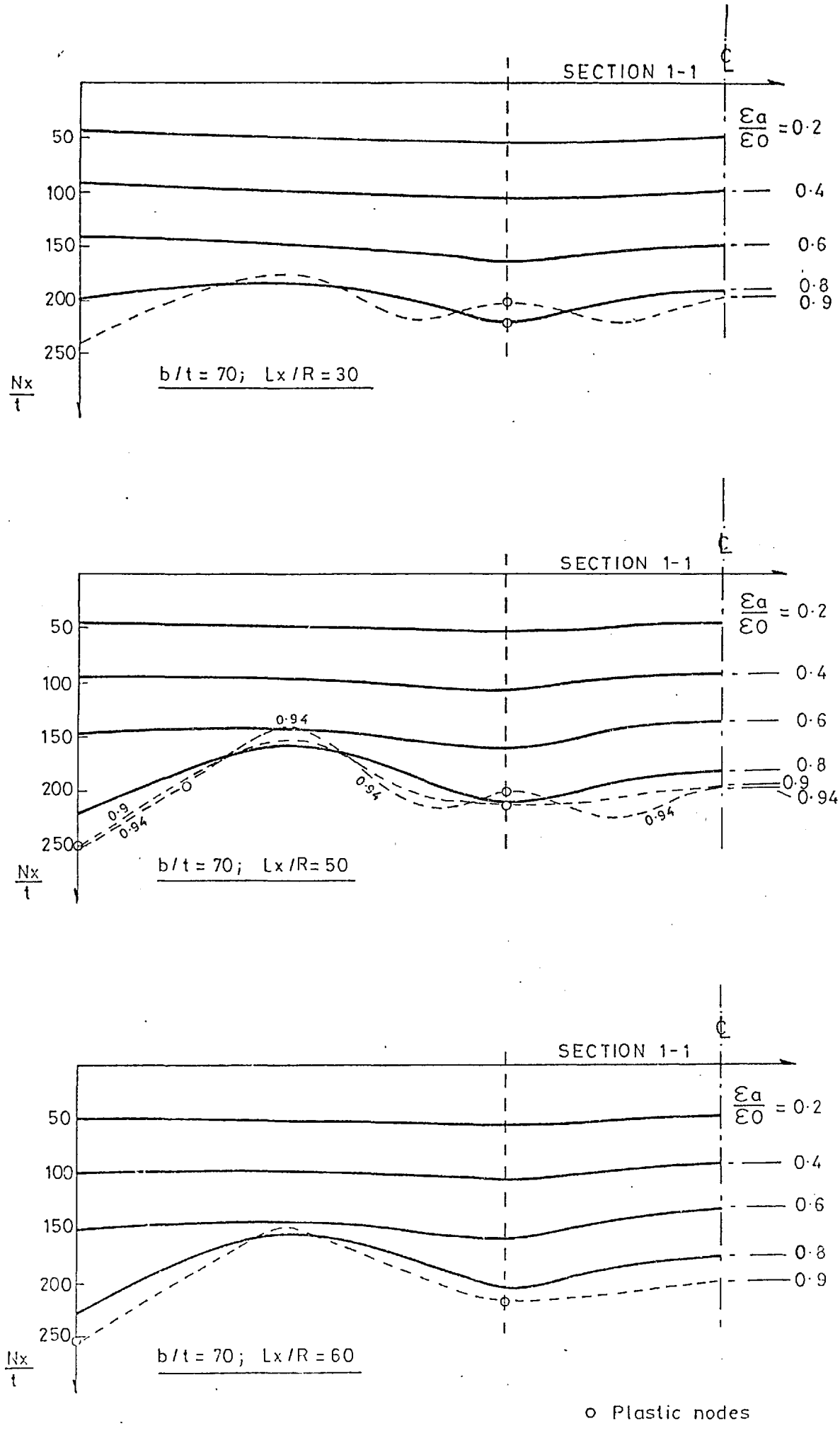

Fig E23 Direct stresses at mid-span for increments of applied strain

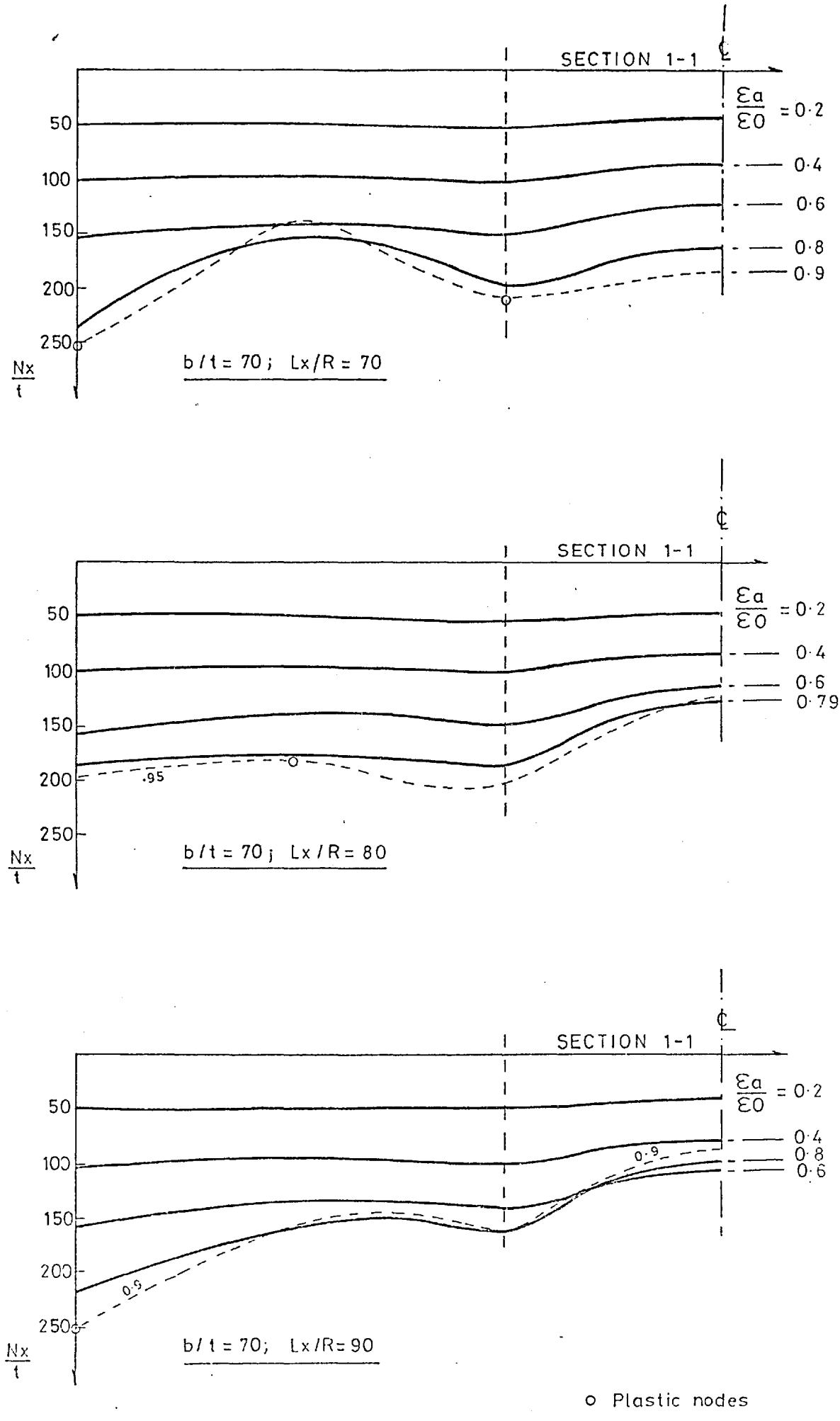

Fig E24 Direct stresses at mid-span for increments of applied strain

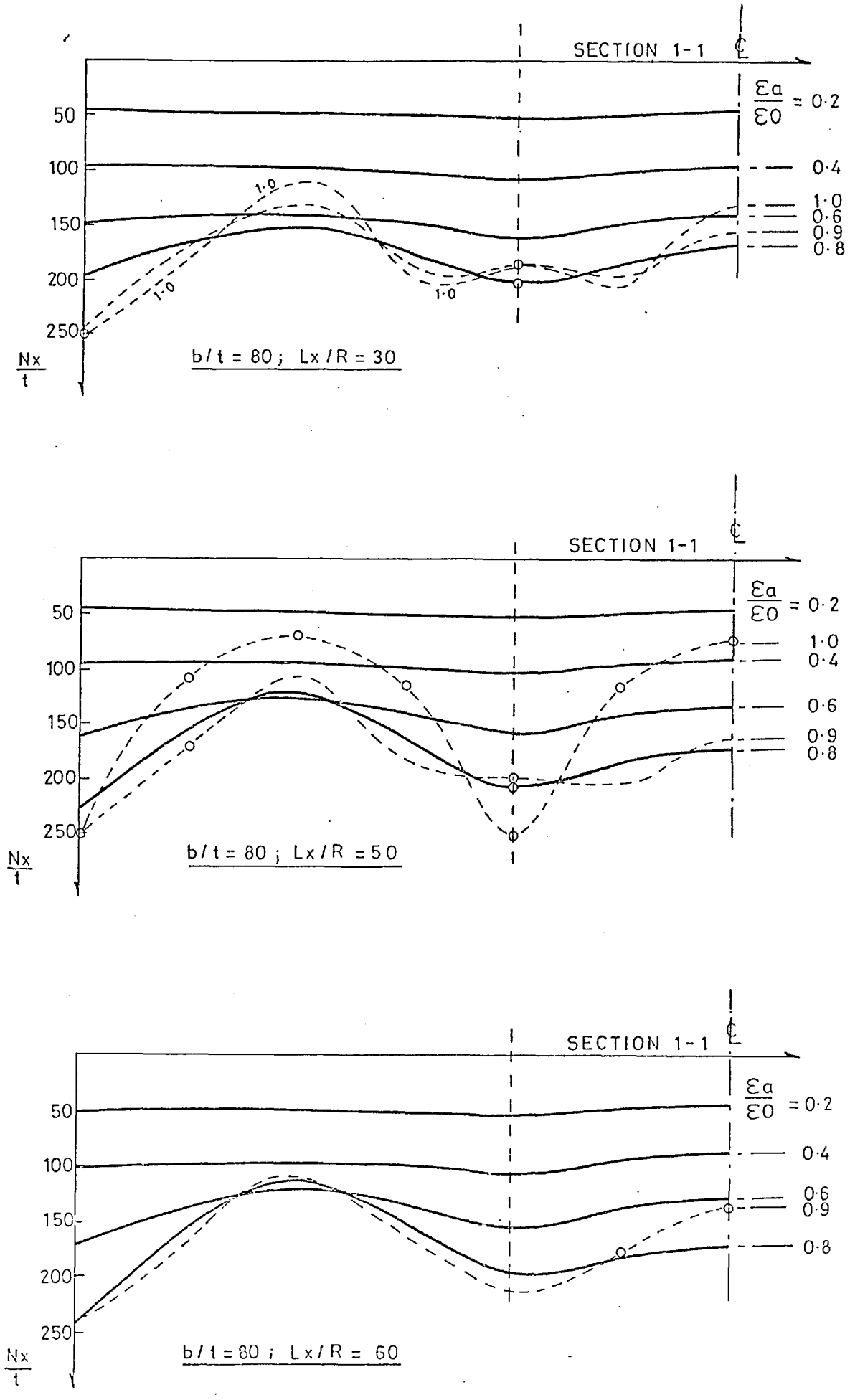

o Plastic nodes

Fig E25 Direct stresses at mid-span for increments of applied strain

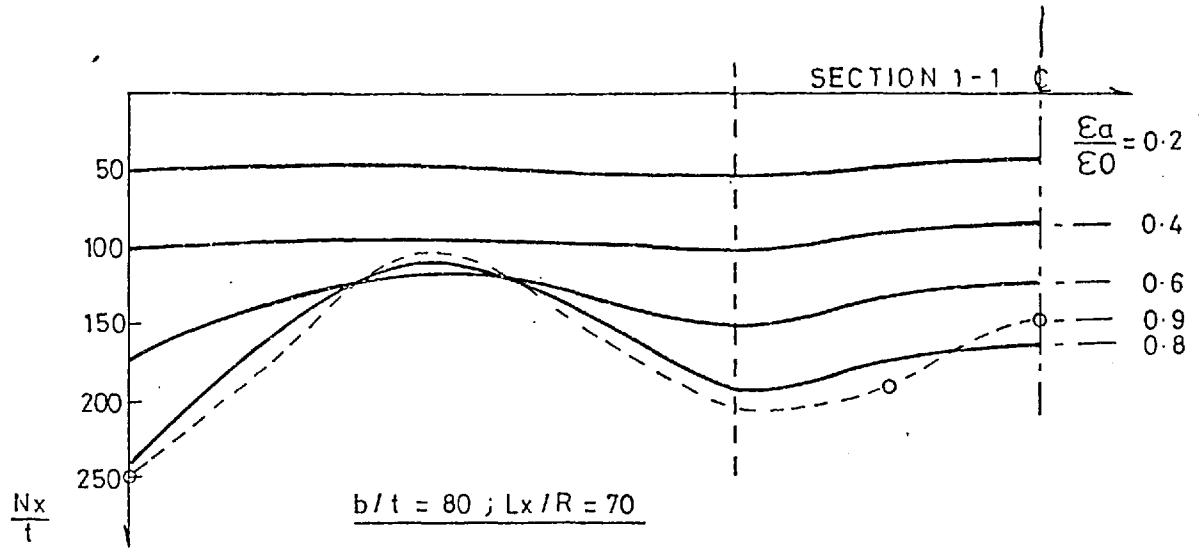

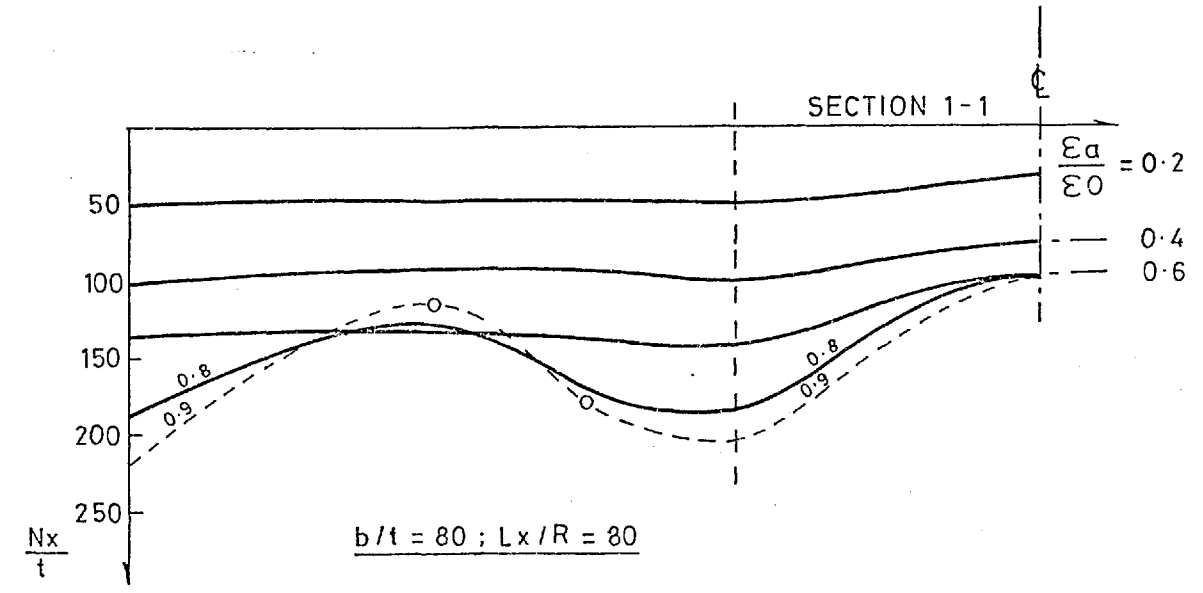

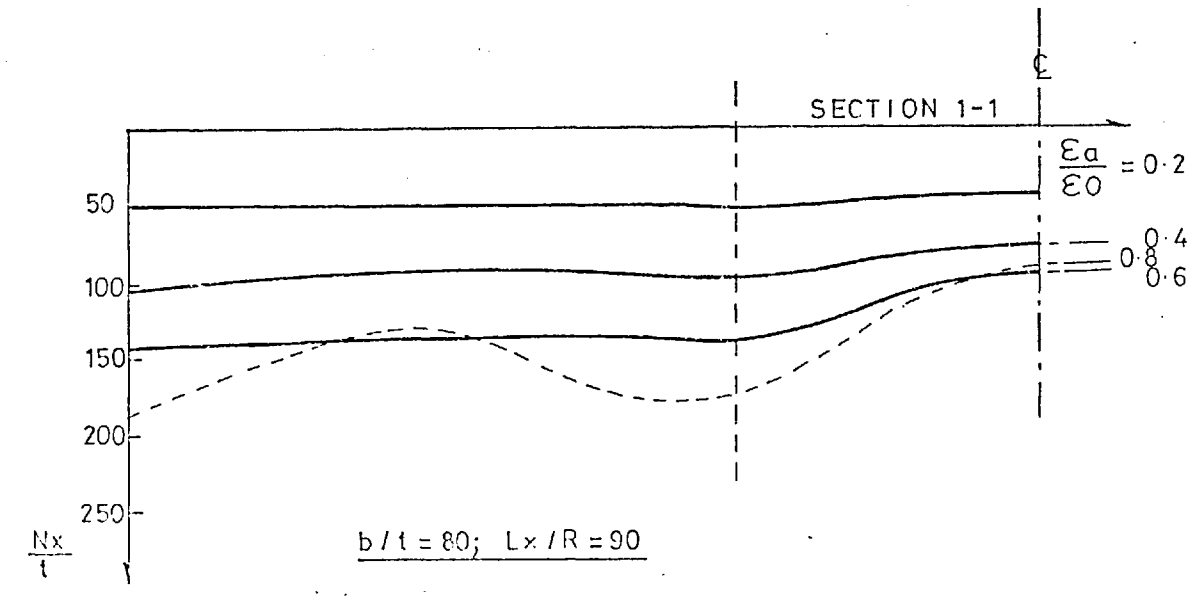

o Plastic nodes

Fig E26 Direct stresses at mid-span for increments of applied strain

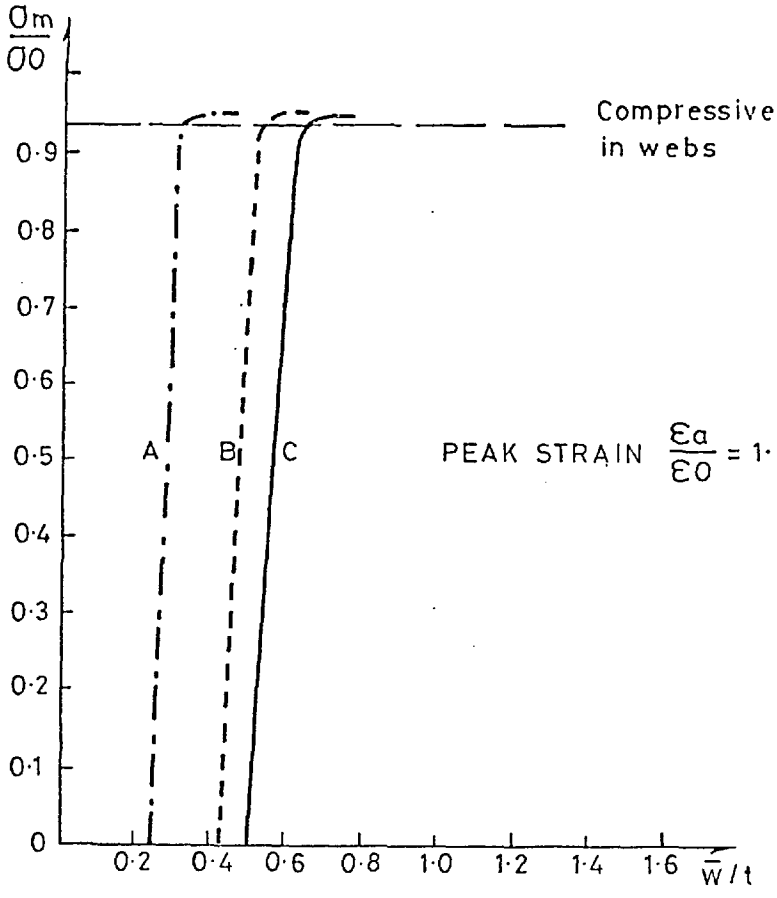

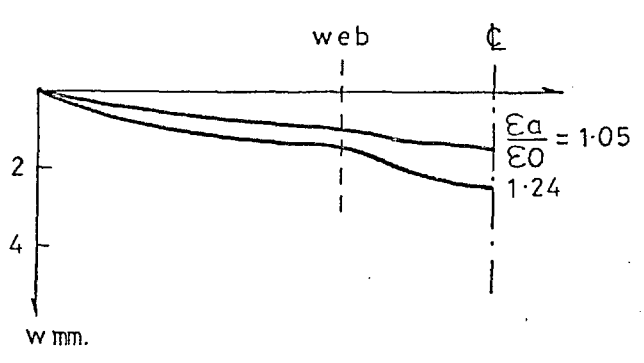

SECTION 1-1

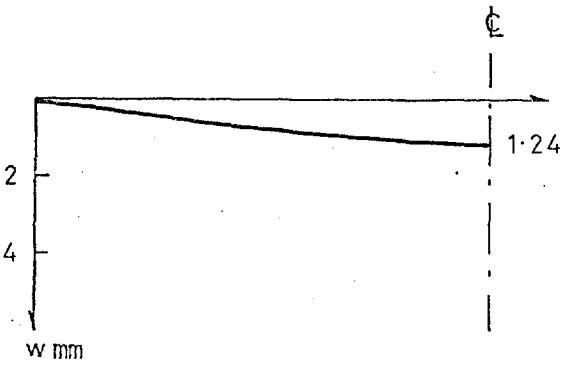

SECTION 3-3

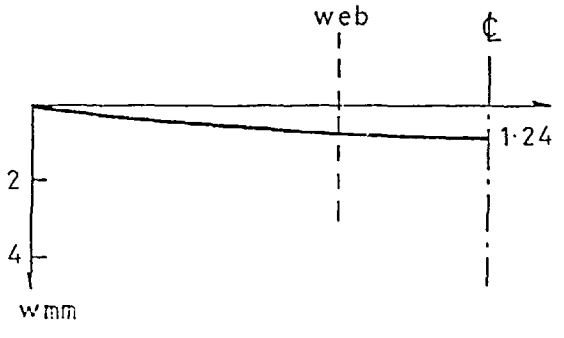

SECTION 2-2

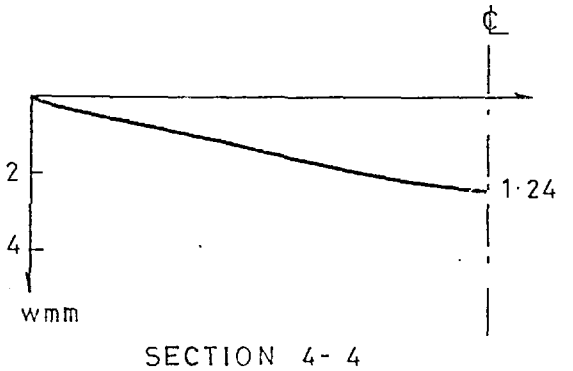

SECTION 4-4

Fig E27 Mean edge stress versus mid-span deflections and deflection profiles for b/t = 30 and Lx/R= 30 (Lx/R= 50 and Lx/R= 60 similar)

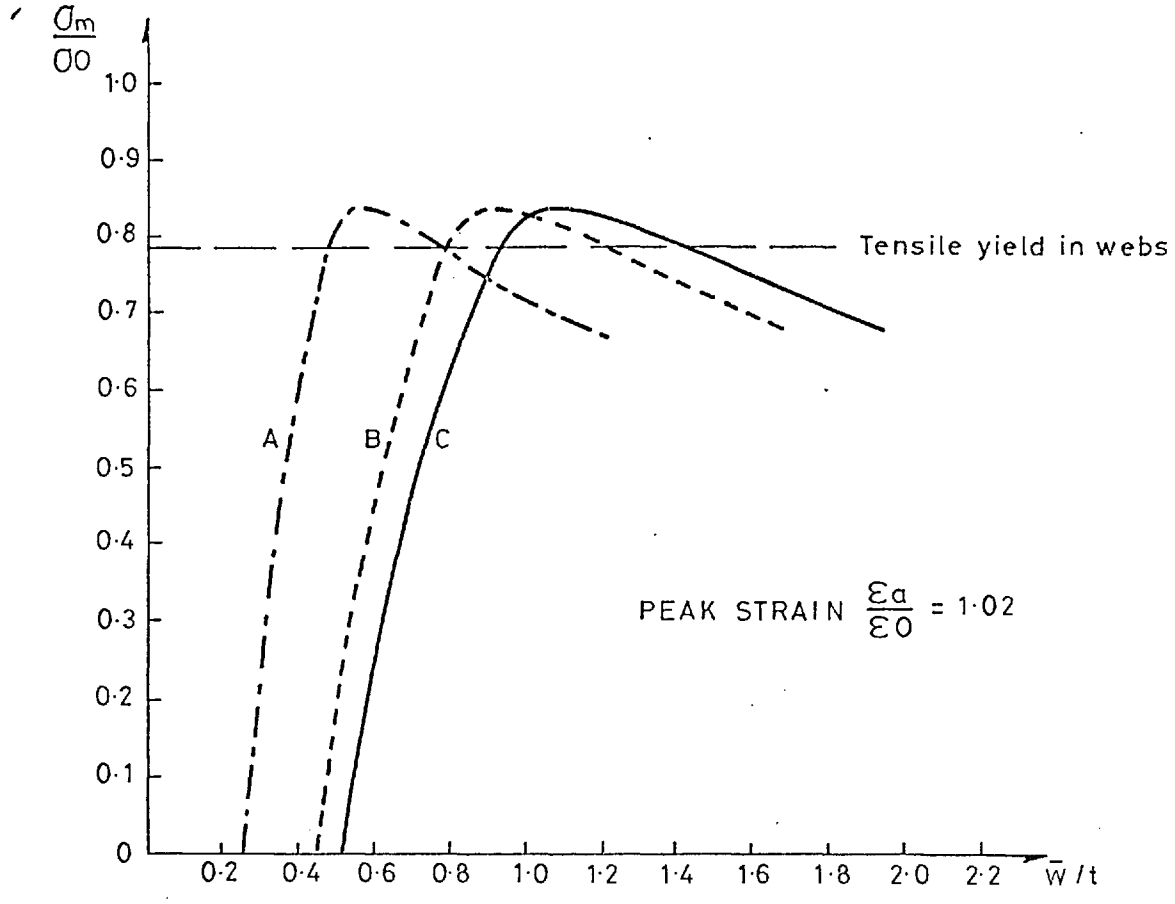

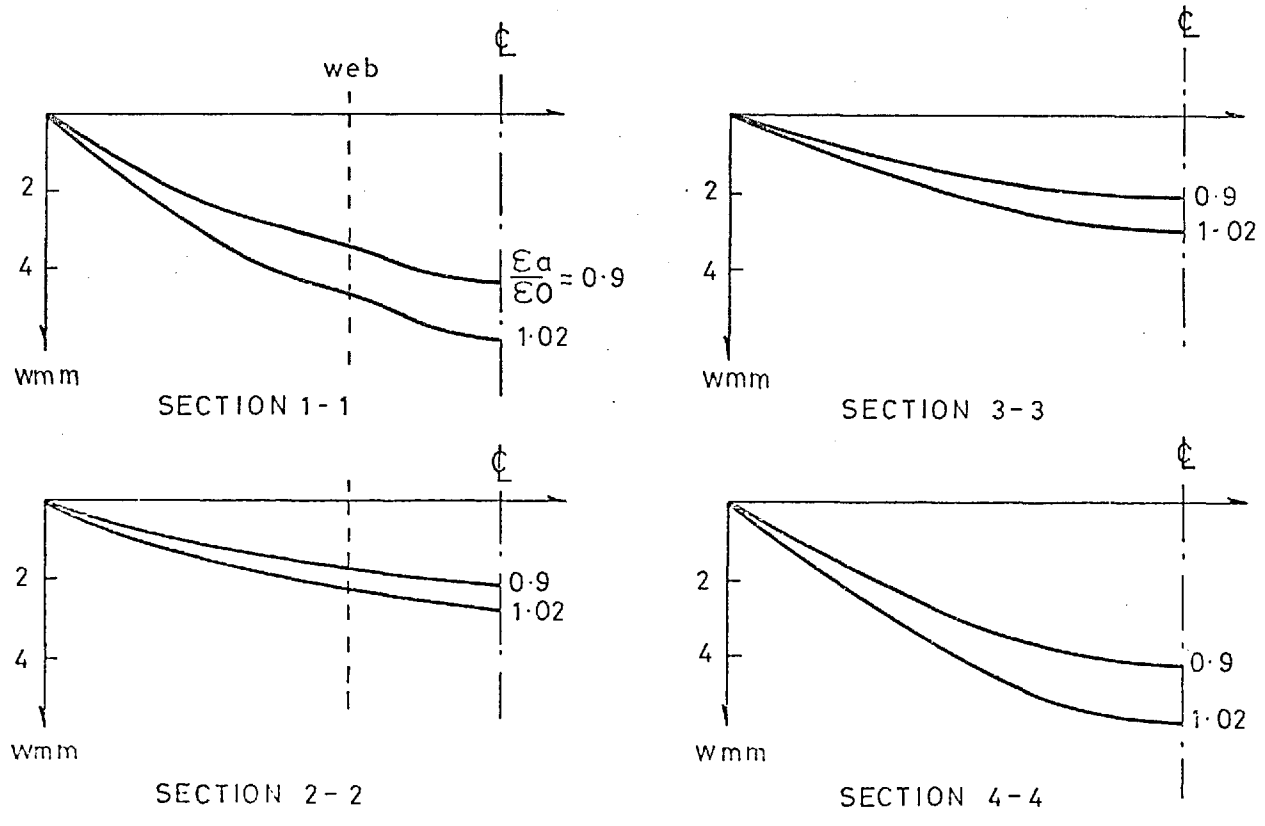

Fig E28 Mean edge stress versus mid-span deflections and deflection profiles for b/t = 30 and L_x/R = 70

(L_x/R = 80 similar)

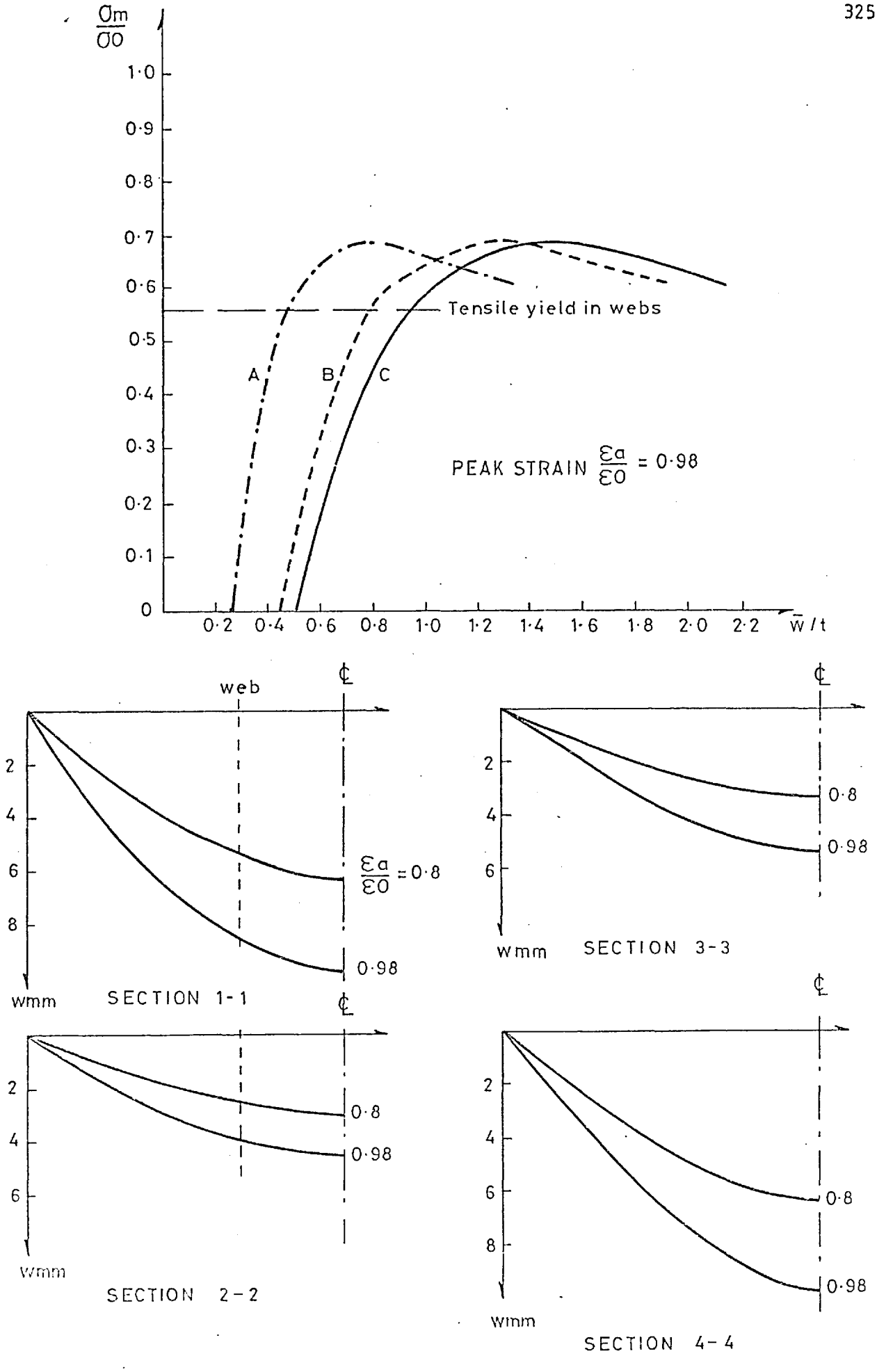

Fig E29 Mean edge stress versus mid-span deflections and deflection profiles for b/t = 30 and L_x/R = 90

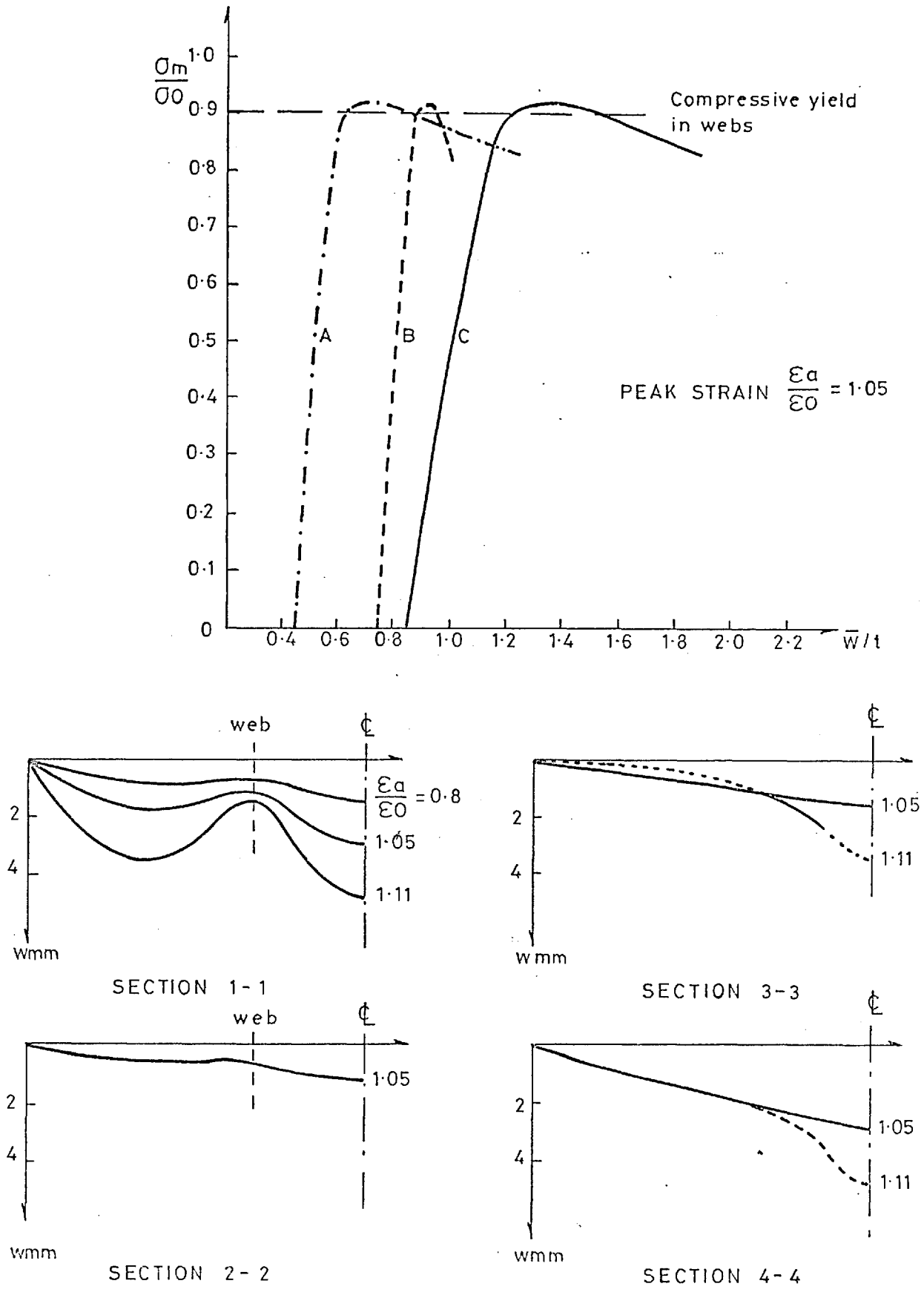

Fig E30 Mean edge stress versus mid-span deflections and deflection profiles for b/t = 50 and Lx/R = 30 (Lx/R = 50 similar)

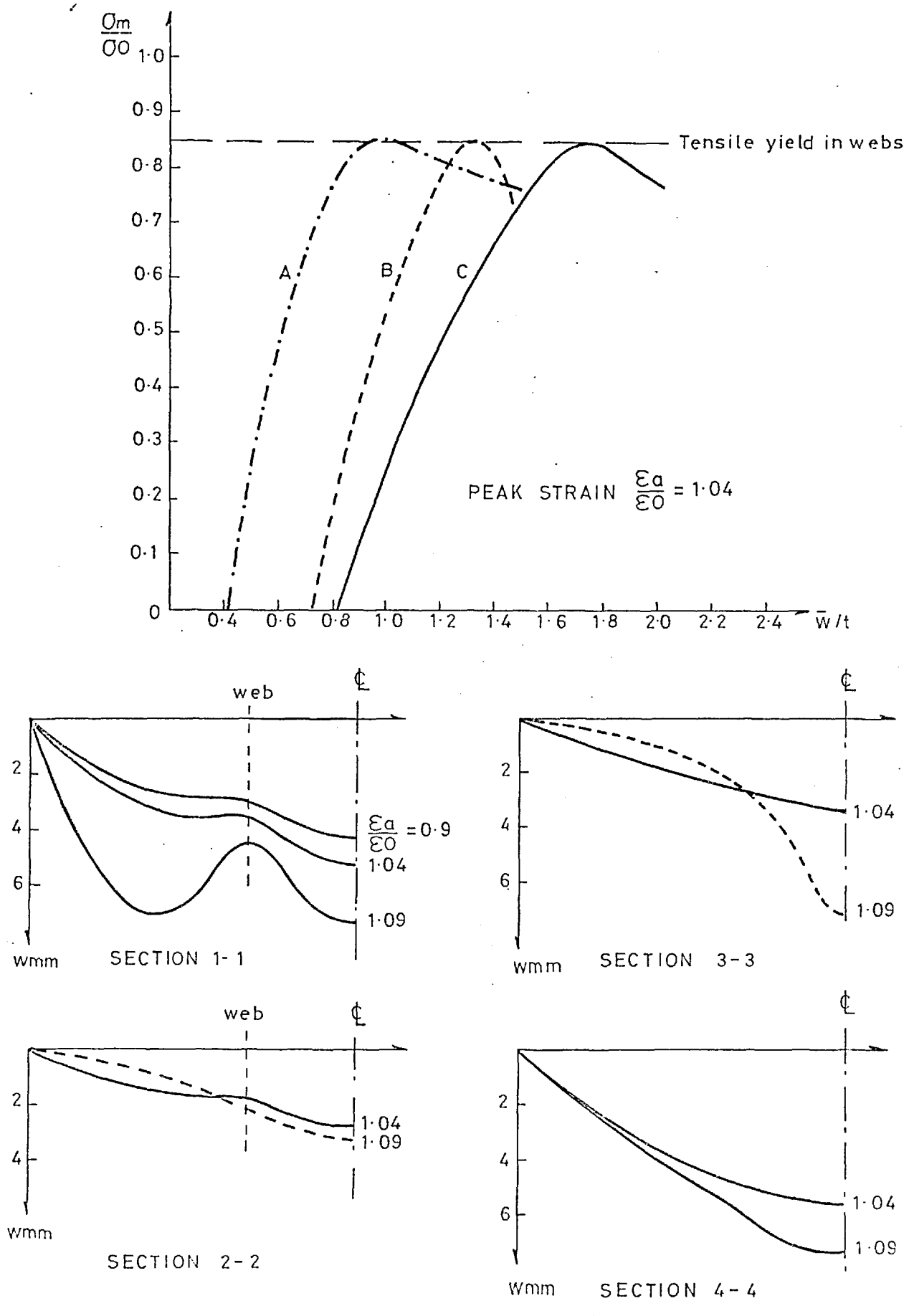

Fig E31 Mean edge stress versus mid-span deflections and deflection profiles for b/t = 50 and L_x/R = 60

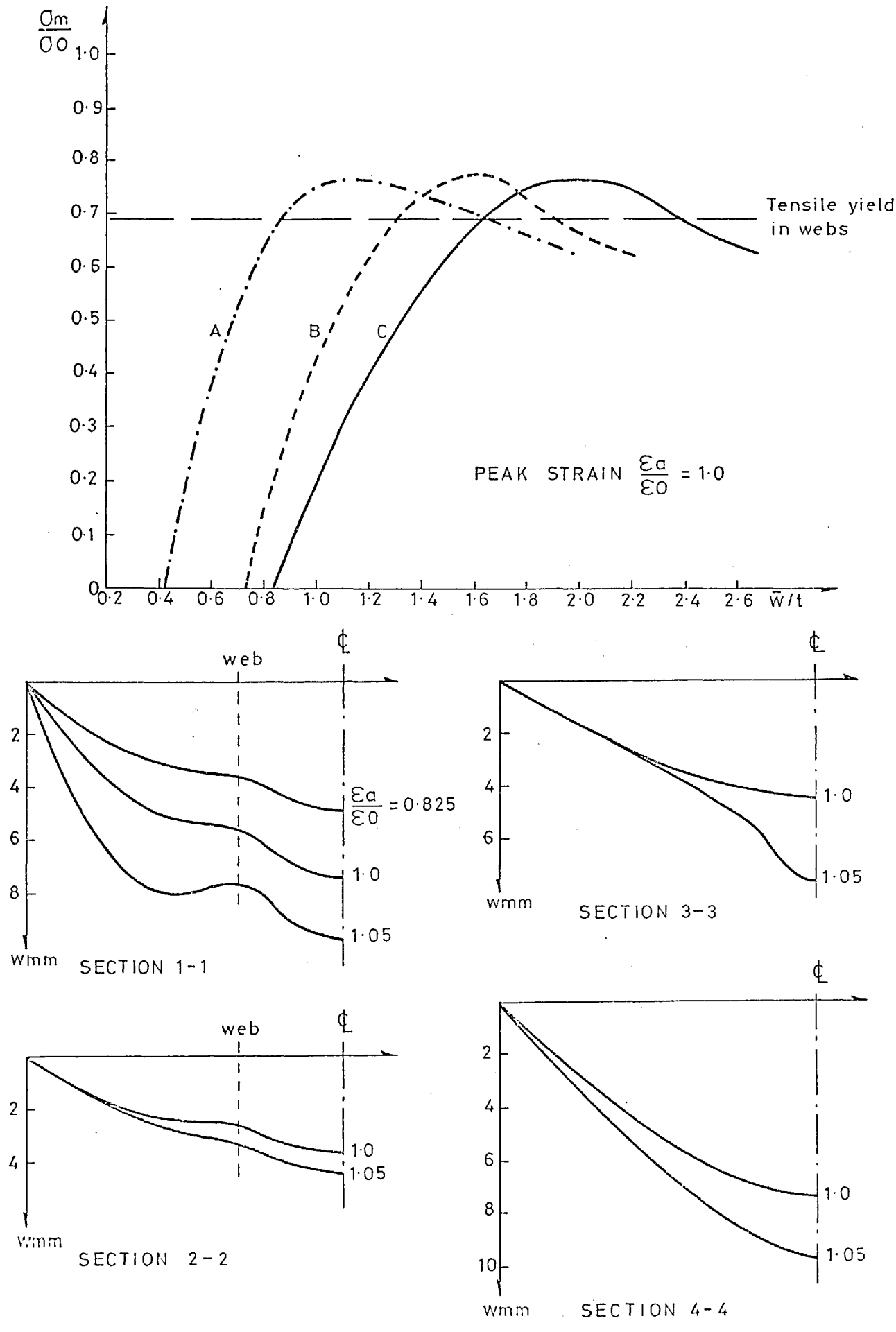

Fig E32 Mean edge stress versus mid-span deflections and deflection profiles for b/t = 50 and Lx/R = 70

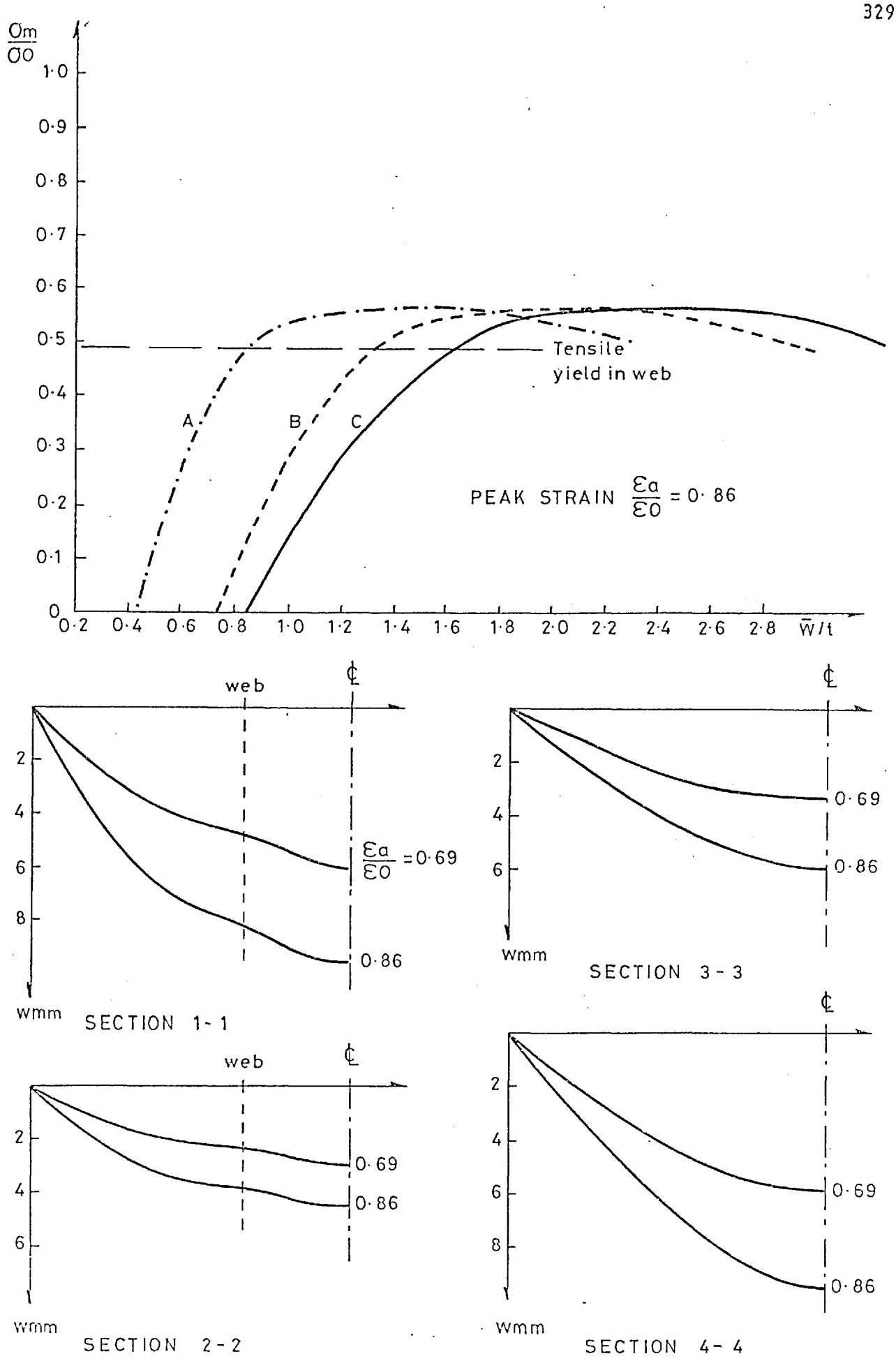

Fig E33 Mean edge stress versus mid-span deflections and deflection profiles for b/t = 50 and Lx/R = 90 (Lx/R = 80 similar)

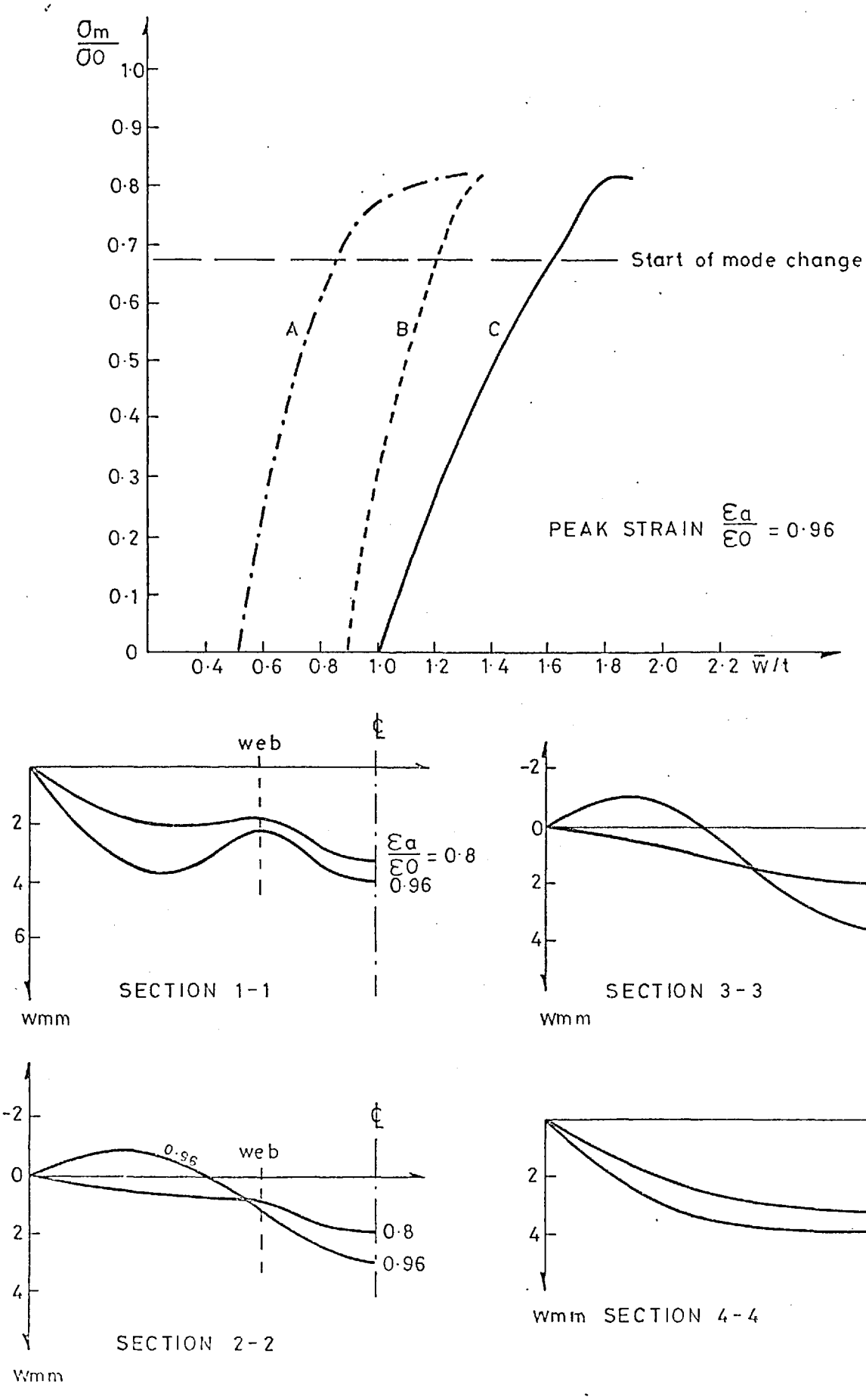

Fig E34 Mean edge stress versus mid-span deflections and deflection profiles for b/t = 60 and Lx/R = 50 (Lx/R=30 and 60 similar)

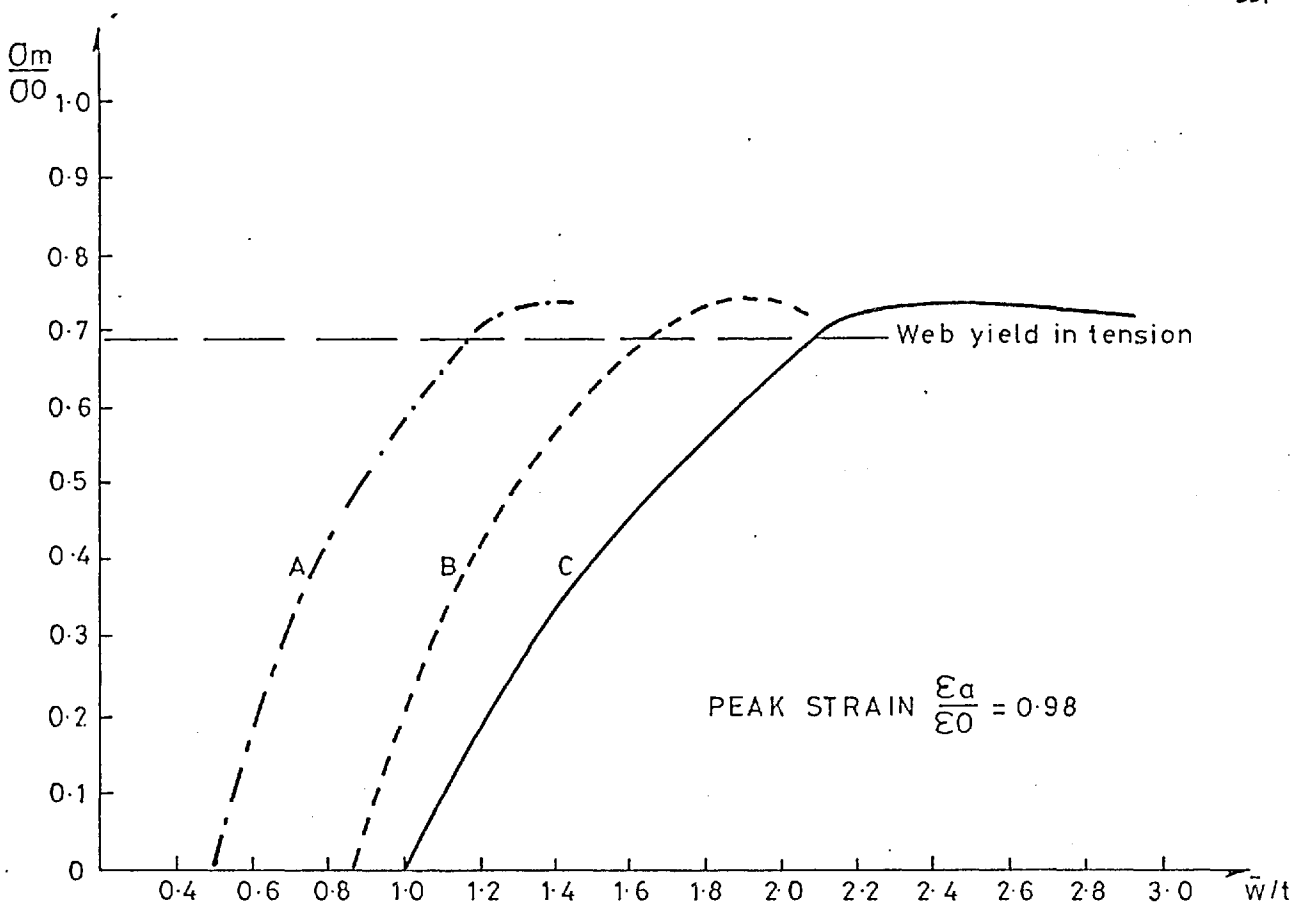

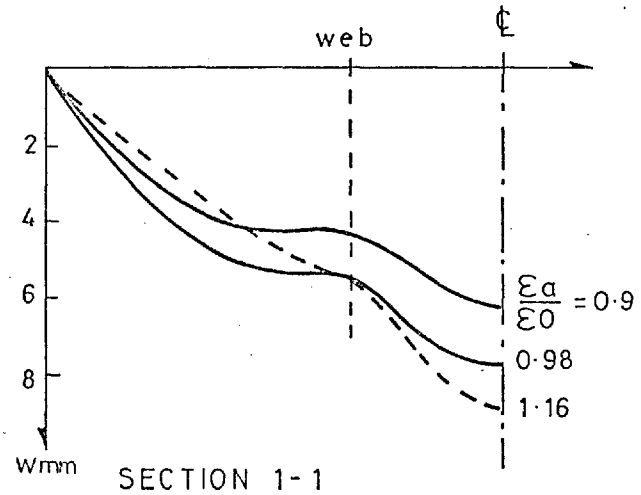

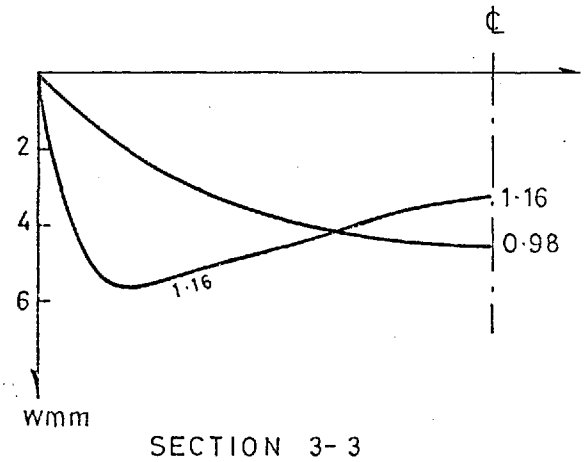

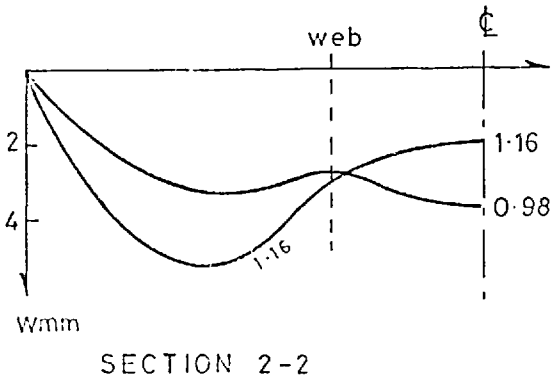

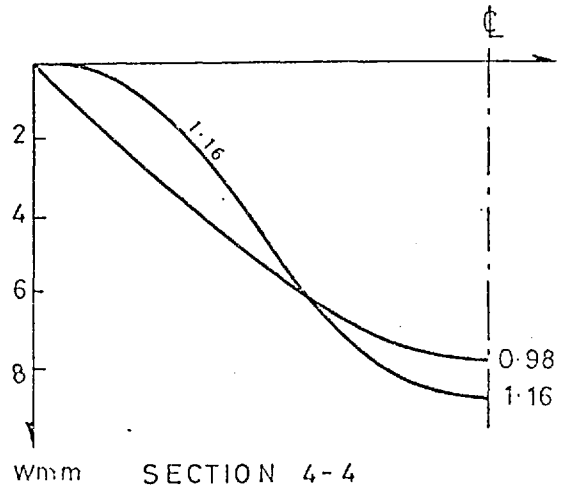

Fig E35 Mean edge stress versus mid-span deflections and deflection profiles for b/t = 60 and L_x/R=70

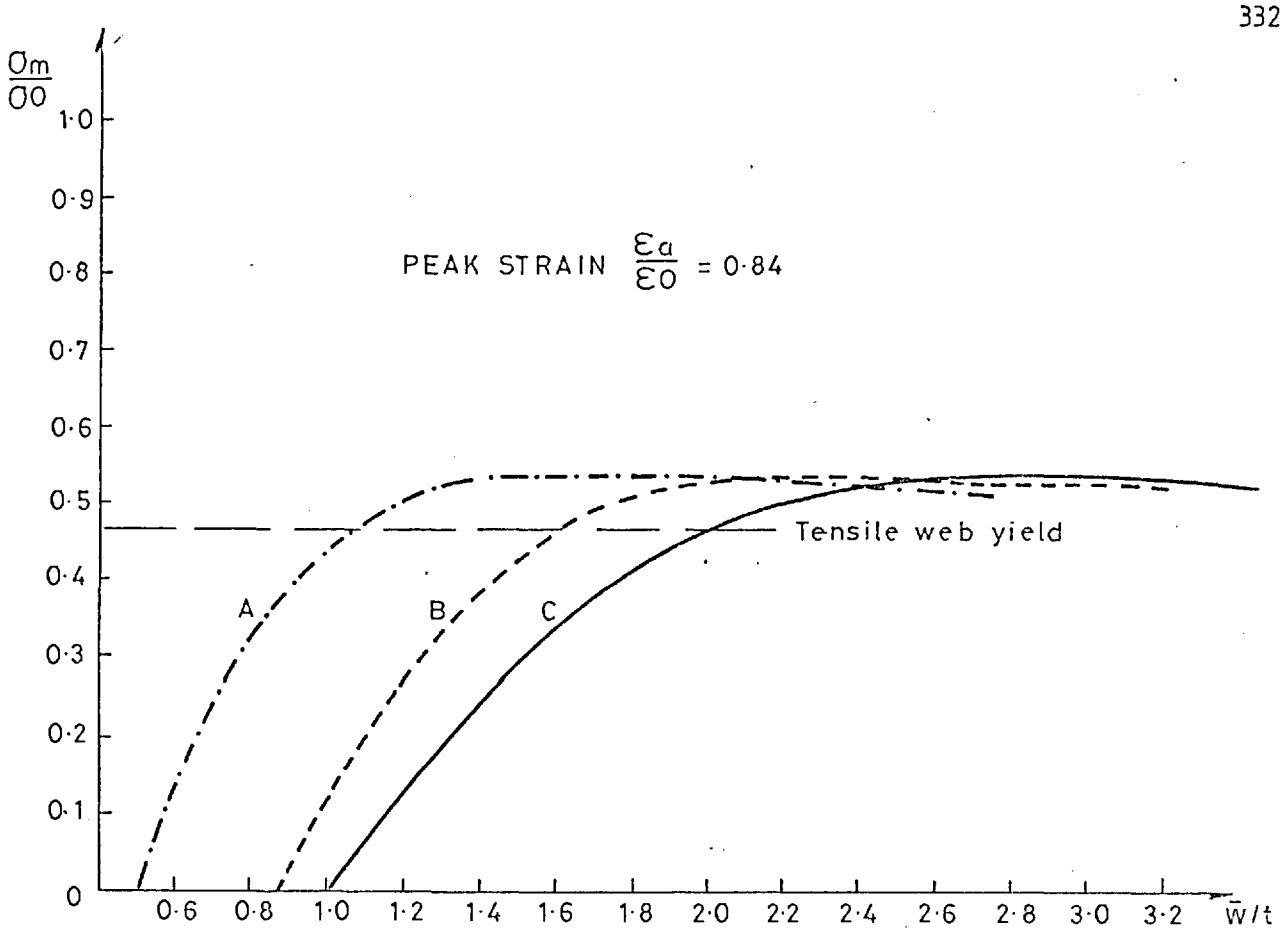

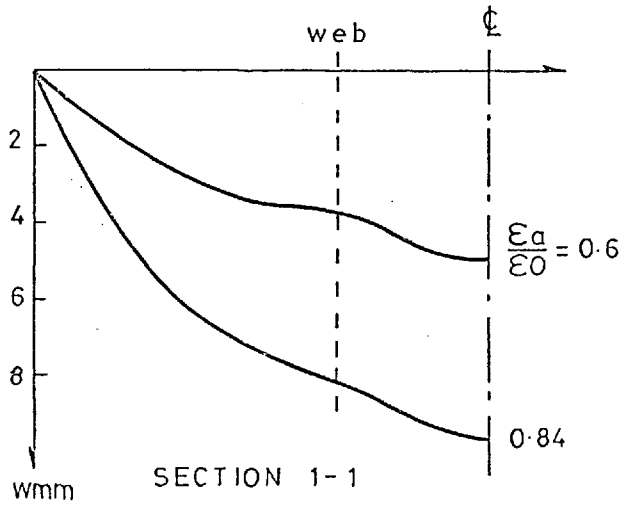

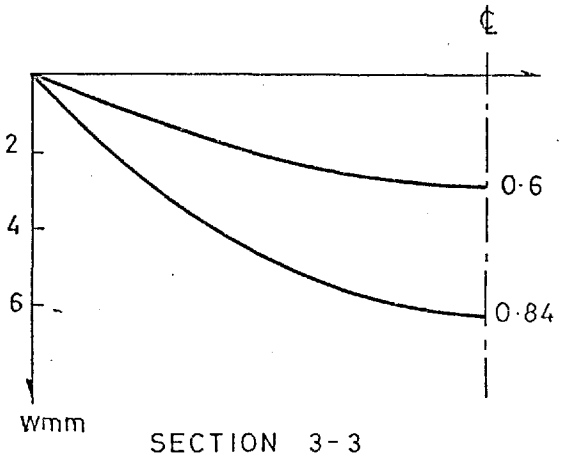

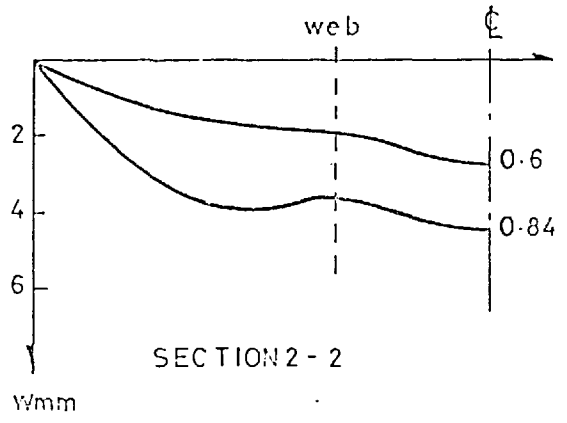

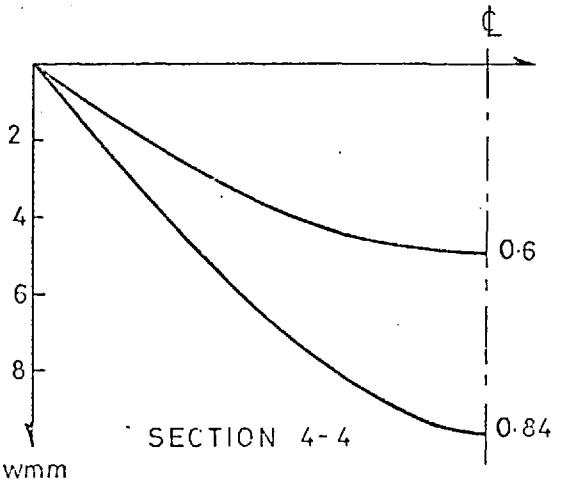

Fig E36 Mean edge stress versus mid-span deflections and deflection profiles for b/t = 60 and Lx/R = 90 (Lx/R = 80 similar)

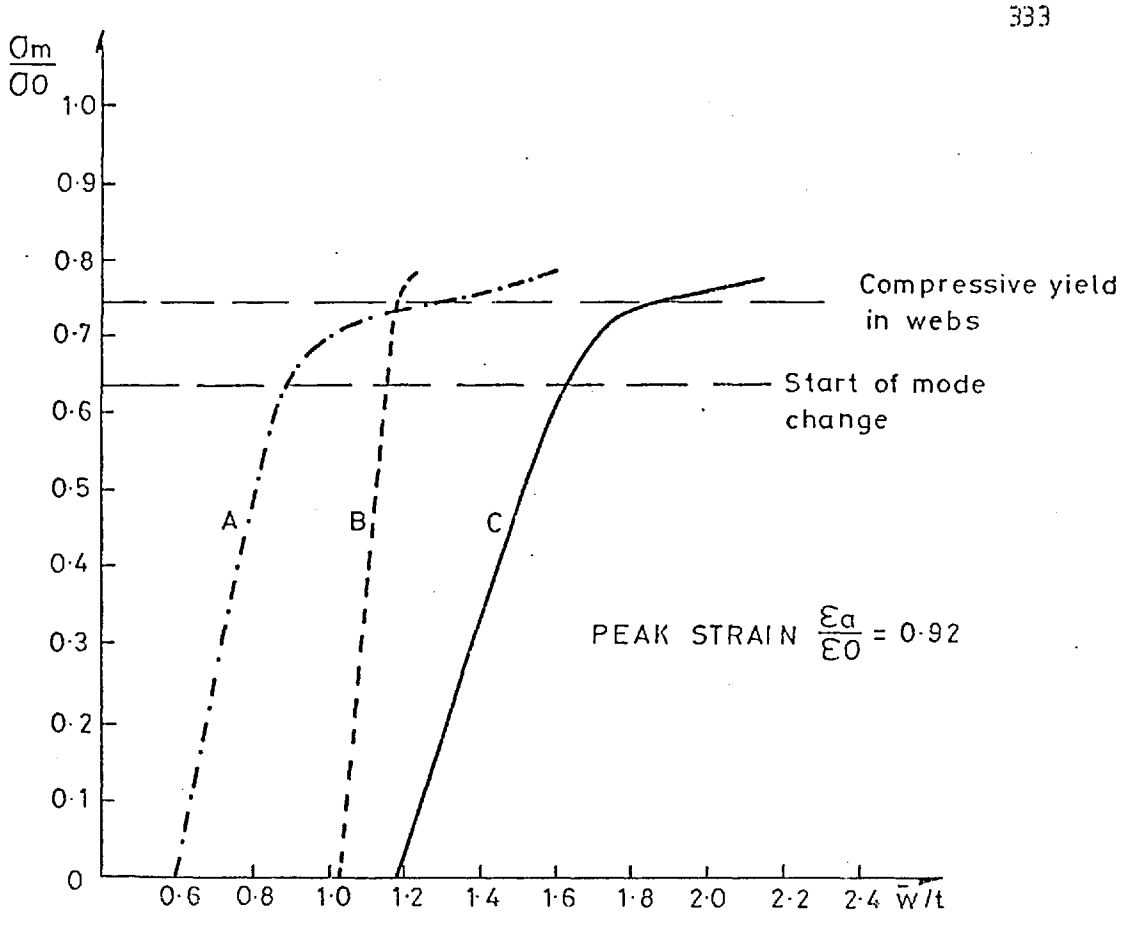

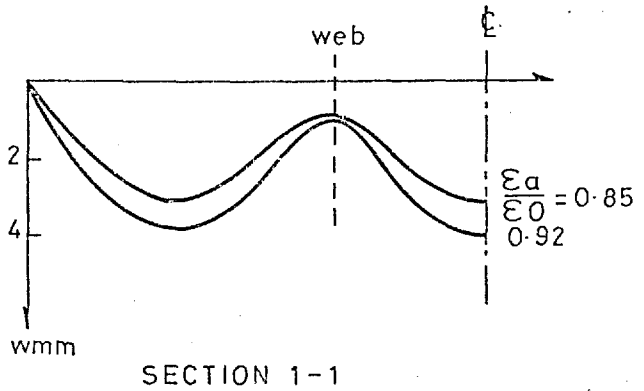

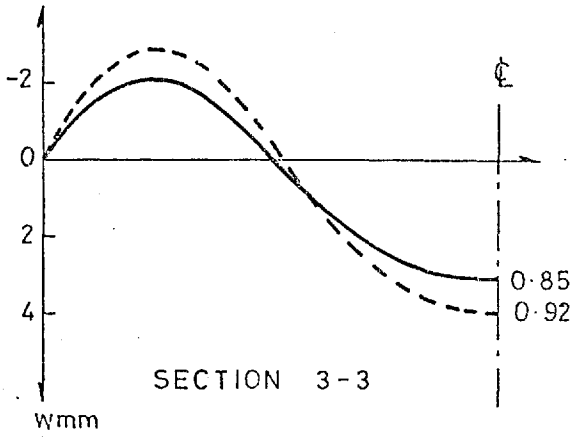

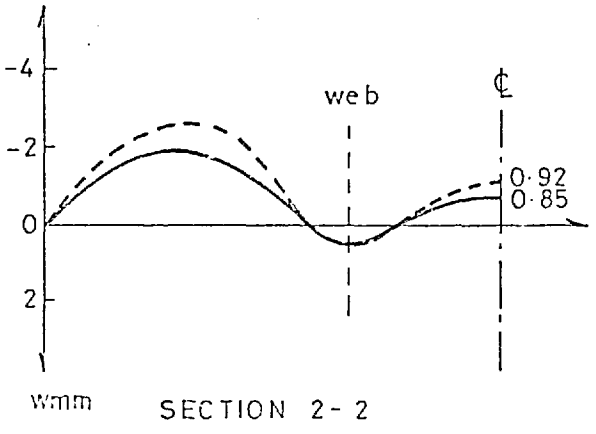

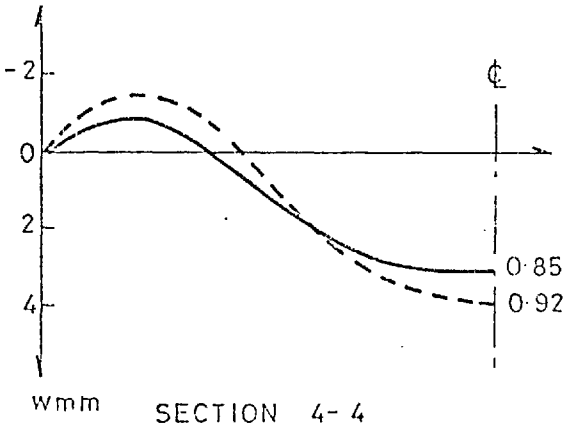

Fig E37 Mean edge stress versus mid-span deflections and deflection profiles for $b/t = 70$ and $L_x/R = 30$

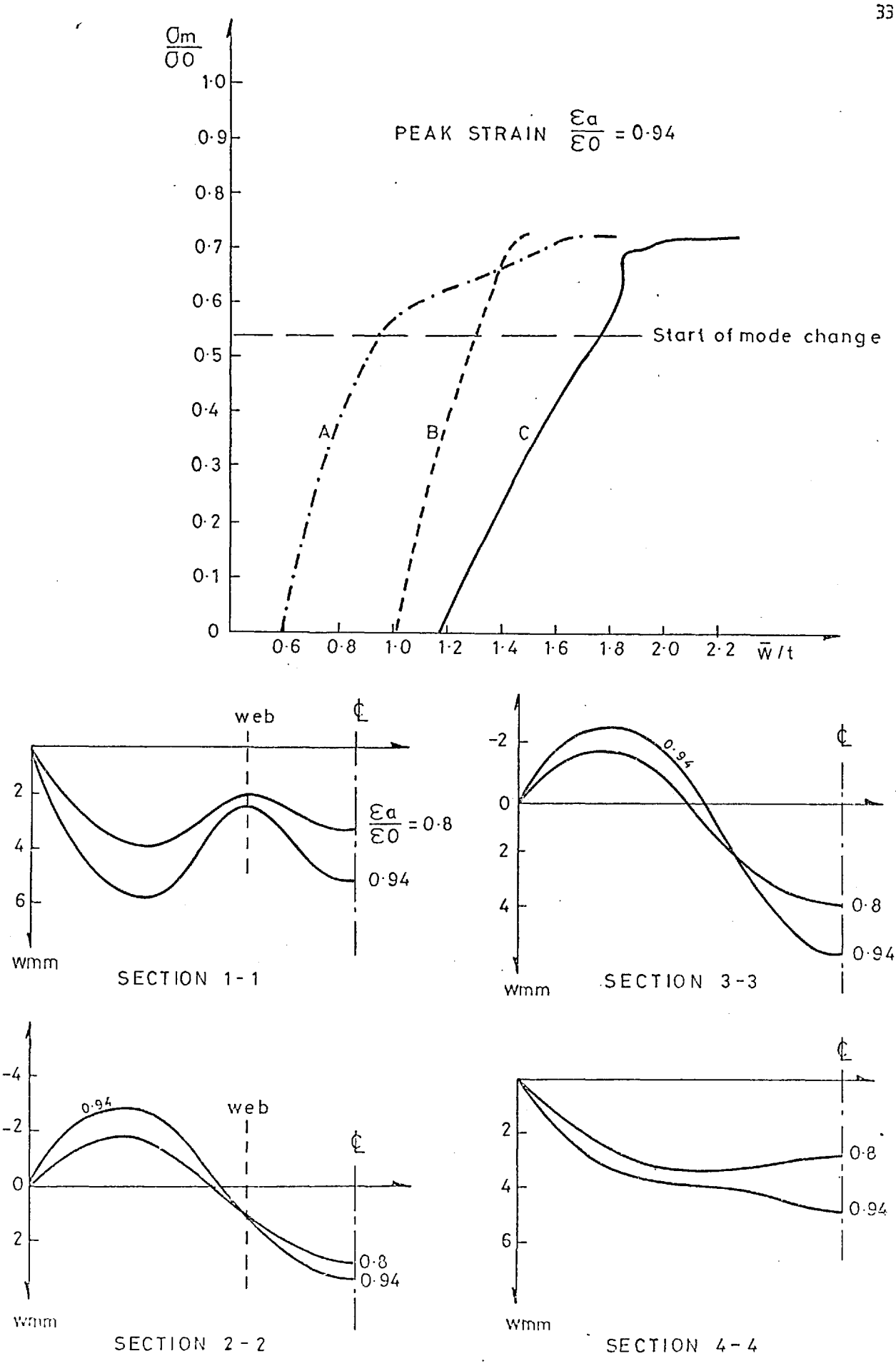

Fig E38 Mean edge stress versus mid-span deflections and deflection profiles for b/t = 70 and L_x/R = 50 (L_x/R = 60 and 70 similar)

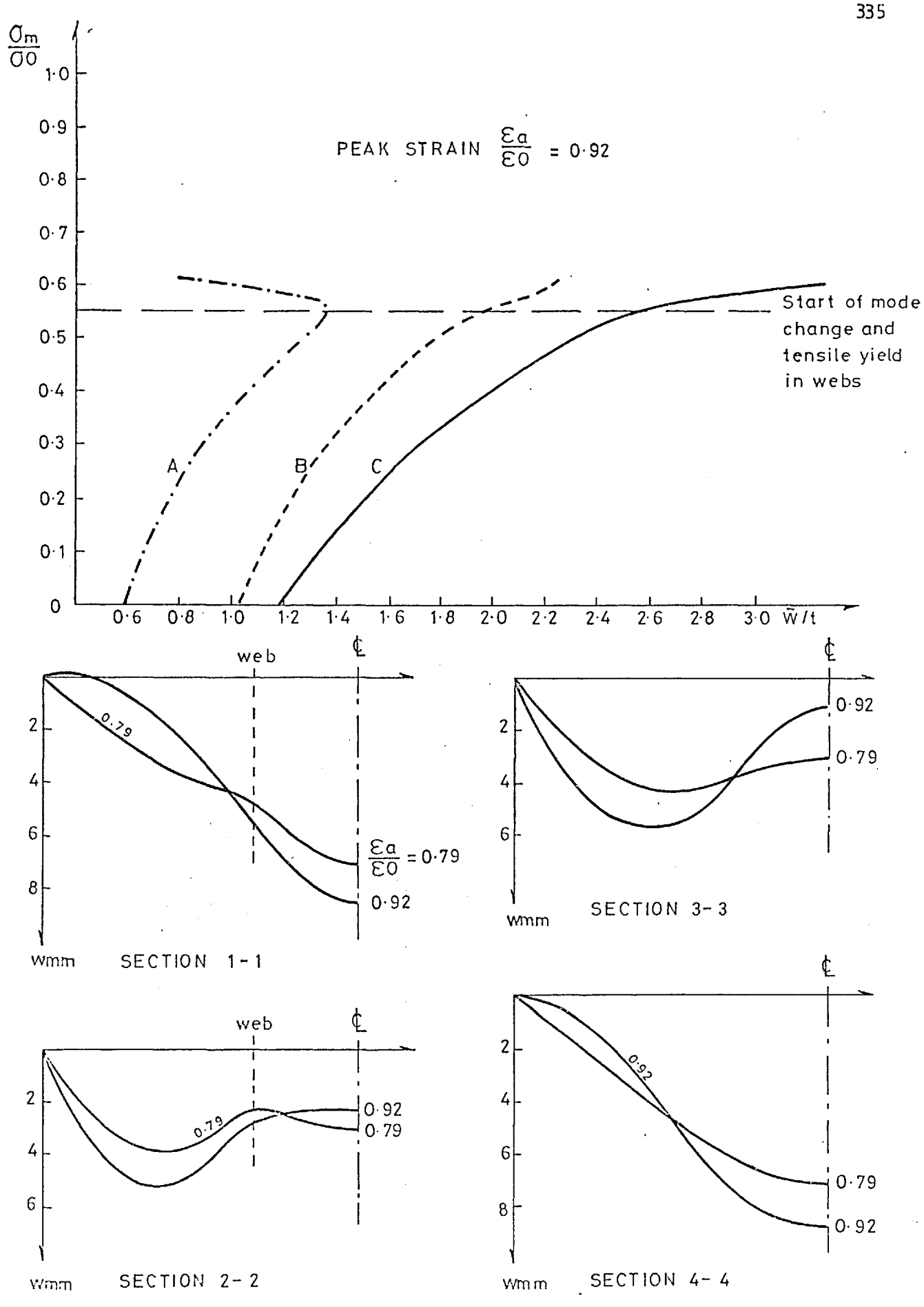

FigE39 Mean edge stress versus mid-span deflections and deflection profiles for b/t = 70 and Lx/R = 80

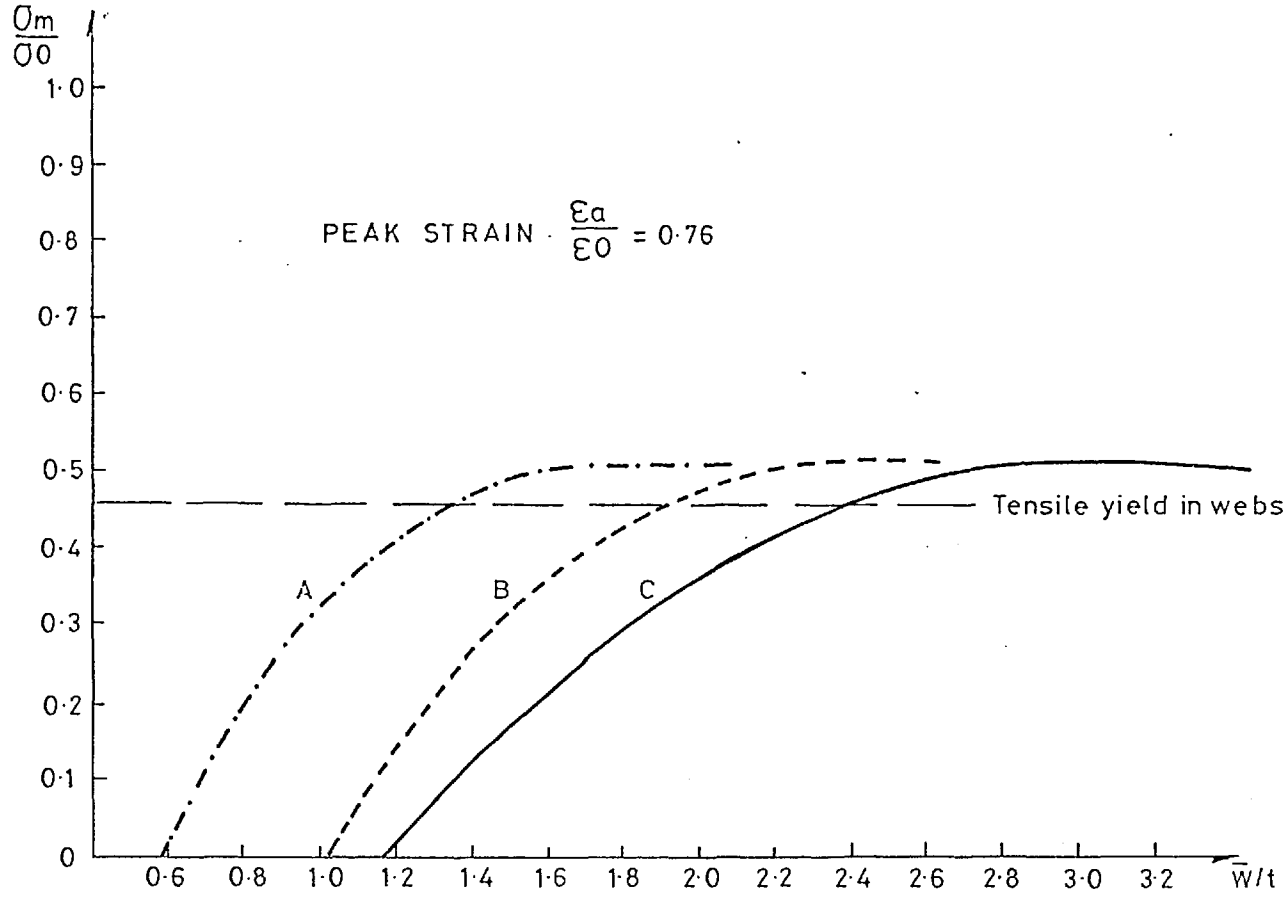

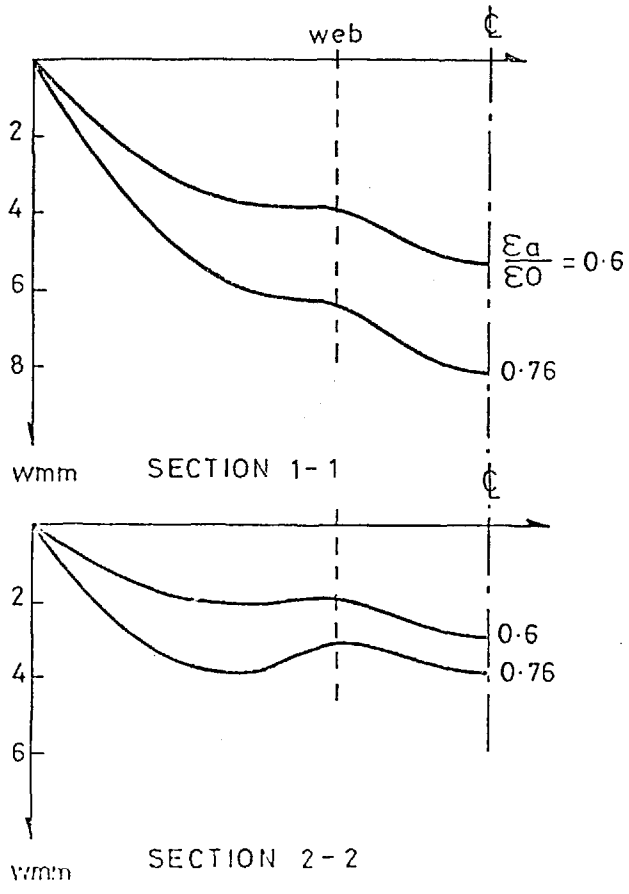

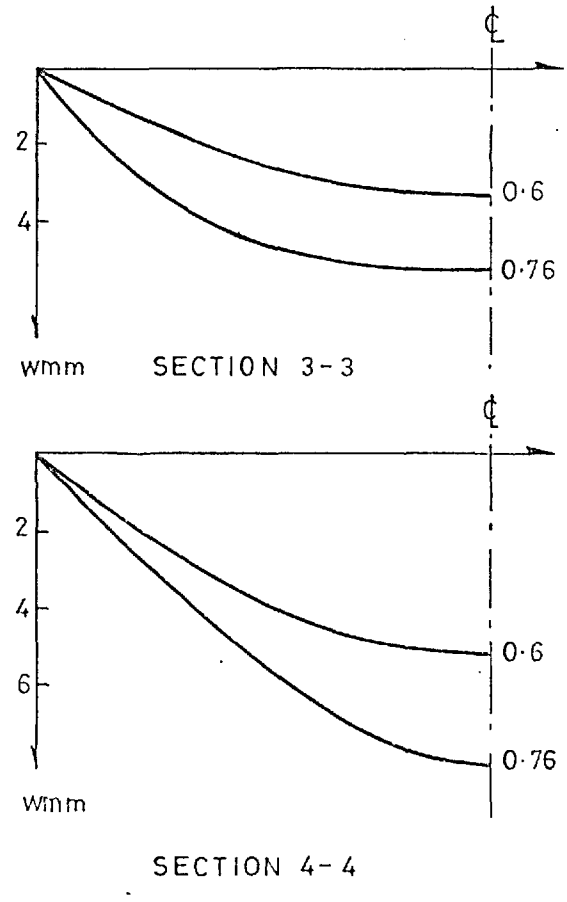

Fig E40 Mean edge stress versus mid-span deflections and deflection profiles for b/t = 70 and Lx/R = 90

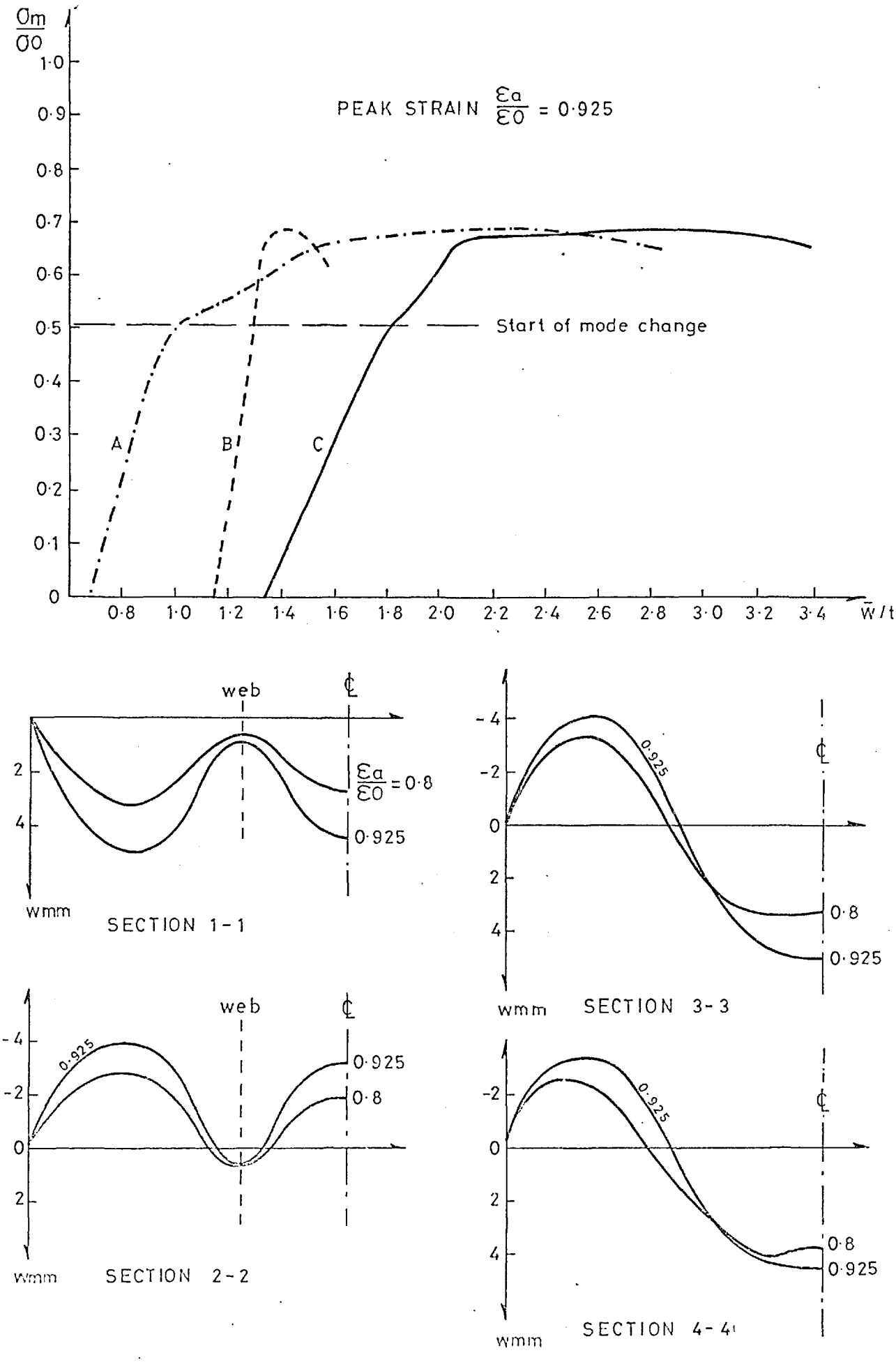

Fig E41 Mean edge stress versus mid-span deflections and deflection profiles for b/t = 80 and Lx/R=30

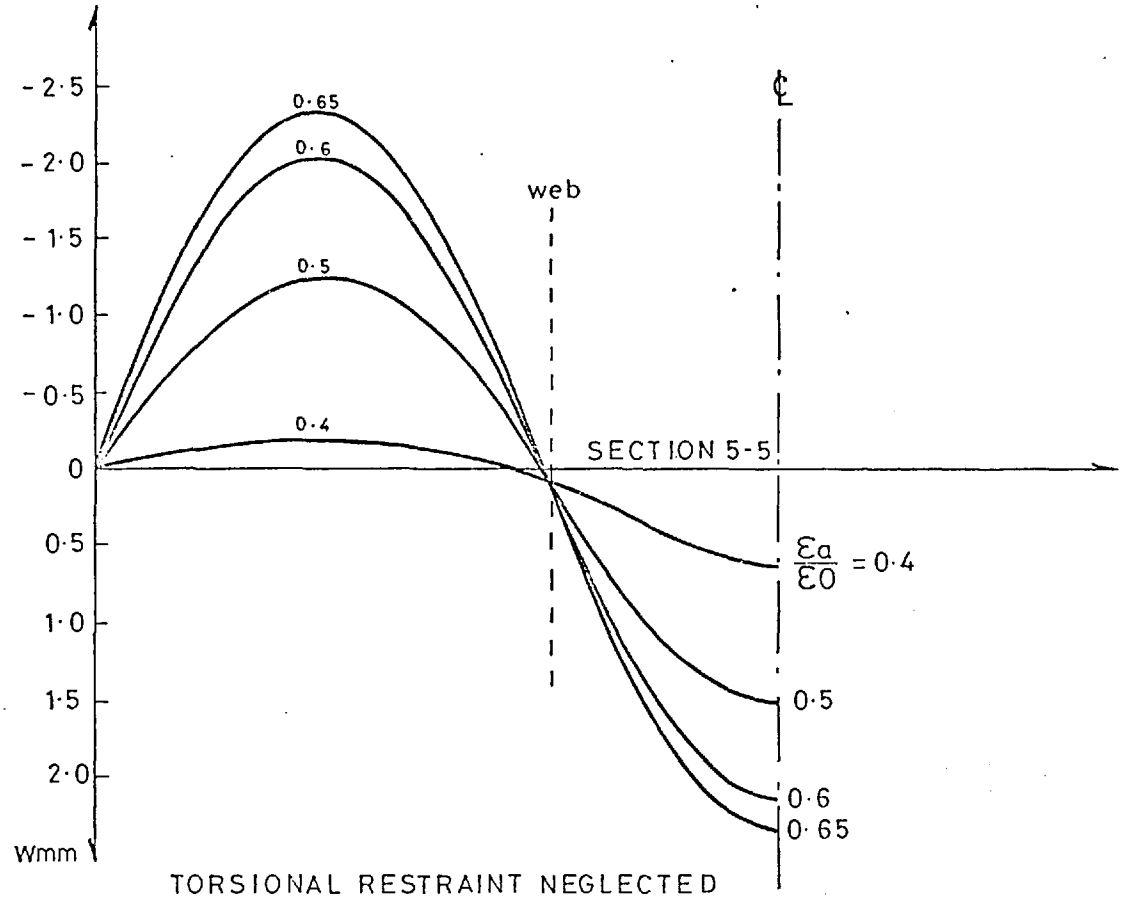

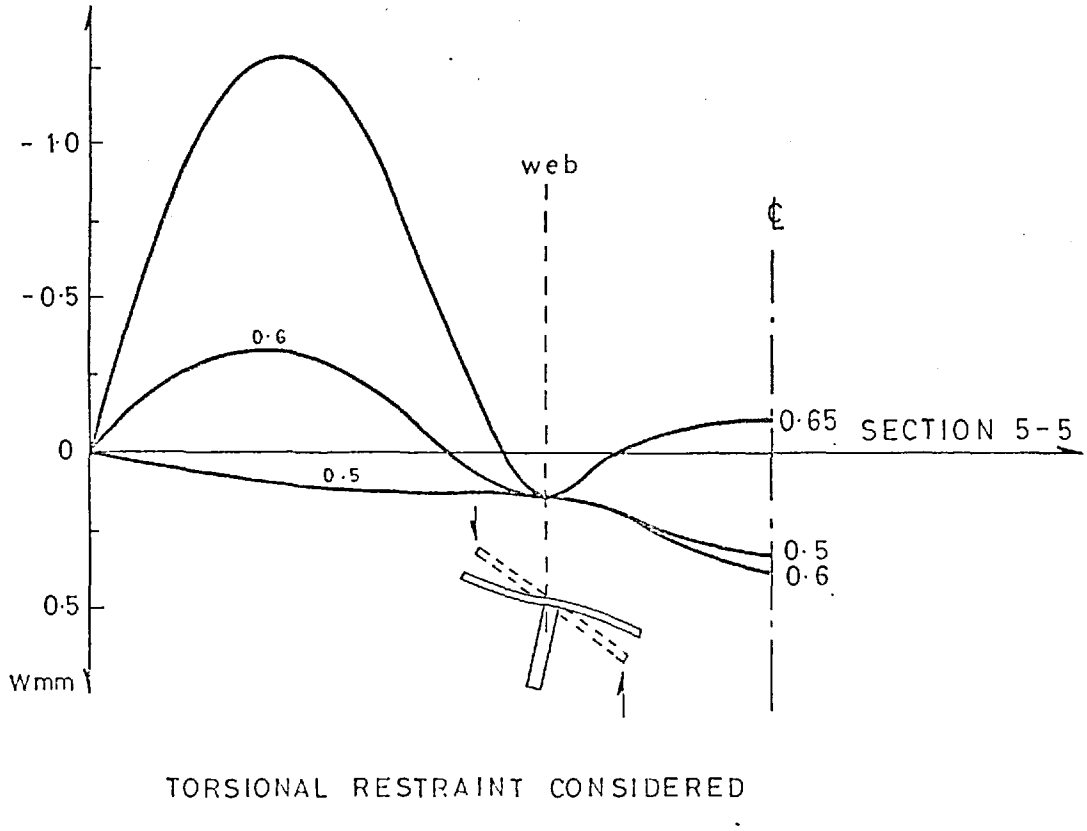

Fig E42 The effect of web torsional stiffeness on the plate
b/t = 80 Lx/R = 30

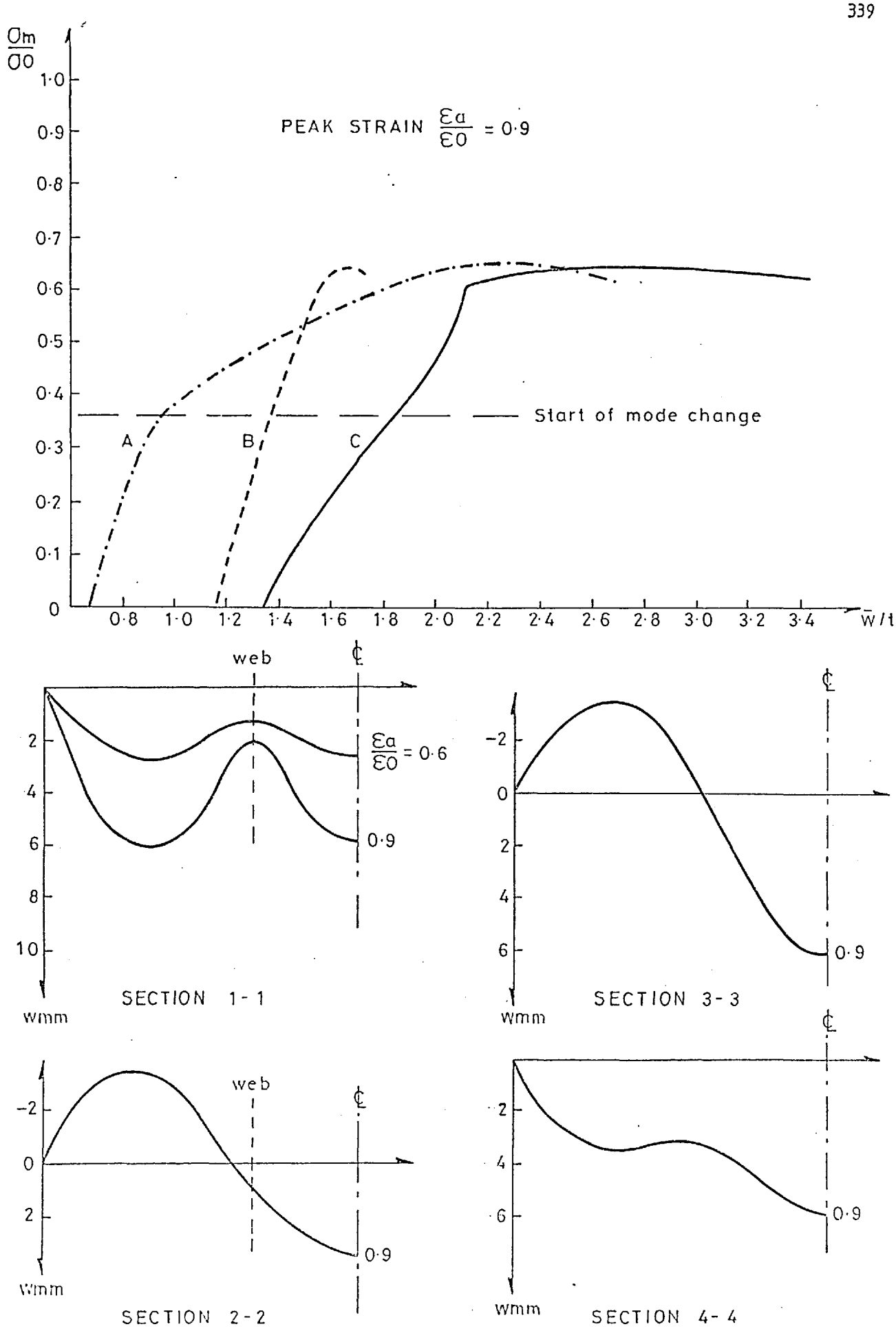

Fig E43 Mean edge stress versus mid-span deflections and deflection profiles for b/t = 80 and L_x/R=50

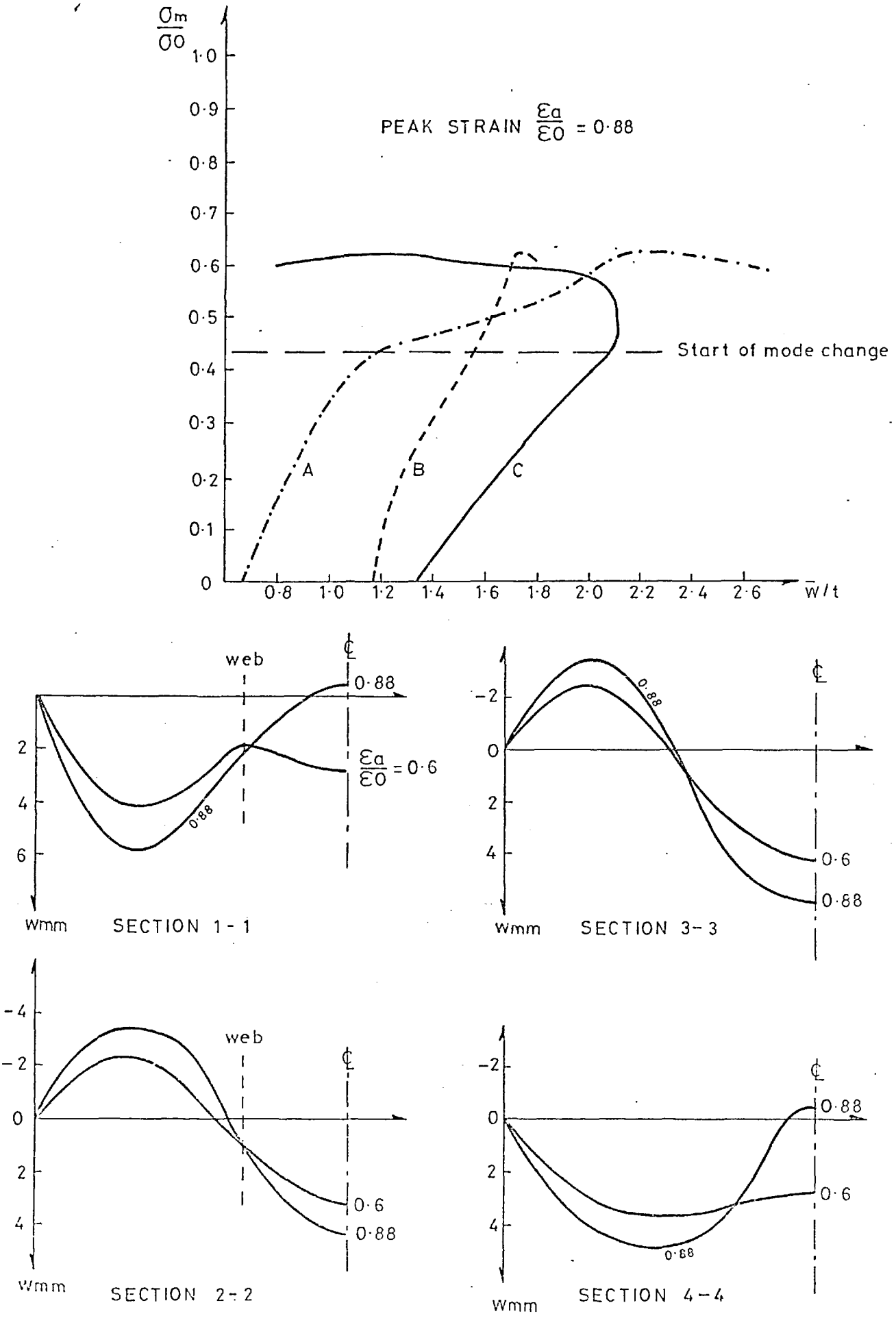

Fig E44 Mean edge stress versus mid-span deflections and deflection profiles for b/t = 80 and Lx/R = 60 (Lx/R = 70 similar)

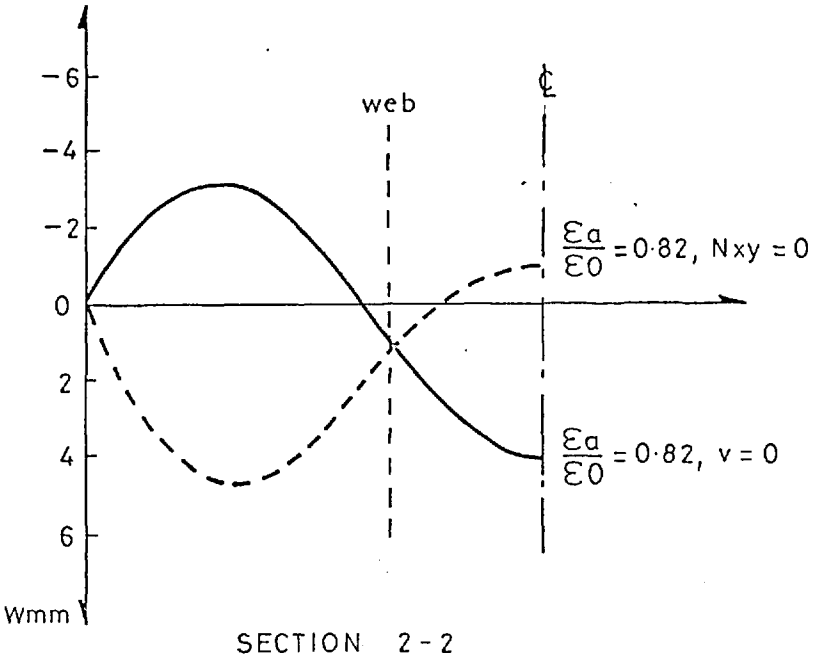

SECTION 2-2

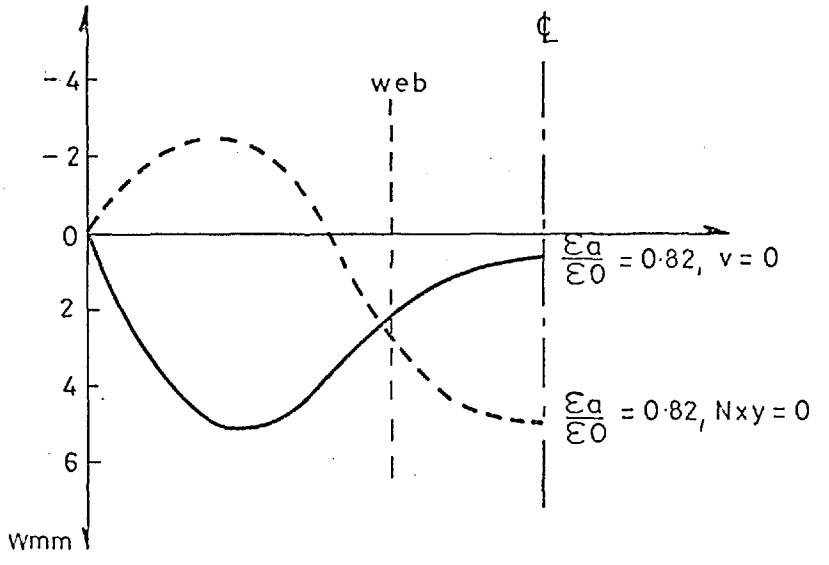

SECTION 1-1

Fig E45 Effect of shear restraint along the loaded edge for b/t = 80 and Lx/R=60

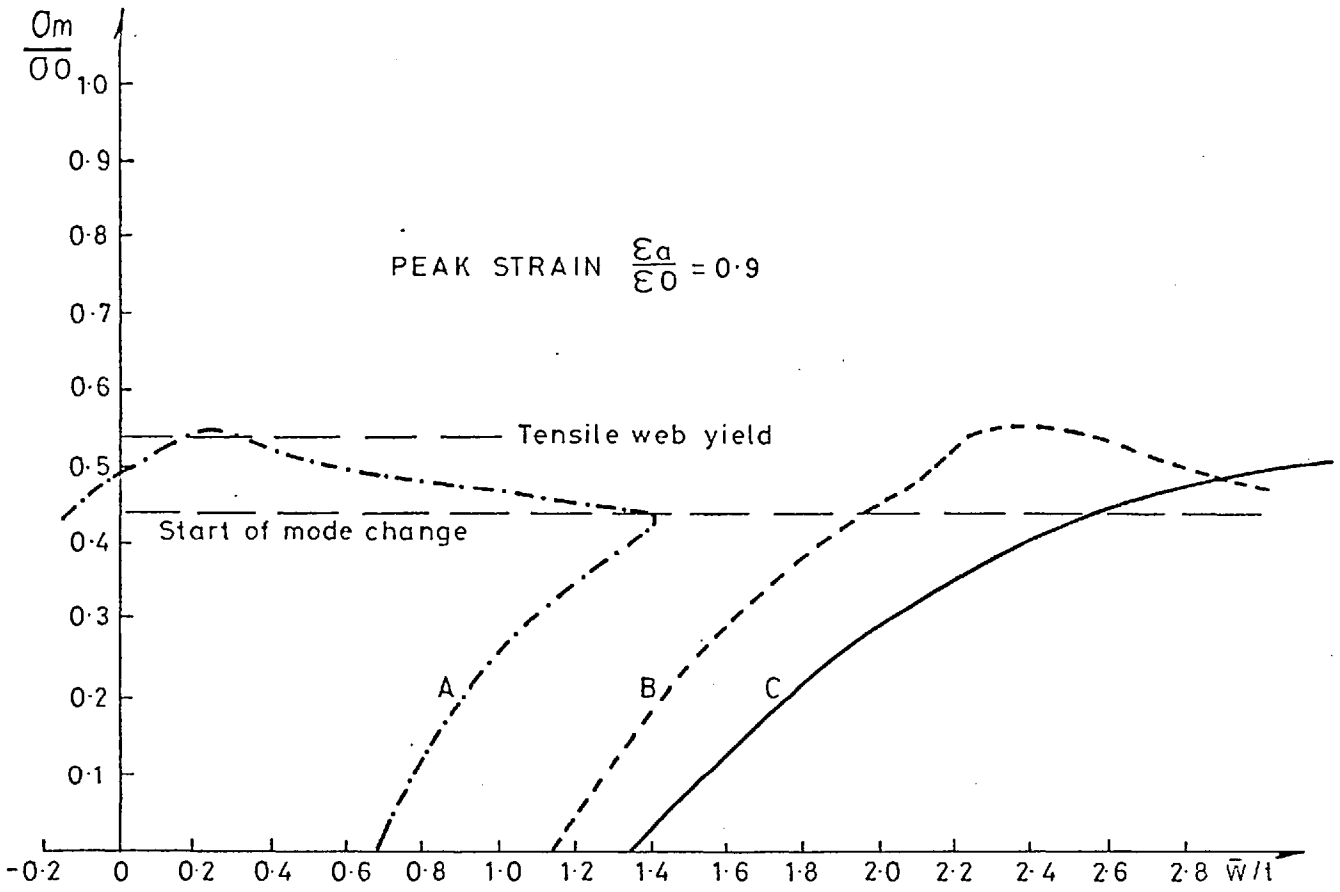

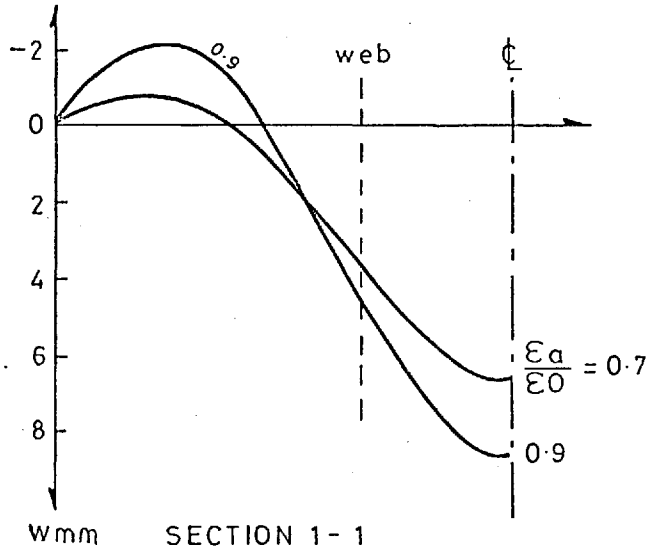

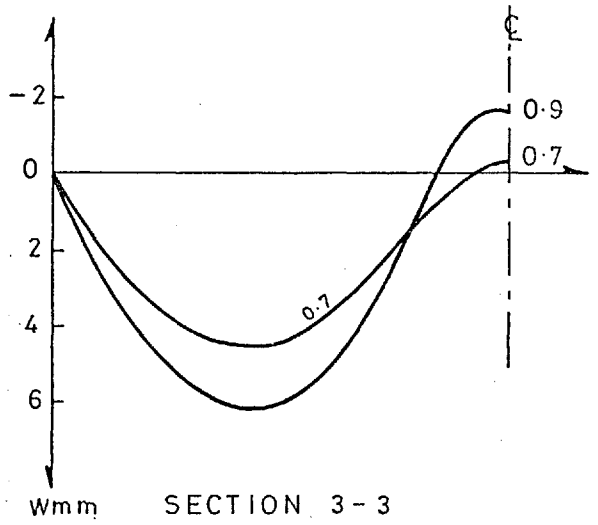

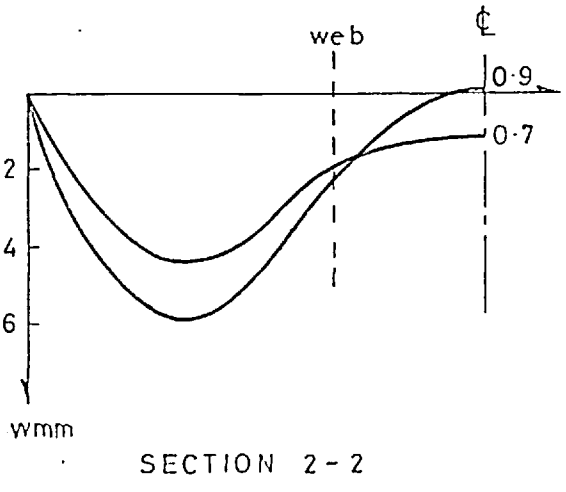

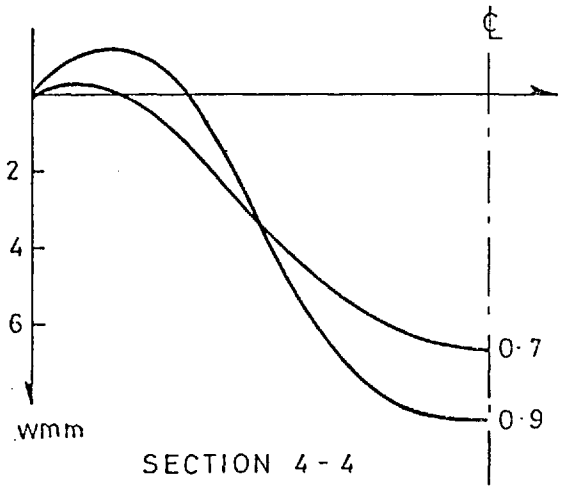

Fig E46 Mean edge stress versus mid-span deflections and deflection profiles for b/t = 80 and Lx/R=80 (Lx/R=90 similar)

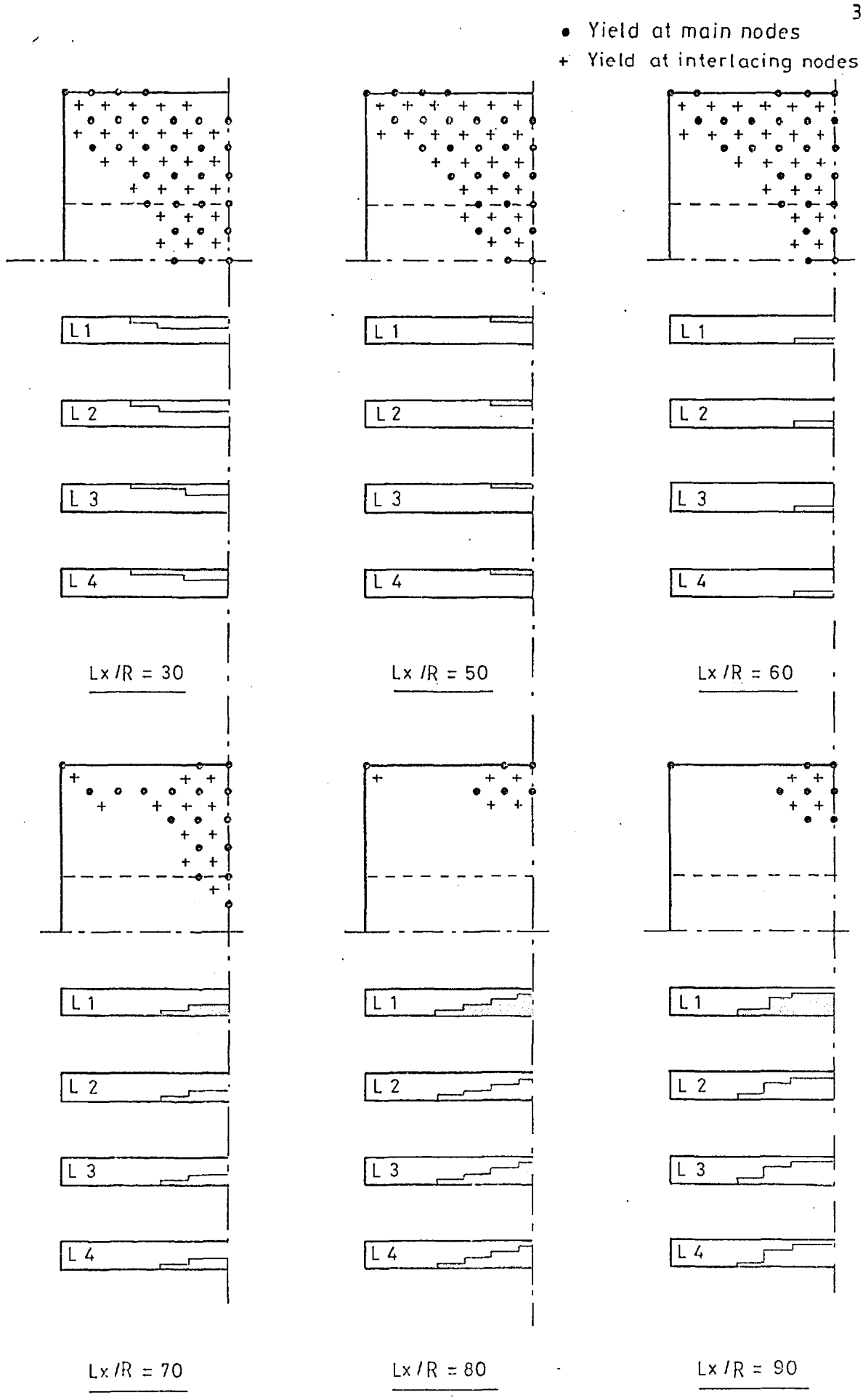

Fig E47 Yield zones at peak stress for plates of b / t = 30

• Yield at main nodes
+ Yield at interlacing nodes

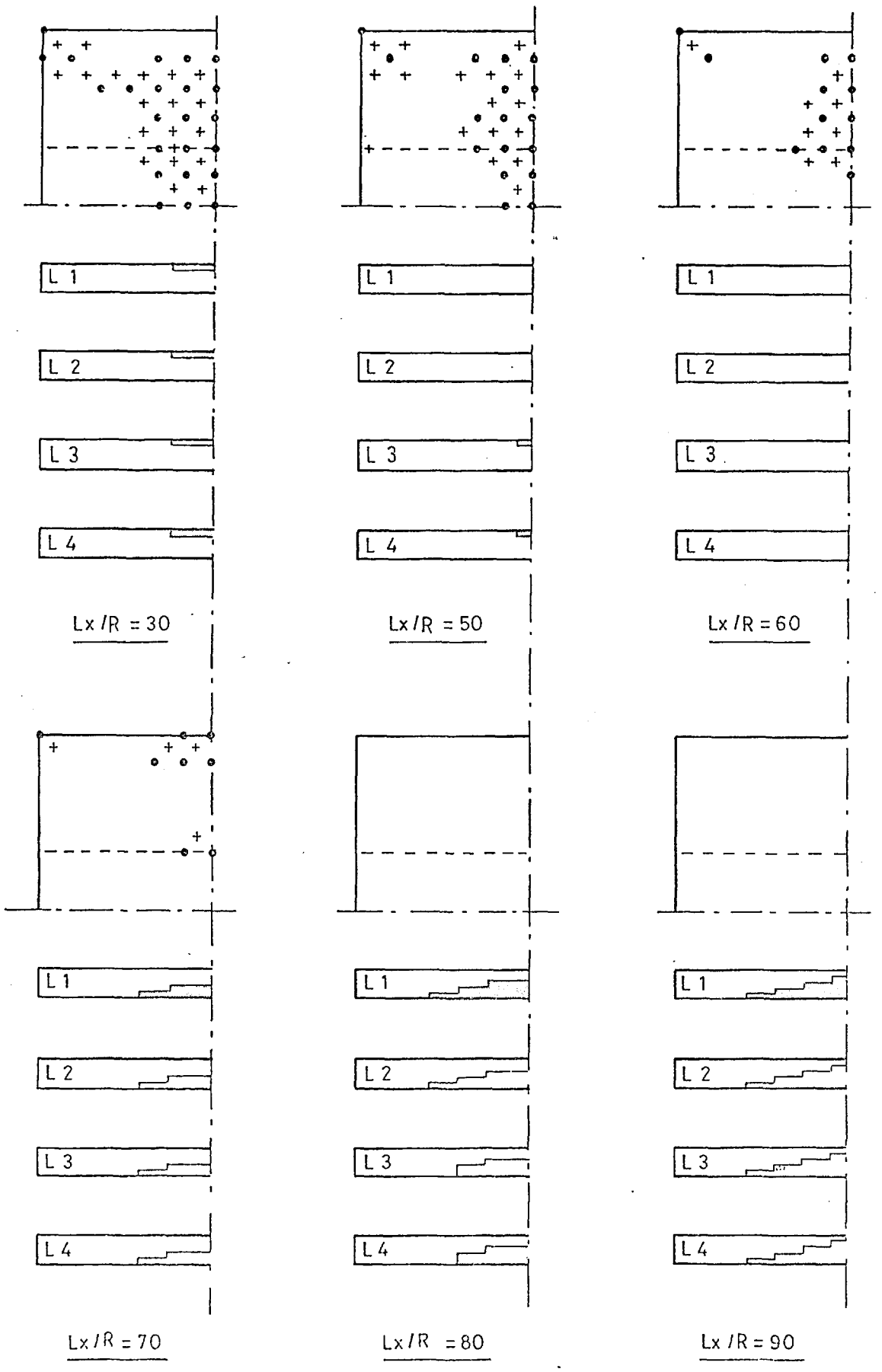

Fig E48 Yield zones at peak stress for plates of b/t = 50

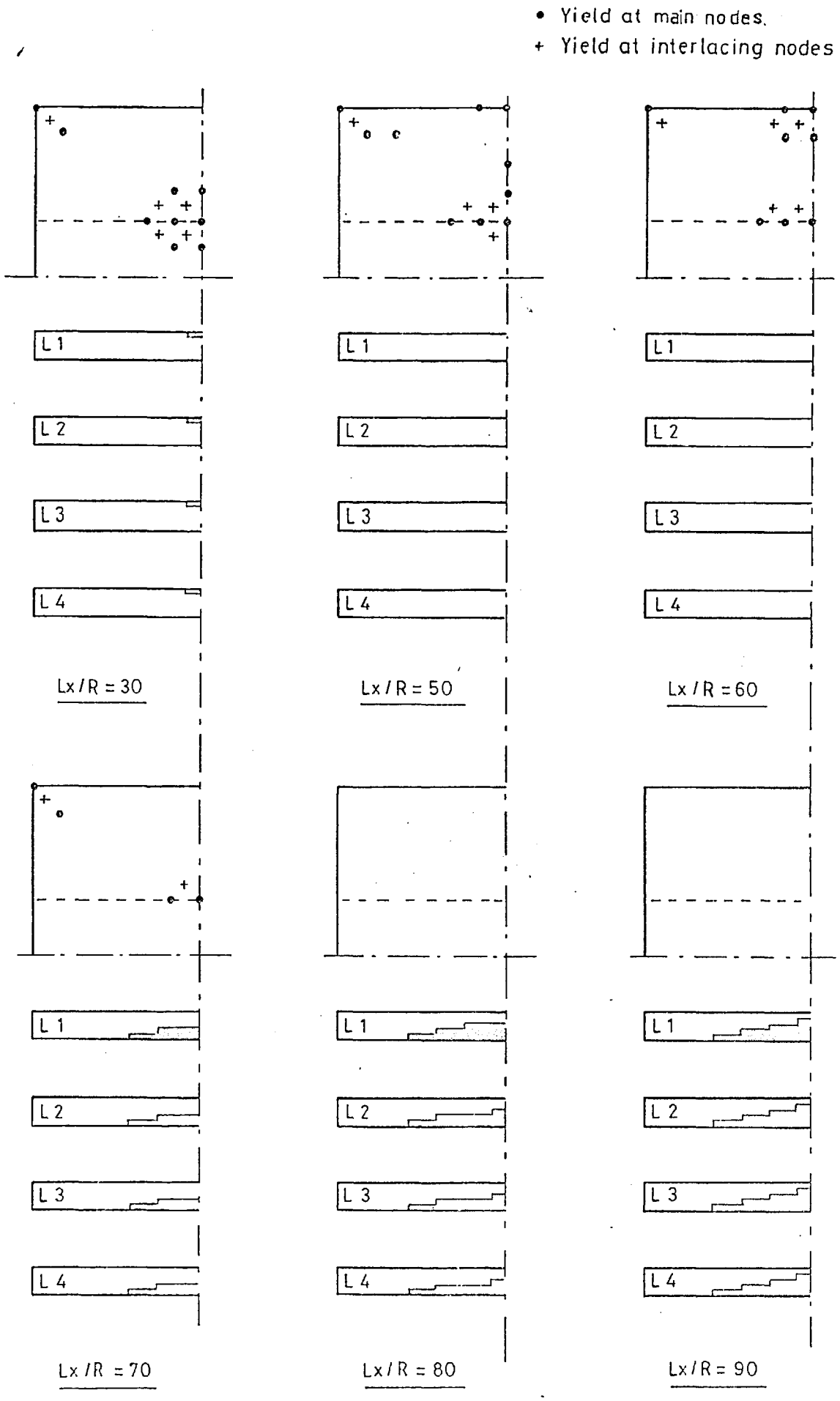

Fig E49 Yield zones at peak stress for plates of b/t = 60

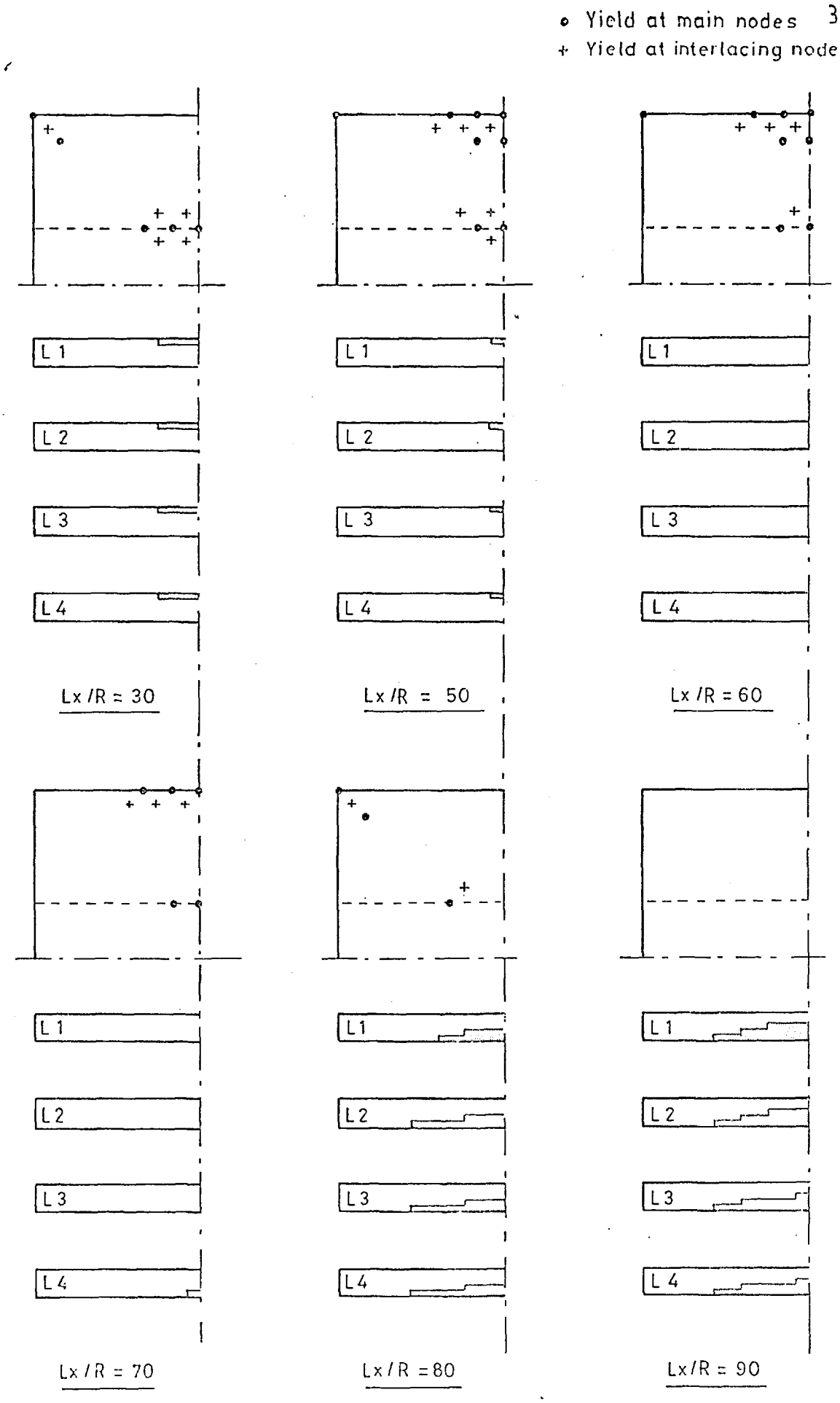

Fig E50 Yield zones at peak stress for plates of b/t = 70

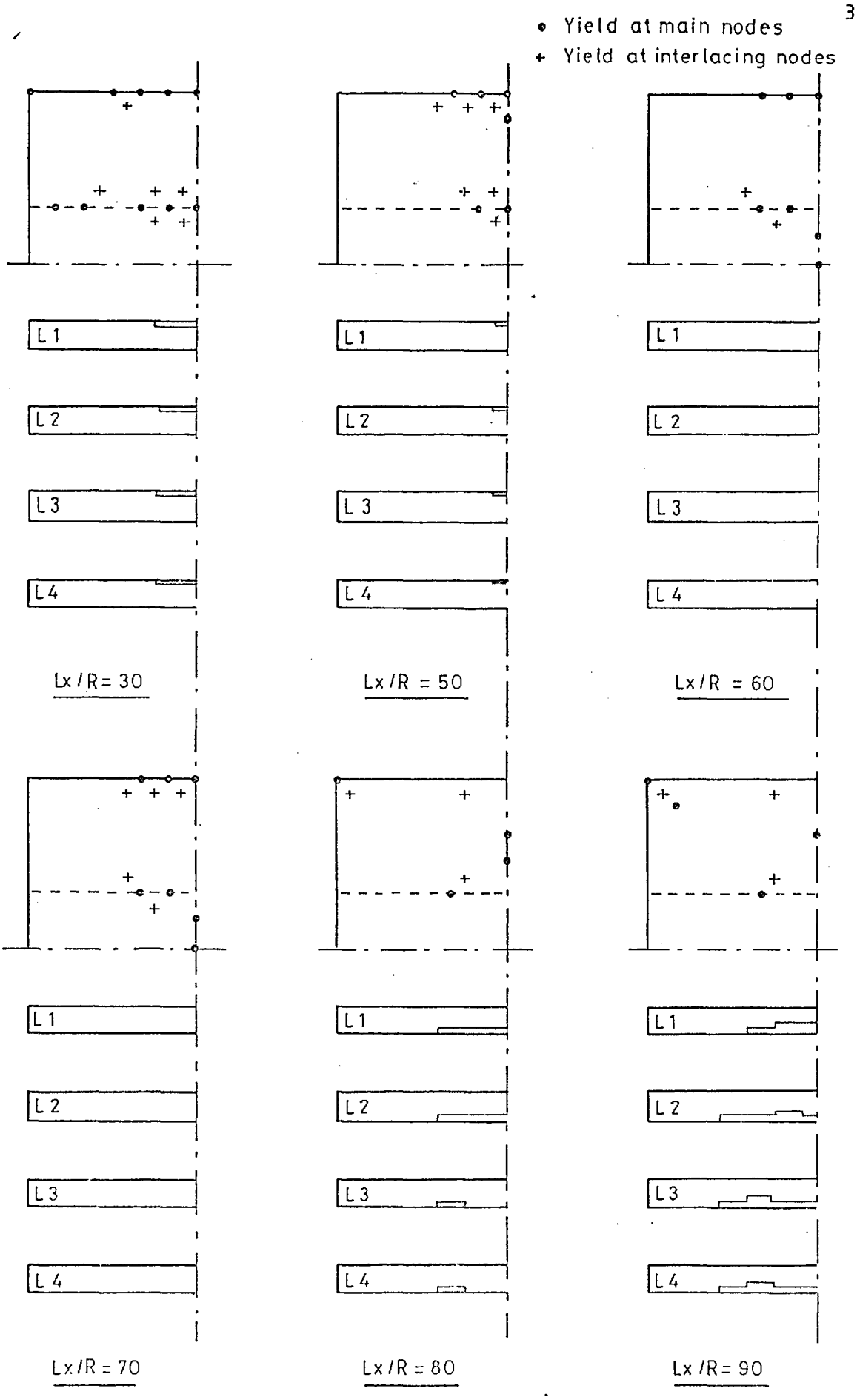

Fig E51 Yield zones at peak stress for plates of b/t = 80

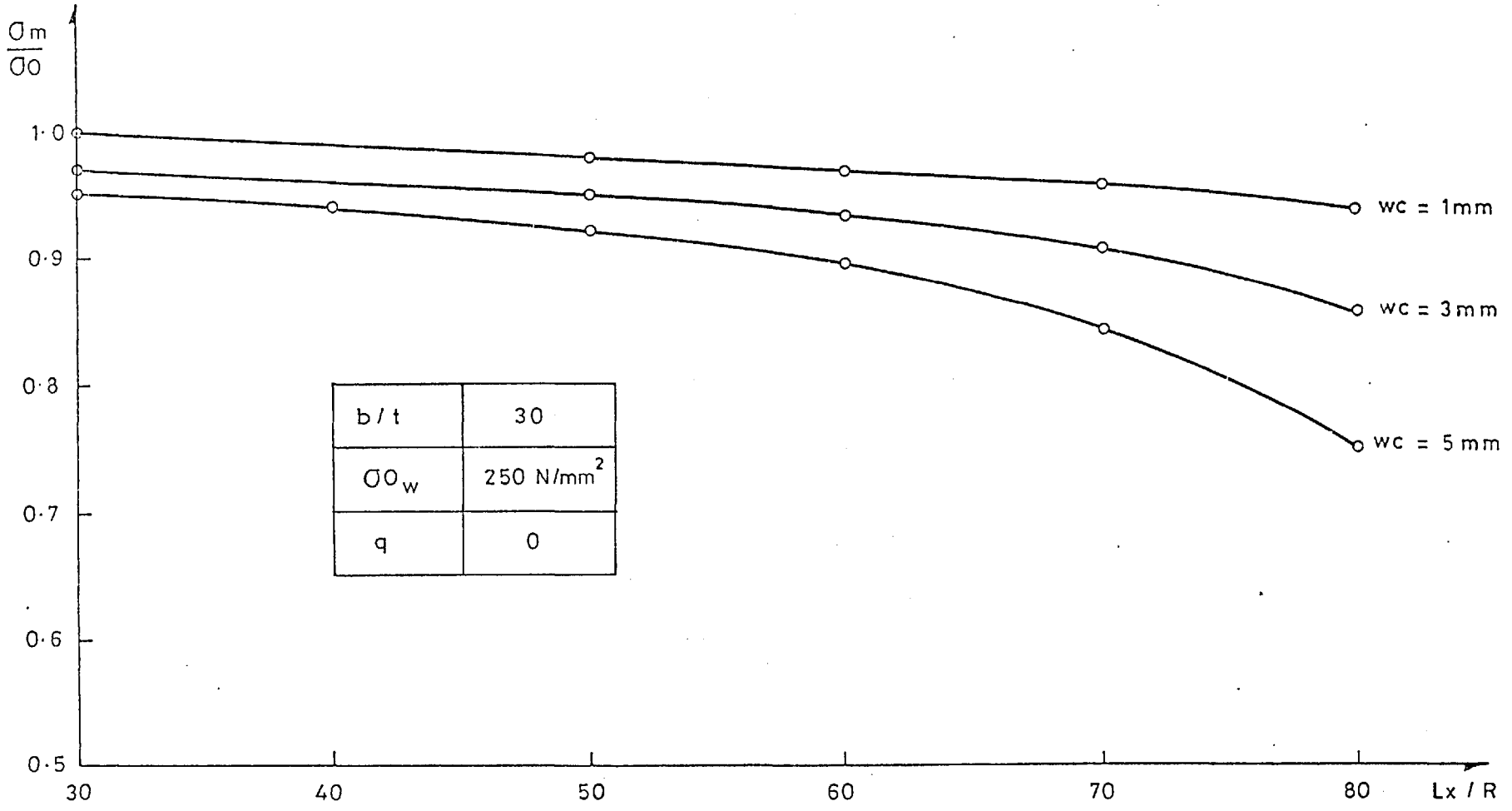

FigE52 Initial deformation study. Summary of peak loads

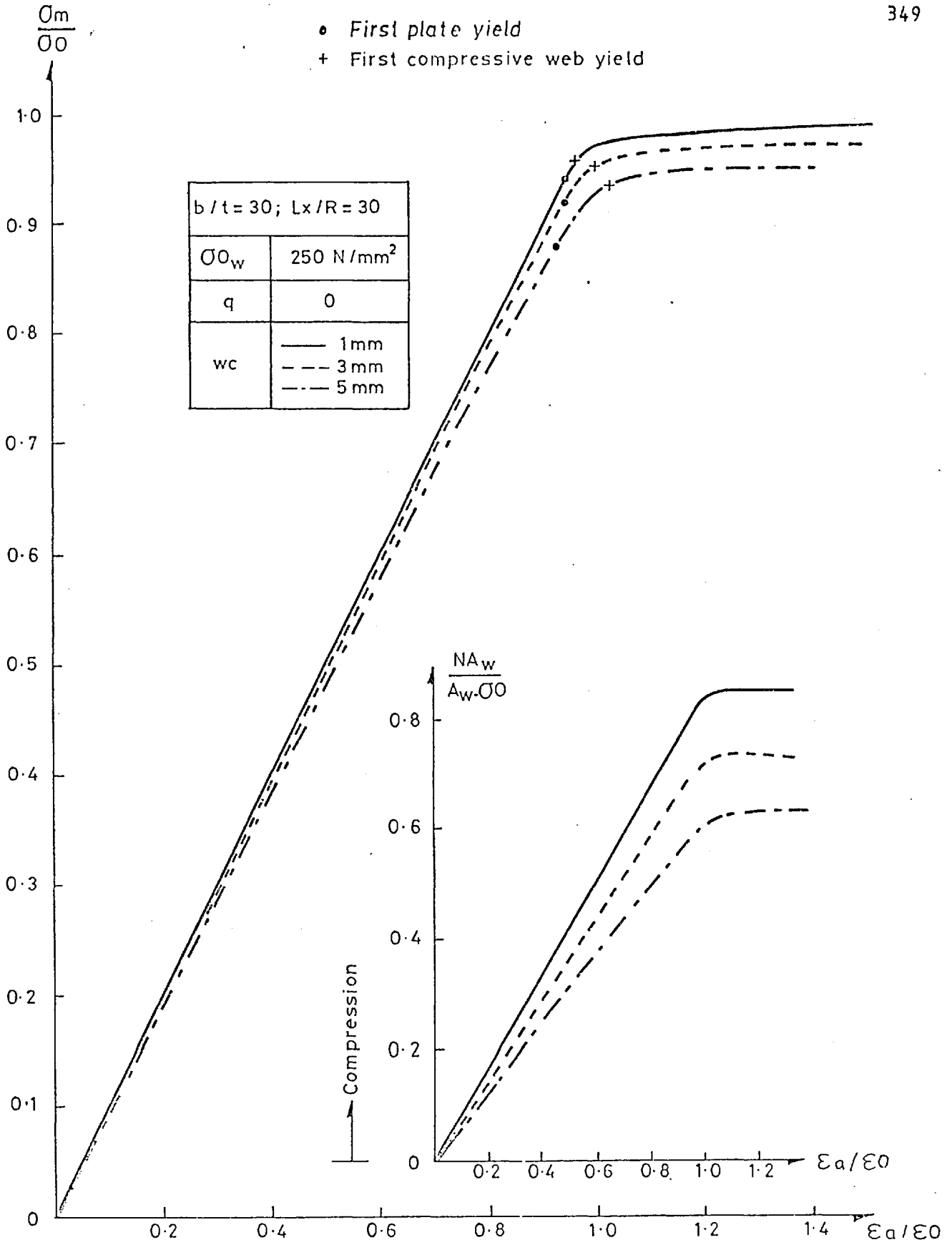

Fig E53 Initial deformation study. Mid-span stress in the webs and mean edge stress in the gross section versus applied strain for b/t = 30 and Lx/R = 30

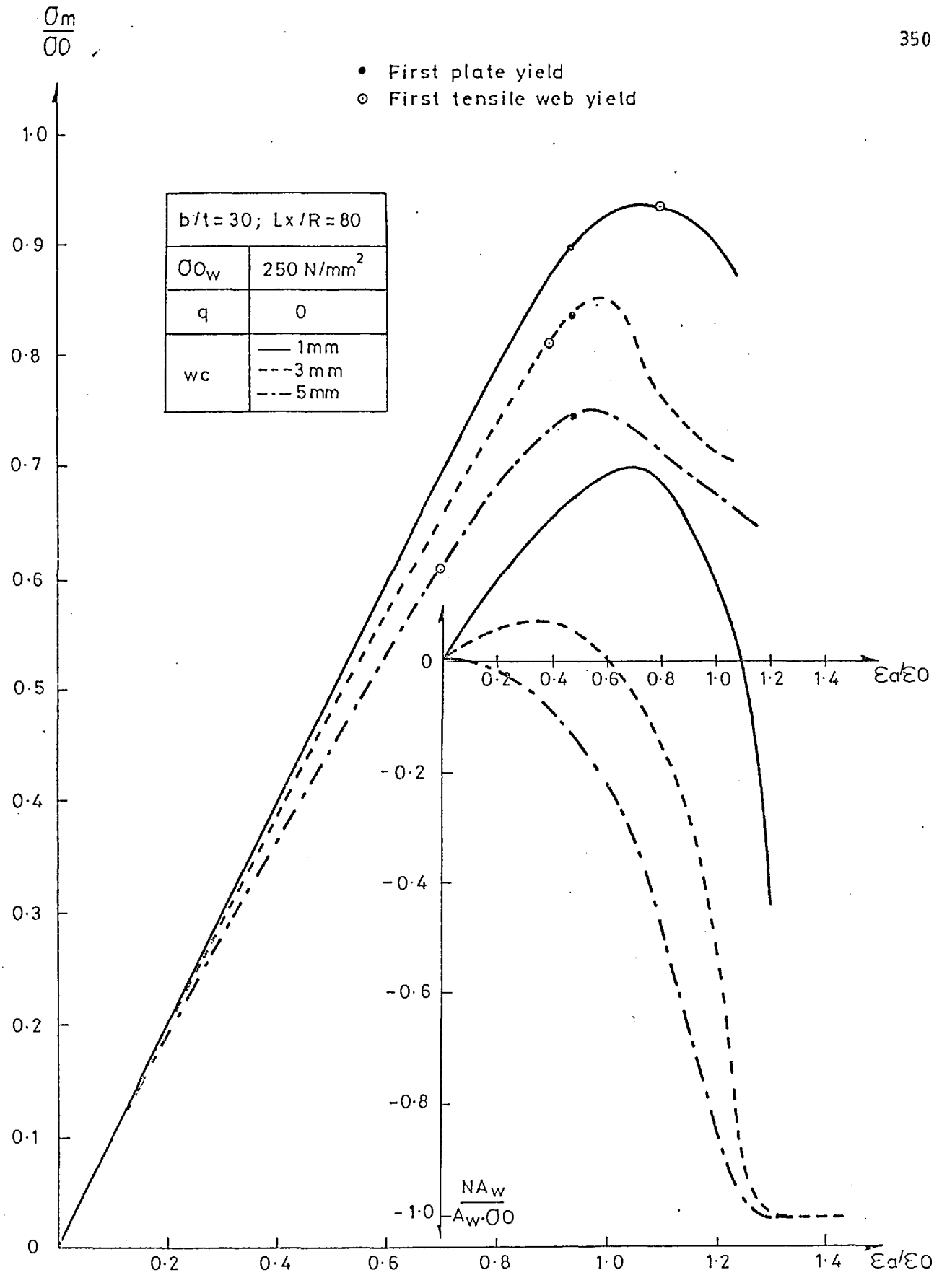

Fig E54 Initial deformation study. Mid-span stress in the webs and mean edge stress in the gross section versus applied strain for b/t = 30 and Lx/R = 80

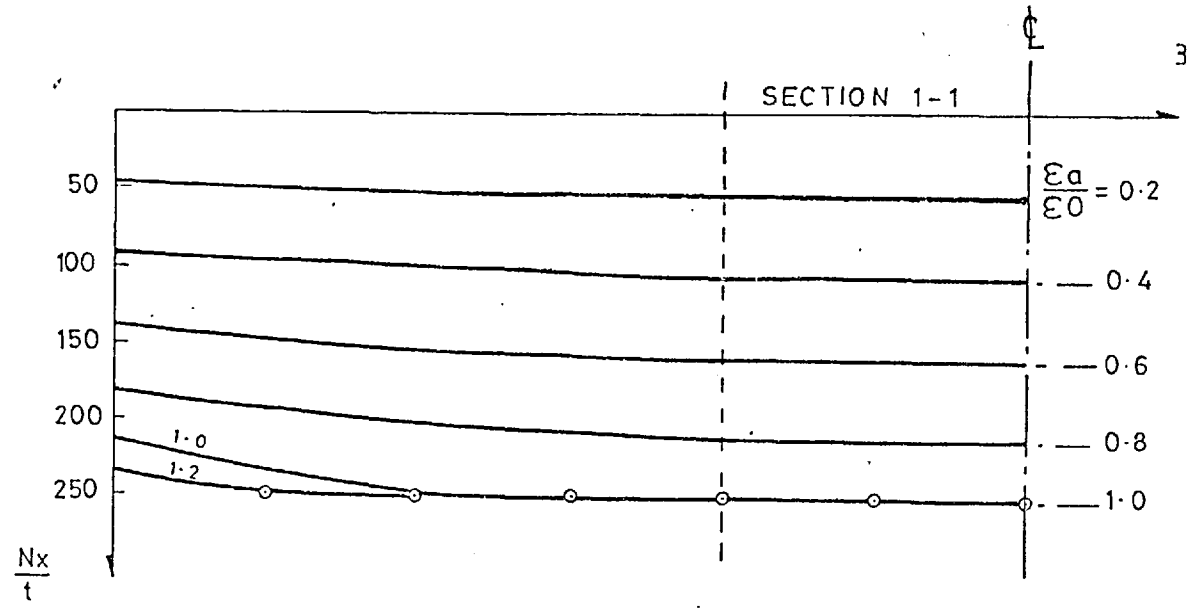

b/t = 30; Lx/R = 30; wc = 1 mm

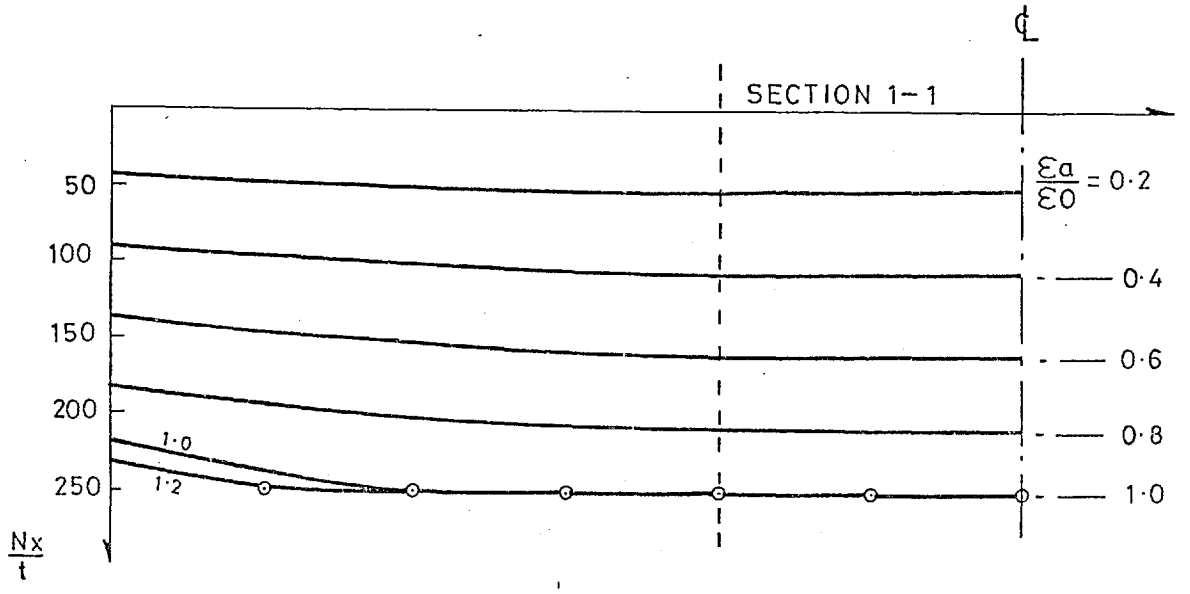

b/t = 30; Lx/R = 30; wc = 3 mm

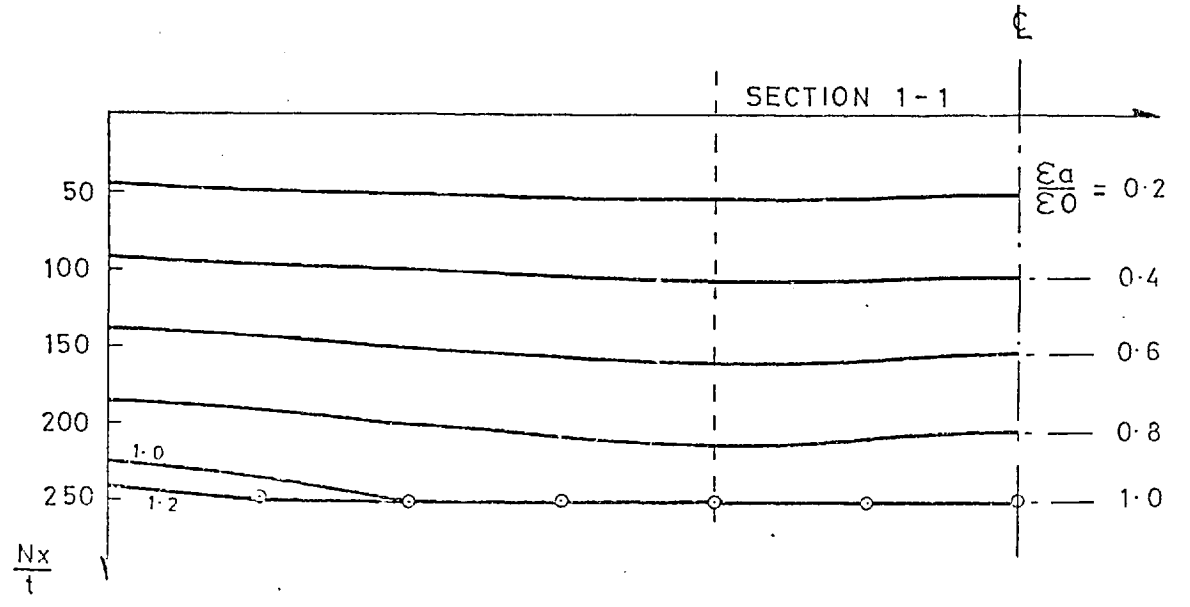

b/t = 30; Lx/R = 30; wc = 5 mm

⊙ Plastic nodes

Fig E55 Initial deformation study. Direct stresses at mid-span for increments of applied strain

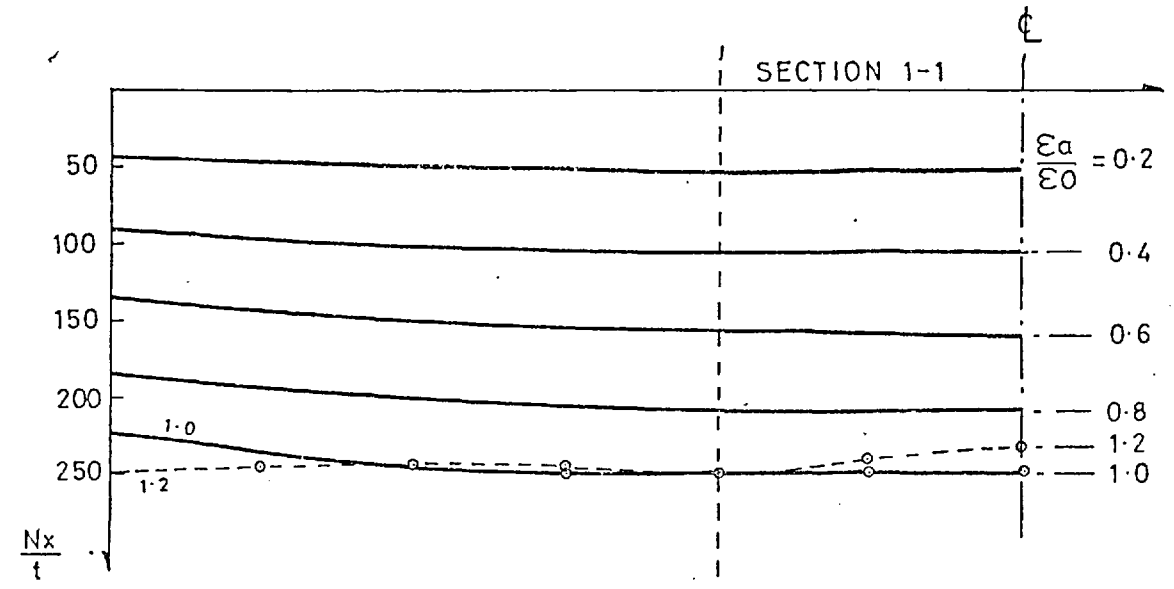

b/t = 30; Lx/R = 80; wc = 1mm

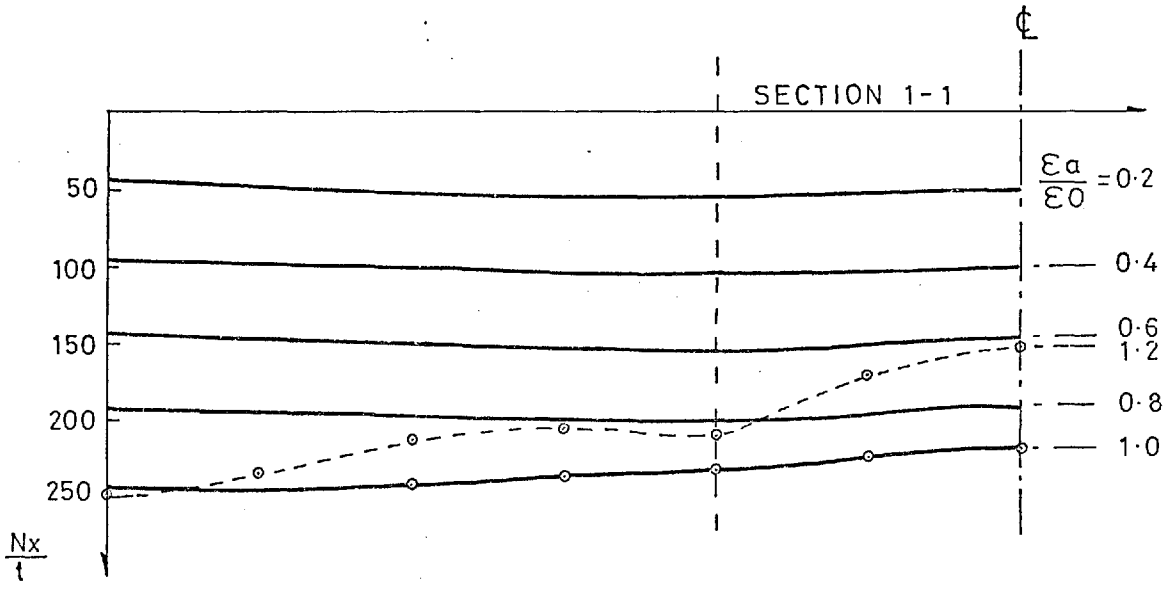

b/t = 30; Lx/R = 80; wc = 3mm

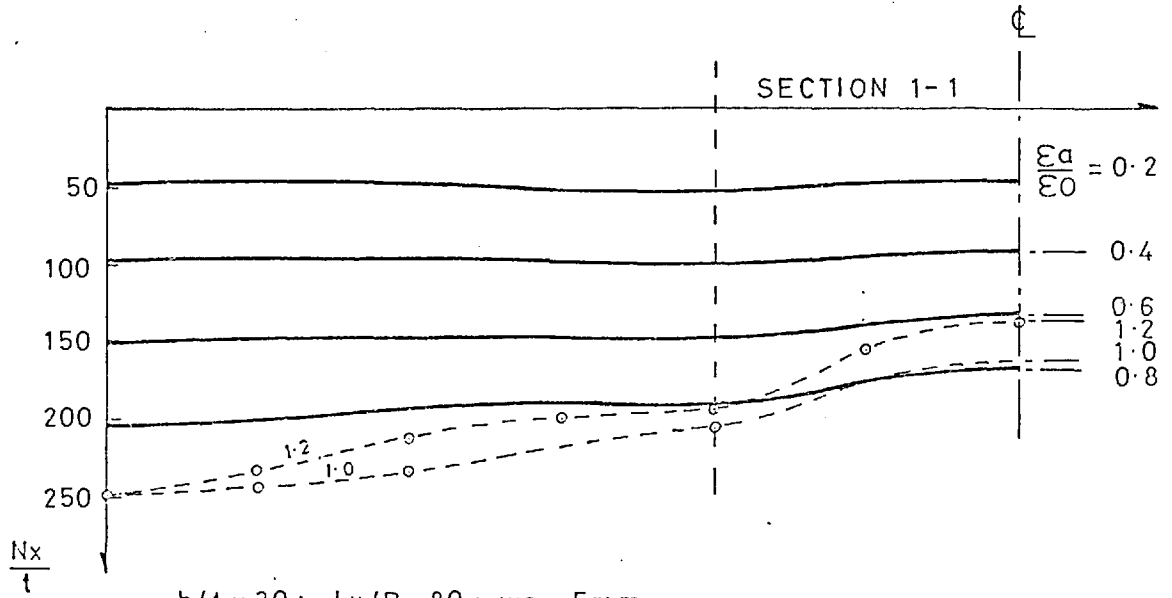

b/t = 30; Lx/R = 80; wc = 5mm

o Plastic nodes

Fig E56 Initial deformation study. Direct stresses at mid-span for increments of applied strain

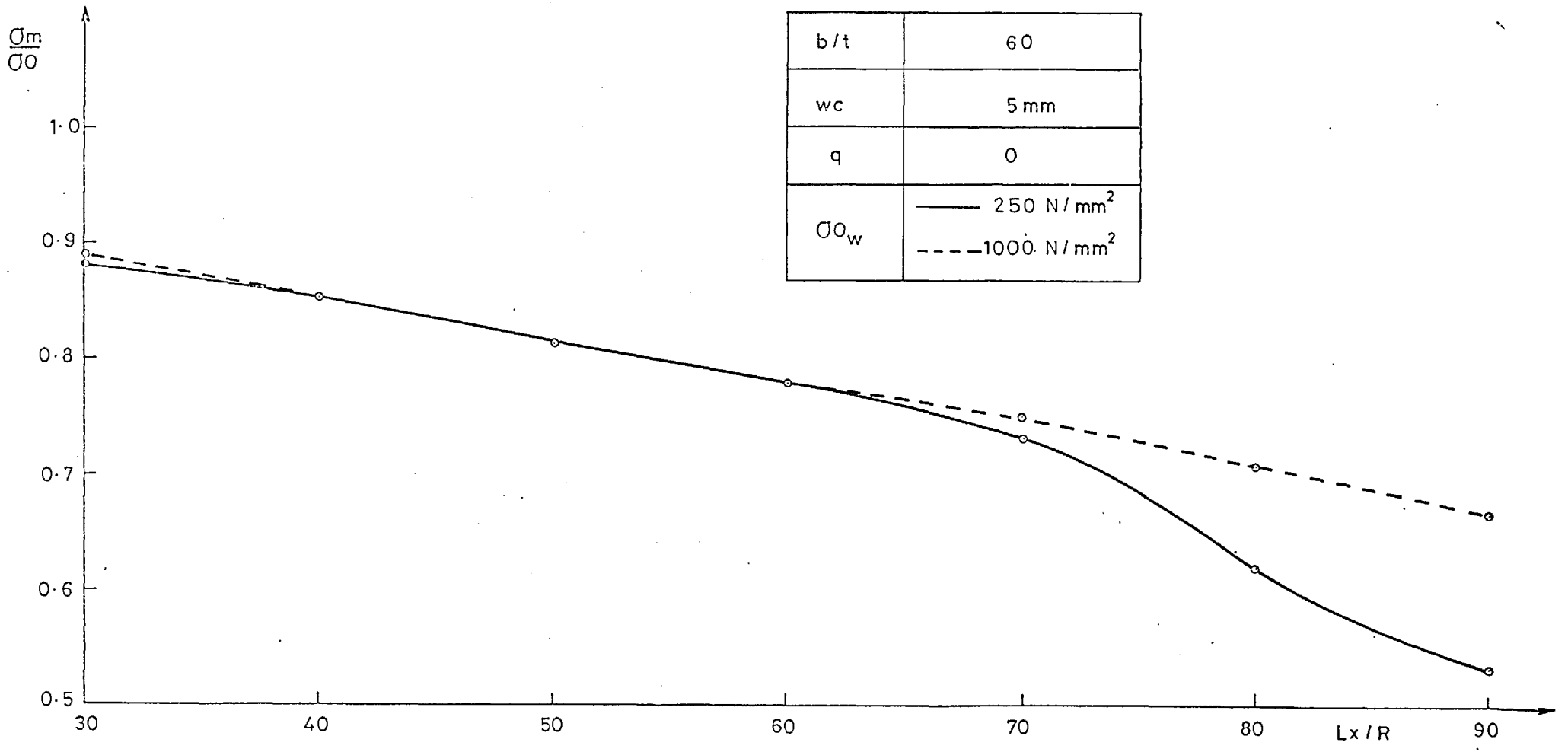

Fig E 57 Hybrid plates. Summary of peak loads

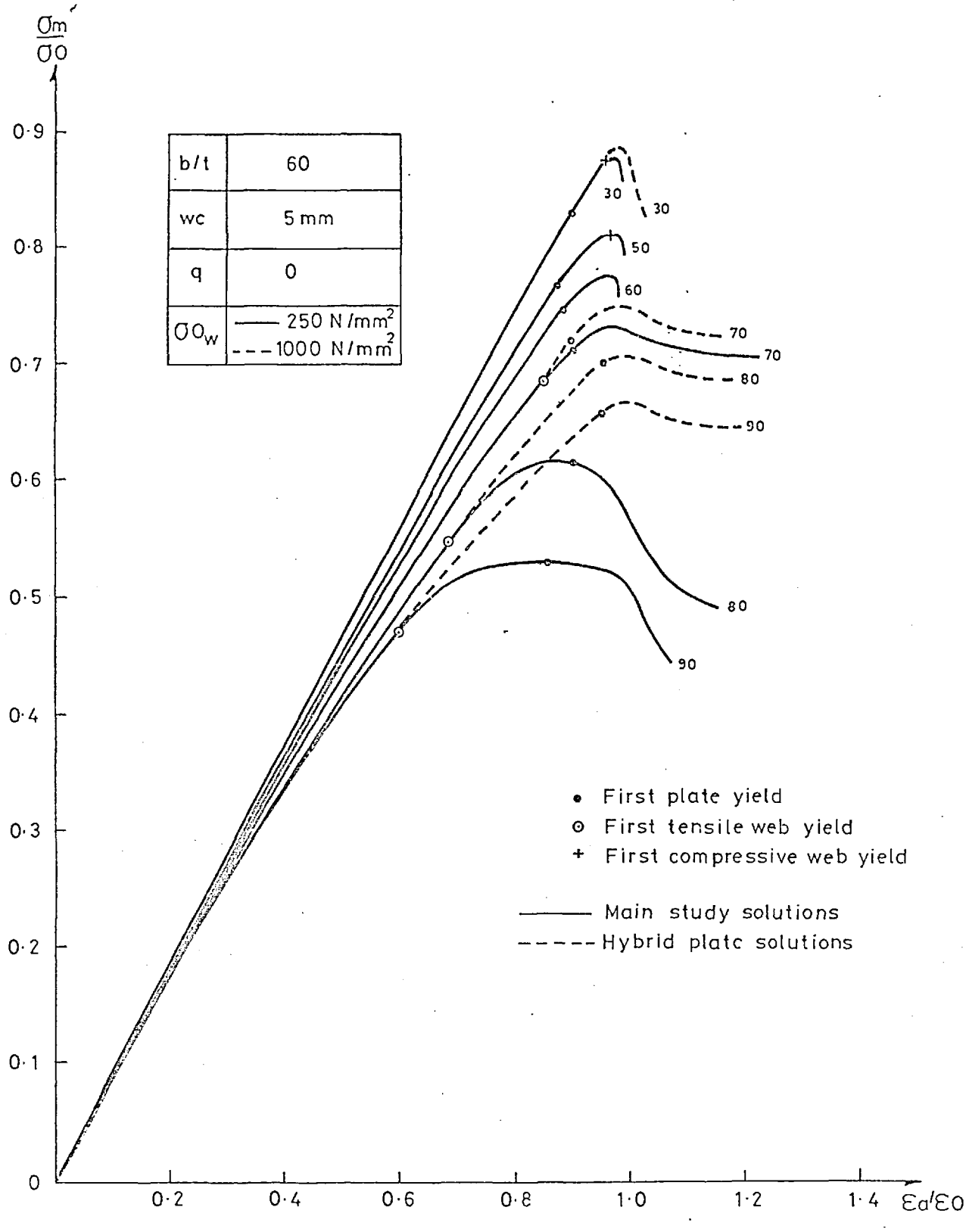

Fig E58 Hybrid plates. Mean edge stress in the gross section versus applied strain for $b/t = 60$ and $L_x/R = 30$ to 90

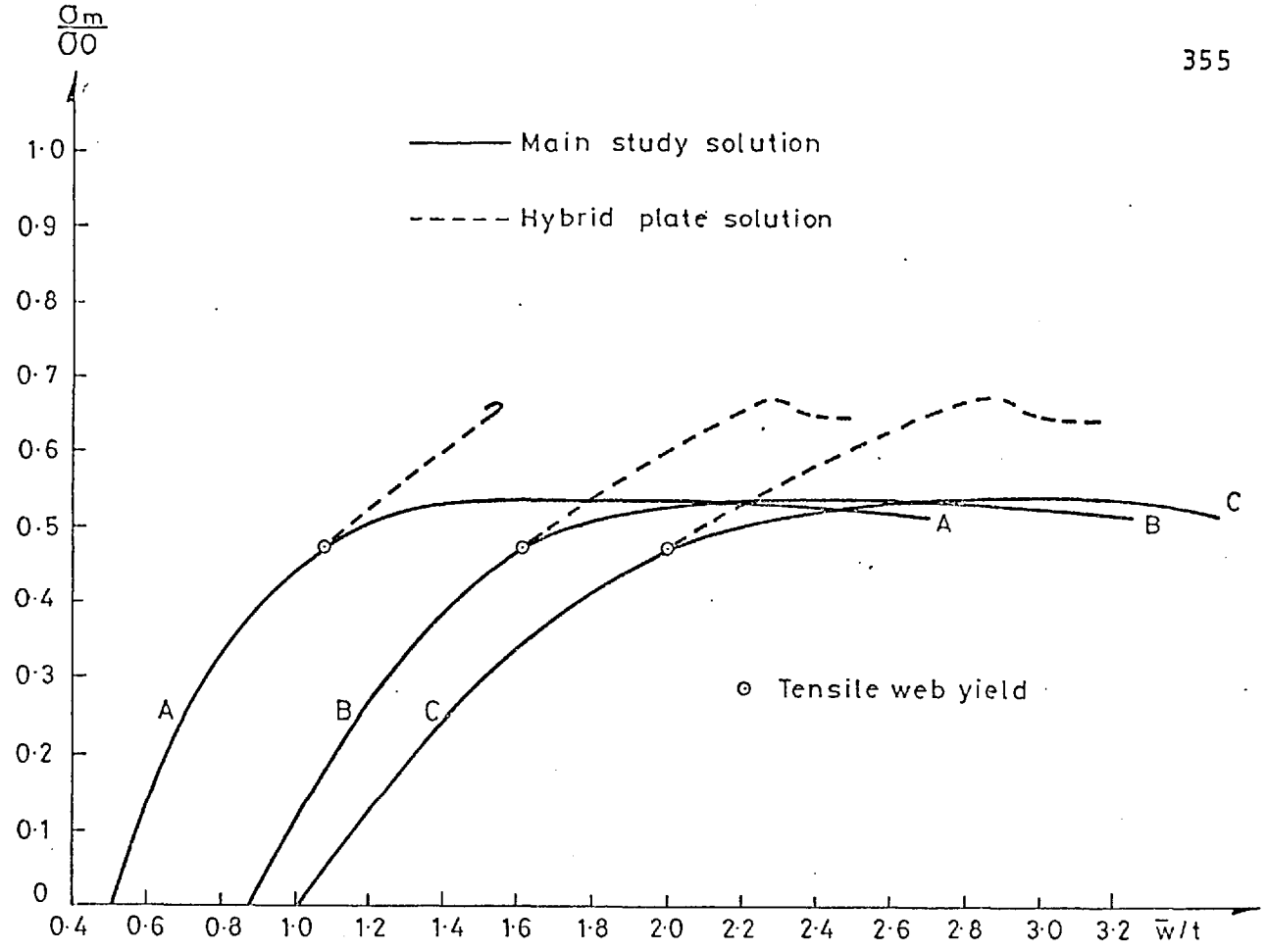

HYBRID PLATE b/t = 60 ; Lx/R = 90

LOAD-DEFLECTION CURVES

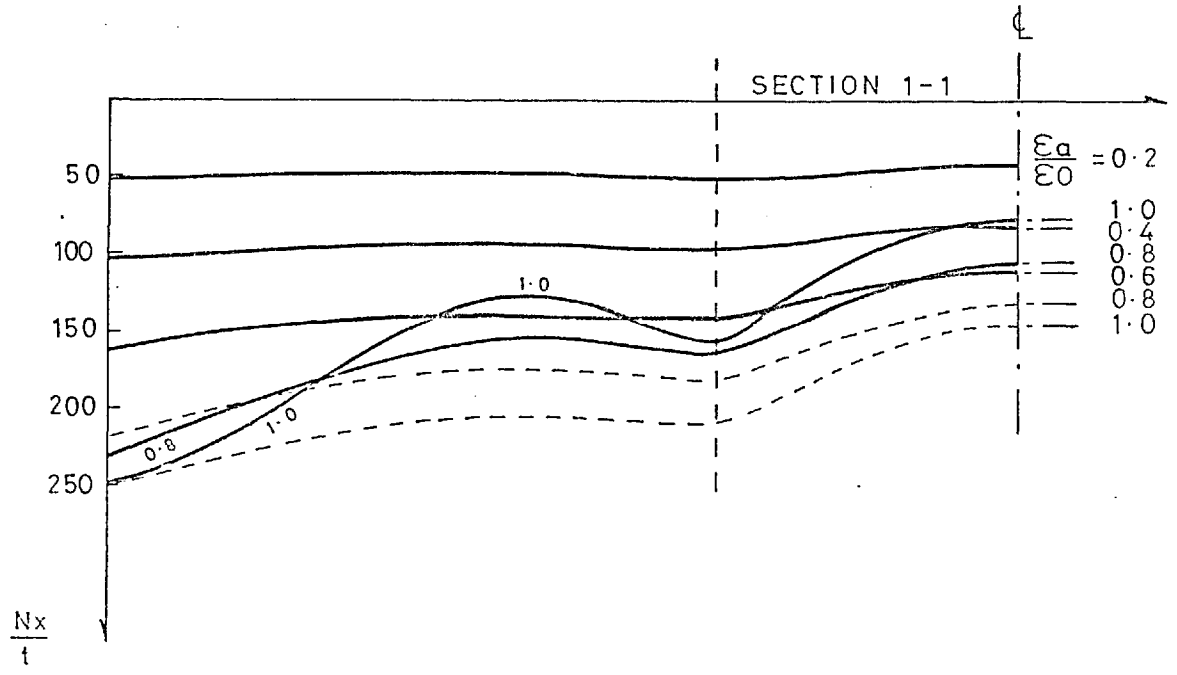

HYBRID PLATE b/t = 60; Lx/R = 90

DIRECT STRESSES AT MID-SPAN FOR INCREMENTS OF APPLIED STRAIN

Fig E 59

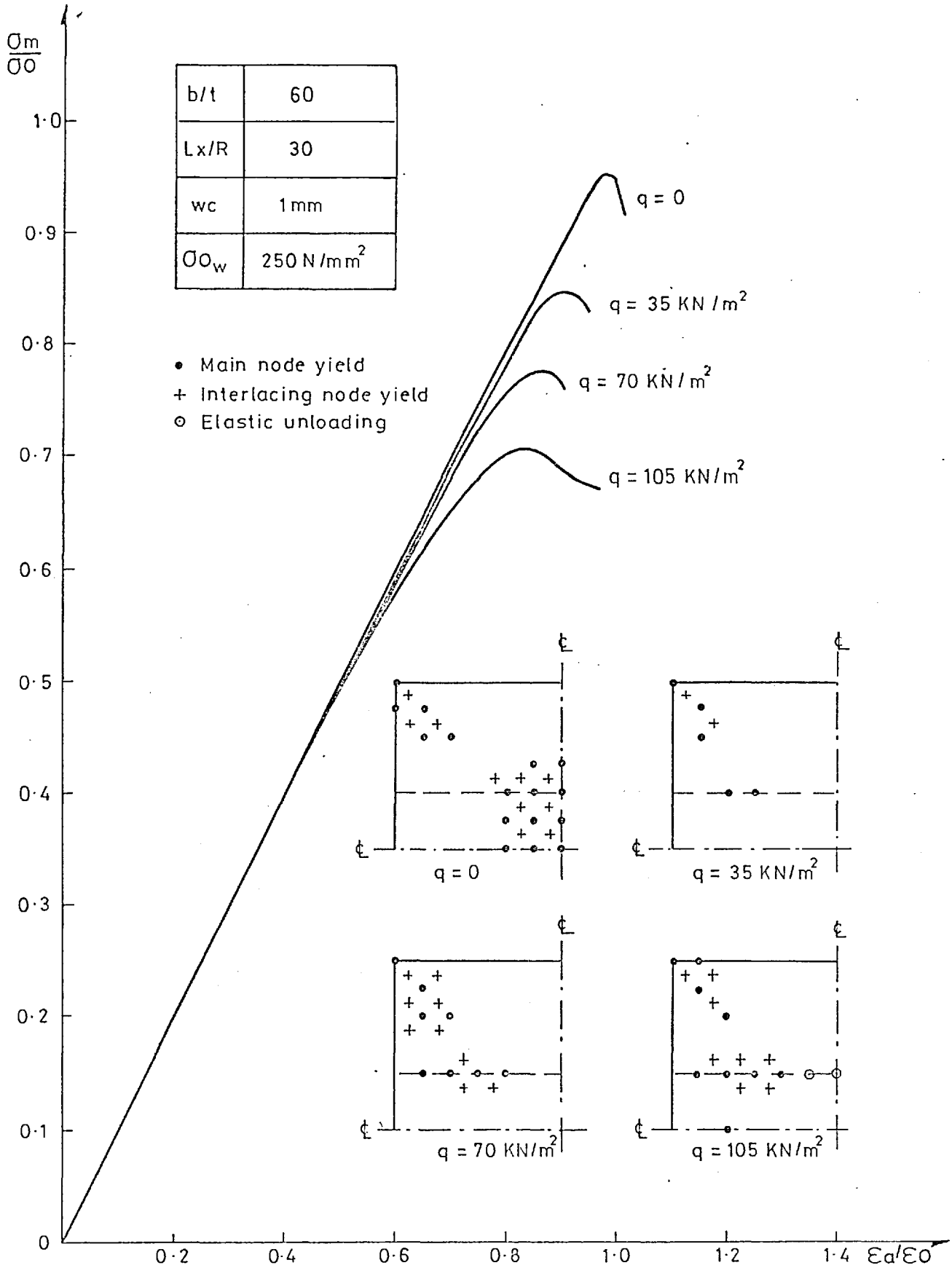

Fig E 60 Combined lateral and in-plane loading. Mean edge stress versus applied strain and peak load yield zones

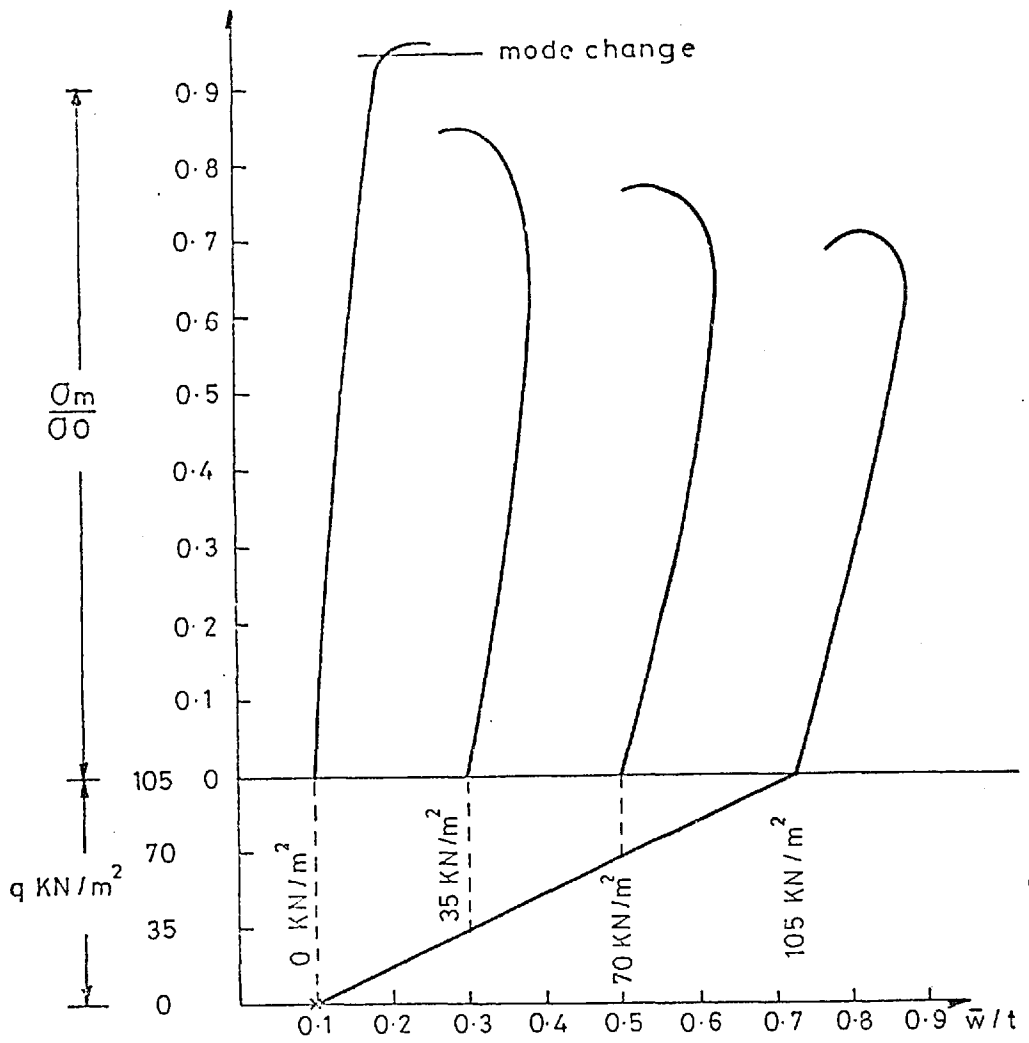

LOAD-DEFLECTION CURVES FOR POINT A

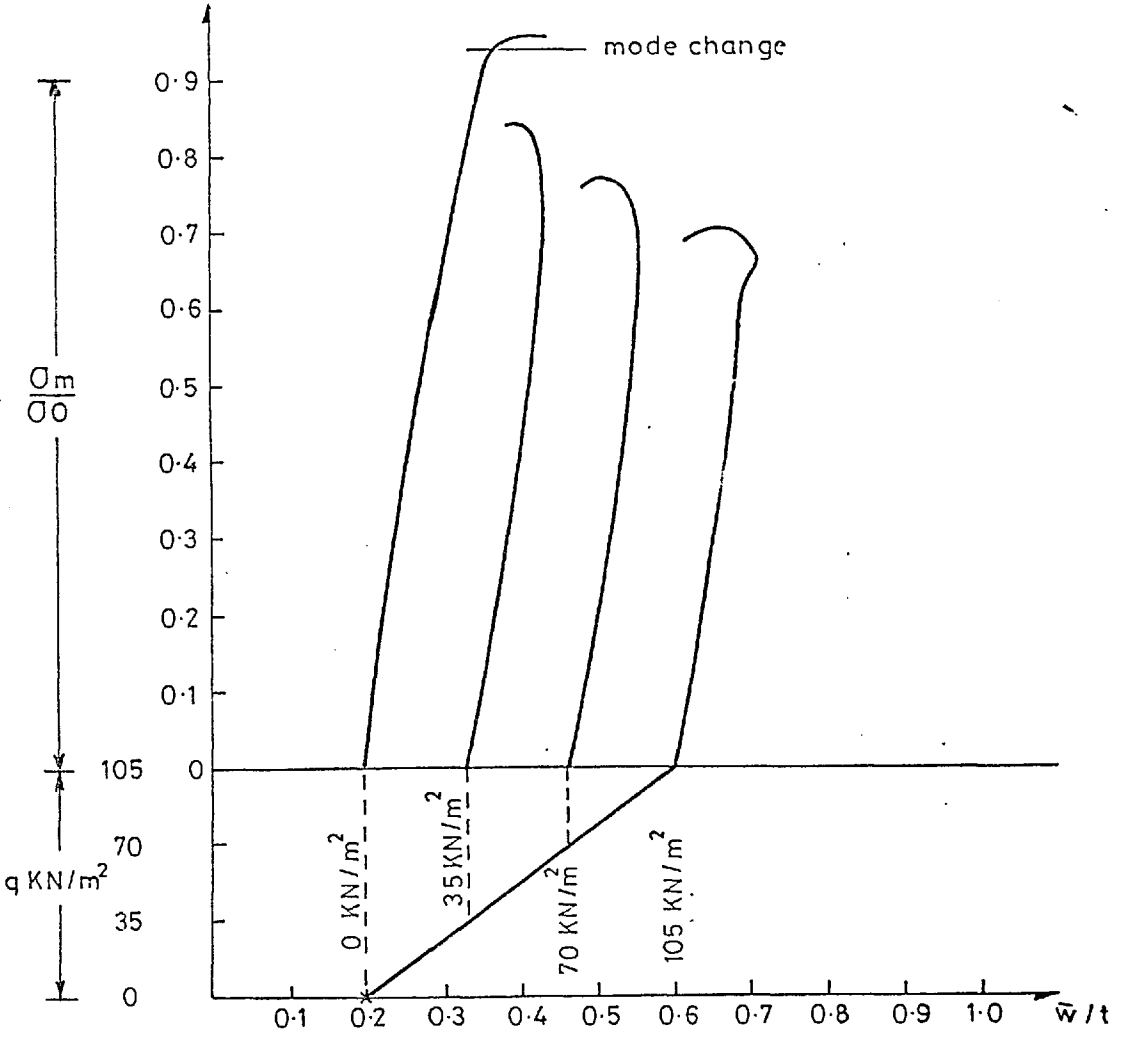

LOAD-DEFLECTION CURVES FOR POINT C.

Fig E 61 Combined lateral and in-plane loading. Load-deflection curves